Evaluating biotic and abiotic controls on plant stomatal conductance using mathematical models

A Dissertation Presented

by

Kenneth Davidson

to

The Graduate School

in Partial Fulfillment of the

Requirements

for the Degree of

Doctor of Philosophy

in

Ecology and Evolution

Stony Brook University

December 2023

Stony Brook University

The Graduate School

Kenneth Davidson

We, the dissertation committee for the above candidate for the

Doctor of Philosophy degree, hereby recommend

acceptance of this dissertation.

Shawn P. Serbin – Dissertation Advisor
Ecologist, Environmental and Climate Science Department
Brookhaven National Laboratory

Alistair Rogers - Chairperson of Defense
Senior Scientist, Environmental and Climate Science Department
Brookhaven National Laboratory

Heather J. Lynch
Professor, Department of Ecology and Evolution

Jennifer A. Holm
Research Scientist, Climate & Ecosystem Sciences Division
Lawrence Berkeley National Laboratory

This dissertation is accepted by the Graduate School

Celia Marshik
Dean of the Graduate School

Abstract of the Dissertation

Evaluating biotic and abiotic controls on plant stomatal conductance using mathematical models

by

Kenneth Davidson

Doctor of Philosophy

in

Ecology and Evolution

Stony Brook University

2023

Vegetation acts as a substantial link between the geosphere and atmosphere, mediating transpiration (E), and carbon assimilation (A). At the center of this process lie stomata, small pores which actively regulate the rate of CO_2 and H_2O diffusion between vegetation and the environment. This process, known as stomatal conductance (g_{sw}) helps set the upper limit on E, and through stomatal limitation on A, is a strong determinant of net primary productivity. A series of mathematical models have been developed to predict the sensitivity of g_{sw} to environmental factors, which have been incorporated into land surface models (LSMs). Despite the clear importance of accurately representing g_{sw} in LSMs, major uncertainty remains in the factors influencing the model parameters related to g_{sw} (the stomatal slope and stomatal intercept), particularly in how they are estimated from data, their temporal consistency, and their degree of variation within plant functional types (PFTs). In this dissertation, utilizing a combination of experimental manipulation, observational study, and mathematical and statistical modeling, I assess these three main sources of stomatal parameter uncertainty. My findings demonstrate that when unaccounted-for, branch excision combined with prolonged wait time can substantially impact the estimation of stomatal slope, with consequences for modeled transpiration. Further, I show that in a tropical evergreen forest, stomatal parameters exhibit diurnal variation, with water use efficiency (WUE) increasing throughout the day, however among leaves of different age classes, stomatal behavior is similar. In a temperate deciduous forest, where leaf ontogeny is closely match with seasonality, I show that stomatal and photosynthetic parameters display substantial variation across the growing season. I next demonstrate that stomatal parameters measured in the Arctic differ substantially from default LSM assumptions, and when updated parameters are applied to the model, ecosystem-scale WUE decreases significantly. Finally, using Bayesian modeling, I calculate a set of PFT specific stomatal parameters which can be used to parameterize LSMs, or serve as informative priors for future Bayesian model development. Overall, I demonstrate the effects of several biotic and abiotic drivers of variation in stomatal parameters, which contribute to significant uncertainty in LSM representation of instantaneous g_{sw} and evapotranspiration.

Dedication Page

To my parents for inspiring my sense of scientific curiosity, and to my wife for encouraging me to never give up on my goals.

Table of Contents

List of Figures vii
List of Tables xiv
Acknowledgements xvi

Chapter 1: Introduction 1

Chapter 2: Late-day measurement of excised branches results in uncertainty in the estimation of two stomatal parameters derived from response curves in *Populus deltoides* Bartr. × *Populus nigra* L 6
2.1 – Abstract 6
2.2 – Introduction 7
2.3 – Materials and Methods 9
2.4 – Results 16
2.5 – Discussion 17
2.6 – Figures 27
2.7 – Tables 33

Chapter 3: Short-term variation in leaf-level water use efficiency in a tropical forest 35
3.1 – Abstract 35
3.2 – Introduction 36
3.3 – Materials and Methods 39
3.4 – Results 44
3.5 – Discussion 47
3.6 – Figures 54
3.7 – Tables 64

Chapter 4: Seasonal trends in leaf level photosynthetic capacity and water use efficiency in a North American Eastern deciduous forest and their impact on canopy-scale gas exchange 66
4.1 – Abstract 66
4.2 – Introduction 67
4.3 – Materials and Methods 70
4.4 – Results 75
4.5 – Discussion 79
4.6 – Figures 85
4.7 – Tables 94

Chapter 5: Improving the parameterization of Arctic stomatal traits in a land surface model using empirical field observations and optimality theory 96
5.1 – Abstract 96
5.2 – Introduction 97
5.3 – Materials and Methods 100
5.4 – Results 110

Table of Contents

5.5 – Discussion 115
5.6 – Figures 125
5.7 – Tables 136

Chapter 6: An analysis of global parameters of stomatal behavior using Bayesian modeling ..138
6.1 – Abstract 138
6.2 – Introduction 139
6.3 – Materials and Methods 143
6.4 – Results 146
6.5 – Discussion 151
6.6 – Figures 161
6.7 – Tables 168

Chapter 7: Conclusion 174

Bibliography 182

Appendix 1: Supporting information for Chapter 2 217
Appendix 2: Supporting information for Chapter 3 222
Appendix 3: Supporting information for Chapter 4 246
Appendix 4: Supporting information for Chapter 5 254
Appendix 5: Supporting information for Chapter 6 262

List of Figures

Figure 2.1 - Schematic example of a stomatal response curve 27

Figure 2.2 - Effect of excision, time of day, and their interaction on the fitted value of stomatal slope 28

Figure 2.3 - Comparisons of the interactive effects of excision and time of day on stomatal parameters 29

Figure 2.4 - Effect of excision and time of day on foliar traits 30

Figure 2.5 - Model simulation of rates of photosynthesis and stomatal conductance over a diurnal course 31

Figure 2.6 - Observed and predicted dynamics of stomatal conductance for the diurnal course on August 10, 2020 32

Figure 3.1 - Geographic location of the crane site within the San Lorenzo Protected Forest and monthly climate averages collected at the site between 1997 and 2019 54

Figure 3.2 - Schematic representation of the response curve method 55

Figure 3.3 - Examples of the three phenological stages for four of the six species in this study .56

Figure 3.4 - Species specific averages of hourly photosynthesis, stomatal conductance, vapor pressure deficit at the leaf surface, and irradiance 57

Figure 3.5 - Validation plots of observed values of leaf level g_s versus model predicted data for the model based on response curve derived g_0 and g_1, the model based on survey derived g_0 and g_1, and the survey model with an inclusion of a time-of-day effect on g_1 58

Figure 3.6 - Fitted values of g_1 by species from the response and survey methods 59

Figure 3.7 - Simulated canopy scale E (g H_2O s^{-1}) at 15 min time points for *Guatteria dumetorum*, *Miconia borealis*, *Terminalia amazonia*, and *Vochysia ferruginea* on the 20th of February 2020 60

Figure 3.8 - Fitted values of g_1 for response curve data, and data from survey measurements 61

Figure 3.9 - Trends in fitted values of g_1 by time-of-day and species. g_1 decreases significantly with increasing time-of-day for all six species investigated 62

Figure 3.10 - Comparison of estimated mean total daily E (kg H_2O m^{-2} ground area) using the three models (Note A2.1) 63

List of Figures

Figure 4.1 - Schematic representation of sampling method and estimation of stomatal response parameters 85

Figure 4.2 - Fitted values of g_1 for response curve data, and data from survey measurements 86

Figure 4.3 - Average monthly estimates of four important physiological parameters 87

Figure 4.4 - Linear relationships between the maximum carboxylation capacity of Rubisco normalized to 25°C ($V_{cmax.25}$) and dark respiration rate normalized to 25°C ($R_{dark.25}$) and foliar functional traits. 88

Figure 4.5 - Linear relationships between the stomatal intercept (g_0) and slope parameter (g_1) from the Unified Stomatal Optimization model, and foliar photosynthetic and hydraulic traits ..89

Figure 4.6 - Relationships between monthly mean meteorological conditions and monthly mean physiological traits by species-group 90

Figure 4.7 - Model estimates for total monthly canopy transpiration using two different model parametrizations 91

Figure 4.8 - Model estimates for total monthly canopy net carbon assimilation using two different model parametrizations 92

Figure 4.9 - Total canopy net assimilation per unit ground area, for four of the most common species-groups present at Black Rock Forest 93

Figure 5.1 - Map of the four Next Generation Ecosystem Experiment - Arctic sites in Alaska, USA 125

Figure 5.2 - Comparison of ELM default and observed parameter values for arctic C_3 grass and broadleaf deciduous boreal shrub plant functional types 126

Figure 5.3 - Relationships between leaf traits, microclimatic conditions, and ELM parameter estimates obtained in this study 127

Figure 5.4 - Comparison of predicted ecosystem carbon and water fluxes between simulations in which different combinations of parameters were modified to correspond with field observations 128

Figure 5.5 - Comparison of mean annual response for simulations in which different combinations of parameters were modified to correspond with field observations 129

Figure 5.6 - Parameter variance decomposition based on an ensemble of 1000 simulations for each site 130

List of Figures

Figure 5.7 - Theoretical response functions for the effect of different soil moisture formulations on photosynthesis and stomatal conductance with different combinations of stomatal slope and intercept selected.....131

Figure 5.8 - Comparison of predicted ecosystem carbon and water fluxes between simulations in which different soil moisture stress formulations were applied 132

Figure 5.9 - Comparison of model predicted, and flux tower observed, ecosystem scale exchanges of carbon and water by month at the BEO site 133

Figure 5.10 - Comparison of model predicted, and flux tower observed, ecosystem scale exchanges of carbon and water by month at the Council site.....134

Figure 5.11 - Ecosystem scale water use efficiency (WUE; above ground net primary productivity/ vegetative transpiration; g C m^{-2} mm H_2O^{-1}), for all eight model variations at all four sites.....135

Figure 6.1 - Geographic and climatological extent of the data used in this study 161

Figure 6.2 - Observed versus model predicted g_{sw} (mol m^{-2} s^{-1}) for the three empirical models broken out by PFT group 162

Figure 6.3 - PFT specific estimates for stomatal slope and intercept and their relative uncertainty 163

Figure 6.4 – Köppen-Geiger Climate Zone specific estimates for stomatal slope and intercept and their relative uncertainty 164

Figure 6.5 - Evaluation of the effect of measurement methodology on estimates of stomatal slope and intercept and their relative uncertainty 165

Figure 6.6 - Observed versus model predicted g_{sw} (mol m^{-2} s^{-1}) for the three empirical models broken out by data source 166

Figure 6.7 - Correlations between estimated stomatal slope and leaf traits across all PFTs and species 167

Figure A1.1 - Diagnostic plots for g_s, A, and C_i across an expected range of irradiance, leaf temperature, and VPD_{air}.....217

Figure A1.2 - Comparison of values of C_i at each level of irradiance within a stomatal response curve.....218

Figure A2.1 - Histograms of VPD_{air} recorded by the STRI metrological station positioned on top of the canopy crane from 06:00-18:30 for the duration of the study and recorded inside the cuvette of the LI-6800 during survey measurements.....222

List of Figures

Figure A2.2 – Stomatal response regression fit following the form of Equation 3.2 of individual observations of from response curve data, and survey derived data.....223

Figure A2.3 - Histograms showing the distribution of individual observations of photosynthesis, stomatal conductance, vapor pressure deficit at the leaf surface, and irradiance, collected during diurnal survey measurements, divided out by time of day and by species 224

Figure A2.4 - Observed versus predicted fluxes of canopy scale *E* for *Guatteria dumetorum*, *Miconia borealis*, *Terminalia amazonia*, and *Vochysia ferruginea* using three different methods to derive stomatal parameters 225

Figure A2.5 - g_0 comparisons between different methods reveal a similar trend of elevated survey parameter estimates for four of the six species 226

Figure A2.6 - The relationship between response curve derived g_1 and g_0 and LMA, Ψ_{leaf}, and successional stage 227

Figure A2.7 – The relationship between leaf water potential and model residual (difference between observed and predicted g_s) for the survey model including a time-of-day effect.....228

Figure A2.8 - Relationship between leaf phenological stage and $V_{c,\max.25}$, and $R_{dark.25}$, for the six species in this study 229

Figure A2.9 - Simulations of daily canopy *E* by species when using different leaf phenology distributions.....230

Figure A2.10 - g_1 as estimated from response curves collected with decreasing (saturating to 0 μmol PAR) and increasing (0 μmol PAR to saturating) levels of irradiance 231

Figure A2.11 - Comparison of fitted values for g_1 and g_0 by species for curves conducted in the morning (07:00-12:00) and afternoon (12:01-18:00) 232

Figure A2.12 – Estimated g_1 versus length of response curve measurement.....233

Figure A2.13 - Calibration plots for the curve derived data, and the survey derived data used to build the models of g_1 and g_0 234

Figure A2.14 - Mean estimated intercellular carbon mole fraction (C_i) by species and leaf age 235

Figure A2.15 - Conceptual illustration of the link between stomatal slope, and water use efficiency.....236

Figure A2.16 – Observed vs predicted g_s when a Ψ_{leaf} penalty is applied (upper panels, Note A2.3), and when no penalty is applied (lower panels).....237

List of Figures

Figure A2.17 - Reduction in potential g_s between Equation A2.1(100% at any Ψ_{leaf}) and Equation A2.3 as a function of Ψ_{leaf} for four species 245

Figure A3.1 - Evaluation of individual residuals for the maple and white oak species-groups .246

Figure A3.2 – Average monthly estimates of leaf mass per area, leaf dry matter content, elemental nitrogen per unit mass, elemental nitrogen per unit area, ratio of foliar carbon to nitrogen, stomatal density, the ratio between the dark respiration rate normalized to 25°C, and the maximum carboxylation capacity of Rubisco normalized to 25°C by species-group for the 2021 growth season.....247

Figure A3.3 - Frequency distributions of the level of the relative strength of the stomatal limitation on photosynthesis 248

Figure A3.4 - Relationships between leaf to air VPD, PAR, and air temperature, and the level of stomatal limitation on photosynthesis.....249

Figure A3.5 - Average monthly relative water deficit at turgor loss, and predawn Ψ_{leaf} by species-group for the 2021 growth season 250

Figure A4.1 - Model output for carbon dynamics during regular spin up phase 253

Figure A4.2 – Relationships between parameters used in ensemble simulations.....254

Figure A4.3 - Above ground responses for simulations in which different β_t factor functions were tested 255

Figure A4.4 - Below ground responses for simulations in which different β_t factor functions were tested 256

Figure A4.5 - Comparison of model predicted, and observed, site level soil moisture content by day of year.....257

Figure A4.6 - Theoretical relationships between assimilation rate transpiration rates when ELM default and updated parameters for stomatal slope and intercept are used.....258

Figure A5.1 - Caterpillar plots of posterior chains and histograms of posterior distributions for PFT specific slope and intercept using the BWB model and informative priors 262

Figure A5.2 – Caterpillar plots of posterior chains and histograms of posterior distributions for PFT specific slope and intercept using the Medlyn model and informative priors 263

Figure A5.3 - Caterpillar plots of posterior chains and histograms of posterior distributions for PFT specific slope and intercept using the Lamour model and informative priors 264

List of Figures

Figure A5.4 - Caterpillar plots of posterior chains and histograms of posterior distributions for PFT specific slope and intercept using the BWB model and uninformative priors.....265

Figure A5.5 - Caterpillar plots of posterior chains and histograms of posterior distributions for PFT specific slope and intercept using the Medlyn model and uninformative priors 266

Figure A5.6 - Caterpillar plots of posterior chains and histograms of posterior distributions for PFT specific slope and intercept using the Lamour model and uninformative priors 267

Figure A5.7 – Caterpillar plots of posterior chains and histograms of posterior distributions for PFT specific slope and intercept using the Lamour model and uninformative priors for slope an intercept, but informative priors for $R_{d.25}$.....268

Figure A5.8 - Caterpillar plots of posterior chains and histograms of posterior distributions for climate zone specific slope and intercept using the BWB model and uninformative priors 269

Figure A5.9 - Caterpillar plots of posterior chains and histograms of posterior distributions for climate zone specific slope and intercept using the Medlyn model and uninformative priors....270

Figure A5.10 - Caterpillar plots of posterior chains and histograms of posterior distributions for climate zone specific slope and intercept using the Lamour model and uninformative priors ...271

Figure A5.11 - Caterpillar plots of posterior chains and histograms of posterior distributions for measurement method specific slope and intercept using the BWB model and uninformative priors 272

Figure A5.12 – Caterpillar plots of posterior chains and histograms of posterior distributions for measurement method specific slope and intercept using the Medlyn model and uninformative priors 273

Figure A5.13 - Caterpillar plots of posterior chains and histograms of posterior distributions for measurement method specific slope and intercept using the Lamour model and uninformative priors 274

Figure A5.14 - The effect of using informative versus uninformative priors on PFT specific estimates of stomatal slope and intercept 275

Figure A5.15 - PFT specific correlations between estimated stomatal slope and leaf traits which were significant 276

List of Tables

Table 2.1 - Fixed effects components from the mixed effects models tested 33

Table 2.2 - Linear effect means and contrast estimates for the interactive effects of excision and time of day 34

Table 3.1 - Values for species-specific photosynthetic and conductance parameters and canopy scaling factors used in simulations of leaf-level A and g_s.....64

Table 3.2 - Fixed effects components from the mixed effects models tested 65

Table 4.1 - Average species-group-specific values for photosynthetic and conductance parameters used in fixed model simulations of canopy E and NPP, and approximate date of leaf out and leaf coloration 94

Table 4.2 - Estimates of monthly mean stomatal limitation on photosynthesis (I) and the proportions of observations (1 hr model timestep) where limitation occurs 95

Table 5.1 - Species specific estimates of stomatal and photosynthetic parameters 136

Table 5.2 - Default and updated ELM parameter values for Arctic PFTs 137

Table 6.1 - List of models evaluated as part of this study.....168

Table 6.2 - Goodness of fit of the three stomatal models in predicting g_{sw} when validated using an external dataset 171

Table 6.3 - Model summary for the PFT specific models 172

Table A1.1 - Parameters used in the coupled photosynthesis, conductance, and energy balance models used for simulations in this study 219

Table A1.2 - Biochemical and functional properties estimated for each treatment group 220

Table A1.3 - Fixed effects components from the mixed effects model comparing photosynthetic parameters to leaf structural properties 221

Table A2.1 - Parameter estimates and their standard error for the response curve model.....239

Table A2.2 - Parameter estimates and their standard error for the survey model.....240

Table A2.3 - Parameter estimates and their standard error for the survey + time-of-day model 241

Table A2.4 - Species specific Weibull function values corresponding to xylem conductivity versus Ψ_{stem} 244

List of Tables

Table A3.1 - Group specific parameters used in the coupled photosynthesis, conductance, and energy balance models used for simulations in this study 251

Table A3.2 - Values for mean monthly photosynthetic and conductance parameters by species-group 252

Table A4.1 - Updated PFT specific values for F_{LNR} to account for corrections to α_{R25} and F_{NR} as recommended by Rogers, (2014) 259

Table A4.2 - Probability density functions used to simulate prior distributions for ensemble model.....260

Table A4.3 - Probability density functions used to simulate prior distributions for ensemble model.....261

Table A5.1 - Links to the datasets used in this study, and their associated manuscripts 277

Table A5.2 - Model summary for the PFT specific models using uninventive priors 278

Acknowledgments

There are so many people to thank who assisted with and enabled the completion of this dissertation. It was a long, and at times winding road, and I could not have made it to the end without a great deal of guidance and support.

Thank you to my BNL committee members, Shawn Serbin and Alistair Rogers, for your mentorship, scientific insights, and feedback, and for taking the time to work with me to hone my analytical and communication skills. Coming to BNL to do my PhD was one of the best choices of my scientific career.

Thank you to Heather Lynch, not only for serving on my committee, but also for her masterful coaching in all things statistics and policy. I have benefited greatly from her instruction.

Thank you to my external committee member Jennifer Holm, for agreeing to help me learn the ropes of Earth System Modeling. Your insights into the development of my latter two chapters have been extremely helpful.

Thank you to all my TEST Group colleagues, past and present. Daryl, Jeremiah, Kim, Andrew, Cherry, Julien, Angie, Baily, Jin, Ran, and Keith. You have all been influential in so many aspects of my research, either through close mentorship, technical assistance, or just being there to bounce ideas off of. I will always remember the memories we have made together in the office, lab, and field.

Thank you to my peers at SBU who shared in this academic journey with me. Anna M., José, Rachael, Nicolette, Jannet, Paul, Julia, Alison, Anna T., Bill, Ashley, and Carlos. You have all contributed to the sense of camaraderie and belonging I feel within the E&E department.

To my external collaborators and colleagues, from NGEE-Tropics; Joe Wright, Alfonso Zambrano, Matrijn Slot, Edwin Andrades, Nate McDowell, Alex Pivovaroff, and Brett Wolfe, from NGEE-Arctic; Fengming Yuan, Benjamin Sulman, Daniel Ricciuto, and Coleen Iverson, and from Black Rock Forest; Katie Terlizzi, Matthew Munson, Grayson Badgley, and Matthew Brady. You have all contributed your time, skills, and intellects to the success of this research.

This work was supported by the Biological and Environmental Research Program within the US Department of Energy's Office of Science, through the NGEE - Tropics project (contract no. DE – SC0012704 to BNL), and the NGEE – Arctic project (contract no. DE- SC0012704 to BNL), the Black Rock Forest Consortium (David Redden Conservation Science Fund), and by the Stony Brook University Department of Ecology and Evolution graduate student support funding (Lawrence B. Slobodkin Graduate Research Fund and Graduate Excellence Fund).

The text of this dissertation in part is a reprint of materials as they appear in the journals New Phytologist and Tree Physiology. This work is in the Public Domain in the US, and additional permission to use this material in this dissertation has been granted by the journal publishers, John Wiley & Sons, Inc., and Oxford University Press.

Chapter 1: Introduction

Of the processes required to simulate the role of vegetation in influencing and mediating Earth's climate, few are more central than vegetative gas exchange. The vegetative layer serves to regulate approximately 61% of the global flux of water to the atmosphere via transpiration (*E*; Schlesinger & Jasechko, 2014), and the majority of the input of carbon from the atmosphere to the biosphere and geosphere via photosynthetic carbon assimilation (*A*; Ainsworth & Rogers, 2007). In addition, vegetative gas exchange also plays a critical role in terrestrial energy balance via its impact on sensible and latent heat flux (Duveiller *et al.*, 2018). The challenge of mathematically modeling *A* and stomatal conductance to water vapor (g_{sw}) has occupied the intellects of scientists for the better part of 60 years, ever since Bassham, Benson, and Calvin used radio tagged C^{14} isotopes to trace the path of carbon through the photosynthetic apparatus and into assimilated carbohydrates (Bassham & Calvin, 1960). A great deal of modern plant physiological research focuses on developing, parameterizing, and improving mathematical models of *A* and g_{sw} incorporated into Land Surface Models (LSMs), which are process-rich mechanistic representations of the terrestrial biosphere used to model the dynamics, responses, and feedbacks of vegetation to the climate system (Fisher *et al.*, 2018; Lawrence *et al.*, 2019; Fisher & Koven, 2020).

While the representation of *A* in LSMs is relatively well constrained (Rogers *et al.*, 2017c), for the most part simulated using the Farquhar von Caemmerer Berry (FvCB) biochemical model of steady state photosynthetic assimilation (Farquhar *et al.*, 1980), large uncertainties remain regarding the representation of g_{sw} in LSMs (Dietze *et al.*, 2014; Jefferson *et al.*, 2017; Ricciuto *et al.*, 2018). Stomatal behavior is key to the understanding of long-term limitations on both *A* and *E*, as stomata set the upper limit on CO_2 diffusion into the intercellular airspace (Long & Hällgren, 1993), and act as the main means of vegetation to regulate water loss via transpiration (Farquhar & Wong, 1984). Stomatal restrictions on CO_2 diffusion can lead to limitations on photosynthetic assimilation (McDowell *et al.*, 2006) and can even lead to carbon starvation and plant mortality (McDowell, 2008; McDowell *et al.*, 2019). Likewise, lack of stomatal control (e.g., infinite g_{sw}), can lead to excess loss of water via transpiration, which can have a myriad of physiological, structural, and biochemical consequences for the plant, including turgor loss (Scholander *et al.*, 1964; Brodribb *et al.*, 2003; Bartlett *et al.*, 2012), cavitation and embolism of the xylem (Tyree & Sperry, 1989; Jones & Sutherland, 1991; Klein *et al.*, 2018), and non-stomatal reductions in

photosynthetic performance (Dewar *et al.*, 2018; Gourlez de la Motte *et al.*, 2020; Sabot *et al.*, 2022). Thus, uncertainties in models of stomatal behavior will have an impact on carbon and water flux estimates, with additional implications for the calculation of energy balance.

The majority of stomatal models used in LSMs are constructed around the linearity of the A-g_{sw} relationship (Damour *et al.*, 2010; Miner *et al.*, 2017), first demonstrated experimentally by Wong *et al.*, (1979). Empirical stomatal modeling followed (Farquhar & Wong, 1984), which was furthered by Ball *et al.*, (1987) who showed that the balance of the A-g_{sw} relationship is mediated in part by the difference in humidity between the leaf surface (representing the sub-stomatal region) and the atmosphere. From these observations, Ball and colleagues (1987) arrived at a model with two parameters, a stomatal slope which governs the relationship between the stomatal index (a multivariate term combining photosynthetic rate, CO_2 concentration, and atmospheric water demand) and g_{sw}, and the stomatal intercept, which is equivalent to the expected g_{sw} when net photosynthesis is zero. Much of the subsequent model development has arisen from investigations into g_{sw} behavior under dynamic growth conditions (e.g., changes in VPD, temperature, light, and soil moisture), and has been guided by the overriding theory that stomata have evolved to limit water loss while maximizing carbon gain. First proposed by Cowan & Fraquhar, (1977; Equation 1.1), this theory of optimal stomatal behavior suggests that the ratio of the partial derivative of E with respect to A is maintained, yielding λ, the marginal cost (in terms of water) for a unit of carbon gain. In simpler terms, λ represents the optimal water use efficiency (WUE) for a given leaf or plant.

Equation 1.1
$$\frac{\partial E}{\partial A} = \lambda$$

Optimality assumptions have been incorporated into a number of empirical stomatal models, most notably the unified stomatal optimization model (USO; Medlyn *et al.*, 2011), where the value for the stomatal slope parameter is approximately inversely proportional to WUE. Other more mechanistic models assess the impact of soil, root, or xylem water limitations on g_{sw} by applying an empirical scaling factor to one of the model parameters which adjusts g_{sw} in proportion to the water supply limitation, typically estimated from a metric such as leaf or soil water potential (Anderegg *et al.*, 2017; Rogers *et al.*, 2017; Tuzet *et al.*, 2003). Further still, some more advanced optimality-based models not only consider the water cost of carbon in terms of hydraulic limitation, but also consider the effect of g_{sw} on future biochemical limitations on photosynthesis (Hölttä *et al.*, 2017; Dewar *et al.*, 2018; Wang *et al.*, 2020b).

Regardless of the exact stomatal conductance model used, uncertainties in model parameterizations will still be propagated into LSM predictions of carbon, water, and energy cycling, as the principal determinant of stomatal model performance is the parameterization of the stomatal slope and intercept (Héroult *et al.*, 2013; Lin *et al.*, 2015; Wolz *et al.*, 2017; Franks *et al.*, 2018; Wu *et al.*, 2019b). Of the uncertainties related to stomatal model parameterization, three of the most common are (1) uncertainty in how stomatal parameters are estimated from data; (2) uncertainty in the temporal consistency of stomatal parameters; and (3) uncertainty in the degree of parameter variation, both within and among plant functional types (PFTs). In this dissertation, using a combination of experimental and observational data evaluated against expected model response, I investigate all three of these sources of uncertainty across various scales and ecosystems.

In chapter 2, I present the results of an experiment in which I test an often-overlooked aspect of measurement methodology (Santiago & Mulkey, 2003; Verryckt *et al.*, 2020; Missik *et al.*, 2021), namely if the estimation of the stomatal slope and intercept are impacted by predawn branch excision. I found that predawn branch excision did not significantly affect measured slope and intercept when measured within 4h of excision, however after this threshold, stomatal slope decreased by an average of 25% in excised branches. When this 25% difference in stomatal slope was applied to a model of canopy gas exchange, modeled transpiration was 18% lower over a simulated diurnal period.

In chapter 3, motivated by the finding that leaf age is an important determinant of photosynthetic capacity in evergreen tropical forests (Wu *et al.*, 2016), I assess possible physiological and mechanistic controls on the estimation of the stomatal slope and stomatal intercept parameters, using diurnal gas exchange surveys and leaf-level response curves of six tropical broadleaf evergreen tree species. I find that stomatal slope and intercept varied between leaves of different phenological stages, however there was no consistent trend in among-species stomatal parameters with leaf age, making a uniform and unidirectional leaf age effect on stomatal traits difficult to justify in a model of canopy transpiration. I also identified a diurnal trend associated with stomatal slope and intercept that significantly improved model projections of diurnal trends in transpiration.

In chapter 4, motivated by the lack of explicit seasonality in WUE in most LSMs, I investigated seasonal patterns in leaf-level physiological, hydraulic, and anatomical properties in a deciduous

temperate forest ecosystem. I found that the maximum carboxylation capacity of the enzyme rubisco (V_{cmax}) and the stomatal slope were seasonally variable, taking on a peaked distribution, however their patterns were not temporally synchronized. I show that seasonal progression of V_{cmax} was primarily driven by changes in leaf structural and anatomical characteristics, while seasonal changes in stomatal slope were most strongly related to changes in V_{cmax} and leaf hydraulics. Further, I demonstrate that when using a seasonally variable V_{cmax} and stomatal slope to parameterize a canopy scale gas exchange model, seasonally aggregated A and E are increased by 3% and 16% respectively.

In chapter 5, motivated by a lack of physiological and trait data measured on Arctic vegetation, I collected stomatal response curves on eight arctic plant species, across a range of environmental conditions, and used these data to estimate five key foliar model parameters for the two default arctic PFTs used in the E3SM land model (ELM). I also tested widely held assumptions about stomatal optimality by modifying the way in which soil moisture stress influences instantaneous g_{sw} and evapotranspiration in ELM. I found that when I used updated parameters in ELM, ecosystem-scale water use efficiency decreased significantly across all four of the simulation sites, primarily because of substantially higher simulated E. The measured stomatal intercept parameter was observed to be 400-500% higher than the model default, thus contributing to the largest effect, leading to a substantial increase in the baseline rate of E.

Lastly, in chapter 6, I assembled a dataset consisting of 27723 unique observations across 198 species measured at 66 locations globally, and using Bayesian modeling, investigated patterns of within- and among-PFT variation in stomatal parameters. My motivation for this analysis was to assess if global variation in stomatal slope and intercept could be predictably associated with PFT, climate and/or leaf traits. In addition, I use these data to assess the efficacy of three common empirical stomatal models, which have yet to be compared head-to-head across a diverse dataset. My findings broadly suggest that for non-woody PFTs, stomatal slope and intercept vary predictably according to optimal resource allocation theory, however in PFTs which occupy the same bioclimatic region, PFT specific estimates of stomatal slope and intercept may be confounded by co-occurring climatic factors and leaf trait associations. Additionally, there was no difference in model goodness of fit between models of g_{sw} which use an RH vs a VPD function, however, when gross photosynthesis was used in place of net photosynthesis, the model failed to reproduce g_{sw} observations at a higher rate, particularly in non-woody PFTs.

Overall, with this dissertation, I demonstrate how multiple sources of parametric and model structural uncertainty related to stomatal conductance can contribute to uncertainty in LSM representation of carbon, water, and energy cycles. Such uncertainties include unknown effects of leaf age or ontogeny on stomatal slope and intercept, unknown relationships between PFT and bioclimatic variables which may influence assumptions about PFT-level stomatal traits, and unknown effects of soil moisture stress on leaf gas exchange, which may be incorrectly represented in current LSMs. By identifying these uncertainties, which in large part stem from biotic and abiotic factors which influence stomatal behavior at the species or PFT-level, I aim to help guide future model development with respect to correctly representing these processes. In particular, many of the relationships identified in this dissertation could be added to existing LSMs so that they more closely approximate stomatal processes or mechanisms (e.g., effect of leaf ontogeny on stomatal slope). My findings broadly underscore the need to closely consider the methods used when deriving stomatal parameters, the assumptions implicit in leaf-level models of stomatal conductance, and the simplification of natural diversity in traits required when PFT specific stomatal parameters are derived. Further, I demonstrate the implications (in terms of model output) associated with each model update when they are applied to fully coupled LSMs, providing a practical assessment of each modification, which may help guide the modeling community as to the value of making a model update.

Chapter 2: Late day measurement of excised branches results in uncertainty in the estimation of two stomatal parameters derived from response curves in *Populus deltoides* Bartr. x *Populus nigra* L.

2.1 – **Abstract:**

Many terrestrial biosphere models depend on an understanding of the relationship between stomatal conductance and photosynthesis. However, unlike the measurement of photosynthetic parameters, such as the maximum carboxylation capacity, where standard methods (e.g., CO_2 response or AC_i curves) are widely accepted, a consensus method for empirically measuring parameters representing stomatal response has not yet emerged. Most models of stomatal response to environment represent stomatal conductance as being bounded by a lower intercept parameter (g_0), and linearly scaled based on a multivariate term described by the stomatal slope parameter (g_1). Here I employ the widely used Unified Stomatal Optimization model, to test whether g_1 and g_0 parameters are impacted by the choice of measurement method, either on an intact branch, or a cut branch segment stored in water. I measured paired stomatal response curves on intact and excised branches of a hybrid poplar clone (*Populus deltoides* Bartr. x *Populus nigra* L. OP367), measured twice over a diurnal period. I found that predawn branch excision did not significantly affect measured g_0 and g_1 when measured within 4h of excision. Measurement in the afternoon resulted in significantly higher values of g_1 and lower values of g_0, with values changing by 55% and 56% respectively. Excision combined with afternoon measurement resulted in a marked effect on parameter estimates, with g_1 increasing 89% from morning to afternoon and a 25% lower g_1 for cut branches than those measured *in situ*. I also show that in hybrid poplar the differences in parameter estimates obtained from plants measured under different conditions can directly impact models of canopy function, reducing modelled transpiration by 18% over a simulated 12.5-hour period. While these results are only for a single isohydric woody species, my findings suggest that stomatal optimality parameters may not remain constant throughout the day.

2.2 – **Introduction:**

Model representation of the exchange of carbon dioxide and water vapor between vegetative canopies and the atmosphere is a critical component of land surface models (LSMs). Both of these fluxes are fundamentally governed by stomatal control, which balances water loss through transpiration (E) against CO_2 entry into the leaf via photosynthesis (Hetherington & Woodward, 2003). Many models of stomatal regulation assume that stomatal conductance (g_{sw}), the rate of water vapor exiting leaf stomata, has evolved to be optimal with respect to water use, i.e. plants maximize carbon gain, per unit of water lost (Cowan & Fraquhar, 1977; Damour *et al.*, 2010). This optimal relationship can be represented empirically using the "Unified Stomatal Optimization" model (USO; Medlyn *et al.*, 2011; Eqn. 2.1), which has two derived parameters, g_1 ($kPa^{0.5}$), typically referred to as the stomatal slope, which governs the relationship between the stomatal index (a multivariate term combining photosynthetic rate, CO_2 concentration, and leaf to air vapor pressure deficit) and g_s, and g_0 (mol m^2 s^{-1}) representing the expected stomatal conductance when net photosynthesis is zero. The model also has three measured variables, photosynthetic rate (A, μmol m^2 s^{-1}), the leaf to air vapor pressure deficit (VPD_{leaf}, kPa), and CO_2 concentration at the leaf surface (C_a, mol mol^{-1}). In the USO framework, g_1 is inversely proportional to water use efficiency, abbreviated WUE, and defined as $\partial E/\partial A$. A large g_1 is associated with a plant that loses more water per unit carbon assimilated than a plant with a low g_1.

Equation 2.1. $$g_{sw} = g_0 + 1.6\left(1 + \frac{g_1}{\sqrt{VPD_{leaf}}}\right)\frac{A}{C_a}$$

Despite the fact that A and g_{sw} rates directly impact global carbon and water cycles, their relationship continues to be a large source of variation in current model predictions (Ricciuto *et al.*, 2018). For example, Dietze *et al.* (2014) found that when unconstrained by data, g_1 was the second largest uncertainty in their analysis of global controls on net primary productivity. However, unlike many other photosynthetic parameters that can be derived from gas exchange measurements, no consensus exists on a standard method for estimating g_0 and g_1 (Bernacchi *et al.*, 2013; Sharkey *et al.*, 2007). One common method for assessing stomatal function is a survey-based approach, where rates of A and g_{sw} are measured instantaneously under natural conditions, and g_1 and g_0 are fit from the data with regression analysis (e.g., Lin *et al.*, 2015). Alternatively, many investigators have used a response curve approach for the estimation of stomatal behavior, in which the environment around a leaf (e.g., irradiance, C_a, or VPD_{leaf}) is altered, and the operator

observes how rates of steady state A and g_{sw} respond (Ball *et al.*, 1987; Leakey *et al.*, 2006; Mott, 1988). Unlike survey methods, response curves control for leaf-to-leaf variation in response, and capture a parameter estimate at a fixed point in time, and thus are an appealing method for fitting parameter estimates used in LSMs of vegetation function.

However, stomatal response curves are not without drawbacks, sometimes taking up to a full day to complete for a single leaf (Leakey *et al.*, 2006). This poses a challenge when the species of interest is difficult to access, and for this reason, researchers often sample branches and conduct response curves *ex situ*, utilizing methods such as shotgun sampling (Serbin *et al*. 2014; Burnett *et al*. 2019; 2021), or manual branch pruning (Wu *et al.*, 2019b). However, with these *ex situ* measurements comes the assumption that excision of a branch will not fundamentally alter the response of the parameter of interest, through branch cavitation or other stress responses (Santiago & Mulkey, 2003; Verryckt *et al.*, 2020; Missik *et al.*, 2021).

It is well known that excision can alter wood conduit structure by introducing air into the xylem, which can lead to cavitation and embolism of tissue upstream of the cut (Williamson & Milburn, 1995). Xylem damage can also reduce the volume of water reaching the leaf tissue, altering capacitance (Sperry *et al.*, 1993), potentially influencing the relationship between A and g_s. A number of studies (e.g., Verryckt *et al.*, 2020, Santiago & Mulkey, 2003; Missik *et al.*, 2021; Akalusi *et al.*, 2021) have shown that if branches are immediately recut under water after initial excision, rates of A and g_{sw} may be unaffected. Importantly, however, these studies do not assess changes in the parameters g_1 and g_0, stomatal traits which may be more acutely affected by hydraulic damage if water supply to the leaf is impaired.

A final implicit assumption with the response curve approach is that the measured parameter will be temporally constant, and thus will not change over the length of the measurement. In most cases however, there is a contrast between the apparent parameter measured, and the ideal or nominal value for the parameter. For example it is known that the maximum rate of Rubisco carboxylation normalized to 25ºC ($V_{cmax.25}$) declines over a diurnal time-course due to Rubisco deactivation, leading late day estimation of $V_{cmax.25}$ to be up to 50% lower than the morning value (Salvucci and Anderson 1987; Kobza and Seemann 1989). In addition, Resco de Dios *et al.* (2020) found that changes in the circadian timing of metabolism over diurnal timescales leads to different "optimal" levels of g_s, showing that assuming a fixed optimal level for stomatal parameters is not consistent with observation.

Here I attempt to test two key assumptions of stomatal response curves in a controlled manner, namely that time since branch excision, and the time of day in which a measurement is made will not impact fitted parameter estimates. My objective was to determine if g_1 and g_0 estimations were different between pairs of cut and intact branches, measured across two periods during a day. My specific research questions were; (1) does predawn excision of branches lead to a modified stomatal response to irradiance, compared with the intact *in situ* measurement curves? (2) Is g_1 diurnally dynamic, leading to shifts in WUE over the course of the day? (3) Will use of g_0 and g_1 estimated from excised or late day measurements produce different estimates of leaf scale transpiration?

2.3 – **Materials and Methods:**

Plant material:

In May 2019, 20 cm hardwood stem cuttings of *Populus deltoides* Bartr. X *Populus nigra* L. OP367 (hybrid poplar) were soaked in water until roots formed and transplanted into 210 L pots filled with Pro-Mix M (Premier Tech, Quebec, Canada) potting soil. Plants were grown outside on a fenced concrete pad at Brookhaven National Laboratory (Upton, NY, USA, latitude: 40.8834319, longitude: -72.870103, elevation: 18 m above sea level). Mean annual temperature at the site is 10.3ºC, and mean annual precipitation is 1244.6 mm. During the period of study average temperature was 22.3ºC, and the site received a total of 114.3 mm of precipitation. Data collection took place during the second year of growth. During spring and summer, pots were irrigated every other day to field capacity to prevent soil from drying to the point at which the plants would experience soil water stress. During this period, three fertilizer treatments of Peters Professional 15-16-17 (ICL Specialty Fertilizers, Dublin, Ohio, USA) were applied, the last of which occurred seven days before the first measurements were taken. At each application, approximately 4.5 L of fertilizer mix was injected into the soil using a Dosatron D14MZ10 Fertilizer Injector (Dosatron International Inc., Clearwater, FL, USA), set to a mix rate of 200 ppm with the injector set at a 1:100 ratio fertilizer to water.

Measurements took place from July 15 – August 21, 2020. For each measurement day two plants were selected, and on each plant two equivalent branches were identified, one which would be excised predawn and the other to serve as an intact control. Prior to excision, a target leaf was identified and flagged on each of the four candidate branches. The target leaves were matched so

that within each plant, leaves were of the same approximate size, color, phenological stage, and leaf plastochron index (LPI) (Erickson & Michelini, 1957; Meicenheimer, 2014; Rogers *et al.*, 2012), a measure of the approximate age of a leaf based on its proximity to the most distal leaf which has expanded beyond 10 mm in length from base to apex. While the plant-to-plant criteria for leaf selection varied, the target leaves were always the most recently fully expanded, physiologically mature, and undamaged leaves. LPI ranged from 8-15, indicating that all leaves were physiologically mature and fully expanded. In this way, although the total plant to plant variation in target leaves was considerable, within each plant the target leaves were as closely matched as possible.

Predawn (approximately 30 minutes prior to nautical twilight) on the day of each measurement, two approximately 2.5 m candidate branches were cut for each of two plants. These branches would serve as the cut treatment for both the morning (AM) and afternoon (PM) measurement period. Each branch segment was then placed in a bucket containing 22 L of water, and immediately recut under water to prevent cavitation or embolism of the xylem (Wheeler *et al.*, 2013; Sperry, 2013). This method serves to remove embolized tissue, and allows for xylem tension to be relieved by drawing liquid water into the cut, thereby restoring the hydraulic driving gradient within the branch (Venturas *et al.*, 2015). Each recut consisted of removing at least 50 cm of material to provide a sufficient buffer between the site of the second cut and any embolized xylem (Wolfe *et al.*, 2016). After branches had been recut, they measured approximately 2 m in length. I chose to make my initial branch cuts predawn as that is when water potential is closest to zero, no photosynthesis is occurring, ambient temperatures were low, and the branches and the intact plants were experiencing no thermal stress.

Cut branches were stored under ambient metrological conditions adjacent to their parent individual from the time of cutting until gas exchange measurement commenced. After gas exchange the four measured leaves were sampled for fresh mass and area. Fresh mass was taken on an ER-60A digital balance (A&D Weighing San Jose, CA, USA) and area was calculated from digital photographs with a scale reference and subsequently post processed using the software application ImageJ (v1.53a, National Institutes of Health, Bethesda, MD, USA). Dry mass was recorded after samples were dried to constant mass at 60°C. Leaf mass per area (LMA) was calculated as dry mass divided by the total leaf area. In total 32 curves were conducted (16 pairs).

Gas exchange measurements

All gas exchange measurements were conducted using one of two LI-6800 portable photosynthesis systems (LI-COR Inc., Lincoln, NE, USA) with either a Multiphase Flash Fluorometer leaf chamber (6800-01A) (first 16 curves) or a "Small Light Source" leaf chamber (6800-02) for the remaining curves. I found no significant effect of chamber type on either g_0 or g_1 estimates. For all measurements, the color spectrum of the irradiance was 90% red, 10% blue. Both LI-6800s were factory calibrated by the manufacturer three months prior to use and were running the same version of the operating system (v 1.14.05).

Stomatal response curves followed previously established methods (Leakey *et al.*, 2006) in which irradiance was systematically adjusted in order to propagate changes in A, while holding VPD_{leaf} and C_a constant (Fig. 2.1). Before beginning the collection of all experimental stomatal response curves, 10 irradiance response curves were conducted on randomly selected individuals at a leaf temperature of 30°C to determine the overall response of A to various levels of irradiance. From these curves, the response of A to irradiance was subdivided into 10 approximately equal levels representing the full range of irradiance and their corresponding levels of A, ranging from light saturated photosynthesis (A_{sat}), to respiratory CO_2 release in the dark (R_{dark}). The final irradiance levels chosen were as follows (1500, 900, 700, 450, 250, 175, 90, 40, 20, 0 μmol m^{-2} s^{-1}). I chose to decrease irradiance on a sun adapted leaf, rather than increase irradiance for a dark-adapted leaf as in general, stomata are known to react more slowly to increases in irradiance than decreases in irradiance (Lawson & Blatt, 2014; Lawson & Vialet-Chabrand, 2019), presumably as a mechanism to maximize carbon gain in unstable conditions (Lawson *et al.*, 2012; Drake *et al.*, 2013; McAusland *et al.*, 2016). Thus, by conducting response curves by decreasing irradiance, I estimate that the time to complete a single curve was reduced by approximately half. While the direction of a change in irradiance (increase vs decrease) does impact instantaneous water use efficiency (iWUE; $A_n g_s^{-1}$) immediately following the change in irradiance, this will have no impact on the steady state levels of A and g_{sw} required to estimate g_1 and g_0.

Before the collection of each individual g_{sw} response curve, a leaf temperature and VPD_{leaf} level was chosen that would be representative of the mean external environment for that day for the full length of the curve. As each curve took 5-6 hours to complete, leaf temperature set-point values often had to be higher than ambient air temperature in the morning to prevent reaching the dew point temperature later in the day when cooling was necessary. On average for the morning

curves, T_{leaf} was 28.1ºC and VPD_{leaf} was 1.15 kPa. For the afternoon curves, mean T_{leaf} was 30.2ºC and mean VPD_{leaf} was 1.25 kPa. C_a was set to 400 μmol CO_2 mol^{-1} so that the level of CO_2 at the leaf surface was approximately equivalent to the level of CO_2 outside the leaf chamber. C_a, VPD_{leaf}, and T_{leaf} were held constant for the entirety of each curve so that A and g_{sw} response between curves were comparable and related only to the leaf-to-leaf variation at a given irradiance level on the experimental plants. An automatic logging program was used to collect a data point every 10 seconds for the duration of measurements, and the devices were set to automatically match sample and reference gas analyzers every 10 minutes.

Each curve began at 1500 PPFD (μmol m^{-2} s^{-1}). After a 1-hour acclimation and stabilization period, PPFD was dropped to the next lowest irradiance level, and leaves were allowed to acclimate to this new irradiance level for a minimum of 25 minutes. After the 25-minute acclimation period, A and g_{sw} levels were monitored for stability in both leaves, after which the process was repeated until measurements at all 10 irradiance levels had been completed. For each irradiance level an average of the 5 log points prior to a change in irradiance constituted that measurement. Irradiance level was dropped for both branches simultaneously so that any external influences of ambient irradiance or wind on the curves would be equivalent between branches. Overall, both branches responded similarly to changes in irradiance, with negligible differences in stabilization times between treatments. Two pairs of curves were conducted per day, the morning treatment (~07:30-13:30 EST, hereafter AM treatment) and the afternoon treatment (~13:30-18:30 EST, hereafter PM treatment).

Estimation of stomatal conductance parameters

Stomatal response was evaluated using the USO model (Medlyn *et al.*, 2011) (Equation 2.1). Using the USO model, data can be fit to estimate the two main parameters, a stomatal slope (g_1) and an intercept (g_0). The g_0 parameter represents the expected g_{sw} when A_{net}=0, which will occur at a PPFD equivalent to the light compensation point. The g_1 parameter represents the slope of the relationship between g_{sw} and a combined term including C_a, VPD_{leaf}, and A, sometimes termed the stomatal index.

Equation 2.1 can be rewritten as a linear model where g_1 is the slope term, and g_0 is the intercept term, as in other Ball-Berry type model formulations (e.g., Ball *et al.*, 1987; Leuning, 1995; Katul *et al.*, 2010; Equation 2.2; Fig. 2.1b). g_1 and g_0 are mathematically identical in

Equation 2.1 and 2.2, however Equation 2.2 provides for simpler graphical depiction of the data and will be used throughout.

Equation 2.2. $$g_{sw} - \frac{1.6A}{C_a} = g_0 + g_1 * \left(\frac{1.6A}{C_a\sqrt{VPD_{leaf}}}\right)$$

Typically, the model parameters g_0 and g_1 are simultaneously fitted so that the model best represents the observations. However, several authors have shown a strong correlation between the estimates of g_0 and g_1 which can lead to interdependency in their estimation (Damour *et al.*, 2010; Duursma *et al.*, 2019), which can bias estimates of g_1 based on g_0. Alternatively, other authors (e.g., Leuning, 1995) have suggested to use another method where g_0 is fixed either as 0, or as a given positive value to minimize the impact of g_0 on g_1 estimation. To account for this concern, I used two approaches to fit g_0 and g_1. In the first approach, both g_0 and g_1 are simultaneously estimated for each treatment group, and both g_0 and g_1 are reported. In the second approach, a population value for g_0 was estimated by extrapolating g_{sw} at a value of $A_n = 0$ from points just above and below the light compensation point for each curve, then taking the mean of these values for the full population of curves (hereafter $g_{0,population}$; 0.037 mol m^{-2} s^{-1}). Then, using $g_{0,population}$ as the intercept, g_1 was estimated for each treatment group. For models which use $g_{0,population}$ as the intercept, only the g_1 value is reported.

Leaf biochemical analysis for modeling synthesis

To estimate V_{cmax} I used the "one-point method" (De Kauwe *et al.*, 2016, Equation 2.3), which has shown comparable results to traditional AC_i curves in this species (Burnett *et al.*, 2019):

Equation 2.3. $$V_{cmax} = \frac{A_{sat}}{\left(\frac{C_i - \Gamma^*}{C_i + K_m} - 0.015\right)}$$

where K_m is the Michaelis–Menten constant (404.9 μmol mol^{-1}), Γ* is the CO_2 compensation point in the absence of mitochondrial respiration, and C_i is the intercellular CO_2 concentration.

The "one-point" data used were the first point on each stomatal response curve, as it was an acclimated, steady state, light saturated measurement at 400 ppm CO_2. V_{cmax} at measurement temperature was then scaled to V_{cmax} at 25°C using a modified Arrhenius equation (Leuning, 2002, Equation 2.4) with the kinetic constants provided in Bernacchi *et al.*, (2001):

Equation 2.4. $$V_{cmax.25} = \frac{C * \exp\left[(H_a/RT_{25})(1 - T_{25}/T_{leaf})\right]}{1 + \exp\left[(S_V T_{leaf} - H_d)/(RT_{leaf})\right]}$$

where $V_{cmax.25}$ is the value of V_{cmax} at the reference temperature (T_{25} = 298.15 K), $V_{cmax.T}$ is the value

of V_{cmax} at the leaf temperature (T_{leaf} in K), H_a, H_d, and S_v are the activation and deactivation energies of the enzyme Rubisco and an entropy term (H_a = 65330 J mol^{-1}, H_d =149250 J mol^{-1}, S_v = 486 J mol^{-1} K^{-1}), R is the ideal gas constant (R = 8.314 J mol^{-1} K^{-1}), and C is a combined term equivalent to $1 + \exp[(S_vT_{25} - H_d)/(RT_{25})]$.

J_{max} at 25°C was then calculated as 1.615 * $V_{cmax.25}$, a ratio observed in values collected from AC_i curves in a previous study on the same individuals (Walker *et al.*, 2021). $R_{dark.T}$ was calculated from dark adapted measurements of A (the final response curve point) and was scaled to 25°C ($R_{dark.25}$) using an inverse Arrhenius equation (Equation 2.5; Bernacchi *et al.*, 2001; Von Caemmerer, 2013):

Equation 2.5.
$$R_{dark.25} = \frac{R_{dark.T}}{\exp\left(\frac{H_a}{(R*T_{25})} - \frac{H_a}{(R*T_{leaf})}\right)}$$

where H_a is the activation energy of mitochondrial respiration (H_a = 46390 J mol^{-1}).

Statistical analysis

To test the effect of branch excision and time of day on g_0 and g_1 I used a mixed effect model, with two fixed effects: excision (cut and intact) and the time of day (AM and PM). I also tested the interaction between these two factors. I have a total of 32 curves (8 cut-AM, 8 intact-AM, 8 cut-PM, 8 intact-PM), each consisting of 10 points for 320 total measurements. However, points within each curve are non-independent, making this an excellent application for mixed models, with leaf considered as a random effect on g_0 and g_1. I also used mixed models to test for an effect of LMA and fresh mass on g_0 and g_1. In all mixed models, I consider a $p < 0.05$ as evidence of a significant result, and the differences between group means were assessed using a post hoc Tukey's HSD test (Tukey, 1949).

Paired sample t-tests were used to compare cut and intact LMA, fresh mass, V_{cmax}, A and C_i. Paired sample t-tests were also used to examine the effect of time of day on the same leaf properties. To examine the effect of leaf on stomatal traits, I constructed linear models of LMA, fresh mass: dry mass, V_{cmax}, and R_{dark} versus g_0 and g_1. Models with a slope not significantly different from 0 were considered to be non-significant.

All analyses were performed using the software package R (v 3.6.2, R Core Team, 2013); mixed models were constructed and tested using the package 'nlme' (v 3.1, Pinheiro *et al.*, 2020) and contrast estimates were analyzed with the package 'emmeans' (v 1.4.8 Lenth *et al.*, 2020).

Leaf Gas exchange simulation

In order to simulate A and g_{sw} in response to ambient environmental conditions, I used a coupled leaf scale steady state assimilation, conductance, and energy balance model included in the R package 'LeafGasExchange' (v 1.0.1 Lamour & Serbin, 2021). The model first simulates environmental conditions at the leaf surface. It uses meteorological data for the study site obtained from the Brookhaven National Lab Meteorological Service (https://www.bnl.gov/weather/), which records air temperature, wind speed, irradiance level, and atmospheric pressure at one-minute time intervals.

I use a leaf energy budget model published by Muir (2019, 2020) to simulate T_{leaf}, C_s, and VPD_{leaf}. This energy budget uses an iterative solving function to estimate T_{leaf} and boundary layer conductance (g_{bw}) by first assuming $T_{leaf} = T_{air} + 1$ºC, $C_s = C_a$, and $VPD_{leaf} = VPD_{air}$, then solving for A, g_s, C_i, $T_{leaf,}$ and g_{bw} accounting for the temperature dependencies of the photosynthetic parameters $R_{dark,}$ V_{cmax}, and J_{max} (Bernacchi *et al*. 2001, Leuning 2002, Bernacchi *et al*. 2003b, Von Caemmerer 2013). Then the model compares the resulting estimation of T_{leaf} to the prior value, and if the values are within 0.1°C, assumes the model has converged. If the values differ by more than 0.1°C, the model is rerun using the updated values of Tleaf, C_s, and VPD_{leaf}.

Stomatal conductance is simulated using the USO model (Medlyn *et al.*, 2011) shown in Equation 2.1. Photosynthesis is simulated using the Farquhar von Caemmerer Berry (FvCB) assimilation model (Farquhar *et al.*, 1980) which assumes that net photosynthesis (A_n) is the minimum of carboxylation limited assimilation (A_c) and RuBp regeneration limited assimilation (A_j), minus the respiration rate that is not attributable to the photorespiratory pathway (R_{dark}). The model uses parameters for the maximum rate of electron transport at 25°C ($J_{max.25}$), maximum rate of carboxylation at 25°C ($V_{cmax.25}$), and the leaf dark respiration rate at 25°C ($R_{dark.25}$) which are scaled to T_{leaf} using an Arrhenius function or an inverse Arrhenius function (Bernacchi et al. 2001, 2003b, Leuning 2002, Von Caemmerer 2013). The model was parameterised using $V_{cmax.25}$, $J_{max.25}$, $R_{dark.25}$, g_0, and g_1 calibrated using the data from this study. For the other parameters necessary to calculate photosynthesis, default parameters for C_3 plant species were chosen (Lamour & Serbin, 2021; Table A1.1). For all model simulations, uncertainty was modeled by rerunning the model using g_1 and g_0 values corresponding to ± SE of the fitted value.

Two different types of models were run using these data, one run simulating A and g_{sw} over a 12-hour time period on each day of data collection, and one using an "average day" which was an

aggregation of the mean daytime metrological parameters at one-minute intervals. I also ran the model across an expected range in leaf temperature, VPD_{leaf}, and irradiance to ensure changes in A, g_s, and C_i were as expected (Fig. A1.1)

2.4 – **Results:**

Stomatal Model Parameters:

When looking at the overall effect of time of day on stomatal parameters I find a significant increase ($F_{2,298}$ = 126.6, p< 0.001) in g_1 by 55% between the AM and PM treatment, and a significant ($F_{2,298}$ = 20.2, p< 0.001) 56% decrease in g_0 between AM and PM treatments. When using $g_{0,population}$ in place of g_0, there was a significant ($F_{2,298}$ = 68.0, p< 0.001) 89% increase in g_1 from AM to PM, a larger effect than seen with the model which considers both g_0 and g_1 (Table 2.1, Fig. 2.2b-c).

Next, when considering the interaction of excision and time of day I find a significant effect on g_1 ($F_{4,294}$ = 64.3, p< 0.001), g_0 ($F_{4,294}$ = 17.1, p< 0.001), and g_1 when using $g_{0,population}$ ($F_{4,298}$ = 68.0, p< 0.001; Table 2.2). The parameter g_1 increased by 49% between AM and PM in the cut treatment (t_{296} = -2.7, p = 0.0334) whereas it only increased by 36% for the intact treatment (t_{296} = -3.5, p = 0.0036, Fig. 2.3c-d). The g_0 parameter followed a similar pattern, with a 66% decrease between AM-cut and PM-cut treatments (t_{296} = 3.9, p < 0.001), however there was no significant difference between AM and PM in the intact treatment (Table 2.2, Fig. 2.3a-b). When $g_{0,population}$ was used, all pairwise comparisons of g_1 were significant, except the comparison between AM-cut and AM-intact treatments (Table 2.2, Fig. 2.3e-f). Across all significant contrast, g_1 was lower in the AM treatment than the PM treatment and lower for the cut treatment than the intact treatment (Fig. 2.2c).

Finally, I observed a significant ($F_{2,298}$ = 71.0, p< 0.001) 9% reduction in g_1 measured on leaves from excised branches respective to leaves from intact branches, and a smaller significant ($F_{2,298}$= 51.7, p<0.001) 6% reduction in g_0. When using $g_{0,population}$ in place of g_0 I observed a significant ($F_{2,300}$= 102.2, p<0.001) 10% reduction in g_1 for the cut treatment over the intact treatment (Table 2.1, Fig. 2.2a). However, these effects of excision are likely due to large differences in treatments in the PM group, as I find no significant differences between AM-cut and AM-intact treatments.

Leaf Traits

Paired sample t-tests revealed no significant ($p < 0.05$) difference in leaf traits (LMA, mass:dry mass ratio, $R_{dark.25}$, $V_{cmax.25}$) between cut and intact leaves or leaves from the AM and PM treatments, aside from a significant ($t_{21.58} = -2.23$, $p = 0.037$) 29.7% increase in $V_{cmax.25}$ from AM to PM (Fig. 2.4a-d). A full list of treatment level leaf trait means, and standard deviations, can be found in Table A1.2.

Differences in leaf structural properties had no significant effect on either g_1 or g_0 parameter estimates (Table A1.3). Both LMA and the ratio of fresh mass to dry mass show no significant relationship with fitted values of g_0 and g_1, suggesting that leaf to leaf variation in these properties was not a cause of other fixed effects trends in g_1 or g_0 (Fig. 2.4e-h).

Simulation of leaf-level *A*, g_{sw}, and *E*

Simulations using the coupled leaf assimilation, stomatal conductance, and energy balance model revealed stark differences in both the shape and overall magnitude of the leaf-level *A* and *E* response (Fig. 2.5). Parametrization has a strong effect on the integrated daily level of *E*, with 2.73 ± 0.4 L m^{-2} for the AM-cut treatment, 2.76 ± 0.4 L m^{-2} for the AM-intact treatment, 3.04 ± 0.3 L m^{-2} for the PM-cut treatment, and 3.32 ± 0.36 L m^{-2} for the PM-intact treatment (Fig. 2.5c). Rates of daily integrated *A* followed a similar pattern with 0.390 ± 0.000039 kg m^{-2} for the AM-cut treatment, 0.387 ± 0.000039 kg m^{-2} for the AM-intact treatment, 0.391 ± 0.00039 kg m^{-2} for the PM-cut treatment, and 0.394 ± 0.00040 kg m^{-2} for the PM-intact treatment (Fig. 2.5d). I also see that when I compare a model which has fixed values of g_1, g_0, $V_{cmax.25}$, $J_{max.25}$, and $R_{dark.25}$, and a model where these values are dynamic with time of day (AM group values used from 06:00-13:00 and PM group values used from 13:01-18:30), the dynamic model produces estimates of *E* and *A* that are 8.6% and 1.1% respectively lower than the model which assumes fixed values.

2.5 – **Discussion:**

Here I demonstrate that predawn excision, combined with late day measurement, can strongly influence parameter estimates of g_0 and g_1 in hybrid poplar. I show that in the PM treatment, excision of a branch leads to a 25% lower g_1 estimate than in an intact control, suggesting that WUE may increase as the result of branch excision. However, if measurements were made within four hours of branch excision, I observed no significant difference in measured g_0 or g_1. I also see

that over the diurnal course g_0 decreases by 55% and g_1 increases by 56%, irrespective of treatment. These differences mean that if PM-cut branches are used to derive values of g_1 for models of intact branches, this can result in up to a 34% overestimation of leaf-level g_{sw} for AM and mid-day periods. If extended over the course of a full day, the differences in estimated g_1 between PM-intact and AM-cut branches led to a modeled level of transpiration that is 18% higher than would be simulated when using AM-cut measurements alone.

Excision effect on g_1 and g_0:

When looking at excision alone as a factor influencing parameter estimates, there was only a small effect of excision on branches, leading to a 10% reduction in g_1 for the cut treatment when compared with the intact treatment. However, when the interaction of excision and time of day are considered together, an important trend immerges. In the morning, g_1 was not significantly different between the cut an intact treatment, however in the afternoon g_1 was 25% lower in the cut treatment than the intact treatment (Fig. 2.3e-f). This finding, that there is no effect of excision on g_1 when measurements are within four hours of branch removal, is critical as it reinforces the validity of using *ex situ* measurements of excised branches for physiological study (Leakey *et al.*, 2006; Verryckt *et al.*, 2020; Missik *et al.*, 2021). This observation also highlights that while excision does not impact g_1 early in the day, over time the effect of excision becomes more pronounced.

This is, to my knowledge, the first study which directly compares the stomatal property g_1 between cut and intact branches, as typically one measurement method is chosen without any cross comparison on the effect excision has on rates of A or g_{sw}. While other studies have examined excision effects (Santiago & Mulkey, 2003; Leakey *et al.*, 2006; Verryckt *et al.*, 2020; Missik *et al.*, 2021) none have addressed the potential effects of excision on the stomatal parameter g_1 or g_0. Missik *et al*., (2021) investigates rates of A and g_{sw} relative to time since excision, finding that for the three species studied, rates of A decline by between 25-63%, and rates of g_{sw} decline by 31-43%. Missik and colleagues (2021) also examine the literature for similar studies, finding that of 13 previous studies which examine excised branches, only one examines a quantitative difference in rates of A and g_s. That study (Santiago & Mulkey, 2003) examines the impact of excision on both sustained rates of A and on photosynthetic response curves in 10 tropical canopy tree species. Santiago and Mulkey (2003) suggest that an excision induced decline in g_{sw} may be the cause of

their observed decline in A, however they lack strong evidence for this claim. Leakey *et al*., (2006) measured rates of A and g_{sw} in excised leaves of soybean (*Glycine max* [L.]) in order to parametrize a model of crop photosynthesis and transpiration. Leakey and colleagues, (2006) then tested the parametrization of these laboratory derived data by comparing measured and modeled rates of g_{sw} finding that they were highly correlated, with a non-significant bias. Finally, Verryckt *et al*., (2020) explores the effect of excision on rates of A in tropical species. However they do not examine any impact of excision on rates of g_s, limiting the comparisons that can be drawn between their work and this study.

In addition to the effect of excision on g_1 I also observe a difference in g_0 between treatments, with g_0 being slightly (6%) lower for the cut group than the intact group. This finding, that g_0 is lower for the cut treatment, aligns well with existing stomatal (Cowan & Fraquhar, 1977) and hydraulic (Katul *et al*. 2003) optimality frameworks, which suggest that a lower g_0 is a more water use efficient behavior, as any g_{sw} at values of $A_{net} \leq 0$ is water "wasted" with no net photosynthetic gain, unless as offsetting thermal stress alone (Cowan, 1978; Cowan & Fraquhar, 1977; Blackman *et al.*, 2016; Miner *et al.*, 2017; Martin-StPaul *et al.*, 2017). While it is not biologically possible for g_{sw} to be exactly equal to 0 due to cuticular leakage and incomplete stomatal closure (Duursma *et al.*, 2019) lower g_0 is commonly associated with species in arid regions where any loss of water with no gain in carbon is maladaptive (Duursma *et al.*, 2019; Kerstiens, 1996; Machado *et al.*, 2021; Martin-StPaul *et al.*, 2017). Based on this reasoning, I expected a decrease in g_1 to be accompanied with a concurrent drop in g_0. However, I did not observe this pattern in any of my comparisons. This unexpected finding may be because the hybrid poplar I used in this study is an agricultural variety, bread for fast biomass accumulation, and thus its stomatal dynamics may not be adapted for maximum water retention at low irradiance.

Time of day effect on g_1 and g_0:

In their optimization model of stomatal function, Cowan and Fraquhar (1977) assume that water use efficiency (λ), and therefore the g_1 parameter is constant over a given period of time, typically between a day and a growth season. This model assumes that a plant's stomata will always be operating at the lowest rate of g_{sw} for a given rate of A and thus the function $\partial E/\partial A$ is minimized. Alternatively, hydraulic theory suggests that WUE may increase throughout the day as the "cost" of water increases due to increased evaporative demand, and the "demand" for carbon

decreases due to water transport limitation (Katul *et al.*, 2003). In this study I observed a lower mean g_0 and higher mean g_1 estimate from PM curves than for AM curves, suggesting that WUE decreased throughout the day, while stomatal behavior at low irradiance became more conservative. Here I explore two factors which may contribute to the observed diurnal trends in g_1 and g_0.

First, I observed an increase in $V_{cmax.25}$ from AM to PM (Table A1.2), which could influence the estimation of g_1 and g_0. In this study $V_{cmax.25}$ is fit using the "one-point method" (De Kauwe *et al.*, 2016) either at ~08:00 (AM) or ~13:00 (PM), rather than traditional AC_i curves. In looking at the data used to estimate $V_{cmax.25}$ I see that when correcting for the effect of leaf temperature, rates of $A_{sat.25}$ are significantly different between AM and PM groups, with the AM group having lower mean $A_{sat.25}$ than the PM group. However, rates of C_i are not different between groups (Fig. A1.2), nor are uncorrected rates of A_{sat}, suggesting that the AM group may be facing a temperature limitation on activity of the enzyme Rubisco rather than a limitation due to the supply of carbon reaching the site of carboxylation (Harrison *et al.*, 2010; Resco de Dios *et al.*, 2016). This is further supported by the fact that mean rates of g_{sw} are not different between AM and PM groups.

Many authors have reported an afternoon decline in $V_{cmax.25}$ (Singsaas *et al.*, 2000; Kets *et al.*, 2010; Nascimento & Marenco, 2013; Stinziano *et al.*, 2020), while an afternoon increase in $V_{cmax.25}$ is rather unusual. However, the afternoon increase may be the result of a more complete activation of Rubisco at the start of the PM measurement (~13:00) compared to the AM (~08:00) leading to a suppressed apparent maximum capacity in the AM group. Slow activation of Rubisco in *Populus* species has previously been observed (Roden & Pearcy, 1993), as well as suppression of rates of activation after initial high light exposure (Kobza & Seemann, 1989).

With a higher $V_{cmax.25}$ I would expect higher rates of A, which could lead to a lower g_1 and thus a higher iWUE if A and g_{sw} did not increase in proportion. However, most plants maintain a fixed ratio of C_i to C_a as mesophyll requirements for photosynthesis create a tight coordination between A and g_{sw} (Wong *et al.*, 1985; Sharkey *et al.*, 2007). Wong *et al.* (1979) also showed that this coordination is robust to changes in photosynthetic capacity, suggesting that changes in $V_{cmax.25}$ should not modulate the A:g_{sw} relationship. I did not observe any significant differences in C_i between AM and PM treatments at equivalent irradiance levels (Fig. A2.2), suggesting that while A may have increased due to higher $V_{cmax.25}$, g_{sw} would have increased in proportion to facilitate the increased stomatal conductance to CO_2 (g_{sc}) (Farquhar *et al.*, 1980), and thus the g_1 estimate

should not have been effected.

A second possible explanation for the increase in g_1 between AM and PM and the decrease in g_0 from AM to PM is the effect of ambient conditions, both metrological and hydraulic, on the measured parameters. Previous field studies of diurnal rates of g_{sw} and sap flux have demonstrated a strong link between canopy scale g_{sw} and ambient VPD (Maruyama & Kuwagata, 2008; Matthews *et al.*, 2017; Miranda *et al.*, 2013), with g_{sw} declining in response to increased VPD. In addition, hydraulic supply theory suggest that at the leaf-level for non-stressed plants, supply of water increases with increased evaporative demand (Buckley, 2017; Damour *et al.*, 2010), meaning that at the same rate of A more water is available, and g_{sw} will be higher.

In my experiment I observed a rapid increase in ambient VPD from 06:00 to 12:30, and a decrease in ambient VPD from 12:31 to 18:00 (Fig. 2.5f). In addition, from previous studies on the same individuals I observed that early in the day xylem tension remains low, and levels off at mid-day levels from 12:30 onward (Serbin *et al.*, 2020). This combination of increasing VPD and low xylem tension may serve to limit rates of g_{sw} for AM leaves, causing them to appear more water use efficient in their stomatal behavior, as for the same rate of A, morning curves had lower g_{sw} thus on average a higher fitted value for g_1 (Fig. 2.2c). Likewise for g_0, points from the AM curves were measured on or around solar noon, while for the PM curves, the g_0 points were measured around 18:30. When considering the ambient conditions at these two time points, it is not surprising that I see a 56% decrease in g_0 between AM and PM, as the ambient xylem flux at noon would be much higher than the flux late in the day when the solar zenith angle is much more obtuse (Fig. 2.6). This drop also follows the expectations of hydraulic supply and demand, which would assume a drop in g_0 over the diurnal course, concurrent with declining water reserves, and carbon demands (Duursma *et al.*, 2019; Lombardozzi *et al.*, 2017).

Finally, I do not believe that length of the measurement or differences in enclosure time are contributing to the patterns observed, as both AM and PM curves took approximately the same length of time to complete and were stepped through changes in irradiance at the same time.

<u>Interaction of excision and time of day could reveal a progressive effect of hydraulic stress on stomatal parameters:</u>

When the effect of treatment and time of day are jointly assessed, a temporal trend emerges. g_1 increases from AM to PM in both treatments, indicative of a time-of-day effect in both

treatments. Interestingly, however, g_1 increases more for the intact branches than the cut branches between AM and PM (Fig. 2.2c). There are several possible explanations for this asymmetrical response. (1) It could be due to a bias in the amount of leaf area outside the measurement chamber, as intact branches had a significantly higher portion of their total leaf area experiencing ambient conditions than the cut treatment. (2) Due to hydraulic segmentation of woody tissue, the cumulative resistance across the water column of a cut branch will be lower than the resistance felt over the entire canopy of a tree (Pivovaroff *et al.*, 2014), which would manifest in a greater diurnal hydraulic driving gradient for the intact treatment, and thus a comparably higher stomatal slope difference from AM to PM. (3) Cut branches have been disconnected from root soil moisture signaling, which may dampen natural diurnal dynamics in stomatal response related to ABA signaling or hydraulic conductivity (Christmann *et al.*, 2007; Cochard *et al.*, 1996; Huber *et al.*, 2019). (4) The cutting of branches may have triggered the onset of xylem cavitation and failure (Tyree & Sperry, 1989). A reduction in xylem sapwood area would result in less water reaching the leaves under the same xylem tension, as the total tension would be dispersed over a comparably smaller xylem area. If less water was reaching the leaves, g_{sw} would be lower and thus a lower g_1 estimate would be observed. It is possible that all four factors are working in concert to produce the observed effect, however without xylem sapflow measurements, it is impossible to know exactly what the driving dynamic is.

The other interesting temporal trend is the difference in excision effect from AM to PM. In the AM group of plants, there was no significant difference in g_1 between cut and intact leaves, while for the PM group, g_1 was 25% higher in the intact treatment than the cut treatment. This suggests that while excision does not seem to bias the measurement results early in the day when the plants are experiencing lower levels of water stress, as time goes on, the effect of excision becomes more pronounced, leading the cut branches to exhibit a markedly more water use efficient stomatal behavior. This response of increased iWUE, associated with stomatal limitation as a result of water stress, has been well documented in the past (Franks *et al.*, 1998; Klein, 2014), and may either be associated with embolism of the tissue adjacent to the cut (Tyree & Sperry, 1989; Santiago & Mulkey, 2003), or a larger influence of hydraulic stress due to the removal of tissue and thus material over which to resist xylem tension (Pivovaroff *et al.*, 2014). This change in water use efficiency is in line with my expectations that predawn cutting, along with significant storage or wait time before a long response curve could alter the observed stomatal behavior, and thus bias

the parameter estimates obtained.

Interestingly however, g_0 does not follow the same pattern as g_1 with no statistical difference in g_0 between excision treatments in the PM group, (albeit a 53% lower g_0 for the cut branches than the intact branches). This suggests that the excision effect on stomata is more acutely seen at higher g_{sw} levels, and that both treatments are already behaving in a physiologically optimal fashion under low irradiance (Duursma *et al.*, 2019). It has been well documented that maximum g_{sw} is limited by leaf (Schulze & Hall, 1982; Brodribb *et al.*, 2003; Klein, 2014) and soil (Thomas *et al.*, 1999; Manzoni *et al.*, 2011; Héroult *et al.*, 2013) water stress, with the magnitude of the reduction in g_{sw} larger at higher rates of conductance. Therefore, if excision is contributing to hydraulic constraint within the xylem transport pathway, maximum g_{sw} at high irradiance should be more acutely limited than g_{sw} levels across all irradiance conditions (Anderegg *et al.*, 2017).

There are several possible explanations for these treatment and temporal effects on g_0 and g_1. As mentioned before, the initial predawn cut may have been an impetus for xylem damage, which under increased diurnal xylem tension, continued to propagate throughout the day, becoming more acute in the PM treatment. "Runaway" cavitation and embolism of the xylem (Hölttä *et al.*, 2009; Sperry *et al.*, 1993; Tyree & Sperry, 1989) effectively reduces the total xylem conduit area, limiting water supply to the leaves, and distributes the same amount of tension over less xylem area. These factors result in a reduction of apparent g_{sw} rates compared to leaves supplied by intact xylem tissue, as less water is available at the site of conductance (Sperry *et al.*, 1993).

Increased xylem tension also serves to decrease leaf water potential, which can trigger stomatal closure as Ψ_{leaf} approaches Ψ_{leaf} at turgor loss point (Martin-StPaul *et al.*, 2017). This is especially apparent in species which behave more isohydric (Klein, 2014), such as the poplar clone used in this study (Cocozza *et al.*, 2010; Johnson *et al.*, 2002). Isohydric plants are thought to have superior stomatal adjustment capacity compared with anisohydric plants, and as a consequence, more closely link their stomatal opening to ambient stress conditions, closing stomata at high VPD, and low Ψ_{leaf} or Ψ_{soil} (Klein, 2014).

Alternatively, levels of abscisic acid (ABA) or another stress signaling hormone could have been building over the day, with the effects becoming more pronounced for the PM group than the AM group. Like Ψ_{leaf} influenced stomatal closure, hormonal stomatal closure is linked to an external stressor such as leaf water stress, thermal stress, or excision stress (Tombesi *et al.*, 2015; Wilkinson & Davies, 2002). The predicted isohydric response to any such stressor would be to

reduce stomatal aperture to safeguard against xylem damage and cellular turgor loss, both of which are difficult to recover from, and costly in terms of carbon resource allocation (Klein *et al.*, 2018; McDowell *et al.*, 2019).

When comparing between these two possible explanations for a lower g_{sw}:A ratio for the PM group, I find more evidence in support of hydraulic limitation than reduced stomatal aperture. In previous studies of these individuals there were no detectable differences in Ψ_{leaf} or survey rates of g_{sw} from morning to midday (Serbin *et al.*, 2020), suggesting that this species does not alter its stomatal behavior in response to heat or moisture stress. A reduction in stomatal aperture while maintaining the same rate of A would reduce C_i, as for the same rate of A less CO_2 is being supplied to the site of carboxylation. However, I found no significant difference in either A or C_i between any cut-intact pair at any level of irradiance (Fig. A1.2). This suggests that stomatal aperture and thus g_{sw} was not affected by excision, leading hydraulic limitation to be the most plausible cause of the effect observed, a similar finding to other excision studies (Santiago & Mulkey, 2003; Missik *et al.*, 2021). This could also explain the incongruence between an effect on g_1 but not g_0, as the effect of hydraulic limitation would be more acute under high irradiance, as xylem tension scales with evaporative demand (Cai *et al.*, 2020; Schulze *et al.*, 1985; Tang & Boyer, 2008).

Impact of parameter assumptions on leaf-level simulations:

Results from simulations of hybrid poplar using the coupled assimilation, stomatal conductance, and energy balance model revealed that methodological choice in parametrization resulted in significant differences in both the diurnal pattern of g_{sw}, and the integrated transpiration over a simulated diurnal cycle (Fig. 2.5, Fig. A1.1). Simulated rates of A and g_{sw} correspond closely to previous studies of poplar species which find mean rates of A at 20 μmol m^{-2} s^{-1} and g_{sw} at 0.35 mol m^{-2} s^{-1} (Bernacchi, *et al*. 2003a, Cseke *et al*. 2009, Rogers *et al*. 2012). Across all six simulations, g_{sw} exhibited a marked midday decline, which is brought on by an increased VPD as the air warms (El-Sharkaway & Cock, 1984; Dai *et al.*, 1992; Tardieu & Davies, 1993; Merilo *et al.*, 2018). This decline in g_{sw} results in stomatal limitation on A, regulating the shape of the photosynthetic response (Bernacchi, *et al*. 2003a). The use of a dynamic simulation reveals that the parameters g_0 and g_1 strongly regulate both E and A, as an afternoon increase in g_1 leads to a nearly 33% increase in rates of g_s. As expected, the parametrizations which resulted in higher fitted values of g_1 and g_0, produced higher sustained simulated rates of both g_{sw} and A, while still

maintaining the same pronounced overall diurnal pattern representative of irradiance and VPD trends (Fig. 2.5a). When considering total transpiration over a diurnal (06:00-18:30) period, choice of parametrization has a strong effect on the total level of transpiration in poplar, with values ranging from 2.73 L m^{-2} day^{-1} for the AM-cut treatment, to 3.32 L m^{-2} day^{-1} for the PM-intact treatment (Fig. 2.5c). While this difference is small compared to the day-to-day variation expected in *E* (Bauerle *et al.*, 2009), this consistent 18% difference taken over a full growth season would represent a large uncertainty in the rate of transpiration of a plant canopy. In addition, the two predictions from the intact treatment (and their associated error) are largely different, suggesting that choice regarding time of day of measurement has serious ramifications on g_1 and g_0 in poplar, as well as predicted model output.

Conclusions:

In ecophysiology it is often necessary to assume that single leaf, *ex situ* measurements of gas exchange are broadly comparable to *in situ*, whole canopy dynamics, if the proper precautions (e.g., predawn excision and recutting under water) are taken, and assumptions (e.g., the hydraulic dynamics of a cut branch are equivalent to an intact branch) are minimized. While it has been shown that *ex situ* measurement does not alter photosynthesis (Verryckt *et al.*, 2020) and may even be the better option for AC_i curves (Ainsworth *et al.*, 2003), it is currently unknown what approach is most suitable for long duration response curves used to estimate g_1 (Damour *et al.*, 2010) and g_0 (Duursma *et al.*, 2019). Here I show that in cases where measurements are made early in the day, or a short time post excision, *ex situ* stomatal response parameters estimated from *ex situ* response curves match those obtained from *in situ* response curves (Fig. 2.3). However, I also demonstrate that choices regarding experimental design, and failure to consider the strong diurnal effect on hydraulic driving gradients can confound comparisons of results (Fig. 2.5).

While this study only investigated stomatal dynamics in a single isohydric woody species, I none the less show that if the aim of stomatal response curves is to ascertain a single nominal value for a species or group of interest, the exact sampling method must be carefully considered. It may be preferable to average measurements across the diurnal period, rather than conduct all curves at one time point during the day. If the time since excision is not recorded, conclusions about plant to plant or species to species differences in parameters may be of limited value. Therefore, failure to consider potential stomatal parameter measurement uncertainties, together with other

uncertainties and known variation in parameters across space and time, on downstream leaf-, canopy-, and ecosystem-scale processes, have the potential to introduce considerable uncertainties into the modeling of plant carbon and water cycling (Dietze et al. 2014; Rogers *et al.*, 2017c)

2.6 – **Figures:**

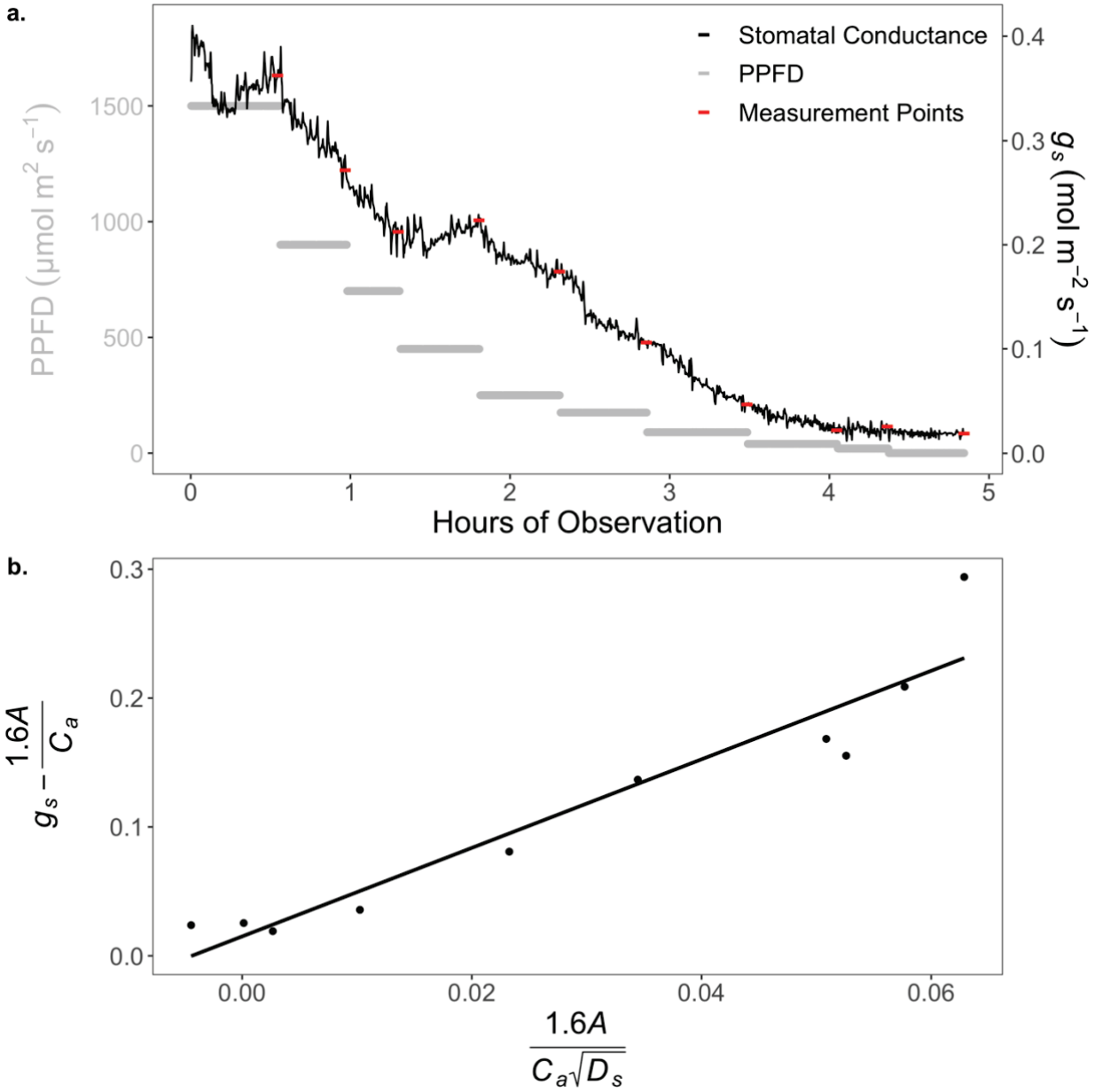

Figure 2.1: Overall format of the stomatal response curve approach in which irradiance is reduced in a stepwise manner, and rates of stomatal conductance (g_s) decline in response. (a) Example of a curve in which rates of g_s reached steady state at each light level. Red points on the response curve correspond to the mean value for that irradiance level extracted for subsequent analysis. Even at steady state levels of g_s, there is still a great degree of observation-to-observation variation. (b) Standard visualization of the data from the curve conducted in (a). Plotting this way allows for a linear approximation of the g_1 and g_0 parameters, which are the slope and intercept respectively of the best fit line.

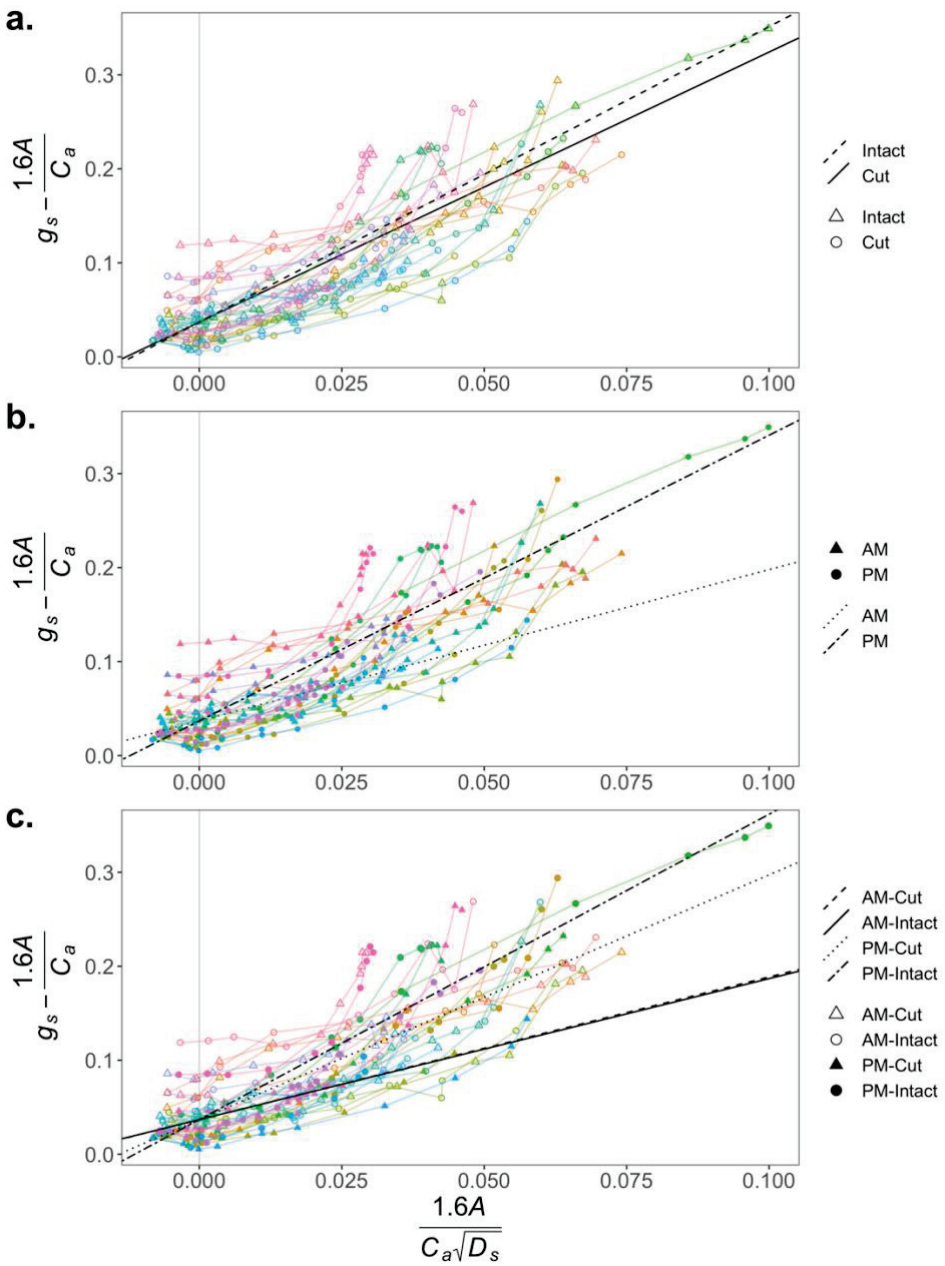

Figure 2.2: Effect of (a) excision and (b) time of day, and their interaction (c) on the fitted value of g_1 from the USO model, when g_0 is set to $g_{0,population}$ (0.037 mol m^2s^{-1}). Both excision and time of day produced a significant fixed effects relationship, with a 10% reduction in estimated g_1 for excised branches (a), and an 89% increase in g_1 from the AM treatment to the PM treatment (b). For the interaction (c) all contrast level differences are significant, except for the difference between cut and intact treatments during the AM time period. Notably, for the PM time period, predicted g_1 for the cut treatment was 25% less than the intact treatment, suggesting that the measurements are not comparable. Points connected by a colored line indicate that they were collected together as part of the same response curve. Points of the same color have the same random effects structure applied. Grey vertical line denotes the point of light compensation ($A_n = 0$)

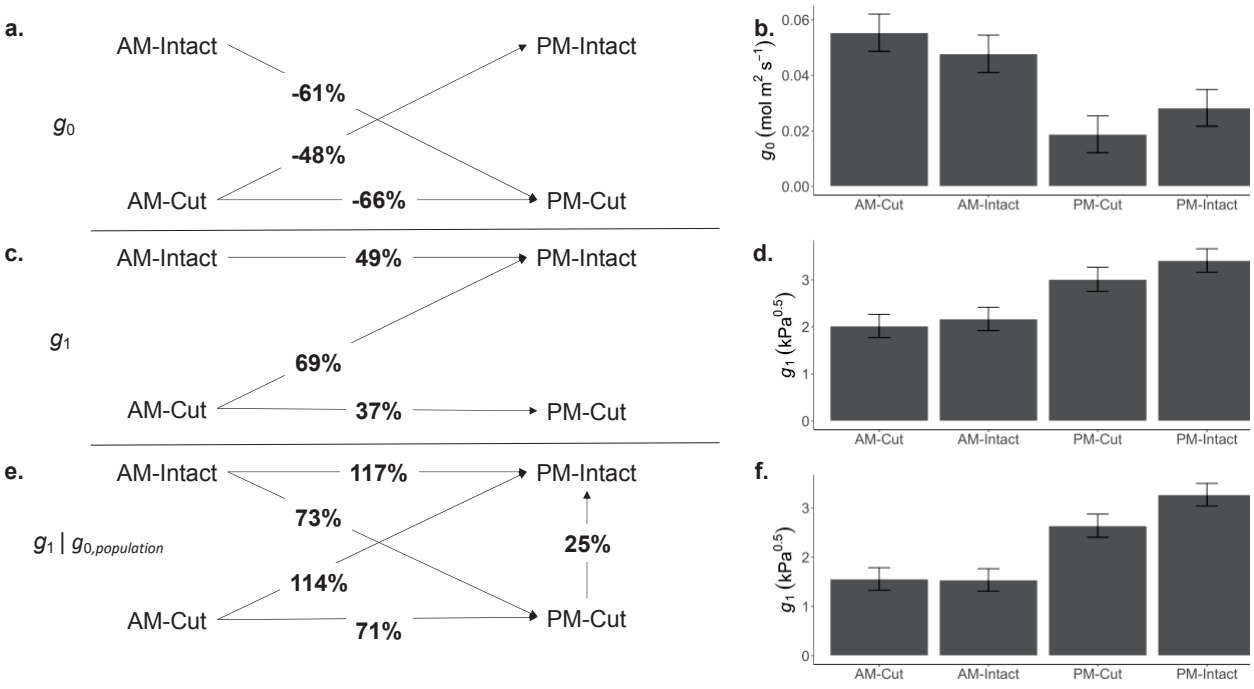

Figure 2.3: Comparisons of the interactive effects of excision and time of day on stomatal parameters. Percent difference between all six linear contrasts and absolute values and their error for (a-b) g_0 estimates, (c-d) g_1 estimates, and (e-f) g_1 estimates when g_0 is set to $g_{0,population}$. All differences reported in panels a, c, and e by percentage are significant. Error bars in panels b, d, and f are ± 2 SE, n=8. Full statistics and values for all effects are reported in Table 2.2.

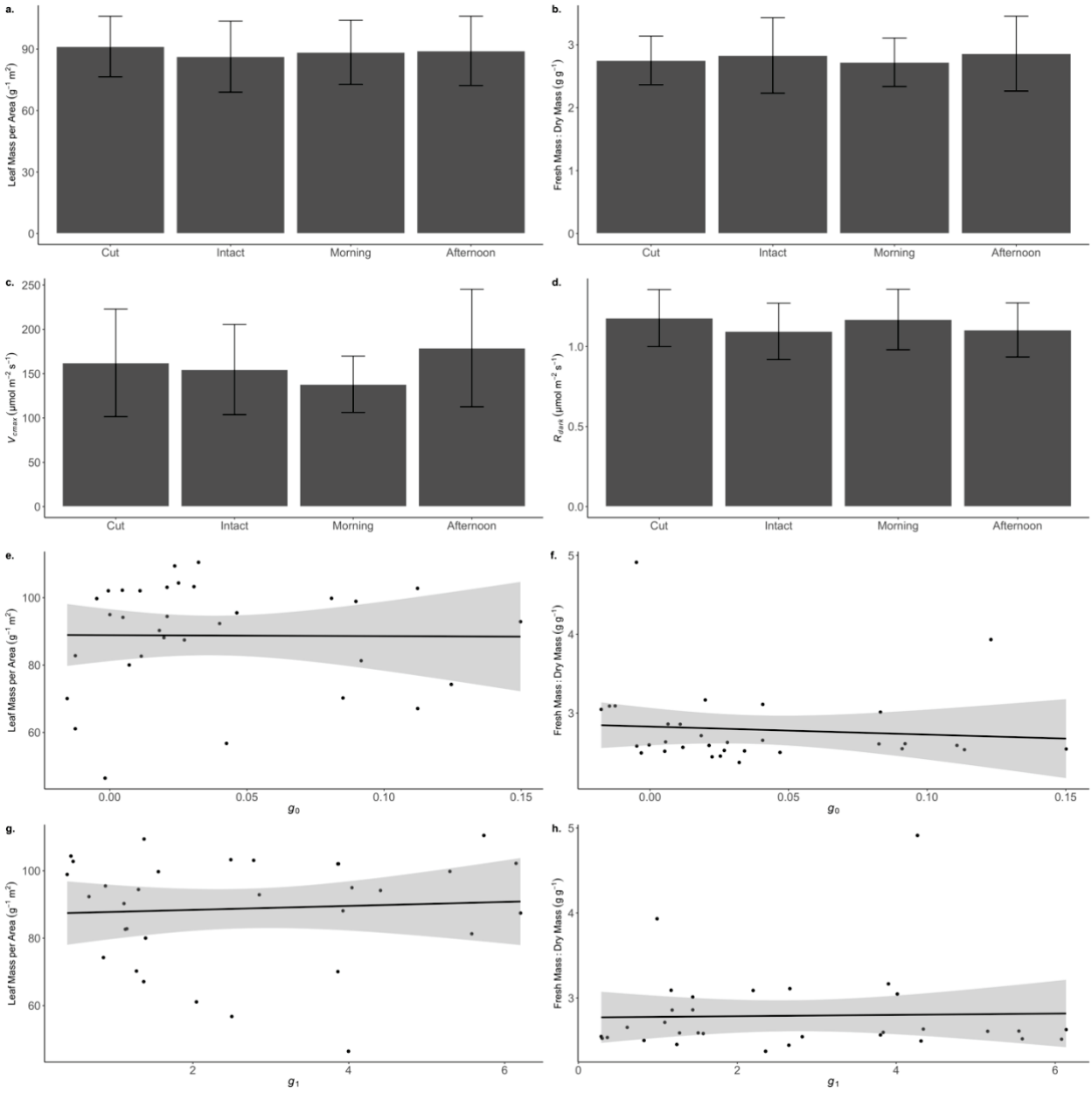

Figure 2.4: Leaf traits do not vary between cut and intact leaves or between leaves measured in the AM and PM groups with no significant effect on the estimated stomatal response parameters. Mean leaf mass per area (a), and fresh mass, dry mass ratio (b) are not different between treatments, however there is a large among plant variation in these values. There is a significant difference in V_{cmax} (c) between AM and PM groups, however there is no difference between cut and intact groups. For R_{dark} (d) there are no significant differences either between AM and PM groups or cut and intact groups. Leaf structural properties have no significant relationship with g_0 (e-f) or g_1 (g-h) estimates within curves.

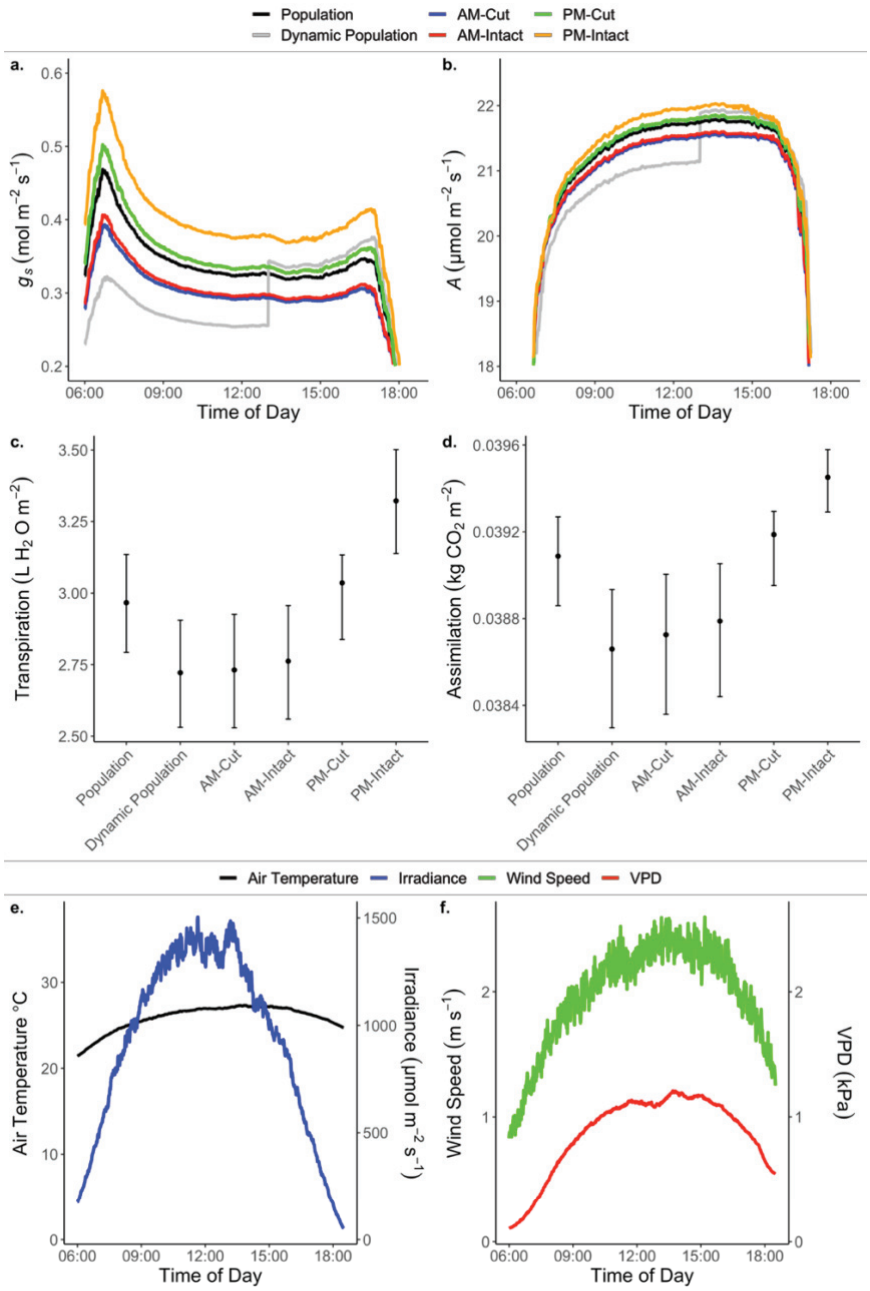

Figure 2.5: Coupled leaf gas exchange model simulation results of rates of photosynthesis (A) and stomatal conductance (g_s) given metrological data for an "average day" (06:00-18:30) during the period of measurement. Diurnal trends in (a) g_s and (b) A response for six different model runs conditioned on the mean g_1 and g_0 from the four treatments, the mean of all the data irrespective of treatment (population), and an dynamic model with the mean of the AM group used from 06:00-13:00 and the PM group used from 13:01-18:30. g_s rates respond strongly to the level of irradiance, temperature (e), VPD, and wind (f) which work in concert to produce a pronounced mid-day depression in g_s. Rates of A between model runs are different indicating stomatal limitation on A for the models with lower g_1 and g_0 parameter estimates. Total expected canopy (c) transpiration as a function of diurnal g_s and VPD, and (d) assimilation as a function of irradiance and leaf temperature. Error bars represent model runs using parameters ± 2 SE of their fitted means.

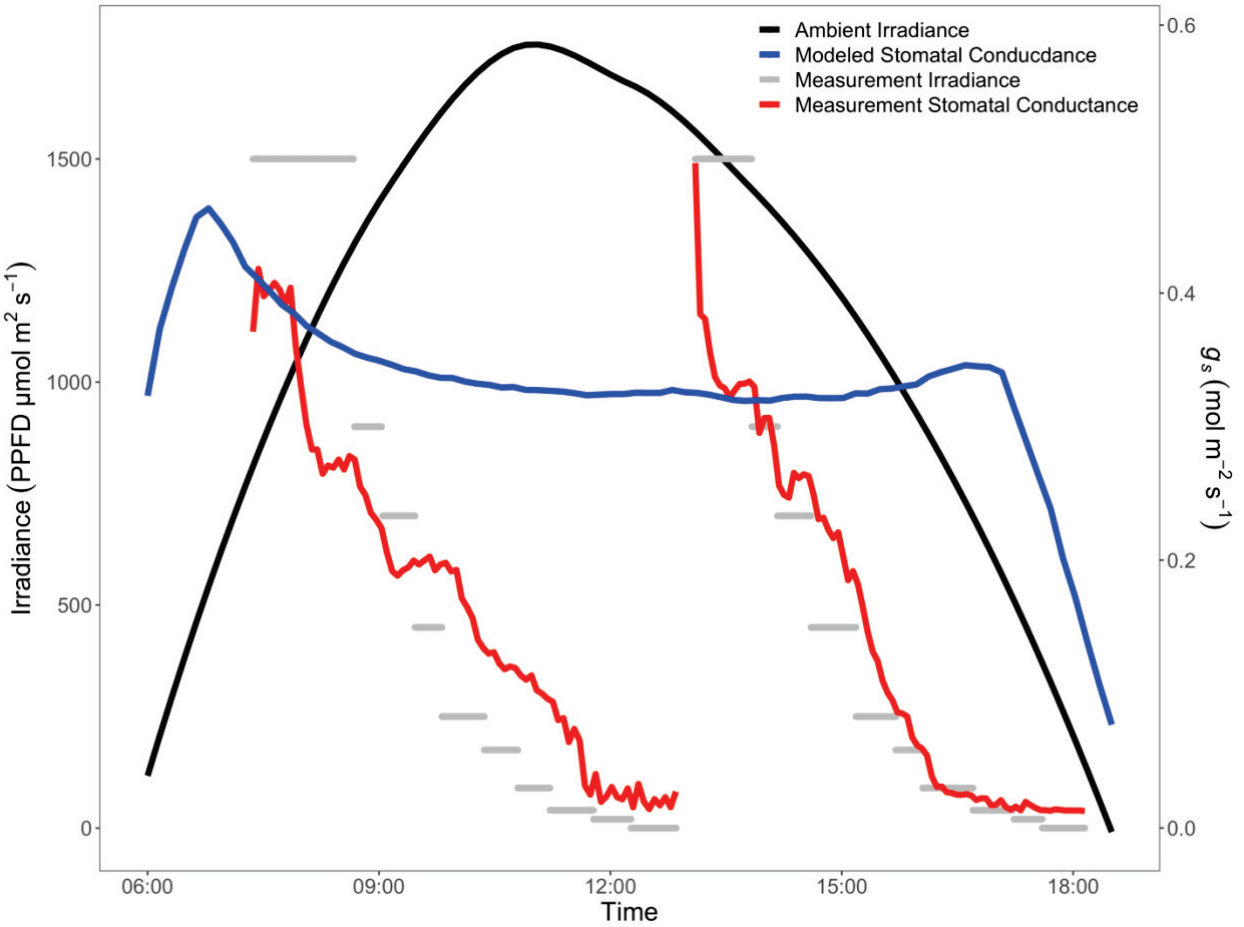

Figure 2.6: Observed experimental and predicted natural dynamics of light and rates of stomatal conductance (g_s)measured on August 10, a typical day of measurement. Black and blue trend lines are the ambient PPFD and predicted rates of g_s based on metrological data and photosynthetic parameters (see methods). Note that the mid-day decline in g_s is due to an increase in VPD, rather than an effect of rates of *A*. Data in grey and red are the measurement PPFD and corresponding rates of g_s measured on intact leaves on the same day.

2.7 – **Tables:**

Table 2.1: Fixed effects components from the mixed effects models tested. Effects denoted with +0 are from the model where g_0 was $g_{0,population}$.

Model	Numerator df, Denominator df	F-value	Random effect SD	p-value	Contrast	Mean	SE	% difference
$g_0 \sim$ excision	2, 298	51.730	0.022	<0.001	g_0: Cut	0.037	0.0060	6%
					g_0: Intact	0.039	0.0060	
$g_1 \sim$ excision	2, 289	71.011	0.840	<0.001	g_1: Cut	2.54	0.233	9%
					g_1: Intact	2.76	0.231	
$g_1 \sim$ excision + 0	2, 300	102.177	0.917	<0.001	g_1: Cut	2.87	0.221	10%
					g_1: Intact	3.15	0.219	
$g_0 \sim$ time	2, 298	20.151	0.016	<0.001	g_0: AM	0.052	0.0063	-56%
					g_0: PM	0.023	0.0062	
$g_1 \sim$ time	2, 298	126.615	0.607	<0.001	g_1: AM	2.10	0.240	55%
					g_1: PM	3.26	0.243	
$g_1 \sim$ time + 0	4, 289	68.035	0.691	<0.001	g_1: AM	1.61	0.231	89%
					g_1: PM	3.04	0.233	

Table 2.2: Linear effect means and contrast estimates for the interactive effects of excision and time of day. Model denoted with +0 is the model where g_0 was $g_{0,population}$. Bolded values are significant with an alpha cutoff of 0.05. Sign (+/-) on the effect size indicates the direction of the comparison.

Model	Numerator df	F-value	Random effect SD	p-value	Effect	Mean	SE	Contrast	Effect size	t-value	p-value
g_0 ~ excision:time	4, 294	17.052	0.016	<0.001	AM-Cut	0.0556	0.00663	AM-Cut vs PM-Cut	-66%	3.941	**<0.001**
					AM-Intact	0.048	0.00665	AM-Cut vs AM-Intact	-14%	1.474	0.455
					PM-Cut	0.0189	0.00654	AM-Intact vs PM-Cut	-61%	-3.118	**0.011**
					PM-Intact	0.029	0.00658	AM-Cut vs PM-Intact	-48%	2.852	**0.024**
								PM-Cut vs PM-Intact	-53%	-2.038	0.176
								AM-Intact vs PM-Intact	-40%	2.033	0.178
g_1 ~ excision:time	4, 294	64.272	0.606	<0.001	AM-Cut	2.02	0.252	AM-Cut vs PM-Cut	49%	-2.731	**0.034**
					AM-Intact	2.18	0.252	AM-Cut vs AM-Intact	8%	-0.935	0.786
					PM-Cut	3.01	0.259	AM-Intact vs PM-Cut	37%	2.304	0.099
					PM-Intact	3.41	0.253	AM-Cut vs PM-Intact	69%	-3.883	**<0.001**
								PM-Cut vs PM-Intact	13%	-2.271	0.107
								AM-Intact vs PM-Intact	36%	-3.451	**0.004**
g_1 ~ excision:time + 0	4, 298	68.0350	0.727	<0.001	AM-Cut	1.52	0.23	AM-Cut vs PM-Cut	71%	-3.284	**0.006**
					AM-Intact	1.50	0.23	AM-Cut vs AM-Intact	-1.3%	0.135	0.999
					PM-Cut	2.60	0.238	AM-Intact vs PM-Cut	73%	3.335	**0.005**
					PM-Intact	3.25	0.231	AM-Cut vs PM-Intact	114%	-5.309	**<0.0001**
								PM-Cut vs PM-Intact	25%	-5.055	**<.0001**
								AM-Intact vs PM-Intact	117%	-5.364	**<.0001**

Chapter 3: Short-term variation in leaf-level water use efficiency in a tropical forest

3.1– **Abstract:**

The representation of stomatal regulation of transpiration and CO_2 assimilation is key to forecasting terrestrial ecosystem responses to global change. Given its importance in determining the relationship between forest productivity and climate, accurate and mechanistic model representation of the relationship between stomatal conductance to water (g_{sw}) and assimilation is crucial. Here I assess possible physiological and mechanistic controls on the estimation of the g_1 (stomatal slope, inversely proportional to water use efficiency) and g_0 (stomatal intercept) parameters (from the Unified Stomatal Optimization model), using diurnal gas exchange surveys and leaf-level response curves of six tropical broadleaf evergreen tree species. g_1 estimated from *ex situ* response curves averaged 50% less than g_1 estimated from survey data. While g_0 and g_1 varied between leaves of different phenological stages, the trend was not consistent among species. I identified a diurnal trend associated with g_1 and g_0 that significantly improved simplified canopy-scale model projections of diurnal trends in transpiration. The accuracy of modelled g_{sw} can be improved by accounting for variation in stomatal behavior across diurnal periods, and between measurement approaches, rather than focusing on phenological variation in stomatal behavior. Additional investigation into the primary mechanisms responsible for diurnal variation in g_1 will be required to account for this phenomena in land surface models.

3.2 – **Introduction:**

Properly parameterizing Earth system models (ESMs) is of vital importance to forecasting terrestrial ecosystems' responses to novel future climates (Rogers *et al.*, 2017c). In particular, the ESM representation of the terrestrial biosphere in land-surface models (LSMs) used to predict the dynamics, responses, and feedbacks of vegetation to the climate system is a critical requirement for climate modeling (Bonan, 2008). This includes the representation of photosynthetic carbon assimilation (*A*), which directly determines ecosystem net carbon uptake (Ainsworth & Rogers, 2007). Transpiration (*E*), which is a dominant flux in the hydrologic cycle (Schlesinger & Jasechko, 2014), is fundamentally governed by stomatal conductance (g_{sw}), which regulates both *A* and *E* (Meidner & Mansfield, 1968; Hetherington & Woodward, 2003; Lawson & Vialet-Chabrand, 2019). Despite the large influence of g_{sw} on global carbon and water cycles, parametrization of g_{sw} in models remains one of the largest uncertainties in current predictions of net ecosystem productivity (Dietze *et al.*, 2014; Bauerle *et al.*, 2014; Jefferson *et al.*, 2017; Franks *et al.*, 2018; Ricciuto *et al.*, 2018).

The LSMs that are commonly used in Earth system models tend to represent g_{sw} using an assumed linear relationship between g_{sw} and *A* where the slope parameter governs the ratio of g_{sw}:*A* (Damour *et al.*, 2010). The majority of these formulations are phenomenological (e.g., Wong *et al.*, 1979; Farquhar & Wong, 1984; Ball *et al.*, 1987; Leuning, 1995; Damour *et al.*, 2010), however, Medlyn *et al.*, (2011) argued that the relationship could be modeled in terms of stomatal optimality theory. The principal of stomatal optimization is that the evolution of vascular plants has prioritized maximizing *A*, per unit of water lost via *E* (Cowan & Fraquhar, 1977; Cowan, 1978). Stated in terms of water, stomatal regulation should minimize g_{sw} so that *E* is minimized for a given amount of *A,* at least during periods of water limitation. This is mathematically represented by $\partial E/\partial A = \lambda$, where $1/\lambda$ represents the whole plant water use efficiency (WUE). This relationship is conceptualized in the "Unified Stomatal Optimization model" (USO; Medlyn *et al.*, 2011; Eqn. 3.1).

Equation 3.1.
$$g_{sw} = g_0 + 1.6\left(1 + \frac{g_1}{\sqrt{VPD_{leaf}}}\right)\frac{A}{C_a}$$

Unlike phenomenological models, the g_1 term in the USO model relates directly to optimality

theory (Cowan & Fraquhar, 1977; Cowan, 1978). The stomatal slope term (g_1) is approximately inversely proportional to WUE. The stomatal intercept (g_0) is the expected g_{sw} when net assimilation (A_{net}) = 0 and occurs at an irradiance level equivalent to the light compensation point. The g_0 parameter was an empirical addition, intended to help constrain the model and ensure predicted g_{sw} is always positive, rather than a feature predicted by optimality (Duursma *et al.*, 2019). The other terms in the USO model relate to environmental conditions, including the leaf-to-air vapor pressure deficit (VPD_{leaf}) and the CO_2 concentration at the leaf surface (C_a). Previously, Wu *et al.*, (2019b) tested four different stomatal model formulations in the wet tropics and found that the USO model was best suited to represent g_{sw} in this system.

Data used to fit the USO model can be collected either by taking survey measurements at ambient conditions (Bernacchi *et al.*, 2006; Lin *et al.*, 2015; Wu *et al.*, 2019b) or by the use of a response curve method (Ball *et al.*, 1987; Leuning, 1995; Leakey *et al.*, 2006; Domingues *et al.*, 2014; Wolz *et al.*, 2017; Davidson *et al.*, 2022; Lamour *et al.*, 2022). In the survey method, *in situ* measurements of instantaneous gas exchange from many individual leaves are collectively used to fit a regression from which g_1 and g_0 are obtained. In the curve method, slow irradiance, vapor pressure deficit (VPD), or CO_2 response curves are used to illicit stomatal response, usually on a cut branch segment. For this approach it is typical to calculate g_0 and g_1 for an individual leaf.

Much of the work to date on assessing variation of stomatal parameters has focused on specific biotic or abiotic drivers. Research into the effects of drought, soil moisture (Héroult *et al.*, 2013), and temperature (Lin *et al.*, 2015; Wolz *et al.*, 2017) have shown that, in some systems, the abiotic control on g_1 may be stronger than any biotic controls (Zhou *et al.*, 2014, 2016). Other work has linked leaf phenology and photosynthetic properties in tropical evergreen forests, where the rate of leaf production and leaf longevity both influence leaf function (van Schaik *et al.*, 1993). Leaves with longer average lifespans have reduced maximum carboxylation capacity of the enzyme Rubisco (V_{cmax}) as compared with shorter lived leaves (Kitajima *et al.*, 1997b, 2002). Similarly, Wu *et al.*, (2016) found that V_{cmax} changed over the lifetime of tropical leaves, and this leaf-age variation is an important factor to consider when modeling tropical forest carbon assimilation (Wu *et al.*, 2017). Yet, it remains to be seen what impact leaf phenology has on stomatal parameters in tropical species. A strong phenological partitioning of leaf-level stomatal response, if it occurs, would most likely be an important development for ESMs given the large impact phenology has on terrestrial carbon dynamics (De Weirdt *et al.*, 2012). This is especially true for evergreen

tropical forests, where leaves are found across a particularly wide range of phenological stages and where phenological changes drive a large variation in seasonal carbon uptake (Wu *et al.*, 2016, 2017).

Other research has focused on the temporal consistency of stomatal parameters (Resco de Dios *et al.*, 2020), or the conditions in which the g_{sw} response should be optimized (Katul *et al.*, 2010). Plants may optimize their stomatal operation across a variety of time scales, from near instantaneous response to stimuli such as sunflecks (Way & Pearcy, 2012; Campany *et al.*, 2016), diurnal responses such as those to drying soil (Knapp, 1993; Zhang *et al.*, 2018), and long-term responses such as those which optimize water and nutrient uptake by roots (Franklin, 2007). Thus, whole plant WUE is the integration of all these factors, with leaf-level WUE lying at the end of a hierarchy of responses (Katul *et al.*, 2010). Wu *et al.*, (2019b) addressed the seasonal consistency of tropical WUE by analyzing dynamics of g_1 during a drought event and found that species specific g_1 did not significantly vary by month, suggesting that at the whole canopy scale WUE is stable through time. However, the diurnal consistency of leaf-level WUE in this system remains untested. If they occur, diurnal adjustments in WUE may be in response to rapidly changing external stimuli such as changes in VPD during the day (Katul *et al.*, 2009), or may be the consequence of shifting water supply and carbon demand dynamics within the leaf (Bonan *et al.*, 2014; Dewar *et al.*, 2018). Understanding the degree to which WUE varies diurnally, and the main mechanisms which regulate these diurnal changes, may be helpful in developing more representative and robust process-based models of g_{sw} and E in tropical broadleaf evergreen forests.

In this study, I measured leaf gas exchange on six evergreen tropical tree species to identify key biotic and abiotic controls on stomatal parameters and WUE. I had four main objectives: 1) compare survey and *ex situ* response curve derived g_0 and g_1 to assess whether these two commonly used approaches provide comparable estimates of the key parameters; 2) determine if g_0 and g_1 vary with leaf phenological stage; 3) assess if g_0 and g_1 vary over a diurnal period; and 4) conduct simulations within a simplified canopy-scale model to understand the impacts of parameterization on E, comparing the estimated flux to a model benchmark derived from sap flux measurements. By addressing these four objectives, my goal was to develop a more detailed process-based understanding of stomatal function in wet tropical forests and identify several key axes of biotic and abiotic variation which could be targeted for further investigation.

3.3 – **Materials and Methods:**

Site and species description

Data collection occurred from January 6 to March 23, 2020, in the San Lorenzo Protected Forest (9.281°N, 79.974°W), on the Colón Province on the Republic of Panama's Caribbean coast (Fig. 3.1). The site is characterized as a wet lowland (130 m ASL) tropical forest, with a mean annual temperature of 23.4°C and an average of 3330 mm of rainfall (Paton, 2020).I used a crane operated by the Smithsonian Tropical Research Institute (STRI) for canopy access. Six tree species were selected for study, chosen to span early, mid, and late successional growth strategies (Table 3.1). For each species, I sampled from two trees that were exposed to full sun throughout the day. Four of the trees had previously been instrumented for measurement of sap flux.

Gas exchange and leaf trait data collection

Gas exchange measurements were carried out using five LI-6400XT portable photosynthesis systems using a 6400-02(B) LED light source and an LI-6800 portable photosynthesis system using a Multiphase Flash Fluorometer leaf chamber (6800-01A) (LI-COR Biosciences, Lincoln NE, USA). For all measurements the color spectrum of the irradiance was set to a fixed ratio of 90% red:10% blue.

I used two different methods of gas exchange: an *ex situ* response curve approach and an *in situ* survey approach. Stomatal response curves on cut branch segments were carried out as described previously (Leakey *et al.*, 2006; Davidson *et al.*, 2022; Lamour *et al.*, 2022). Upper canopy, fully sun exposed branches were cut predawn and immediately recut under water to ease xylem tension and prevent embolism (Sperry, 2013). I recut a total of at least 50 cm back from the first cut to remove open vessels (Wolf *et al.*, 2016) with final branch lengths of approximately 1.5 m. Cut branches were transferred in buckets to a shaded (~150 μmol PAR) location where all response curves were carried out. Each species was measured on 10-15 different days, spread across the duration of the field campaign. For each curve, irradiance level was reduced from saturating down to 0 μmol m^{-2} s^{-1} PPFD in a stepwise fashion every 20-40 min (Fig. 3.2a; Lamour *et al.*, 2022). The irradiance value at saturation was derived for each species using photosynthetic response curves collected at multiple locations from across the top of each canopy (Lamour *et al.*, 2021b; Rogers *et al.*, 2021).

Survey measurements followed previous approaches (Rogers *et al.*, 2004; Wu *et al.*, 2019b).

Fully sunlight top-of-canopy leaves were measured with the LI-6800. Before each measurement, the conditions within the leaf chamber were set to match ambient air temperature (22.8-32.6ºC), CO_2 concentration (~400 ppm), and irradiance (3 – 2400 µmol PAR). The relative humidity in the leaf chamber was maintained at 70% for all measurements, a level which allowed for VPD_{air} to be close to mean daytime conditions (Paton, 2020, Fig. A2.1), while minimizing condensation risk in the instrument. Each survey measurement consisted of a 30-90 second stabilization period, followed by five measurements of A and g_{sw} at five second intervals, which were then averaged to produce a single data point.

Surveys were carried out from 0630h (approximate sunrise) to 1830h (approximate sunset) across eight different days. Two survey schemes were used, one in which I measured as many leaves as possible at three positions on a single tree crown for 40 minutes every hour for four hours, and a second where each of the 12 tree crowns (two per species, three positions per tree) was measured as many times as possible for 12 minutes, replicating this pattern five times in a 12-hour period. The aim of the first scheme was to assess the diurnal dynamics of a single species on a given day, while the aim of the second scheme was to broadly survey the forest. I used the data from the first scheme to parameterize my models (see Note A2.1), and data from the second scheme, along with Wu *et al.*, (2019b), to validate my models.

Immediately following the single species gas exchange survey measurements the leaf was cut at the base of the petiole, and stored in a humid, cool, dark box for further processing (Leach *et al.*, 1982; Rodriguez-Dominguez *et al.*, 2022). Processing included using a Scholander-type pressure chamber to measure leaf water potential (Ψ_{leaf}; Scholander *et al.*, 1964). Following measurement of Ψ_{leaf}, samples were dried to constant mass and weighed to determine leaf mass area (LMA; dry leaf mass per unit leaf area). Measured leaves were classified into one of three phenological stages, young, mature, or old (Table 3.1, Fig. 3.3).

Reflectance spectroscopy

I used a full range spectroradiometer (PSR 3500+, Spectral Evolution, Inc., Lawrence, MA, USA) together with an LC-RP-Pro leaf clip foreoptic (Spectra Vista Corporation, Poughkeepsie, NY, USA) containing an internal, full-spectrum calibrated light source to measure leaf reflectance on all leaves following completion of stomatal response curves. The reflectance data were used to estimate $V_{cmax.25}$ and $J_{max.25}$ using the spectral methods and model presented in Lamour *et al.*,

(2021).

Sap flux measurement

Sap flux velocity (cm s^{-1}) data were collected for four of the 12 study trees. Sap flux velocity was measured with Granier-type sensors (Model PS-TDP8, PlantSensors, Nakara, Australia), which use heat dissipation to empirically infer sap flux velocity (Granier, 1987). Each tree was instrumented with two sensors, located at breast height, and positioned perpendicular to each other at a depth of 2 cm into the sapwood of the trees. Raw temperature data were processed in the R package 'AquaFlux' (v 1.0.0 Speckman, 2019) to derive sap flux velocity. VPD data obtained on site from the STRI meteorological station was used to normalize minimum flux. Sap flux velocity data were multiplied by sapwood area (Meinzer *et al*., 2001) to derive sap flow (g s^{-1}) at 15-minute intervals, with the assumption that velocity was consistent across the sapwood radial profile. In total there were 42 diurnal (05:30-18:30) periods of complete sap flux coverage for each of the four study trees during the period of study (Pivovaroff *et al.*, 2021).

Estimation of conductance parameters

Stomatal response was evaluated using the USO model (Medlyn *et al.*, 2011, Fig. 3.2b, Equation 3.1, Note A2.1). g_1 represents the slope in the relationship shown in Equation 3.2, a reconfiguration of Equation 3.1 where g_1 directly acts as the slope between g_{sw} and A, C_a, and VPD_{leaf}. The parameters g_1 and g_0 are mathematically identical in Equations 3.1 and 3.2 (Lamour *et al.*, 2022), however Equation 3.2 provides for simpler graphical depiction of the data.

Equation 3.2. $$g_{sw} - \frac{1.6*A}{C_a} = g_0 + g_1 * \frac{1.6*A}{\sqrt{VPD_{leaf}}}$$

As with any linear model, a limited range of measured g_{sw} can affect the model fit by introducing uncertainty in the regression (g_1). The wider the range of the data, the lower the uncertainty in the fit of the model slope, assuming that the variation around the mean slope is consistent (e.g., no heteroscedasticity). For response curve data, I captured a full range of conductance values, as I am theoretically measuring g_{sw} from its maximum (light saturated) value to its minimum (dark adapted) value. A limited range of g_{sw} can also lead to uncertainty in estimating a value for g_0, especially if most measurements occurred far above the light compensation point. To keep analysis consistent between datasets, I chose to fit g_0 for the survey dataset rather than prescribe a value (Duursma *et al.*, 2019).

R_{dark} was calculated from dark adapted measurements of A_{net} (the final response curve point) and was scaled to 25°C ($R_{dark.25}$) using an inverse Arrhenius equation (Equation 3.3; Bernacchi *et al.*, 2001; Von Caemmerer, 2013):

Equation 3.3. $$R_{dark.25} = \frac{R_{dark}}{\exp\left(\frac{H_a}{(R*T_{25})} - \frac{H_a}{(R*T_{leaf})}\right)}$$

where H_a is the activation energy of mitochondrial respiration (H_a = 46390 J mol^{-1}), and R is the ideal gas constant (R = 8.314 J mol^{-1} K^{-1}).

Canopy *E* simulations

As a method of evaluating the performance of different stomatal parameterizations against a benchmark data set, I modeled canopy scale *E* response to ambient environmental conditions. I chose not to evaluate the model performance in simulating canopy scale *A*, as I have no benchmark which to compare model estimates. I used the R package 'LeafGasExchange' (v 1.0.1, Lamour & Serbin, 2021), which includes a coupled leaf scale steady state assimilation, conductance, energy balance, and radiation interception model. Details of model parameters and equations used can be found in Note A2.2.

The leaf gas exchange model simulates environmental conditions around the leaf using local meteorological data (Paton, 2020). To simulate the radiation environment at the leaf surface the model uses the radiation interception model developed by Norman, (1979), which partitions incoming radiation into direct and diffuse streams. In each simulation I assumed six canopy layers with a uniform distribution of leaf area index (LAI) between layers (Béland & Baldocchi, 2021). To simulate wind speed within the canopy I assumed an exponential decrease with LAI within the canopy following the model presented in Equation 14 in Buckley *et al.*, (2014). Values for $V_{cmax.25}$, $J_{max.25}$, $R_{dark.25}$, g_0, and g_1, estimated as described above, were averaged by species and by phenological stage (Table 3.1). In each model run, uncertainty was simulated by rerunning the model using g_1 and g_0 values corresponding to ± 1 SE of the fitted value.

Leaf-level estimates of *E* were scaled to the canopy by first summing across canopy layers, then multiplying by total canopy area as estimated using the allometric function presented in Martínez Cano et al., (2019). LAI estimates were made for each species (Condit *et al.*, 1996; Sirri *et al.*, 2019), which allow for an appropriate accounting of leaf area per ground area.

I then conducted a model simulation sensitivity analysis to explore the potential impacts of

biotic variation on emergent, canopy scale *E*. To do this, I simulated different canopies with different combinations of leaf phenological classes, with leaf physiological properties based on leaf phenological stage. For this analysis I assumed "natural" conditions were a 15-80-5% partitioning between young, mature, and old leaves, an estimate that is in line with Wu *et al.*, (2017b). I compared the simulation results for canopy scale *E* with measured sap flow as a benchmark. Here I expected that there was a delay between flux measured at the base of the tree and *E* in the canopy, so I averaged flux across a 15 minute interval to minimize this discrepancy (Meinzer *et al.*, 2003)

Statistical analysis

To compare g_1 and g_0 estimates between tree species and phenological stages within tree species I used mixed effects models constructed and analyzed in the R package 'nlme' (v 3.1, Pinheiro *et al.*, 2020). For response curve data, the leaf served as the random effect, while for survey data, the location within the canopy of the tree served as the random effect. For all data I considered the species and phenological stage as fixed effects. The equations and coefficients for the mixed models can be found in Note A2.1 and Table A2.1-3.

To examine which of my three statistical models (response curve, survey, survey + time-of-day; Note A2.1) predicts leaf-level g_{sw} most accurately, I performed a validation of the fixed effects components of the models using two additional survey derived datasets, one which was collected on four separate days during the 2020 field campaign (described above as scheme 2), and a second data set collected by Wu *et al.*, (2019b) at the same site in 2016 (Rogers *et al.*, 2021). I then used validation statistics (r^2, RMSE, likelihood ratio test) to determine which model predicted g_{sw} most accurately.

I assessed the effect of species and species:leaf phenological stage on $V_{cmax.25}$, $R_{dark.25}$, and the effect of LMA, Ψ_{leaf}, and successional stage on g_1 and g_0 using ANOVA and post-hoc Tukey tests. Finally, I compared canopy level transpiration simulations using ANOVA at the species level, and a post-hoc Tukey's honest significant difference test to distinguish significance between factor levels. All analysis was performed using the R open source software environment (v 3.6.2, R Core Team, 2013).

3.4 – **Results:**

Gas exchange dynamics of diurnal surveys and response curves

Here I present the results from an analysis of 80 stomatal response curves (Fig. A2.2a) and 665 survey data points (Fig. 3.4; Lamour *et al.*, 2021b). Both A and g_{sw} respond strongly to the diurnal cycle of irradiance during the survey measurements (Fig. 3.4). VPD_{leaf} also exhibits a diurnal trend, peaking around solar noon, due to higher leaf temperatures, and a small increase in VPD_{air} (Fig. A2.1). Stomatal response curves can be used to examine potential maximum photosynthetic and stomatal fluxes. Here I see that among species, there is significant variation in maximum g_{sw}, with *Brosimum utile, Cecropia insignis*, and *Miconia borealis* having maximum g_{sw} values up to three times that of the other three species (Fig. A2.2b).

I can compare the relationship between g_{sw} and environmental conditions for both datasets (Fig. A2.2). I see that not only do the survey data have a larger overall range of conductance, but there is also more within-species variation in conductance for a given set of environmental conditions. I can also see the non-linearity of the response curve data, explored in detail by Lamour *et al.*, (2022), which is much less pronounced for the survey data set.

Model comparison and validation

I evaluated the accuracy of the models built on the different datasets (response curve, survey, survey + time-of-day), first assessing their calibration scores, and then by predicting g_{sw} measured by the survey method at the same site in 2016 (Rogers *et al.*, 2021) and using the 2020 validation dataset. In the calibration phase, the survey and survey + time-of-day models can be compared directly as they are derived using the same data set. The model including a time-of-day effect on g_1 and g_0 has an improved calibration r^2 (0.80 vs 0.75) a lower RMSE (0.0564 vs 0.0627 mol m^{-2} s^{-1}), a lower AIC score (-1844 vs -1741) and a likelihood ratio test reveals the models were significantly different ($p < 0.001$). However, during the validation phase, the model calibrated on the survey dataset without a time-of-day effect performed the best, with the lowest RMSE, and the highest validation r^2 (Fig. 3.5).

g_1 values estimated using the response curve dataset were significantly ($p < 0.001$) lower than when they were estimated using the survey data set (Fig. 3.6). On average, the response curves produced estimates of g_1 which were 50% lower than estimates obtained from survey data. Only in the species *Brosimum utile* was there no significant difference in estimated g_1 (Fig. 3.6).

Finally, I simulated canopy scale *E* for all six species to compare how the different methods of deriving stomatal parameters perform in a modeling context at the larger whole-tree scale. Four of the six species also had scaled sap flux velocity measurements (Pivovaroff *et al.*, 2021) to compare the modeled *E* allowing us to benchmark results (Fig. 3.7). I found that when comparing estimated and observed *E,* the survey + time-of-day parameterization had the lowest RMSE (0.013 g H_2O m^{-2} s^{-1}) followed by survey (0.014 g H_2O m^{-2} s^{-1}), and the response curve method (0.022 g H_2O m^{-2} s^{-1}) (Fig. A2.3). All three methods closely tracked changes in irradiance. However, the two survey methods captured the magnitude of the change in canopy *E* more closely than the response curve method (Fig. 3.7).

Effect of leaf phenological stage on estimated stomatal parameters

For the response curve data set, both g_1 and g_0 varied by tree species ($p < 0.001$) and phenological stage ($p = 0.009$) with a significant stage:species interaction ($p < 0.001$, Figs. 3.8a, A2.4, Table 3.2). For the survey data set, g_0 varied by tree species ($p < 0.001$), phenological stage ($p < 0.001$) with a significant stage:species interaction ($p < 0.001$, Fig. A2.4, Table 3.2) but g_1 only varied among tree species ($p < 0.001$; Fig. 8b, Table 3.2).

When assessing the differences between the interactive effects of phenological stage and species on g_1 for response curves I only found four significant effects, *Brosimum utile* young and mature ($p = 0.003$, 66.9% decrease), *Miconia borealis* young and mature ($p = 0.006$, 61.2% decrease), *Miconia borealis* young and old ($p = 0.041$, 49.7% decrease), and *Cecropia insignis* young and old ($p = 0.007$, 111% increase). I also used response curve data to investigate continuous relationships between g_0 and g_1 with other related leaf physiological traits, but did not observe a significant effect of LMA, Ψ_{leaf}, or successional stage on g_1 or g_0 (Fig. A2.5, A2.6).

Finally, I analyzed the interactive effects of phenological stage and species on $V_{cmax.25}$ and $R_{dark.25}$, derived from leaf spectroscopy. The relationships between stage and $R_{dark.25}$ ($p < 0.001$) and stage and $V_{cmax.25}$ ($p < 0.001$) were significant, ~40% decrease in values between the mature and old phenological stages (Fig. A2.7, Table 3.1).

Investigation of a time-of-day effect

Using the survey dataset (Fig. 3.4), I tested if the time-of-day influenced g_0 and g_1. I found a significant decline in g_1 from morning to evening for the six species ($p < 0.05$, Table 3.2). g_1 was

on average 2.5 times higher in the early morning than in the late afternoon, however, the magnitude of the decline differed between species (Fig. 3.9). Unlike g_1, g_0 did not differ by the time-of-day for the six species ($p = 0.432$).

Canopy level transpiration simulations

To assess the impact of data collection methodology on simplified canopy-scale model performance, I compared estimates of mean daytime E for the six species, three methods and sap flux benchmark (when available, Fig. 3.10). I assumed a constant flux of E for each 15 min interval and averaged E for each 12-hour diurnal period. For five of the six species the survey data produce significantly higher ($p < 0.001$) estimates of E than for the response curve data (*Brosimum utile* =26.0%, *Cecropia insignis*= 87.1%, *Guatteria dumetorum* = 124.9%, *Terminalia amazonia* =107.4%, and *Vochysia ferruginea* = 44.3% increase). In *Miconia borealis* there was no significant difference between E as estimated from curve derived values, and E as estimated from survey derived values ($p = 0.152$), even though in *Miconia borealis* the g_1 value estimated from response curves was nearly half that of the g_1 value estimated from survey measurements (Fig. 3.6). However, g_0 values for *Miconia borealis* were especially low with no significant difference between curve and survey-based estimates (Fig. A2.4), and *Miconia borealis* has a saturating irradiance which was 50% higher than the other five species in this study (Rogers *et al.*, 2021).

I also found no significant differences between the survey approaches for any of the six species. In all four species for which I have a benchmark, the benchmark and survey estimates showed strong correspondence with estimates being statistically indistinguishable ($p > 0.05$).

Finally, I examined the impact of leaf phenological stage distribution assumptions on the modeling of canopy E (Fig. A2.8). For this analysis I reran the simplified canopy-scale model prescribing different distributions of leaf phenology, including even (33.3% young, 33.3% mature, 33.3% old), all-young, all-mature, and all-old. Interestingly, I found no significant differences in predicted daily canopy transpiration between the even phenology distribution, the "natural" (15% young, 80% mature, 5% old) phenology distribution, or the all-mature phenology distribution for any species when using any of the three models (response curve, survey, survey + time-of-day) of stomatal parameters. However, when modeled using a single phenological stage, I see strong variation in estimates of daily E (Fig. A2.8) with daily estimates of E varying by up to 150% in some species.

3.5 – **Discussion:**

A key step toward reducing ESM uncertainty is to account for the abiotic and biotic effects on the stomatal parameters g_0 and g_1. In this study I demonstrate that *ex situ* stomatal response curves and *in situ* survey style measurements produce statistically different estimations of stomatal parameters in tropical broadleaf evergreen forests (Fig. 3.6). These differences in parameterization resulted in large (between 26% and 125%) differences in simulated fluxes of water (Fig. 3.10). Further, I found that leaf phenology plays a role in regulating stomatal traits, however this role was not consistent across species (Fig. 3.8, A2.4) was not observed consistently using the different measurement approaches (Fig. 3.6), and, for a given methodology, did not drive variation in modelled E (Fig. A2.8). I also observed a consistent decline in g_1 during the photoperiod (Fig. 3.9), with g_1 declining by an average of 250%. When these results are taken together and used to model forest function, I found that models using stomatal parameters derived from *ex situ* response curves significantly underestimated canopy level E both at instantaneous time scales (Fig. A2.3) and across a full dry season (Fig. 3.7), and that while leaf traits do vary among leaf phenological stage, models which only include mature vegetation perform similarly to those that explicitly simulate three leaf stages (Fig. A2.8).

Derivation of stomatal model parameters is highly sensitive to the method of data collection

One of the clearest observations from this study is the significant difference in fitted values of g_1 between response curves and survey style measurements. In five of the six species studied, g_1 was significantly lower (50% reduction) for response curves than for survey measurements (Fig. 3.6). I explore several possible mechanistic explanations for the observed difference in g_1 estimates.

All response curves were measured on excised branch segments. While previous work on tropical tree species has shown that excision does not impair photosynthetic function (Verryckt *et al.*, 2020) stomata will be affected more acutely by hydraulic damage than chloroplasts if branches are not allowed to sufficiently rehydrate before measurement (Wolf *et al.*, 2016; Lawson & Vialet-Chabrand, 2019). This decline in g_{sw}, without a commensurate decline in A (Davidson *et al.*, 2022) may result in a decrease in estimated g_1. An excision effect was previously observed in plants collected from the same site as this study, where levels of A and g_{sw} diminished from pre-excision values within 60 minutes of branch removal (Santiago & Mulkey, 2003). Here, the researchers

attributed excision induced embolism as the likely mechanism underlaying their result. Missik *et al.*, (2021) found that immediately following excision, levels of g_{sw} were reduced by up to 62% in woody deciduous trees, again attributing this decline to embolism. However, in both studies branches were cut during the daytime when transpiration fluxes are higher, and the risk of embolism is much greater (Sperry, 2013). Further, Santiago & Mulkey, (2003) limited their experiment to just 60 minutes, which may not be sufficient time for branches to rehydrate and acclimate to a new leaf-level environment. Other studies (e.g., Meng & Arp, 1993; Miyazawa *et al.*, 2011) have found mixed, and sometimes contrasting effects of excision on gas exchange measurements.

A more relevant comparison may be drawn between this study and Davidson *et al.*, (2022) who, in a comparison of cut and uncut branch segments, demonstrated that in a woody deciduous species when excision is carried out predawn, stomatal behavior is not significantly altered in leaves measured within 8h of excision. I observed no significant difference in g_0 or g_1 estimated from curves conducted in the morning (07:00-12:00) and the afternoon (12:01-18:00) local time (Fig. A2.9) suggesting that excision stress did not alter stomatal function over the course of measurements. In addition, longer duration response curves were correlated with higher estimates of g_1 (Fig. A2.10), again suggesting that a stress response is not accumulating during measurement.

It is also possible that the direction of the response curve (increasing irradiance versus decreasing irradiance), combined with an asymmetrical response of stomata to long term changes in irradiance (Lawson & Blatt, 2014) may have led to the negative bias observed for g_1. To test this, I collected response curves in both directions on a similar set of tropical species (Fig. A2.11) however I did not observe any evidence for a negative bias associated with curves in which irradiance is reduced.

There could also be error associated with the survey measurements. Accurate survey assessment of the A:g_{sw} relationship relies upon the assumption that levels of A and g_{sw} are at a steady state (Hölttä *et al.*, 2017), and are acclimated to the environment surrounding the leaf, however errors when selecting an appropriate level of PPFD, VPD_{leaf}, or C_a will cause alteration of the leaf-level environment. Taking irradiance as an example; if an incorrect level of irradiance is chosen, the level of assimilation will change rapidly in response to the new irradiance, however the stomatal response will lag, which will alter the estimate of g_1. Stomata are known to react more slowly to increases in irradiance than decreases in irradiance (Lawson & Vialet-Chabrand, 2019).

This means that if, on average, I misestimated irradiance in the same proportion (equal under and over-estimation), I would expect a slightly lower WUE (higher g_1) for survey data, which is consistent with my findings (Fig. 3.6). This issue of improperly estimated irradiance is not insignificant, as irradiance can fluctuate dramatically, particularly under cloudy conditions (Fig. 3.7), which may lead to errors matching the natural environment to the leaf chamber conditions.

A final factor to consider is the leaf-to-leaf variability implicit in each measurement type, with survey measurements consisting of roughly 10 times the number of individual leaves as response curves (Fig. A2.2). Survey measurements showed a slightly poorer performance, and a significantly higher variance, in an internal model calibration than curve derived measurements (Fig. A2.12, Tables A2.1 and A2.2). This may be due to the larger leaf-to-leaf variability captured using the survey method, or it could be due to unstable ambient conditions at the time of measurement which can create noise in survey data (Fig. A2.2b and S13c-d). When the two models were validated using an external dataset comprised of ~120 new individual leaf estimates per species, both models had similar residual variation, while the response curve model exhibited a clear bias, underestimating levels of g_{sw} (Fig. 3.5).

Clearly, both methods have benefits and drawbacks, and neither is free from error. Survey style measurements can integrate the diurnal dynamics of stomatal response, which may be an appealing feature for those who model stomatal response to a range of multivariate environmental conditions. Response curves capture stomatal response at truly stabilized conditions, which while stability of environment rarely occurs in nature, is useful for developing generalizable parameter estimates which can be used in ESMs.

<u>The effect of leaf phenology and traits on g_0 and g_1</u>

Previous work documenting phenological changes in leaf properties in wet evergreen tropical forest found a strong effect of leaf phenology on V_{cmax} (Kitajima *et al.*, 1997b; Wu *et al.*, 2017). This change in V_{cmax} leads to a change in potential A, and an assumed commensurate change in the potential g_{sw}, driven by changes in leaf-level metabolism (Tobin & Rogers, 1992; Wingler *et al.*, 2004). However, if the relationship between A and g_{sw} is not coordinated across leaf development, g_1 will vary between leaf phenological stages. Theoretically, a phenology related increase in g_1, as observed in *Cecropia insignis* (Fig. 3.8a) may be adaptative as a means of maximizing the photosynthetic efficiency of older vegetation. If V_{cmax} declines in older vegetation, as I observe in

this study (Fig. A2.7), I may also expect an increase in g_1 as a higher level of intercellular carbon (C_i) is required for the same rate of A. However, in this study I did not find evidence across all species for a consistent effect of leaf phenological stage or relative leaf age on g_1 or g_0 (Fig. 3.8). Here I explore two possible explanations for the lack of an effect observed in this study.

In the USO model, the relationship between A and g_{sw} is the chief control on the g_1 parameter. Coordination between A and g_{sw} means that for a given level of A, there is a given level of g_{sw} and thus a given level of C_i. Conversely, if A and g_{sw} lack coordination, at a given level of A, g_{sw}, and thus C_i, can vary. Therefore, tight coordination between A and g_{sw} will result in leaves maintaining a fixed ratio of C_i:C_a across changes in photosynthetic capacity (Wong *et al.*, 1979, 1985; McDowell *et al.*, 2006). I did not find significant differences in C_i:C_a across any of the phenological stages across species (Fig. A2.14), suggesting that although V_{cmax} may shift with leaf phenology (Fig. A2.7a), g_{sw} will change in proportion to supply and maintain a stable level of intercellular CO_2 (Long & Hällgren, 1993). This coordination in V_{cmax} and g_{smax} (g_{sw} at saturating irradiance) is indicative of stable WUE or g_1 across phenological stages (Fig. 3.8). However, this does not suggest a lack of optimization of carbon capture through ontogeny. Even though the ratio of A and g_{sw} does not change with leaf phenology, V_{cmax} changes with leaf phenology (Fig. A2.7a).

Time-of-day effect on g_1

While g_1 is often thought to be fixed over daily to seasonal timescales (Medlyn *et al.*, 2011), others suggest that at the leaf-level g_1 may vary over shorter, diurnal time scales (Katul *et al.*, 2010). Daytime adjustments in g_1 may be driven by rapidly changing external stimuli such as irradiance (Way & Pearcy, 2012; Campany *et al.*, 2016), or VPD and C_a (Katul *et al.*, 2009), to which individual leaves may alter their stomatal response in order to maximize assimilation, or minimize water loss. Supply and demand dynamics may also effect stomatal behavior, with a reduction in the water supply to the substomatal cavity (Bonan *et al.*, 2014), leading to a more conservative response. Here I observed declining g_1 over the diurnal periods for all six species (Fig. 3.9).

A decreased supply of water to the leaf late in the day (Venturas *et al.*, 2017), may be the most likely explanation for the observed decrease in g_1. In this case, lower g_{sw} at the same level of stomatal index, (a term representing A at a combination of leaf-level environmental conditions) would result in a decrease in the fitted value of g_1 (Fig. A2.15). These findings are consistent with

other studies of stomatal response (Manzoni *et al.*, 2011) which suggest that WUE responds to short-term changes in the supply of water. Longer term adjustments in WUE in response to seasonal or yearly drought, do not appear to be occurring at this site (Wu *et al.*, 2019b).

The finding that g_1 declines throughout the day is also consistent with models of stomatal optimality which apply a penalty on stomatal opening, either in the form of vascular damage (Wolf *et al.*, 2016; Sperry *et al.*, 2017; Anderegg *et al.*, 2018), or in non-stomatal limitations on A (Hölttä *et al.*, 2017; Dewar *et al.*, 2018; Kennedy *et al.*, 2019). Many of these models apply a function where stomata reduce their aperture in response to Ψ_{leaf} (Klein, 2014). To investigate if Ψ_{leaf} can help explain the diurnal dynamics of g_1, I implemented the optimality model described in Anderegg *et al.*, (2018). This model applies a reduction in estimated g_{sw} which is proportional to the assumed decline in stem xylem conductivity with increasing Ψ_{leaf} (see also Note A2.3). However, I found that the Ψ_{leaf} penalty from Anderegg *et al.*, (2018) poorly explained observed patterns of g_{sw} (Fig. A2.16). Examination of stomatal model residuals versus measured Ψ_{leaf} (Fig. A2.6) demonstrates that Ψ_{leaf}, as an explanatory factor alone, is not capable of explaining the variation in g_1 observed, consistent with previous observations (Wu *et al.*, 2019b). As an alternative to Ψ_{leaf} based models, many ESMs use a β_t factor, dictated by soil moisture, to downregulate V_{cmax} and g_{sw}. Recently, Li *et al.*, (2022) tested the applicability of a β_t factor at the same site in this study and found that, like Anderegg *et al.*, (2018), it over penalized drought-related loss of productivity. Several other hydraulic parameters such as hydraulic capacitance, and leaf hydraulic conductance may be more pertinent, and may play a larger role in stomatal regulation, however I lack those data in this current study.

The low morning WUE observed across all species may be the result of circadian resonance (Green *et al.*, 2002) whereby sunrise anticipation linked to a plant's endogenous rhythm may prime stomata to achieve their largest opening early in the day. This behavior, in systems with a fixed photoperiod, is thought to be adaptive as a means of maximizing carbon assimilation (Resco de Dios *et al.*, 2016). Higher than optimal morning g_{sw} would lead to elevated estimates of g_1, which is consistent with previous findings that suggest circadian regulation fails to help to optimize diurnal variations in stomatal conductance (Resco de Dios *et al.*, 2020).

The failure of a time-of-day effect to significantly improve predictions of g_{sw} (Fig. 3.5) suggests that while an overall pattern of declining g_1 is expected, the magnitude of the decline each day is the byproduct of abiotic processes that I may not have fully captured in this study, such as

dynamics in the soil-plant-atmosphere continuum (Zhang *et al.*, 2018), or an effect of ABA on regulating stomata (McAdam & Brodribb, 2015). Without these data, and a more detailed understanding of the response of stomata to small changes in VPD (Buckley, 2016) it may not be possible to model diurnal fluctuations in WUE. Thus, I recommend future research explore diurnal shifts in g_1 in greater detail, as an understanding of the mechanisms behind these dynamics has the potential to significantly advance model representation of canopy *E*.

Impact of measurement method on models of canopy function

Our simulations of canopy *E* revealed that using parameters derived from response curves leads to a systematically underestimated (26-125%) diurnal flux (Figs. 3.7, 3.10), consistent with the external model validation (Figs. 3.5, A2.3). This underestimation is in part attributable to lower g_1 values from response curves (Fig. 3.6) which limit daytime *E*, due to the assumption that at an irradiance level greater than saturating, $g_{sw} = g_{s\max}$.

All three models underestimate the level of *E* at low irradiance as the simulations assume that any time irradiance is below the light compensation point, $g_{sw}=g_0$. However, this assumption may be flawed due to the combination of cuticular conductance and stomatal leakage (Machado *et al.*, 2021), measurement artifacts (Duursma *et al.*, 2019) or unaccounted for transpiration from stored crown water supplies (Meinzer *et al.*, 2003). The integrated diurnal flux of water (Fig. 3.10) also reveals a large impact of parameterization, with the survey method producing species level values of *E* between 9% and 77% higher than model output using response curve derived parameters, underscoring the impact that g_1 can have on model estimation of ecosystem function (Dietze *et al.*, 2014) and reinforcing the need for careful choices with regard to the method used to estimate g_1.

Finally, in my assessment of the impact of selected phenological distribution on simulations of canopy *E* (Fig. A2.8) I observed no significant difference in daily *E* between models run using a natural leaf distribution an even phenological distribution or an all-mature distribution. Previous work in the Brazilian Amazon has suggested that appropriate estimation of leaf phenological distribution is essential for accurate estimation of gross primary productivity (GPP), and canopy A_{net} (Wu *et al.*, 2016, 2017). The fact that the models of *E* are not sensitive to leaf age distribution may be due in part to the limited role leaf phenology plays in stomatal traits (Fig. A2.8), with the majority of between phenological stage variation being modeled as variation in V_{cmax} (Fig. A2.7,Wu *et al.*, 2019a). While V_{cmax} plays a role in determining g_{sw} and therefore *E*, variation in

the g_1 and g_0 parameters would be expected to manifest in larger variation in E (Rogers *et al.*, 2017c). My findings underscore the need to closely consider the method used, and assumptions implicit to that method, when parameterizing generic PFTs, or when applying trait based approaches to ESMs (Van Bodegom *et al.*, 2012).

3.6 – **Figures:**

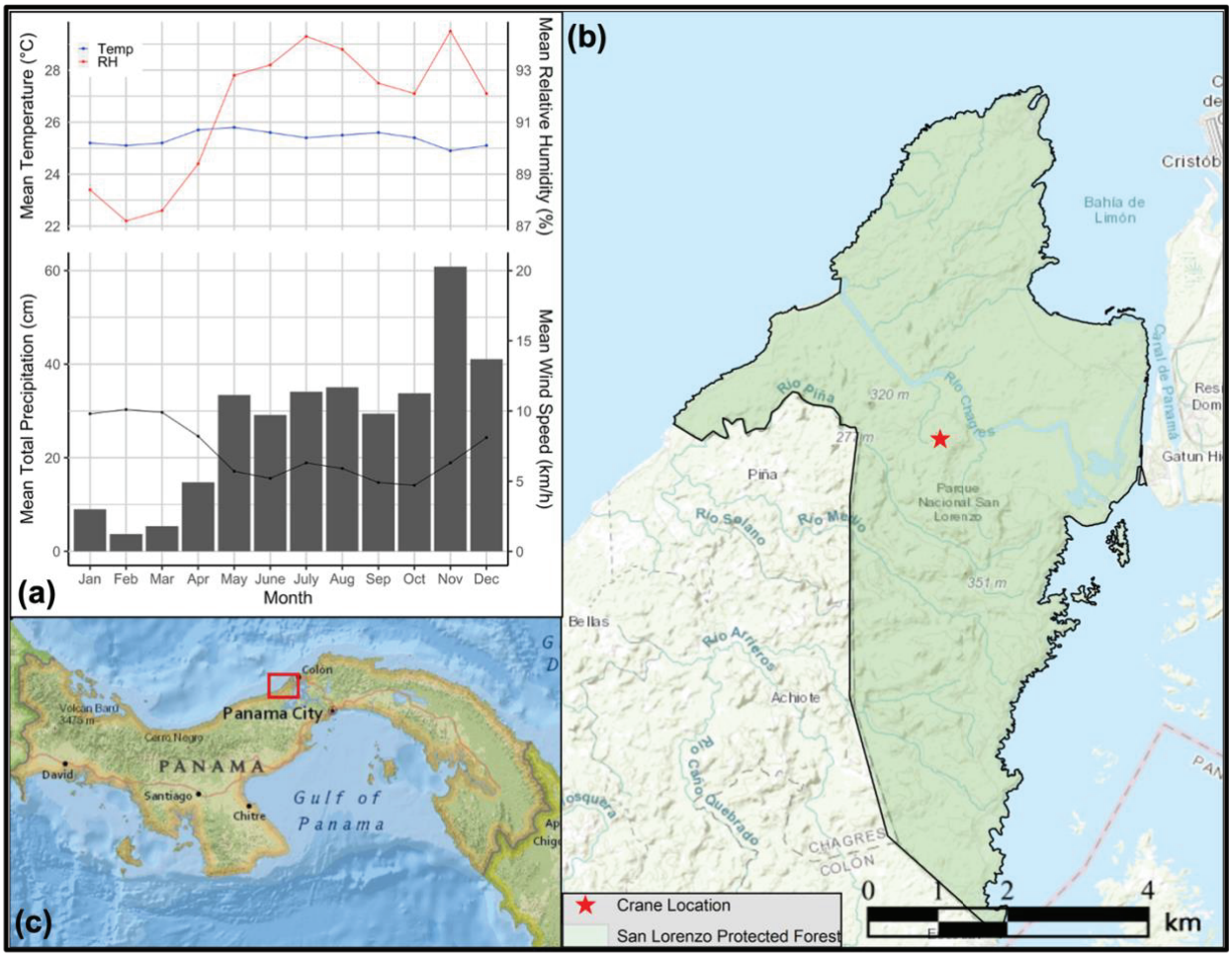

Figure 3.1: Geographic location of the crane site within the San Lorenzo Protected Forest and monthly climate averages collected at the site between 1997 and 2019. The period between January and April is considered the dry season, with less than 20% of annual rainfall (black bars). During the period of study, mean temperature was 25.5°C and mean daily precipitation was 1.3 mm. Basemap sources: National Geographic and Esri.

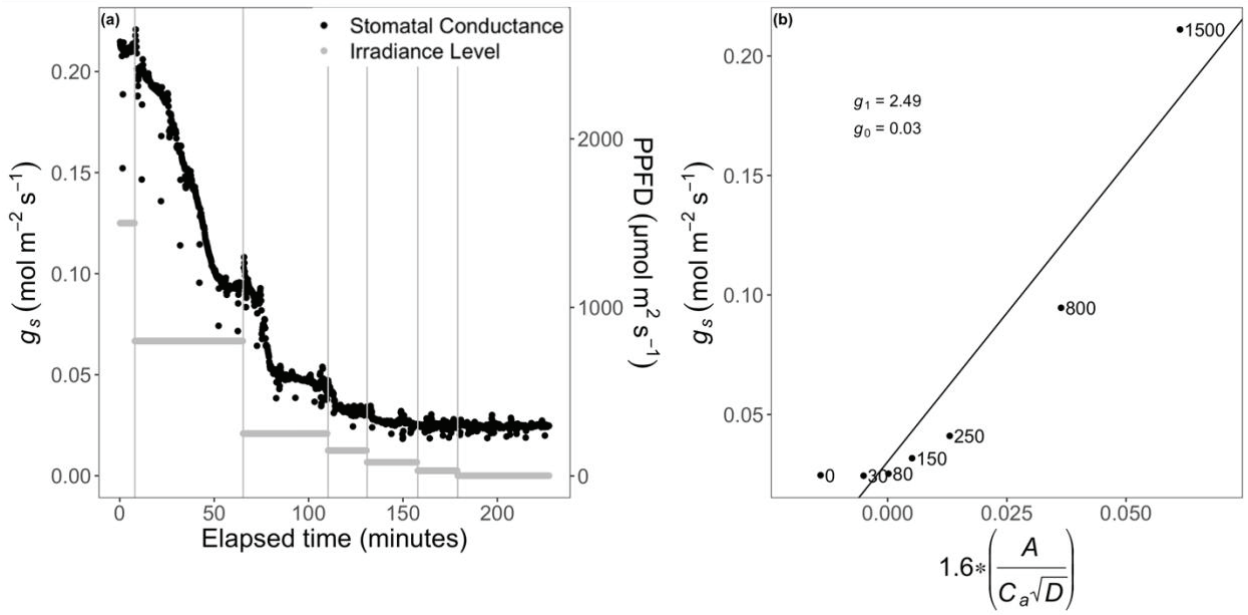

Figure 3.2: Schematic representation of the response curve method. (a.) raw data from a response curve, with each black point representing an observation of g_s. At each irradiance level (horizontal grey bars) stomatal conductance (g_s) drops then stabilizes, at which point irradiance is reduced to the next level (vertical grey bars). Across all irradiance levels, leaf temperature and VPD_{leaf}, were held constant and close to ambient conditions. The CO_2 inside the leaf chamber was maintained at 400 µmol mol^{-1}. (b.) a typical regression fit of the points extracted from the seven irradiance levels, and the g_1 and g_0 estimates produced from this curve. In this example, the non-linearity of the response curve data, explored in detail by Lamour *et al.*, (2022), is readily apparent. For data analysis, many curves are combined to obtain one overall regression, with each curve acting as a random effect on the overall g_1 and g_0 estimates.

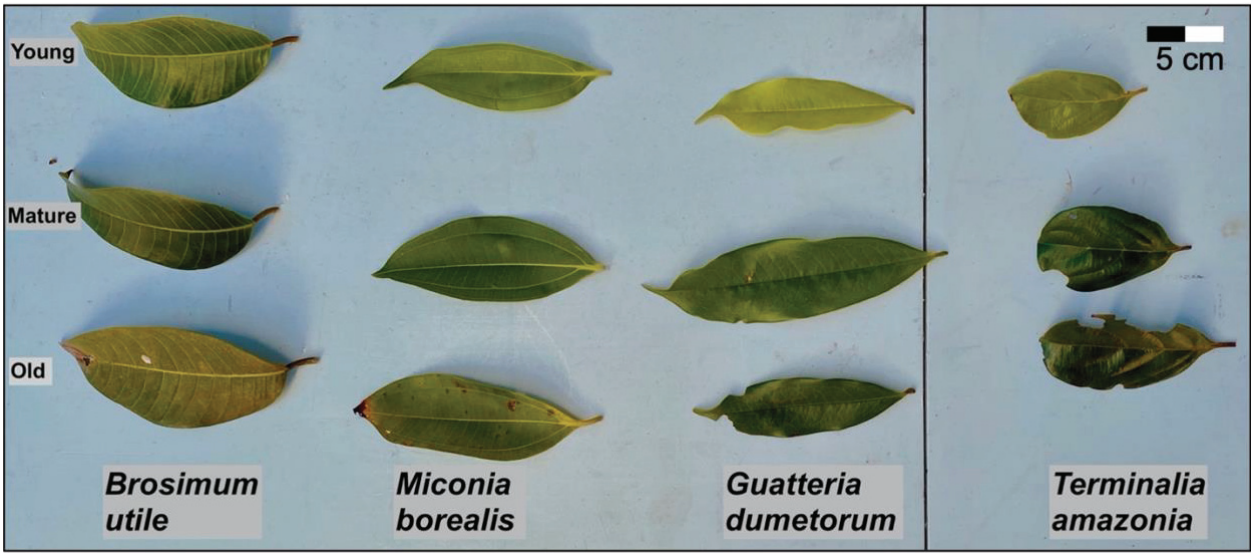

Figure 3.3: Examples of the three phenological stages for four of the six species in this study. Young leaves were characterized as lighter in color, with minimal damage, softer more flexible texture, and a distal position on the branch. Mature leaves comprised the majority of the leaf material, characterized as fully expanded, having an intermediate color and texture as well as an intermediate position. Old leaves were very scarce for most species and tended to have minor surface damage, were dark in color, and were in extreme proximal positions on branches.

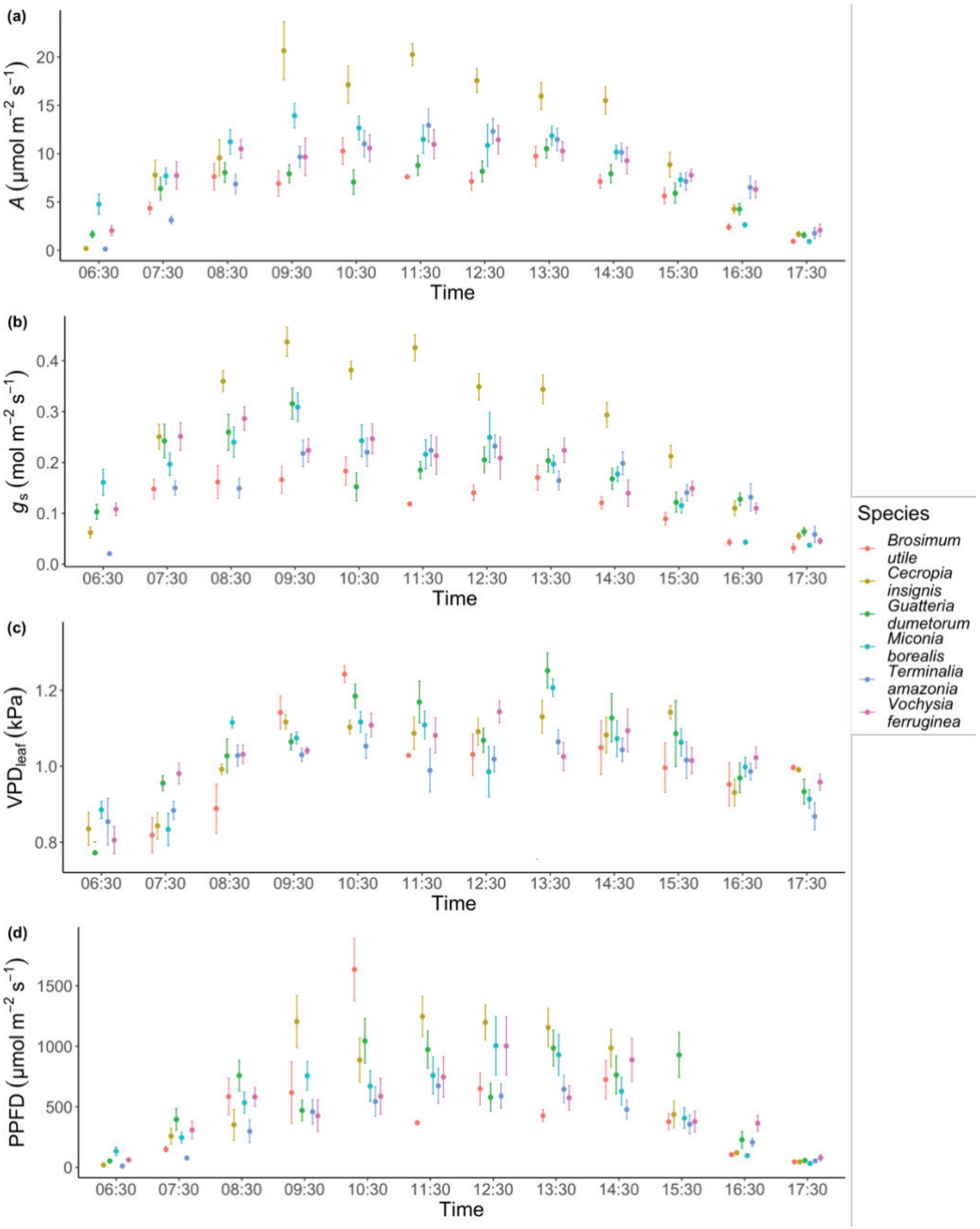

Figure 3.4: Species specific averages of hourly (a) photosynthesis, (b) stomatal conductance, (c) vapor pressure deficit at the leaf surface, and (d) irradiance collected during diurnal survey measurements. Error bars represent ± 2 SE of the mean.

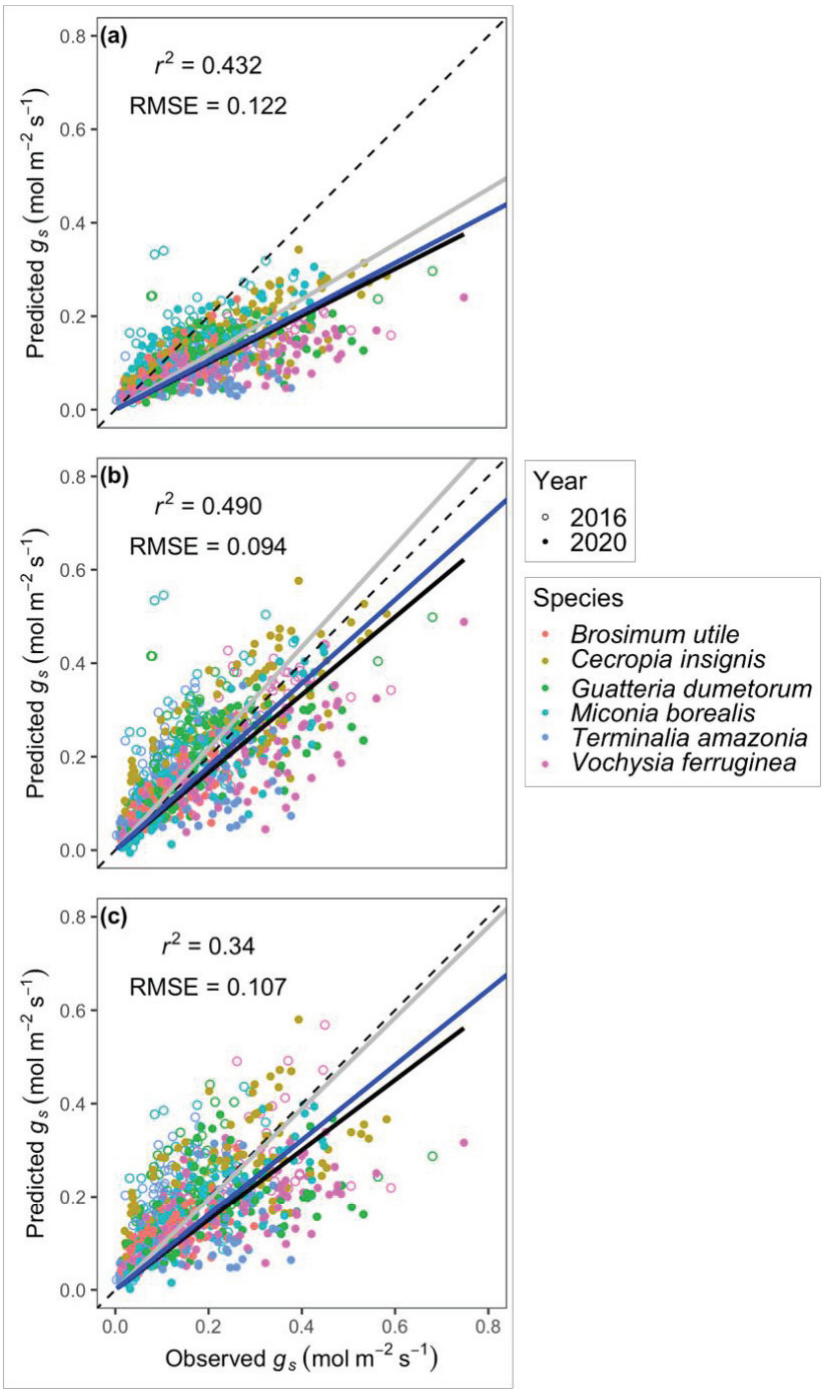

Figure 3.5: Validation plots of observed values of leaf-level stomatal conductance (g_s)versus USO model predicted data for (a.) the model based on response curve derived g_0 and g_1, (b.) the model based on survey derived g_0 and g_1, and (c.) the survey model with an inclusion of a time-of-day effect on g_1. r^2 and RMSE values in each panel show that the survey model improves predictions of g_s over the response curve model, however, the inclusion of the time-of-day effect slightly worsens model predictive accuracy. Open circles were from the 2016 dataset collected by Wu *et al*. (2019), while filled circles correspond to the 2020 validation data. Solid black, grey, and blue trend lines correspond to the lines of best fit for the 2016 data, 2020 data, and all the data respectively. Dashed black line is a 1:1 reference line.

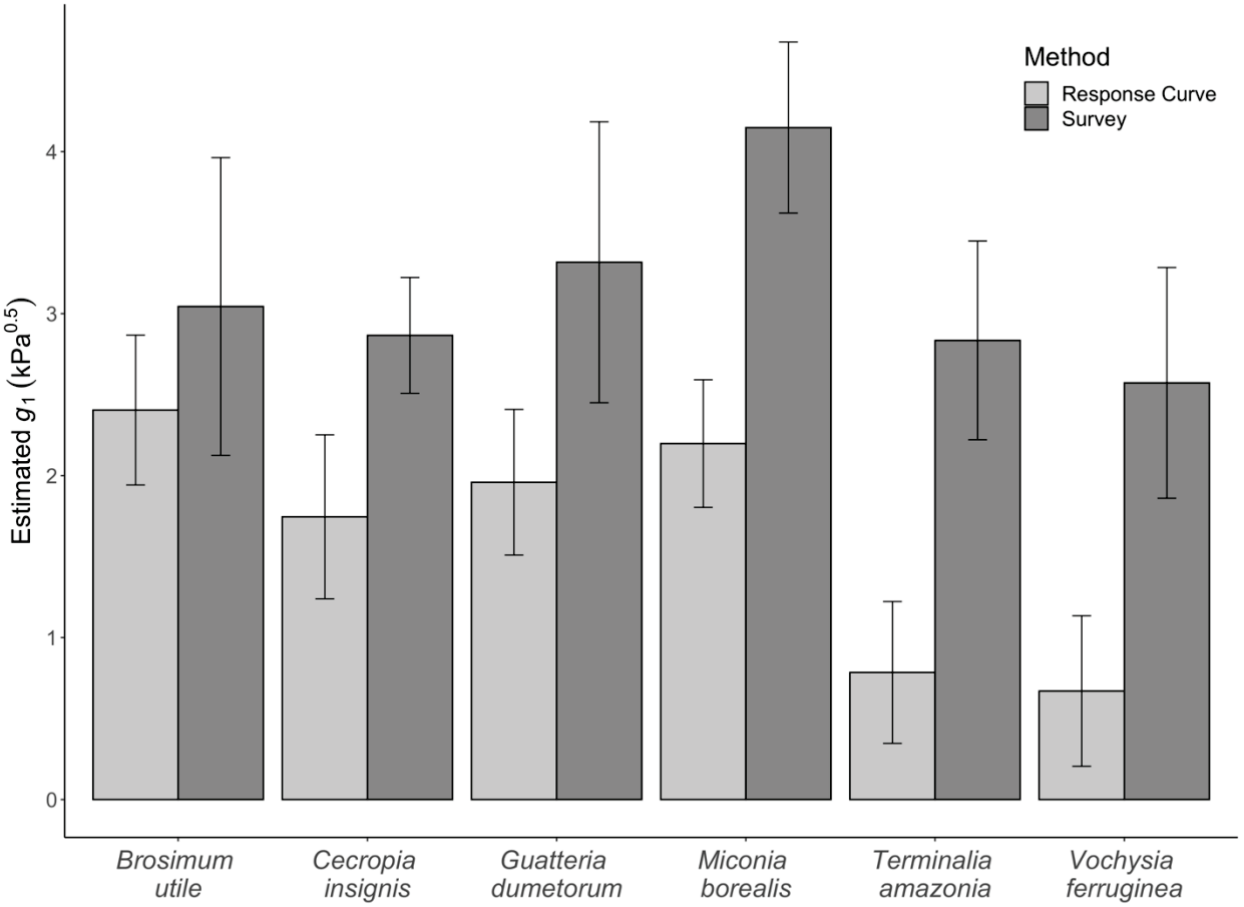

Figure 3.6: Fitted values of g_1 by species from the response and survey methods. For all species other than *Brosimum utile* g_1 from response curves was significantly lower than g_1 estimated from the survey data ($p < 0.001$). Error bars represent ± 2 SE of the mean.

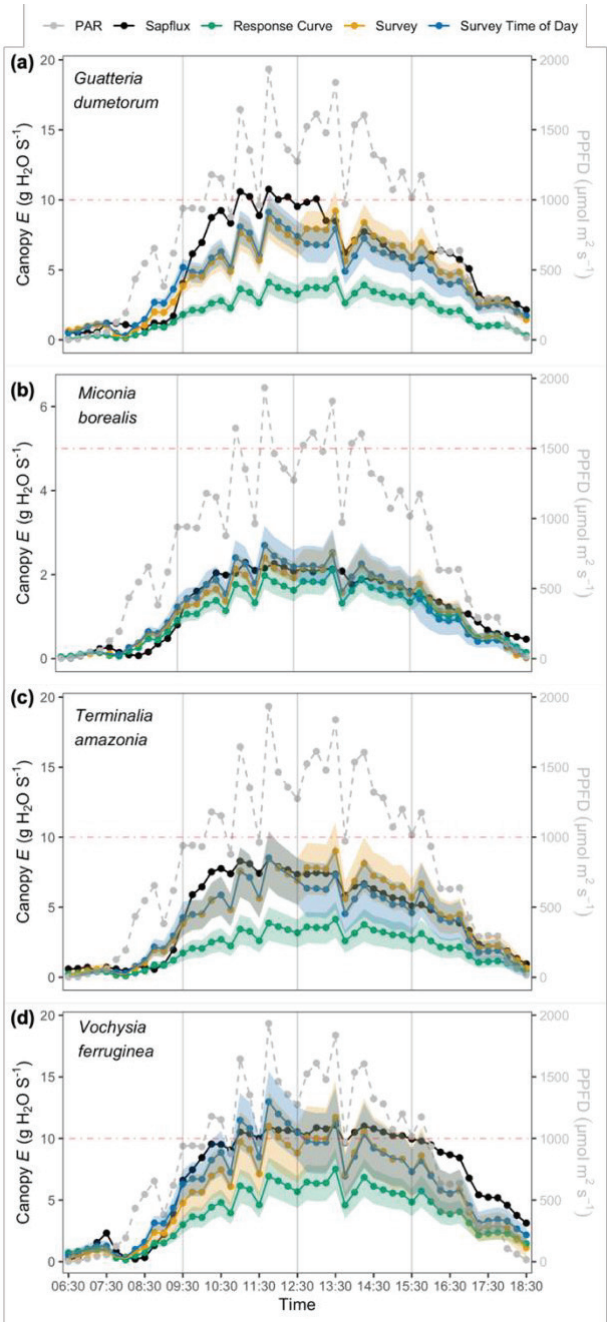

Figure 3.7: Simulated canopy scale E (g H_2O s^{-1}) at 15 min time points for (a.) *Guatteria dumetorum*, (b.) *Miconia borealis,* (c.) *Terminalia amazonia*, and (d.) *Vochysia ferruginea* on the 20th of February 2020. Black points and line represent the sapflux benchmark, green points and line represent response curve derived simulation, gold points and line represent survey derived simulation, and blue points and line represent survey derived simulation with g_1 changing based on time-of-day. Shading around the simulated data represent error propagated into the simulation by using $g_1 \pm 1$ SE of the estimated value. Grey dashed line represents the solar profile (PAR), vertical grey lines show the transition between g_1 values for the survey time-of-day model and horizontal red line shows the level of saturating irradiance for each species.

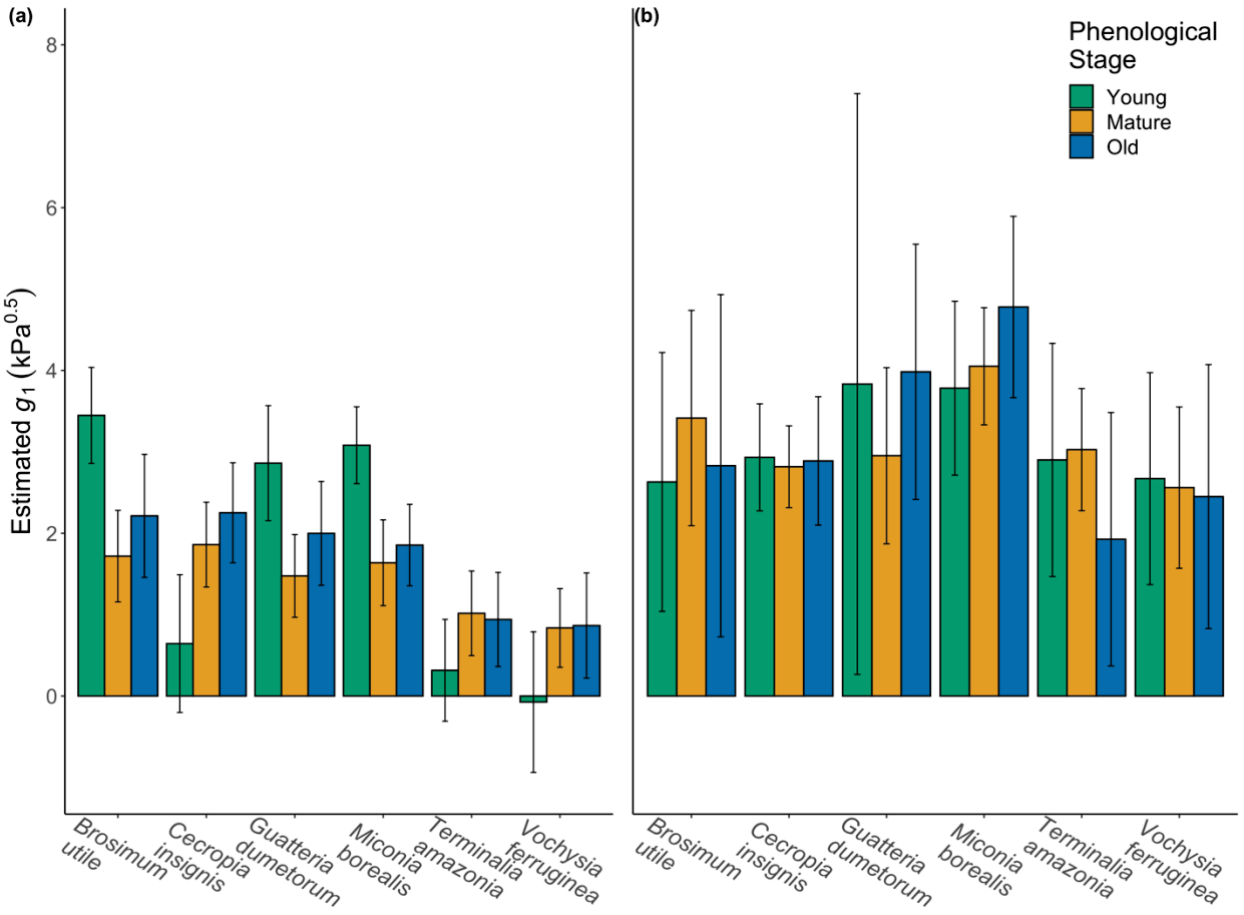

Figure 3.8: Fitted values of g_1 for (a.) response curve data, and (b.) data from survey measurements. Data in panel (a.) are significant to the species and phenological stage levels, while data in panel (b.) were only significant at the species level. Error bars represent ± 2 SE of the mean.

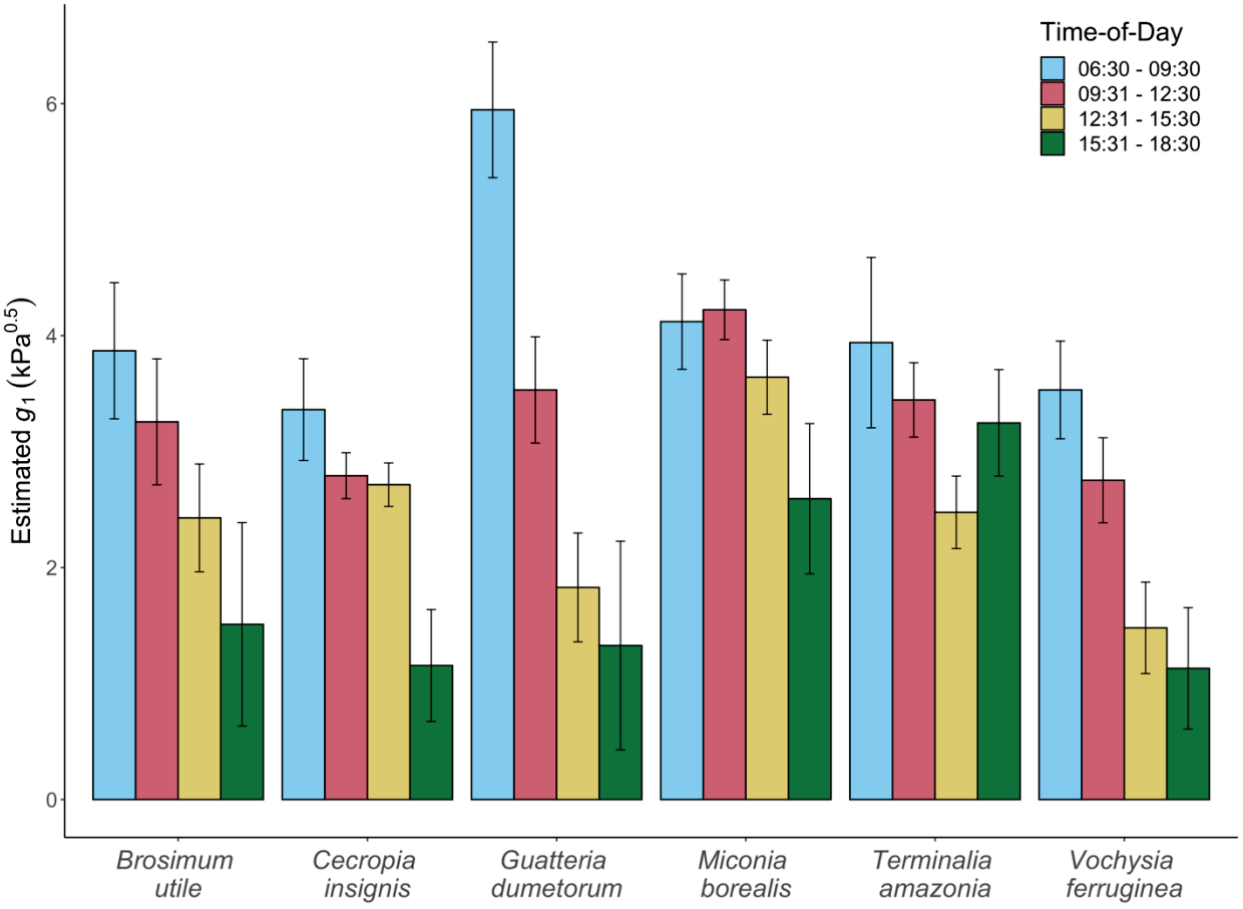

Figure 3.9: Trends in fitted values of g_1 by time-of-day and species. g_1 decreases significantly with increasing time-of-day for all six species investigated. *Brosimum utile*, *Cecropia insignis*, *Guatteria dumetorum*, and *Vochysia ferruginea*, all exhibit a very strong and consistent decline in g_1, whereas *Miconia borealis* and *Terminalia amazonia* exhibit a more moderate decline. Error bars represent ± 2 SE of the mean.

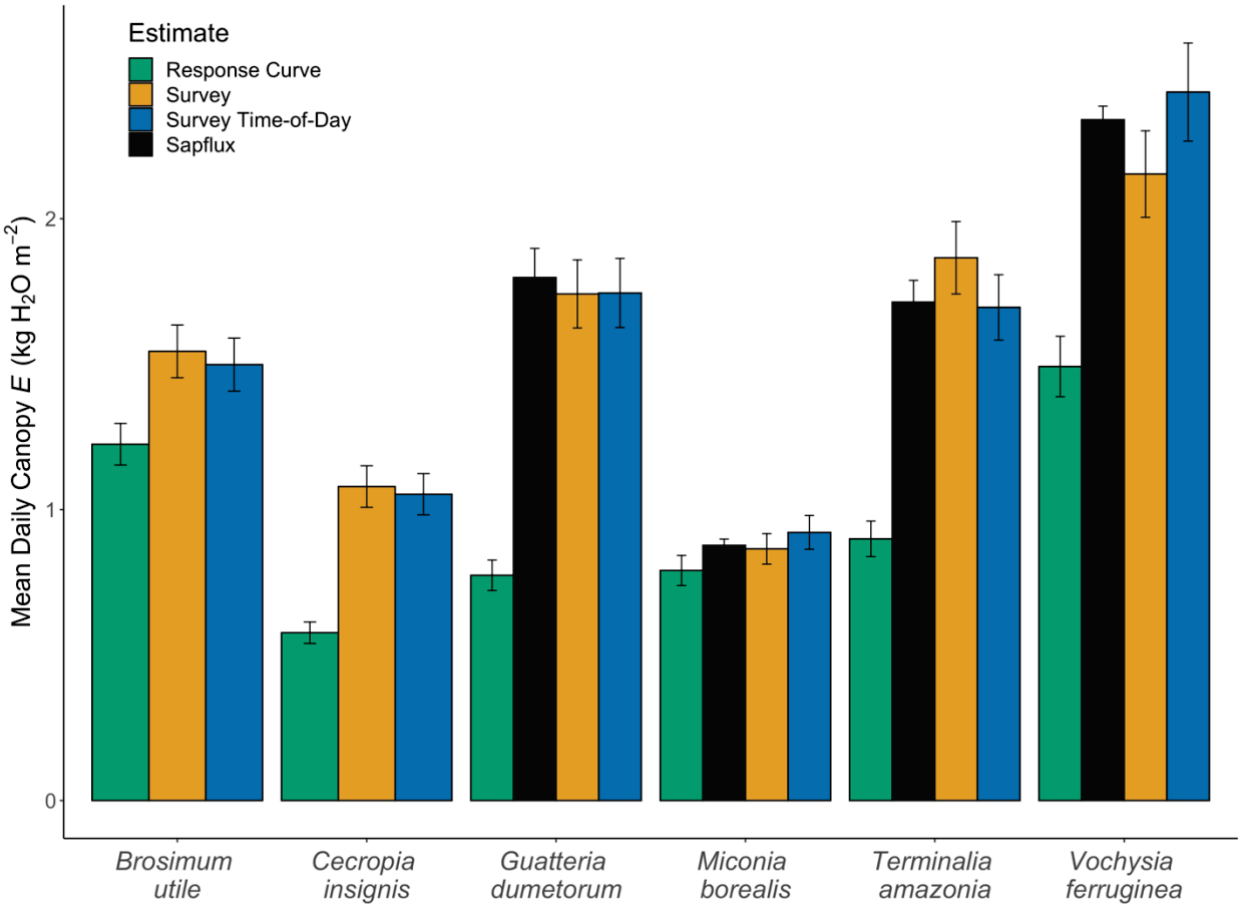

Figure 3.10: Comparison of estimated mean total daily *E* (kg H_2O m^{-2} ground area) using the three models (Note A2.1). Sapflux benchmark values are presented for four of the six species in this study. Mean values are the average integrated total of *E* over the 42 diurnal (05:30-18:30) periods of complete sapflux coverage. Error bars represent ± 2 SE of the mean.

3.7 – **Tables:**

Table 3.1: Values for species-specific photosynthetic and conductance parameters and canopy scaling factors used in simulations of leaf-level A and g_{sw}. For details regarding parameter estimates and tree functional traits, see section 'Canopy E simulations'. Data on leaf lifespan were previously reported in Osnas *et al*. (2018)

Species	$V_{cmax.25}$ (µmol m^{-2} s^{-1})	$J_{max.25}$ (µmol m^{-2} s^{-1})	$R_{dark.25}$ (µmol m^{-2} s^{-1})	g_1 ($kPa^{0.5}$)	g_0 (mol m^{-2} s^{-1})	DBH (cm)	LAI (m^2 m^{-2})	Crown Area (m^2)	Sapwood Area (m^2)	Successional Status	Leaf Lifespan (days)
***Brosimum utile* (Kunth) Oken**	Young: 68.84 Mature: 51.28 Old: 35.22	84.61 60.44 49.17	1.36 1.17 0.89	Response Curve: 2.40 Survey: 3.04	0.013 0.029	-	-	-	-	Late	324
***Cecropia insignis* Liebm.**	Young: 77.48 Mature: 78.70 Old: 60.50	109.48 108.48 89.33	1.50 1.81 1.68	Response Curve: 1.75 Survey: 2.87	0.031 0.107	-	-	-	-	Early	231
***Guatteria dumetorum* R. E. Fr.**	Young: 38.66 Mature: 48.18 Old: 35.79	65.71 67.53 64.71	1.24 0.82 0.97	Response Curve: 1.96 Survey: 3.32	0.028 0.067	59.0	1.5	155.7	0.210	Mid	212
***Miconia borealis* (Bonpl.) DC.**	Young: 64.59 Mature: 71.60 Old: 54.06	106.29 108.38 94.55	1.81 0.92 0.79	Response Curve: 2.20 Survey: 4.15	0.034 0.003	34.0	1.15	74.42	0.080	Mid	189
***Terminalia amazonia* (J.F. Gmel.) Exell**	Young: 70.28 Mature: 77.85 Old: 51.34	106.07 116.16 87.52	1.42 1.14 1.24	Response Curve: 0.78 Survey: 2.83	0.022 0.032	52.9	1.5	134.57	0.174	Mid	160
***Vochysia ferruginea* Mart.**	Young: 46.57 Mature: 57.46 Old: 43.66	76.14 78.47 78.62	1.67 1.18 0.78	Response Curve: 0.67 Survey: 2.57	0.036 0.040	58.0	2.0	153.24	0.204	Mid	215

Table 3.2: Fixed effects components from the mixed effects models tested.

Model[1]	Effect	Numerator df	Denominator df	F-value	p-value
Response Curve	g_0 ~ species	6	607	94.30	< 0.0001
	g_0 ~ stage	2	607	10.30	< 0.001
	g_0 ~ stage:species	10	607	3.13	< 0.001
	g_1 ~ species	6	607	110.67	< 0.001
	g_1 ~ stage	2	607	4.73	0.009
	g_1 ~ stage:species	10	607	5.31	< 0.001
Survey	g_0 ~ species	6	629	630.08	< 0.001
	g_0 ~ stage	2	629	25.61	< 0.001
	g_0 ~ stage:species	10	629	9.10	< 0.001
	g_1 ~ species	6	629	118.21	< 0.001
	g_1 ~ stage	2	629	0.08	0.922
	g_1 ~ stage:species	10	629	0.50	0.889
Survey + time-of-day	g_0 ~ species	6	623	764.05	< 0.001
	g_0 ~ stage	2	623	31.06	< 0.001
	g_0 ~ stage:species	10	623	11.04	< 0.001
	g_1 ~ species	6	623	143.35	< 0.001
	g_1 ~ time	3	623	124.29	< 0.001
	g_1 ~ time:species	18	623	8.11	< 0.001

[1]A full description of each model, and the random effects components are provided in Note A2.1.

Chapter 4: Seasonal trends in leaf-level photosynthetic capacity and water use efficiency in a North American Eastern deciduous forest and their impact on canopy-scale gas exchange

4.1– **Abstract:**

Vegetative transpiration (E) and photosynthetic carbon assimilation (A) are known to be seasonally dynamic, with changes in their ratio determining the marginal water-use efficiency (WUE). Despite an understanding that stomata play a mechanistic role in regulating WUE, it is still unclear how stomatal and non-stomatal processes influence changes in WUE over the course of the growing season. As a result, limited understanding of the primary physiological drivers of seasonal dynamics of canopy WUE remains one of the largest uncertainties in earth system model projections of carbon and water exchange in temperate deciduous forest ecosystems. Here I investigated seasonal patterns in leaf-level physiological, hydraulic, and anatomical properties, including the seasonal progress of the Universal Stomatal Optimization model stomatal slope parameter (g_1; inversely proportional to WUE) and the maximum carboxylation rate (V_{cmax}). I found that V_{cmax} and g_1 were seasonally variable, however their patterns were not temporally synchronized. g_1 generally showed an increasing trend until late in the season, while V_{cmax} peaked during the mid-summer months. Seasonal progression of V_{cmax} was primarily driven by changes in leaf structural, and anatomical characteristics, while seasonal changes in g_1 were most strongly related to changes in V_{cmax} and leaf hydraulics. Using a seasonally variable V_{cmax} and g_1 to parameterize a canopy scale gas exchange model increased seasonally aggregated A and E by 3% and 16% respectively.

4.2 – **Introduction:**

Vegetation regulates the exchanges of water vapor to the atmosphere via transpiration (*E*) and the uptake of carbon from the atmosphere via photosynthetic carbon assimilation (*A*), thus models which aim to predict carbon and water balance across space and through time must account for the temporal and spatial variation in *E* and *A* (Blyth *et al.*, 2021). Accounting for the seasonal variability associated with these processes is a major challenge for earth system models (ESMs) which often employ trait-based proxies to represent seasonal progression in potential for transpiration and assimilation (Rogers *et al.*, 2017c). However, these proxies may not fully capture the mechanisms underpinning the drivers of seasonal variation in *E* and *A*, nor do they accurately address how variation in *E* and *A* may co-vary over the course of a growing season. This critical knowledge gap hampers the predictive accuracy of ESMs and has been identified as an area for model improvement (Jefferson *et al.*, 2017).

ESMs represent *E* and *A* using a system of equations (e.g., Farquhar *et al.*, 1980) that link photosynthetic carbon gain (von Caemmerer & Farquhar, 1981) to water loss via stomata (Ball *et al.*, 1987; Medlyn *et al.*, 2011). The marginal variation of *A* and *E*, known as the water use efficiency ($\partial A/\partial E$, WUE), is represented in the unified stomatal optimization model (Medlyn *et al.*, 2011) as the inverse of the stomatal slope parameter (g_1, $kPa^{0.5}$). Thus, the relationship between *A* and stomatal conductance (g_{sw}) for a given set of environmental conditions is dictated by g_1, combined with the value of the stomatal intercept (g_0, mol m^2 s^{-1}, the expected g_{sw} when net assimilation [A_{net}] is zero). Among the parameters necessary to estimate *A* (Bernacchi *et al.*, 2013) are the maximum carboxylation rate of the enzyme Rubisco (V_{cmax}, μmol m^{-2} s^{-1}), and the rate of respiratory CO_2 release in the dark (R_{dark}, μmol m^{-2} s^{-1}). While accurate estimation of stomatal and photosynthetic parameters is essential to properly represent the role of vegetation in regulating net primary productivity (NPP) and transpiration across space and time, a general lack of paired foliar trait and physiology data (e.g., Wright *et al.*, 2004; Kattge *et al.*, 2011) across diverse plant functional types (PFTs) still hampers modeling efforts (Reich *et al.*, 2007). In particular, lack of process-based knowledge for representing PFT specific parametrization of stomatal traits, remains one of the largest uncertainties in current model predictions of the functioning of North American forests (Dietze *et al.*, 2014; Jefferson *et al.*, 2017; Ricciuto *et al.*, 2018).

Accounting for seasonal variability associated with photosynthetic and stomatal parameters is

an additional challenge when parameterizing models (Wilson *et al.*, 2000a, 2001; Xu & Baldocchi, 2003; Grassi *et al.*, 2005; Wang *et al.*, 2008; Ow *et al.*, 2010; Stokes *et al.*, 2010; Bauerle *et al.*, 2012; Way & Montgomery, 2015; Ali *et al.*, 2015; Chu *et al.*, 2018; Burnett *et al.*, 2021b). Given the lack of seasonal data, some modeling efforts use trait-based proxies to represent seasonal change in photosynthetic capacity (Rogers *et al.*, 2017c) such as seasonal trends in foliar nitrogen content or leaf mass per area (LMA) as a proxy for seasonal trends in V_{cmax} (Ellsworth & Reich, 1993; Medlyn *et al.*, 1999; Meir *et al.*, 2002; Misson *et al.*, 2006). These models, which use the principle of optimal allocation of nitrogen such that photosynthetic potential is maximized (Quebbeman & Ramirez, 2016), have recently been shown to be capable of explaining up to 83% of seasonal variation in V_{cmax} globally (Jiang *et al.*, 2020). However, trait-based relationships are known to vary considerably by PFT (Kattge *et al.*, 2009), or by the fraction of nitrogen allocated to Rubisco (Luo *et al.*, 2021). Other models prescribe a value for V_{cmax}, which can be modified seasonally in conjunction with bioclimatic factors such as growth temperature (Medvigy *et al.*, 2009), photoperiod (Bauerle *et al.*, 2012), or soil moisture (Wang *et al.*, 2022). In some cases (Ali *et al.*, 2015; Smith *et al.*, 2019) this latter method has been shown to be superior to trait-based approaches.

While there has been considerable effort dedicated to assessing mechanisms of seasonal variation in V_{cmax}, much less is known about the seasonal or ontogenetic patterns of leaf WUE, where the effects of season, drought, and phenology are often interrelated. Past work has mostly focused on drought effects (Sala & Tenhunen, 1996; Xu & Baldocchi, 2003; Grassi & Magnani, 2005; Héroult *et al.*, 2013; Sperlich *et al.*, 2016; Xie *et al.*, 2016), finding that seasonal increases in WUE are associated with progressive drought stress. In studies without a pronounced seasonal drought effect (Zhu *et al.*, 2011; Sanchez *et al.*, 2013; Miao *et al.*, 2021), WUE has been observed to decrease as leaves approached senescence, with a late season peak in stomatal slope. Further, models of foliar transpiration which account for leaf ontogeny suggest that cuticular leakage and incomplete stomatal closure contribute to elevated g_0 at the start and end of the growth season (Gee & Federer, 1972; Wardle & Short, 1983; Kane *et al.*, 2020). Recently, Jin *et al.*, (2022) demonstrated that phenology of leaf area index (LAI) can be used to improve seasonal characterization of canopy g_1 which, led to improved predictions of seasonal E. Additional work has linked stomatal traits with seasonal climatic conditions, such as growth season temperature

(Jin *et al.*, 2017) or photoperiod (Bauerle *et al.*, 2012). Evidence also suggests that moisture availability and atmospheric humidity may partially regulate WUE seasonality, explaining up to 35% of the global variation in g_1 (Lin *et al.*, 2015).

Despite some remaining uncertainties surrounding the seasonality of leaf physiology, variation in photosynthetic capacity associated with a seasonal scalar has been incorporated into a number of common ESMs (Krinner *et al.*, 2005; Medvigy *et al.*, 2009; Oleson *et al.*, 2013) and optimality schemes (Sabot *et al.*, 2022; Prikaziuk *et al.*, 2023) via a seasonal modification of the V_{cmax} parameter. Debate still remains, however, regarding the correct function used to represent this seasonal change (Medvigy *et al.*, 2013; Chen *et al.*, 2021; Mengoli *et al.*, 2022). Modification of V_{cmax} affects both rates of A and g_{sw}, and thus has the potential to indirectly alter WUE. However, aside from models which temporarily reduce g_0, g_1, or both in response to a soil moisture stress β_t-factor (De Kauwe *et al.*, 2013; Rogers *et al.*, 2017c; Li *et al.*, 2022), no ESMs, to my knowledge, directly alter WUE through a modification of stomatal parameters associated with leaf ontogeny or environmental conditions.

In this study, I measured the seasonal patterns of a suite of foliar parameters related to WUE (g_1 and g_0) and photosynthetic capacity scaled from measurement temperature to 25°C ($V_{cmax.25}$, and $R_{dark.25}$) in four tree species-groups (Table 4.1) that are common to the Northeastern United States and have high economic and ecological value. I collected data on foliar physiology and leaf traits every three weeks for the full 2021 growing season and used these data in a canopy-scale gas exchange model, based on the USO stomatal model and the FvCB photosynthesis model. I address four key research questions: (1) What are the seasonal patterns in foliar WUE and photosynthetic parameters? (2) What are the biotic and abiotic controls of foliar physiological trait development, and how do they relate to the anatomical, structural, and hydraulic changes associated with leaf ontogeny? (3) Does ontogeny modify the assumed linear relationships between photosynthetic parameters and leaf traits, and can these linear relationships be extended to stomatal parameters as well? (4) How does a model parameterization which explicitly considers seasonal dynamics of WUE and photosynthetic capacity impact the modeling of transpiration (E) and canopy carbon assimilation (A) compared with a model parameterization which holds WUE and photosynthetic capacity constant at the seasonal mean value?

4.3 – **Materials and Methods:**

Study site and species:

All data were collected at the Black Rock Forest (BRF), a 1550 ha protected, secondary growth forest located in the Hudson Highlands Region of New York (Fig. 4.1a). The site has a humid, sub-tropical climate, receiving an average of 1.2 m of precipitation per growth season, and with a mean growth season temperature of 23.4°C (Turnbull *et al.*, 2001; Schuster *et al.*, 2008; Fig. 4.2). I collected data from three sites within the forest, each with similar soil and species composition (Fig. 4.1a). The forest is dominated by deciduous species, with a composition of ~67% oaks, ~31% non-oak deciduous hardwoods, and ~2% conifers (Schuster *et al.*, 2008; Falxa-Raymond *et al.*, 2012), with a mean LAI of 4.59 ± 0.12 m^2 m^{-2}, measured in July using an LAI-2200 (LI-COR Inc., Lincoln, NE, USA). Roughly every three weeks between May 17 and October 15, 2021, I collected data on six deciduous hardwood species, which I aggregated into four groups (hereafter "groups") based on functional type (see Table 4.1 for details). During each sample collection, I targeted the most fully expanded and physiologically mature leaf on each sampled branch with the aim of measuring the same cohort of leaves over the course of a growing season.

Branches were collected via shotgun sampling (Serbin *et al.*, 2014b; Burnett *et al.*, 2021b), using a 12-gauge shotgun and steel bird shot (Fig. 4.1b). All branch sampling occurred between nautical twilight and sunrise. Once branches fell, they were immediately recut under water to prevent cavitation or embolism of the xylem. After an initial 20 cm cut was made, multiple smaller cuts (5-15 cm) were made to progressively ease xylem tension (Sperry, 2013). After processing, all branch segments measured between 100 and 200 cm.

Gas exchange:

Gas exchange measurements were conducted in the laboratory using three LI-6800 and two LI-6400XT portable photosynthesis systems (LI-COR Inc., Lincoln, NE, USA). For all measurements, the color spectrum of the irradiance was the same (90% red, 10% blue). I conducted stomatal response curves to estimate stomatal and photosynthetic parameters (Ball *et al.*, 1987; Leakey *et al.*, 2006; Davidson *et al.*, 2022). With this method, irradiance is adjusted to propagate changes in A, while maintaining a constant level of sample CO_2 concentration (C_a) and VPD_{leaf} within each response curve (Fig. 4.1c). Using previously published data on the response of A to irradiance for the study species (Dreyer *et al.*, 2001), I estimated the full range of irradiance,

ranging from light-saturated photosynthesis (A_{sat}), to respiratory CO_2 release in the dark (R_{dark}). All measurements were made at a leaf temperature of 24-27ºC, and with VPD_{leaf} between 0.8 and 1.4 kPa. On average, T_{leaf} was 26.25ºC and VPD_{leaf} was 1.07 kPa. Data were automatically logged every 10 seconds for the duration of measurements. After a 1-hour acclimation and stabilization period at the first irradiance level, light was reduced to the next lowest irradiance level, and leaves were allowed to acclimate to this new irradiance level for a minimum of 20 minutes until rates of A and g_{sw} reached a steady state. This process was repeated until measurements at all 11 irradiance levels had been completed. For each irradiance level, an average of the 5 log points prior to a change in irradiance represented each measurement point.

After gas exchange measurements were taken, I used a cork borer to obtain leaf discs of a known area, and measured leaf disc fresh mass. These discs were then dried to a constant mass in a 60ºC oven and weighed to obtain dry mass. I then estimated LMA (dry mass/leaf area) and leaf dry matter content (LDMC; dry mass/fresh mass). Finally, a subset of the dried leaf samples were ground, and elemental nitrogen and carbon was quantified using a 2400 Series II CHN analyzer (PerkinElmer, Waltham, MA, USA) to estimate nitrogen as expressed on an area and mass basis (N_{area}, N_{mass}).

Leaf hydraulics:

In addition to gas exchange, I measured a suite of leaf-level hydraulic properties on all collected branches to determine how changes in leaf hydraulics related to other physiological changes associated with leaf ontogeny. Once each branch was collected, a leaf was immediately removed at the base of the petiole, and sealed in an airtight, humid, cool, dark box for transport to the laboratory. Leaf water potential (Ψ_{leaf}) was measured with a Scholander type pressure chamber (Scholander *et al.*, 1964). This measurement of predawn Ψ_{leaf} served as a quantitative assessment of branch hydraulic stress, and enabled prescreening of branches prior to other measurements (Rodriguez-Dominguez *et al.*, 2022).

I also performed pressure-volume (PV) curves on one leaf from each branch following the method of Bartlett *et al.*, (2012). Branches were rehydrated for a period of 1.5 hours prior to analysis. Using a razor, leaf samples were removed from the rehydrated branches and Ψ_{leaf} and sample mass were recorded. Samples were then allowed to dry for 10 hours, with Ψ_{leaf} and sample

mass recorded 8-12 times during this period. After this, samples were dried to constant mass in a 60ºC oven, and a dry mass value was recorded. I assessed the relationship between the water potential and relative water content using the R package 'pvldcurve' (v 1.2.6; Raesch, 2020) to determine the turgor loss point (Ψ_{TLP}), relative water deficit at the turgor loss point (RWD_{TLP}, %), and the bulk elastic modulus (ε).

Stomatal anatomy:

Using a thin layer of clear coat nail varnish, I obtained impressions of the abaxial side of two leaves per branch sample. Images of these impressions were captured using a stage microscope with a digital camera attachment (Nikon ECLIPSE Ci/Ni, Tokyo, Japan) at 400x magnification. Using these images, I estimated stomatal density (number of stomata per mm^2) and stomatal area, (length x width of the guard cells), averaging these measurements by group for each month.

Estimation of gas exchange parameters:

The stomatal parameters g_1 and g_0 were estimated using the Unified Stomatal Optimization model (USO, Medlyn *et al.*, 2011, Equation 4.1).

Equation 4.1. $$g_{\mathrm{sw}} = g_0 + 1.6\left(1 + \frac{g_1}{\sqrt{VPD_{\mathrm{leaf}}}}\right)\frac{A}{C_a}$$

where g_0 represents the expected g_{sw} when A_n=0, C_a and VPD_{leaf} are the leaf surface CO_2 concentration and vapor pressure deficit respectively, and g_1 is a slope parameter inversely proportional to WUE ($\partial E/\partial A$).

I estimated V_{cmax} for each leaf using the "one-point method" (De Kauwe *et al.*, 2016, Equation 4.2), where I allowed time for full acclimation to the light environment. This approach has shown comparable results to traditional AC_i curves in other eastern deciduous species (Burnett *et al.*, 2019):

Equation 4.2. $$V_{cmax} = \frac{A_{sat}}{\left(\frac{C_i - \Gamma^*}{C_i + K_m} - 0.015\right)}$$

where K_m is the Michaelis–Menten constant (404.9 μmol mol^{-1}; Table A3.1; Bernacchi *et al.*, 2001), Γ* is the CO_2 compensation point in the absence of mitochondrial respiration (42.75 μmol mol^{-1}; Table A3.1; Bernacchi *et al.*, 2001), and C_i is the intercellular CO_2 concentration.

I used the initial acclimated, steady state, light-saturated point of each stomatal response curve for my measurement of A_{sat} and its corresponding C_i. To scale V_{cmax} at measurement temperature to V_{cmax} at 25°C ($V_{cmax.25}$), I used a modified Arrhenius equation (Leuning, 2002, Equation 4.3) with kinetic constants specific to each group (Table A3.1; Dreyer *et al.*, 2001):

Equation 4.3. $$V_{cmax.25} = \frac{V_{cmax.T}}{C*\exp\left[\left(\frac{H_a}{RT_{25}}\right)*\left(\frac{1-T_{25}}{T_{leaf}}\right)\right]*1+\exp\left[\frac{(S_V T_{leaf}-H_d)}{RT_{leaf}}\right]}$$

where $V_{cmax.25}$ is the value of V_{cmax} at the reference temperature (T_{25} = 298.15 K), $V_{cmax.T}$ is the value of V_{cmax} at the leaf temperature (T_{leaf} in K), H_a, H_d, and S_v are the activation and deactivation energies of the enzyme Rubisco and an entropy term (J mol^{-1}; J mol^{-1}; J mol^{-1} K^{-1}), R is the ideal gas constant (R = 8.314 J mol^{-1} K^{-1}), and C is a combined term equivalent to 1 + exp[($S_v T_{25}$ − H_d)/(RT_{25})].

Finally, R_{dark} was calculated from dark-adapted measurements of A (the final stomatal response curve point) and was scaled to 25°C ($R_{dark.25}$) using an inverse Arrhenius equation (Equation 4.4; Bernacchi *et al.*, 2001; Von Caemmerer, 2013):

Equation 4.4. $$R_{dark.25} = \frac{R_{dark}}{\exp\left(\frac{H_a}{(R*T_{25})} - \frac{H_a}{(R*T_{leaf})}\right)}$$

where H_a is the group-specific activation energy of mitochondrial respiration (Table A3.1; J mol^{-1}).

<u>Canopy assimilation and transpiration simulations:</u>

To assess how seasonality in photosynthetic and stomatal parameters may impact simulated rates of canopy E and A, I used the function 'f.GPPT' included in the R package 'LeafGasExchange' (v 1.0.1; Lamour & Serbin, 2021) which combines a coupled leaf-scale steady

state assimilation (Farquhar *et al.*, 1980), conductance (Medlyn *et al.*, 2011), and energy balance model (Muir, 2019b). The scaling of gas exchange from the leaf to the canopy is made using the Norman (1979) radiation model as implemented by Bonan (2019) to partition incoming radiation into direct and diffuse streams for each of 10 canopy layers. The gas exchange of the sun and shade leaves is then aggregated for each layer to calculate the canopy scale A and E. Details regarding model parameters and equations used can be found in Lamour *et al.*, (2023).

I ran the model at 1-hour time increments from May 15 to October 15, 2021, using local meteorological data (Fig. 4.2). For all simulations I modeled the canopy as being made up of ten layers (Béland & Baldocchi, 2021), having a non-uniform, top weighted distribution of LAI between layers (Bonan, 2015). LAI for each layer was scaled from the measured peak-season average (4.59 m^2 m^{-2}).

I ran two different versions of the model, one in which values of $V_{cmax.25}$, $R_{dark.25}$, g_0, and g_1 were consistent across the season, corresponding to the group average values (hereafter fixed model; Table 4.1), and a second model where values of $V_{cmax.25}$, $R_{dark.25}$, g_0, and g_1 were both month- and group-specific (hereafter variable model; Table A3.2). Other photosynthetic constants used in the model of photosynthesis (Farquhar *et al.*, 1980) can be found in Table A3.1. I investigated modeled results at a monthly interval, and across the full season to compare the effect that model choice had on estimation of E and NPP.

Stomatal limitation of assimilation:

To estimate stomatal limitation on canopy assimilation I reran the variable model, removing the effect of stomata by setting g_1 to infinity. This means that g_{sw} is unbounded from A, so for all rates of A, C_i is not a limiting factor. The resulting assimilation ($A_{\text{infinite}g_{sw}}$) can be compared to the variable model estimate for assimilation (A_{observed}) to calculate stomatal limitation on net photosynthesis (I; Equation 4.5; Farquhar & Sharkey, 1982; Long & Bernacchi, 2003; Slot & Winter, 2017).

Equation 4.5. $$I = 1 - \frac{A_{\text{observed}}}{A_{\text{infinite}g_{sw}}}$$

Here a value of $I = 0$ represents no stomatal limitation on A (where $C_i = C_a$) while a value of $I = 1$

represents complete stomatal limitation on A.

Statistical analysis:

To compare how estimates of $V_{cmax.25}$, $R_{dark.25}$, g_0, and g_1 varied across successive months I used mixed effects models constructed and analyzed in the R package 'nlme' (v 3.1; Pinheiro *et al.*, 2020). In total I had 2,681 observations of A and g_{sw}, collected from 240 individual leaves. For $V_{cmax.25}$, and $R_{dark.25}$, sampling site acted as the random effect, while for g_0, and g_1, which are both estimated from multiple non-independent observations per leaf, both individual leaf and sampling site served as the random effect. For all data I considered the species-group and month of observation as fixed effects. I plotted the residual error relative to the group mean as a means of verifying that the two species in the maple and white oak groups were physiologically similar (Fig. A3.1).

I next used linear models to assess the assumed relationships between leaf-level traits (N_{area}, LMA, LDMC, stomatal density, RWD_{TLP}) and the leaf-level physiological parameters $V_{cmax.25}$, $R_{dark.25}$, g_0, and g_1. I also investigated if linear relationships existed between different combinations of physiological parameters (e.g., a relationship between g_1 and $V_{cmax.25}$). I next used Spearman's Rank Correlation tests to investigate the relationships between monthly average meteorological variables and physiological parameters. To account for the increased probability of Type I error associated with multiple comparisons of the same parameter (12 comparisons per parameter), I applied a Bonferroni correction to adjust the α required to establish significance from the nominal value of 0.05 to 0.004 for both the linear models and the correlation tests. All analysis was performed using the R open-source software environment (v 3.6.2, R Core Team, 2013).

4.4 – **Results:**

Seasonal patterns of leaf physiological parameters:

I observed significant seasonal and group effects for all four parameters (Table 4.1 and A3.2). For most groups, $V_{cmax.25}$ exhibited a significant ($p < 0.05$) mid-season peak rising to the highest rate in July before declining later in the season (Fig. 4.3a). The one exception to this pattern was maple, which displayed rates of $V_{cmax.25}$ that remained fairly constant through the season with no significant differences among months.

$R_{dark.25}$ showed a contrasting seasonal pattern to that of $V_{cmax.25}$ with high values at the beginning of the season and reaching a mid-season minimum in either July (white oak) or August, before recovering to approximately half of the early season values by October (Fig. 4.3b). All four groups showed significant ($p < 0.001$) overall variation, with a significant decrease in estimated rates of $R_{dark.25}$ between May and the mid-summer minimum in all four groups. The proportion of $R_{dark.25}$ to $V_{cmax.25}$ also varied considerably across the season, with the ratio reaching its maximum in either August or September for all groups (Fig. A3.2g).

Similar to $R_{dark.25}$, g_0 values for all four groups began the season at a peak before declining between June and September (Fig. 4.3d). This decline was significant ($p < 0.05$) for all four groups, however birch remained variable between 0.88 and 1.88 μmol m^{-2} s^{-1}. For maple, there was a significant ($p < 0.05$) recovery of g_0 between August and October, as rates returned to approximately 60% of their May values.

The g_1 for oak and maple increased significantly ($p < 0.001$) from an early season low to a peak in October (Fig. 4.3c). This pattern was most pronounced in red oak, which experienced a near tripling of g_1 (1.19 to 3.32 $kPa^{0.5}$) between June and October. Birch g_1 increased significantly ($p < 0.05$) between May and June, however, unlike the other groups, the g_1 value remained relatively constant for the remainder of the season.

Overall, when leaf gas exchange parameters were averaged over the full growing season, there was significant ($p < 0.001$) variation among groups for some traits (Table 4.1). $V_{cmax.25}$ was relatively consistent between groups, except for red oak which had a non-statistically significant 40% higher rate. Birch and maple both exhibited significantly lower leaf respiration than the oaks. For the g_1 parameter, the species-groups clustered into three groupings, with white oak and maple having significantly lower g_1 (higher WUE) than birch and red oak. Finally, birch differed from the other three groups, with a rate of g_0 nearly three times higher than the other groups.

In general, among-leaf variation for each given group was fairly consistent across successive months (Fig. 4.3). For the oak groups, $V_{cmax.25}$ varied the most among months, with a peak in July (Fig. 4.3a), while white oak displayed significant among leaf variation in $R_{dark.25}$ in May and June (Fig. 4.3b). Among-leaf variation in g_1 and g_0 was comparable across all six months of study, however birch exhibited substantially more leaf-to-leaf variation in g_0 than the other three groups (Fig. 4.3d).

Trait-trait and trait-environment relationships:

Next, I examined the linear relationships between a suite of functional, structural, anatomical, and hydraulic leaf traits which are assumed to explain some of the variation observed in the physiological parameters ($V_{cmax.25}$, $R_{dark.25}$, g_1, g_0). I found a significant, yet weak (R^2 = 0.23) positive relationship between N_{area} and $V_{cmax.25}$ (Fig. 4.4a), and a slightly weaker (R^2 = 0.18) negative relationship between LMA and $V_{cmax.25}$ (Fig. 4.4c). The observed month-to-month variation in $R_{dark.25}$ was best explained by stomatal density (R^2 = 0.45; Fig. 4.4b) and LDMC (R^2 = 0.44; Fig. 4.4d), however these relationships are primarily influenced by early-season measurements on immature leaves when $R_{dark.25}$ was at its seasonal maximum. Neither the variation in $V_{cmax.25}$ nor $R_{dark.25}$ could be statistically explained by any of the hydraulic parameters tested.

Variation in stomatal parameters was less well explained by variation in traits with the only significant ($p < 0.004$) relationship observed between g_0 and the relative water deficit at turgor loss point (R^2=0.71, Fig 4.5a). However, I found that variation in both $R_{dark.25}$ (R^2=0.60, Fig 4.5d) and $V_{cmax.25}$ (R^2=0.85, Fig 4.5b) explained some of the variation in g_1. In addition, g_0 was also linearly related to $R_{dark.25}$ (R^2=0.67, Fig 4.5c). Seasonal variation in g_0 and g_1 could not be explained by Ψ_{TLP} or ε derived from PV curves.

Finally, I analyzed the relationships between the physiological parameters and five ambient environmental variables averaged by month: mean daytime (sunrise to sunset) irradiance, mean daytime temperature, mean daytime VPD, mean total 24-hour precipitation, and mean 24-hour soil moisture content (SMC) (Fig. 4.6). Mean daytime temperature best explained variability in parameter estimates, with a positive relationship with $V_{cmax.25}$ (ρ = 0.45; Fig. 4.6e), and negative relationship with $R_{dark.25}$ (ρ = -0.57; Fig. 4.6f) and g_0 (ρ = -0.65; Fig. 4.6h). Mean daily irradiance also helped explain monthly variability in $R_{dark.25}$ (ρ = 0.50; Fig. 4.6b) and had a negative relationship with g_0 (ρ = -0.49; Fig. 4.6c). VPD, precipitation, and SMC were not significantly correlated with any of the four physiological parameters (Fig. 4.6i-t), however there was a general positive relationship between SMC, g_0, and $R_{dark.25}$.

Model results:

The simulation of canopy E using a variable model parameterization (Fig. 4.7) resulted in a 63.4% higher rate of E in May compared to the fixed model, owing to the comparably poorer

stomatal control of early season leaves (higher g_0 and lower g_1; Fig. 4.3c-d), compared with the full season average values of g_0 and g_1. Conversely, toward the middle and end of the growing season (August-September), rates of canopy E were 46.7 and 34% higher respectively for the model which used fixed photosynthetic and stomatal parameters. Much of this variation is driven by the variable model having rates of $V_{cmax.25}$ that declined significantly and rates of $R_{dark.25}$ that increased significantly after the mid-season growth peak in July (Fig. 4.3a-b, A3.2g), while for the fixed model, $V_{cmax.25}$ and $R_{dark.25}$ were constant over the entire simulation period.

In my simulation of canopy A, I observed a similar effect to that of E, with the variable model predicting 53.7% lower mean canopy A in May (Fig. 4.8). This reduced rate of A in the variable model is the result of the significantly lower than average rate of $V_{cmax.25}$ and higher than average rate of $R_{dark.25}$ in May (Fig. 4.3a-b). The shape of the seasonal response was also different between the two models, with the variable model capturing a midseason peak in net assimilation while the fixed model predicted a progressive decline in net assimilation from the first two months to the end of the growth season (Fig. 4.8). Interestingly, this decline in the fixed model appeared to be driven solely by climatic factors such as ambient temperature and irradiance level, rather than a biotic or physiological process (Fig. 4.2).

When the two models are compared over the full 2021 growth season, accounting for the relative abundance of each group, it was possible to estimate total net assimilation and transpiration per unit ground area. The fixed parameter model estimates a five-month total of 88.68 kg H_2O released and 1.67 kg CO_2 assimilated per meter of ground. The variable parameter model estimates a five-month total of 103.05 kg H_2O released and 1.73 kg CO_2 assimilated per meter of ground, values that are 16% and 3% higher respectively than the fixed model.

Finally, I can examine the degree to which g_{sw} limits A during model simulations (Table 4.2). A was most limited by g_{sw} in red oak (46.3% of observations), followed by maple (37.7%), white oak (25.4%), and birch (19.6%), and was most limited in July (56.6%) and least in October (2.7%). Stomatal limitation occurs more frequently in the afternoon than in the morning, with the highest average I calculated between 14:00-15:00 (Fig. A3.3). All four groups appear to have equal diurnal distributions of I. Stomatal limitation is associated with periods of higher irradiance, VPD, and air temperature (Fig. A4.4) in all four groups, however the strength of the association varies among groups. When I compare seasonal assimilation between the model with and without stomatal

limitation, I find that on average, stomata limit potential assimilation by 10-20% (Fig. 4.9).

4.5 – **Discussion:**

I investigated the seasonal patterns of four physiological parameters, essential for accurate modeling of vegetation-atmosphere interactions and which are known or assumed to vary with leaf phenology. I sought to explore the biotic and abiotic factors associated with seasonal trends in physiological parameters, and consider the effects that a time-varying parametrization would have on models of canopy E and A. My results reveal a mid-growth season peak in $V_{cmax.25}$ for all four groups investigated, which coincides closely with the seasonal minimum in dark respiration rate (Fig. 4.3a-b), while g_1 progressively decreased over the season in three of the four groups (Fig. 4.3c). Photosynthetic parameters closely track seasonal trends in leaf structural, nutritional, and anatomical characteristics (Fig. 4.4), while stomatal parameters are correlated most strongly with changes in the $V_{cmax.25}$ and the relative water deficit at the point of turgor loss (Fig. 4.5). Further, the lack of coordination between $V_{cmax.25}$ and maximum stomatal conductance (g_{sw}max) as evidenced by dynamic stomatal limitation across leaf phenology (Table 4.2), suggest that the seasonal dynamics of WUE observed here are the result of variable stomatal behavior, rather than a passive stomatal response to changes in assimilation potential. The simulations indicate that there is a clear need for models to more explicitly account for seasonality in both photosynthetic and stomatal parameters for temperate broadleaf deciduous forest species (Fig. 4.7-4.8). I show that over the full 2021 season, the model with a time-varying parametrization results in a 16% higher cumulative E and a 3% higher cumulative A (Fig. 4.9) with differences most pronounced in the shoulder seasons (e.g., spring leaf flush), which are expected to be strongly impacted by climate change.

Seasonal variability and ontogenetic controls of photosynthetic capacity:

The photosynthetic parameters $V_{cmax.25}$ and $R_{dark.25}$ displayed a strong seasonality across the 2021 growth season for all four groups studied (Fig. 4.3ab). This is comparable to other studies in eastern deciduous forests (Wehr *et al.*, 2016; Yang *et al.*, 2020), where $V_{cmax.25}$ followed a peaked response, with a peak slightly after the summer solstice (Fig. 4.2a, 4.3a) at the period of full leaf expansion. While the seasonal maximum in $V_{cmax.25}$ did not correspond with the maximum day length or maximum daily irradiance (Fig. 4.2a) as has been demonstrated previously (Wilson *et*

al., 2000a, 2001; Grassi *et al.*, 2005; Bauerle *et al.*, 2012), it did correspond to the period of highest daytime air temperature and VPD (Fig. 4.2b-c). This is a similar seasonal pattern observed in previous studies of temperate ecosystems (Medvigy *et al.*, 2013; Luo *et al.*, 2021) in which daytime air temperature was the strongest determinant of ecosystem productivity and photosynthetic capacity. Consistent precipitation and SMC over the growth season (Fig. 4.2d-e) may also contribute to the lack of a seasonal decline in $V_{cmax.25}$ as has been observed in studies of drought-prone ecosystems (Bauerle *et al.*, 2012; Zhou *et al.*, 2014; Granda *et al.*, 2020; Gourlez de la Motte *et al.*, 2020). Of the five meteorological variables investigated here, mean daytime air temperature best explained seasonal progression of $V_{cmax.25}$ and $R_{dark.25}$ (Fig. 4.6e-f). This tight coupling between $V_{cmax.25}$ and $R_{dark.25}$ is expected given that the enzyme Rubisco constitutes a considerable proportion of total foliar protein (Atkin *et al.*, 2000; Cannell, 2000; Amthor, 2000; O'Leary *et al.*, 2019), and recently both $V_{cmax.25}$ and $R_{dark.25}$ were shown to acclimate in unison to changes in growth temperature (Wang *et al.*, 2020a). However, here I observed a ratio of $R_{dark.25}$ to $V_{cmax.25}$ which is seasonally dynamic (Fig. A3.2g), calling into question the long-held model assumption that $R_{dark.25}$ should be ~1.5% of $V_{cmax.25}$ (Collatz *et al.*, 1991).

In addition to abiotic conditions, several biotic traits also showed a significant correlation with photosynthetic capacity. This included a linear relationship between both N_{area} and LMA and $V_{cmax.25}$ (Fig. 4.3ac). Like $V_{cmax.25}$, N_{area} peaked in the middle of the summer (Fig. A3.2d), which is unsurprising given the often observed linear relationship between foliar nitrogen content and $V_{cmax.25}$ (Ellsworth & Reich, 1993; Misson *et al.*, 2006; Rogers, 2014; Evans & Clarke, 2019). LMA increased rapidly from May to June and continued to increase to a maximum value at the end of the season, just prior to senescence (Fig. A3.2a), in agreement with previous literature suggesting a strong positive relationship between seasonal phenology and LMA (Grassi *et al.*, 2005; Wright *et al.*, 2006; Hikosaka *et al.*, 2007), and also observed in similar deciduous forests located in the northeastern United States (Yang *et al.*, 2016). This linear relationship between $V_{cmax.25}$, N_{area}, and LMA suggests that not only are these relationships robust across leaf ontogeny, but also that nitrogen use efficiency is constant across the growth season (Wilson *et al.*, 2001).

I also observed a positive linear relationship between stomatal density and $R_{dark.25}$ (Fig. 4.4b), with both traits reaching seasonal minimums in mid-summer, after full leaf expansion. Interestingly however, I found no significant relationship between stomatal density and g_1, g_0, or

g_{sw}max, all three of which have been extensively documented in previous among-species studies of natural vegetation and cultivated crops (Franks & Beerling, 2009; Franks *et al.*, 2009; Bertolino *et al.*, 2019; Machado *et al.*, 2021). The lack of a within-species link between stomatal density and stomatal parameters, along with the relationship between stomatal density and $R_{dark.25}$ suggests that these changes, while both associated with leaf ontogeny, themselves may not be causally linked. Finally, I observed a negative relationship between $R_{dark.25}$ and LDMC (Fig. 4.4d), a relationship widely reported in studies of the global leaf economic spectrum (LES; Wright *et al.*, 2004; Reich, 2014).

Seasonal variability and ontogenetic controls of stomatal behavior:

In this study, I found that *I*, which is associated with higher air temperatures and VPD (Fig. A3.3i-l), is highest in the middle of the season, declining as leaves senesce (Table 4.2). Likewise, I observed a seasonal decline in foliar WUE (increasing g_1, Fig. 4.3c) in three of four groups. Several previous studies of other deciduous species (e.g., Wilson *et al.*, 2000b; Xu & Baldocchi, 2003; Grassi & Magnani, 2005) have observed contrasting trends, such as increasing *I* and decreasing or stable WUE throughout the season. However, the three above studies occurred in warm climates, with a pronounced seasonal drought effect, and in one case (Xu & Baldocchi, 2003) focused on a drought-adapted species, a strong contrast with the seasonally cold and wet conditions present at BRF (Fig. 4.2). The presence of a seasonal decline in WUE is not without some established support. In similar forests to BRF, both Sang *et al.*, (2011) and Burnett *et al.*, (2021) observed a seasonal decline in WUE, with an early season maximum and late season minimum. The seasonal shifts in WUE observed here may be driven by ontogenetic processes, such as a seasonal shift from conservative stomatal behavior to protect new vegetation (Gimeno *et al.*, 2019) toward more profligate behavior to maximize carbon assimilation prior to leaf senescence (Brodribb & Holbrook, 2003; Sanchez *et al.*, 2013; Burnett *et al.*, 2021b).

Previous studies (De Kauwe *et al.*, 2015a; Duursma *et al.*, 2019) have called into question the biophysical interpretation of the g_0 parameter, suggesting that depending upon the method used to derive it, it may represent error in fitting rather than an actual biological trait. However, in this study I measure the full response of stomatal conductance to changes in irradiance above and below the light compensation point (Fig. 4.1d), which enables us to observe actual daytime rates

of g_{sw} at and around g_0. While g_0 is not predicted by optimality theory (Cowan & Fraquhar, 1977) g_0 nonetheless represents a true biophysical parameter with a mechanism similar to minimum conductance, the lower bound of the possible range of g_{sw} (Duursma *et al.*, 2019). The g_0 measured in this study can be interpreted as a mechanistic parameter representing water loss both from the cuticular pathway (Márquez *et al.*, 2021, 2022), and from incomplete stomatal closure (Machado *et al.*, 2021) when A_n is zero. Thus, seasonal changes in g_0 reflect seasonal changes in the rate of water loss from the leaf during conditions when photosynthesis is no longer leading to net carbon gain.

Leaf ontogenetic changes may influence the patterns of g_0 I observed, and which have been observed in other studies of oak species (Granda *et al.*, 2020). During the first measurement period, all four groups had a markedly higher g_0 (up to 8x) than their respective mid-season average. Recent evidence from a study of red oaks suggests that the majority of this early season foliar water loss comes from cuticular leakage in immature leaves, rather than lack of stomatal control (Kane *et al.*, 2020). The small uptick in g_0 observed in October may be the result of the onset of leaf senescence, which has long been associated with a decrease in stomatal control (Gee & Federer, 1972; Wardle & Short, 1983).

The seasonal patterns of g_1 and g_0 observed in this study may be partially explained by the seasonal progression of climate factors (Fig. 4.2). In all four groups, g_1 declined linearly as a function of mean daytime irradiance (Fig. 4.6c), while g_0 declined with increasing mean daytime air temperature (Fig. 4.6h). Interestingly, monthly trends of VPD and precipitation were not significantly correlated with either g_1 or g_0, while monthly SMC showed a weak, yet non-significant, positive association with g_0 (Fig. 4.6t). This latter finding however, may have more to do with the mesic conditions at the start and end of the growing season when g_0 was higher. The overall trends in g_0 and g_1 I observed run in contrast to predictions of hydraulic theory (Martínez-Vilalta & Garcia-Forner, 2017; Anderegg, 2018), which suggests that periods of drought and high VPD, especially toward leaf senescence (Pantin *et al.*, 2012) should reduce Ψ_{leaf}, and thus reduce g_1 and g_0. However, during the study VPD, precipitation, and SMC remained relatively consistent across the season (i.e., no major periods of drought), and do not appear to have an impact on predawn Ψ_{leaf} (Fig. A3.5b). I did observe a positive relationship between g_0 and the relative water deficit at the turgor loss point (RWD_{TLP}, Fig. 4.5a), suggesting a potential water stress mitigation

strategy, as leaves which lose more water at or below net-zero assimilation require more relative water loss before losing turgidity. Seasonal patterns of RWD_{TLP} follow the same pattern as predawn Ψ_{leaf} (Fig. A3.5), reinforcing the adaptive role stomata play in buffering against the risk of hydraulic damage (Bartlett *et al.*, 2016).

Monthly mean g_1 and g_0 also exhibited linear relationships with photosynthetic parameters (Fig. 4.5bd). Most notably, g_1 was positively associated with $V_{cmax.25}$, and negatively associated with $R_{dark.25}$. It has long been assumed that a tight coordination between rates of A and g_{sw} results in a fixed ratio of C_i:C_a, even as photosynthetic capacity changes (Wong *et al.*, 1979, 1985; McDowell *et al.*, 2006), as although $V_{cmax.25}$ may shift with leaf phenology, the rate of g_{sw} will change in proportion to supply and maintain a stable level of intercellular CO_2 (Long & Hällgren, 1993). These changes also have the effect of reducing the potential for g_{sw} to limit A (Drake *et al.*, 2017). If present, a coordination between $V_{cmax.25}$ and $g_{sw\max}$ would result in stable g_1 and I across leaf phenology, however these data, and that of a similar study (Burnett *et al.*, 2021b) do not support such a coordination. This suggests that the seasonal dynamics of WUE observed here are the result of dynamic stomatal behavior, rather than a passive stomatal response to changes in assimilation potential.

Implications for land-surface modeling:

Applying my findings of the seasonality in $V_{cmax.25}$, $R_{dark.25}$, g_1, and g_0 significantly altered model output for both E and A (Figs. 4.7-4.8), consistent with other studies that considered the effect of seasonality in models (Wang *et al.*, 2004; Bauerle *et al.*, 2012; Medvigy *et al.*, 2013; Burnett *et al.*, 2021b). My model parameterization differs somewhat from other studies, both in how I chose to apply seasonality, and the values I used for my fixed model. Both Bonan *et al.*, (2011) and Burnett *et al.*, (2021) use a maximum or solstice value for $V_{cmax.25}$ in their model without seasonality, which results in a seasonal model with a value of $V_{cmax.25}$ which is always less than or equal to the non-seasonal model. Unsurprisingly, Bonan *et al.*, (2011) found that implementing seasonality reduced NPP by about 8%, while Burnett *et al.*, (2021) found a smaller, yet still significant effect of seasonality which reduced cumulative canopy A. Medvigy *et al.*, (2013) applied a function scaling $V_{cmax.25}$ based on photoperiod, and found that simulating seasonality resulted in a 3% increase in NPP, the same increase to A as I observed in this study.

Unlike previous studies, which have primarily focused on the impact of seasonality on carbon assimilation, I was also interested in the effect that a variable g_1 and g_0 would have on seasonal simulations of E. The use of variable stomatal parameters reveals a substantial underestimation of early season E compared to the fixed model (Fig. 4.7), leading to a 16% higher total seasonal transpiration rate for the variable model than the fixed model. I also observe that stomatal limitation on A plays a small yet significant role in regulating seasonal assimilation, on average reducing potential A by 10-20% (Fig. 4.9), reinforcing the importance of appropriate estimation of stomatal parameters in earth system modeling (De Kauwe *et al.*, 2015a).

Based on the findings presented in this study and others (e.g., Medvigy *et al.*, 2013; Burnett *et al.*, 2021), there is a clear need for models to account for seasonality in both photosynthetic and stomatal parameters, with emphasis given toward ensuring that photosynthetic and stomatal parameters correctly scale with one another. The increasing development of models which predict physiology according to climatic optimality principles (Smith *et al.*, 2019; Caldararu *et al.*, 2020; Cooley *et al.*, 2022) provides an opportunity for the modeling community to move away from models which use a seasonal mean value or fixed model parameters. While this study provides a semi-empirical model at a single site for a single season, I nonetheless advocate for future studies which move toward a true mechanistic representation of how parameters, at the intersection of leaf ontogeny and climate, change seasonally. Accomplishing a reparameterization of models will be a difficult task, yet one which will substantially improve our collective understanding of land-atmosphere interactions across diverse geographical regions and variable environmental conditions.

4.6 – **Figures:**

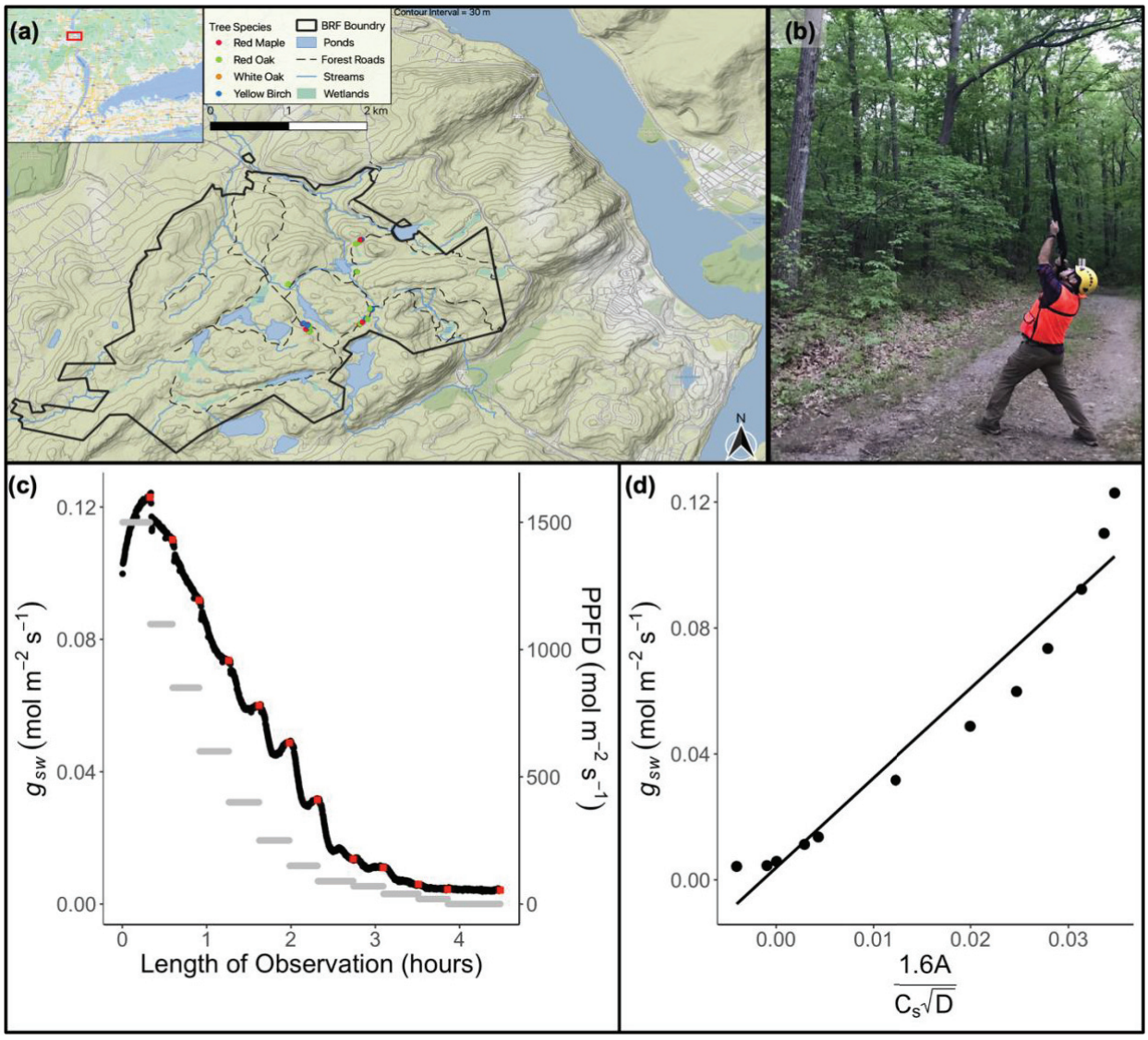

Figure 4.1: Schematic representation of sampling method and estimation of stomatal response parameters. (a) geographic location of Black Rock Forest (41.45°N, 74.01°W, 110-450 m above sea level), and distribution of study trees at the site; (b) using a 12-gauge shotgun to sample upper canopy vegetation; (c) raw data from the response of stomatal conductance (g_{sw}) to decreasing irradiance, with black points representing individual observations of g_{sw}, red points representing the final extracted rates of g_{sw}, and horizontal gray bars representing irradiance levels (1500, 900, 700, 450, 250, 175, 90, 40, 20, 0 µmol m^{-2} s^{-1}); (d) regression fit of the g_{sw} values extracted from the curve in panel (c) versus the leaf-level environmental conditions at the time of measurement. C_s and D are the leaf surface CO_2 concentration and vapor pressure deficit respectively, and A is the net photosynthetic rate.

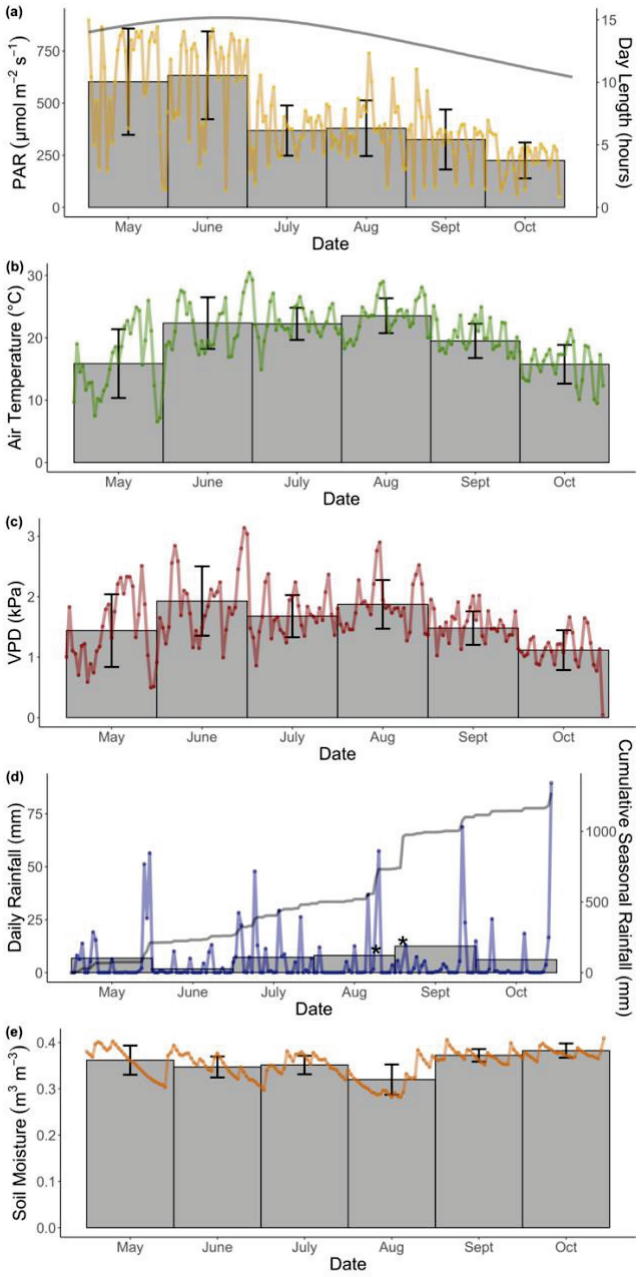

Figure 4.2: Meteorological conditions at Black Rock Forest for the 2021 growth season. Data in panels (a-d) are an average from two meteorological stations within the forest, each recording hourly average measurements, while data in panel (e) come from the ERA5-Land reanalysis dataset (Muñoz Sabater, 2019). Daytime is defined as the interval from local sunrise to sunset. During the period of study mean daily temperature was 19.7°C and total precipitation was 1.1 m (a) mean daytime irradiance (photosynthetically active radiation) and day length, (b) mean daytime air temperature, (c) mean daytime vapor pressure deficit (VPD), (d) total daily (24-hour) and cumulative seasonal rainfall, and (e) mean daily (24-hour) volumetric soil moisture content. For all plots individual points are single day observations, and grey bars are monthly average with error bars representing 2 SE of the mean. Asterisks in panel (d) are abnormal rainfall events (not plotted), Aug. 22 (125 mm) and Sept. 1 (222 mm).

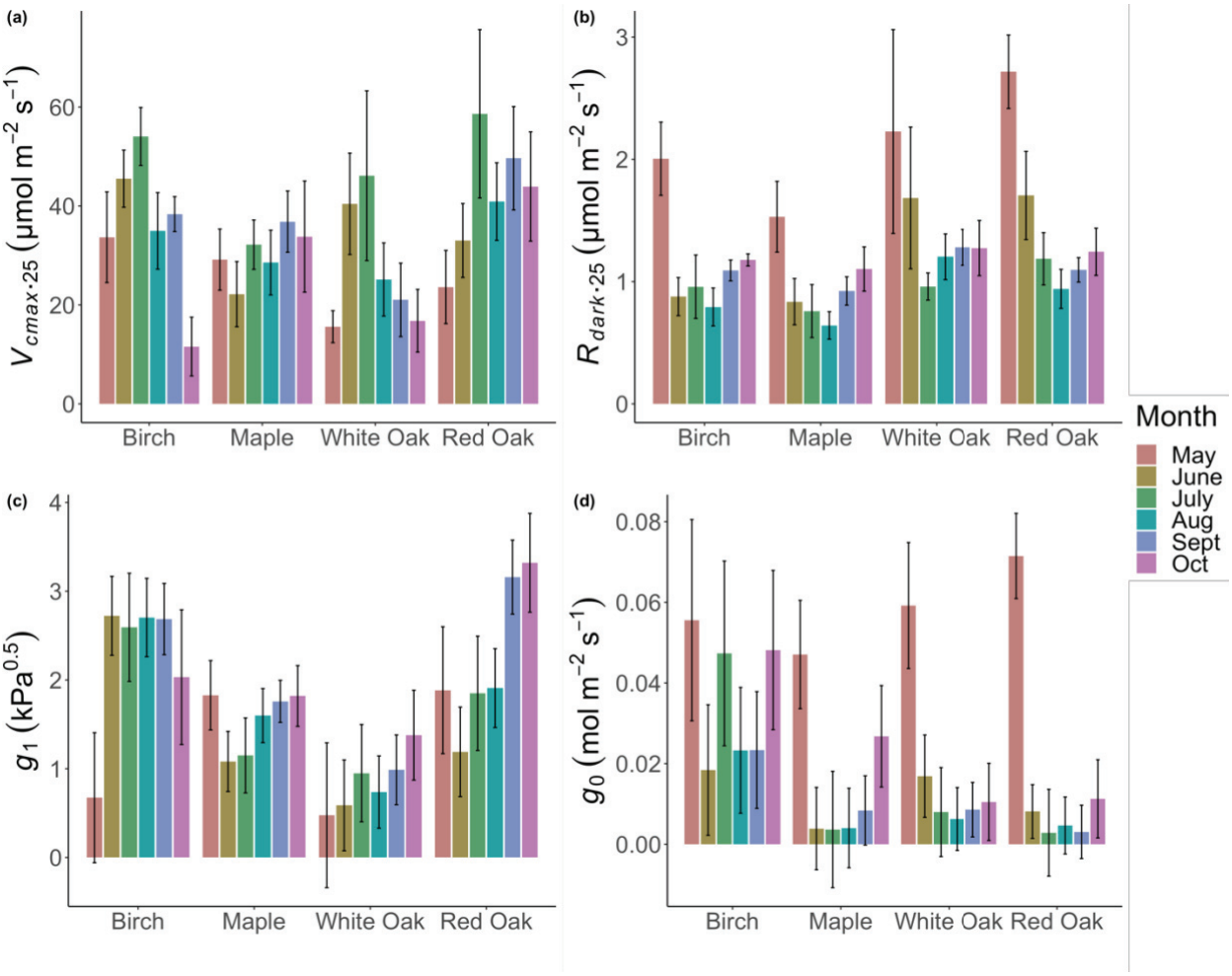

Figure 4.3: Average monthly estimates of four important physiological parameters. (a) the maximum carboxylation capacity of Rubisco normalized to 25°C ($V_{cmax.25}$), (b) dark respiration rate normalized to 25°C ($R_{dark.25}$), (c) the stomatal slope parameter (g_1) and (d) stomatal intercept parameter (g_0) of the Unified Stomatal Optimization model (Medlyn et al. 2011) measured throughout the growth season in four tree groups in the Black Rock Forest. Data shown are mean ± 2 SE (n=9-12; see Table S2 for further details).

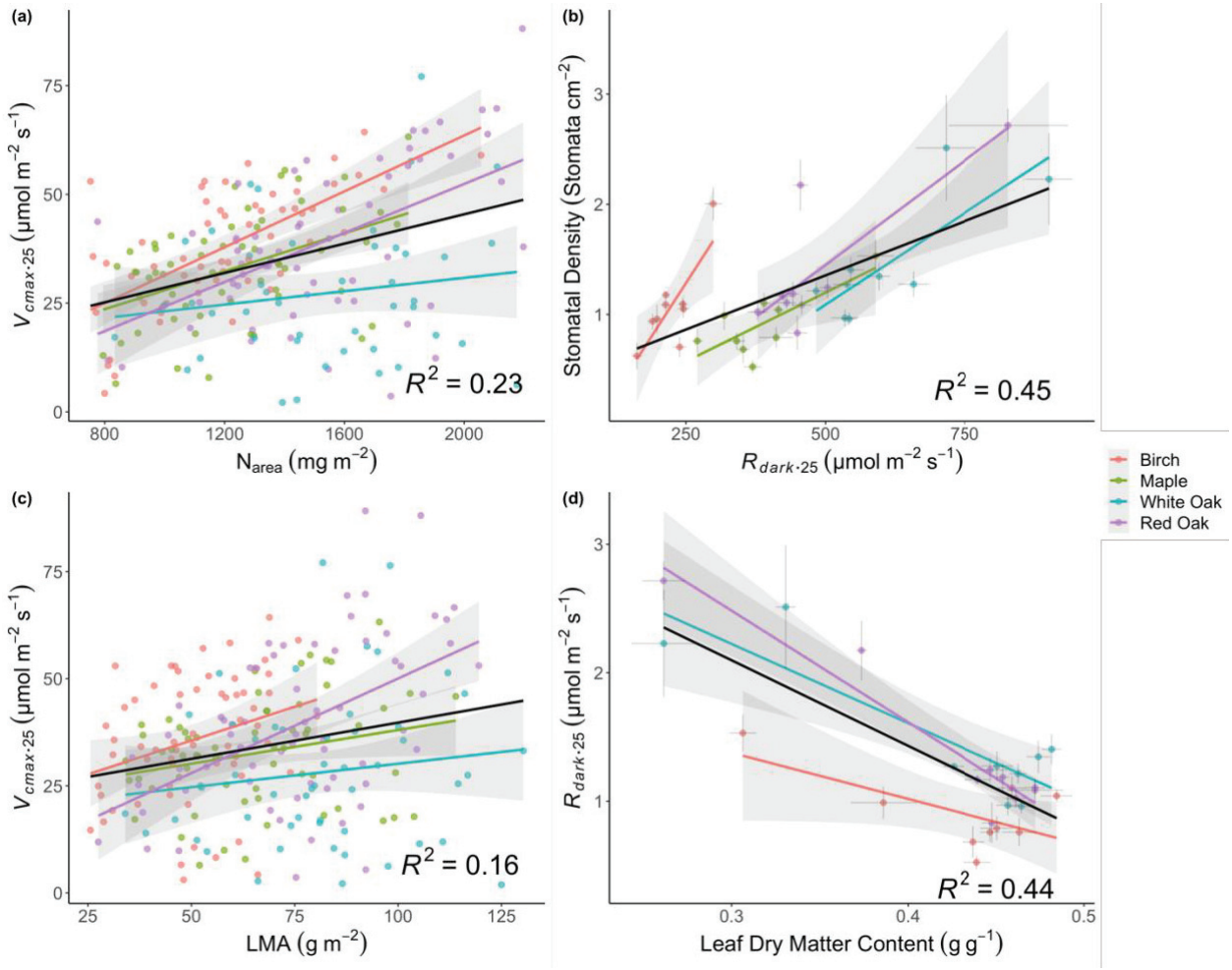

Figure 4.4: Linear relationships between the maximum carboxylation capacity of Rubisco normalized to 25°C ($V_{cmax.25}$) and dark respiration rate normalized to 25°C ($R_{dark.25}$) and foliar functional traits. $V_{cmax.25}$ versus (a) foliar elemental nitrogen per unit area, and (c) leaf mass per area, and $R_{dark.25}$ versus (b) stomatal density and (d) leaf dry matter content. Points in panels (a) and (c) represent individual observations, while points in panels (b) and (d) are mean monthly observations with error bars ± 2 SE (n=9-12 see Table S2 for further details). Data for maple are excluded from panel (d) as the slope of the relationship was not significantly different from zero. Points to the extreme left in panel (d) and extreme right in panel (b) come from the start and end of the growth season. The black trend line is the overall relationship, while colored lines and shroud are the species-group specific relationships and prediction interval. All relationships shown are significant ($p < 0.004$).

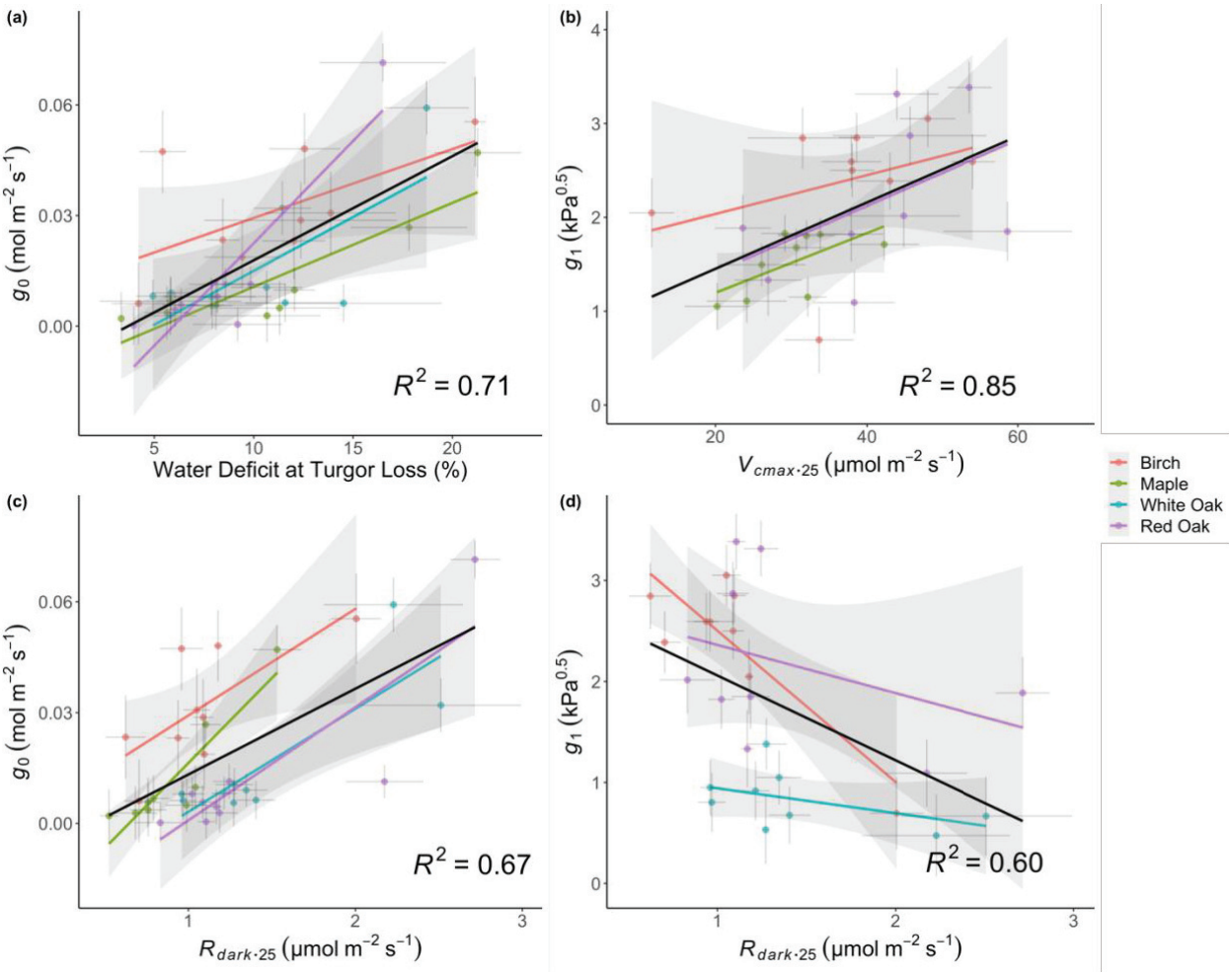

Figure 4.5: Linear relationships between the stomatal intercept (g_0) and slope parameter (g_1) from the Unified Stomatal Optimization model (Medlyn et al. 2011), and foliar photosynthetic and hydraulic traits. g_0 versus (a) relative water deficit at the point of turgor loss, and (c) dark respiration rate normalized to 25°C ($R_{dark.25}$), and g_1 versus (b) the maximum carboxylation capacity of Rubisco normalized to 25°C ($V_{cmax.25}$) and (d) $R_{dark.25}$. Points are mean monthly observations with error bars ± 2 SE (n=9-12; see Table S2 for further details). The black trend line is the overall relationship, while colored lines and shroud are the species-group specific relationships and prediction interval. All relationships shown are significant ($p < 0.004$).

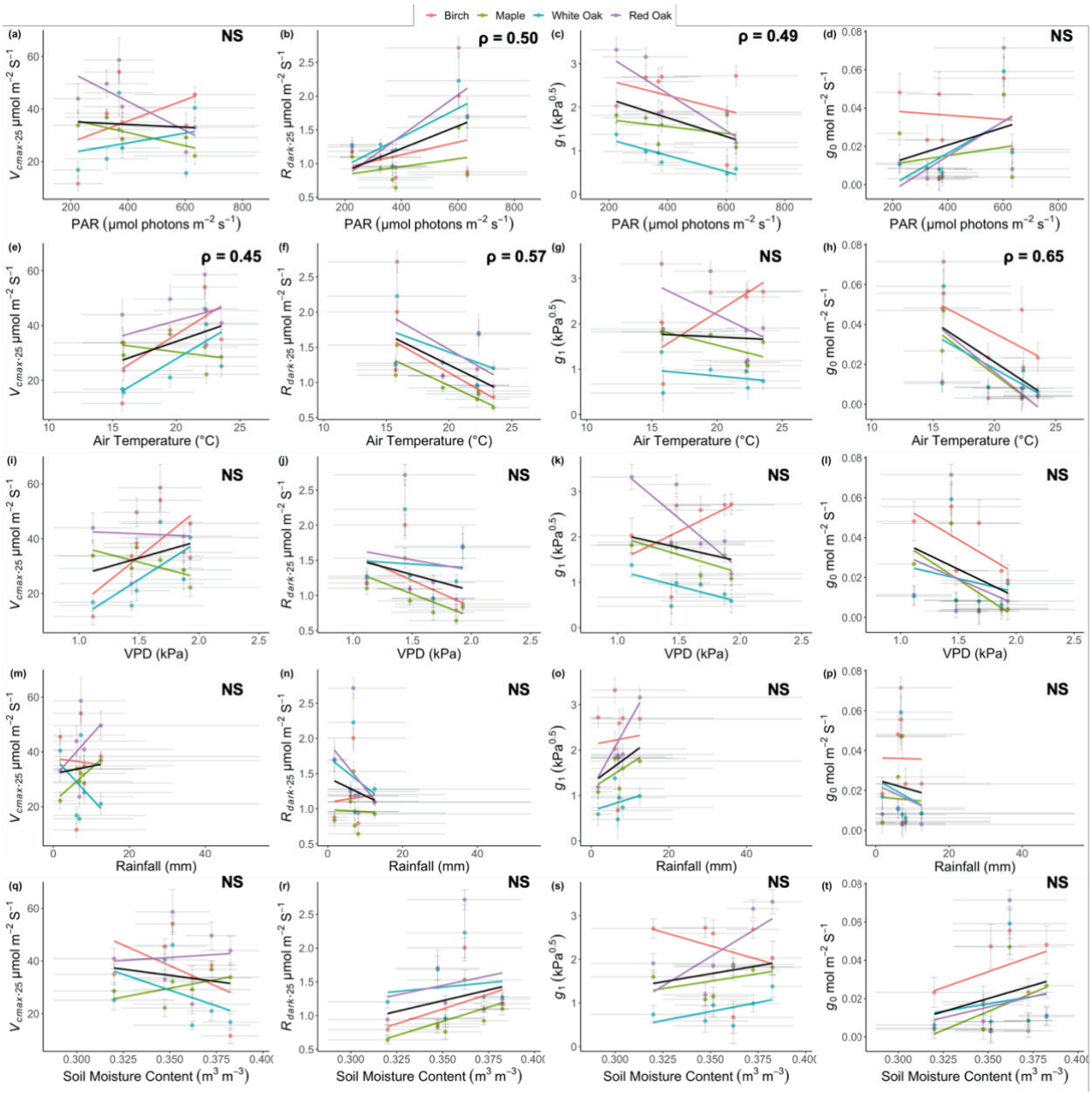

Figure 4.6: Relationships between monthly mean meteorological conditions (daytime PAR, daytime air temperature, daytime VPD, total 24-hour total precipitation, 24-hour soil moisture content) and monthly mean physiological traits (the maximum carboxylation capacity of Rubisco normalized to 25°C ($V_{cmax.25}$), the dark respiration rate normalized to 25°C ($R_{dark.25}$), the stomatal slope parameter (g_1) and the stomatal intercept parameter (g_0) of the Unified Stomatal Optimization model) by species-group. Points represent monthly average estimates with error bars ± 2 SE. The black trend line is the overall relationship, while colored lines are species-group specific relationships. Values for ρ in each panel represent the overall correlation coefficient (NS= not significant; $p < 0.004$).

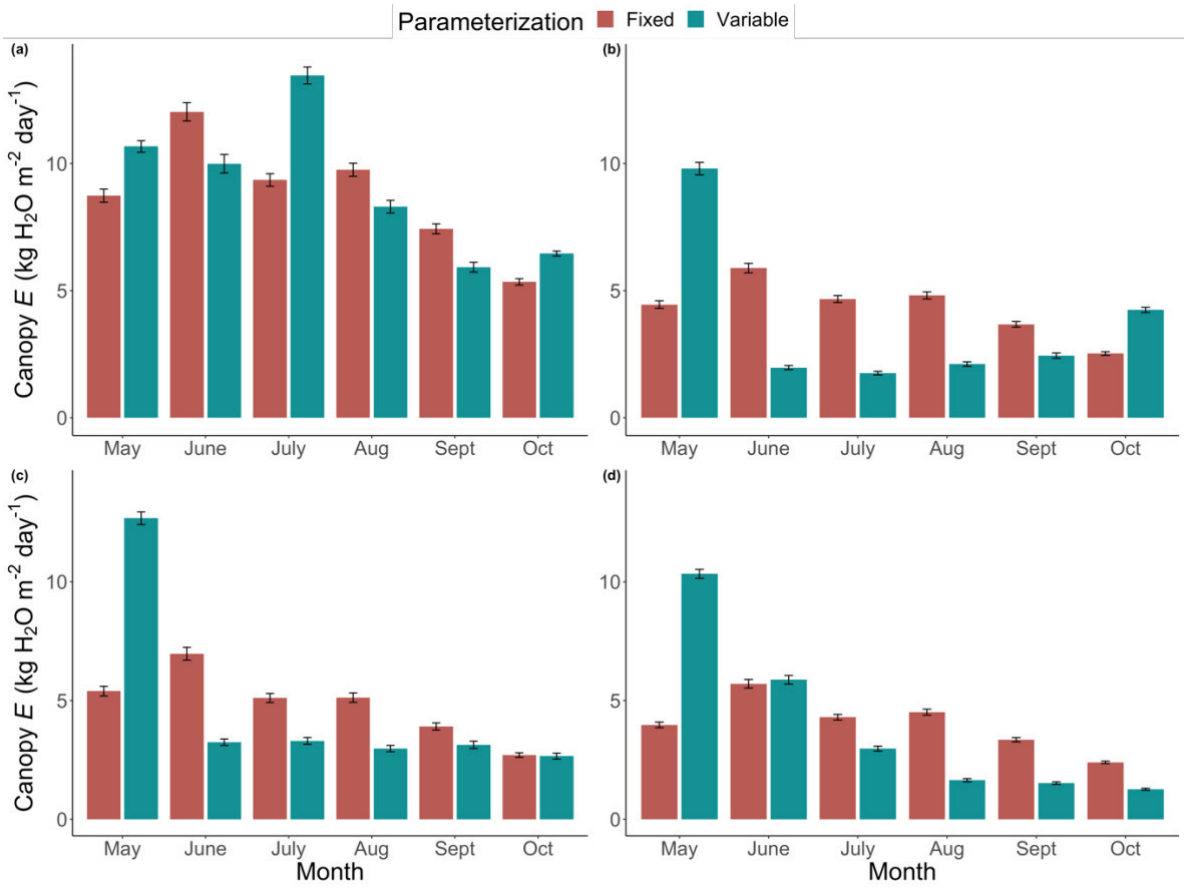

Figure 4.7: Model estimates for total monthly canopy transpiration using two different model parametrizations. (a) birch, (b) maple, (c) red oak, and (d) white oak. In the fixed model, values for the four key physiological parameters (the maximum carboxylation capacity of Rubisco normalized to 25°C ($V_{cmax.25}$), the dark respiration rate normalized to 25°C ($R_{dark.25}$), the stomatal slope parameter (g_1) and the stomatal intercept parameter (g_0) of the Unified Stomatal Optimization model) are the same between months. In the variable model, physiological parameters are month specific (see Table S2 for further details). Error bars are ± 2 SE of the mean monthly estimate (n=30-31).

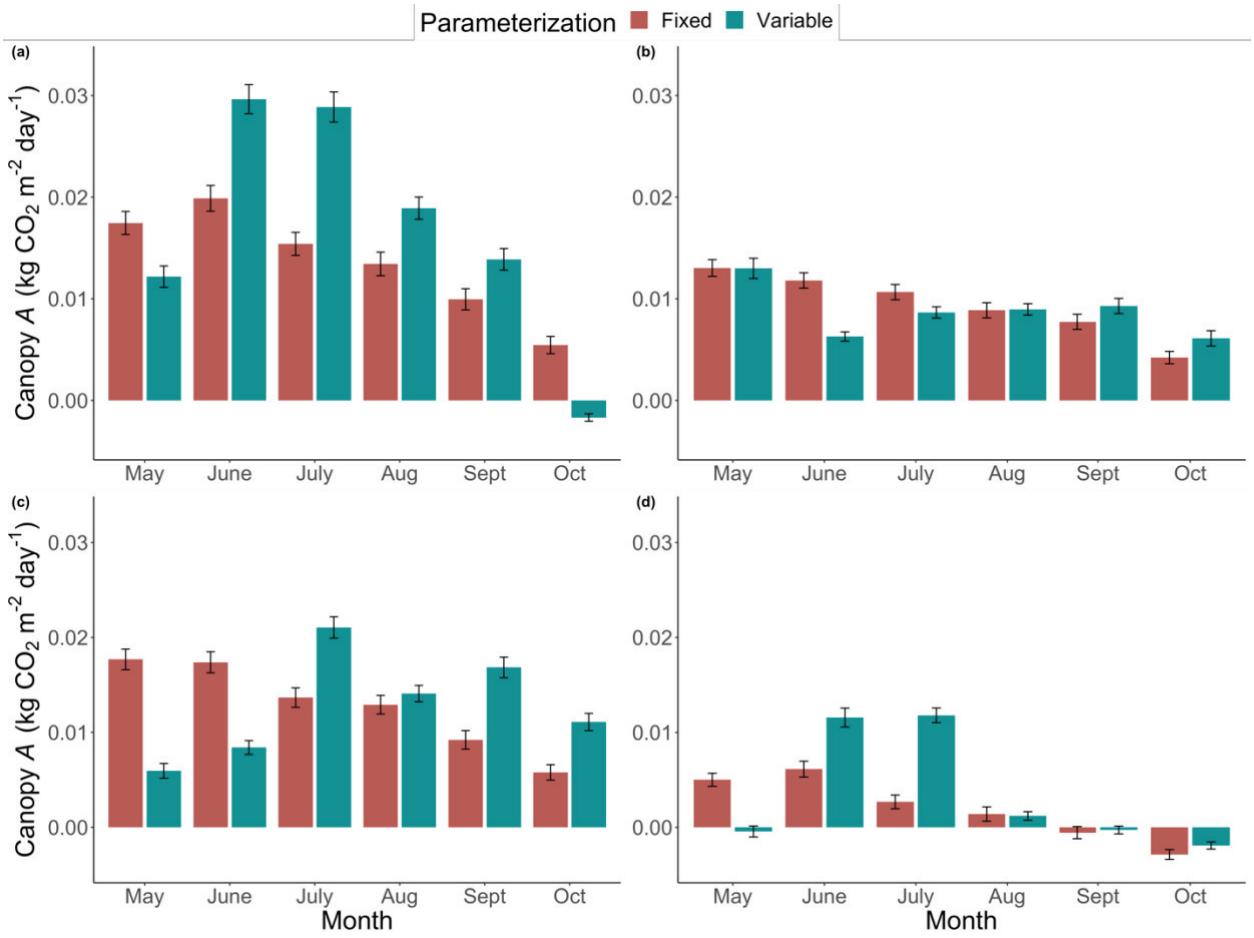

Figure 4.8: Model estimates for total monthly canopy net carbon assimilation using two different model parametrizations. (a) birch, (b) maple, (c) red oak, and (d) white oak. In the fixed model, values for the four key physiological parameters (the maximum carboxylation capacity of Rubisco normalized to 25°C ($V_{cmax.25}$), the dark respiration rate normalized to 25°C ($R_{dark.25}$), the stomatal slope parameter (g_1) and the stomatal intercept parameter (g_0) of the Unified Stomatal Optimization model) are the same between months. In the variable model, physiological parameters are month specific (see Table S2 for further details). Error bars are ± 2 SE of the mean monthly estimate (n=30-31).

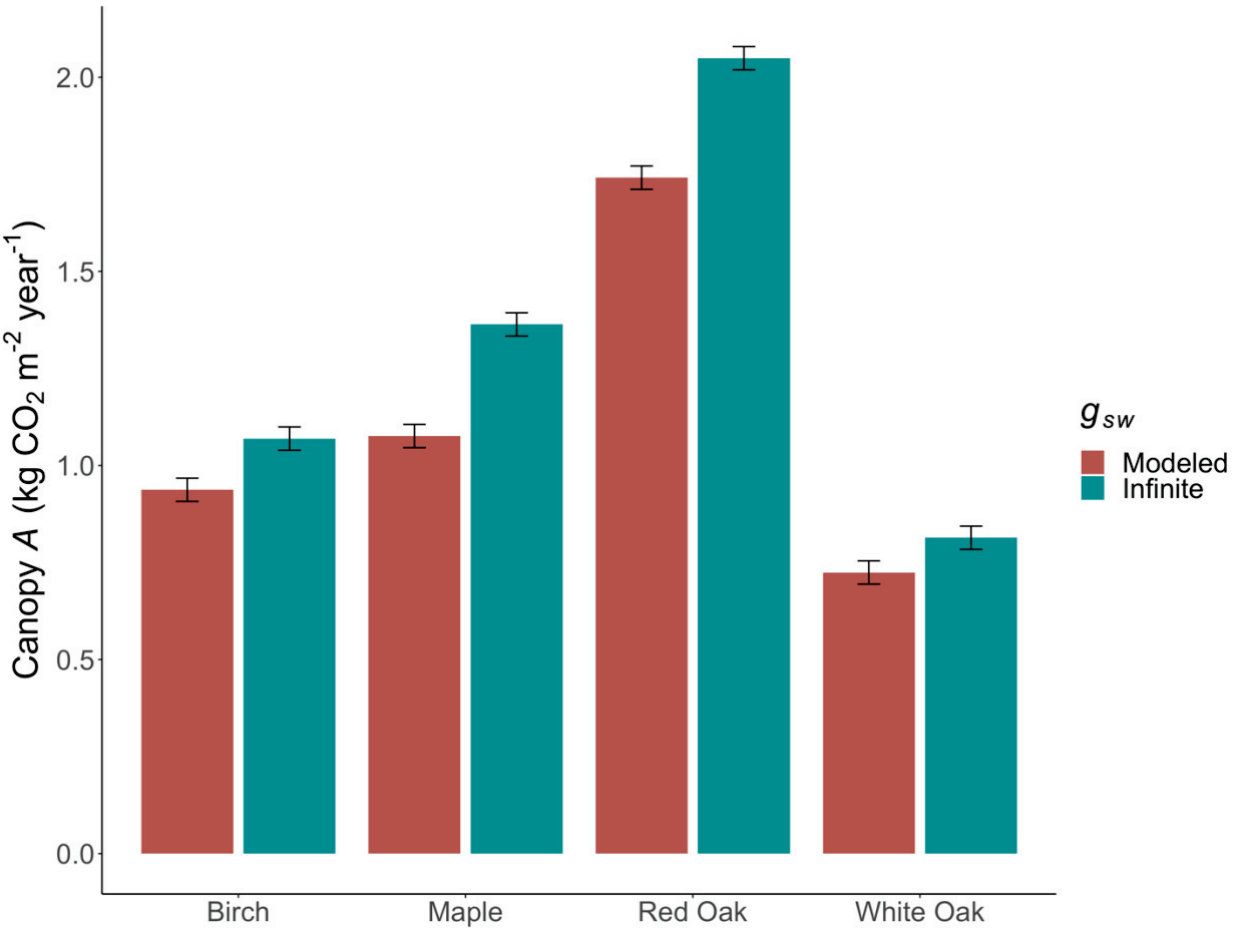

Figure 4.9: Total canopy net assimilation per unit ground area, for four of the most common species-groups present at Black Rock Forest. Bars in blue represent a model run when g_1 was set to infinity, removing stomatal limitation on potential assimilation. Bars in red represent the standard variable model run. Error bars are ± 2 SE of the mean.

4.7 – **Tables:**

Table 4.1: Average species-group-specific values for photosynthetic and conductance parameters used in fixed model simulations of canopy *E* and NPP, and approximate date of leaf out and leaf coloration. Each sample represents an independent leaf-level estimate. Values in parentheses are the SE of the species-group mean estimate. Superscript letters indicate significant ($P < 0.05$) pairwise differences between parameter estimates obtained from post hoc Tukey tests.

Group	Species	Sample Size	$V_{cmax.25}$ (µmol m^{-2} s^{-1})	$R_{dark.25}$ (µmol m^{-2} s^{-1})	g_1 ($kPa^{0.5}$)	g_0 (mol m^{-2} s^{-1})	Leaf-out (DOY)	Leaf coloration (DOY)
Birch	*Betula alleghaniensis* Britt.	69	35.92^{A} (1.9)	1.06^{A} (0.05)	2.47^{A} (0.13)	0.033^{A} (0.0046)	131	257
Maple	*Acer rubrum* L. *Acer saccharum* Marshall	68	32.91^{A} (1.59)	0.96^{A} (0.05)	1.45^{B} (0.08)	0.011^{B} (0.0017)	126	263
White Oak	*Quercus alba* L. *Quercus montana* Willd.	66	28.09^{A} (2.42)	1.34^{B} (0.07)	0.91^{C} (0.12)	0.012^{B} (0.0026)	139	286
Red Oak	*Quercus rubra* L.	69	39.74^{A} (2.41)	1.34^{B} (0.08)	1.95^{A} (0.14)	0.013^{B} (0.0029)	124	273

Table 4.2: Estimates of monthly mean stomatal limitation on photosynthesis (*I*) and the proportions of observations (1 hr model timestep) where limitation occurs.

Group	Month	Mean value of *I*	Proportion of observations *I* > 0 (%)
Birch	May	0.221	7.2
	June	0.231	32.0
	July	0.086	24.1
	Aug	0.142	31.9
	Sept	0.087	10.3
	Oct	-	0.0
Maple	May	0.208	20.5
	June	0.374	61.3
	July	0.240	58.7
	Aug	0.306	52.1
	Sept	0.177	15.0
	Oct	0.168	3.3
White Oak	May	0.418	3.9
	June	0.221	39.8
	July	0.103	62.1
	Aug	0.201	22.9
	Sept	0.268	0.7
	Oct	-	0.0
Red Oak	May	0.177	23.9
	June	0.276	63.0
	July	0.163	83.2
	Aug	0.191	65.8
	Sept	0.174	19.7
	Oct	0.128	6.6

Chapter 5: Improving the parameterization of Arctic stomatal traits in a land surface model using empirical field observations and optimality theory

5.1 – **Abstract:**

Earth system models are the primary tool to forecast the complex coupling between the surface and atmosphere, where the underlying land surface models (LSMs) provide the means to simulate the contributions of the terrestrial ecosystems to nutrient, carbon, water, and energy cycles. Of the vegetation processes simulated within LSMs, stomatal conductance (g_{sw}) is one of the most critical processes to represent correctly as it fundamentally governs the exchange of carbon and water between the atmosphere and the vegetative layer. In this study, I collected stomatal response curves on eight Arctic plant species, across a range of environmental conditions, and used these data, along with an accompanying foliar biochemical analysis to estimate five key foliar model parameters for the two default Arctic plant functional types (PFTs) used in the E3SM land model (ELM). By using these updated parameter values within ELM, I was able to assess the impact of revised parameters on modeled carbon cycling and transpiration (E). Further, I tested three alternative soil moisture stress functions, which more correctly simulate the process by which soil moisture stress effects leaf-level water use efficiency (WUE). I found that when these updated parameters were applied to ELM, ecosystem scale WUE decreased significantly across all four study sites. Further, when modeled gross primary production and latent heat flux were compared with flux tower data, a significant temporal mismatch between the model and observations was identified, potentially due to an incorrect phenology scheme in ELM. My findings highlight the importance of accurately representing stomatal response to biotic and abiotic factors when modeling Arctic ecosystems, and the importance of parameterizations that are tailored to Arctic PFTs.

5.2 – **Introduction:**

The Arctic ecosystem is experiencing unparalleled warming as the result of global climate change (Rantanen *et al.*, 2022), with impacts on dynamics of seasonal albedo, precipitation and snowpack, and sea ice cover and formation (Winton, 2006; Hinzman *et al.*, 2013; Jenkins & Dai, 2021). In turn, these altered climatic factors have a substantial impact on vegetation and soils, which have caused an overall "greening" of the Arctic (Myers-Smith *et al.*, 2020), increased shrub cover in many ecosystems (Myers-Smith *et al.*, 2011a; Mekonnen *et al.*, 2021), and accelerated permafrost thaw that has the potential to release trapped CO_2 and methane, hastening the climate feedback (Koven *et al.*, 2011; Schuur *et al.*, 2015). Earth system models (ESMs) are one of the key tools ecologists possess to forecast these multifaceted impacts of climate change (Flato, 2011), with land surface models (LSMs) used to simulate the complex contributions of the terrestrial ecosystems to nutrient, carbon, water, and energy cycles (Fisher & Koven, 2020). This is accomplished by simulating processes such as detailed vegetation physiology, growth and turnover, soil biogeochemical processes such as plant and soil carbon cycling, landcover change, disturbance, and surface and subsurface hydrology (Lawrence *et al.*, 2019). Of the vegetation processes simulated within LSMs, stomatal conductance to water (g_{sw}) is one of the most critical processes to represent correctly as it fundamentally governs the exchange of carbon and water between the atmosphere and vegetative layer (Franks *et al.*, 2018). Limitations imposed by stomata help set the upper limit on water loss via transpiration (E), and through stomatal limitation on photosynthesis (A), g_{sw} is a strong determinant of net primary productivity (NPP; Zhang et al., 2019). As such, uncertainty in the model parameters related to stomatal conductance (the stomatal slope and stomatal intercept) contribute to some of the largest model uncertainties in current projections of carbon and water cycling in LSMs (Dietze *et al.*, 2014; Jefferson *et al.*, 2017; Rogers *et al.*, 2017c; Ricciuto *et al.*, 2018; Lemordant *et al.*, 2018).

The Energy Exascale Earth System Model (E3SM; Golaz *et al.*, 2019) Land Model v2 Arctic (hereafter ELM; Ricciuto *et al.*, 2018) inherits its default configuration for stomatal conductance from the Community Land Model (CLM) 4.5 (Oleson *et al.*, 2013), and uses the Ball Woodrow Berry (BWB) model of stomatal conductance (Ball *et al.*, 1987). In the BWB model, g_{sw} is assumed to scale linearly based on a function which includes A, CO_2 concentration, and relative humidity (RH) at the leaf surface. The BWB model has two fitted parameters, a slope parameter which

governs the ratio of g_s: $f(A,CO_2,RH)$, and an intercept parameter which sets the minimum level for g_{sw} at conditions at or below the light compensation point for photosynthesis (Damour *et al.*, 2010). ELM also inherits the same default plant functional type (PFT) classifications as CLM 4.5, with PFT specific values for stomatal slope and intercept (Oleson *et al.*, 2013). Of relevance to the Arctic ecosystem are the "broadleaf deciduous boreal shrub" (BDBS), and "C_3 arctic grass" (CAG) PFTs, which by default have the same value for stomatal slope (9 [unitless]) and stomatal intercept (10000 μmol m^{-2} s^{-1}; Sellers *et al.*, 1996).

To date, there have been very few studies which have attempted to quantify stomatal conductance or stomatal traits in the Arctic (Rogers *et al.*, 2022), with most previous work focusing on boreal trees rather than shrubs or graminoids (e.g., Landhäusser *et al.*, 1996; Dang *et al.*, 1998; Kropp *et al.*, 2017). Likely one of the most complete datasets assessing stomatal parameters in the high Arctic comes from the global synthesis by Lin *et al.*, (2015), which included data from 8 Arctic species collected on the north slope of Alaska. Results from this study suggest that when estimated using the Medlyn stomatal model (USO; Medlyn *et al.*, 2011) estimated stomatal slope of Arctic PFTs are approximately half of their respective temperate and tropical counterparts. The researchers attribute this marked difference to two factors; first, in the USO model formulation stomatal slope should be roughly proportional to Γ^* (CO_2 compensation point in absence of photorespiration) due to the exponential temperature dependence of Γ^* (Bernacchi *et al.*, 2001). Second, an increase in the viscosity of water at the lower temperatures experienced in the Arctic should decrease the carbon "cost" of transporting water (Prentice *et al.*, 2014), thus reducing the USO stomatal slope estimate because of its inverse proportionality with water use efficiency. While the Lin *et al.*, (2015) analysis is a promising step forward, it lacks a large spatial coverage of Arctic data and only includes observations of a single shrub species at a single site.

Likewise, the data from Lin *et al.*, (2015) cannot be used to estimate the stomatal intercept parameter because it lacks paired A and g_{sw} data collected at and around the light compensation point (De Kauwe *et al.*, 2015b; Duursma *et al.*, 2019). As such, Lin *et al.*, (2015) assumed that the stomatal intercept value was zero for all species and ecosystems. Not only does this assumption impact the estimation of stomatal slope (Duursma *et al.*, 2019), it also may be a significant oversimplification of the physiology of Arctic vegetation. Previous studies of non-Arctic vegetation have shown that stomatal intercept may be higher at lower temperatures (Anfodillo *et*

al., 2002; Duarte *et al.*, 2016), and lower VPD levels (Drake *et al.*, 2018), and that shorter growing seasons may lead to reduced cuticular development and thus higher stomatal intercept (Fernández *et al.*, 2017). Clearly more data are needed in order to properly parameterize stomatal intercept, and evaluate its importance in models of Arctic vegetation.

In addition to the stomatal slope and intercept, ELM also regulates g_{sw} through the use of a multiplicative scaler term (0-1), known as the β_t factor or "BTRAN" (Oleson *et al.*, 2013). The β_t factor is applied to the stomatal intercept, the maximum carboxylation capacity of the enzyme rubisco ($V_{c\max}$; μmol m^{-2} s^{-1}) and the respiration rate (R_d; μmol m^{-2} s^{-1}) and is intended to account for the reductions in g_{sw} and A imposed by soil moisture limitation (Sellers *et al.*, 1996). The value of β_t is calculated based on soil moisture availability, and PFT specific rooting and stomatal closure parameters (see Methods section "Default Land Model Configuration"), with no modifications yet applied for Arctic specific PFTs. Empirical studies to support a reduction in stomatal intercept as a function of soil water stress have produced mixed conclusions (e.g., Liozon *et al.*, 2000; Xu & Baldocchi, 2003; Misson *et al.*, 2006) which may be partially attributable to the interrelation between leaf age, seasonality and drought in many study systems (Miner *et al.*, 2017). However, in a study of boreal trees in Siberia, (Kropp *et al.*, 2017) found that past precipitation and permafrost depth significantly impacted canopy conductance and transpiration. While, to my knowledge, no studies have directly addressed the accuracy of the β_t factor in the Arctic, numerous studies have found that its application may lead to an overestimated drought-related reduction in productivity and transpiration when compared with observations from the tropics (Powell *et al.*, 2013; Li *et al.*, 2022) and in global assessments (Bonan *et al.*, 2011; Kennedy *et al.*, 2019). Other more mechanistic functions may better represent the impact of soil moisture stress on transpiration, such as applying the reduction in g_{sw} by altering the stomatal slope (e.g., Anderegg *et al.*, 2017), simulating water transport through the xylem with a hydraulic model (e.g., Sperry & Love, 2015; Kennedy *et al.*, 2019) or via a model which accounts for a chemical drought stress signal such as abscisic acid (Huber *et al.*, 2019).

In this study, I collected full range (saturating irradiance to dark) stomatal response curves on eight Arctic plant species, across a range of environmental conditions. I used these data, along with an accompanying foliar biochemical analysis to estimate stomatal slope, stomatal intercept, $R_{dark.25}$, $V_{c\max.25}$, SLA_0, F_{LNR}, and C_{NL} for the two Arctic PFTs used in ELM. By applying these

refined parameter estimates to ELM I was able to address the following research questions: 1) How different are observed and default gas exchange parameter values in ELM? 2) How does observed variation in the estimation of gas exchange parameters relate to local microclimatic conditions experienced by Arctic vegetation, and are there any associations between stomatal parameters and leaf traits which can be exploited for parametrizing new Arctic PFTs? 3) What impact does revising gas exchange parameter values used in ELM have on predictions of NPP and *E*? 4) Can our newfound understanding of arctic stomatal conductance, along with widely held assumptions about stomatal optimality, be used to improve the way soil moisture stress is represented in ELM?

5.3 – **Materials and Methods:**

Study Sites and Measurements

All data in this study were collected at one of three Next-Generation Ecosystem Experiments Arctic (NGEE-Arctic) project (https://ngee-arctic.ornl.gov/) field sites (Fig. 5.1) which were established in 2010 to assist the US Department of Energy's effort to evaluate Earth system model representation of Arctic ecosystems. The northernmost NGEE-Arctic site (hereafter BEO) is located in Utqiaġvik, AK within the bounds of the Barrow Environmental Observatory, along the coast of the Beaufort Sea. The BEO site consists of coastal lowland polygonal tundra, with continuous permafrost and low vegetation biomass density and diversity (Fig. 5.1a), conditions which represent approximately 30% of the Arctic and sub-Arctic (Walker *et al.*, 2018). Mean growth season (June-August) temperature at the BEO site is 3.2ºC and mean annual precipitation is 173 mm $year^{-1}$ with the majority of the precipitation occurring during the growth season (Liljedahl *et al.*, 2011). The other two sites where I collected data (hereafter Teller and Kougarok) are located on the Seward Peninsula of Alaska, and represent the transition zone between Arctic and boreal ecosystems (Epstein *et al.*, 2004). These sites are hilly, vegetated with a mix of shrub and grass species, and represent conditions present in approximately 40% of the Arctic and sub-Arctic (Walker *et al.*, 2018). Unlike the BEO site, the sites on the Seward Peninsula have a thick, carbon rich active layer of soils, discontinuous permafrost (Schuur *et al.*, 2015). At the Kougarok site, vegetation varies by position along the hillslope (Sulman *et al.*, 2021), with a large community of *Alnus* shrubs present below the hillcrest (Salmon *et al.*, 2019; Fig. 5.1b). The Kougarok site has

an average summer (July) temperature of 11ºC and receives an average of 102.1 mm of rainfall per summer (Hinzman *et al.*, 2003). The Teller site comprises a hillslope watershed with notable solifluction features, and is dominated by *Salix* shrubs, wet sedges, and dwarf shrubs with vegetation distribution linked closely to subsurface properties and soil wetness (Léger *et al.*, 2019; Yang *et al.*, 2021; Fig. 5.1c). Mean growth season (June-August) temperature at the Teller site is 8.8ºC and mean growth season precipitation is 167 mm (Fick & Hijmans, 2017). A third NGEE-Arctic site (hereafter Council) is also present on the Seward Peninsula however no data were collected here in this study. The Council site is characterized by lowland wet, warm, and discontinuous permafrost with extensive thermal erosion and drained thermokarst lakes. The Council site has an average summer (July) temperature of 11.4ºC and receives an average of 317.2 mm of rainfall per summer (Hinzman *et al.*, 2003).

To characterize stomatal traits, I collected stomatal response curves (e.g., Leakey *et al.*, 2006; Davidson *et al.*, 2022; Lamour *et al.*, 2022) on intact leaves of the most abundant vegetation types at each site (Table 5.1). Vegetation measured at the BEO site consisted of both C3 Arctic Grass and boreal deciduous shrub PFTs, while data collection at the two Seward Peninsula sites focused only on the shrub PFT. At the Seward Peninsula sites, leaf gas exchange measurements were made using two LI-6800 gas exchange systems, while at the BEO site measurements were made using four LI-6400XT gas exchange systems (LI-COR Biosciences, Lincoln, NE USA). Equipment at both sites had recently (within two years) been calibrated, zeroed on a common gas standard at the start of the campaign, and were running the latest available version of the operating system.

The experimental protocol for stomatal response curves was identical at all three sites. Following enclosure of the sample in the leaf chamber, the leaf was allowed to stabilize to conditions for a minimum of 40 min. For the duration of the curve, the CO_2 concentration, leaf temperature, and relative humidity (LI-6800 only) inside the leaf chamber were held constant. A sample CO_2 level of 400 μmol mol^{-1} was chosen so that sample CO_2 would be close to ambient, and leaf temperatures were maintained near to ambient temperature while preventing condensation from forming inside the instrument. For the first measurement, leaves were acclimated to 1500 μmol m^{-2} s^{-1} of photosynthetically active radiation (PAR). Subsequently, the irradiance level was successively reduced (500, 200, 75 and 0 μmol m^{-2} s^{-1}) and irradiance was maintained for a minimum of 30 min or until stomatal conductance had stabilized. Following completion of each

curve, the leaf sample was removed from the chamber and the leaf area was measured. In cases where the leaf did not fill the leaf chamber aperture, results were recalculated to adjust for leaf area. For samples collected in Utqiaġvik, a LI-COR LI-3100C leaf area meter was used to estimate leaf area, while for Seward Peninsula samples, a flatbed scanner and image processing software (ImageJ v 1.53) was used to estimate leaf area. Samples were then dried in a 60ºC drying oven, and once constant mass had been achieved, were reweighed, ground, and processed for elemental nitrogen and carbon content using a 2400 Series II CHN analyzer (PerkinElmer, Waltham, MA, USA). This biochemical analysis was used to estimate the leaf carbon-to-nitrogen ratio (CN_L, g C g^{-1} N) and the top of canopy specific leaf area (SLA_0, m^2 leaf area g^{-1} C). For complete gas exchange and biochemistry datasets, as well as additional details on experimental protocols, see (Rogers *et al.*, 2023; Davidson & Serbin 2022).

Stomatal slope (m) and intercept (b) parameters were estimated by regressing estimated g_{sw} against leaf-level conditions using the Ball-Woodrow-Berry model of stomatal conductance (Ball *et al.*, 1987; Equation 5.1).

Equation 5.1.
$$g_{sw} = \left(\frac{A*Rh}{C_a} * m\right) + b$$

where A is the net photosynthesis rate (μmol m^{-2} s-1), Rh is the relative humidity of the air at the leaf surface (%) and C_a is the CO_2 concentration at the leaf surface (μmol mol^{-1}).

Leaf respiratory CO_2 release in the dark (R_{dark}) was calculated using the final stomatal response curve point as a dark-adapted measurements of A. R_{dark} was scaled to 25°C ($R_{dark.25}$) using an inverse Arrhenius equation (Bernacchi *et al.*, 2001; Von Caemmerer, 2013; Equation 5.2):

Equation 5.2.
$$R_{dark.25} = \frac{R_{dark}}{\exp\left(\frac{H_a}{(R*T_{25})} - \frac{H_a}{(R*T_{leaf})}\right)}$$

where H_a is the activation energy of mitochondrial respiration (H_a = 46390 J mol^{-1}), and R is the ideal gas constant (R = 8.314 J mol^{-1} K^{-1}).

I then estimated V_{cmax} for each leaf using the "one-point method" (De Kauwe *et al.*, 2016; Equation 5.3). For this calculation, I used the initial acclimated, steady state, light-saturated point

of each stomatal response curve for my measurement of light saturated photosynthesis (A_{sat}, μmol m^{-2} s^{-1}) and its corresponding intercellular CO_2 concentration (C_i, μmol mol^{-1}) and the values of R_{dark} as estimated from Equation 5.2. Previous work on Arctic species has shown that V_{cmax} estimates obtained following this protocol are close to those obtained using traditional AC_i curves (Burnett *et al.*, 2019):

Equation 5.3. $$V_{cmax} = (A_{sat} + R_{dark})\frac{(C_{i-\Gamma^*})}{(C_i+K_m)}$$

where K_m is the Michaelis–Menten constant (404.9 μmol mol^{-1}), Γ* is the CO_2 compensation point in the absence of mitochondrial respiration (42.75 μmol mol^{-1}), and C_i is the intercellular CO_2 concentration (μmol mol^{-1}).

To scale V_{cmax} at measurement temperature to V_{cmax} at 25°C ($V_{cmax.25}$), I used a modified Arrhenius equation (Leuning, 2002; Equation 5.4):

Equation 5.4. $$V_{cmax.25} = \frac{V_{cmax.T}}{C*\exp\left[\left(\frac{H_a}{RT_{25}}\right)*\left(\frac{1-T_{25}}{T_{leaf}}\right)\right]*1+\exp\left[\frac{(S_V T_{leaf}-H_d)}{RT_{leaf}}\right]}$$

where $V_{cmax.25}$ is the value of V_{cmax} at the reference temperature (T_{25} = 298.15 K), $V_{cmax.T}$ is the value of V_{cmax} at the leaf temperature (T_{leaf} in K), H_a, H_d, and S_v are the activation and deactivation energies of the enzyme Rubisco and an entropy term (H_a= 65330 J mol^{-1}, H_d = 149250 J mol^{-1}, and S_v = 485 J mol^{-1} K^{-1}), and C is a combined term equivalent to $1 + \exp[(S_V T_{25} - H_d)/(RT_{25})]$.

To obtain species, PFT, site-species, and site-PFT estimates of stomatal slope and intercept I utilized mixed models in which individual has a random effect on slope and intercept. This method accounts for the fact that when collecting stomatal response curves, points within one curve are non-independent. For comparable estimates of $V_{cmax.25}$ and $R_{dark.25}$ mixed models are not required as all estimates are independent.

In addition to leaf trait measurement, I collected several microclimatic variables at the two Seward Peninsula sites. Leaf surface temperature prior to measurement was assessed using a SI-121-SS Narrow Field of View Infrared Radiometer (Apogee Instruments Inc., Logan, UT USA). Soil moisture content was measured at the four cardinal positions 0.5 m from the base of each

shrub using a HydroSense II Handheld Soil Moisture Sensor (Campbell Scientific, Logan, UT USA). The depth to the permafrost layer was assessed by inserting a thaw-depth probe into the ground until it reached the freezing layer. Finally, using a differential GPS I measured the elevation of each plant, which, within a given location, serves as a stand in for several microclimatic factors such as slope, aspect, topographic wetness, and soil type.

Default Land Model Configuration

In this section I briefly provide an overview of the stomatal and photosynthesis components of ELM which are relevant to the analysis in this study. Default parameter values for all PFT specific parameters described in this section can be found in Table 5.2. A more detailed description of the ELM model, including changes that have been made since ELM v2 Arctic branched from CLM 4.5 (Oleson *et al.*, 2013), which are primarily related to nutrient cycling and limitation, can be found in Ricciuto *et al.*, (2018), Yang *et al.*, (2019), and Burrows *et al.*, (2020).

In ELM, vegetation is divided into two components representing the sunlit and shaded fractions, each solved separately using the average fraction of absorbed photosynthetically active radiation (Φ^{sun} and Φ^{shade}, W m^{-2}). Within each of these components, leaf stomatal conductance (g_{sw}, inverse of stomatal resistance r_s), and photosynthesis (A) are coupled and iteratively solved for, until the values for C_i converge (e.g., Collatz et al., 1991). Canopy conductance (G_s; Equation 5.5) and canopy photosynthesis (A_{canopy}; Equation 5.6) are solved accounting for the leaf area in each partial canopy layer (sun and shade):

Equation 5.5. $$G_s = (g_{sw}^{sun} + g_b)L^{sun} + (g_{sw}^{shade} + g_b)L^{shade}$$

Equation 5.6. $$A_{canopy} = A^{sun}L^{sun} + A^{shade}L^{shade}$$

where L^{sun} and L^{shade} are the leaf area index (LAI, m^2 m^{-2}) of the sun and shade fractions respectively, and g_b is the boundary layer conductance which is related to PFT specific leaf aerodynamic characteristics (Oleson *et al.*, 2013).

For C3 plants, photosynthesis in ELM is calculated based on the Farquhar von Caemmerer Berry (FvCB) model (Farquhar *et al.*, 1980), with modifications described by Bonan *et al.*, (2011). In this model, net photosynthesis (A_{net}) is the minimum of the rubisco limited rate of carboxylation

(A_c, μmol m^{-2} s^{-1}, Equation 5.7), the RuBP regeneration limited rate of carboxylation (A_j, μmol m^{-2} s^{-1}, Equation 5.8), and the product export limited rate of carboxylation (A_p, μmol m^{-2} s^{-1}, Equation 5.9), less the value of respiration (R_d, μmol m^{-2} s^{-1}).

Equation 5.7. $$A_c = \frac{V_{cmax}(C_i - \Gamma^*)}{C_i + K_c(1 + o_i/K_o)}$$

where o_i is the internal leaf O_2 partial pressure (o_i = 0.209 * atmospheric pressure, Pa) and K_c and K_o are the Michaelis-Menten constants for CO_2 and O_2 respectively (Pa).

Equation 5.8. $$A_j = \frac{J(C_i - \Gamma^*)}{4C_i + 8\Gamma^*}$$

where J is the electron transport rate (μmol m^{-2} s^{-1}).

Equation 5.9. $$A_p = 3T_p$$

where T_p is the triose phosphate utilization rate (μmol m^{-2} s^{-1}) and is given as 0.167*V_{cmax}. R_d is considered to be 0.015*V_{cmax}. Temperature scaling of all parameters (e.g., K_c to $K_{c.25}$) and rates (e.g., V_{cmax} to $V_{cmax.25}$) are described in detail by Bonan *et al.*, (2011).

In ELM, $V_{cmax.25}$ is derived as a function of leaf nitrogen (N) content and specific leaf area (Thornton & Zimmermann, 2007; Equation 5.10):

Equation 5.10. $$V_{cmax.25} = N_a F_{LNR} F_{NR} a_{R25}$$

where N_a is area-based leaf nitrogen concentration (g N m^{-2} leaf area), F_{LNR} is the fraction of leaf nitrogen in rubisco (g N in rubisco g^{-1} N), F_{NR} is the mass ratio of total rubisco molecular mass to nitrogen in rubisco (F_{NR} =7.16 g rubisco g^{-1} N in rubisco), and a_{R25} is the specific activity of rubisco at 25°C (a_{R25} = 60 μmol g^{-1} rubisco s^{-1}). N_a in Equation 5.10 is derived based on the inverse of the leaf carbon-to-nitrogen ratio (CN_L, g C g^{-1} N) multiplied by the top of canopy specific leaf area (SLA_0, m^2 leaf area g^{-1} C, Equation 5.11):

Equation 5.11. $$N_a = \frac{1}{C_{NL} * SLA_0}$$

Both CN_L and SLA_0 are PFT specific parameters.

Stomatal conductance in ELM is calculated based on a modification of the BWB model (Ball *et al.*, 1987, 1987; Equation 5.1), with the addition of a soil stress factor (Equation 5.12):

Equation 5.12. $$g_{\mathrm{sw}} = \left(\frac{A * h_s}{C_a / P_{atm}} * m\right) + b * \beta_t$$

where P_{atm} is the atmospheric pressure (Pa), h_s is the leaf surface humidity calculated as the vapor pressure at the leaf surface divided by the saturation vapor pressure inside the leaf at the measurement temperature, and β_t is a soil water stress function. It should be noted that in conditions when $\beta_t \leq 1$ it is also applied to V_{cmax} and R_d as a means of reducing A_n.

The soil water stress factor β_t is calculated across cumulative (1 to i) soil layers and is based on soil moisture content, and a set of PFT specific root distribution and stress response factors (Sellers *et al.*, 1996; Equation 5.13).

Equation 5.13. $$\beta_t = \sum_i w_i r_i$$

where w_i and r_i are the wilting factor and rooting fraction respectively for layer i. The wilting factor is calculated based on the soil matric potential (ψ_i, mm), the PFT specific soil water potential at which stomata are fully open (ψ_o, mm) and closed (ψ_c, mm) and the effective porosity of the soil based on the fraction of soil occupied by ice (Equation 5.14):

Equation 5.14. $$w_i = \begin{cases} \frac{\psi_c - \psi_i}{\psi_c - \psi_o}\left[\frac{\theta_{sat,i} - \theta_{ice,i}}{\theta_{sat,i}}\right] \leq 1 & \text{for } T_i > T_f - 2 \;\&\; \theta_{liq,i} > 0 \\ 0 & \text{for } T_i \leq T_f - 2 \; or \; \theta_{liq,i} \leq 0 \end{cases}$$

where θ_{sat}, θ_{ice}, and θ_{liq} are the proportion of saturated, frozen, and liquid water in the soil respectively, and T_i and T_f are the soil temperature of layer i and the freezing soil temperature

respectively. The fraction of root distributed to each soil layer is a function of the PFT specific parameter r_i (Equation 5.15):

Equation 5.15. $r_i =$

$$\begin{cases} 0.5\left[\exp\left(-r_a z_{h,i-1}\right) + \exp\left(-r_b z_{h,i-1}\right) - \exp\left(-r_a z_{h,i}\right) - \exp\left(-r_b z_{h,i}\right)\right] & \text{for } 1 \le i < N_{level} \\ 0.5\left[\exp\left(-r_a z_{h,i-1}\right) + \exp\left(-r_b z_{h,i-1}\right)\right] & \text{for } i = N_{level} \end{cases}$$

Where $z_{h,i}$ is the depth (m) from the ground surface to the depth at which layers i and $i + 1$ touch, and r_a and r_b are PFT specific root distribution parameters (Zeng, 2001).

Modifications to the Land Model Configuration

As originally conceptualized, the PFT specific photosynthetic and stomatal parameters used in ELM were chosen to broadly represent C3 and C4 vegetation types (Wullschleger *et al.*, 2014). However, this framework overgeneralizes the physiology of Arctic vegetation, and may lead to significant bias in model estimates of *E* and NPP (Dietze *et al.*, 2014; Jefferson *et al.*, 2017; Ricciuto *et al.*, 2018). To account for the unique physiology of the two Arctic PFTs in ELM, I reparameterized seven critical parameters used in ELM, based on previous literature and site observations across three Arctic sites (Table 5.2). Parameter adjustments for CN_L, and SLA_0 come from direct measurements of these foliar traits, collected in this study (see section "Study Sites and Measurements"), and in previous work across all NGEE-Arctic field sites (Rogers *et al.*, 2017b; Serbin *et al.*, 2023). Estimates for stomatal slope, stomatal intercept, and F_{LNR} were obtained from gas exchange measurements collected in this study (see section "Study Sites and Measurements"), and complemented with additional gas exchange collected between 2012-2019 (Rogers *et al.*, 2017a, 2020). Rooting parameters were modified from their nominal values based on data collected by (Iversen *et al.*, 2015) which reports the maximum rooting depth of several Arctic plant species. These new root parameters not only better represent Arctic specific PFTs, but also prevent the root depth distribution from extending below the simulated active layer.

Along with PFT specific parameter modifications, I also updated two model constants related to Rubisco stoichiometry, as recommended by Rogers, (2014). These constants were the specific activity of Rubisco at 25ºC (α_{R25} = 7.3 μmol CO_2 g^{-1} Rubisco s^{-1}) and the mass ratio of total Rubisco

molecular mass to nitrogen in Rubisco (F_{NR}= 6.22 g Rubisco g^{-1} N in Rubisco). Because the product of these parameters, along with N_a and F_{LNR} equal $V_{cmax.25}$ (Equation 5.10), it is also necessary to update the value of each PFT's F_{LNR} so that the model projected carbon flux is not affected by this stochiometric correction. To do this, I used the default PFT specific values of $V_{cmax.25}$ and N_a (itself derived from SLA_0 and C_{NL}; Equation 5.11), along with the updated α_{R25} and F_{NR}, rearranging Equation 5.10 to solve for corrected F_{LNR}. A full list of corrected F_{LNR} values can be found in Table A4.1. It should be noted that the values of corrected F_{LNR} are now higher than before, and in some cases (e.g., crop PFTs) now represent biologically unreasonable values. ELM sources its PFT specific values of $V_{cmax.25}$ from Kattge *et al*., (2009), which cites a single data source for crop PFT $V_{cmax.25}$ (n=9). It is likely that the crop PFT specific $V_{cmax.25}$ value from Kattge *et al*., (2009), when paired with an N_a value from a separate source (not specified in the ELM technical documentation), led to an improbably high F_{LNR}, which had previously been difficult to detect due to the incorrect α_{R25} and F_{NR} in ELM. While the F_{LNR} values for crop PFTs will not have any impact on the Arctic simulations carried out in this study, I none the less recommend that future work focus on evaluation of crop PFT $V_{cmax.25}$ and N_a, in a manner similar to the analysis presented in the section "Comparing observations to default ELM parameter values."

In addition to parameter modifications, I also tested three new applications of the soil water stress function (β_t) to the photosynthetic and stomatal model equations (Table A4.2). This included modifying the function so that β_t reduces stomatal slope rather than intercept, the removal of the β_t effect on V_{cmax} and R_d, and a combination of both of these effects. These modifications were chosen so that the impact of soil water stress on stomatal function would more closely approximate real world stomatal processes (Damour *et al.*, 2010; Duursma *et al.*, 2019), without fundamentally altering the equations used to simulate gas exchange in ELM.

Description of Model Simulations

All simulations were begun with 200 years of accelerated decomposition spin up, followed by 600 years of regular spinup (Thornton & Rosenbloom, 2005; Koven *et al.*, 2013), and a transient period from 1850-2014. To ensure proper mixing of soil nutrient pools, I examined model output during the regular spin up phase to ensure that carbon stocks were stable (< 3% disequilibrium of total ecosystem carbon; Fig. A4.1).

I conducted two different simulation experiments to test the effects of updated parameter

values and β_t formulations on model output (Table A4.2). For the first experiment, I ran 20 single member simulations (five per site), modifying a group of parameters at a time at each of the four NGEE-Arctic field sites (Fig. 5.1). The first four model simulations (MS-0) were baseline simulations using unmodified ELM parameter values. The next 12 simulations (MS-1, MS-2, and MS-3) were each run using modified photosynthetic (F_{LNR}, SLA_0, C_{NL}), stomatal (m and b), and rooting (r_a, and r_b) parameters respectively. The final four simulations in the first experiment (MS-4) included modified values for all seven parameters assessed in this study (m, b, SLA_0, F_{LNR}, C_{NL}, r_a, and r_b).

I next ran an ensemble simulation consisting of 1000 different combinations of the seven parameters modified during the single member model runs. These parameters were randomly drawn from distributions parameterized according to observations with their variance expanded to sample values outside of the observed parameter space (Table A4.3). These random samples were subsequently adjusted using Sobol' sequences to achieve a quasi-random distribution of data which evenly fills the parameter space (Fig. A4.2; Sobol', 1967). Then to assess the impact of each of the parameters on among ensemble member variance, I estimated the Sobol' first order indices for each of the seven parameters using a B-spline smoothing approach (Ratto & Pagano, 2010).

The second experiment was focused on the effect of the β_t parameter on E and NPP. This experiment consisted of three sets of four single member simulations (MS-5, MS-6, and MS-7) in which the function for applying the β_t parameter to the photosynthetic and stomatal equations was adjusted (Table A4.2).

Finally, I compared my various model outputs, to two different observational data sets as a means of benchmarking the effect of my modifications to ELM. The first of these datasets was comprised of the AmeriFlux FLUXNET data products from the Barrow (US-NGB; Torn & Dengel, 2021) and Council (US-NGC; Torn & Dengel, 2022) flux tower sites. Here I compared gross primary productivity (GPP; as partitioned using the “nighttime method”; Reichstein *et al.*, (2005), latent heat flux, and net ecosystem exchange (NEE) between the flux tower and the model. Because of a temporal mismatch between model projections (1850-2014) and flux tower observations (US-NGB: 2012-2017, US-NGC: 2015-2017) I chose to look at data aggregated by month thereby minimizing the effect of any given year’s meteorology on the comparisons. The second benchmark dataset was volumetric soil moisture content (SMC) from the ERA5-Land

reanalysis product (Muñoz Sabater, 2019). For this comparison, I restricted both datasets to the period between April 1st and September 30th for site years 2000-2014, averaging across years to arrive at a mean SMC for each day of the year.

5.4 – **Results:**

Difference in the estimated parameter values and ELM model defaults

Comparison between the parameter values measured as part of this study, and the default values used in ELM reveal large differences between model assumptions and field observations. Estimated stomatal slope for the BDBS and CAG PFTs were 7.9 and 4.2 respectively, values which are 11.2% and 53.4% lower than the default value of 9 used in ELM (Fig. 5.2a). As with stomatal slope, observed values for stomatal intercept were significantly different than the model assumption of 1000 μmol m^{-2} s^{-1} (Fig. 5.2b), with BDBS exceeding the default by 490% (59046 μmol m^{-2} s^{-1}), and CAG exceeding the default by 395% (49540 μmol m^{-2} s^{-1}).

For leaf structural traits, estimated SLA_0 for the BDBS and CAG PFTs were 0.023 and 0.032 m^2 g^{-1}, 21.9% lower and 9.4% higher respectively than the ELM default of 0.03 m^2 g^{-1} (Fig. 5.2e). Values of C_{NL} observed in this study were 17.1% (BDBS = 20.72 g C g^{-1} N) and 15.0% lower (CAG = 21.25 g C g^{-1} N) than the ELM default of 25 g C g^{-1} N (Fig. 2d). Finally, estimated F_{LNR} for CAG was identical to the ELM default value (0.1993 g N in rubisco g^{-1} N) while for BDBS it was 46.5% lower, at 0.1066 g N in rubisco g^{-1} N (Fig. 5.2c).

Variation in the parameter estimates explained by microclimate and leaf traits

To assess possible abiotic sources of within PFT variation in parameter estimates, I examined the linear relationships between the model parameters b, m, SLA_0, F_{LNR}, and C_{NL}, the foliar traits $g_{s\max}$, $V_{cmax.25}$, and $R_{dark.25}$, and four common microclimatic factors, SMC, thaw depth, elevation, and leaf surface temperature. For the analysis of microclimatic factors, I focused on the Seward Peninsula sites which exhibit strong spatial variation in topography, soil moisture, and active layer depth (Grosse *et al.*, 2011). I found that elevation, which, in an Arctic tundra ecosystem, is associated with multiple microclimatic factors such as slope, aspect, topographic wetness, and soil type, helped to explain between 20% and 39% of overall variation in stomatal traits (b, m, and $g_{s\max}$), while variation in SMC explained between 12% and 22% of variation in b and $R_{dark.25}$

respectively (Fig. 5.3). Observed variation in *b* was positively associated with elevation ($R^2 = 0.22$, $p < 0.001$; Fig. 5.3a) and negatively associated with SMC ($R^2 = 0.12$, $p = 0.002$; Fig. 5.3e). Among-sample variation in both *m* ($R^2 = 0.20$, $p < 0.001$; Fig. 5.3b) and $g_{s\max}$ ($R^2 = 0.39$, $p < 0.001$; Fig. 5.3c) were both positively associated with elevation. The only non-stomatal parameter whose variation could be explained by microclimate was $R_{dark.25}$ which was positively associated with soil moisture content ($R^2 = 0.22$, $p < 0.001$; Fig. 5.3d). Neither thaw depth nor leaf surface temperature helped to explain any significant variation in parameter estimates (not shown).

Next, I examined the linear relationships between different combinations of leaf traits and model parameters as a means of testing core model assumptions about trait relationships. I found that stomatal slope was positively associated with SLA_0 ($R^2 = 0.27$, $p < 0.001$; Fig. 5.3f), and was negatively associated with $R_{dark.25}$ ($R^2 = 0.40$, $p < 0.001$; Fig. 5.3g). Interestingly, neither the relationship between N_a and $V_{cmax.25}$ or the relationship between $R_{dark.25}$ and $V_{cmax.25}$ were significant (Fig. 5.3h&i). This was true both when all data were pooled, and when the relationship was examined for each PFT separately. ELM assumes that $R_{dark.25} = 0.015 * V_{cmax.25}$.

Impacts of revised parameter estimates on predictions of NPP and *E*

I next assessed how the updated parameter estimates would affect ELM simulations by comparing ELM run with modified parameters to a base case at each of the four NGEE-Arctic field sites (Fig. 5.4). Compared with the baseline simulation (MS-0), transpiration rates for the simulation with all seven parameters adjusted (MS-4) were between 16.9% (Teller) and 57.6% (Kougarok) higher than the base case at their respective sites (Fig. 5.4b). Of the parameters responsible for this effect, the increase in transpiration was clearly most strongly influenced by updated stomatal parameters (*m* and *b*). The ELM runs with only *m* and *b* modified showed comparably higher rates of g_{sw} (Fig. 5.5b), while for three of the four sites, the assimilation rate was less than or equal to the baseline (Fig. 5.5a). Interestingly, this apparent increase in the ratio of g_{sw}:A_n is opposite of what would be expected when the stomatal slope parameter is reduced, however the five to sixfold increase in stomatal intercept (Fig. 5.2b) is likely offsetting any increase in water use efficiency that would result from a reduced *m*. Modifications to the rooting parameters (*ra* and *rd*), also appeared to slightly increase *E*, most likely through a reduced soil moisture stress effect (Fig. 5.5d). This effect was particularly pronounced early in the growth season, and was larger at the Kougarok and Teller sites, which have thicker active layers and

experience lower overall soil moisture stress. Between the four sites, the effect of the foliar parameters alone on transpiration was highly variable, with updated F_{LNR}, C_{NL} and SLA_0 reducing E at Kougarok, and Teller, increasing E at the BEO, and resulting in no change at Council (Fig. 5.4b). These differences were likely due to the different PFT compositions of the four sites, with Kougarok and Teller having a higher relative abundance of BDBS. Reduced F_{LNR}, C_{NL} and SLA_0 for the BDBS PFT resulted in lower LAI (Fig. 5.5c), which reduced both assimilation and stomatal conductance per unit ground area (Fig. 5.5a&b).

At all four sites, modeled rates of NPP for the simulation with seven parameters adjusted were lower than the base case at each site (BEO = 5.6%, Council = 16.6%, Kougarok = 2.9%, Teller = 15.4%). Unlike E, which was strongly affected by the m and b parameters across all four sites, the drivers of this reduced NPP at each site appear to be more variable. At the BEO site, modification to F_{LNR}, C_{NL} and SLA_0 increased assimilation, $V_{cmax.25}$, and LAI while modification to m and b reduced assimilation and LAI and had no impact on $V_{cmax.25}$ (Fig. 5.5c&e). Like the BEO site, the Council site experienced increased assimilation and LAI when F_{LNR}, C_{NL} and SLA_0 were modified, however unlike the BEO site, modified m and b parameters led to an increased assimilation and no relative change to LAI (Fig. 5.5c). At both sites, modifications to the root parameters had minimal effect, other than a slightly reduced effect of β_t early and late in the growing season (Fig. 5.5d). At both the Kougarok and Teller sites, modifying F_{LNR}, C_{NL} and SLA_0 resulted in a strong reduction in NPP, the consequence of a drop in LAI and assimilation (Fig. 5.5a&c). In addition, modifications to the root parameters increased LAI, assimilation, and $V_{cmax.25}$, which resulted in a slightly increased NPP for these simulations (Fig. 5.5c&e).

Next, to quantify the influence of each parameter on model output, I ran an ensemble of 1000 simulations for each site, and performed a variance decomposition on the resulting output. For each ensemble member, values for m, b, F_{LNR}, C_{NL}, SLA_0, ra, and rd were randomly drawn from a quasi-random distribution of data, which evenly fills the parameter space, and approximates the distribution of observed values for each parameter (Fig. A4.2; Sobol', 1967). I then estimated the Sobol' first order indices for each of the seven parameters using a B-spline smoothing approach (Ratto & Pagano, 2010). The first order indices for the seven traits were capable of explaining just over half of variance in E (55.7-59.9%), while for NPP the seven parameters explained between half and a third (50.2-29.4%) of among model variance across all 1000 ensembles (Fig. 5.6a&b).

Variance in *E* among ensemble members was most heavily explained by variation in the F_{LNR} parameter (24.2-28.8%), followed by *b* (11.4-15.4%), *m* (9.0-11.0%), C_{NL} (3.0-7.4%), and SLA_0 (0.7-1.8%; Fig. 5.6a). Cumulatively, the rooting parameters *ra* and *rd* explained less than 1% of among ensemble variation in *E.* Unsurprisingly, variation in NPP among ensemble members was most dominated by variation in the photosynthetic and structural traits, with F_{LNR} explaining 25.5-39.7% of among ensemble variance in NPP, and C_{NL} explaining 2.0-8.7% of among ensemble variance in NPP (Fig. 5.6b). Stomatal traits had relatively limited explanatory power, 0.8-1.4% for *b* and 0.7-1.1% for *m*. Surprisingly SLA_0 explained less than 0.1% of among ensemble variance at each of the four sites, while *ra* and *rd* each explained less than 0.001% of among ensemble variance. For model predicted *E,* average among ensemble variance was 26%-206% higher than inter-annual (model years 2000 and 2014) variation while for NPP among ensemble variance was 21-142% higher (Fig. 5.6c&d).

Impacts of β_t function on predictions of NPP and *E*

In addition to the model simulations outline above, I also tested three alternative formulations for how the β_t was applied to the photosynthetic and stomatal equations (Equation 5.12, Table A4.2) and the resulting effects on model projections of *E* and NPP. In the first of these alternative formulations (MS-5), the direct effect of β_t on photosynthesis and respiration was removed, allowing for stomatal limitation on C_i to dictate the reduction in A_n expected under conditions of soil moisture stress (Fig. 5.7b). The second alternative model (MS-6) applies the effect of β_t to the stomatal slope parameter, rather than stomatal intercept, thus reducing *m* with increasing soil moisture stress (Fig. 5.7c). The final alternative function (MS-7) is a combination of the two previous approaches, removing the direct effect of β_t on photosynthesis and respiration, and applying the effect of β_t to *m* rather than *b* (Fig. 5.7d).

Across all four sites, the three alternative β_t functions resulted in a significant increase in cumulative annual *E*, as compared to the baseline formulation (Fig. 5.8b). However, within each site there was no significant among-model difference in predicted *E*. On average the three alternative β_t functions resulted in a flux of *E* which was 35.6% higher than the default model at the BEO, 35.2% higher at Council, 58.2% higher at Kougarok, and 16.2% higher at Teller. This increased *E* appears to be the result of increased stomatal conductance for the three alternative models (Fig. A4.3b), which either results from lower limitation on baseline conductance rates, as

is the case for the models which switch the effect of β_t to m (MS-6 and MS-7), or from higher assimilation potential when the β_t restriction on photosynthesis and respiration was removed (MS-5 and MS-7).

The effect of the three alternative β_t functions on NPP was much more variable than for E, both within and among sites (Fig. 5.8a). At the BEO, site MS-5 and MS-7 resulted in significantly higher NPP than the baseline (MS-4), while MS-6 slightly reduced NPP. This increased NPP for MS-5 and MS-7 likely stems directly from the higher assimilation potential when the β_t effect on $V_{c\max}$ is removed. At the Council site, which experiences the highest soil moisture stress of the three sites located on the Seward Peninsula (Fig. A4.4b) each of the three alternative β_t functions reduced NPP by 16.5-22.1% compared with the baseline. Likewise, at the Teller site, MS-5, MS-6, and MS-7 each reduced NPP by approximately 17.9%. A possible explanation for this unexpected drop in NPP may come from altered belowground dynamics, such as a higher soil moisture content at Teller (Fig. A4.4a) or lower soil organic nitrogen and carbon (Fig. A.4c&d), which may act in concert to limit assimilation. At Kougarok, the three alternative β_t functions had minimal effect on model projected NPP.

Model benchmarking

As a means of benchmarking the effect of the modifications to ELM, I compared ELM outputs to flux tower observations (Fig. 5.9 and 5.10) and a soil moisture reanalysis product (Fig. A4.5). At both the BEO and the Council site, model projected GPP substantially exceeded flux observations in May and June, and was substantially less than flux observations in April, August, and September (Fig. 5.9a and 5.10a). At both sites, July values of GPP were most similar between the model and flux tower observations. For latent heat flux (Fig. 5.9b and 5.10b), differences between model projections and observations, the BEO and Council sites exhibit contrasting trends. At the BEO site, model projected latent heat flux was less than flux observations in April and May, similar in June, and greater than flux observations in July, August, and September. By contrast at the Council site, model projected laten heat flux in April was less than flux observations, before exceeding it in May, June, and July, and having similar yet slightly lower values in August and September. When looking at NEE data (Fig. 5.9c and 5.10c), across all model parameterizations, ELM projections indicate that the land surface should act as a net carbon source in April, August, and September, while acting as a sink in May, June and July (Council only). However, flux tower

observations at the BEO indicate that the land surface is a net carbon sink from April through September, while at Council the land acts as a sink between April and August before becoming a source in September. Clearly, these results indicate that there is a substantial temporal mismatch between ELM projections and flux tower observations (Fig. 5.9 and 5.10). In addition, within-month difference between ELM projections and flux tower observations far exceeds the among-model variation introduced by updating parameter values and modifying the β_t function.

Next, I compared volumetric soil moisture data as simulated by ELM with the ERA5-Land reanalysis product (Muñoz Sabater, 2019; Fig. A4.5). Similar to the flux tower comparison, I see a major temporal mismatch between model projections of SMC and reanalysis data, specifically at the three Seward Peninsula sites. At all three of these sites, model simulated SMC is at its lowest point around DOY 160, which is when the ERA5 data suggest that SMC should reach its maximum value (Fig. A4.5b-d). Unlike the flux tower comparisons, among ELM model variation in projected SMC is of a similar magnitude to the difference between ELM and ERA5 data for the Council and Kougarok sites. At the BEO site, ELM projected SMC is substantially (~24%) lower than the ERA5 SMC, and exhibits a slight temporal mismatch with peak seasonal SMC in ELM occurring around DOY 110, while peak season SMC for the ERA5 data occurs around DOY 150 (Fig. A4.5a). At the Teller site, ELM projected SMC is substantially (~80%) higher than the ERA5 SMC.

5.5 – **Discussion:**

Within the land surface modeling community, it is recognized that the utility and predictive accuracy of a model is only as good as the assumptions made when determining its parameter values (Fisher & Koven, 2020). These limitations become increasingly more apparent in the Arctic, where historically trait observations have been limited (Rogers *et al.*, 2022), and the distinctive diversity and assemblage of plant functional groups leads to unique interactions between cycles of nutrients, water, carbon, and energy not observed in temperate or tropical zones (Chapin *et al.*, 1996; Wullschleger *et al.*, 2014; Bjorkman *et al.*, 2018; Thomas *et al.*, 2019). In this study I attempt to rectify some of the shortcomings in ELM's parametrization of vegetation traits related to carbon and water exchange by estimating new parameter values, and testing the impact of the revised parameterizations on model outputs. I demonstrate that there are large

discrepancies between the Arctic default gas exchange parameters, which ELM largely inherited from a generic woody C_3 PFT (Oleson *et al.*, 2013), and parameters estimated from field observations (Fig. 5.2). In particular, the stomatal parameters *b* and *m* were 395-490% higher and 11.2-53.4% lower than their respective ELM defaults. I also show that the observed variation in some parameters appears to be associated with microclimatic factors (Fig. 5.3a-e), in particular elevation and soil moisture content, which explain between 20% and 39% of overall variation in stomatal traits. When parameter values were updated to reflect field observations, modeled NPP was 2.9%-15.4% lower, and *E* was 6.9%-57.6% higher than the base case at each site (Fig. 5.4a-b), suggesting that as currently parameterized, ELM overestimates the water use efficiency of Arctic vegetation (Fig. 5.11). Further, when the β_t function, which governs the gas exchange response to soil moisture stress, was modified to more realistically account for the impact of water stress on leaf gas exchange (Fig. 5.7), NPP was further reduced at two of the four sites, while *E* was increased across all four sites (Fig. 5.8). Variance decomposition of an ensemble of 1000 model runs indicated uncertainty in F_{LNR} explains the plurality of among ensemble variation in both *E* and NPP, with the stomatal traits *b* and *m* explaining the next most variation in *E*, and C_{NL} explaining the next most variation in NPP (Fig. 5.6). Finally, when compared to flux tower and reanalysis derived benchmark datasets (Fig. 5.9, 5.10, and A4.5), modifications to ELM appear to contribute less to overall model error than the overall disconnect between the model and seasonality.

Comparing observations to default ELM parameter values

The disparity between model default parameter values and those measured in this study not only highlights the unique physiology of high latitude vegetation (Van De Weg *et al.*, 2013; Rogers *et al.*, 2017d), but also underscores the knowledge gap in physiological ecology between temperate and Arctic species (Rogers *et al.*, 2022). Traditionally, across both modeling and physiology literature, stomatal intercept is frequently assumed as zero or another small value (Duursma *et al.*, 2019), and as such often not considered to be of physiological importance because it constitutes such a small percentage of total stomatal conductance (Šantrůček *et al.*, 2004). However, by measuring the full response of stomatal conductance to changes in irradiance above and below the light compensation point, I can observe actual daytime rates of g_{sw} at the intercept, indicating that

for the two Arctic PFTs *b* is between four and five-fold higher than the model default of 1000 μmol m^{-2} s^{-1} (Fig. 5.2b). Previous studies have challenged the biological interpretation of the stomatal intercept, suggesting that as used in models it is a fitting artifact rather than a real biophysical parameter (De Kauwe *et al.*, 2015a,b). While *b* is not predicted by optimality theory (Cowan & Fraquhar, 1977) it nonetheless represents a true biophysical parameter with a mechanism similar to minimum conductance, the lower bound of the possible range of g_{sw} - (Duursma *et al.*, 2019) representing water loss both from the cuticular pathway (Márquez *et al.*, 2021, 2022), and from incomplete stomatal closure (Machado *et al.*, 2021) when A_n is zero or VPD is high. The elevated stomatal intercept of Arctic vegetation may play an adaptive role in maintaining leaf energy balance, as has been observed in temperate species experiencing heat stress (Schuster *et al.*, 2016; Drake *et al.*, 2018). Previous studies of Arctic vegetation have revealed substantial thermoregulatory capacity of tall shrubs (Myers-Smith *et al.*, 2011b; Bring *et al.*, 2016; Yang *et al.*, 2021), which may be aided by elevated baseline rates of stomatal conductance. Alternatively, the long photoperiod experienced by Arctic vegetation, in concert with low VPD and high soil water availability, may have led Arctic vegetation to evolve comparably poorer control of stomata at low light and high VPD conditions (Anfodillo *et al.*, 2002; Fernández *et al.*, 2017). The interplay between stomatal slope and intercept is also notable. Observed stomatal slope was significantly lower than the ELM default value (Fig. 5.2a), which is typically considered to be indicative of a higher leaf-level WUE (Ball *et al.*, 1987; Medlyn *et al.*, 2011). However, when this lower slope is combined with the significantly elevated stomatal intercept of Arctic vegetation, the expected ratio of *E* to *A* is higher (lower WUE) than the model default across part, or all, of the range of the relationship (Fig. A4.6).

Observed leaf structural and biochemical parameters were closer than stomatal traits to ELM default values. Notably, observed F_{LNR} for the CAG PFT was identical to the model default, despite previous reports that Arctic vegetation may have an apparent F_{LNR} 2-3x higher than what is prescribed by some LSMs (Rogers *et al.*, 2017d; Fig. 5.2c). While some species measured in this study exhibited higher than expected $V_{cmax.25}$ (which along with C_{NL} and SLA_0 is used to calculate F_{LNR}; Equation 5.10 & 5.11; Table 5.1), when aggregated by PFT the resulting F_{LNR} estimate matched the default, as corrected using updated values for α_{R25} and F_{NR} (Rogers, 2014; Table A4.1). Observed F_{LNR} for the BDBS PFT corresponded well with previous estimates made on other

Arctic shrub species (Bubier *et al.*, 2011; Van De Weg *et al.*, 2013), indicating that as currently parameterized, ELM is overestimating the contribution of foliar N to Rubisco for this PFT. Estimates for SLA_0 and C_{NL} also agreed well with previous literature (Rogers *et al.*, 2017d; Sulman *et al.*, 2021) and, in contrast with F_{LNR}, within-PFT variation for these parameters appears to be more limited (Fig. 5.2c-d).

Relationships between microclimate, leaf traits, and parameter estimates

The data reveal a positive relationship between three stomatal traits and elevation, which is robust within all three shrub species studied (Fig. 5.3 a-c). Previous work assessing factors that contribute to Arctic plant range expansion have identified topographic conditions (elevation and slope) as critical determinants of shrub distribution (Ropars & Boudreau, 2012; Tape *et al.*, 2012; Mekonnen *et al.*, 2021; Yang *et al.*, *in prep*) in particular with *Alnus* and *Salix* genera occupying distinctive elevational bands. *Alnus* is more structured by elevation than *Salix*, as it is able to occupy rocky, more nutrient poor soils as the result of a symbiotic relationship with N-fixing bacteria (Salmon *et al.*, 2019; Chen *et al.*, 2020). In my field measurements, *Alnus* shrubs were located in two distinct elevational bands at the Kougarok site, with taller upslope individuals rooted in drier more rocky soils, and lower stature "savannah" individuals rooted among wet tussocks (Salmon *et al.*, 2019; Sulman *et al.*, 2021). Interestingly, the higher elevation *Alnus* shrubs have a higher stomatal slope, intercept, and $g_{s\max}$ (Fig. 5.3a-c), suggesting that even though they are in drier soils, they have a lower water use efficiency than the lowland savannah *Alnus* shrubs. While I did not observe any significant relationships between canopy temperature and stomatal traits for these individuals, this higher baseline rate of water release may be adaptative as a thermoregulatory mechanism to prevent overheating and keep these taller, more exposed shrubs within their optimal temperature range for photosynthesis (Michaletz *et al.*, 2015, 2016; Fauset *et al.*, 2018). At the Teller site, the relationship between SMC and elevation is less apparent, with *Salix* communities occurring in long interconnected patches, which often span a larger range of elevation. Clearly more work is needed to understand the interplay between elevation and related abiotic factors, such as permafrost depth, snow distribution, and disturbances, however this finding of a link between elevation and within and among species stomatal traits strengthens the argument that elevation, and other correlated microclimatic variables, are an important determinant of Arctic shrub distribution.

The implication of the relationship between SMC and stomatal intercept is also intriguing. While it has long been known that soil moisture stress will reduce stomatal conductance (Meidner & Mansfield, 1968; Wong *et al.*, 1979), universal relationships between drought stress and *b* or minimum stomatal conductance ($g_{sw\min}$) remain elusive (Drake *et al.*, 2018; Duursma *et al.*, 2019; Cavender-Bares *et al.*, 2020). From an optimal water use prospective (e.g., Cowan & Fraquhar, 1977; Cowan, 1978; Hari *et al.*, 1986; Buckley, 2020) any stomatal flux at *b* is considered wasted water, as it yields no compensatory carbon gain, and thus the stomatal intercept is seen as a consequence of incomplete stomatal closure rather than an active component of stomatal regulation. However, this discounts the role that stomata play in both leaf thermoregulation (Michaletz *et al.*, 2015, 2016) and maintenance of tension within the xylem to enable water transport (Tyree & Sperry, 1989). The negative relationship I observe here between SMC and stomatal intercept (Fig. 5.3e) may thus be a consequence of variation in stomatal anatomy or some other non-regulatory stomatal trait, rather than an adaptation of individuals in wetter soil toward more conservative stomatal control. It is also interesting to note that the negative relationship between SMC and stomatal intercept I observe is opposite of how the β_t function restricts g_{sw}. β_t decreases with increasing moisture stress reducing *b* and thus the overall calculation of stomatal conductance.

In addition to its relationship with environmental variables I also found that variation in *m* was associated with SLA_0 and $R_{dark.25}$ (Fig. 5.2f-g) suggestive of the fact that leaves with a higher resource investment (Wright *et al.*, 2004) should be more conservative in their WUE. While there is limited data to drawn comparisons with from the Arctic, the same association between stomatal slope and leaf resource investment has been observed in tropical systems (Wu *et al.*, 2019b; Lamour *et al.*, 2022). Further, I found no relationship between N_a and $V_{c\max.25}$ (Fig. 5.3h). At the global scale, N_a and $V_{c\max.25}$ are strongly associated, which has led some LSMs to calculate PFT-specific $V_{c\max.25}$ or F_{LNR} from their linear relationship with N_a (Medlyn *et al.*, 1999; Kattge *et al.*, 2009; Walker *et al.*, 2014; Luo *et al.*, 2021). At the local scale, these relationships may not be stable, as other nutrients, such as phosphorous may limit productivity more than nitrogen (Feng & Dietze, 2013; Ali *et al.*, 2015; Croft *et al.*, 2017), however, it remains to be determined if phosphorous is a limiting resource across the Arctic. Finally, I observed that $R_{dark.25}$ was not significantly associated with $V_{c\max.25}$ (Fig. 5.2i), in contrast to the ELM assumption that $R_{dark.25}$

should be 1.5% of $V_{cmax.25}$ (Oleson *et al.*, 2013). This finding agrees with other previous studies of non-Arctic vegetation, where the association between $R_{dark.25}$ and $V_{cmax.25}$ was not stable across the growth season (Davidson *et al.*, 2023a), along gradients of canopy depth (Souza *et al.*, 2021; Lamour *et al.*, 2023d), or among species with variation in wood density (Lamour *et al.,* 2023b). Further efforts to develop associations between leaf traits and model parameters will be essential for mapping within-PFT parameter variation across the landscape (Šantrůček *et al.*, 2004; Duursma *et al.*, 2019; Langford *et al.*, 2019; Yang *et al.*, 2021) or when estimating parameters for new Arctic PFTs (Sulman *et al.*, 2021).

Modifications to ELM: impact on ecosystem scale water and carbon cycles

When ELM parameters related to leaf gas exchange are updated to reflect field observations, projected ecosystem scale WUE (above ground NPP/E) is significantly reduced at all four sites (Fig. 5.11). Likewise, use of alternative β_t functions further moderately reduces ecosystem WUE at all sites except for the BEO site where two of the β_t functions led to an increase in ecosystem WUE. These declines in ecosystem WUE are primarily the result of a significant increase in simulated rates of transpiration, in conjunction with a small reduction in simulated NPP (Fig. 5.4 and 5.8). Interestingly, at the leaf scale, field observations suggest that by default ELM should underestimate WUE, as the observed stomatal slope is less than the default value for both BDBS and ACG PFTs (Fig. 5.2a). However, the 390-490% increase in the stomatal intercept observed in this study (Fig. 5.2b), suggests that the base rate of vegetative water loss in the Arctic is significantly higher than previously estimated, leading to a lower overall ecosystem scale WUE. The relatively minor changes in ecosystem scale WUE resulting from the alternative β_t functions at the Kougarok and Teller sites are reflective of the overall lower soil moisture stress at those sites, while at the BEO and Council sites, soil moisture stress has the potential to reduce assimilation and transpiration by 70 and 25% respectively (Fig 5.8). The removal of this substantial reduction in assimilation capacity in two of the three β_t functions results in a strong increase in above ground NPP at the BEO site, and thus concomitant increase in ecosystem WUE.

This altered WUE could have important consequences on long term projections of modelled vegetation function at local to global scales. Within the Arctic, a decrease in ecosystem WUE could lead to a greater drought or thermal stress vulnerability (Beck & Goetz, 2012; Zona *et al.*, 2014; Lu *et al.*, 2022), particularly for species and functional groups adapted toward more

anisohydric stomatal behavior (Sade *et al.*, 2012), which may lead to a dynamic restructuring of vegetation composition, particularly across landscapes with gradients in soil water availability (Bring *et al.*, 2016; Black *et al.*, 2021). In addition, increased transpiration would likely have major impacts on surface and subsurface hydrology (Troch *et al.*, 2009; Lique *et al.*, 2016; Knauer *et al.*, 2017). An Arctic ecosystem with a significantly increased latent heat flux could also affect global patterns of surface cooling, and heatwave development in previously unforeseen ways (Kala *et al.*, 2016).

Recently, using a combination of eddy flux and soil moisture data, Zona *et al.*, (2022) showed that physiological limitations induced by soil water deficits may limit peak vegetation productivity in the Arctic, however current LSM configurations may not capture this decline (Le Roux *et al.*, 2013; Gonsamo *et al.*, 2019; Feng *et al.*, 2021). Further model modifications, beyond the three alternative β_t functions tested in this study, will be necessary for the effect of soil moisture stress to appropriately propagated to ELM. Additional improvement of the β_t function could come from an Arctic specific parametrization of the ψ_o and ψ_c parameters, which represent the soil matric potential at which stomata should be fully open and fully closed (Equation 5.14). Like the *m* and *b* parameters, the default ψ_o and ψ_c used in ELM come from generic C3 PFTs (Sellers *et al.*, 1996; Oleson *et al.*, 2013), thus representing an obvious avenue for model improvement. Alternatively, the β_t function could be replaced by a hydrodynamic model (e.g., Xu *et al.*, 2016; Christoffersen *et al.*, 2016; Kennedy *et al.*, 2019) that explicitly represents the flux of water from the soil to the atmosphere through various plant tissues. Hydrodynamic models also have the potential to better represent differences in PFT specific root and xylem architecture, such as the ability of shrubs to access water in deeper soil layers (Cahoon *et al.*, 2016), and hydraulicly redistribute this water into shallower layers where it may be accessed by graminoids (Prieto *et al.*, 2012). While hydrodynamic models have seen limited application in the Arctic and face limitations in how they represent the physiological changes associated with frost tolerance (Lambert *et al.*, 2022), they none the less represent an enticing path forward for future Arctic specific model development.

Model validation and variance decomposition

Using variance decomposition of an ensemble of 1000 simulations at each site, I was able to quantify the contribution of each of the seven measured parameter to model uncertainty (Fig. 5.6).

Across all four sites the F_{LNR} parameter contributed to the largest proportion of variance in both E and NPP. While it is expected that F_{LNR} would have a strong influence on NPP through its association with carboxylation capacity, the finding that F_{LNR} explained a larger amount of among ensemble variation in E than either of the two stomatal parameters is surprising. While assimilation capacity plays a role in determining g_{sw} and therefore E, variation in the stomatal parameters, especially the stomatal slope parameter, would be expected to manifest in larger variation in E (Dietze *et al.*, 2014; Rogers *et al.*, 2017c). However, given that these estimates of proportion of variance explained are first order, univariate estimates (Ratto & Pagano, 2010), they may mask the overall uncertainty contributed by stomatal parameters in conjunction with other parameters examined. This analysis also demonstrates that model sensitivity to a parameter, in conjunction with its prior uncertainty determines the importance of a variable. For example, SLA_0, which has impacts on LAI and N_a (Fisher *et al.*, 2019) and thus is expected to contribute to a significant proportion of model variance in NPP, explained < 1% of variance in each site (Fig. 5.7). This may be due in part to the low prior uncertainty in SLA_0 (Fig. 5.2e), that, when propagated to the ensembles, limits its contribution to overall uncertainty. However, it is important to note that using prior uncertainty alone to estimate parameter importance may lead to incorrect conclusions (LeBauer *et al.*, 2013). Future efforts to estimate model variance due to novel parameters should focus on data assimilation approaches (Luo *et al.*, 2011; Liu *et al.*, 2021), which will allow researchers to limit parameter space via the use of informed priors, thus ensuring ecologically feasible ranges of parameters are considered (Beven & Freer, 2001). Likewise, multivariate relationships between parameters (e.g., Fig. 5.3f-g) can be explicitly considered to more appropriately approximate real world parameter interactions.

When the results of the modifications to ELM are compared to model benchmarks from flux tower data, I see that among model differences in GPP, latent heat flux, and NEE are relatively small compared to the differences between the model and field observations (Fig. 5.9 and 5.10). In particular, I observe a substantial asynchrony in both the magnitude and timing of ecosystem carbon and water fluxes, with ELM simulating a substantially more peaked response of early season productivity before a more rapid decline in the fall (Fig. 5.9a and 5.10). This disconnect between the model and observations may be due to incorrect temperature response functions applied to the photosynthetic model (Rogers *et al.*, 2017d), or may be due to an incorrect

phenology scheme regulating spring leaf expansion and decline after the solstice (Schwartz & others, 2003; Myers-Smith *et al.*, 2020). The use of temperature response functions derived from temperate vegetation types may bias the calculation of temperature specific model parameters, such as apparent $V_{c\max}$, and could lead to unrealistically high GPP early in the season when $V_{c\max}$ is expected to peak (Oleson *et al.*, 2013; Fig. A4.3a). Likewise, ELM uses a seasonal-deciduous phenology algorithm, based on accumulated growing-degree-days (GDD; White *et al.*, 1997), which regulates timing and magnitude of fluxes between carbon and nitrogen storage, transfer, and flux pools. This scheme, which only considers the effect of air temperature, may be inadequate to represent the complex contributions of snowmelt, soil temperature, and the insulating capacity of snow to the timing of spring leaf flush (Kelsey *et al.*, 2021). In addition, recent evidence from across the Alaskan tundra suggests that a modified GDD model which includes a maximum temperature threshold that best represent the phenology of tundra species (Elmendorf & Hollister, 2023).

Data from remote sensing platforms has the capacity to better constrain ELM representation of temperature response of photosynthesis and the dynamics impacting leaf phenology across the Arctic (Yang *et al.*, 2022). The use of satellite derived solar-induced chlorophyll fluorescence data as a proxy for GPP may allow for seasonal tracking of trends in apparent $V_{c\max}$, which could help to inform temperature response functions (Chen *et al.*, 2023). Similarly, high temporal and spatial resolution data derived from uncrewed areal systems may prove essential from understanding the complex environmental contributions to the timing and onset of leaf flushing and senescence (Assmann *et al.*, 2020).

Conclusions:

In this study, I used field derived observations, collected at three sites across the Alaskan Arctic, to update PFT specific parameters related to leaf-level gas exchange and biochemistry. These updated parameters resulted in a significant decrease in ecosystem scale WUE, brought about mainly by a substantial increase in predicted transpiration. When observed variance in parameters was propagated to an ensemble of models, uncertainty in F_{LNR} led to the most among model variance in both E and NPP, suggesting that more work should be done to constrain this critical parameter in Arctic vegetation. Further, when updated ELM predictions were compared

with flux tower observations, a substantial mismatch in seasonality of GPP, latent heat flux, and NEE was observed. Clearly, more effort will be needed to improve ELM representation of Arctic plant physiology, particularly with respect to the seasonal timing of phenology, and better constraint of Arctic specific temperature responses.

5.6 – **Figures:**

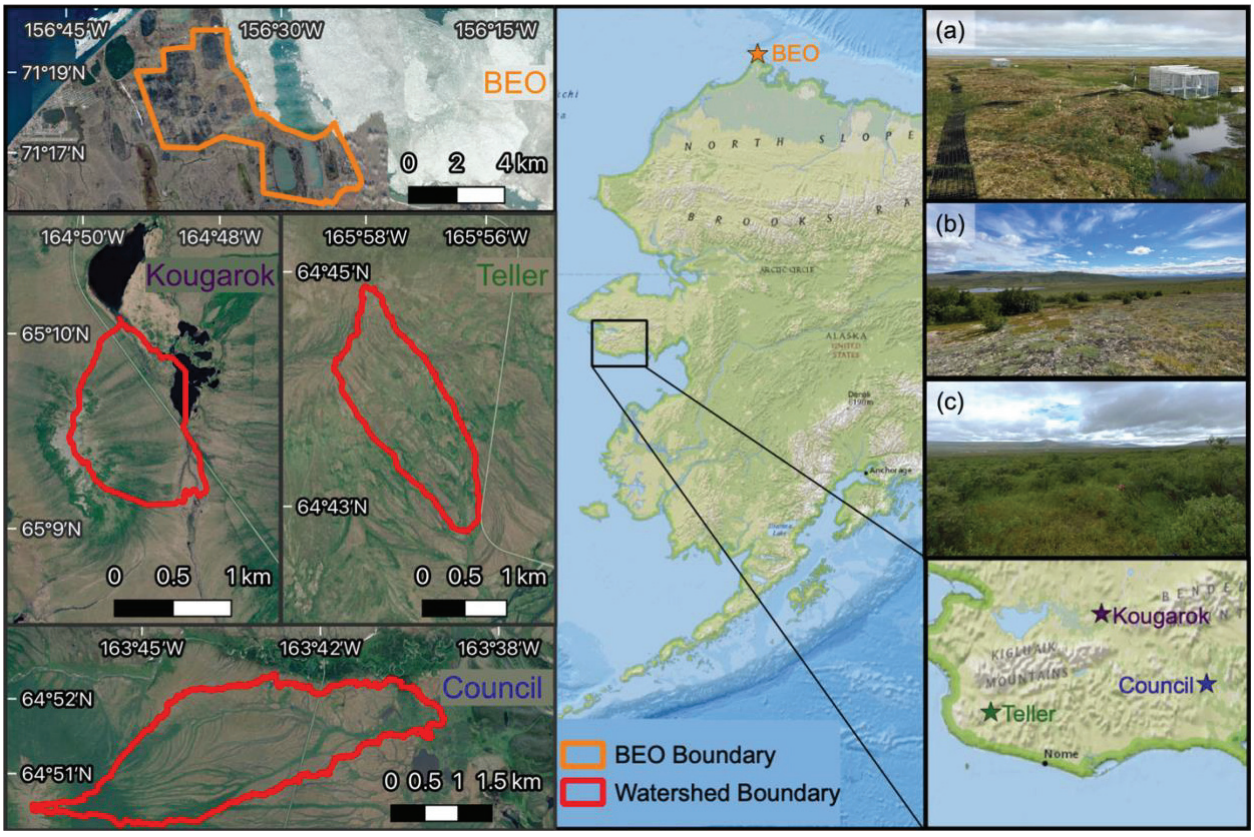

Figure 5.1: Map of the four Next Generation Ecosystem Experiment- Arctic sites in Alaska, USA. The Kougarok, Teller, and Council sites are all located on the Seward Peninsula, while the BEO site is located above the Arctic Circle in Utqiaġvik. Inset (a), northward view across the BEO illustrating the polygonal tundra landscape and low stature vegetation. Inset (b), eastward view across the Kougarok watershed, with tall upslope *Alnus* shrubs in the foreground. Inset (c), southward view across the Teller watershed with lines of medium stature *Alnus* shrubs flanking the view. Satellite imagery obtained from Alaska Imagery GeoPortal. Basemap imagery obtained from ESRI and National Geographic.

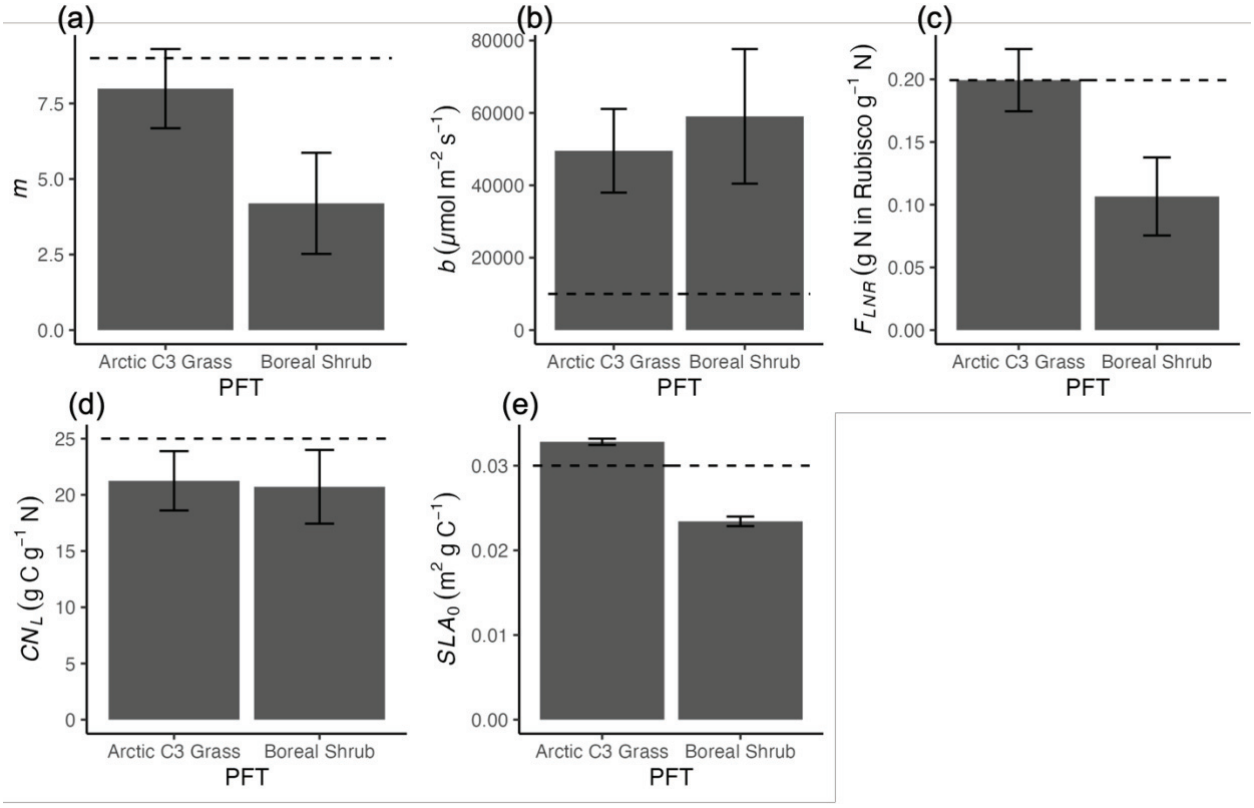

Figure 5.2: Comparison of ELM default (dashed lines) and observed parameter values (grey bars) for Arctic C_3 grass and broadleaf deciduous boreal shrub plant functional types. (a) stomatal slope (unitless; m), (b) stomatal intercept (μmol m^{-2} s^{-1}; b), (c) fraction of leaf nitrogen in rubisco (g N in rubisco g^{-1} N; F_{LNR}), (d) leaf carbon-to-nitrogen ratio (g C g^{-1} N; CN_L) and (e) top of canopy specific leaf area (m^2 g^{-1}; SLA_0). Dashed lies are ELM defaults, while grey bars are mixed model estimates from PFT-specific parameters accounting for species as a random factor. Error bars are ± 2 SE (n=62 and 68 see Table 1 for further details).

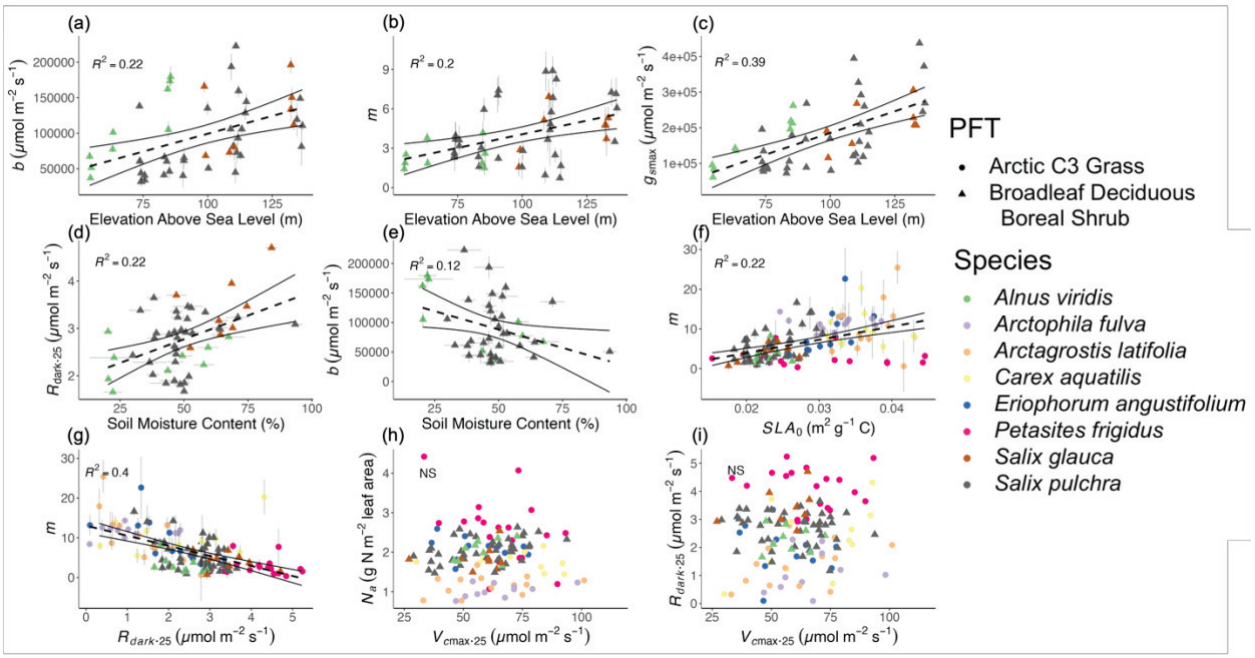

Figure 5.3: Relationships between leaf traits, microclimatic conditions, and ELM parameter estimates obtained in this study. Trait x environment relationships include (a) stomatal intercept (µmol m^{-2} s^{-1}; *b*), (b) stomatal slope (unitless; *m*), and (c) maximum stomatal conductance (µmol m^{-2} s^{-1}; g_{smax}), versus elevation above sea level, a stand in for other associated microclimatic variables, and (d) dark respiration rate normalized to 25°C (µmol m^{-2} s^{-1}; $R_{dark.25}$), and (e) *b* versus mean soil moisture content. Trait x trait relationships include *m* as a function of (f) top of canopy specific leaf area (m^2 g^{-1}; SLA_0), and (g) $R_{dark.25}$, and (h) area-based leaf nitrogen concentration (g N m^{-2} leaf area; N_a) and (i) $R_{dark.25}$ as a function of the maximum carboxylation capacity of the enzyme rubisco normalized to 25°C (µmol m^{-2} s^{-1} ;$V_{cmax.25}$). Dashed lines are the lines of best fit for the linear model (y~x) and black lines are the 95% confidence interval for the estimate. Relationships in panels a-g are significant ($p < 0.001$). Error bars around each point represent ± 2 SE of the estimate.

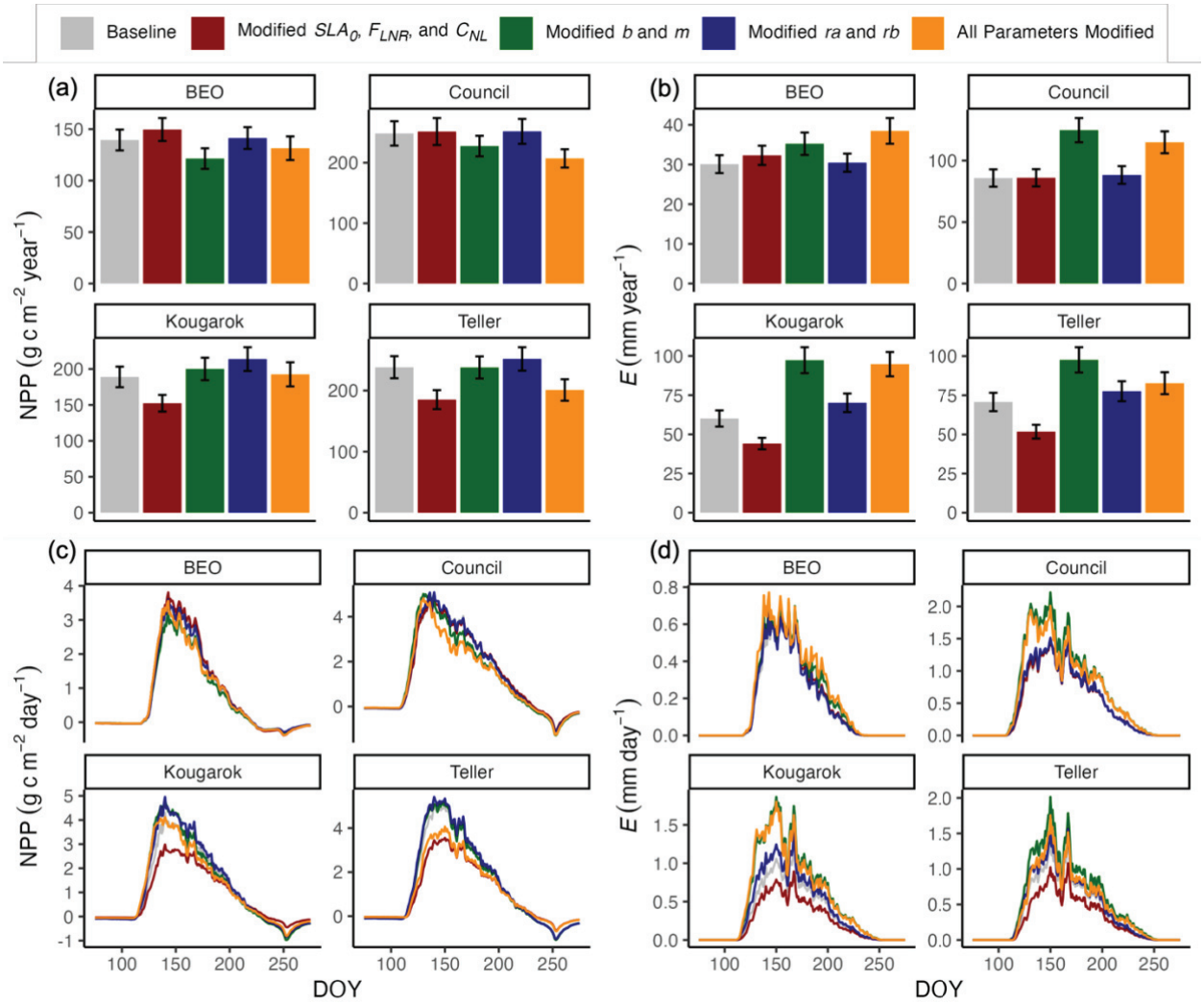

Figure 5.4: Comparison of predicted ecosystem carbon and water fluxes between simulations in which different combinations of parameters were modified to correspond with field observations. Upper panels depict average cumulative annual (a) net primary productivity (g C m^{-2} year^{-1}; NPP) and (b) vegetative transpiration (mm year^{-1}; E) over the period from 1850 to 2014. Lower panels depict average daily (c) NPP and (d) E, from DOY 75-275. Data in grey represent the model with no modifications (MS-0), data in red are simulations in which the fraction of leaf nitrogen in rubisco (F_{LNR}), the leaf carbon-to-nitrogen ratio (CN_L) and the top of canopy specific leaf area (SLA_0) have been modified (MS-1), data in green are simulations in which the stomatal slope (m) and intercept (b) have been modified (MS-2), data in blue are simulations in which the root depth distribution parameters (ra and rb) have been modified (MS-3), and data in orange are simulations in all seven parameters were modified (MS-4). Each subpanel represents one of the simulations sites. Error bars for the upper panels represent ± 2 SE of the mean annual value.

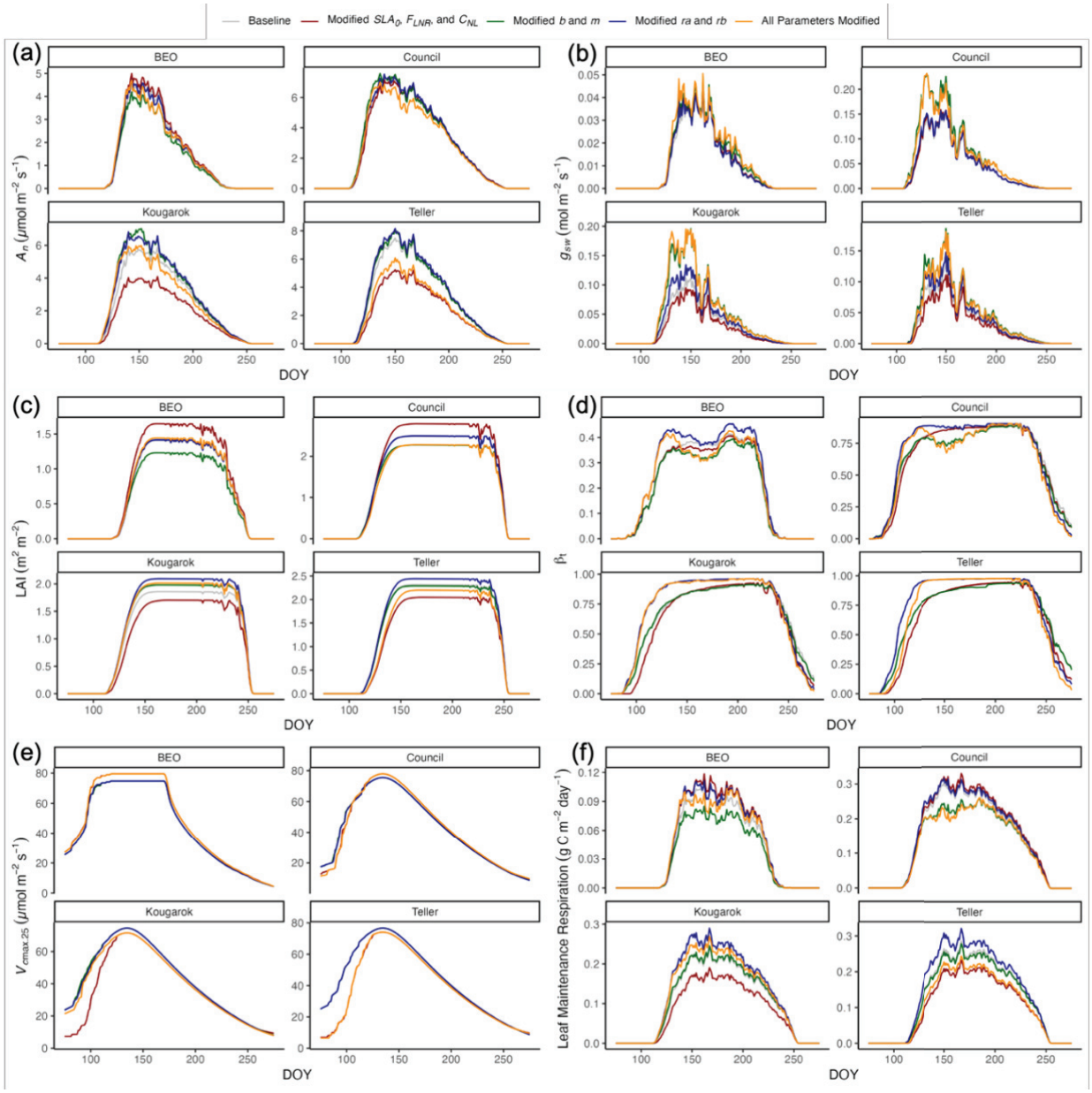

Figure 5.5: Comparison of mean annual response for simulations in which different combinations of parameters were modified to correspond with field observations. Average daily (a) photosynthetic carbon assimilation (µmol m^{-2} s^{-1}; A_n), (b) stomatal conductance (mol m^{-2} s^{-1}; g_s), (c) leaf area index (m^2 m^{-2}; LAI), (d) soil moisture stress factor (unitless; β_t), (e) maximum carboxylation capacity of the enzyme rubisco normalized to 25°C (µmol m^{-2} s^{-1} ;$V_{cmax.25}$) and (f) leaf maintenance respiration (g C m^{-2} day^{-1}). Averages for each day of the year were taken over the period from 1850 to 2014. Data in grey represent the model with no modifications, data in red are simulations in which the fraction of leaf nitrogen in rubisco (F_{LNR}), the leaf carbon-to-nitrogen ratio (CN_L) and the top of canopy specific leaf area (SLA_0) have been modified, data in green are simulations in which the stomatal slope (m) and intercept (b) have been modified, data in blue are simulations in which the root depth distribution parameters (ra and rb) have been modified, and data in orange are simulations in all seven parameters were modified. Each subpanel represents one of the simulations sites.

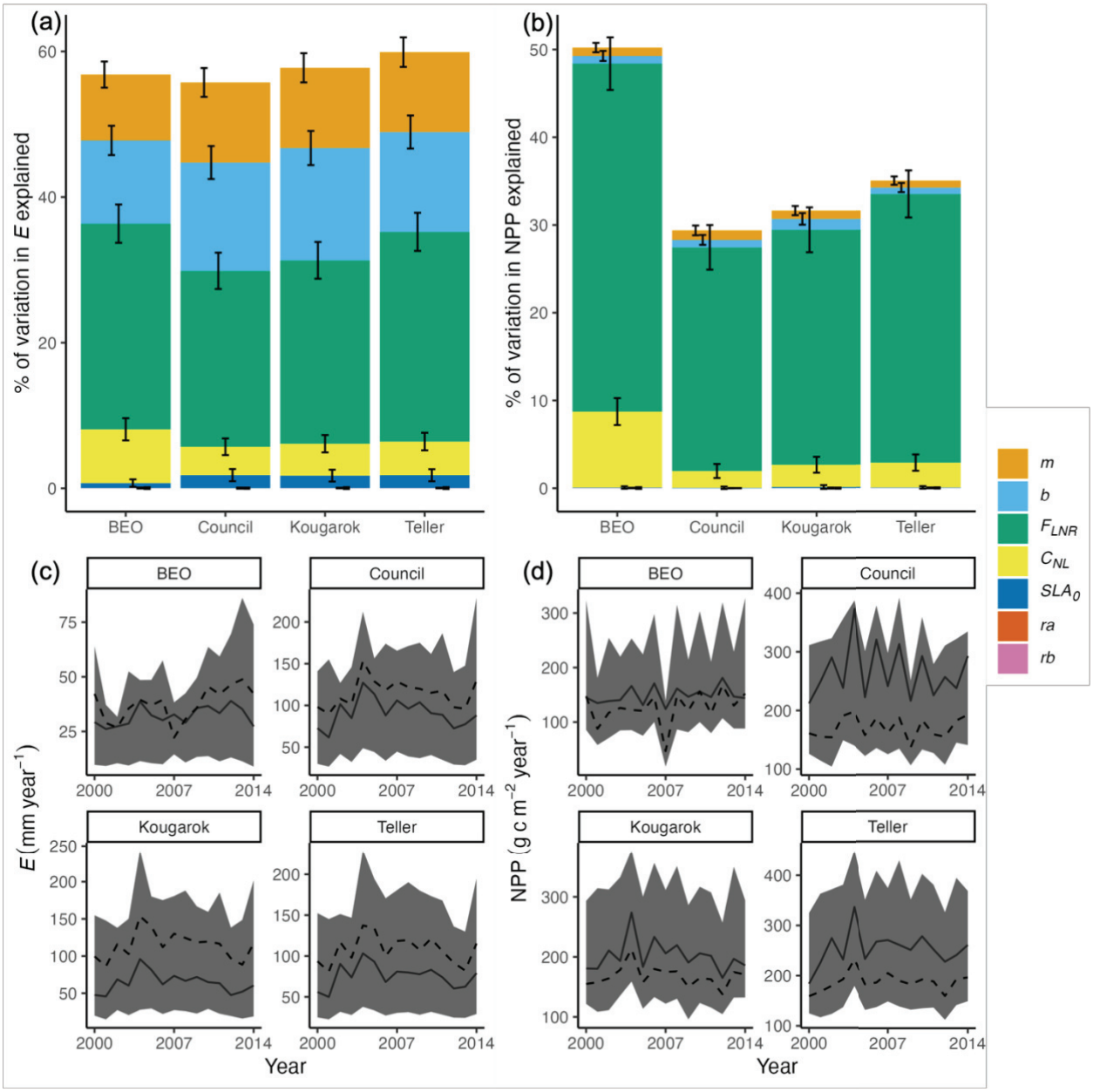

Figure 5.6: Parameter variance decomposition based on an ensemble of 1000 simulations for each site. Percent variance in (a) transpiration and (b) NPP explained by the first order Sobal' indices for each of the seven parameters modified in the study. Error bars represent the 95% confidence interval of the estimate. Interannual variation in (c) transpiration and (d) NPP among the ensembles. Solid line represents the mean of the 1000 ensembles, grey shroud represents the middle 95% quartile, and the dashed line represents the model prediction with parameters updated to reflect observations (MS-4).

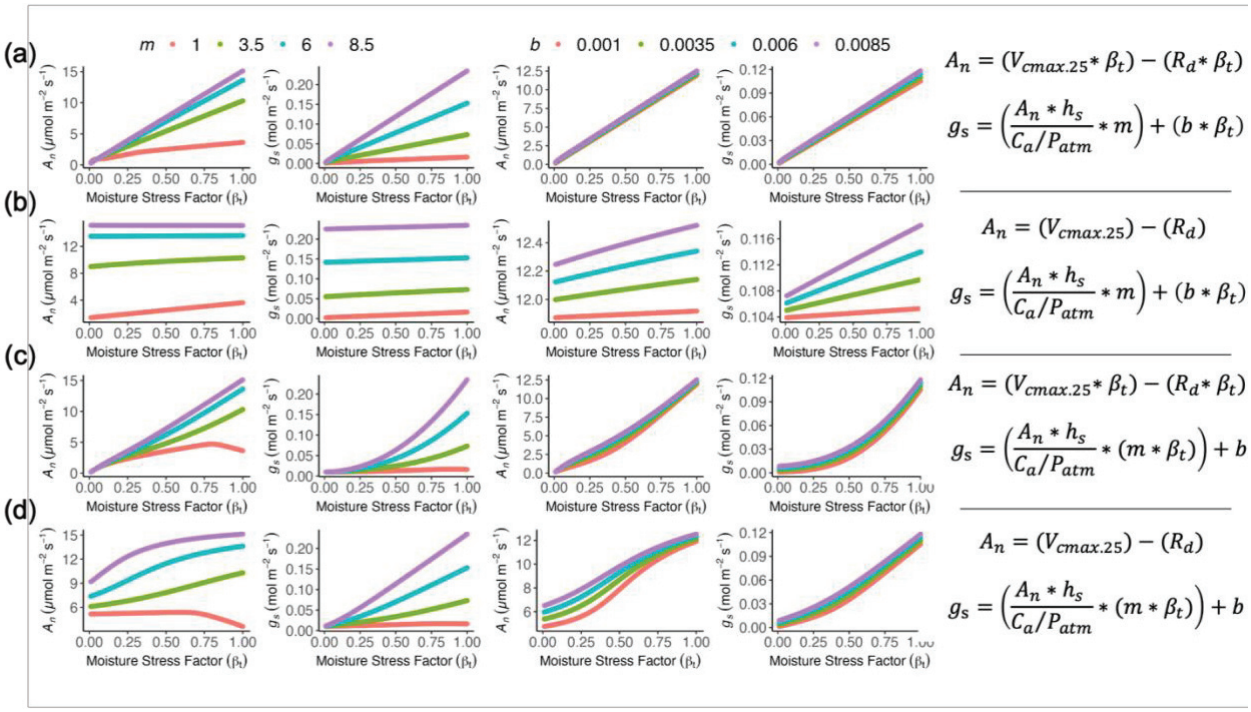

Figure 5.7: Theoretical response functions for the effect of different soil moisture stress (β_t factor) formulations on photosynthesis (A_n) and stomatal conductance (g_s) with different combinations of stomatal slope (m) and intercept (b) selected. The upper row (a) is the default configuration of ELM (MS-4), where β_t is applied to the maximum carboxylation capacity of rubisco (V_{cmax}), the dark respiration rate (R_d) and b. The second row (b) depicts modifications made under MS-5, where the direct effect of β_t on photosynthesis and respiration was removed. The third row (c) depicts the effects of MS-6, where β_t is applied to m, rather than b. The final row (d) depicts the effects of MS-7 which removes the direct effect of β_t on V_{cmax} and R_d, and applys the effect of β_t on m rather than b. For all simulations PAR= 1000 µmol m^{-2} s^{-1}, air temperature= 27ºC, relative humidity= 70%, air CO_2 concentration = 400 ppm, and V_{cmax} = 54.0 µmol m^{-2} s^{-1}.

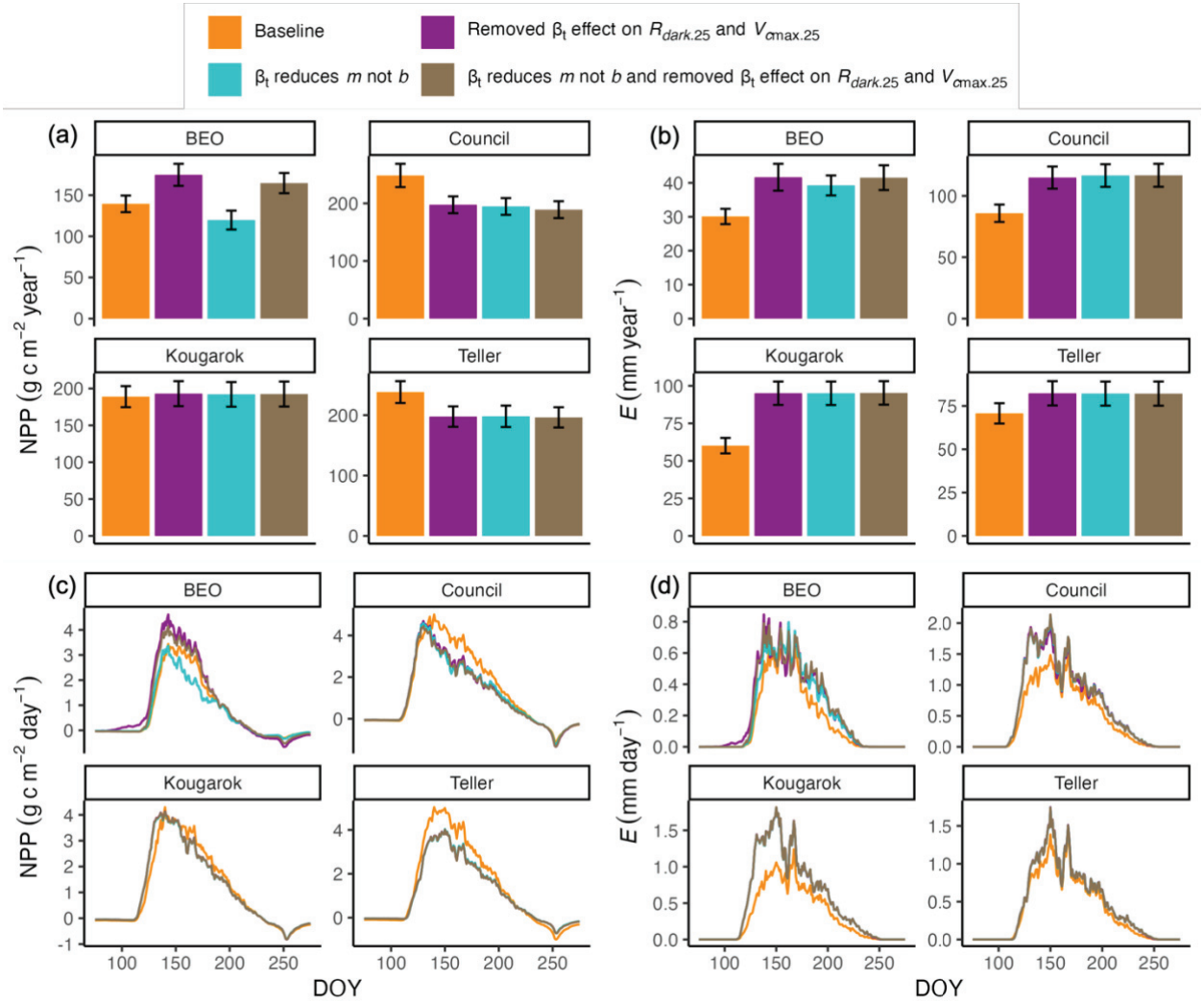

Figure 5.8: Comparison of predicted ecosystem carbon and water fluxes between simulations in which different soil moisture stress (β_t factor) formulations were applied. Upper panels depict average cumulative annual (a) net primary productivity (g C m^{-2} $year^{-1}$; NPP) and (b) vegetative transpiration (mm $year^{-1}$; *E*) over the period from 1850 to 2014. Lower panels depict average daily (c) NPP and (d) *E*, from DOY 75-275. Data in orange are simulations in which the β_t function has not been modified (MS-4), data in magenta represent the model where the direct effect of β_t on photosynthesis and respiration has been removed (MS-5), data in teal represent the model where β_t has been applied to the stomatal slope (*m*), rather than the stomatal intercept (*b*) (MS-6), and data in brown represent the model where the direct effect of β_t on photosynthesis and respiration has been removed and effect of β_t has been switched from *b* to *m* (MS-7). In all simulations, the fraction of leaf nitrogen in rubisco (F_{LNR}), the leaf carbon-to-nitrogen ratio (CN_L), the top of canopy specific leaf area (SLA_0), the root depth distribution parameters (*ra* and *rb*), *m* and *b* have been modified to correspond with field observations.

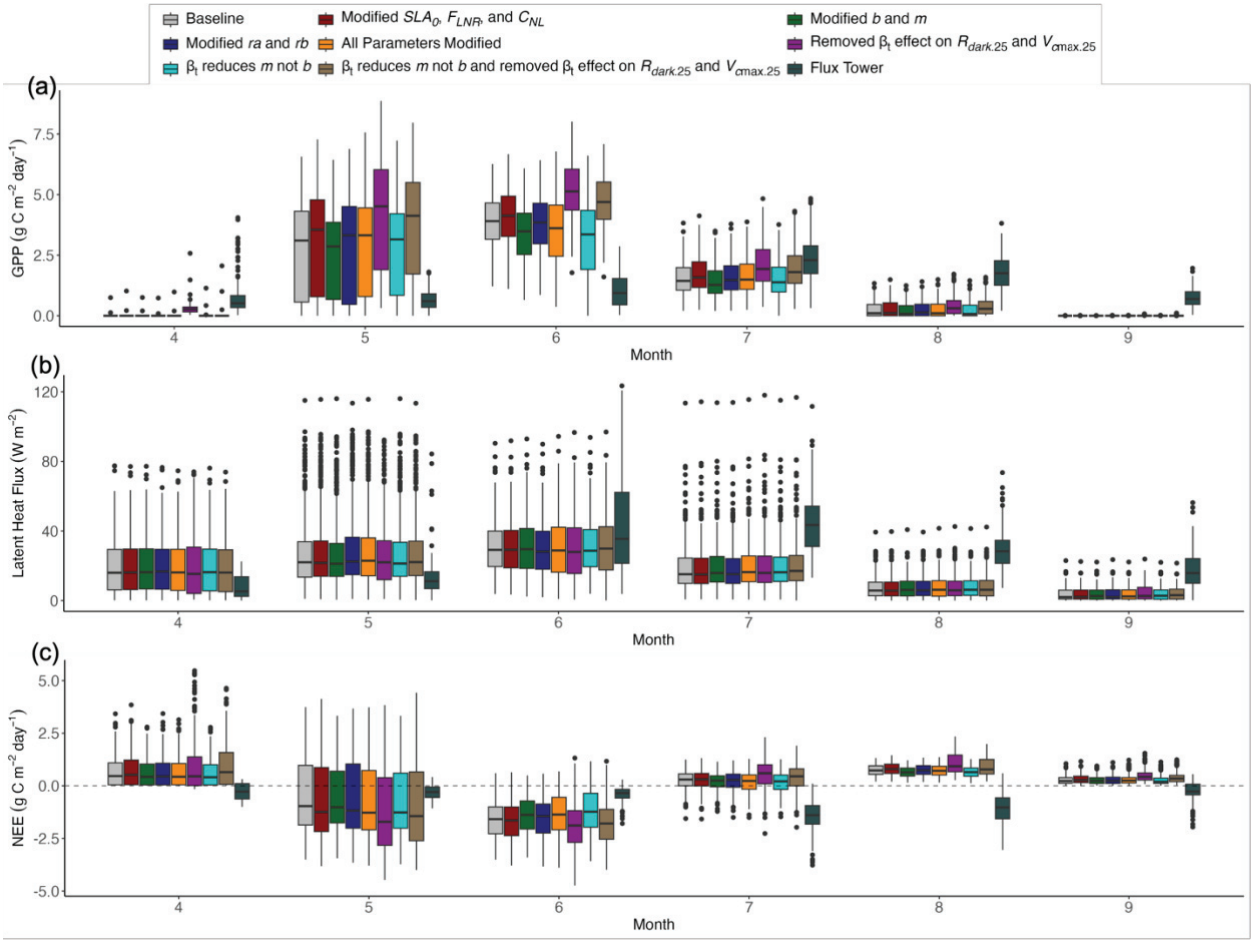

Figure 5.9: Comparison of ELM predicted, and flux tower observed, ecosystem scale exchanges of carbon and water by month at the BEO site. (a) gross primary productivity (g C m^{-2} day^{-1}; GPP) as partitioned using the "nighttime" method, (b) latent heat flux (W m^{-2}) and (c) net ecosystem exchange (g C m^{-2} day^{-1}; NEE). Data in light grey represent the model with no modifications (MS-0), data in red are simulations in which the fraction of leaf nitrogen in rubisco (F_{LNR}), the leaf carbon-to-nitrogen ratio (CN_L) and the top of canopy specific leaf area (SLA_0) have been modified (MS-1), data in green are simulations in which the stomatal slope (m) and intercept (b) have been modified (MS-2), data in blue are simulations in which the root depth distribution parameters (ra and rb) have been modified (MS-3), and data in orange are simulations in all seven parameters were modified (MS-4), data in magenta represent the model where the direct effect of β_t on photosynthesis and respiration has been removed (MS-5), data in teal represent the model where β_t has been applied to the m, rather than b (MS-6), and data in brown represent the model where the direct effect of β_t on photosynthesis and respiration has been removed and effect of β_t has been switched from b to m (MS-7). Data in dark grey come from the AmeriFlux FLUXNET data product from the Barrow (US-NGB; Torn & Dengel, 2021) flux tower site.

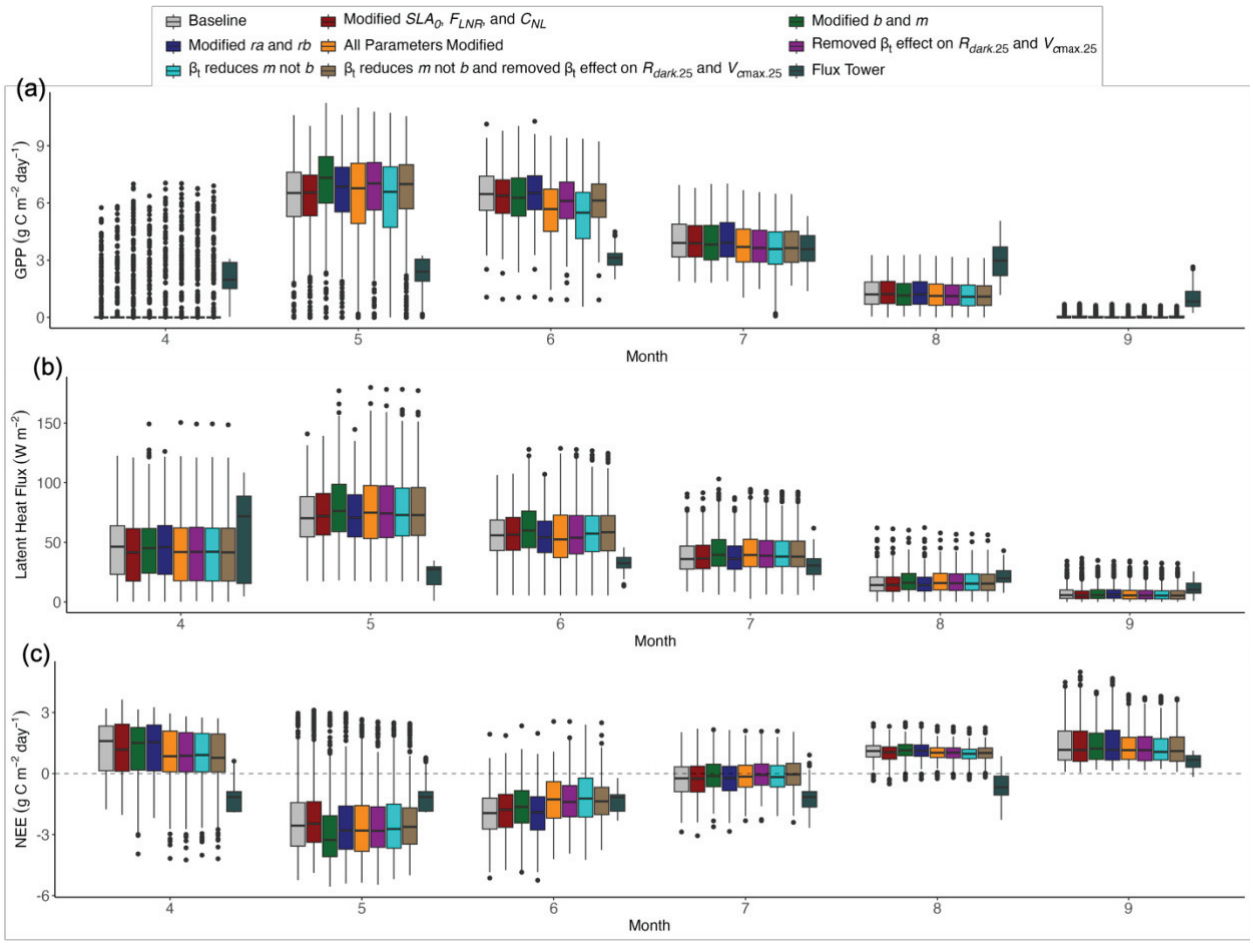

Figure 5.10: Comparison of ELM predicted, and flux tower observed, ecosystem scale exchanges of carbon and water by month at the Council site. (a) gross primary productivity (g C m^{-2} day^{-1}; GPP) as partitioned using the "nighttime" method, (b) latent heat flux (W m^{-2}) and (c) net ecosystem exchange (g C m^{-2} day^{-1}; NEE). Data in light grey represent the model with no modifications (MS-0), data in red are simulations in which the fraction of leaf nitrogen in rubisco (F_{LNR}), the leaf carbon-to-nitrogen ratio (CN_L) and the top of canopy specific leaf area (SLA_0) have been modified (MS-1), data in green are simulations in which the stomatal slope (m) and intercept (b) have been modified (MS-2), data in blue are simulations in which the root depth distribution parameters (ra and rb) have been modified (MS-3), and data in orange are simulations in all seven parameters were modified (MS-4), data in magenta represent the model where the direct effect of β_t on photosynthesis and respiration has been removed (MS-5), data in teal represent the model where β_t has been applied to the m, rather than b (MS-6), and data in brown represent the model where the direct effect of β_t on photosynthesis and respiration has been removed and effect of β_t has been switched from b to m (MS-7). Data in dark grey come from the AmeriFlux FLUXNET data product from the Council (US-NGC; Torn & Dengel, 2022) flux tower site.

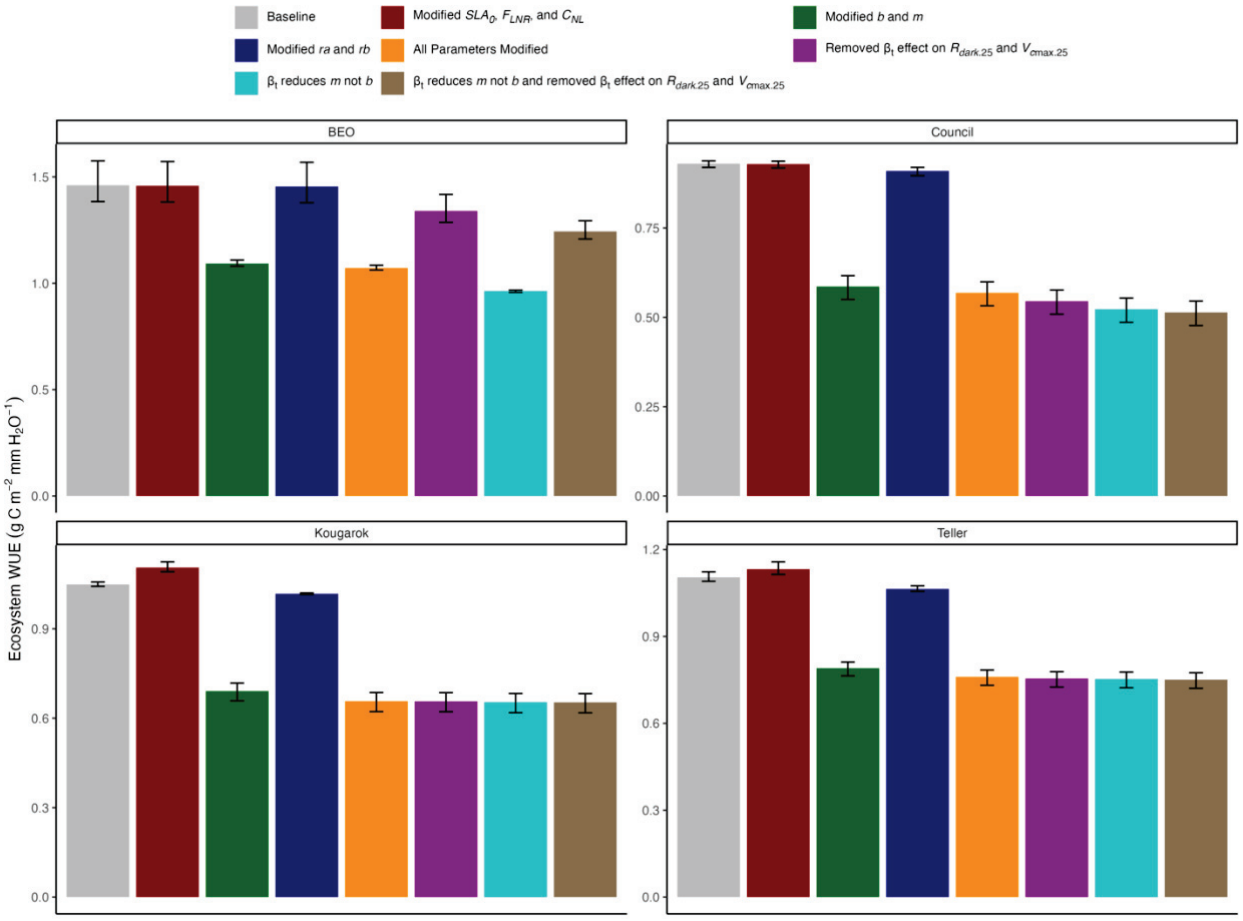

Figure 5.11: Ecosystem scale water use efficiency (WUE; above ground net primary productivity/ vegetative transpiration; g C m^{-2} mm H_2O^{-1}), for all eight model variations at all four sites. Data in light grey represent the model with no modifications (MS-0), data in red are simulations in which the fraction of leaf nitrogen in rubisco (F_{LNR}), the leaf carbon-to-nitrogen ratio (CN_L) and the top of canopy specific leaf area (SLA_0) have been modified (MS-1), data in green are simulations in which the stomatal slope (m) and intercept (b) have been modified (MS-2), data in blue are simulations in which the root depth distribution parameters (ra and rb) have been modified (MS-3), and data in orange are simulations in all seven parameters were modified (MS-4), data in magenta represent the model where the direct effect of β_t on photosynthesis and respiration has been removed (MS-5), data in teal represent the model where β_t has been applied to the m, rather than b (MS-6), and data in brown represent the model where the direct effect of β_t on photosynthesis and respiration has been removed and effect of β_t has been switched from b to m (MS-7).

5.7 – **Tables:**

Table 5.1: Average species specific estimates of stomatal and photosynthetic parameters, as estimated from this study and as previously reported by Rogers *et al*., (2017a, 2022). Values in parentheses are the standard error of the mean estimates.

Species	**PFT**	**n**	$R_{dark.25}$ (µmol m^{-2} s^{-1})	$V_{cmax.25}$ (µmol m^{-2} s^{-1})	***b*** (µmol m^{-2} s^{-1})	***m*** (unitless)	g_{smax} (µmol m^{-2} s^{-1})
Alnus viridis (Chaix) DC.	DBS	9	2.34 (0.14)	55.31 (3)	106000 (18000)	2.4 (0.33)	157000 (23000)
Arctophila fulva (Trin.) Rupr. ex Andersson	ACG	11	0.26 (0.44)	65.25 (4.45)	13000 (4000)	11.07 (0.41)	141000 (10000)
Arctagrostis latifolia (R. Br.) Griseb.	ACG	14	1.17 (0.28)	64.83 (6.3)	51000 (13000)	10.68 (1.67)	207000 (18000)
Carex aquatilis Wahlenb.	ACG	12	0.57 (0.76)	68.88 (5.7)	67000 (20000)	8.57 (1.69)	191000 (24000)
Eriophorum angustifolium Honck.	ACG	12	1.95 (0.26)	53.2 (4.87)	18000 (6000)	9.33 (1.62)	154000 (27000)
Petasites frigidus (L.) Fr.	ACG	19	4.09 (0.17)	66.07 (3.57)	87000 (11000)	2.6 (0.46)	149000 (13000)
Salix glauca L.	DBS	8	3.43 (0.24)	57.31 (3.46)	123000 (17000)	4.38 (0.58)	210000 (21000)
Salix pulchra Cham.	DBS	45	2.69 (0.09)	59.45 (2.28)	98000 (7000)	5.68 (0.56)	198000 (15000)

Table 5.2: Default and updated ELM parameter values for Arctic PFTs.

	ELM default parameters		Updated parameters	
Parameter (abbreviation, units)	**Broadleaf Deciduous Boreal Shrub**	**Arctic C3 Grass**	**Broadleaf Deciduous Boreal Shrub**	**Arctic C3 Grass**
Stomatal slope (*m*, unitless)	9	9	4.19	7.9
Stomatal intercept (*b*, µmol m^{-2} s^{-1})	10000	10000	59046	49540
Leaf carbon-to-nitrogen ratio (CN_L, g C g^{-1} N)	25	25	20.72	21.25
Fraction of leaf nitrogen in rubisco (F_{LNR}, g N in rubisco g^{-1} N)	0.1993	0.1993	0.1066	0.1993
Top of canopy specific leaf area (SLA_0, m^2 leaf area g^{-1} C)	0.030	0.030	0.023	0.032
Root distribution parameter a (r_a, m^{-1})	7.0	1.5	13.0	11.0
Root distribution parameter b (r_b, m^{-1})	11.0	2.0	10.0	9.0

Chapter 6: An analysis of global parameters of stomatal behavior using Bayesian modeling

6.1 – **Abstract:**

Accurate prediction of stomatal conductance to water (g_{sw}) represents one of the largest uncertainties in current model representation of ecosystem function, because of the dual role of stomata in limiting transpiration of water to the atmosphere and fixation of carbon by the biosphere (A). This relationship between E and A is theoretically constrained by the marginal carbon cost of water use, which has been represented mathematically in several empirical stomatal models via variation in the stomatal slope and intercept parameters. Land Surface Models (LSMs) incorporate variation in stomatal parameters as a means of differentiating stomatal behavior and water use efficiency between different plant functional types (PFTs) or biomes. However, these estimates often come from small scale studies, conducted in a single location, or assessing a limited number of species, and thus may poorly represent the dynamics of a diverse PFT used in an LSM. To address this, I assembled a large gas exchange dataset, consisting of measurements taken across the globe, and use these data to test 13 Bayesian models for the prediction of the stomatal slope and intercept parameters from three common empirical g_{sw} models. I find that for the non-woody PFTs, stomatal slope and intercept vary predictably according to optimal resource allocation theory, however in PFTs that occupy the same bioclimatic region there are substantial overlaps in the credible intervals for parameter estimates. Further, I find that of the three empirical models tested, two (the Ball-Woodrow-Berry and Medlyn models) performed well while the third (the Lamour model) failed to reproduce g_{sw} observations particularly in non-woody PFTs. Both stomatal slope and intercept also appear to be influenced in part by the bioclimatic zone in which they reside, however these associations are weaker than the PFT specific trends. Finally in testing associations between stomatal slope and leaf traits that had previously been reported in small scale studies or within a single PFT, I found that across all three models, stomatal slope was associated with the maximum carboxylation capacity of the enzyme rubisco normalized to 25ºC ($V_{c\max.25}$), and for the Lamour model, stomatal slope varied with leaf carbon isotope discrimination ($\delta^{13}C$; ‰). In reporting my posterior estimates for stomatal slope an intercept, I hope to provide a dataset which can be used to develop informative priors for future Bayesian models of g_{sw}.

6.2 – **Introduction:**

Across most of the Earth's land surface, vegetative exchange of carbon, water and energy are the central processes governing land atmosphere interactions (Sellers *et al.*, 1997; Pitman, 2003). This coupling between terrestrial and atmospheric pools of matter and energy is mediated by plants via the processes of photosynthesis (A), transpiration (E), and respiration (R_d), with the former two processes ultimately governed by stomatal conductance (g_{sw}; Hetherington & Woodward, 2003; Buckley *et al.*, 2017). Stomata are the main conduit through which atmospheric carbon dioxide (CO_2) enters the leaf and reaches the sites of carboxylation (Long & Hällgren, 1993), meaning that the rate of g_{sw} helps to set the upper bound on both A and net primary productivity (NPP). In addition, stomatal opening causes water vapor to be transpired to the atmosphere, which exerts a major impact on the rate of soil water depletion (Bonan *et al.*, 2014), and also impacts canopy energy balance by transferring energy from the canopy to the atmosphere in the form of latent heat flux (Collatz *et al.*, 1991). Estimates suggest that E accounts for >60% of annual land surface water flux (Schlesinger & Jasechko, 2014; Li *et al.*, 2019), while NPP is responsible for sequestering approximately a third of total anthropogenic carbon emissions (Le Quéré *et al.*, 2016), reinforcing the regulatory role stomata play in global biogeochemical cycling. Accurate estimation of g_{sw} is therefore essential when simulating global fluxes of carbon and water and, as such, improving the representation of g_{sw} in land surface models (LSMs) has recently become an area of intensive study (Lin *et al.*, 2015; Miner *et al.*, 2017; Wolz *et al.*, 2017; Lamour *et al.*, 2022; Sabot *et al.*, 2022; Li *et al.*, 2022).

Of the wide array of leaf-level stomatal models proposed in the literature (Damour *et al.*, 2010; Wang *et al.*, 2020b; Sabot *et al.*, 2022), most are essentially empirical or semi-empirical, that is conceptualized around a physiological hypothesis but constrained based on observations. Unlike truly mechanistic models, which are designed to simulate exact hydrodynamic or biochemical processes and thus require detailed knowledge of underlying physiological mechanisms, the stomatal schemes most often employed in LSMs (Jarvis, 1976; Ball *et al.*, 1987; Leuning, 1995; Medlyn *et al.*, 2011) use empirical functions developed based on observed relationships between stomatal conductance and environmental drivers (Damour *et al.*, 2010). Most of these empirical models share a common framework in which g_{sw} responds to a combination of atmospheric water demand, leaf demand for CO_2, and soil, root, or xylem water limitations (Gao *et al.*, 2002; Manzoni

et al., 2011; De Kauwe *et al.*, 2015b). Atmospheric demand is typically expressed as a function of vapor pressure deficit (VPD) or relative humidity (RH), while the leaf demand for CO_2 is normally expressed as a ratio of A and the CO_2 concentration at the leaf surface (C_a). Soil, root, or xylem water limitations are subsequently simulated by applying an empirical scaling factor to one of the model parameters that adjusts g_{sw} in proportion to the water supply limitation, typically estimated it from a metric such as leaf (Ψ_l) or soil (Ψ_s) water potential (Tuzet *et al.*, 2003; Rogers *et al.*, 2017c; Anderegg *et al.*, 2017).

Often, empirical stomatal models assume that the relationship between A and g_{sw} is a linear function. That is, provided that the leaf-level environment (e.g., VPD, C_a, Ψ_l) remains constant, and A and g_{sw} are both at a steady state, A will change in proportion to a change in g_{sw}. This linear form results in two estimated parameters, the stomatal slope which determines the relationship between g_{sw} and the leaf-level environmental conditions and the stomatal intercept, which represents the expected level of g_{sw} when either the leaf demand for CO_2 reaches zero (i.e., at the light compensation point of net photosynthesis; A_n) or the atmospheric water demand exceeds a critical threshold. From a physiological context, the stomatal slope represents the sensitivity of stomata to the environment, while the stomatal intercept is used to describe a metric of minimum conductance, which includes water loss via cuticular conductance or transpiration through incompletely closed stomata (Machado *et al.*, 2021; Márquez *et al.*, 2021, 2022).

The application of empirical models of stomatal conductance to LSMs offers several advantages. Chiefly, empirical functions, when coupled with a model of assimilation (e.g., Farquhar *et al.*, 1980) provide a convenient means to estimate stomatal conductance using readily available, or easily estimated, environmental variables such as VPD, irradiance, air temperature, and wind speed. This is in contrast to mechanistic models, which typically require an estimate of more specialized physiological measurements such as whole plant hydraulic conductivity (Jones & Sutherland, 1991), guard cell turgor pressure (Dewar, 1995), or concentration of abscisic acid (Li *et al.*, 2006). In addition, many of the variables required to parameterize the A - g_{sw} relationship are often reported in datasets of gas exchange (Kattge *et al.*, 2011; Ely *et al.*, 2021), allowing empirical models to be broadly applied across a wide range of plant species and environmental conditions. However, there are limits to empirical approaches, stemming primarily from their dependance on statistical relationships derived from a calibration dataset, which may not be

applicable or generalizable across different plant species, growth stages, and environmental conditions (Verhoef & Egea, 2014), and may even introduce numerical instability to the model through unrealistic feedbacks between the stomata and the environment (Sabot *et al.*, 2022). Additionally, empirical models often oversimplify the complex interactions between stomatal conductance and environmental factors, pushing all the uncertainty onto the estimation of a limited number of parameters (De Kauwe *et al.*, 2013; Wolz *et al.*, 2017; Wu *et al.*, 2019b; Davidson *et al.*, 2023b), such that minor uncertainty in parameterization often scales to significant model uncertainty at regional to global scales (Smith & Dukes, 2013; Héroult *et al.*, 2013; Lin *et al.*, 2015; Franks *et al.*, 2018). Thus, decisions made with regard to parameterization often represent the largest source of error in many model representation of land atmosphere interactions (Dietze *et al.*, 2014; Bauerle *et al.*, 2014; Jefferson *et al.*, 2017; Franks *et al.*, 2018; Ricciuto *et al.*, 2018).

While there has long been an understanding that stomatal behavior is variable both between and among species (Meidner & Mansfield, 1968; Jarvis, 1976; Ball, 1988), LSMs historically considered variation in stomatal model parameters in a very limited capacity, only distinguishing between C3 or C4 photosynthetic pathways (De Kauwe *et al.*, 2015b; Franks *et al.*, 2018). Subsequently, enabled by studies of stomatal behavior at finer organizational scales (Lin *et al.*, 2015; Franks *et al.*, 2017; Wolz *et al.*, 2017) and collation of existing literature values (Miner *et al.*, 2017), LSMs have begun specifying PFT-specific parameters in an attempt to reduce model uncertainty in carbon and water cycle projections (Fisher *et al.*, 2018; Fisher & Koven, 2020; Koven *et al.*, 2020). PFT-specific parameterizations are an important model improvement, however some studies have demonstrated significant within-species variation in stomatal behavior (Ono *et al.*, 2013; Miner & Bauerle, 2017; Davidson *et al.*, 2023a), which can even exceed among-PFT variation in some cases (Wolz *et al.*, 2017). In addition to variability within species, questions remain about the effect of climatic variables, such as growing season temperature and soil moisture, on stomatal behavior (Medlyn *et al.*, 2011; Prentice *et al.*, 2014). It is yet unclear whether a PFT scheme which explicitly considers biome (e.g., Arctic or tropical) along with growth form (e.g., graminoid or tree) is preferable to a scheme that considers the continuous effect of environment on stomatal traits (Lin *et al.*, 2015; Franks *et al.*, 2018). Further, efforts to identify relationships between stomatal parameters and leaf traits that are assumed to be mechanistically associated with A and g_{sw} (Wright *et al.*, 2004) have only produced weak correlations, which are

often restricted to a specific PFT, stomatal model, or biome (Franks *et al.*, 2018; Wu *et al.*, 2019b; Lamour *et al.*, 2022). Finally, a comprehensive comparison of the ability of different methodologies (e.g., survey style measurements and response curves) for obtaining stomatal parameters has yet to be performed, primarily because of the wide variety of accepted approaches for fitting stomatal parameters and the often opaque reporting of methodology when data are aggregated into large datasets (Miner *et al.*, 2017; Ely *et al.*, 2021).

In this study, I attempt to advance our understanding of the factors responsible for global variation in stomatal model parameters by collating a large dataset (> 27700 observations) of gas exchange measurements, and using these data to develop and test a series of hierarchical Bayesian models for the prediction of stomatal slope and intercept across various levels of organization. I focus on three empirical models. The first of these models (Ball *et al.*, 1987; hereafter the BWB model) is one of the most widely used and adapted empirical models, serving as the default stomatal module in numerous LSMs (Oleson *et al.*, 2013; FATES Development Team, 2019). The second model (Medlyn *et al.*, 2011; hereafter the Medlyn model) was developed from stomatal optimality theory (Cowan & Fraquhar, 1977), which posits that stomata should be evolved to minimize loss of water relative to carbon gain, such that the stomatal slope parameter should be conserved within growth forms and climates. The third model (Lamour *et al.*, 2022; hereafter the Lamour model), was developed out of observation that existing empirical models failed to capture the nonlinearity of g_{sw}, especially at low and high irradiance. My objectives for this study were (1) to evaluate the efficacy of the three aforementioned empirical stomatal models for predicting g_{sw} across a diverse dataset; (2) evaluate the effects of growth form, growth climate, and leaf traits on estimates of stomatal parameters across the three models; and (3) develop a set of posterior estimates of stomatal slope and intercept which can be used as informative priors for future Bayesian models of g_{sw}. By addressing these three objectives, my goal was to develop a more detailed understanding of the driving factors behind large scale differences in stomatal behavior across a wide diversity of vegetation types. In addition, by using Bayesian methods, which are increasingly gaining traction in the physiological modeling and hydraulics communities (Mackay *et al.*, 2012; Ewers, 2013 Lahiri *et al.*, 2019; Xiao *et al*., 2021; Pandey *et al*., 2021; Niu *et al*., 2022; Aros-Mualin *et al.*, 2023), the posterior estimates obtained in this study can be used in future LSM parameterizations, and also serve as a starting point for subsequent studies that use Bayesian

inference to estimate model parameters.

6.3 – **Materials and Methods:**

Data Collection and Processing:

All the gas exchange data used in this study come from previously published, and publicly available, datasets, a list of which can be found in Table A5.1. I carried out a systematic search of multiple data repositories including the Dryad Data Repository (datadryad.org), the Environmental Data Initiative (edirepository.org), the Environmental System Science Data Infrastructure for a Virtual Ecosystem (ESS-DIVE) repository (ess-dive.lbl.gov), and the TRY Plant Trait Database (try-db.org), using key words such as "stomatal slope", "stomatal intercept", "stomatal response", and "stomatal optimality." In addition, I use the expansive dataset collated by Lin *et al.*, (2015), which to date is the largest single publicly available source of survey style gas exchange measurements. I chose to focus on datasets rather than compiling a list of previously estimated values of stomatal slope and intercept for three reasons. First, using raw data allowed me to apply Bayesian inference, rather than ascribing an effect size onto parameters which had previously been calculated. Second, having access to raw data allowed me to perform my own independent quality checking and control process, and allowed me to extract data from the control groups in studies where an experimental manipulation was applied. Third, because the process of archiving raw gas exchange data is a relatively recent practice (Ely *et al.*, 2021), this allowed me to focus on data which had not previously been included in other synthesis studies (Miner *et al.*, 2017).

After aggregating the raw data, I carried out a significant quality checking and control process. I first removed all data with an artificial experimental manipulation (e.g., artificial drought, elevated CO_2), as well as removing any data with biologically improbable values (e.g., C_i or $g_{sw} \leq 0$). Next, I plotted A vs g_{sw} for each unique species, and visually inspected the data, removing outlier ($\geq 3\ \sigma$ from the mean) measurements. I also removed data for any species which demonstrated a negative relationship between A and g_{sw}, a biologically improbable relationship that is indicative of measurement error. In situations where critical environmental data (e.g., leaf temperature) were missing from the data, I either used a standard value as recorded in the accompanying published manuscript, or in some cases contacted the dataset author directly for clarification. Finally, all species with 10 or fewer measurement points were removed from the data

set. After processing, the resulting dataset consisted of 27723 unique observations across 198 species measured at 66 locations globally (Fig. 6.1).

Next, all species level data were categorized into one of 15 PFT classifications, based on the default PFTs used in CLM 4.5 (Oleson *et al.*, 2013). This classification scheme broadly divides vegetation based on growth form (e.g., shrub, grass, tree, crop), and where appropriate, latitude zone (e.g., Arctic, boreal, temperate, tropical), leaf habit (e.g., deciduous or evergreen), leaf type (e.g., needleleaf or broadleaf), and photosynthetic pathway (e.g., C3 or C4). I then classified each measurement location into its respective Köppen-Geiger Climate Zone (Köppen, 1936), using the database provided within the "kcg" R package (v1.0.0.2, Bryant *et al.*, 2017). Data were also grouped by measurement type, either being classed as a response curve, such as a CO_2, light, or VPD response curve, or designated as survey style measurements, which are instantaneous measurements of gas exchange, with conditions inside the measurement chamber set to match ambient conditions. Finally, I categorized the growth conditions of the plants based on whether they were grown in an agricultural field, a glasshouse, grown in pots, or were naturally grown.

In addition to gas exchange data, I also aggregated a dataset corresponding to species level trait data, which I obtained from the TRY database (Kattge *et al.*, 2011). I chose to focus on four leaf traits, specific leaf area (SLA; $mm^2\ mg^{-1}$), foliar nitrogen per unit leaf area (N_a; $g\ m^{-2}$), the maximum carboxylation capacity of the enzyme rubisco normalized to 25ºC ($V_{cmax.25}$; $\mu mol\ m^{-2}\ s^{-1}$), and leaf carbon isotope discrimination ($\delta^{13}C$; ‰). All four of these traits have been previously associated with stomatal behavior in smaller scale syntheses (Rogers *et al.*, 2017c; Franks *et al.*, 2018; Wu *et al.*, 2019b; Lamour *et al.*, 2022), and thus represent a promising starting point for assessing global relationships with stomatal behavior.

Stomatal model descriptions:

To characterize stomatal behavior in this study I investigated three different empirical stomatal models. The BWB model (Ball *et al.*, 1987; Equation 6.1)

Equation 6.1. $$g_{\mathrm{sw}} = \left(\frac{A*Rh}{C_a} * m\right) + b$$

has two parameters, a stomatal slope parameter (m; unitless) and intercept parameter (b; $mol\ m^{-2}\ s^{-1}$). In the BWB model A is the net photosynthesis rate ($\mu mol\ m^{-2}\ s^{-1}$), Rh is the relative humidity of the air at the leaf surface (%) and C_a is the CO_2 concentration at the leaf surface ($\mu mol\ mol^{-1}$).

The Medlyn model (Medlyn *et al.*, 2011; Equation 6.2)

Equation 6.2. $$g_{sw} = g_0 + 1.6\left(1 + \frac{g_1}{\sqrt{VPD_{leaf}}}\right)\frac{A}{C_a}$$

also has two parameters, a stomatal slope parameter (g_1; $kPa^{0.5}$) and intercept parameter (g_0; mol m^{-2} s^{-1}), and like in the BWB model, A in the Medlyn model is the net photosynthesis rate (µmol m^{-2} $s^{-}1$). However, the Medlyn model uses leaf surface VPD (VPD_{leaf}; kPa) in place of relative humidity.

Like the previous two models, the Lamour model (Lamour *et al.*, 2022; Equation 6.3)

Equation 6.3. $$g_{sw} = g_0 + g_1 \frac{1.6}{\sqrt{VPD_{leaf}}}\frac{A_g^2}{C_a}$$

also has two parameters, a stomatal slope parameter (g_1; µmol m^{-2} s^{-1} $kPa^{0.5}$) and an intercept parameter (g_0; mol m^{-2} s^{-1}). Similar to the Medlyn model the Lamour model uses the leaf surface VPD. However, unlike both the BWB and Medlyn models, the Lamour model uses gross photosynthesis (A_g) in place of net photosynthesis. Therefore, when estimating g_{sw} from gas exchange data where net photosynthesis is typically reported, a respiration term (either dark respiration, [R_{dark}], or day respiration [R_{day}]) must be subtracted from the net photosynthesis value. In addition, the interpretation of g_0 in the Lamour model is different from the former two models. In the Lamour model g_0 is equivalent to $g_{sw,dark}$, while in both the BWB and Medlyn models b/g_0 is equivalent to g_{sw} at the light compensation point.

Bayesian Model Descriptions:

I tested 13 Bayesian models investigating different combinations of effects on the stomatal model parameters. Details of each model, including its fixed and random effects, and prior assumptions are described in Table 6.1. All models were assembled and tested using the software JAGS (v. 4.3.0, Plummer, 2017), a Gibbs sampling program designed for the analysis of hierarchal models. JAGS was accessed via the R software environment (v. 3.3.2, R Core Team, 2013), using the packages "R2Jags" (v. 0.5-7 Su & Yajima, 2015) and "rjags" (v. 4-6, Plummer *et al.*, 2016). For each model I ran 6 chains, with a thinning rate of 1, discarding 90% of the data (900,000 – 9,000,000) as a burn in. All models were run with a minimum of 1,000,000 draws from the posterior. If chains failed to converge after the initial 1,000,000 iteration run, the model was rerun with the number of posterior samples increased to a maximum of 10,000,000 draws from the

posterior. Convergence of MCMC chains was assessed via a combination of visual inspection using the R package "MCMCvis" (v. 0.15.5, Youngflesh *et al.*, 2022, Fig. A5.1-A5.13) and assessment of the $\hat{R}$ parameter (> 1.05 indicates potential lack of convergence, Vehtari *et al.*, 2021).

Prior estimates of PFT-specific stomatal slope and intercept were obtained from the synthesis study of Miner *et al.*, (2017), which reports species specific values of stomatal slope and intercept for the BWB and Medlyn models. Since the Lamour model was only recently published, I lack a good data source from which to draw informative priors. However, I estimated PFT-specific Lamour model g_1 based on the Medlyn model values reported in Miner *et al.*, (2017), applying a linear correction of $g_{1,\text{Lamour}} = 0.05 + 0.07 * g_{1,\text{Medlyn}}$. In addition, prior estimates of PFT specific respiration ($R_{\text{d.25}}$; μmol m^{-2} s^{-1}) were estimated by aggregating species level $R_{\text{d.25}}$ values from the TRY database (Kattge *et al.*, 2011), and estimating the mean and variance for each PFT. Before being applied to the Lamour model, the temperature normalized values of $R_{\text{d.25}}$ are scaled to leaf temperature using an inverse Arrhenius equation (Equation 6.4; Bernacchi *et al.*, 2001):

Equation 6.4. $$R_{d.Tleaf} = R_{d.25} exp^{(H_a/(R*(Tleaf+273-15)) - H_a/(R*298.15))}$$

where H_a is the activation energy of mitochondrial respiration (H_a = 46 390 J mol−1), R is the ideal gas constant (R = 8.314 J mol−1 K−1), and T_{leaf} is the leaf temperature in ºC.

As a means of testing the goodness of fit of competing models, I randomly split the data into two data sets, a calibration set which contains approximately 80% of the data and a validation set with approximately 20% of the data. This split was done at the species level, so each species is represented in both data sets. Then for each model a validation marginal R^2, and RMSE, was calculated, allowing models to be compared for how faithfully they recreate observed data. When comparing among posterior estimates for parameters within a model, I consider non-overlap of 95% credible intervals as evidence of a significant difference between effects.

6.4 – **Results:**

PFT effects on stomatal behavior

One of the primary objectives of this study was to compare the efficacy of the three stomatal models using a diverse dataset, which included data from multiple biomes, and which spans many

PFTs. To accomplish this, I estimated PFT specific model parameters for each of the three stomatal models, and used these data to estimate g_{sw} across a range of environmental conditions. These predictions were then compared to observations from a separate validation dataset which contains the same species and measurement locations as the calibration dataset (Fig. 6.2). Overall, I found that both the BWB and Medlyn models had similar goodness of fit across the full dataset (BWB: $R^2 = 0.715$, RMSE = 0.0770 mol m^{-2} s^{-1}; Medlyn: $R^2 = 0.733$, RMSE = 0.0744 mol m^{-2} s^{-1}), while the Lamour model performed substantially worse ($R^2 = 0.386$, RMSE = 0.572 mol m^{-2} s^{-1}).

When these comparisons were broken out by PFT (Table 6.2), some interesting trends emerged. Across all three models, g_{sw} predictions were the least accurate in the Arctic/boreal PFTs, with predictions of g_{sw} for the broadleaf deciduous boreal shrub, C3 Arctic grass, and needleleaf evergreen boreal tree giving some of the lowest R^2 and highest RMSE across models. Surprisingly, the broadleaf deciduous boreal tree performed the best of all the PFTs across all three models, however this PFT was only represented by a single species (*Fagus sylvatica*) in the dataset, and thus its PFT specific parameters were also species-specific parameters. In addition, while the BWB and Medlyn models have comparable performance across most of the PFTs, this does not hold true in the Arctic/boreal region (Fig. 6.2a-c), where the Medlyn model has a substantially better performance, particularly within the broadleaf deciduous boreal shrub PFT. The Lamour model performed particularly poorly for the non-woody/crop PFTs, especially in the C4 grass and C3 crop PFTs where its RMSE was 0.8839 and 3.2281 mol m^{-2} s^{-1} respectively. This was mainly the result of substantial overprediction of g_{sw} for these PFTs (Fig. 6.2f), which is not seen in any of the other models or for any other group.

I next examined the PFT specific estimates of stomatal slope and intercept, and their uncertainty for each model (Fig. 6.3, Table 6.3). Among PFTs, I observed substantial differences in the posterior mean estimate for stomatal slope (Fig. 6.3a-c), however few of these differences were significant (i.e., non-overlap of 95% credible intervals). Of the differences which were significant, C3 non-Arctic grass has a significantly (~100-500%, 21.42 and 8.42 $kPa^{0.5}$) higher stomatal slope than all other PFTs when estimated with the BWB and Medlyn models, and C4 grass had a significantly lower stomatal slope (~70-90%, 3.99 and 2.19 $kPa^{0.5}$) than all other non-woody PFTs when estimated with the BWB and Medlyn models. Stomatal slope was also significantly (~50%) higher in the evergreen tropical PFT than the deciduous tropical PFT when

estimated with the BWB and Medlyn models (Fig. 6.3a-b). When using the Lamour model, posterior mean estimates for stomatal slope had substantial uncertainty, and as such, there were no significant differences observed, despite the nearly 10 times difference in values between the highest and lowest estimates.

Differences in posterior mean estimates for stomatal intercept were more pronounced with several significant among PFT differences observed (Fig. 6.3d-f). For both the BWB and Medlyn models, stomatal intercept was significantly different between the C3 Arctic grass, broadleaf deciduous boreal shrub, and needleleaf boreal tree PFTs (Fig. 6.3d,e). Similarly, for both the BWB and Lamour models there were significant differences in stomatal intercept between all four non-woody/crop PFTs (Fig. 6.3d,f). There was much less variation among the PFTs within the temperate and tropical groups, however in general the evergreen PFTs tended to have lower intercepts than their equivalent deciduous counterparts in the temperate group.

While between model comparisons of stomatal slope for the same PFT cannot be drawn due to differences in units, it is none the less intriguing to see that the relative magnitude of the stomatal slope values are consistent between the three models, especially between the BWB and Medlyn models (Table 6.3). As for stomatal intercept, while the values are the same (mol H_2O m^{-2} s^{-1}) the interpretation of the values are different. Stomatal intercept in the Lamour model is equivalent to dark adapted g_{sw} ($g_{sw,\mathrm{dark}}$), and thus is expected to be lower than the stomatal intercept from the BWB or Medlyn model. However, PFT specific stomatal intercepts as predicted by the Lamour model are on average 52% higher than the BWB model, and 65% higher than the Medlyn model (Fig. 6.3d-f).

Finally, I wanted to assess the influence that using informed priors from the literature would have on posterior estimates of stomatal slope and intercept. To do this, I reran each of the PFT specific models using an uninformative prior assumption for stomatal slope. For the Lamour model, a second variation was run where in addition to the uninformative slope, an uninformative prior for the respiration value was supplied. In general, the choice of an informative prior had little influence on the posterior distribution, with mean values of stomatal slope either being the same or slightly higher for the informed model (Fig. A5.14a-c, Table A5.2). Stomatal intercept, which itself is drawn from an uninformative prior, appears not to be affected by the prior estimate for stomatal slope (Fig. A5.14d-f).

Climatological effects on stomatal behavior

A potential alternative to modeling variation in stomatal traits based on PFT is to consider differences in stomatal behavior intrinsic to different growth environments (Lin *et al.*, 2015; Franks *et al.*, 2018). To investigate this, I ran three additional models which estimated stomatal slope and intercept based on the Köppen-Geiger Climate Zone (Köppen, 1936), which divides the globe into 30 bioclimatic zones, based on environmental conditions and the types of vegetation which are known to occur in the region. The data collected in this study represent 16 of the 30 Köppen-Geiger zones, and cover each of the main five classification groupings. Overall, I found that while there was a clear signal of climatological structuring in estimated stomatal slope for the BWB and Medlyn models (Fig. 6.4a,b), there were no significant differences in estimated stomatal slope between climate zones. In general, stomatal slope was higher in zones with a higher overall mean annual temperature, and tended to decrease with decreasing aridity, however these trends were weak, and within each zone there was substantial variability around the mean estimate.

For stomatal intercept, parameter estimates appear to be more highly influenced by the Köppen-Geiger zone, with substantial and significantly different values observed in contrasting climates (Fig. 6.4d-f). Of particular note is the substantially higher estimate for the polar tundra zone in the BWB and Medlyn models, which is almost 50% higher than the next highest intercept value (Fig. 6.4d&e). Within the tropical grouping for the BWB and Medlyn models, the monsoon sub-class also exhibited a significantly higher intercept than either the rainforest or savannah sub-class. For the Lamour model, stomatal intercept decreased significantly with increasing growing season temperature in the continental group, and was significantly higher in the temperate climate zones with a wet summer (Fig. 6.4f).

As with the PFT models, comparing stomatal slope and intercept between models for the same climate zone is hampered by differences in units. However, just as with the PFT models, the relative magnitudes of the stomatal slope values are consistent between the three empirical models (Fig. 6.4a-c). Stomatal intercept estimates are more variable, with contrasting magnitudes for some of the groups, in particular in the continental, temperate, and arid zones (Fig. 6.4d-f). Again, stomatal intercepts as predicted by the Lamour model are on average 50-60% higher than those of the BWB or Medlyn models (Fig. 6.4d-f).

Methodological effects on stomatal behavior

To examine the effect of measurement methodology on the estimation of stomatal parameters I ran an additional three models which separately estimated the fixed effect of measurement type (response curve or survey measurement), and PFT on stomatal slope and intercept. Given that only 21% of the total dataset was made up of response curve derived data, I chose to restrict this analysis to only the PFTs which contained both data types, increasing the proportion of response curve derived data to 31%. Comparing estimates within PFTs, there were small differences in the posterior mean estimate for stomatal slope (Fig. 6.5a-c, and larger differences in the posterior mean estimate for stomatal intercept (Fig. 6.5d-f), which hold across all three empirical stomatal models. In particular, stomatal slope was higher for the survey derived data in the broadleaf deciduous temperate tree (BWB and Medlyn), broadleaf evergreen tropical tree (BWB, Medlyn, and Lamour), and needleleaf evergreen temperate tree (BWB and Medlyn) PFTs, while it was lower in the broadleaf deciduous tropical tree PFT (BWB, Medlyn, and Lamour). However, none of the differences in stomatal slope between methods were deemed statistically significant, because of substantial overlap in the 95% credible intervals of the posterior distributions. For stomatal intercept, across all four PFTs and all three empirical models, the estimated posterior mean was lower for the curve derived data than the survey derived data, with significant differences observed in the broadleaf deciduous temperate tree (BWB, Medlyn, and Lamour), broadleaf deciduous tropical tree (BWB and Lamour), and broadleaf evergreen tropical tree (BWB, Medlyn, and Lamour) PFTs.

I next compared model predicted and observed g_{sw} to assess the impact of methodology on predicting g_{sw} for a novel dataset (Fig. 6.6). For this comparison I used the validation dataset, predicting curve derived data using parameters fit from survey data and vice versa. For both the BWB and Medlyn models, using parameters derived from survey data to predict g_{sw} from response curves yielded better estimates than the using parameters derived from response curves to predict g_{sw} obtained via survey (Fig. 6.6). In particular, the parameters derived from response curves, when applied to the survey dataset led to underestimation of g_{sw} at high values, leading to a higher RMSE (BWB: 0.0487 vs 0.0846 mol m^{-2} s^{-1}; Medlyn: 0.0556 vs 0.0915 mol m^{-2} s^{-1}), and a lower R^2 (BWB: 0.696 vs 0.573; Medlyn: 0.695 vs 0.526). For the Lamour model, results were more mixed (Fig. 6.6e&f). Here, applying survey derived parameters to response curve data led to a slightly lower

validation R^2 (0.323 vs 0.334) but a higher RMSE (0.0798 vs 0.1081 mol m^{-2} s^{-1}). Parameters obtained from the survey dataset appear to predict a somewhat flat response of g_{sw}, suggesting that estimated stomatal slope may be too high, while parameters obtained from the response curve dataset led to significant heteroscedasticity in the predictions.

Predicting species level stomatal slope based on leaf traits

One of the major focuses of stomatal model development over the past 10 years has been attempting to derive relationships between stomatal parameters and leaf traits (Lin *et al.*, 2015; Rogers *et al.*, 2017c; Franks *et al.*, 2018; Wu *et al.*, 2019b; Lamour *et al.*, 2022). Here I advance this line of investigation by assessing the association between species specific stomatal slope estimates and four leaf traits which previously were found to correlate with stomatal behavior (Fig. 6.7). Of the twelve relationships investigated (three stomatal models across four traits), only four produced a significant correlation across all PFTs. I observed a positive association between $V_{cmax.25}$ and stomatal slope using the BWB (df = 77, $p < 0.001$, $r = 0.367$) and Medlyn models (df = 77, $p = 0.003$, $r = 0.325$) and a negative relationship with the Lamour model (df = 77, $p = 0.017$, $r = -0.267$). I also observed a negative relationship between ^{13}C isotope discrimination and stomatal slope for the Lamour model (df = 79, $p < 0.001$, $r = -0.368$). All other relationships across all PFTs were not significantly correlated.

Looking within individual PFTs I found four significant correlations after correcting the alpha level significance cutoff to account for multiple comparisons ($p \leq 0.0125$). In the broadleaf evergreen tropical tree PFT, there was a negative relationship between SLA and stomatal slope for the BWB model (df = 44, $p = 0.007$, $r = -0.388$; Fig. A5.15a) and a negative relationship between ^{13}C isotope discrimination and stomatal slope for the Lamour model (df = 24, $p = 0.008$, $r = -0.500$; Fig. A5.15c). In the broadleaf deciduous temperate tree PFT, I observed a negative relationship between N_a and stomatal slope for the Lamour model (df = 26, $p = 0.003$, $r = -0.530$; Fig. A5.15d). Finally for the broadleaf evergreen shrub PFT, I observed a positive relationship between SLA and stomatal slope for the Medlyn model (df = 11, $p = 0.005$, $r = 0.600$; Fig. A5.15b).

6.5 – **Discussion:**

Accurate and context specific estimations of the parameters used in empirical stomatal

conductance models are essential when attempting to simulate photosynthesis and transpiration across a wide range of conditions and PFTs. Here, using a large dataset of gas exchange measurements (Fig. 6.1), I evaluated the efficacy of three empirical stomatal models, and assess some of the factors responsible for global variation in stomatal model parameters. My results suggest that when considered across a wide range of PFTs and growth environments, both the BWB and Medlyn models produce comparable posterior distributions of PFT specific stomatal slope and intercept (Fig. 6.3), leading to equivalent predictive ability (Fig. 6.2). Posterior distributions for the Lamour model are more variable, with a large overlap in credible intervals of contrasting PFTs (Fig. 6.3c&f). Further, predictions of g_{sw} from the Lamour model fail to recreate observations at a higher rate than either the BWB or Medlyn models. Both stomatal slope and intercept also appear to be influenced in part by the bioclimatic zone in which they reside (Fig. 6.4), however these associations are weaker than the PFT specific trends. When the effect of measurement methodology on parameter estimates was examined, estimated stomatal intercept was significantly lower when estimated from curve derived data than from survey derived data (Fig. 6.5). Additionally, in an external model validation, both the BWB and Medlyn models performed better when using parameters fitted from survey data, while the Lamour model performed better when validated using parameters fitted from response curves (Fig. 6.6). Widespread and universally applicable relationships between leaf traits and stomatal behavior remain elusive, as I observed only weak correlations between $V_{cmax.25}$ and stomatal slope for the BWB, Medlyn and Lamour models, and a negative correlation between ^{13}C isotope discrimination and stomatal slope for the Lamour model (Fig. 6.7).

Several previous studies have found that when compared against each other, the BWB and Medlyn models produce similar estimates of g_{sw} (Miner *et al.*, 2017; Wolz *et al.*, 2017; Wu *et al.*, 2019b), with differences in predictive capacity arising from differences in genotypic specific response (Dos Santos *et al.*, 2023) or how each model performs under conditions of soil moisture deficit (Wang *et al.*, 2018). Similarly, in the process of programing the Medlyn model into the FATES dynamic vegetation demography model, Li *et al.*, (2022) demonstrated that under conditions where VPD $\leq$ 1.5, the Medlyn and BWB models predict nearly identical rates of transpiration, and only begin to diverge in their predictions as VPD increases and g_{sw} declines toward the stomatal intercept. My findings broadly agree with this, as across the full validation

dataset, predictions based on both the BWB and Medlyn models had similar goodness of fit (Fig. 2), and the overall magnitude of the PFT specific posterior means were similar between the models (Fig. 6.3a,b,d,e). However, for the Arctic/boreal PFTs the BWB model performed substantially worse, potentially as the result of the unique low RH, low VPD conditions common in the Arctic (Massmann *et al.*, 2019).

The fact that the Medlyn model explicitly considers the effect of VPD, rather than RH, may make it a more appealing choice for use in LSMs or other climate forecasting tools (Rogers *et al.*, 2017c). RH is not predicted to substantially change into the future, while VPD is expected to increase with atmospheric warming (Sato *et al.*, 2015). Concurrently, an increase in VPD may suppress photosynthesis while increasing transpiration, leading to lower ecosystem water use efficiency (Li *et al.*, 2023). Further, the use of a VPD type model may be more appealing from a physiological/mechanistic perspective as an increase in VPD is directly proportional to atmospheric demand for water, and thus mimics stomatal mechanics (Aphalo & Jarvis, 1991; Streck, 2003; Eamus *et al.*, 2008; Op De Beeck *et al.*, 2010). While recognizing that the BWB model has an extensive history as the g_{sw} model at the core of many contemporary LSMs (Oleson *et al.*, 2013; Knauer *et al.*, 2017; Franks *et al.*, 2018), and as such there is a great deal of literature from which to sample parameters (Miner *et al.*, 2017), I none the less would advocate for a transition toward implementing VPD type models (such as the Medlyn or Lamour models) in future LSM development.

The failure of the Lamour model to accurately reproduce stomatal dynamics for both the Arctic/boreal PFTs and the non-woody/crop PFTs (Fig. 6.2c&f) is somewhat surprising given that the Lamour model exhibited superior performance to the Medlyn model across several datasets in its initial and subsequent validations (Lamour *et al.*, 2022, 2023b). One possible explanation for this discrepancy comes from the use of A_g in the Lamour model, rather than A_n as had previously been the norm in prior stomatal conductance models (Ball *et al.*, 1987; Leuning, 1995; Katul *et al.*, 2009; Medlyn *et al.*, 2011; but see also Yin & Struik, 2009). When fitting gas exchange data to an A_g type model, the respiration rate (either R_{day} or R_{dark}) must be subtracted from A_n in order to estimate the correct rate of assimilation. This respiration rate can be assessed at different levels of organization, (e.g., leaf, species, PFT, absolute), however here I chose to fit the respiration rate as a PFT specific parameter to mirror the form of most LSMs (Wullschleger *et al.*, 2014). In doing

so, it is possible that an inappropriate leaf or species-specific respiration was applied to some of the measurements, thus biasing the estimation of A_g. Since assimilation is expected to have the largest influence on g_{sw} of any model constituent (Medlyn *et al.*, 2011; Duursma *et al.*, 2019), this may explain the heteroscedasticity I observed in g_{sw} predictions when using the Lamour model (Fig. 6.2c,f,i,l).

Uncertainty associated with the temperature response of respiration may also contribute to some of the issues observed with the Lamour model. A single value for the activation energy of mitochondrial respiration (H_a) was used to scale $R_{d.25}$ to $R_{d.Tleaf}$ (Equation 6.4), for all PFTs, however H_a is known to vary based on growth temperature (Kattge & Knorr, 2007). In particular, activation energies for Arctic vegetation are known to be lower than those estimated for temperate species (Rogers *et al.*, 2017d), which may potentially explain the especially poor performance of the Lamour model in the Arctic (Fig. 6.2c). The poor estimation of g_{sw} for the C3 crop PFT is also notable (Fig. 6.2f, Table 2). Of the 15 PFTs examined, the C3 crop had the highest mean A_n (24.45 μmol m^{-2} s^{-1}), and g_{sw} (0.514 mol m^{-2} s^{-1}), and it is possible that by taking the square of the A_g term, the Lamour model is substantially overpredicting g_{sw} for this PFT. Model validation tests are useful for evaluating the overall ability of a model to reproduce observations, and assessing which conditions result in the largest model predictive uncertainty, however a true test of model performance would be to integrate the Lamour model into a fully coupled LSM and evaluate its effect on predictions of primary productivity and evapotranspiration (e.g., Li *et al.*, 2022).

Variation in stomatal slope and intercept by PFT (Fig. 6.3) aligned well with previous efforts to categorize stomatal traits by PFT for use in LSMs (Lin *et al.*, 2015; Miner *et al.*, 2017; Franks *et al.*, 2018). In particular, PFT specific stomatal slope (Fig. 6.3a-c) appears to reflect, in part, variation in the carbon cost of water use, with longer lived PFTs such as trees and shrubs possessing lower stomatal slopes than shorter lived herbaceous species. Lower stomatal slopes are associated with higher water use efficiency (Buckley *et al.*, 2017), which would be the expected resource use and allocation strategy for PFTs with longer lifespans and which invest more heavily in foliar tissue (Wright *et al.*, 2004; Prentice *et al.*, 2014). The one exception to this trend is the C4 grass PFT, which across the three models has a lower stomatal slope than the other herbaceous PFTs, owed in part to its unique photosynthetic pathway (Beale *et al.*, 1999). I also observed a higher stomatal slope for the evergreen tropical tree PFT than the deciduous tropical tree PFT

across all three models (Fig. 6.3a-c), which suggests that tropical trees which seasonally shed their leaves are behaving in a more water use efficient manner than those which produce new leaves year-round. This reinforces previous work suggesting that in seasonally dry tropical ecosystems, foliar traits and water use efficiency differ based on leaf phenology, with deciduous phenologies tending to have higher water use efficiencies (Jackson *et al.*, 1995; Kitajima *et al.*, 1997a; Choat *et al.*, 2006; Hasselquist *et al.*, 2010; Ávila-Lovera *et al.*, 2019).

Differences in posterior mean estimates for stomatal intercept (Fig. 6.3d-f) appear less structured by growth form than stomatal slope. This may be a consequence of the variable interpretation of the stomatal intercept in both the BWB and Medlyn models, where the intercept includes both stomatal conductance associated with low irradiance (less than the level of light compensating photosynthesis), as well as cuticular conductance (Duursma *et al.*, 2019; Machado *et al.*, 2021; Márquez *et al.*, 2022). As such, a number of studies have called for replacing stomatal intercept with a true estimate of minimum stomatal conductance ($g_{sw,\text{min}}$), as such a formulation would better represent nonlinearity in the response of stomata to low irradiance (Barnard & Bauerle, 2013; De Kauwe *et al.*, 2015a; Lombardozzi *et al.*, 2017; Duursma *et al.*, 2019; Lamour *et al.*, 2022). In the Lamour model, stomatal intercept is equivalent to $g_{sw,\text{dark}}$, which can be thought of as the rate of g_{sw} for a dark adapted leaf. However, stomatal intercept estimates from the Lamour model were on average twice as large as estimates for the BWB or Medlyn models, which suggests that the use of a PFT mean R_d value, rather than a leaf specific R_d value may be influencing the fit. The role of stomatal intercept in models of g_{sw} is an active area of research (Duursma *et al.*, 2019), and one that I believe needs a stronger consideration as new g_{sw} schemes are developed and incorporated into LSMs

Variation in stomatal slope and intercept by climate zone (Fig. 6.4) in part agrees with previous studies which have suggested that stomatal traits should be associated with bioclimatic factors (Lin *et al.*, 2015; Franks *et al.*, 2018). In such a classification scheme, the combined (and potentially contrasting) effects of moisture and temperature must be considered. It is typically assumed that stomatal slope should increase with growth temperature, in part due to its dependance on Γ^* in the Medlyn and Lamour models (Medlyn *et al.*, 2011), and also because of the higher water carbon cost for transporting colder, more viscous xylem water (Prentice *et al.*, 2014). On the other hand, lower moisture environments are expected to bring about a lower stomatal slope

because vegetation will have evolved to be more water use efficient (De Kauwe *et al.*, 2015b). Here I found that stomatal slope tended to be higher in zones with a higher overall mean annual temperature, and tended to decrease with decreasing aridity, broadly agreeing with theory (Fig. 6.4a-c). However, these trends were relatively weak, and may be confounded by a diversity of growth forms within each climate zone.

Expectations of the interrelationship between temperature and humidity on stomatal intercept are less clearly defined in the literature, as traditionally, across both modeling and physiology literature, stomatal intercept is frequently assumed as zero or another small value (Šantrůček *et al.*, 2004; Duursma *et al.*, 2019). When stomatal intercept is quantified, it is often in terms of cuticular conductance, or $g_{sw,\min}$. Research from tropical systems (Slot *et al.*, 2021) suggest that $g_{sw,\min}$ does not differ among species growing along a gradient in rainfall, nor does it increase with leaf temperature (below 50ºC). Further, studies of plants growing in the Brazilian Cerrado suggest that minimum conductance is associated with carbon assimilation rates, such that a tradeoff exists between plants which maximize their assimilation potential, at the risk of a higher rate of cuticular water loss (Machado *et al.*, 2021). The lack of clear structuring in stomatal intercept observed in this study may be reflective of a diversity of stomatal intercept among species or PFTs existing in the same climate zone.

The elevated stomatal intercept observed for polar tundra vegetation may play an adaptive role in maintaining leaf energy balance, as has been observed in temperate species experiencing heat stress (Schuster *et al.*, 2016; Drake *et al.*, 2018). Alternatively, the long photoperiod experienced by polar vegetation, in concert with low VPD and high soil water availability, may have led tundra species to evolve comparably poorer control of stomata at low light and high VPD conditions (Anfodillo *et al.*, 2002; Fernández *et al.*, 2017). As for the species growing in the tropical monsoon climate, previous studies have suggested strong seasonality in stomatal traits in association with moisture availability (Igarashi *et al.*, 2015), with less strict stomatal control during the moist growing season following monsoons. Variation of both the stomatal slope and intercept in highly seasonal climates, such as the polar tundra, savannah, and tropical monsoon region merits additional study, as a single nominal value for stomatal behavior may be inappropriate in such climate zones.

By examining the effect of measurement methodology on the estimation of stomatal

parameters (Fig. 6.5), I directly address a question repeatedly raised in stomatal modeling studies, if response curves will produce the same stomatal parameter estimates as survey measurements (Dang *et al.*, 1998; Damour *et al.*, 2010; Miner *et al.*, 2017; Davidson *et al.*, 2022, 2023b; Lamour *et al.*, 2023b). At issue here are two relevant considerations, whether rates of A and g_{sw} are at a true "steady state" when measurements are made, and if the total range of expected conditions (PAR, VPD, C_a) are measured. Proponents of response curves typically argue that despite their laborious nature, these measurements ensure that gas exchange is stabilized, and allow manipulation of a single environmental variable at a time (Falge *et al.*, 1996; Bunce, 2000; Gutschick & Simonneau, 2002; Medlyn *et al.*, 2005; Héroult *et al.*, 2013; Gimeno *et al.*, 2016). Proponents of the survey approach argue that when determining stomatal parameters, measurements should focus only on the range of leaf-level conditions that occur in the environment of interest, and that by assessing g_{sw} over time, natural dynamics in stomatal behavior are captured (Ball, 1988; Collatz *et al.*, 1991; Dang *et al.*, 1998; Damour *et al.*, 2010; Davidson *et al.*, 2023b).

Here I found that differences in methodology led to substantial differences in estimated stomatal parameters (Fig. 6.5), in particular with curve derived data leading to lower stomatal intercept estimates than survey data (Fig. 6.5d-f). While stabilization of A and g_{sw} may contribute in part to these differences, the range of environment over which the two methods cover is clearly different between measurement types. In terms of measured PAR, while the range of values are comparable, the median value for the response curve dataset is 33% of the survey dataset (298.0 μmol m^{-2} s^{-1} PAR vs 918.0 μmol m^{-2} s^{-1} PAR) indicating that the curve data more heavily focused on lower values of PAR. Previously when focusing on PAR < 150 μmol m^{-2} s^{-1}, several researchers observed a nonlinearity in the g_{sw} response, which could lead to inaccurately low stomatal slope and intercept estimates (Ball, 1988; Leuning, 1990, 1995; Barnard & Bauerle, 2013; Lamour *et al.*, 2022). This effect of nonlinearity may be biasing parameter estimates for the response dataset, with 37% of the data measured with PAR < 150 μmol m^{-2} s^{-1}. Interestingly though, stomatal intercepts for the Lamour model, which was developed to account for nonlinearity in the g_{sw} response (Lamour *et al.*, 2022), are also significantly lower when fit using curve derived data (Fig. 6.5f), which suggests that other differences in the dataset may be influencing parameter fits.

When parameters derived using each method were validated against data collected using the opposite method (Fig. 6.6), survey derived parameters better represented response curve data (Fig.

6.6a,c,e) than response curve parameters representing survey data (Fig. 6.6b,d,f). This is not surprising given that curve derived data tend to have less variability in g_{sw} for a given set of environmental conditions, due to better controls on steady state gas exchange (Miner *et al.*, 2017; Davidson *et al.*, 2023b). This can be seen when assessing the heteroscedasticity of the observed vs predicted g_{sw}; curve derived data have less scatter, and lower RMSE values across the range of conditions (Fig. 6.6a,c,e). Looking specifically at the Lamour model (Fig. 6.6e-f), it appears that the survey derived stomatal slope and intercept correspond particularly poorly with the data, and lead to a strong bias for overpredicting low g_{sw} values and underpredicting high g_{sw} values. This may be a consequence of the fact that in the Lamour model the stomatal intercept is equivalent to $g_{sw,\text{dark}}$ and is therefore the lower bound of possible g_{sw}. Therefore if a calibration dataset is used in which the estimated $g_{sw,\text{dark}}$ is above any observed g_{sw} values for the validation dataset, those predictions will automatically be artificially high (see also Fig. 6.2c,f,i,l). Neither the BWB or Medlyn model suffer from this drawback, as for both of these models predicted g_{sw} is able to drop below the stomatal intercept when values of A_n drop below 0 μmol m^{-2} s^{-1}.

While choice of specific measurement methodology may be dependent on other experimental considerations, such as ease of access to upper canopy branches (Verryckt *et al.*, 2020; Missik *et al.*, 2021; Davidson *et al.*, 2022), researchers should nonetheless be cognizant of the potential biases introduced by their chosen method. When aggregating data collected using different methods, consideration of the environmental variability and data stability associated with each data type should be assessed (Miner *et al.*, 2017). Therefore, I caution against the mixing of data types, methods, or models without first considering the simplifying assumptions inherent to each.

Of the relationships between stomatal slope and leaf traits assessed in this study, only four were found to be significant when assessed across all PFTs (Fig. 6.7). In their investigation of the response of stomatal conductance to seasonal drought in the tropics, Wu *et al.*, (2019) observed that stomatal slope as fitted with the BWB and Medlyn models was negatively correlated with leaf mass per unit area (inverse of SLA). Across the three models tested in this study, I found no overall relationship between stomatal slope and SLA (Fig. 6.7j-l), however in the broadleaf evergreen shrub PFT, I observed a positive association between SLA and stomatal slope for the Medlyn model (Fig. A5.15b). In contrast, for the broadleaf evergreen tropical tree PFT, I observed a negative relationship between SLA and stomatal slope as fit using the BWB model (Fig. A5.15a).

This negative correlation, which has the opposite sign to what was found by Wu *et al.*, (2019), suggests that thinner, lower density leaves should have a higher water use efficiency. This finding runs directly in contrast to predictions of optimal resource allocation, which suggest that leaves and structures which require a higher construction cost should be more efficient with respect to their resource use (Terashima *et al.*, 2001; Prentice *et al.*, 2014). One possible explanation for this apparent tradeoff is that thinner leaves will experience larger shifts in leaf temperature (Michaletz *et al.*, 2015, 2016), and thus must be more water use efficient to compensate for extra thermoregulatory water loss. However, the fact that this tradeoff does not appear to be present in deciduous tropical tree species may suggest that it is a statistical artifact rather than an adaptive strategy.

When deriving and testing their non-linear g_{sw} model Lamour *et al.*, (2022) found that stomatal slope was negatively associated with $V_{cmax.25}$ and N_a. Here I find that for both the BWB and Medlyn models, stomatal slope is positively associated with $V_{cmax.25}$ (Fig. 6.7a-b), and using the Lamour model stomatal slope is negatively associated with $V_{cmax.25}$ (Fig. 6.7c). Across all three models, I observed no significant correlation between stomatal slope and N_a (Fig. 6.7d-f). However, for the broadleaf deciduous temperate tree PFT, I observed a negative relationship between Lamour model stomatal slope and N_a (Fig. A5.15d). While Lamour *et al.*, (2022) do not provide any mechanistic insight into the association between stomatal slope and $V_{cmax.25}$ or N_a, their association likely stems from coordination in rates of A and g_{sw} leading to an optimal ratio of intercellular to atmospheric CO_2 (C_i/C_a), which correlates with leaf-level water use efficiency (Farquhar *et al.*, 1989; McDowell *et al.*, 2006; Franks *et al.*, 2018). It is unclear as to why the sign of the correlation differs between models, however issues associated PFT specific R_d estimates (as discussed above) may contribute to error when estimating species specific Lamour stomatal slope.

In their evaluation of the BWB and Medlyn models for use in LSMs, Franks *et al.*, (2018) suggests that through its association with rainfall and C_i/C_a, $\delta^{13}C$ should be associated with stomatal slope such that the more negative the value of $\delta^{13}C$, the higher the stomatal slope. When tested in this study, I found that across all PFTs, stomatal slope (as fitted by the Lamour model) and $\delta^{13}C$ were negatively correlated (Fig. 6.7i), in agreement with Franks *et al.*, (2018). Further, I observed a strong negative correlation between Lamour stomatal slope and $\delta^{13}C$ in the broadleaf evergreen tropical tree PFT (Fig. A5.15c). These associations provide a potential means of

estimating global variation in stomatal slope through its association with leaf physiology, rather than the standard approach of estimating group specific stomatal parameters (De Kauwe *et al.*, 2015a; Lin *et al.*, 2015, this study) which is often constrained by our understanding of biome boundaries and PFTs.

6.6 – **Figures:**

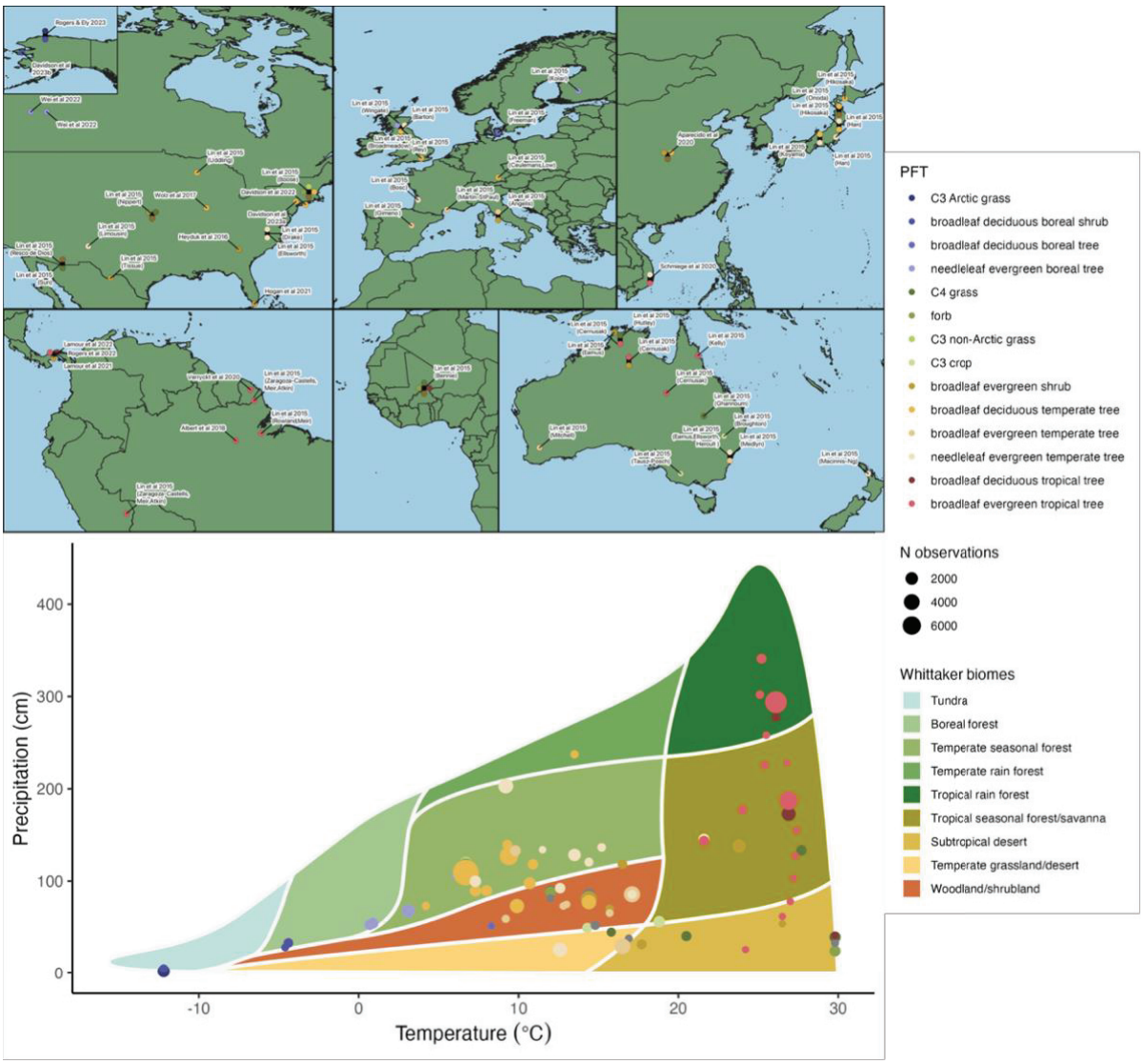

Figure 6.1: Geographic and climatological extent of the data used in this study. Panel (a) shows the sampling location of each dataset, along with the plant functional types (PFTs) present at each location. When multiple PFTs co-occur, they are displayed offset from their exact geographic points. Direct links to each dataset can be found in Table A5.1. Panel (b) shows the Whittaker biome of each constituent dataset. Estimates of location specific temperature and precipitation come from the WorldClim dataset, version 2.1 (https://www.worldclim.org/data/worldclim21.html). Whittaker biome extents are based on Ricklefs (2008).

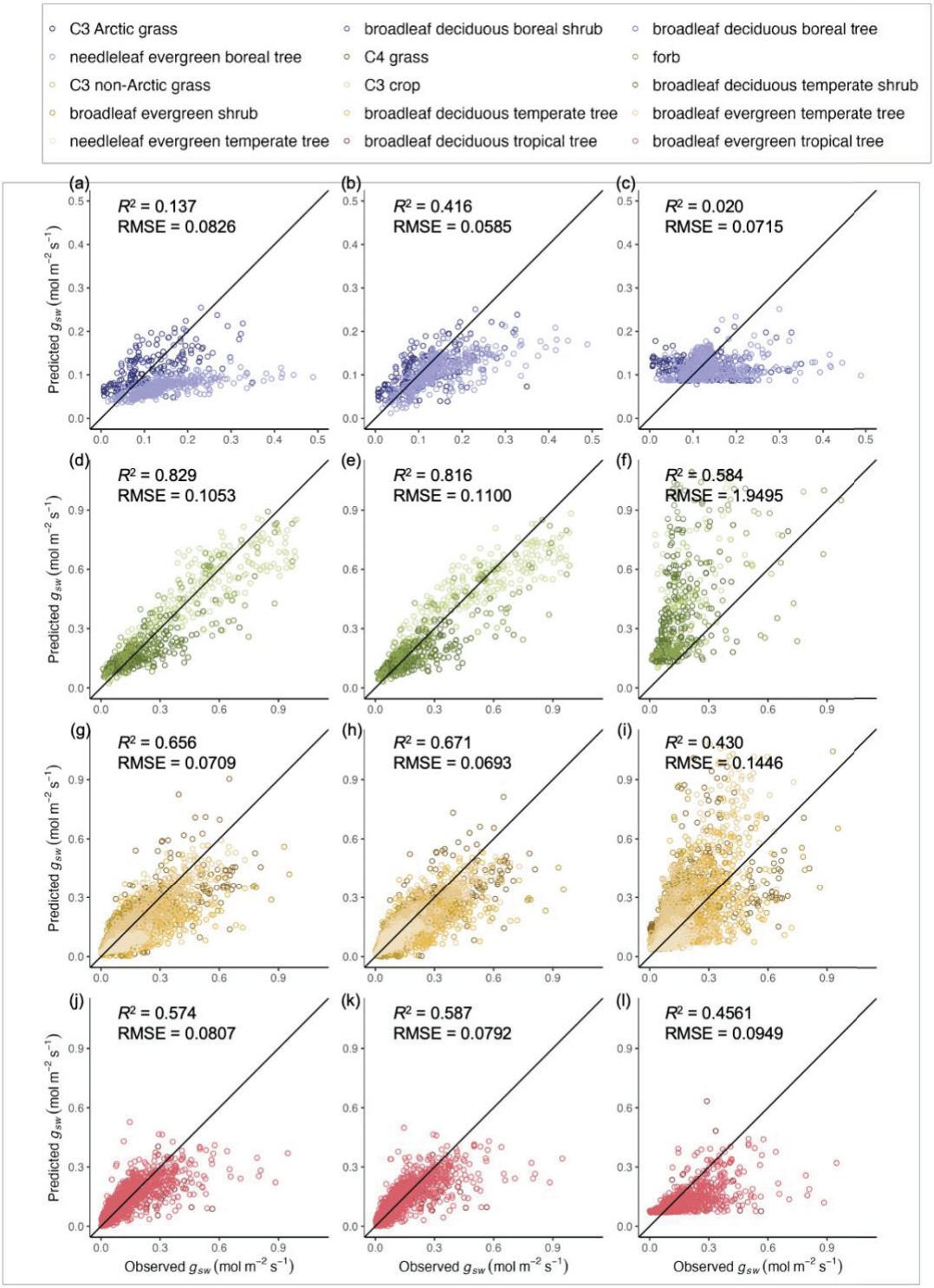

Figure 6.2: Observed versus model predicted g_{sw} (mol m^{-2} s^{-1}) for the three empirical models broken out by PFT group. Panels (a), (d), (g), and (j) show predictions using the BWB model, panels (b), (e), (h), and (j) show predictions using the Medlyn model, and panels (c), (f), (i), and (l) show predictions using the Lamour model. All observed g_{sw} values come from the validation dataset, which contains approximately 20% of the data and was excluded from the calibration dataset. For each panel a marginal R^2, and RMSE is reported. Black diagonal lines in each panel are the 1:1 reference line.

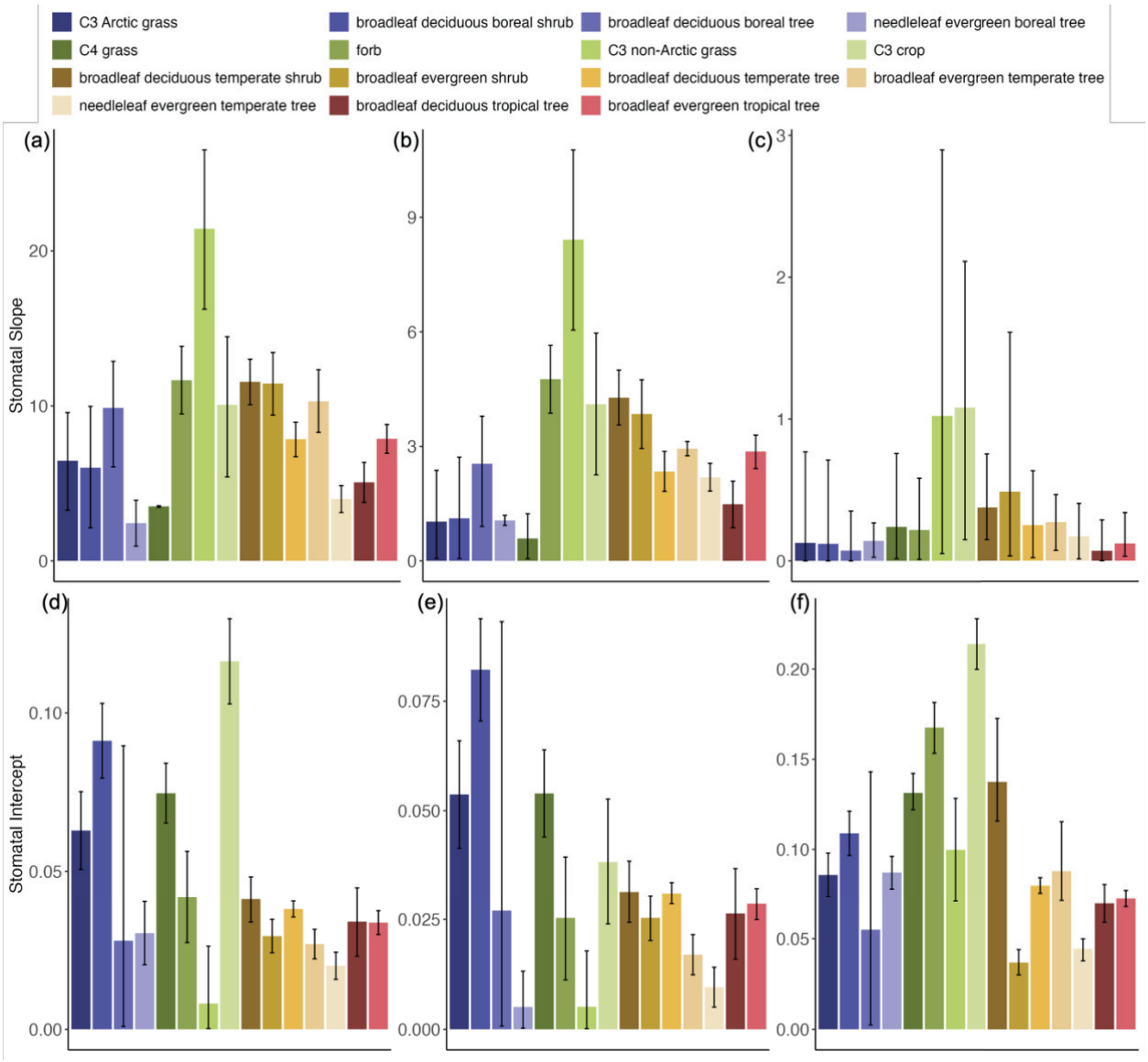

Figure 6.3: PFT specific estimates for stomatal slope (a-c) and intercept (d-f) and their relative uncertainty. Data in panels (a) and (d) are fit using the BWB model, data in panels (b) and (e) are fit using the Medlyn model, and data in panels (c) and (f) are fit using the Lamour model. Error bars represent the 95% credible interval for the estimate mean.

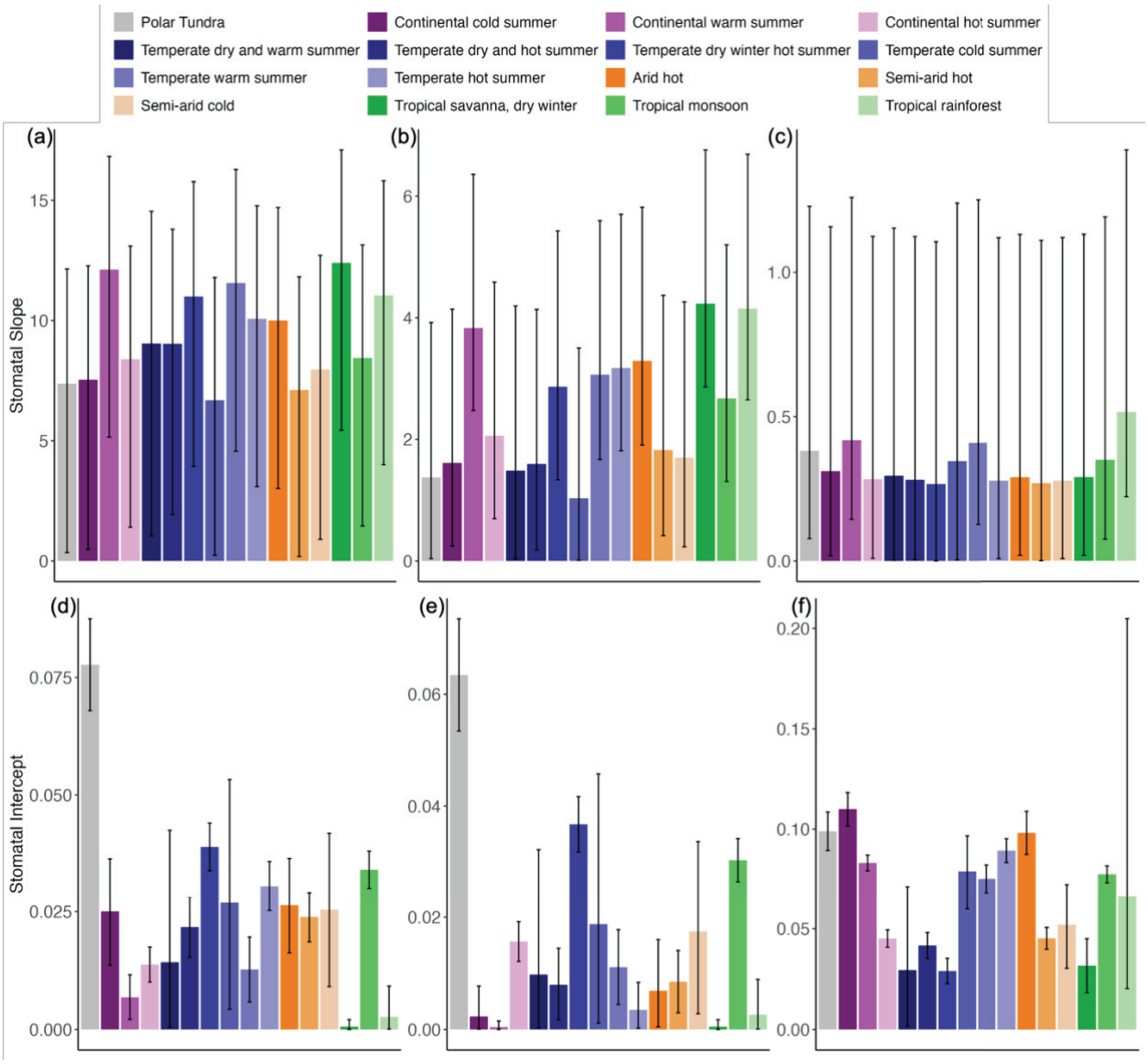

Figure 6.4: Köppen-Geiger Climate Zone specific estimates for stomatal slope (a-c) and intercept (d-f) and their relative uncertainty. Data in panels (a) and (d) are fit using the BWB model, data in panels (b) and (e) are fit using the Medlyn model, and data in panels (c) and (f) are fit using the Lamour model. Error bars represent the 95% credible interval for the estimate mean.

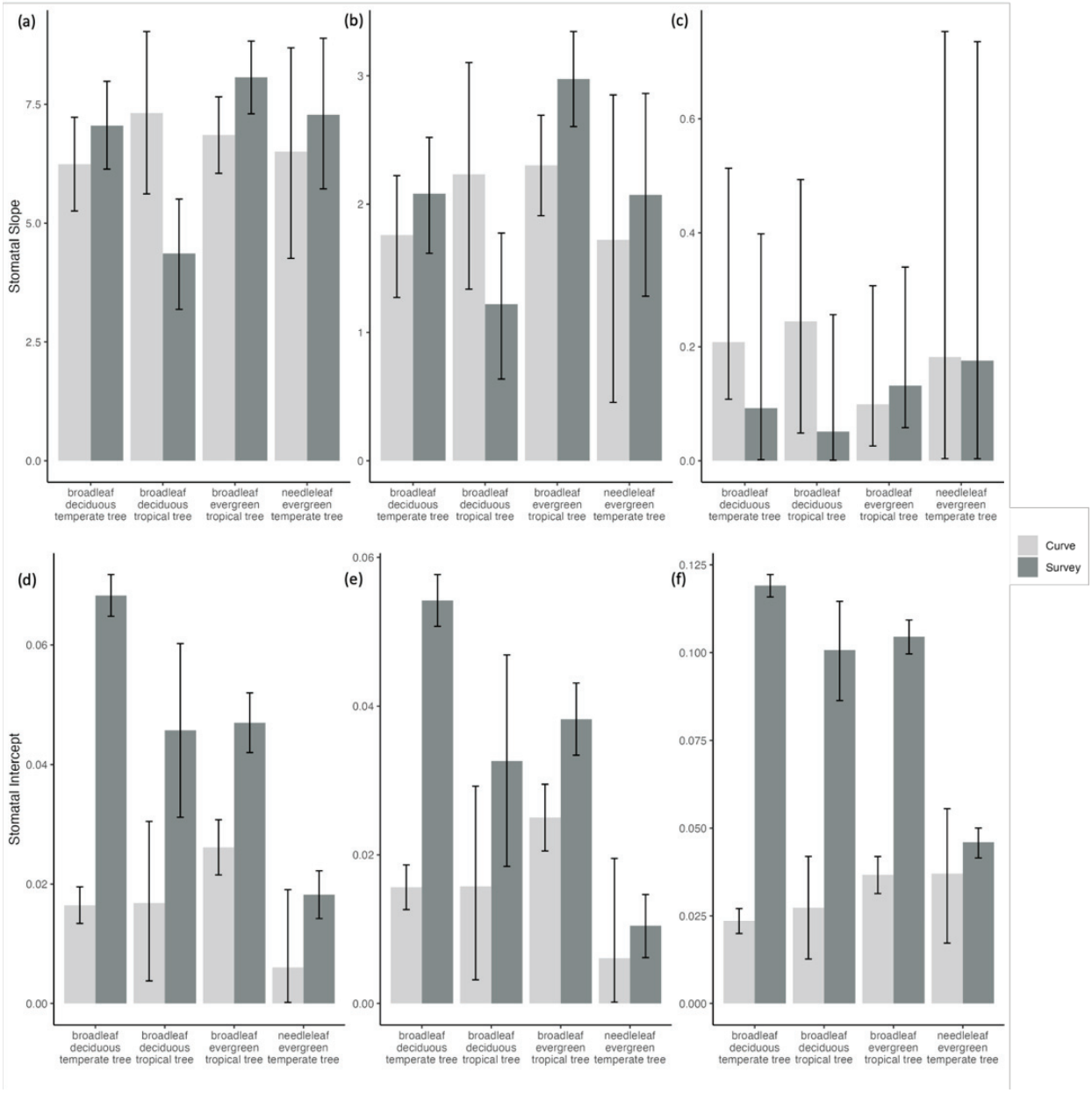

Figure 6.5: Evaluation of the effect of measurement methodology on **e**stimates of stomatal slope (a-c) and intercept (d-f) and their relative uncertainty. Data in panels (a) and (d) are fit using the BWB model, data in panels (b) and (e) are fit using the Medlyn model, and data in panels (c) and (f) are fit using the Lamour model. Curve derived data are any data in which stomatal response was elicited via successive manipulation of the leaf-level environment (e.g., VPD, irradiance, CO_2). Survey derived data are any data in which gas exchange was measured under ambient conditions successively on the same leaf or across multiple leaves on the same individual plant. Error bars represent the 95% credible interval for the estimate mean.

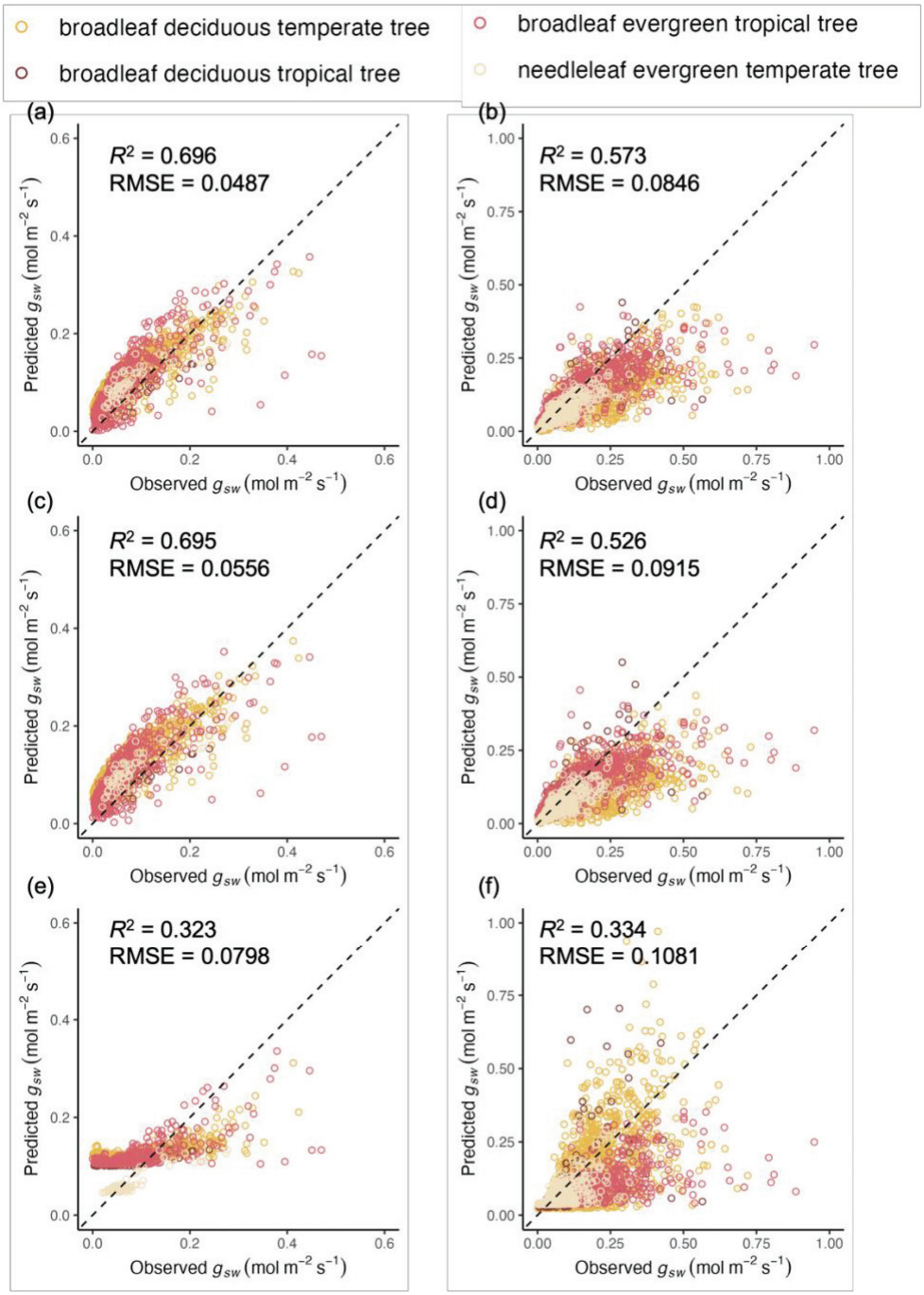

Figure 6.6: Observed versus model predicted g_{sw} (mol m^{-2} s^{-1}) for the three empirical models broken out by data source. Panels (a), (c), and (e) show response curve derived g_{sw} observations against predictions made using survey derived parameters. Panels (b), (d), and (f) show survey derived g_{sw} observations against predictions made using response curve derived parameters. Panels (a) and (b) correspond to the BWB model, panels (c) and (d) correspond to the Medlyn model, and panels (e) and (f) correspond to the Lamour model. All observed g_{sw} values come from the validation dataset, which contains approximately 20% of the data that was excluded from the calibration dataset. For each panel a marginal R^2, and RMSE is reported. Black dashed lines in each panel are the 1:1 refence line.

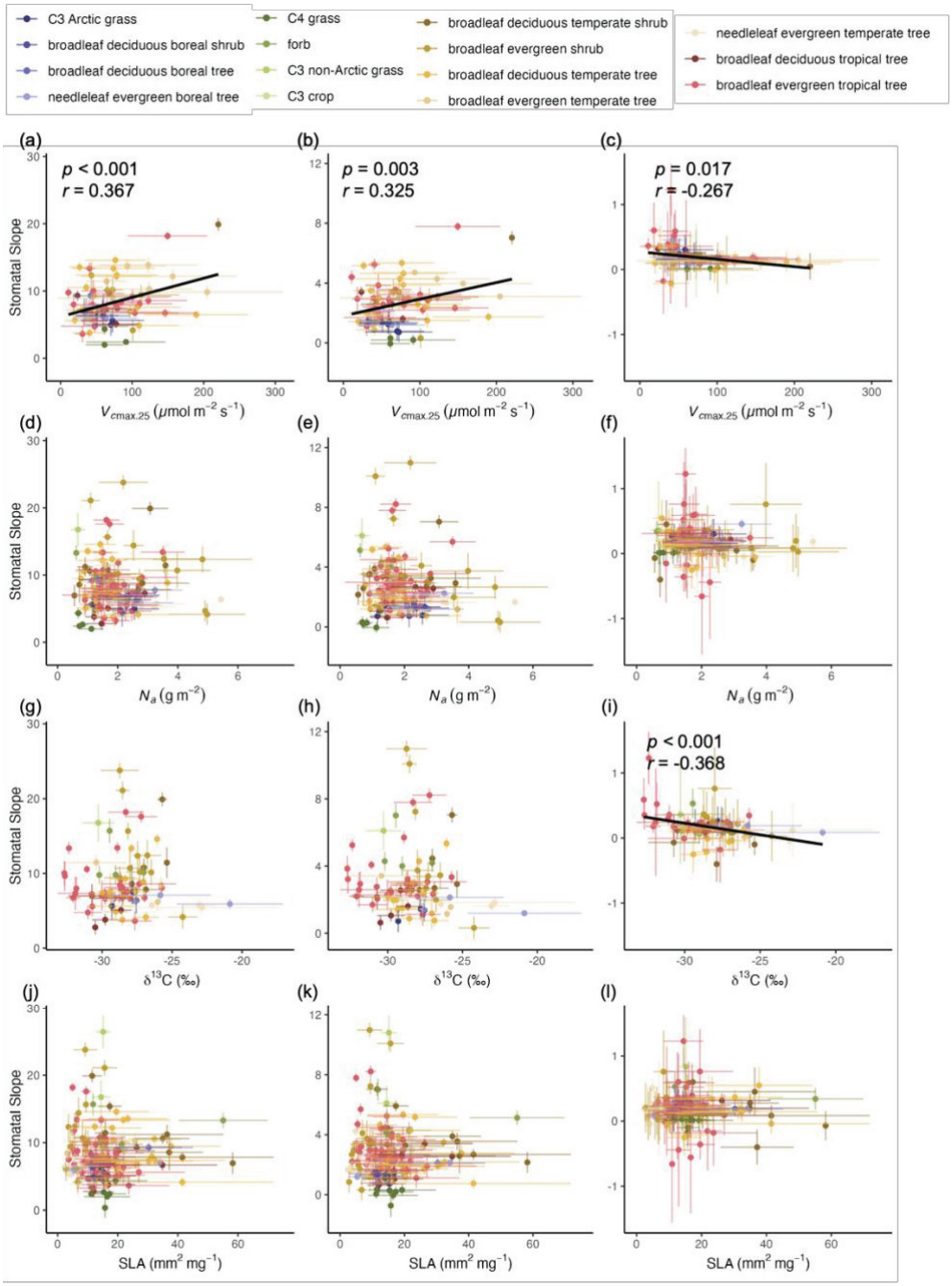

Figure 6.7: Correlations between estimated stomatal slope and leaf traits across all PFTs and species. Relationship between stomatal slope and (a-c) the maximum carboxylation capacity of the enzyme rubisco normalized to 25ºC ($V_{cmax.25}$; µmol m^{-2} s^{-1}), (d-f) foliar nitrogen content per unit area (N_a; g m^{-2}), (g-i) foliar carbon isotope discrimination ($\delta^{13}C$; ‰), and (j-l) specific leaf area (SLA; mm^2 mg^{-1}). Panels (a), (d), (g), and (j) correspond to the BWB model, panels (b), (e), (h), and (k) correspond to the Medlyn model, and panels (c), (f), (i), and (l) correspond to the Lamour model. Lines of best fit are shown for relationships which were significant. Horizontal error bars are ± 2 SE of the mean species-specific trait estimate. Vertical error bars are the 95% credible interval for the species level estimate of stomatal slope. The reported *r* value is the Pearson correlation coefficient.

6.7 – **Tables:**

Table 6.1: List of models evaluated as part of the study. For each model fixed and random effects groups are identified. All models were fit using the calibration data set which consisted of 80% of the data chosen at random. For the first two models, one alternative version of each was tested, in which only uninformative priors for μ_1 were supplied; $\mu_1 \sim N(5.0,10.0)[0]$. For the third model, two alternative versions of the model were tested. In the first of the two alternatives, uninformative priors for μ_1 were supplied; $\mu_1 \sim N(0.4,1.0)[0]$. In the second alternative model, uninformative priors were supplied for both μ_1 and μ_2; $\mu_1 \sim N(0.4,1.0)[0]$ and $\mu_2 \sim N(1.0,0.1)[0]$.

Model Equation	Fixed Effects	Random Effects	g_{sw} Model	Priors†
$\boldsymbol{g_{sw,i,j,k} = \left(\mu_{0,PFT_j}\right) + \left(\frac{A_{n_i} * Rh_i}{C_{a_i}} * \left(\mu_{1,PFT_j} + \alpha_{species_k}\right)\right) + \varepsilon_i}$	$m \sim$ PFT = μ_1 $b \sim$ PFT = $\mu 0$	$m \sim$ Species = α	BWB	$\mu_0 \sim N(0.01000, 1.000)[0]$ $\mu_{1,\text{BDBS}} \sim N(10.5000, 10.000)[0]$ $\mu_{1,\text{BDBT}} \sim N(5.000, 10.000)[0]$ $\mu_{1,\text{BDTmS}} \sim N(5.000, 10.000)[0]$ $\mu_{1.\text{BDTmT}} \sim N(7.4158, 17.933)[0]$ $\mu_{1,\text{BDTrT}} \sim N(5.0000, 10.000)[0]$ $\mu_{1,\text{BES}} \sim N(6.4486, 13.492)[0]$ $\mu_{1,\text{BETmT}} \sim N(5.0000, 10.000)[0]$ $\mu_{1,\text{BETrT}} \sim N(7.9427, 25.264)[0]$ $\mu_{1,\text{C3AG}} \sim N(5.0000\ 10.000)[0]$ $\mu_{1,\text{C3C}} \sim N(11.7330, 63.077)[0]$ $\mu_{1,\text{C3nAG}} \sim N(9.2386, 21.238)[0]$ $\mu_{1,\text{C4G}} \sim N(3.5115, 0.025)[0]$ $\mu_{1,\text{NEBT}} \sim N(6.2110, 1.837)[0]$ $\mu_{1,\text{NETmT}} \sim N(4.658, 0.842)[0]$ $\mu_{1,\text{Forb}} \sim N(10.1372, 0.512)[0]$ $\alpha \sim N(0.000, 1.000)$ $\varepsilon \sim N(0.000, 0.0100)$
$\boldsymbol{g_{sw,i,j,k} = \left(\mu_{0,PFT_j}\right) + 1.6\left(1 + \frac{\left(\mu_{1,PFT_j} + \alpha_{species_k}\right)}{\sqrt{VPD_{leaf_i}}}\right)\frac{A_{n_i}}{C_{a,i}} + \varepsilon_i}$	$g_1 \sim$ PFT = μ_1 $g_0 \sim$ PFT = $\mu 0$	$g_1 \sim$ Species = α	Medlyn	$\mu_0 \sim N(0.01000, 1.000)[0]$ $\mu_{1,\text{BDBS}} \sim N(5.0000, 10.000)[0]$ $\mu_{1,\text{BDBT}} \sim N(5.000, 10.000)[0]$ $\mu_{1,\text{BDTmS}} \sim N(4.8200, 10.000)[0]$ $\mu_{1,\text{BDTmT}} \sim N(5.4675, 1.653)[0]$ $\mu_{1,\text{BDTrT}} \sim N(5.0000, 10.000)[0]$ $\mu_{1,\text{BES}} \sim N(4.3300, 2.015)[0]$ $\mu_{1,\text{BETmT}} \sim N(2.9400, 0.096)[0]$ $\mu_{1,\text{BETrT}} \sim N(3.6211, 1.718)[0]$ $\mu_{1,\text{C3AG}} \sim N(5.0000\ 10.000)[0]$ $\mu_{1,\text{C3C}} \sim N(4.4333, 1.380)[0]$ $\mu_{1,\text{C3nAG}} \sim N(5.2500, 10.000)[0]$ $\mu_{1,\text{C4G}} \sim N(1.6200, 10.000)[0]$ $\mu_{1,\text{NEBT}} \sim N(1.0550, 0.0685)[0]$ $\mu_{1,\text{NETmT}} \sim N(2.5860, 0.5124)[0]$ $\mu_{1,\text{Forb}} \sim N(4.1433, 0.8656)[0]$ $\alpha \sim N(0.000, 1.000)$ $\varepsilon \sim N(0.000, 0.0100)$

† PFT abbreviations are as follows: BDBS = broadleaf deciduous boreal shrub, BDBT= broadleaf deciduous boreal tree, BDTmS = broadleaf deciduous temperate shrub, BDTmT = broadleaf deciduous temperate tree, BDTrT = broadleaf deciduous tropical tree, BES = broadleaf evergreen shrub, BETmT = broadleaf evergreen temperate tree, BETrT = broadleaf evergreen tropical tree, C3AG = C3 Arctic grass, C3C = C3 crop, C3nAG = C3 non-Arctic grass, C4G = C4 grass, NEBT = needleleaf evergreen boreal tree, NETmT = needleleaf evergreen temperate tree, Forb= forb.

Table 6.1 (cont.): List of models evaluated as part of the study. For each model fixed and random effects groups are identified. All models were fit using the calibration data set which consisted of 80% of the data chosen at random. For the first two models, one alternative version of each was tested, in which only uninformative priors for μ_1 were supplied; $\mu_1 \sim N(5.0,10.0)[0]$. For the third model, two alternative versions of the model were tested. In the first of the two alternatives, uninformative priors for μ_1 were supplied; $\mu_1 \sim N(0.4,1.0)[0]$. In the second alternative model, uninformative priors were supplied for both μ_1 and μ_2; $\mu_1 \sim N(0.4,1.0)[0]$ and $\mu_2 \sim N(1.0,0.1)[0]$.

Model Equation	Fixed Effects	Random Effects	g_{sw} Model	Priors†
$$g_{sw,i,j,k} = \left(\mu_{0,PFT_j}\right) + 1.6\left(1 + \frac{\left(\mu_{1,PFT_j} + \alpha_{species_k}\right)}{\sqrt{VPD_{leaf_i}}}\right) * \frac{\left(A_{n_i} - \left(\mu_{2,PFT_j} + \beta_{species_k}\right)\right)^2}{C_{a,i}} + \varepsilon_i$$	$g_1 \sim$ PFT = μ_1 $g_0 \sim$ PFT = μ_0 $R_d \sim$ PFT = μ_2	$g_1 \sim$ Species = α $R_d \sim$ Species = β	Lamour	$\mu_0 \sim N(0.0100, 1.000)[0]$ $\mu_{1,\text{BDBS}} \sim N(0.4000, 1.000)[0]$ $\mu_{1,\text{BDBT}} \sim N(0.4000, 1.000)[0]$ $\mu_{1,\text{BDTmS}} \sim N(0.3874, 1.000)[0]$ $\mu_{1,\text{BDTmT}} \sim N(0.4327, 1.653)[0]$ $\mu_{1,\text{BDTrT}} \sim N(0.4000, 1.000)[0]$ $\mu_{1,\text{BES}} \sim N(0.3531, 2.015)[0]$ $\mu_{1,\text{BETmT}} \sim N(0.2558, 0.096)[0]$ $\mu_{1,\text{BETrT}} \sim N(0.3035, 1.718)[0]$ $\mu_{1,\text{C3AG}} \sim N(0.4000, 1.000)[0]$ $\mu_{1,\text{C3C}} \sim N(0.306, 1.380)[0]$ $\mu_{1,\text{C3nAG}} \sim N(0.4175, 1.000)[0]$ $\mu_{1,\text{C4G}} \sim N(0.1634, 1.000)[0]$ $\mu_{1,\text{NEBT}} \sim N(0.1239, 0.0685)[0]$ $\mu_{1,\text{NETmT}} \sim N(0.2310, 0.5124)[0]$ $\mu_{1,\text{Forb}} \sim N(0.3400, 0.8656)[0]$ $\mu_{2,\text{BDBS}} \sim \Gamma(1.3989, 1.809)$ $\mu_{2,\text{BDBT}} \sim \Gamma(1.2643, 1.250)$ $\mu_{2,\text{BDTmS}} \sim \Gamma(2.0874, 0.829)$ $\mu_{2,\text{BDTmT}} \sim \Gamma(1.3593, 1.000)$ $\mu_{2,\text{BDTrT}} \sim \Gamma(2.6084, 0.645)$ $\mu_{2,\text{BES}} \sim \Gamma(3.0375, 0.737)$ $\mu_{2,\text{BETmT}} \sim \Gamma(2.3096, 0.657)$ $\mu_{2,\text{BETrT}} \sim \Gamma(3.8529, 0.487)$ $\mu_{2,\text{C3AG}} \sim \Gamma(3.1666, 1.498)$ $\mu_{2,\text{C3C}} \sim \Gamma(0.7511, 1.351)$ $\mu_{2,\text{C3nAG}} \sim \Gamma(1.0796, 1.039)$ $\mu_{2,\text{C4G}} \sim \Gamma(11.5250, 0.326)$ $\mu_{2,\text{NEBT}} \sim \Gamma(1.1630\ 1.568)$ $\mu_{2,\text{NETmT}} \sim \Gamma(1.5637, 0.871)$ $\mu_{2,\text{Forb}} \sim \Gamma(1.4168, 0.985)$ $\alpha \sim N(0.000, 1.000)$ $\beta \sim N(0.000, 0.1000)$ $\varepsilon \sim N(0.000, 0.0100)$
$$g_{sw,i,j,k} = \left(\mu_{0,Climate\ Zone_j}\right) + \left(\frac{A_{n_i} * Rh_i}{C_{a_i}} * \left(\mu_{1,Climate\ Zone_j} + \alpha_{Growth\ Form_k}\right)\right) + \varepsilon$$	$m \sim$ Climate Zone = μ_1 $b \sim$ Climate Zone = μ_0	$m \sim$ Growth Form = α	BWB	$\mu_0 \sim N(0.01000, 1.000)[0]$ $\mu_1 \sim N(5.0000, 10.000)[0]$ $\alpha \sim N(0.000, 1.000)$ $\varepsilon \sim N(0.000, 0.0100)$
$$g_{sw,i,j,k} = \left(\mu_{0,Climate\ Zone_j}\right) + 1.6\left(1 + \frac{\left(\mu_{1,Climate\ Zone_j} + \alpha_{Growth\ Form_k}\right)}{\sqrt{VPD_{leaf_i}}}\right) * \frac{A_{n_i}}{C_{a,i}} + \varepsilon_i$$	$g_1 \sim$ Climate Zone = μ_1 $g_0 \sim$ Climate Zone = μ_0	$g_1 \sim$ Growth Form = α	Medlyn	$\mu_0 \sim N(0.01000, 1.000)[0]$ $\mu_1 \sim N(5.0000, 10.000)[0]$ $\alpha \sim N(0.000, 1.000)$ $\varepsilon \sim N(0.000, 0.0100)$

† PFT abbreviations are as follows: BDBS = broadleaf deciduous boreal shrub, BDBT= broadleaf deciduous boreal tree, BDTmS = broadleaf deciduous temperate shrub, BDTmT = broadleaf deciduous temperate tree, BDTrT = broadleaf deciduous tropical tree, BES = broadleaf evergreen shrub, BETmT = broadleaf evergreen temperate tree, BETrT = broadleaf evergreen tropical tree, C3AG = C3 Arctic grass, C3C = C3 crop, C3nAG = C3 non-Arctic grass, C4G = C4 grass, NEBT = needleleaf evergreen boreal tree, NETmT = needleleaf evergreen temperate tree, Forb= forb.

Table 6.1 (cont.): List of models evaluated as part of the study. For each model fixed and random effects groups are identified. All models were fit using the calibration data set which consisted of 80% of the data chosen at random. For the first two models, one alternative version of each was tested, in which only uninformative priors for μ_1 were supplied; $\mu_1 \sim N(5.0,10.0)[0]$. For the third model, two alternative versions of the model were tested. In the first of the two alternatives, uninformative priors for μ_1 were supplied; $\mu_1 \sim N(0.4,1.0)[0]$. In the second alternative model, uninformative priors were supplied for both μ_1 and μ_2; $\mu_1 \sim N(0.4,1.0)[0]$ and $\mu_2 \sim N(1.0,0.1)[0]$.

Model Equation	Fixed Effects	Random Effects	g_{sw} Model	Priors†
$g_{sw,i,j,k,l} = \left(\mu_{0,Climate\ Zone_j}\right) + 1.6\left(1 + \frac{\left(\mu_{1,Climate\ Zone_j} + \alpha_{Growth\ Form_k}\right)}{\sqrt{VPD_{leaf_i}}}\right) * \frac{\left(A_{n_i} - \left(\mu_{2,Climate\ Zone_j} + \beta_{species_l}\right)\right)^2}{C_{a,i}} + \varepsilon_i$	$g_1 \sim$ Climate Zone $= \mu_1$ $g_0 \sim$ Climate Zone $= \mu_0$ $R_d \sim$ Climate Zone $= \mu_2$	$g_1 \sim$ Growth Form $= \alpha$ $R_d \sim$ Species $= \beta$	Lamour	$\mu_0 \sim N(0.0100, 1.000)[0]$ $\mu_1 \sim N(0.4000, 1.000)[0]$ $\mu_2 \sim N(1.0000, 0.1000)[0]$ $\alpha \sim N(0.000, 1.000)$ $\beta \sim N(0.000, 0.1000)$ $\varepsilon \sim N(0.000, 0.0100)$
$g_{sw,i,j,k,l} = \left(\mu_{0,PFT_j} + \mu_{2,Method_k}\right) + \left(\frac{A_{n_i} * Rh_i}{C_{a_i}} * \left(\mu_{1,PFT_j} + \mu_{3,Method_k} + \alpha_{Species_l}\right)\right) + \varepsilon_i$	$m \sim$ PFT $= \mu_1$ $m \sim$ Method $= \mu_2$ $b \sim$ PFT $= \mu_0$ $b \sim$ Method $= \mu_3$	$m \sim$ Species $= \alpha$	BWB	$\mu_0 \sim N(0.01000, 1.000)[0]$ $\mu_2 \sim N(0.01000, 1.000)[0]$ $\mu_1 \sim N(5.0000, 10.000)[0]$ $\mu_3 \sim N(5.0000, 10.000)[0]$ $\alpha \sim N(0.000, 1.000)$ $\varepsilon \sim N(0.000, 0.0100)$
$g_{sw,i,j,k,l} = \left(\mu_{0,PFT_j} + \mu_{2,Method_k}\right) + 1.6\left(1 + \frac{\left(\mu_{1,PFT_j} + \mu_{3,Method_k} + \alpha_{Species_l}\right)}{\sqrt{VPD_{leaf_i}}}\right)\frac{A_{n_i}}{C_{a,i}} + \varepsilon_i$	$g_1 \sim$ PFT $= \mu_1$ $g_1 \sim$ Method $= \mu_2$ $g_0 \sim$ PFT $= \mu_0$ $g_0 \sim$ Method $= \mu_3$	$g_1 \sim$ Species $= \alpha$	Medlyn	$\mu_0 \sim N(0.01000, 1.000)[0]$ $\mu_2 \sim N(0.01000, 1.000)[0]$ $\mu_1 \sim N(5.0000, 10.000)[0]$ $\mu_3 \sim N(5.0000, 10.000)[0]$ $\alpha \sim N(0.000, 1.000)$ $\varepsilon \sim N(0.000, 0.0100)$
$g_{sw,i,j,k,l} = \left(\mu_{0,PFT_j} + \mu_{3,Method_k}\right) + 1.6\left(1 + \frac{\left(\mu_{1,PFT_j} + \mu_{4,Method_k} + \alpha_{Species_l}\right)}{\sqrt{VPD_{leaf_i}}}\right) * \frac{\left(A_{n_i} - \left(\mu_{2,PFT_j} + \mu_{5,Method_k} + \beta_{species_l}\right)\right)^2}{C_{a,i}} + \varepsilon_i$	$g_1 \sim$ PFT $= \mu_1$ $g_1 \sim$ Method $= \mu_4$ $g_0 \sim$ PFT $= \mu_0$ $g_0 \sim$ Method $= \mu_3$ $R_d \sim$ PFT $= \mu_2$ $R_d \sim$ Method $= \mu_5$	$g_1 \sim$ Species $= \alpha$ $R_d \sim$ Species $= \beta$	Lamour	$\mu_0 \sim N(0.0100, 1.000)[0]$ $\mu_1 \sim N(0.4000, 1.000)[0]$ $\mu_2 \sim N(1.0000, 0.1000)[0]$ $\mu_3 \sim N(0.0100, 1.000)[0]$ $\mu_4 \sim N(0.4000, 1.000)[0]$ $\mu_5 \sim N(1.0000, 0.1000)[0]$ $\alpha \sim N(0.000, 1.000)$ $\beta \sim N(0.000, 0.1000)$ $\varepsilon \sim N(0.000, 0.0100)$

† PFT abbreviations are as follows: BDBS = broadleaf deciduous boreal shrub, BDBT= broadleaf deciduous boreal tree, BDTmS = broadleaf deciduous temperate shrub, BDTmT = broadleaf deciduous temperate tree, BDTrT = broadleaf deciduous tropical tree, BES = broadleaf evergreen shrub, BETmT = broadleaf evergreen temperate tree, BETrT = broadleaf evergreen tropical tree, C3AG = C3 Arctic grass, C3C = C3 crop, C3nAG = C3 non-Arctic grass, C4G = C4 grass, NEBT = needleleaf evergreen boreal tree, NETmT = needleleaf evergreen temperate tree, Forb= forb.

Table 6.2: Goodness of fit of the three stomatal models in predicting g_{sw} when validated using an external dataset. Data are broken out by PFT, with identical observed g_{sw} for each of the three models. Values reported are the marginal R^2 and the root mean squared error (mol m^{-2} s^{-1}).

PFT	BWB R^2	Medlyn R^2	Lamour R^2	BWB RMSE	Medlyn RMSE	Lamour RMSE
C3 Arctic grass	0.31	0.334	0.175	0.0535	0.0524	0.0767
broadleaf deciduous boreal shrub	0.277	0.331	0.05	0.0632	0.0616	0.0725
broadleaf deciduous boreal tree	0.966	0.994	0.956	0.0138	0.0284	0.0583
needleleaf evergreen boreal tree	0.516	0.474	0.032	0.0904	0.0592	0.0704
C4 grass	0.571	0.51	0.331	0.0798	0.0845	0.8839
forb	0.768	0.763	0.627	0.1275	0.1337	0.3959
C3 non-Arctic grass	0.599	0.584	0.314	0.0836	0.085	0.2862
C3 crop	0.772	0.763	0.582	0.1226	0.1271	3.2281
broadleaf evergreen shrub	0.518	0.442	0.438	0.0821	0.0875	0.133
broadleaf deciduous temperate shrub	0.574	0.637	0.182	0.1243	0.1145	0.379
broadleaf deciduous temperate tree	0.563	0.606	0.43	0.0754	0.0718	0.0996
broadleaf evergreen temperate tree	0.808	0.766	0.577	0.0598	0.0677	0.1848
needleleaf evergreen temperate tree	0.665	0.691	0.445	0.0345	0.0261	0.0339
broadleaf deciduous tropical tree	0.485	0.546	0.226	0.0791	0.0772	0.0982
broadleaf evergreen tropical tree	0.584	0.595	0.488	0.0808	0.0795	0.0945

Table 6.3: Model summary for the PFT specific models. For each stomatal model, parameter mean, standard deviation, and 2.5%, 50% and 97.5% quantiles are shown. For a full description of the models see Table 6.1.

Parameter	PFT	BWB					Medlyn					Lamour				
		mean	SD	2.5%	50%	97.5%	mean	SD	2.5%	50%	97.5%	mean	SD	2.5%	50%	97.5%
Stomatal Slope	C3 Arctic grass	0.063	0.006	0.051	0.063	0.075	0.054	0.006	0.041	0.054	0.066	0.086	0.006	0.074	0.086	0.098
Stomatal Slope	broadleaf deciduous boreal shrub	0.091	0.006	0.079	0.091	0.103	0.082	0.006	0.071	0.082	0.094	0.109	0.006	0.097	0.109	0.121
Stomatal Slope	broadleaf deciduous boreal tree	0.028	0.024	0.001	0.021	0.09	0.027	0.025	0.001	0.02	0.093	0.055	0.039	0.002	0.049	0.143
Stomatal Slope	needleleaf evergreen boreal tree	0.03	0.005	0.02	0.03	0.04	0.005	0.004	0	0.004	0.013	0.087	0.005	0.078	0.087	0.096
Stomatal Slope	C4 grass	0.075	0.005	0.065	0.075	0.084	0.054	0.005	0.044	0.054	0.064	0.131	0.005	0.122	0.131	0.142
Stomatal Slope	forb	0.042	0.007	0.027	0.042	0.056	0.025	0.007	0.011	0.025	0.039	0.168	0.007	0.153	0.168	0.181
Stomatal Slope	C3 non-Arctic grass	0.008	0.007	0	0.006	0.026	0.005	0.005	0	0.004	0.018	0.1	0.014	0.071	0.1	0.128
Stomatal Slope	C3 crop	0.116	0.007	0.103	0.116	0.13	0.038	0.007	0.024	0.038	0.053	0.214	0.007	0.2	0.214	0.228
Stomatal Slope	broadleaf evergreen shrub	0.029	0.003	0.024	0.029	0.035	0.025	0.003	0.02	0.025	0.031	0.037	0.004	0.03	0.037	0.044
Stomatal Slope	broadleaf deciduous temperate shrub	0.041	0.004	0.034	0.041	0.048	0.031	0.004	0.024	0.031	0.038	0.137	0.02	0.116	0.126	0.172
Stomatal Slope	broadleaf deciduous temperate tree	0.038	0.001	0.035	0.038	0.04	0.031	0.001	0.029	0.031	0.034	0.08	0.002	0.075	0.08	0.084
Stomatal Slope	broadleaf evergreen temperate tree	0.027	0.002	0.022	0.027	0.031	0.017	0.002	0.012	0.017	0.022	0.088	0.017	0.072	0.077	0.115
Stomatal Slope	needleleaf evergreen temperate tree	0.02	0.002	0.016	0.02	0.024	0.01	0.002	0.005	0.01	0.014	0.045	0.003	0.038	0.045	0.05
Stomatal Slope	broadleaf deciduous tropical tree	0.034	0.006	0.023	0.034	0.045	0.026	0.005	0.016	0.026	0.037	0.07	0.005	0.059	0.07	0.08
Stomatal Slope	broadleaf evergreen tropical tree	0.034	0.002	0.03	0.034	0.037	0.029	0.002	0.025	0.029	0.032	0.073	0.002	0.068	0.073	0.077
Stomatal Intercept	C3 Arctic grass	6.46	1.612	3.272	6.478	9.572	1.028	0.618	0.07	0.969	2.37	0.127	0.219	0	0.042	0.769
Stomatal Intercept	broadleaf deciduous boreal shrub	6.016	1.996	2.131	6.005	9.97	1.116	0.723	0.061	1.027	2.717	0.12	0.199	0	0.041	0.711
Stomatal Intercept	broadleaf deciduous boreal tree	9.867	1.722	6.072	10.004	12.878	2.545	0.724	0.901	2.614	3.789	0.073	0.096	0	0.034	0.352
Stomatal Intercept	needleleaf evergreen boreal tree	2.437	0.754	0.951	2.436	3.914	1.061	0.067	0.929	1.061	1.193	0.141	0.062	0.025	0.14	0.268
Stomatal Intercept	C4 grass	3.511	0.025	3.463	3.511	3.56	0.586	0.312	0.058	0.568	1.235	0.24	0.178	0.016	0.198	0.757
Stomatal Intercept	forb	11.659	1.115	9.478	11.668	13.844	4.761	0.452	3.87	4.762	5.648	0.218	0.16	0.01	0.177	0.583
Stomatal Intercept	C3 non-Arctic grass	21.427	2.62	16.242	21.435	26.515	8.416	1.203	6.048	8.418	10.766	1.022	0.744	0.051	0.89	2.898
Stomatal Intercept	C3 crop	10.074	2.327	5.417	10.09	14.467	4.104	0.931	2.254	4.106	5.967	1.081	0.57	0.149	1.027	2.112
Stomatal Intercept	broadleaf evergreen shrub	11.442	1.03	9.407	11.447	13.449	3.85	0.459	2.946	3.85	4.746	0.487	0.37	0.034	0.407	1.611
Stomatal Intercept	broadleaf deciduous temperate shrub	11.552	0.748	10.078	11.555	13.015	4.275	0.366	3.562	4.274	4.997	0.376	0.155	0.149	0.348	0.753
Stomatal Intercept	broadleaf deciduous temperate tree	7.853	0.566	6.725	7.856	8.949	2.34	0.267	1.823	2.337	2.869	0.251	0.158	0.022	0.221	0.635
Stomatal Intercept	broadleaf evergreen temperate tree	10.294	1.023	8.294	10.292	12.335	2.941	0.095	2.755	2.941	3.127	0.273	0.091	0.074	0.281	0.466
Stomatal Intercept	needleleaf evergreen temperate tree	3.992	0.442	3.122	3.994	4.851	2.191	0.186	1.828	2.191	2.556	0.172	0.104	0.013	0.161	0.404
Stomatal Intercept	broadleaf deciduous tropical tree	5.068	0.658	3.773	5.069	6.355	1.484	0.311	0.868	1.486	2.089	0.07	0.081	0	0.041	0.288
Stomatal Intercept	broadleaf evergreen tropical tree	7.879	0.474	6.942	7.883	8.803	2.866	0.223	2.419	2.868	3.296	0.122	0.082	0.032	0.096	0.34

Table 6.3 (cont.): Model summary for the PFT specific models. For each stomatal model, parameter mean, standard deviation, and 2.5%, 50% and 97.5% quantiles are shown. For a full description of the models see Table 6.1.

Parameter	PFT	BWB					Medlyn					Lamour				
		mean	SD	2.5%	50%	97.5%	mean	SD	2.5%	50%	97.5%	mean	SD	2.5%	50%	97.5%
R_{d25}	C3 Arctic grass	-	-	-	-	-	-	-	-	-	-	4.067	1.484	1.377	4.008	7.103
R_{d25}	broadleaf deciduous boreal shrub	-	-	-	-	-	-	-	-	-	-	3.258	1.327	0.711	3.268	5.844
R_{d25}	broadleaf deciduous boreal tree	-	-	-	-	-	-	-	-	-	-	2.019	1.548	0.12	1.664	5.929
R_{d25}	needleleaf evergreen boreal tree	-	-	-	-	-	-	-	-	-	-	5.181	0.989	3.156	5.203	7.069
R_{d25}	C4 grass	-	-	-	-	-	-	-	-	-	-	1.957	0.685	0.939	1.831	3.602
R_{d25}	forb	-	-	-	-	-	-	-	-	-	-	1.542	0.778	0.123	1.721	2.769
R_{d25}	C3 non-Arctic grass	-	-	-	-	-	-	-	-	-	-	1.374	0.786	0.111	1.318	3.039
R_{d25}	C3 crop	-	-	-	-	-	-	-	-	-	-	6.23	1.079	3.83	6.298	8.225
R_{d25}	broadleaf evergreen shrub	-	-	-	-	-	-	-	-	-	-	0.446	0.259	0.096	0.395	1.1
R_{d25}	broadleaf deciduous temperate shrub	-	-	-	-	-	-	-	-	-	-	2.419	0.74	1.341	2.236	4.092
R_{d25}	broadleaf deciduous temperate tree	-	-	-	-	-	-	-	-	-	-	2.073	0.604	1.208	1.896	3.351
R_{d25}	broadleaf evergreen temperate tree	-	-	-	-	-	-	-	-	-	-	1.25	0.44	0.345	1.275	2.058
R_{d25}	needleleaf evergreen temperate tree	-	-	-	-	-	-	-	-	-	-	1.113	0.532	0.204	1.083	2.239
R_{d25}	broadleaf deciduous tropical tree	-	-	-	-	-	-	-	-	-	-	0.774	0.398	0.165	0.72	1.685
R_{d25}	broadleaf evergreen tropical tree	-	-	-	-	-	-	-	-	-	-	1.158	0.327	0.595	1.126	1.879

Chapter 7: Conclusion

Efforts to accurately simulate leaf-level gas exchange, and particularly stomatal conductance to water vapor (g_{sw}), in Land Surface Models (LSMs) have routinely been hampered by large model uncertainties (Dietze *et al.*, 2014; Jefferson *et al.*, 2017; Ricciuto *et al.*, 2018). These uncertainties can either be parametric, stemming from variation in data collection and reporting methodology (Santiago & Mulkey, 2003; Miner *et al.*, 2017; Verryckt *et al.*, 2020; Missik *et al.*, 2021), and data representativeness (De Kauwe *et al.*, 2015a; Lin *et al.*, 2015; Wolz *et al.*, 2017), or structural, related to the simplifying assumptions required when deriving empirical models of g_{sw} (Damour *et al.*, 2010; Medlyn *et al.*, 2011; Franks *et al.*, 2018; Duursma *et al.*, 2019; Lamour *et al.*, 2022). As the famous saying by statistician George Box goes, "All models are wrong, some are useful." In this dissertation, I attempt to improve the "usefulness" of stomatal models as used in LSMs by addressing four main areas of model uncertainty: (1) uncertainty in how stomatal parameters are estimated from different data types using different measurement methodology; (2) uncertainty in the temporal consistency, both diurnally and over leaf ontogeny, of stomatal parameters; (3) uncertainty in the degree of parameter variation, both within and between plant functional types (PFTs); and (4) structural uncertainty related to how different empirical models represent stomatal behavior to atmospheric demand for water, and the linearity of the stomatal response. Much of this work highlights the widespread differences in stomatal behavior among vegetation types and environmental settings and the degree to which stomatal parameters are not fixed values, rather display considerable variation depending on a multitude of biotic and abiotic factors.

An often-overlooked aspect when deriving parameters for use in stomatal models is the influence that measurement methodology may have on the estimate. Unlike many other parameters that can be derived from gas exchange measurements (e.g., the maximum carboxylation capacity of the enzyme rubisco normalized to 25ºC; $V_{cmax.25}$) no consensus exists on a standard method for estimating stomatal slope or intercept (Sharkey *et al.*, 2007; Damour *et al.*, 2010; Bernacchi *et al.*, 2013; Miner *et al.*, 2017; Duursma *et al.*, 2019). One common method for assessing stomatal function is a survey-based approach, where rates of A and g_{sw} are measured instantaneously under natural conditions, and stomatal slope and intercept are fit from the data with regression analysis (e.g., Lin *et al.*, 2015). Alternatively, many investigators have used a response curve approach for

the estimation of stomatal behavior, in which the environment around a leaf (e.g., irradiance, atmospheric CO_2 concentration, or vapor pressure deficit) is altered, and the operator observes how rates of steady state A and g_{sw} respond (Ball *et al.*, 1987; Leakey *et al.*, 2006; Mott, 1988). Historically, there has been debate as to whether response curves and survey style measurements produce comparable estimates of stomatal slope and intercept (Dang *et al.*, 1998; Damour *et al.*, 2010; Miner *et al.*, 2017; Davidson *et al.*, 2022, 2023b; Lamour *et al.*, 2023b). Proponents of response curves typically argue that despite their laborious nature, these measurements ensure that gas exchange is stabilized, and allow manipulation of a single environmental variable at a time (Falge *et al.*, 1996; Bunce, 2000; Gutschick & Simonneau, 2002; Medlyn *et al.*, 2005; Héroult *et al.*, 2013; Gimeno *et al.*, 2016). Proponents of the survey approach argue that when determining stomatal parameters, measurements should focus only on the range of leaf-level conditions that occur in the environment of interest, and that by assessing g_{sw} over time, natural dynamics in stomatal behavior are captured (Ball, 1988; Collatz *et al.*, 1991; Dang *et al.*, 1998; Damour *et al.*, 2010; Davidson *et al.*, 2023b). In this dissertation, I directly compare parameters derived from response curves against those obtained via survey estimates (Chapter 3 and Chapter 6). In both of those comparisons I found that response curves tended to produce lower overall estimates of stomatal slope and intercept than survey-based estimation. While the exact mechanisms leading to a reduced stomatal slope for response curves remains unknown, this analysis illustrates that the methods may not be comparable, especially when data are mixed. If the aim of an experiment is to ascertain a single nominal value of stomatal slope or intercept for a species or group of interest, the exact sampling method must be carefully considered. If the investigator requires an exact estimate of stomatal slope and intercept for a given leaf or individual, response curves may be preferable. Conversely, if the aim of the experiment is to survey a wide array of vegetation, or capture dynamics under natural conditions, the survey approach would be preferred. Regardless, if unreported, failure to consider assumptions inherent to either measurement type, and the potential stomatal parameter uncertainties associated with each method, have the potential to introduce considerable uncertainties into the modeling of plant carbon and water cycling (Dietze *et al*. 2014; Rogers *et al.*, 2017c).

A further methodological complication arises when measurements are made on branches or leaves which have been excised from their parent individual. With this measurement approach

comes the assumption that excision of a branch will not fundamentally alter the response of the stomatal parameters, through xylem cavitation or other stress responses (Santiago & Mulkey, 2003; Verryckt *et al.*, 2020; Missik *et al.*, 2021). As with the response curve vs survey measurement debate, there is no single consensus on the effect of excision on stomatal parameters. Although it has been shown that *ex-situ* measurement does not alter photosynthesis (Verryckt *et al*. 2020) and may even be the better option for CO_2 response curves (Ainsworth *et al*. 2003), it is currently unknown what approach is most suitable for long duration response curves used to estimate stomatal parameters. As a means of testing the impact of excision on estimated stomatal parameters, I conducted an experiment in which stomatal response curves were measured on cut and intact branch segments, and stomatal parameters were compared (Chapter 2). This analysis revealed that predawn branch excision does not significantly affect estimated stomatal slope and intercept when measured within 4-6h of excision, suggesting that when stomatal parameters are assessed within the first half of the day, methodology does not contribute to uncertainty in parameter estimates. This is an important finding as it validates the use of response curves on cut branch segments, provided that sufficient precautions are taken (e.g., predawn excision, recutting under water, early day measurement). However, if the time since excision is not recorded, conclusions about plant-to-plant or species-to-species differences in parameters may be of limited value and may introduce significant uncertainty into modeled canopy transpiration and productivity.

In addition to uncertainty due to methodology, temporal variation in the slope and intercept parameters may introduce substantial model parametric uncertainty. Plants may optimize their stomatal operation across a variety of time scales, from near instantaneous response to stimuli such as sunflecks (Way & Pearcy, 2012; Campany *et al.*, 2016), diurnal responses such as those to drying soil (Knapp, 1993; Zhang *et al.*, 2018), and long-term responses such as those which optimize water and nutrient uptake by roots (Franklin, 2007). Diurnal adjustments in stomatal parameters may be in response to rapidly changing external stimuli such as changes in VPD during the day (Katul *et al.*, 2009), or may be the consequence of shifting water supply and carbon demand dynamics within the leaf (Bonan *et al.*, 2014; Dewar *et al.*, 2018). In my research in the wet tropics (Chapter 3), I identified a diurnal trend in stomatal slope and intercept, with values of both parameters decreasing throughout the diurnal course. While the main mechanism behind this

decline is unclear, it may be caused by decreased supply of water to the canopy late in the day (Venturas *et al*., 2017) which is consistent with models of stomatal optimality, which apply a penalty on stomatal opening in the form of vascular damage (Wolf *et al*., 2016; Sperry *et al*., 2017; Anderegg *et al*., 2018). Similarly, circadian resonance in stomata (Green *et al*., 2002; Resco de Dios *et al*., 2016; 2020) may help to explain some of the stomatal dynamics observed. However, when dynamic stomatal traits were applied to a reduced complexity land surface model, the model failed to significantly improve predictions of canopy transpiration. While an overall pattern of declining stomatal slope throughout the day is expected, the magnitude of the decline each day is the by-product of abiotic processes that I may not have fully captured in the model, such as dynamics in the soil–plant- atmosphere continuum (Zhang *et al*., 2018), or an effect of abscisic acid on regulating stomata (McAdam & Brodribb, 2015). Thus, further efforts to model diurnal adjustments in stomatal traits should focus on the process or mechanism responsible for the adjustment, rather than attempting to replicate the pattern within the model. The latter approach may bring model prediction closer to observation, but will do little to reduce overall model uncertainty, especially in novel ecosystem or climate regimes.

Like diurnal variability, stomata may also be variable seasonally or through leaf ontogeny. Such variability in stomatal parameters has been associated with long term changes in leaf traits or seasonal progression of climatological factors (Kitajima *et al.*, 2002; Bauerle *et al.*, 2012; Rogers *et al.*, 2017c; Anderegg, 2018; Burnett *et al.*, 2021b). In an attempt to account for variations in stomatal conductance through time, some models have begun to represent of stomatal parameters as seasonally dynamic (Blyth *et al.*, 2021). This is as opposed to more traditional model schemes which assume seasonal changes in g_{sw} are passive and arise as the result of changes in A rather than changes in stomatal slope and intercept. When assessing the question of seasonality of stomatal parameters in a temperate deciduous forest ecosystem (Chapter 4), I found stomatal slope and intercept were seasonally variable, driven chiefly by seasonal changes in the capacity for carbon assimilation, and leaf hydraulic properties. While limited to a single season for a single ecosystem, these findings illustrate that there is a clear need for models to account for temporal variation in both photosynthetic and stomatal parameters, with emphasis given toward ensuring that photosynthetic and stomatal parameters correctly scale with one another. Of particular importance here are the shoulder seasons (e.g., spring leaf out and fall lead senescence), when

parameters change rapidly, and where model timing may be inaccurate due to issues associated with model representation of phenology (Estiarte & Peñuelas, 2015). Accomplishing a reconfiguration of models to account for ontogenetic shifts in stomatal parameters will be a difficult task, yet one which will substantially reduce model parametric uncertainty in representation of land-atmosphere interactions across diverse geographical regions and variable environmental conditions.

A final source of model parametric uncertainty assessed in this dissertation has to do with estimating stomatal traits at the PFT level. While there has long been an understanding that stomatal behavior is variable both between and among species (Meidner & Mansfield, 1968; Jarvis, 1976; Ball, 1988), only recently have efforts been made to categorize stomatal parameters by PFT for use in LSMs (Lin *et al.*, 2015; Franks *et al.*, 2017; Miner *et al.*, 2017; Wolz *et al.*, 2017). PFT-specific parameterizations are an important model improvement, however some studies have demonstrated significant within-species variation in stomatal behavior (Ono *et al.*, 2013; Miner & Bauerle, 2017; Davidson *et al.*, 2023a), which, in some cases, can even exceed among PFT variation (Wolz *et al.*, 2017). In addition, due to a lack of data from which parameter estimates can be obtained, some LSMs use parameters for a default C3 plant in place of a PFT specific parameter set (De Kauwe *et al.*, 2015b; Franks *et al.*, 2018). In an assessment of stomatal traits in two Arctic PFTs which had yet to be specifically parameterized (Chapter 5), I found that observed stomatal slope and intercept were significantly different from the model default, and when updated parameters were applied to the model, ecosystem-scale water use efficiency decreased significantly, primarily because of substantially higher simulated transpiration. The disparity between LSM default parameter values and those measured not only highlights the unique physiology of high latitude vegetation (Rogers *et al*., 2017; Van De Weg *et al*., 2013), but also underscores the knowledge gap in physiological ecology between temperate and Arctic species (Rogers *et al*., 2022). In addition, by assessing multiple traits within the same PFT simultaneously, unique trait x trait relationships can be identified which may be useful when developing associations between leaf traits and model parameters, or mapping within-PFT parameter variation across the landscape (Šantrůček *et al.*, 2004; Duursma *et al.*, 2019; Langford *et al*., 2019; Yang *et al*., 2021). Clearly, more work is required to assess PFT specific parameterizations in ecosystems which lack a track record of data collection, as a method for

reducing parametric uncertainty in those ecosystems. Alternatively, modelers should consider whether applying trait or climatological based approximations for parameters of interest is preferable when data from the target ecosystem is lacking (Van Bodegom *et al.*, 2012; Franks *et al.*, 2018). While such approaches may be appealing for filling ecological knowledge gaps, they may introduce further parametric uncertainty, stemming from extending assumptions about parameter relationships into novel ecosystems.

Finally, model structural uncertainty is important to quantify at both the leaf and canopy scale. Sources of structural uncertainty include the response of stomata to soil moisture stress or atmospheric demand, and the assumption of linearity in the stomatal response. Investigations into a reduction in stomatal intercept as a function of soil water stress have produced mixed conclusions (e.g., Liozon *et al*., 2000; Misson *et al*., 2006; Xu & Baldocchi, 2003) that may be partially attributable to the interrelation between leaf age, seasonality and drought in many study systems (Miner *et al.*, 2017). Other more mechanistic functions have been proposed to better represent the impact of soil moisture stress on transpiration, such as applying a reduction in g_{sw} by altering the stomatal slope (e.g., Anderegg *et al*., 2017), simulating water transport through the xylem with a hydraulic model (e.g., Kennedy *et al*., 2019; Sperry & Love, 2015) or via a model which accounts for a chemical drought stress signal such as abscisic acid (Huber *et al.*, 2019), yet the data with which to fit these models are often absent. Tests investigating the way in which the soil moisture stress influences instantaneous g_{sw} and evapotranspiration in the E3SM Land Model (ELM) (Chapter 5), suggest that when stomatal slope rather than stomatal intercept is reduced as a function of soil moisture stress, ecosystem-scale water use efficiency increases as predicted by stomatal optimality theory (Cowan & Fraquhar, 1977). Such modifications to ELM bring model structure more in line with known, or assumed, physiological processes and are important to investigate across a diverse set of environmental conditions.

In addition to modifying model structure to account for soil moisture stress, various empirical stomatal model formulations exist, with differences in how they simulate atmospheric demand for water (RH vs VPD). Models which explicitly consider the effect of VPD, rather than RH, may be preferable for use in LSMs or other climate forecasting tools (Rogers *et al.*, 2017c), as RH is not predicted to substantially change into the future, while VPD is expected to increase with atmospheric warming (Sato *et al.*, 2015). Further, the use of a VPD type model may be more

appealing from a physiological/mechanistic perspective as an increase in VPD is directly proportional to atmospheric demand for water, and thus mimics stomatal mechanics (Aphalo & Jarvis, 1991; Streck, 2003; Eamus *et al.*, 2008; Op De Beeck *et al.*, 2010). When comparing the efficacy of three empirical g_{sw} models (Chapter 6) I found no difference in model goodness of fit between RH and VPD type models, suggesting that the choice of RH vs VPD may not contribute to model structural uncertainty. This is in line with Li *et al.*, (2022), who demonstrated that under conditions where VPD $\leq$ 1.5, VPD and RH type models predict nearly identical rates of transpiration, and only begin to diverge in their predictions as VPD increases and g_{sw} declines toward the stomatal intercept.

A final model structural component to consider is the linearity of the stomatal response. Several researchers have observed, at the leaf-level, a nonlinearity in the g_{sw} response, which could lead to inaccurately low stomatal slope and intercept estimates (Ball, 1988; Leuning, 1990, 1995; Barnard & Bauerle, 2013; Lamour *et al.*, 2022). This effect of nonlinearity is often present at low (< 150 μmol photons m^{-2} s^{-1}) and high (> saturating) irradiance, and was observed numerous times in this dissertation (Chapter 2-4). In response to this finding of non-linearity, several empirical stomatal models have been proposed, notably the model of Lamour *et al.*, (2022), which is based on the Unified Stomatal Optimization (USO) model (Medlyn *et al*., 2011), however uses squared gross assimilation (A_g^2) in place of net assimilation (A_n). When comparing the efficacy of linear and non-linear empirical g_{sw} models (Chapter 6) I found that the Lamour model failed to accurately reproduce stomatal dynamics across several PFTs and environments. This is somewhat surprising given that the Lamour model exhibited superior performance to the USO model across several datasets in its initial and subsequent validations (Lamour *et al.*, 2022, 2023b), however issues estimating a PFT specific respiration term (which is required when estimating A_g from A_n), may have contributed to the especially poor performance of the Lamour model at predicting leaf-level g_{sw} for this dataset. Such model validation tests are useful for evaluating the overall ability of a model to reproduce observations, and assessing which conditions result in the largest model predictive uncertainty, however a true test of model performance would be to integrate the Lamour model (or any other non-linear model to be tested) into a fully coupled LSM and evaluate its effect on predictions of primary productivity and evapotranspiration (e.g., Li *et al.*, 2022). Until such a test is conducted, the true impact of uncertainty associated with the non-linearity in the g_{sw}

response will remain incompletely quantified. Addressing model structural uncertainties will be critical as LSMs continue to develop and become more complex. Uncertainty related to transpiration estimations will likely have major impacts on surface and subsurface hydrology (Troch *et al.*, 2009; Lique *et al.*, 2016; Knauer *et al.*, 2017), and could also affect global patterns of surface cooling, and heatwave development in previously unforeseen ways (Kala *et al.*, 2016).

In summary, failure to consider potential model parametric uncertainties in stomatal traits (e.g., methodological, temporal, among-species), together with other uncertainties associated with model structure, have the potential to introduce considerable uncertainties into the modeling of plant carbon, water, and energy cycling (Dietze et al. 2014; Rogers *et al.*, 2017c). By identifying these uncertainties, which in large part stem from assumptions about the biotic and abiotic factors influencing stomatal behavior at the species or PFT level, future models may be able to account for these uncertainties. By recognizing these assumptions, and attempting to quantify the uncertainty associated with them, we can work toward better representation of these uncertain processes in future land surface models. Such model improvement will not only be important for the development of scientifically sound process-based LSMs, but may prove essential for predicting novel vegetation-atmosphere interactions under a changing future climate.

Bibliography:

Ainsworth EA, Davey PA, Hymus GJ, Osborne CP, Rogers A, Blum H, Nösberger J, Long SP. **2003**. Is stimulation of leaf photosynthesis by elevated carbon dioxide concentration maintained in the long term? A test with *Lolium perenne* grown for 10 years at two nitrogen fertilization levels under *F* ree *A* ir *C* O $_2$ *E* nrichment (FACE): Photosynthetic acclimation of *L. perenne* to elevated [CO $_2$]. *Plant, Cell & Environment* **26**: 705–714.

Ainsworth EA, Rogers A. **2007**. The response of photosynthesis and stomatal conductance to rising [CO $_2$]: mechanisms and environmental interactions: Photosynthesis and stomatal conductance responses to rising [CO $_2$]. *Plant, Cell & Environment* **30**: 258–270.

Akalusi ME, Meng F, P.-A. Bourque C. **2021**. Photosynthetic parameters and stomatal conductance in attached and detached balsam fir foliage. *Plant-Environment Interactions* **2**: 206–215.

Ali AA, Xu C, Rogers A, McDowell NG, Medlyn BE, Fisher RA, Wullschleger SD, Reich PB, Vrugt JA, Bauerle WL, *et al.* 2015. Global-scale environmental control of plant photosynthetic capacity. *Ecological Applications* **25**: 2349–2365.

Amthor J. **2000**. The McCree–de Wit–Penning de Vries–Thornley Respiration Paradigms: 30 Years Later. *Annals of Botany* **86**: 1–20.

Anderegg WRL, Wolf A, Arango-Velez A, Choat B, Chmura DJ, Jansen S, Kolb T, Li S, Meinzer F, Pita P, *et al.* 2017. Plant water potential improves prediction of empirical stomatal models (R Aroca, Ed.). *PLOS ONE* **12**: e0185481.

Anderegg WRL, Wolf A, Arango-Velez A, Choat B, Chmura DJ, Jansen S, Kolb T, Li S, Meinzer FC, Pita P, *et al.* 2018. Woody plants optimise stomatal behaviour relative to hydraulic risk (D Cameron, Ed.). *Ecology Letters* **21**: 968–977.

Anderegg WRL. **2018**. Quantifying seasonal and diurnal variation of stomatal behavior in a hydraulic-based stomatal optimization model. *Journal of Plant Hydraulics* **5**: e001.

Anfodillo T, Di Bisceglie DP, Urso T. **2002**. Minimum cuticular conductance and cuticle features of Picea abies and Pinus cembra needles along an altitudinal gradient in the Dolomites (NE Italian Alps). *Tree Physiology* **22**: 479–487.

Aphalo PJ, Jarvis PG. **1991**. Do stomata respond to relative humidity? *Plant, Cell & Environment* **14**: 127–132.

Aros-Mualin D, Guadagno CR, Silvestro D, Kessler M. 2023. Light, rather than circadian rhythm, regulates gas exchange in ferns and lycophytes. *Plant Physiology* 191: 1634–1647.

Assmann JJ, Myers-Smith IH, Kerby JT, Cunliffe AM, Daskalova GN. **2020**. Drone data reveal heterogeneity in tundra greenness and phenology not captured by satellites. *Environmental Research Letters* **15**: 125002.

Atkin OK, Millar AH, Gardeström P, Day DA. **2000**. Photosynthesis, Carbohydrate Metabolism and Respiration in Leaves of Higher Plants. In: Leegood RC, Sharkey TD, von Caemmerer S, eds. Photosynthesis. Dordrecht, The Netherlands: Springer, 153–175.

Ávila-Lovera E, Urich R, Coronel I, Tezara W. **2019**. Seasonal gas exchange and resource-use efficiency in evergreen versus deciduous species from a tropical dry forest (G Goldstein, Ed.). *Tree Physiology* **39**: 1561–1571.

Ball TJ, Woodrow IE, Berry JA. **1987**. A Model Predicting Stomatal Conductance and its Contribution to the Control of Photosynthesis under Different Environmental Conditions. In: Biggins J, ed. Progress in photosynthesis research. Springer, Dordrecht, 221–224.

Ball TJ. **1988**. *An analysis of stomatal conductance*. Stanford University.

Barnard DM, Bauerle WL. **2013**. The implications of minimum stomatal conductance on modeling water flux in forest canopies: MINIMUM G_S AND WATER FLUX ESTIMATES. *Journal of Geophysical Research: Biogeosciences* **118**: 1322–1333.

Bartlett MK, Klein T, Jansen S, Choat B, Sack L. **2016**. The correlations and sequence of plant stomatal, hydraulic, and wilting responses to drought. *Proceedings of the National Academy of Sciences* **113**: 13098–13103.

Bartlett MK, Scoffoni C, Sack L. **2012**. The determinants of leaf turgor loss point and prediction of drought tolerance of species and biomes: a global meta-analysis: Drivers of plant drought tolerance. *Ecology Letters* **15**: 393–405.

Bassham JA, Calvin M. **1960**. The Path of Carbon in Photosynthesis. In: Biogenesis of Natural Substances. Berkeley, CA: Interscience Publishers.

Bauerle WL, Bowden JD, Wang GG, Shahba MA. **2009**. Exploring the importance of within-canopy spatial temperature variation on transpiration predictions. *Journal of Experimental Botany* **60**: 3665–3676.

Bauerle WL, Daniels AB, Barnard DM. **2014**. Carbon and water flux responses to physiology by environment interactions: a sensitivity analysis of variation in climate on photosynthetic and stomatal parameters. *Climate Dynamics* **42**: 2539–2554.

Bauerle WL, Oren R, Way DA, Qian SS, Stoy PC, Thornton PE, Bowden JD, Hoffman FM, Reynolds RF. **2012**. Photoperiodic regulation of the seasonal pattern of photosynthetic capacity and the implications for carbon cycling. *Proceedings of the National Academy of Sciences* **109**: 8612–8617.

Beale CV, Morison JIL, Long SP. **1999**. Water use efÆciency of C4 perennial grasses in a temperate climate. *Agricultural and Forest Meteorology*.

Beck PSA, Goetz SJ. **2012**. Corrigendum: Satellite observations of high northern latitude vegetation productivity changes between 1982 and 2008: ecological variability and regional differences. *Environmental Research Letters* **7**: 029501.

Béland M, Baldocchi DD. **2021**. Vertical structure heterogeneity in broadleaf forests: Effects on light interception and canopy photosynthesis. *Agricultural and Forest Meteorology* **307**: 108525.

Bernacchi CJ, Bagley JE, Serbin SP, Ruiz-Vera UM, Rosenthal DM, Vanloocke A. **2013**. Modelling C_3 photosynthesis from the chloroplast to the ecosystem: Scaling photosynthesis using models. *Plant, Cell & Environment* **36**: 1641–1657.

Bernacchi CJ, Calfapietra C, Davey PA, Wittig VE, Scarascia-Mugnozza GE, Raines CA, Long SP. **2003a**. Photosynthesis and Stomatal Conductance Responses of Poplars to Free-Air CO_2 Enrichment (PopFACE) during the First Growth Cycle and Immediately Following Coppice. *New Phytologist* **159**: 609–621.

Bernacchi CJ, Leakey ADB, Heady LE, Morgan PB, Dohleman FG, Mcgrath JM, Gillespie KM, Wittig VE, Rogers A, Long SP, *et al.* 2006. Hourly and seasonal variation in photosynthesis and stomatal conductance of soybean grown at future CO_2 and ozone concentrations for 3 years under fully open-air field conditions. *Plant, Cell and Environment* **29**: 2077–2090.

Bernacchi CJ, Pimentel C, Long SP. **2003b**. *In vivo* temperature response functions of parameters required to model RuBP-limited photosynthesis: Modelling RuBP-limited photosynthesis. *Plant, Cell & Environment* **26**: 1419–1430.

Bernacchi CJ, Singsaas EL, Pimentel C, Portis Jr AR, Long SP. **2001**. Improved temperature response functions for models of Rubisco-limited photosynthesis: *In vivo* Rubisco enzyme kinetics. *Plant, Cell & Environment* **24**: 253–259.

Bertolino LT, Caine RS, Gray JE. **2019**. Impact of Stomatal Density and Morphology on Water-Use Efficiency in a Changing World. *Frontiers in Plant Science* **10**: 225.

Beven K, Freer J. **2001**. Equifinality, data assimilation, and uncertainty estimation in mechanistic modelling of complex environmental systems using the GLUE methodology. *Journal of Hydrology* **249**: 11–29.

Bjorkman AD, Myers-Smith IH, Elmendorf SC, Normand S, Rüger N, Beck PSA, Blach-Overgaard A, Blok D, Cornelissen JHC, Forbes BC, *et al.* 2018. Plant functional trait change across a warming tundra biome. *Nature* **562**: 57–62.

Black KL, Wallace CA, Baltzer JL. **2021**. Seasonal thaw and landscape position determine foliar functional traits and whole-plant water use in tall shrubs on the low arctic tundra. *New Phytologist* **231**: 94–107.

Blackman CJ, Pfautsch S, Choat B, Delzon S, Gleason SM, Duursma RA. **2016**. Toward an index of desiccation time to tree mortality under drought: Desiccation time to tree mortality. *Plant, Cell & Environment* **39**: 2342–2345.

Blyth EM, Arora VK, Clark DB, Dadson SJ, De Kauwe MG, Lawrence DM, Melton JR, Pongratz J, Turton RH, Yoshimura K, *et al.* 2021. Advances in Land Surface Modelling. *Current Climate Change Reports* **7**: 45–71.

Bonan G. **2008**. *Ecological climatology: concepts and applications.* Cambridge University Press.

Bonan G. **2015**. *Ecological Climatology: Concepts and Applications*. Cambridge University Press.

Bonan G. **2019**. *Climate change and terrestrial ecosystem modeling*. Cambridge University Press.

Bonan GB, Lawrence PJ, Oleson KW, Levis S, Jung M, Reichstein M, Lawrence DM, Swenson SC. **2011**. Improving canopy processes in the Community Land Model version

4 (CLM4) using global flux fields empirically inferred from FLUXNET data. *Journal of Geophysical Research* **116**: G02014.

Bonan GB, Williams M, Fisher RA, Oleson KW. **2014**. Modeling stomatal conductance in the earth system: linking leaf water-use efficiency and water transport along the soil–plant–atmosphere continuum. *Geoscientific Model Development* **7**: 2193–2222.

Bring A, Fedorova I, Dibike Y, Hinzman L, Mård J, Mernild SH, Prowse T, Semenova O, Stuefer SL, Woo M -K. 2016. Arctic terrestrial hydrology: A synthesis of processes, regional effects, and research challenges. *Journal of Geophysical Research: Biogeosciences* **121**: 621–649.

Brodribb TJ, Holbrook NM, Edwards EJ, Gutiérrez MV. **2003**. Relations between stomatal closure, leaf turgor and xylem vulnerability in eight tropical dry forest trees: Stomatal closure and xylem cavitation. *Plant, Cell & Environment* **26**: 443–450.

Brodribb TJ, Holbrook NM. **2003**. Stomatal Closure during Leaf Dehydration, Correlation with Other Leaf Physiological Traits. *Plant Physiology* **132**: 2166–2173.

Bryant C, Wheeler NR, Rubel F, French RH. **2017**. kgc.

Bubier JL, Smith R, Juutinen S, Moore TR, Minocha R, Long S, Minocha S. **2011**. Effects of nutrient addition on leaf chemistry, morphology, and photosynthetic capacity of three bog shrubs. *Oecologia* **167**: 355–368.

Buckley TN, Martorell S, Diaz-Espejo A, Tomàs M, Medrano H. **2014**. Is stomatal conductance optimized over both time and space in plant crowns? A field test in grapevine (*V itis vinifera*). *Plant, Cell & Environment* **37**: 2707–2721.

Buckley TN, Sack L, Farquhar GD. **2017**. Optimal plant water economy: Optimal plant water economy. *Plant, Cell & Environment* **40**: 881–896.

Buckley TN. **2016**. Stomatal responses to humidity: has the 'black box' finally been opened?: Stomatal responses to humidity. *Plant, Cell & Environment* **39**: 482–484.

Buckley TN. **2017**. Modeling Stomatal Conductance. *Plant Physiology* **174**: 572–582.

Buckley TN. **2020**. *Optimal carbon partitioning reconciles the apparent divergence between optimal and observed canopy profiles of photosynthetic capacity*. Plant Biology.

Bunce JA. **2000**. Responses of stomatal conductance to light, humidity and temperature in winter wheat and barley grown at three concentrations of carbon dioxide in the field: STOMATAL RESPONSES AT ELEVATED CO 2. *Global Change Biology* **6**: 371–382.

Burnett AC, Davidson KJ, Serbin SP, Rogers A. **2019**. The "one-point method" for estimating maximum carboxylation capacity of photosynthesis: A cautionary tale. *Plant, Cell & Environment* **42**: 2472–2481.

Burnett AC, Serbin SP, Lamour J, Anderson J, Davidson KJ, Yang D, Rogers A. **2021**. Seasonal trends in photosynthesis and leaf traits in scarlet oak. **Tree Physiology 41: 1413–1424.**

Burrows SM, Maltrud M, Yang X, Zhu Q, Jeffery N, Shi X, Ricciuto D, Wang S, Bisht G, Tang J, *et al.* 2020. The DOE E3SM v1.1 Biogeochemistry Configuration: Description

and Simulated Ecosystem-Climate Responses to Historical Changes in Forcing. *Journal of Advances in Modeling Earth Systems* **12**.

Cahoon SMP, Sullivan PF, Post E. **2016**. Carbon and water relations of contrasting Arctic plants: implications for shrub expansion in West Greenland (DPC Peters, Ed.). *Ecosphere* **7**.

Cai G, Ahmed MA, Dippold MA, Zarebanadkouki M, Carminati A. **2020**. Linear relation between leaf xylem water potential and transpiration in pearl millet during soil drying. *Plant and Soil* **447**: 565–578.

Caldararu S, Thum T, Yu L, Zaehle S. **2020**. Whole-plant optimality predicts changes in leaf nitrogen under variable CO_2 and nutrient availability. *New Phytologist* **225**: 2331–2346.

Campany CE, Tjoelker MG, von Caemmerer S, Duursma RA. **2016**. Coupled response of stomatal and mesophyll conductance to light enhances photosynthesis of shade leaves under sunflecks: Mesophyll conductance response to light. *Plant, Cell & Environment* **39**: 2762–2773.

Cannell M. **2000**. Modelling the Components of Plant Respiration: Some Guiding Principles. *Annals of Botany* **85**: 45–54.

Cavender-Bares J, Gamon JA, Townsend PA (Eds.). **2020**. *Remote Sensing of Plant Biodiversity*. Cham: Springer International Publishing.

Chapin FS, Bret-Harte MS, Hobbie SE, Zhong H. **1996**. Plant functional types as predictors of transient responses of arctic vegetation to global change. *Journal of Vegetation Science* **7**: 347–358.

Chen A, Ricciuto D, Mao J, Wang J, Lu D, Meng F. **2023**. Improving E3SM Land Model Photosynthesis Parameterization via Satellite SIF, Machine Learning, and Surrogate Modeling. *Journal of Advances in Modeling Earth Systems* **15**: e2022MS003135.

Chen W, Tape KD, Euskirchen ES, Liang S, Matos A, Greenberg J, Fraterrigo JM. **2020**. Impacts of Arctic Shrubs on Root Traits and Belowground Nutrient Cycles Across a Northern Alaskan Climate Gradient. *Frontiers in Plant Science* **11**: 588098.

Chen X, Ciais P, Maignan F, Zhang Y, Bastos A, Liu L, Bacour C, Fan L, Gentine P, Goll D, *et al.* 2021. Vapor Pressure Deficit and Sunlight Explain Seasonality of Leaf Phenology and Photosynthesis Across Amazonian Evergreen Broadleaved Forest. *Global Biogeochemical Cycles* **35**.

Choat B, Ball MC, Luly JG, Donnelly CF, Holtum JAM. **2006**. Seasonal patterns of leaf gas exchange and water relations in dry rain forest trees of contrasting leaf phenology. *Tree Physiology* **26**: 657–664.

Christmann A, Weiler EW, Steudle E, Grill E. **2007**. A hydraulic signal in root-to-shoot signalling of water shortage: Hydraulic signalling of water shortage. *The Plant Journal* **52**: 167–174.

Christoffersen BO, Gloor M, Fauset S, Fyllas NM, Galbraith DR, Baker TR, Kruijt B, Rowland L, Fisher RA, Binks OJ, *et al.* 2016. Linking hydraulic traits to tropical forest

function in a size-structured and trait-driven model (TFS v.1-Hydro). *Geoscientific Model Development* **9**: 4227–4255.

Chu S, Jacobs DF, Sloan JL, Xue L, Wu D, Zeng S. **2018**. Changes in soil properties under Eucalyptus relative to Pinus massoniana and natural broadleaved forests in South China. *Journal of Forestry Research* **29**: 1299–1306.

Cochard H, Bréda N, Granier A. **1996**. Whole tree hydraulic conductance and water loss regulation in Quercus during drought: evidence for stomatal control of embolism? *Annales des Sciences Forestières* **53**: 197–206.

Cocozza C, Cherubini P, Regier N, Saurer M, Frey B, Tognetti R. **2010**. Early effects of water deficit on two parental clones of Populus nigra grown under different environmental conditions. *Functional Plant Biology* **37**: 244.

Collatz GJ, Ball JT, Grivet C, Berry JA. **1991**. Physiological and environmental regulation of stomatal conductance, photosynthesis and transpiration: a model that includes a laminar boundary layer. *Agricultural and Forest Meteorology* **54**: 107–136.

Condit R, Windsor DM, Hubbell SP. **1996**. NPP Tropical Forest: Barro Colorado, Panama, 1969-1990.

Cooley SS, Fisher JB, Goldsmith GR. **2022**. Convergence in water use efficiency within plant functional types across contrasting climates. *Nature Plants* **8**: 341–345.

Cowan IR, Fraquhar GD. **1977**. Stomatal function in relation to leaf metabolism and environment. In: Jennings D, ed. Integration of Activity in the Higher Plant. Cambridge: Cambridge University Press, 471–505.

Cowan IR. **1978**. Stomatal Behaviour and Environment. In: Preston RD, Woolhouse HW, eds. Advances in Botanical Research. Academic Press, 117–228.

Croft H, Chen JM, Luo X, Bartlett P, Chen B, Staebler RM. **2017**. Leaf chlorophyll content as a proxy for leaf photosynthetic capacity. *Global Change Biology* **23**: 3513–3524.

Cseke LJ, Tsai C, Rogers A, Nelsen MP, White HL, Karnosky DF, Podila GK. **2009**. Transcriptomic comparison in the leaves of two aspen genotypes having similar carbon assimilation rates but different partitioning patterns under elevated [CO_2]. *New Phytologist* **182**: 891–911.

Dai Z, Edwards GE, Ku MSB. **1992**. Control of Photosynthesis and Stomatal Conductance in *Ricinus communis* L. (Castor Bean) by Leaf to Air Vapor Pressure Deficit. *Plant Physiology* **99**: 1426–1434.

Damour G, Simonneau T, Cochard H, Urban L. **2010**. An overview of models of stomatal conductance at the leaf level: Models of stomatal conductance. *Plant, Cell & Environment* **39**: 1419–1438.

Dang Q-L, Margolis HA, Collatz GJ. **1998**. Parameterization and testing of a coupled photosynthesis-stomatal conductance model for boreal trees. *Tree Physiology* **18**: 141–153.

Davidson KJ, Lamour J, McPherran A, Rogers A, Serbin SP. **2023a**. Seasonal trends in leaf level photosynthetic capacity and water use efficiency in a North American Eastern deciduous forest and their impact on canopy-scale gas exchange. *New Phytologist*.

Davidson KJ, Lamour J, Rogers A, Ely KS, Li Q, McDowell NG, Pivovaroff AL, Wolfe BT, Wright SJ, Zambrano A, *et al.* 2023b. Short-term variation in leaf-level water use efficiency in a tropical forest. *New Phytologist* **237**: 2069–2087.

Davidson KJ, Lamour J, Serbin SP, Rogers A. **2022**. Late day measurement of excised branches results in uncertainty in the estimation of two stomatal parameters derived from response curves in Populus 3 deltoides Bartr. x Populus nigra L. *Tree Physiology* **42**: 1377–1395.

Davidson K, Serbin S. 2022b. Stomatal response of three Arctic plant species, Seward Peninsula, Alaska, 2022. Next Generation Ecosystem Experiments Arctic Data Collection, Oak Ridge National Laboratory, U.S. Department of Energy, Oak Ridge, Tennessee, USA. Dataset accessed on 2022-10-25 at https://doi.org/10.5440/1975097

De Kauwe MG, Kala J, Lin Y-S, Pitman AJ, Medlyn BE, Duursma RA, Abramowitz G, Wang Y-P, Miralles DG. **2015a**. A test of an optimal stomatal conductance scheme within the CABLE land surface model. *Geoscientific Model Development* **8**: 431–452.

De Kauwe MG, Lin Y-S, Wright IJ, Medlyn BE, Crous KY, Ellsworth DS, Maire V, Prentice IC, Atkin OK, Rogers A, *et al.* 2016. A test of the 'one-point method' for estimating maximum carboxylation capacity from field-measured, light-saturated photosynthesis. *New Phytologist* **210**: 1130–1144.

De Kauwe MG, Medlyn BE, Zaehle S, Walker AP, Dietze MC, Hickler T, Jain AK, Luo Y, Parton WJ, Prentice IC, *et al.* 2013. Forest water use and water use efficiency at elevated CO $_2$: a model-data intercomparison at two contrasting temperate forest FACE sites. *Global Change Biology* **19**: 1759–1779.

De Kauwe MG, Zhou S-X, Medlyn BE, Pitman AJ, Wang Y-P, Duursma RA, Prentice IC. **2015b**. Do land surface models need to include differential plant species responses to drought? Examining model predictions across a mesic-xeric gradient in Europe. *Biogeosciences* **12**: 7503–7518.

De Weirdt M, Verbeeck H, Maignan F, Peylin P, Poulter B, Bonal D, Ciais P, Steppe K. **2012**. Seasonal leaf dynamics for tropical evergreen forests in a process-based global ecosystem model. *Geoscientific Model Development* **5**: 1091–1108.

Dewar R, Mauranen A, Mäkelä A, Hölttä T, Medlyn B, Vesala T. **2018**. New insights into the covariation of stomatal, mesophyll and hydraulic conductances from optimization models incorporating nonstomatal limitations to photosynthesis. *New Phytologist* **217**: 571–585.

Dewar RC. **1995**. Interpretation of an empirical model for stomatal conductance in terms of guard cell function. *Plant, Cell and Environment* **18**: 365–372.

Dietze MC, Serbin SP, Davidson C, Desai AR, Feng X, Kelly R, Kooper R, LeBauer D, Mantooth J, McHenry K, *et al.* 2014. A quantitative assessment of a terrestrial biosphere

model's data needs across North American biomes: PEcAn/ED model-data uncertainty analysis. *Journal of Geophysical Research: Biogeosciences* **119**: 286–300.

Domingues TF, Martinelli LA, Ehleringer JR. **2014**. Seasonal patterns of leaf-level photosynthetic gas exchange in an eastern Amazonian rain forest. *Plant Ecology & Diversity* **7**: 189–203.

Dos Santos JA, Campoe OC, De Souza CR, Marrichi AHC, Carneiro RL, Da Silva PHM, De Mattos EM, Otto MSG, Gonsalez BT. **2023**. Stomatal conductance models in Brazilian forest plantations: genotype and environmental effects on eucalypt and pine forests. *New Forests*.

Drake JE, Power SA, Duursma RA, Medlyn BE, Aspinwall MJ, Choat B, Creek D, Eamus D, Maier C, Pfautsch S, *et al.* 2017. Stomatal and non-stomatal limitations of photosynthesis for four tree species under drought: A comparison of model formulations. *Agricultural and Forest Meteorology* **247**: 454–466.

Drake JE, Tjoelker MG, Vårhammar A, Medlyn BE, Reich PB, Leigh A, Pfautsch S, Blackman CJ, López R, Aspinwall MJ, *et al.* 2018. Trees tolerate an extreme heatwave via sustained transpirational cooling and increased leaf thermal tolerance. *Global Change Biology* **24**: 2390–2402.

Drake PL, Froend RH, Franks PJ. **2013**. Smaller, faster stomata: scaling of stomatal size, rate of response, and stomatal conductance. *Journal of Experimental Botany* **64**: 495–505.

Dreyer E, Le Roux X, Montpied P, Daudet FA, Masson F. **2001**. Temperature response of leaf photosynthetic capacity in seedlings from seven temperate tree species. *Tree Physiology* **21**: 223–232.

Duarte AG, Katata G, Hoshika Y, Hossain M, Kreuzwieser J, Arneth A, Ruehr NK. **2016**. Immediate and potential long-term effects of consecutive heat waves on the photosynthetic performance and water balance in Douglas-fir. *Journal of Plant Physiology* **205**: 57–66.

Duursma RA, Blackman CJ, Lopéz R, Martin-StPaul NK, Cochard H, Medlyn BE. **2019**. On the minimum leaf conductance: its role in models of plant water use, and ecological and environmental controls. *New Phytologist* **221**: 693–705.

Duveiller G, Hooker J, Cescatti A. **2018**. The mark of vegetation change on Earth's surface energy balance. *Nature Communications* **9**: 679.

Eamus D, Taylor DT, Macinnis-Ng CMO, Shanahan S, De Silva L. **2008**. Comparing model predictions and experimental data for the response of stomatal conductance and guard cell turgor to manipulations of cuticular conductance, leaf-to-air vapour pressure difference and temperature: feedback mechanisms are able to account for all observations. *Plant, Cell & Environment* **31**: 269–277.

El-Sharkaway MA, Cock JH. **1984**. Water Use Efficiency of Cassava. I. Effects of Air Humidity and Water Stress on Stomatal Conductance and Gas Exchange1. *Crop Science* **24**: 497–502.

Ellsworth DS, Reich PB. **1993**. Canopy structure and vertical patterns of photosynthesis and related leaf traits in a deciduous forest. *Oecologia* **96**: 169–178.

Elmendorf SC, Hollister RD. **2023**. Limits on phenological response to high temperature in the Arctic. *Scientific Reports* **13**: 208.

Ely KS, Rogers A, Agarwal DA, Ainsworth EA, Albert LP, Ali A, Anderson J, Aspinwall MJ, Bellasio C, Bernacchi C, *et al.* 2021. A reporting format for leaf-level gas exchange data and metadata. *Ecological Informatics* **61**: 101232.

Epstein HE, Beringer J, Gould WA, Lloyd AH, Thompson CD, Chapin FS, Michaelson GJ, Ping CL, Rupp TS, Walker DA. **2004**. The nature of spatial transitions in the Arctic. *Journal of Biogeography* **31**: 1917–1933.

Erickson RO, Michelini FL. **1957**. THE PLASTOCHRON INDEX. *American Journal of Botany* **44**: 297–305.

Estiarte M, Peñuelas J. 2015. Alteration of the phenology of leaf senescence and fall in winter deciduous species by climate change: effects on nutrient proficiency. Global Change Biology **21**: 1005–1017.

Evans JR, Clarke VC. **2019**. The nitrogen cost of photosynthesis. *Journal of Experimental Botany* **70**: 7–15.

Ewers BE. **2013**. Understanding stomatal conductance responses to long-term environmental changes: a Bayesian framework that combines patterns and processes. *Tree Physiology* **33**: 119–122.

Falge E, Graber W, Siegwolf R, Tenhunen JD. **1996**. A model of the gas exchange response of Picea abies to habitat conditions. *Trees* **10**: 277–287.

Falxa-Raymond N, Patterson AE, Schuster WSF, Griffin KL. **2012**. Oak loss increases foliar nitrogen, 15N and growth rates of Betula lenta in a northern temperate deciduous forest. *Tree Physiology* **32**: 1092–1101.

Farquhar GD, Ehleringer JR, Hubick KT. **1989**. Carbon Isotope Discrimination and Photosynthesis. *Annual Review of Plant PhysiologyPlant Molecular Biology* **40**: 503–537.

Farquhar GD, Sharkey TD. **1982**. Stomatal Conductance and Photosynthesis. *Annual Review of Plant Physiology* **33**: 317–345.

Farquhar GD, von Caemmerer S, Berry JA. **1980**. A biochemical model of photosynthetic CO2 assimilation in leaves of C3 species. *Planta* **149**: 78–90.

Farquhar GD, Wong SC. **1984**. An Empirical Model of Stomatal Conductance. *Functional Plant Biology* **11**: 191–210.

FATES Development Team. **2019**. Technical Note for the Functionally Assembled Terrestrial Ecosystem Simulator (FATES).

Fauset S, Freitas HC, Galbraith DR, Sullivan MJP, Aidar MPM, Joly CA, Phillips OL, Vieira SA, Gloor MU. **2018**. Differences in leaf thermoregulation and water use strategies between three co-occurring Atlantic forest tree species: Leaf energy balance of Atlantic forest trees. *Plant, Cell & Environment* **41**: 1618–1631.

Feng X, Dietze M. **2013**. Scale dependence in the effects of leaf ecophysiological traits on photosynthesis: B ayesian parameterization of photosynthesis models. *New Phytologist* **200**: 1132–1144.

Feng X, Fu B, Zhang Y, Pan N, Zeng Z, Tian H, Lyu Y, Chen Y, Ciais P, Wang Y, *et al.* 2021. Recent leveling off of vegetation greenness and primary production reveals the increasing soil water limitations on the greening Earth. *Science Bulletin* **66**: 1462–1471.

Fernández V, Bahamonde HA, Javier Peguero-Pina J, Gil-Pelegrín E, Sancho-Knapik D, Gil L, Goldbach HE, Eichert T. **2017**. Physico-chemical properties of plant cuticles and their functional and ecological significance. *Journal of Experimental Botany* **68**: 5293–5306.

Fick SE, Hijmans RJ. **2017**. WorldClim 2: new 1-km spatial resolution climate surfaces for global land areas. *International Journal of Climatology* **37**: 4302–4315.

Fisher RA, Koven CD, Anderegg WRL, Christoffersen BO, Dietze MC, Farrior CE, Holm JA, Hurtt GC, Knox RG, Lawrence PJ, *et al.* 2018. Vegetation demographics in Earth System Models: A review of progress and priorities. *Global Change Biology* **24**: 35–54.

Fisher RA, Koven CD. **2020**. Perspectives on the Future of Land Surface Models and the Challenges of Representing Complex Terrestrial Systems. *Journal of Advances in Modeling Earth Systems* **12**.

Fisher RA, Wieder WR, Sanderson BM, Koven CD, Oleson KW, Xu C, Fisher JB, Shi M, Walker AP, Lawrence DM. **2019**. Parametric Controls on Vegetation Responses to Biogeochemical Forcing in the CLM5. *Journal of Advances in Modeling Earth Systems* **11**: 2879–2895.

Flato GM. **2011**. Earth system models: an overview. *WIREs Climate Change* **2**: 783–800.

Franklin O. **2007**. Optimal nitrogen allocation controls tree responses to elevated CO_2. *New Phytologist* **174**: 811–822.

Franks PJ, Beerling DJ. **2009**. Maximum leaf conductance driven by CO_2 effects on stomatal size and density over geologic time. *Proceedings of the National Academy of Sciences* **106**: 10343–10347.

Franks PJ, Berry JA, Lombardozzi DL, Bonan GB. **2017**. Stomatal Function across Temporal and Spatial Scales: Deep-Time Trends, Land-Atmosphere Coupling and Global Models. *Plant Physiology* **174**: 583–602.

Franks PJ, Cowan 1 2 I. R., Farquhar GD. **1998**. A study of stomatal mechanics using the cell pressure probe. *Plant, Cell and Environment* **21**: 94–100.

Franks PJ, Drake PL, Beerling DJ. **2009**. Plasticity in maximum stomatal conductance constrained by negative correlation between stomatal size and density: an analysis using *Eucalyptus globulus*. *Plant, Cell & Environment* **32**: 1737–1748.

Franks PJ, Lombardozzi L, Bonan GB, Berry JA, Holbrook NM, Herold N, Oleson KW. **2018**. Comparing optimal and empirical stomatal conductance models for application in Earth system models. *Global Change Biology* **24**: 5708–5723.

Gao Q, Zhao P, Zeng X, Cai X, Shen W. **2002**. A model of stomatal conductance to quantify the relationship between leaf transpiration, microclimate and soil water stress: Modelling stomatal conductance. *Plant, Cell & Environment* **25**: 1373–1381.

Gee GW, Federer CA. **1972**. Stomatal resistance during senescence of hardwood leaves. *Water Resources Research* **8**: 1456–1460.

Gimeno TE, Crous KY, Cooke J, O'Grady AP, Ósvaldsson A, Medlyn BE, Ellsworth DS. **2016**. Conserved stomatal behaviour under elevated CO_2 and varying water availability in a mature woodland (D Whitehead, Ed.). *Functional Ecology* **30**: 700–709.

Gimeno TE, Saavedra N, Ogée J, Medlyn BE, Wingate L. **2019**. A novel optimization approach incorporating non-stomatal limitations predicts stomatal behaviour in species from six plant functional types. *Journal of Experimental Botany* **70**: 1639–1651.

Golaz J, Caldwell PM, Van Roekel LP, Petersen MR, Tang Q, Wolfe JD, Abeshu G, Anantharaj V, Asay-Davis XS, Bader DC, *et al.* 2019. The DOE E3SM Coupled Model Version 1: Overview and Evaluation at Standard Resolution. *Journal of Advances in Modeling Earth Systems* **11**: 2089–2129.

Gonsamo A, Ter-Mikaelian MT, Chen JM, Chen J. **2019**. Does Earlier and Increased Spring Plant Growth Lead to Reduced Summer Soil Moisture and Plant Growth on Landscapes Typical of Tundra-Taiga Interface? *Remote Sensing* **11**: 1989.

Gourlez de la Motte L, Beauclaire Q, Heinesch B, Cuntz M, Foltýnová L, Šigut L, Kowalska N, Manca G, Ballarin IG, Vincke C, *et al.* 2020. Non-stomatal processes reduce gross primary productivity in temperate forest ecosystems during severe edaphic drought. *Philosophical Transactions of the Royal Society B: Biological Sciences* **375**: 20190527.

Granda E, Baumgarten F, Gessler A, Gil-Pelegrin E, Peguero-Pina JJ, Sancho-Knapik D, Zimmermann NE, Resco de Dios V. **2020**. Day length regulates seasonal patterns of stomatal conductance in *Quercus* species. *Plant, Cell & Environment* **43**: 28–39.

Granier A. **1987**. Evaluation of transpiration in a Douglas-fir stand by means of sap flow measurements. *Tree Physiology* **3**: 309–320.

Grassi G, Magnani F. **2005**. Stomatal, mesophyll conductance and biochemical limitations to photosynthesis as affected by drought and leaf ontogeny in ash and oak trees. *Plant, Cell and Environment* **28**: 834–849.

Grassi G, Vicinelli E, Ponti F, Cantoni L, Magnani F. **2005**. Seasonal and interannual variability of photosynthetic capacity in relation to leaf nitrogen in a deciduous forest plantation in northern Italy. **25**: 12.

Green RM, Tingay S, Wang Z-Y, Tobin EM. **2002**. Circadian Rhythms Confer a Higher Level of Fitness to Arabidopsis Plants. *Plant Physiology* **129**: 576–584.

Grosse G, Harden J, Turetsky M, McGuire AD, Camill P, Tarnocai C, Frolking S, Schuur EAG, Jorgenson T, Marchenko S, *et al.* 2011. Vulnerability of high-latitude soil organic carbon in North America to disturbance. *Journal of Geophysical Research* **116**: G00K06.

Gutschick VP, Simonneau T. **2002**. Modelling stomatal conductance of field-grown sunflower under varying soil water content and leaf environment: comparison of three models of stomatal response to leaf environment and coupling with an abscisic acid-based model of stomatal response to soil drying.

Hari P, Mäkelä A, Korpilahti E, Holmberg M. **1986**. Optimal control of gas exchange. *Tree Physiology* **2**: 169–175.

Harrison MT, Kelman WM, Moore AD, Evans JR. **2010**. Grazing winter wheat relieves plant water stress and transiently enhances photosynthesis. *Functional Plant Biology* **37**: 726–736.

Hasselquist NJ, Allen MF, Santiago LS. **2010**. Water relations of evergreen and drought-deciduous trees along a seasonally dry tropical forest chronosequence. *Oecologia* **164**: 881–890.

Héroult A, Lin Y-S, Bourne A, Medlyn BE, Ellsworth DS. **2013**. Optimal stomatal conductance in relation to photosynthesis in climatically contrasting *Eucalyptus* species under drought: Stomatal responses of eucalyptus under drought. *Plant, Cell & Environment* **36**: 262–274.

Hetherington AM, Woodward FI. **2003**. The role of stomata in sensing and driving environmental change. *Nature* **424**: 901–908.

Hikosaka K, Nabeshima E, Hiura T. **2007**. Seasonal changes in the temperature response of photosynthesis in canopy leaves of Quercus crispula in a cool-temperate forest. *Tree Physiology* **27**: 1035–1041.

Hinzman LD, Deal CJ, McGuire AD, Mernild SH, Polyakov IV, Walsh JE. **2013**. Trajectory of the Arctic as an integrated system. *Ecological Applications* **23**: 1837–1868.

Hinzman LD, Kane DL, Yoshikawa K, Carr A, Bolton WR, Fraver M. **2003**. Hydrological variations among watersheds with varying degrees of permafrost. In: Phillips M, Springman SM, Arenson LU, eds. Permafrost. Lisse: A.A. BALKEMA PUBLISHERS, 407–411.

Hölttä T, Cochard H, Nikinmaa E, Mencuccini M. **2009**. Capacitive effect of cavitation in xylem conduits: results from a dynamic model. *Plant, Cell & Environment* **32**: 10–21.

Hölttä T, Lintunen A, Chan T, Mäkelä A, Nikinmaa E. **2017**. A steady-state stomatal model of balanced leaf gas exchange, hydraulics and maximal source–sink flux. *Tree Physiology* **37**: 851–868.

Huber AE, Melcher PJ, Piñeros MA, Setter TL, Bauerle TL. **2019**. Signal coordination before, during and after stomatal closure in response to drought stress. *New Phytologist* **224**: 675–688.

Igarashi Y, Kumagai T, Yoshifuji N, Sato T, Tanaka N, Tanaka K, Suzuki M, Tantasirin C. **2015**. Environmental control of canopy stomatal conductance in a tropical deciduous forest in northern Thailand. *Agricultural and Forest Meteorology* **202**: 1–10.

Iversen CM, Sloan VL, Sullivan PF, Euskirchen ES, McGuire AD, Norby RJ, Walker AP, Warren JM, Wullschleger SD. **2015**. The unseen iceberg: plant roots in arctic tundra. *New Phytologist* **205**: 34–58.

Jackson PC, Cavelier J, Goldstein G, Meinzer FC, Holbrook NM. **1995**. Partitioning of water resources among plants of a lowland tropical forest. *Oecologia* **101**: 197–203.

Jarvis PG. **1976**. The interpretation of the variations in leaf water potential and stomatal conductance found in canopies in the field. *Philosophical Transactions of the Royal Society of London. B, Biological Sciences* **273**: 593–610.

Jefferson JL, Maxwell RM, Constantine PG. **2017**. Exploring the Sensitivity of Photosynthesis and Stomatal Resistance Parameters in a Land Surface Model. *Journal of Hydrometeorology* **18**: 879–915.

Jenkins M, Dai A. **2021**. The Impact of Sea-Ice Loss on Arctic Climate Feedbacks and Their Role for Arctic Amplification. *Geophysical Research Letters* **48**.

Jiang C, Ryu Y, Wang H, Keenan TF. **2020**. An optimality-based model explains seasonal variation in C3 plant photosynthetic capacity. *Global Change Biology* **26**: 6493–6510.

Jin J, Yan T, Wang H, Ma X, He M, Wang Y, Wang W, Guo F, Cai Y, Zhu Q, *et al.* 2022. Improved modeling of canopy transpiration for temperate forests by incorporating a LAI-based dynamic parametrization scheme of stomatal slope. *Agricultural and Forest Meteorology* **326**: 109157.

Jin J, Zhan W, Wang Y, Gu B, Wang W, Jiang H, Lu X, Zhang X. **2017**. Water use efficiency in response to interannual variations in flux-based photosynthetic onset in temperate deciduous broadleaf forests. *Ecological Indicators* **79**: 122–127.

Johnson JD, Tognetti R, Paris P. **2002**. Water relations and gas exchange in poplar and willow under water stress and elevated atmospheric CO 2. *Physiologia Plantarum* **115**: 93–100.

Jones HG, Sutherland RA. **1991**. Stomatal control of xylem embolism. *Plant, Cell and Environment* **14**: 607–612.

Kala J, De Kauwe MG, Pitman AJ, Medlyn BE, Wang Y-P, Lorenz R, Perkins-Kirkpatrick SE. **2016**. Impact of the representation of stomatal conductance on model projections of heatwave intensity. *Scientific Reports* **6**: 23418.

Kane CN, Jordan GJ, Jansen S, McAdam SAM. **2020**. A Permeable Cuticle, Not Open Stomata, Is the Primary Source of Water Loss From Expanding Leaves. *Frontiers in Plant Science* **11**: 774.

Kattge J, Díaz S, Lavorel S, Prentice IC, Leadley P, Bönisch G, Garnier E, Westoby M, Reich P–, Wright IJ, *et al.* 2011. TRY - a global–database of plant traits: TRY - A GLOBAL DATABASE OF PLANT TRAITS. *Global Change Biology* **17**: 2905–2935.

Kattge J, Knorr W, Raddatz T, Wirth C. **2009**. Quantifying photosynthetic capacity and its relationship to leaf nitrogen content for global-scale terrestrial biosphere models. *Global Change Biology*: 16.

Kattge J, Knorr W. **2007**. Temperature acclimation in a biochemical model of photosynthesis: a reanalysis of data from 36 species. *Plant, Cell & Environment* **30**: 1176–1190.

Katul G, Leuning R, Oren R. **2003**. Relationship between plant hydraulic and biochemical properties derived from a steady-state coupled water and carbon transport model: Plant hydraulic and biochemical properties. *Plant, Cell & Environment* **26**: 339–350.

Katul G, Manzoni S, Palmroth S, Oren R. **2010**. A stomatal optimization theory to describe the effects of atmospheric CO2 on leaf photosynthesis and transpiration. *Annals of Botany* **105**: 431–442.

Katul GG, Palmroth S, Oren R. **2009**. Leaf stomatal responses to vapour pressure deficit under current and CO_2 -enriched atmosphere explained by the economics of gas exchange. *Plant, Cell & Environment* **32**: 968–979.

Kelsey KC, Pedersen SH, Leffler AJ, Sexton JO, Feng M, Welker JM. **2021**. Winter snow and spring temperature have differential effects on vegetation phenology and productivity across Arctic plant communities. *Global Change Biology* **27**: 1572–1586.

Kennedy D, Swenson S, Oleson KW, Lawrence DM, Fisher R, Lola da Costa AC, Gentine P. **2019**. Implementing Plant Hydraulics in the Community Land Model, Version 5. *Journal of Advances in Modeling Earth Systems* **11**: 485–513.

Kerstiens G. **1996**. Cuticular water permeability and its physiological significance. *Journal of Experimental Botany* **47**: 1813–1832.

Kets K, Darbah JNT, Sober A, Riikonen J, Sober J, Karnosky DF. **2010**. Diurnal changes in photosynthetic parameters of Populus tremuloides, modulated by elevated concentrations of CO2 and/or O3 and daily climatic variation. *Environmental Pollution* **158**: 1000–1007.

Kitajima K, Mulkey SS, Samaniego M, Joseph Wright S. **2002**. Decline of photosynthetic capacity with leaf age and position in two tropical pioneer tree species. *American Journal of Botany* **89**: 1925–1932.

Kitajima K, Mulkey SS, Wright SJ. **1997**. Decline of photosynthetic capacity with leaf age in relation to leaf longevities for five tropical canopy tree species. *American Journal of Botany* **84**: 702–708.

Kitajima K, Mulkey SS, Wright SJ. **1997**. Seasonal leaf phenotypes in the canopy of a tropical dry forest: photosynthetic characteristics and associated traits. *Oecologia* **109**: 490–498.

Klein T, Zeppel MJB, Anderegg WRL, Bloemen J, De Kauwe MG, Hudson P, Ruehr NK, Powell TL, von Arx G, Nardini A. **2018**. Xylem embolism refilling and resilience against drought-induced mortality in woody plants: processes and trade-offs. *Ecological Research* **33**: 839–855.

Klein T. **2014**. The variability of stomatal sensitivity to leaf water potential across tree species indicates a continuum between isohydric and anisohydric behaviours (S Niu, Ed.). *Functional Ecology* **28**: 1313–1320.

Knapp AK. **1993**. Gas Exchange Dynamics in C^3 and C^4 Grasses: Consequence of Differences in Stomatal Conductance. *Ecology* **74**: 113–123.

Knauer J, Zaehle S, Reichstein M, Medlyn BE, Forkel M, Hagemann S, Werner C. **2017**. The response of ecosystem water-use efficiency to rising atmospheric CO_2 concentrations: sensitivity and large-scale biogeochemical implications. *New Phytologist* **213**: 1654–1666.

Kobza J, Seemann JR. **1989**. Regulation of Ribulose-1,5-Bisphosphate Carboxylase Activity in Response to Diurnal Changes in Irradiance. *Plant Physiology* **89**: 918.

Köppen W. **1936**. The geographic system of climates. In: Geiger W, ed. Handbuch der Klimatologie. Berlin: Borntraeger.

Koven CD, Knox RG, Fisher RA, Chambers JQ, Christoffersen BO, Davies SJ, Detto M, Dietze MC, Faybishenko B, Holm J, *et al.* 2020. Benchmarking and parameter sensitivity of physiological and vegetation dynamics using the Functionally Assembled Terrestrial Ecosystem Simulator (FATES) at Barro Colorado Island, Panama. *Biogeosciences* **17**: 3017–3044.

Koven CD, Riley WJ, Subin ZM, Tang JY, Torn MS, Collins WD, Bonan GB, Lawrence DM, Swenson SC. **2013**. The effect of vertically resolved soil biogeochemistry and alternate soil C and N models on C dynamics of CLM4. *Biogeosciences* **10**: 7109–7131.

Koven CD, Ringeval B, Friedlingstein P, Ciais P, Cadule P, Khvorostyanov D, Krinner G, Tarnocai C. **2011**. Permafrost carbon-climate feedbacks accelerate global warming. *Proceedings of the National Academy of Sciences* **108**: 14769–14774.

Krinner G, Viovy N, de Noblet-Ducoudré N, Ogée J, Polcher J, Friedlingstein P, Ciais P, Sitch S, Prentice IC. **2005**. A dynamic global vegetation model for studies of the coupled atmosphere-biosphere system: DVGM FOR COUPLED CLIMATE STUDIES. *Global Biogeochemical Cycles* **19**: 2003GB002199.

Kropp H, Loranty M, Alexander HD, Berner LT, Natali SM, Spawn SA. **2017**. Environmental constraints on transpiration and stomatal conductance in a Siberian Arctic boreal forest. *Journal of Geophysical Research: Biogeosciences* **122**: 487–497.

Lahiri A, Venkatasubramani PS, Datta A. 2019. Bayesian modeling of plant drought resistance pathway. *BMC Plant Biology* 19: 96.

Lambert MSA, Tang H, Aas KS, Stordal F, Fisher RA, Fang Y, Ding J, Parmentier F-JW. **2022**. Inclusion of a cold hardening scheme to represent frost tolerance is essential to model realistic plant hydraulics in the Arctic–boreal zone in CLM5.0-FATES-Hydro. *Geoscientific Model Development* **15**: 8809–8829.

Lamour J, Davidson KJ, Ely KS, Anderson J, Serbin SP, Rogers A. **2021b**. Leaf gas exchange and fitted parameters, San Lorenzo, Panama, 2020.

Lamour J, Davidson KJ, Ely KS, Anderson JA, Rogers A, Wu J, Serbin SP. **2021a**. Rapid estimation of photosynthetic leaf traits of tropical plants in diverse environmental conditions using reflectance spectroscopy (RE Sharwood, Ed.). *PLOS ONE* **16**: e0258791.

Lamour J, Davidson KJ, Ely KS, Le Moguédec G, Anderson JA, Li Q, Calderón O, Koven CD, Wright SJ, Walker AP, *et al.* 2023d. The effect of the vertical gradients of photosynthetic parameters on the CO_2 assimilation and transpiration of a Panamanian tropical forest. *New Phytologist* **238**: 2345–2362.

Lamour J, Davidson KJ, Ely KS, Le Moguédec G, Leakey ADB, Li Q, Serbin SP, Rogers A. **2022**. An improved representation of the relationship between photosynthesis and stomatal conductance leads to more stable estimation of conductance parameters and improves the goodness-of-fit across diverse data sets. *Global Change Biology* **Accepted**.

Lamour J, Davidson KJ, Ely KS, Li Q, Serbin SP, Rogers A. **2021c**. New calculations for photosynthesis measurement systems: what's the impact for physiologists and modelers? *New Phytologist*: nph.17762.

Lamour J, Serbin SP. **2021**. LeafGasExchange.

Lamour J, Souza DC, Gimenez BO, Higuchi N, Chave, J, Chambers J, Rogers A. 2023b Wood-density has no effect on stomatal control of leaf-level water use efficiency in an Amazonian forest. *Plant, Cell & Environment* **Accepted**.

Landhäusser SM, Wein RW, Lange P. **1996**. Gas exchange and growth of three arctic tree-line tree species under different soil temperature and drought preconditioning regimes. *Canadian Journal of Botany* **74**: 686–693.

Langford ZL, Kumar J, Hoffman FM, Breen AL, Iversen CM. **2019**. Arctic Vegetation Mapping Using Unsupervised Training Datasets and Convolutional Neural Networks. *Remote Sensing* **11**: 69.

Lawrence DM, Fisher RA, Koven CD, Oleson KW, Swenson SC, Bonan G, Collier N, Ghimire B, Kampenhout L, Kennedy D, *et al.* 2019. The Community Land Model Version 5: Description of New Features, Benchmarking, and Impact of Forcing Uncertainty. *Journal of Advances in Modeling Earth Systems* **11**: 4245–4287.

Lawson T, Blatt MR. **2014**. Stomatal Size, Speed, and Responsiveness Impact on Photosynthesis and Water Use Efficiency. *Plant Physiology* **164**: 1556–1570.

Lawson T, Kramer DM, Raines CA. **2012**. Improving yield by exploiting mechanisms underlying natural variation of photosynthesis. *Current Opinion in Biotechnology* **23**: 215–220.

Lawson T, Vialet-Chabrand S. **2019**. Speedy stomata, photosynthesis and plant water use efficiency. *New Phytologist* **221**: 93–98.

Le Quéré C, Andrew RM, Canadell JG, Sitch S, Korsbakken JI, Peters GP, Manning AC, Boden TA, Tans PP, Houghton RA, *et al.* 2016. Global Carbon Budget 2016. *Earth System Science Data* **8**: 605–649.

Le Roux PC, Aalto J, Luoto M. **2013**. Soil moisture's underestimated role in climate change impact modelling in low-energy systems. *Global Change Biology* **19**: 2965–2975.

Leach JE, Woodhead T, Day W. **1982**. Bias in pressure chamber measurements of leaf water potential. *Agricultural Meteorology* **27**: 257–263.

Leakey ADB, Bernacchi CJ, Ort DR, Long SP. **2006**. Long-term growth of soybean at elevated [CO2] does not cause acclimation of stomatal conductance under fully open-air conditions. *Plant, Cell and Environment* **29**: 1794–1800.

LeBauer DS, Wang D, Richter KT, Davidson CC, Dietze MC. **2013**. Facilitating feedbacks between field measurements and ecosystem models. *Ecological Monographs* **83**: 133–154.

Léger E, Dafflon B, Robert Y, Ulrich C, Peterson JE, Biraud SC, Romanovsky VE, Hubbard SS. **2019**. A distributed temperature profiling method for assessing spatial variability in ground temperatures in a discontinuous permafrost region of Alaska. *The Cryosphere* **13**: 2853–2867.

Lemordant L, Gentine P, Swann AS, Cook BI, Scheff J. **2018**. Critical impact of vegetation physiology on the continental hydrologic cycle in response to increasing CO 2. *Proceedings of the National Academy of Sciences* **115**: 4093–4098.

Lenth R, Singmann H, Love J, Buerkner P, Herve M. **2020**. Estimated Marginal Means, aka Least-Squares Means.

Leuning R. **1990**. Modelling Stomatal Behaviour and and Photosynthesis of Eucalyptus grandis. *Functional Plant Biology* **17**: 159–175.

Leuning R. **1995**. A critical appraisal of a combined stomatal-photosynthesis model for C3 plants. *Plant, Cell and Environment* **18**: 339–355.

Leuning R. **2002**. Temperature dependence of two parameters in a photosynthesis model: Temperature dependence of photosynthetic parameters. *Plant, Cell & Environment* **25**: 1205–1210.

Li F, Xiao J, Chen J, Ballantyne A, Jin K, Li B, Abraha M, John R. **2023**. Global water use efficiency saturation due to increased vapor pressure deficit. *Science* **381**: 672–677.

Li Q, Serbin SP, Lamour J, Davidson KJ, Ely KS, Rogers A. **2022**. Implementation and evaluation of the unified stomatal optimization approach in the Functionally Assembled Terrestrial Ecosystem Simulator (FATES). *Geoscientific Model Development* **15**: 4313–4329.

Li S, Assmann SM, Albert R. **2006**. Predicting Essential Components of Signal Transduction Networks: A Dynamic Model of Guard Cell Abscisic Acid Signaling (J Chory, Ed.). *PLoS Biology* **4**: e312.

Li X, Gentine P, Lin C, Zhou S, Sun Z, Zheng Y, Liu J, Zheng C. **2019**. A simple and objective method to partition evapotranspiration into transpiration and evaporation at eddy-covariance sites. *Agricultural and Forest Meteorology* **265**: 171–182.

Liljedahl AK, Hinzman LD, Harazono Y, Zona D, Tweedie CE, Hollister RD, Engstrom R, Oechel WC. **2011**. Nonlinear controls on evapotranspiration in arctic coastal wetlands. *Biogeosciences* **8**: 3375–3389.

Lin Y-S, Medlyn BE, Duursma RA, Prentice IC, Wang H, Baig S, Eamus D, de Dios VR, Mitchell P, Ellsworth DS, *et al.* 2015. Optimal stomatal behaviour around the world. *Nature Climate Change* **5**: 459–464.

Liozon R, Badeck F-W, Genty B, Meyer S, Saugier B. **2000**. Leaf photosynthetic characteristics of beech (Fagus sylvatica) saplings during three years of exposure to elevated CO2 concentration. *Tree Physiology* **20**: 239–247.

Lique C, Holland MM, Dibike YB, Lawrence DM, Screen JA. **2016**. Modeling the Arctic freshwater system and its integration in the global system: Lessons learned and future challenges: MODELING THE ARCTIC FRESHWATER SYSTEM. *Journal of Geophysical Research: Biogeosciences* **121**: 540–566.

Liu Y, Holtzman NM, Konings AG. **2021**. Global ecosystem-scale plant hydraulic traits retrieved using model–data fusion. *Hydrology and Earth System Sciences* **25**: 2399–2417.

Lombardozzi DL, Zeppel MJB, Fisher RA, Tawfik A. **2017**. Representing nighttime and minimum conductance in CLM4.5: global hydrology and carbon sensitivity analysis using observational constraints. *Geoscientific Model Development* **10**: 321–331.

Long SP, Bernacchi CJ. **2003**. Gas exchange measurements, what can they tell us about the underlying limitations to photosynthesis? Procedures and sources of error. *Journal of Experimental Botany* **54**: 2393–2401.

Long SP, Hällgren J-E. **1993**. Measurement of CO2 assimilation by plants in the field and the laboratory. In: Hall DO, Scurlock JMO, Bolhàr-Nordenkampf HR, Leegood RC, Long SP, eds. Photosynthesis and Production in a Changing Environment: A field and laboratory manual. Dordrecht: Springer Netherlands, 129–167.

Lu X, Liang E, Babst F, Camarero JJ, Büntgen U. **2022**. Warming-induced tipping points of Arctic and alpine shrub recruitment. *Proceedings of the National Academy of Sciences* **119**: e2118120119.

Luo X, Keenan TF, Chen JM, Croft H, Colin Prentice I, Smith NG, Walker AP, Wang H, Wang R, Xu C, *et al.* 2021. Global variation in the fraction of leaf nitrogen allocated to photosynthesis. *Nature Communications* **12**: 4866.

Luo Y, Ogle K, Tucker C, Fei S, Gao C, LaDeau S, Clark JS, Schimel DS. **2011**. Ecological forecasting and data assimilation in a data-rich era. *Ecological Applications* **21**: 1429–1442.

Machado R, Loram-Lourenço L, Farnese FS, Alves RDFB, Sousa LF, Silva FG, Filho SCV, Torres-Ruiz JM, Cochard H, Menezes-Silva PE. **2021**. Where do leaf water leaks come from? Trade-offs underlying the variability in minimum conductance across tropical savanna species with contrasting growth strategies. *New Phytologist* **229**: 1415–1430.

Mackay DS, Ewers BE, Loranty MM, Kruger EL, Samanta S. **2012**. Bayesian analysis of canopy transpiration models: A test of posterior parameter means against measurements. *Journal of Hydrology* **432–433**: 75–83.

Manzoni S, Vico G, Katul G, Fay PA, Polley W, Palmroth S, Porporato A. **2011**. Optimizing stomatal conductance for maximum carbon gain under water stress: a meta-analysis across plant functional types and climates: Optimal leaf gas exchange under water stress. *Functional Ecology* **25**: 456–467.

Márquez DA, Stuart-Williams H, Farquhar GD. **2021**. An improved theory for calculating leaf gas exchange more precisely accounting for small fluxes. *Nature Plants* **7**: 317–326.

Márquez DA, Stuart-Williams H, Farquhar GD, Busch FA. **2022**. Cuticular conductance of adaxial and abaxial leaf surfaces and its relation to minimum leaf surface conductance. *New Phytologist* **233**: 156–168.

Martin-StPaul N, Delzon S, Cochard H. **2017**. Plant resistance to drought depends on timely stomatal closure (H Maherali, Ed.). *Ecology Letters* **20**: 1437–1447.

Martínez Cano I, Muller-Landau HC, Wright SJ, Bohlman SA, Pacala SW. **2019**. Tropical tree height and crown allometries for the Barro Colorado Nature Monument, Panama: a comparison of alternative hierarchical models incorporating interspecific variation in relation to life history traits. *Biogeosciences* **16**: 847–862.

Martínez-Vilalta J, Garcia-Forner N. **2017**. Water potential regulation, stomatal behaviour and hydraulic transport under drought: deconstructing the iso/anisohydric concept: Deconstructing the iso/anisohydric concept. *Plant, Cell & Environment* **40**: 962–976.

Maruyama A, Kuwagata T. **2008**. Diurnal and seasonal variation in bulk stomatal conductance of the rice canopy and its dependence on developmental stage. *Agricultural and Forest Meteorology* **148**: 1161–1173.

Massmann A, Gentine P, Lin C. **2019**. When Does Vapor Pressure Deficit Drive or Reduce Evapotranspiration? *Journal of Advances in Modeling Earth Systems* **11**: 3305–3320.

Matthews JSA, Vialet-Chabrand SRM, Lawson T. **2017**. Diurnal Variation in Gas Exchange: The Balance between Carbon Fixation and Water Loss. *Plant Physiology* **174**: 614–623.

McAdam SAM, Brodribb TJ. **2015**. The Evolution of Mechanisms Driving the Stomatal Response to Vapor Pressure Deficit. *Plant Physiology* **167**: 833–843.

McAusland L, Vialet-Chabrand S, Davey P, Baker NR, Brendel O, Lawson T. **2016**. Effects of kinetics of light-induced stomatal responses on photosynthesis and water-use efficiency. *New Phytologist* **211**: 1209–1220.

McDowell N. **2008**. Mechanisms of plant survival and mortality during drought: why do some plants survive while others succumb to drought? *New Phytologist*: 21.

McDowell NG, Adams HD, Bailey JD, Hess M, Kolb TE. **2006**. Homeostatic Maintenance Of Ponderosa Pine Gas Exchange In Response To Stand Density Changes. *Ecological Applications* **16**: 1164–1182.

McDowell NG, Brodribb TJ, Nardini A. **2019**. Hydraulics in the 21 st century. *New Phytologist* **224**: 537–542.

Medlyn BE, Badeck F-W, De Pury DGG, Barton CVM, Broadmeadow M, Ceulemans R, De Angelis P, Forstreuter M, Jach ME, Kellomäki S, *et al.* 1999. Effects of elevated [CO2] on photosynthesis in European forest species: a meta-analysis of model parameters: Photosynthetic acclimation to elevated CO2. *Plant, Cell & Environment* **22**: 1475–1495.

Medlyn BE, Berbigier P, Clement R, Grelle A, Loustau D, Linder S, Wingate L, Jarvis PG, Sigurdsson BD, McMurtrie RE. **2005**. Carbon balance of coniferous forests growing in contrasting climates: Model-based analysis. *Agricultural and Forest Meteorology* **131**: 97–124.

Medlyn BE, Duursma RA, Eamus D, Ellsworth DS, Prentice IC, Barton CVM, Crous KY, De Angelis P, Freeman M, Wingate L. **2011**. Reconciling the optimal and empirical approaches to modelling stomatal conductance. *Global Change Biology* **17**: 2134–2144.

Medvigy D, Jeong S-J, Clark KL, Skowronski NS, Schäfer KVR. **2013**. Effects of seasonal variation of photosynthetic capacity on the carbon fluxes of a temperate deciduous forest: SEASONALITY OF PHOTOSYNTHETIC CAPACITY. *Journal of Geophysical Research: Biogeosciences* **118**: 1703–1714.

Medvigy D, Wofsy SC, Munger JW, Hollinger DY, Moorcroft PR. **2009**. Mechanistic scaling of ecosystem function and dynamics in space and time: Ecosystem Demography model version 2. *Journal of Geophysical Research* **114**: G01002.

Meicenheimer RD. **2014**. The plastochron index: Still useful after nearly six decades. *American Journal of Botany* **101**: 1821–1835.

Meidner H, Mansfield TA. **1968**. *Physiology of stomata.* London: McGraw-Hill.

Meinzer FC, James SA, Goldstein G, Woodruff D. **2003**. Whole-tree water transport scales with sapwood capacitance in tropical forest canopy trees: Water transport scales with sapwood properties in tropical trees. *Plant, Cell & Environment* **26**: 1147–1155.

Meir P, Kruijt B, Broadmeadow M, Barbosa E, Kull O, Carswell F, Nobre A, Jarvis PG. **2002**. Acclimation of photosynthetic capacity to irradiance in tree canopies in relation to leaf nitrogen concentration and leaf mass per unit area: Photosynthetic acclimation in forest canopies. *Plant, Cell & Environment* **25**: 343–357.

Mekonnen ZA, Riley WJ, Berner LT, Bouskill NJ, Torn MS, Iwahana G, Breen AL, Myers-Smith IH, Criado MG, Liu Y, *et al.* 2021. Arctic tundra shrubification: a review of mechanisms and impacts on ecosystem carbon balance. *Environmental Research Letters* **16**: 053001.

Meng F-R, Arp PA. **1993**. Net photosynthesis and stomatal conductance of red spruce twigs before and after twig detachment. *Canadian Journal of Forest Research* **23**: 716–721.

Mengoli G, Agustí-Panareda A, Boussetta S, Harrison SP, Trotta C, Prentice IC. **2022**. Ecosystem Photosynthesis in Land-Surface Models: A First-Principles Approach Incorporating Acclimation. *Journal of Advances in Modeling Earth Systems* **14**.

Merilo E, Yarmolinsky D, Jalakas P, Parik H, Tulva I, Rasulov B, Kilk K, Kollist H. **2018**. Stomatal VPD Response: There Is More to the Story Than ABA. *Plant Physiology* **176**: 851–864.

Miao Y, Cai Y, Wu H, Wang D. **2021**. Diurnal and Seasonal Variations in the Photosynthetic Characteristics and the Gas Exchange Simulations of Two Rice Cultivars Grown at Ambient and Elevated CO2. *Frontiers in Plant Science* **12**: 651606.

Michaletz ST, Weiser MD, McDowell NG, Zhou J, Kaspari M, Helliker BR, Enquist BJ. **2016**. The energetic and carbon economic origins of leaf thermoregulation. *Nature Plants* **2**: 16129.

Michaletz ST, Weiser MD, Zhou J, Kaspari M, Helliker BR, Enquist BJ. **2015**. Plant Thermoregulation: Energetics, Trait–Environment Interactions, and Carbon Economics. *Trends in Ecology & Evolution* **30**: 714–724.

Miner GL, Bauerle WL, Baldocchi DD. **2017**. Estimating the sensitivity of stomatal conductance to photosynthesis: a review: The sensitivity of conductance to photosynthesis. *Plant, Cell & Environment* **40**: 1214–1238.

Miner GL, Bauerle WL. **2017**. Seasonal variability of the parameters of the Ball-Berry model of stomatal conductance in maize (*Zea mays* L .) and sunflower (*Helianthus annuus* L.) under well-watered and water-stressed conditions: Ball-Berry model parameters. *Plant, Cell & Environment* **40**: 1874–1886.

Miranda T, Ebner M, Traiser C, Roth-Nebelsick A. **2013**. Diurnal pattern of stomatal conductance in the large-leaved temperate liana Aristolochia macrophylla depends on spatial position within the leaf lamina. *Annals of Botany* **111**: 905–915.

Missik JEC, Oishi AC, Benson MC, Meretsky VJ, Phillips RP, Novick KA. **2021**. Performing gas-exchange measurements on excised branches - evaluation and recommendations. *Photosynthetica* **59**: 61–73.

Misson L, Tu KP, Boniello RA, Goldstein AH. **2006**. Seasonality of photosynthetic parameters in a multi-specific and vertically complex forest ecosystem in the Sierra Nevada of California. *Tree Physiology* **26**: 729–741.

Miyazawa Y, Tateishi M, Komatsu H, Kumagai T, Otsuki K. **2011**. Are measurements from excised leaves suitable for modeling diurnal patterns of gas exchange of intact leaves? *Hydrological Processes* **25**: 2924–2930.

Mott KA. **1988**. Do Stomata Respond to CO 2 Concentrations Other than Intercellular? *Plant Physiology* **86**: 200–203.

Muir CD. **2019**. tealeaves: an R package for modelling leaf temperature using energy budgets (K Crous, Ed.). *AoB PLANTS* **11**: plz054.

Muir CD. **2019**. Tealeaves: An R package for modelling leaf temperature using energy budgets. *AoB PLaNTS* **11**: 1–10.

Muir CD. **2020**. tealeaves: an R package for modelling leaf temperature using energy budgets.

Muñoz Sabater J. **2019**. ERA5-Land hourly data from 1981 to present.

Myers-Smith IH, Forbes BC, Wilmking M, Hallinger M, Lantz T, Blok D, Tape KD, Macias-Fauria M, Sass-Klaassen U, Lévesque E, *et al.* 2011a. Shrub expansion in tundra ecosystems: dynamics, impacts and research priorities. *Environmental Research Letters* **6**: 045509.

Myers-Smith IH, Hik DS, Kennedy C, Cooley D, Johnstone JF, Kenney AJ, Krebs CJ. 2011b. Expansion of Canopy-Forming Willows Over the Twentieth Century on Herschel Island, Yukon Territory, Canada. *AMBIO* **40**: 610–623.

Myers-Smith IH, Kerby JT, Phoenix GK, Bjerke JW, Epstein HE, Assmann JJ, John C, Andreu-Hayles L, Angers-Blondin S, Beck PSA, *et al.* 2020. Complexity revealed in the greening of the Arctic. *Nature Climate Change* **10**: 106–117.

Nascimento HCS, Marenco RA. 2013. Mesophyll conductance variations in response to diurnal environmental factors in Myrcia paivae and Minquartia guianensis in Central Amazonia. *Photosynthetica* **51**: 457–464.

Niu H, Wang D, Ehsani R, Chen Y. 2022. Tree-level yield estimation using UAV-based vegetation indices and plant physiology-informed machine learning. In: *2022 International Conference on Unmanned Aircraft Systems (ICUAS)*. Dubrovnik, Croatia: IEEE, 1614–1619.

Norman JM. 1979. Modeling the complete crop canopy. In: Barfield G, ed. Modification of the Aerial Environment of Crops. St Joseph, MI: American Society of Agricultural Engineers, 249–277.

O'Leary BM, Asao S, Millar AH, Atkin OK. 2019. Core principles which explain variation in respiration across biological scales. *New Phytologist* **222**: 670–686.

Oleson KW, Lawrence DM, Bonan GB, Drewniak B, Huang M, Levis S, Li F, Riley WJ, Swenson SC, Thornton PE, *et al.* 2013. *Technical Description of version 4.5 of the Community Land Model (CLM)*. Boulder, CO: National Center for Atmospheric Research.

Ono K, Maruyama A, Kuwagata T, Mano M, Takimoto T, Hayashi K, Hasegawa T, Miyata A. 2013. Canopy-scale relationships between stomatal conductance and photosynthesis in irrigated rice. *Global Change Biology* **19**: 2209–2220.

Op De Beeck M, Gielen B, Jonckheere I, Samson R, Janssens IA, Ceulemans R. 2010. Needle age-related and seasonal photosynthetic capacity variation is negligible for modelling yearly gas exchange of a sparse temperate Scots pine forest. *Biogeosciences* **7**: 199–215.

Ow LF, Whitehead D, Walcroft AS, Turnbull MH. 2010. Seasonal variation in foliar carbon exchange in Pinus radiata and Populus deltoides: respiration acclimates fully to changes in temperature but photosynthesis does not: ACCLIMATION OF RESPIRATION BUT NOT PHOTOSYNTHESIS IN TREES. *Global Change Biology* **16**: 288–302.

Pandey AK, Jiang L, Moshelion M, Gosa SC, Sun T, Lin Q, Wu R, Xu P. 2021. Functional physiological phenotyping with functional mapping: A general framework to bridge the

phenotype-genotype gap in plant physiology. *iScience* 24: 102846.

Pantin F, Simonneau T, Muller B. **2012**. Coming of leaf age: control of growth by hydraulics and metabolics during leaf ontogeny. *New Phytologist* **196**: 349–366.

Paton S. **2020**. *Yearly Reports_San Lorenzo Crane*. The Smithsonian Institution.

Pinheiro J, Bates D, DebRoy S, Sarkar D, Heisterkamp S, Bert VW. **2020**. Package 'nlme'.

Pitman AJ. **2003**. The evolution of, and revolution in, land surface schemes designed for climate models. *International Journal of Climatology* **23**: 479–510.

Pivovaroff A, McDowell N, Davies S, Detto M, Wolfe BT, Zambrano A. **2021**. Sap flow data from San Lorenzo, Panama (PA-SLZ) from January - June 2020.

Pivovaroff AL, Sack L, Santiago LS. **2014**. Coordination of stem and leaf hydraulic conductance in southern California shrubs: a test of the hydraulic segmentation hypothesis. *New Phytologist* **203**: 842–850.

Plummer M, Stukalov A, Denwood M. **2016**. rjags.

Plummer M. **2017**. JAGS.

Powell TL, Galbraith DR, Christoffersen BO, Harper A, Imbuzeiro HMA, Rowland L, Almeida S, Brando PM, Costa ACL, Costa MH, *et al.* 2013. Confronting model predictions of carbon fluxes with measurements of Amazon forests subjected to experimental drought. *New Phytologist* **200**: 350–365.

Prentice IC, Dong N, Gleason SM, Maire V, Wright IJ. **2014**. Balancing the costs of carbon gain and water transport: testing a new theoretical framework for plant functional ecology (J Penuelas, Ed.). *Ecology Letters* **17**: 82–91.

Prieto I, Armas C, Pugnaire FI. **2012**. Water release through plant roots: new insights into its consequences at the plant and ecosystem level. *New Phytologist* **193**: 830–841.

Prikaziuk E, Migliavacca M, Su Z (Bob), van der Tol C. **2023**. Simulation of ecosystem fluxes with the SCOPE model: Sensitivity to parametrization and evaluation with flux tower observations. *Remote Sensing of Environment* **284**: 113324.

Quebbeman JA, Ramirez JA. **2016**. Optimal allocation of leaf-level nitrogen: Implications for covariation of V_{cmax} and J_{max} and photosynthetic downregulation: COVARIATION OF V_{cmax} AND J_{max}. *Journal of Geophysical Research: Biogeosciences* **121**: 2464–2475.

R Core Team. **2013**. R: A language and environment for statistical computing.

Raesch A. **2020**. pvldcurve: Simplifies the Analysis of Pressure Volume and Leaf Drying Curves.

Rantanen M, Karpechko AYu, Lipponen A, Nordling K, Hyvärinen O, Ruosteenoja K, Vihma T, Laaksonen A. **2022**. The Arctic has warmed nearly four times faster than the globe since 1979. *Communications Earth & Environment* **3**: 168.

Ratto M, Pagano A. **2010**. Using recursive algorithms for the efficient identification of smoothing spline ANOVA models. *AStA Advances in Statistical Analysis* **94**: 367–388.

Reich PB, Wright IJ, Lusk CH. **2007**. PREDICTING LEAF PHYSIOLOGY FROM SIMPLE PLANT AND CLIMATE ATTRIBUTES: A GLOBAL GLOPNET ANALYSIS. *Ecological Applications* **17**: 1982–1988.

Reich PB. **2014**. The world-wide 'fast–slow' plant economics spectrum: a traits manifesto. *Journal of Ecology*: 27.

Reichstein M, Falge E, Baldocchi D, Papale D, Aubinet M, Berbigier P, Bernhofer C, Buchmann N, Gilmanov T, Granier A, *et al.* 2005. On the separation of net ecosystem exchange into assimilation and ecosystem respiration: review and improved algorithm. *Global Change Biology* **11**: 1424–1439.

Resco de Dios V, Anderegg WRL, Li X, Tissue DT, Bahn M, Landais D, Milcu A, Yao Y, Nolan RH, Roy J, *et al.* 2020. Circadian Regulation Does Not Optimize Stomatal Behaviour. *Plants* **9**: 1091.

Resco de Dios V, Loik ME, Smith R, Aspinwall MJ, Tissue DT. **2016**. Genetic variation in circadian regulation of nocturnal stomatal conductance enhances carbon assimilation and growth: On the function of nocturnal stomatal conductance. *Plant, Cell & Environment* **39**: 3–11.

Ricciuto D, Sargsyan K, Thornton P. **2018**. The Impact of Parametric Uncertainties on Biogeochemistry in the E3SM Land Model. *Journal of Advances in Modeling Earth Systems* **10**: 297–319.

Rocha AV, Loranty MM, Higuera PE, Mack MC, Hu FS, Jones BM, Breen AL, Rastetter EB, Goetz SJ, Shaver GR. **2012**. The footprint of Alaskan tundra fires during the past half-century: implications for surface properties and radiative forcing. *Environmental Research Letters* **7**: 044039.

Roden JS, Pearcy RW. **1993**. Photosynthetic gas exchange response of poplars to steady-state and dynamic light environments. *Oecologia* **93**: 208–214.

Rodriguez-Dominguez CM, Forner A, Martorell S, Choat B, Lopez R, Peters JMR, Pfautsch S, Mayr S, Carins-Murphy MR, McAdam SAM, *et al.* 2022. Leaf water potential measurements using the pressure chamber: Synthetic testing of assumptions towards best practices for precision and accuracy. *Plant, Cell & Environment* **45**: 2037–2061.

Rogers A, Allen DJ, Davey PA, Morgan PB, Ainsworth EA, Bernacchi CJ, Cornic G, Dermody O, Dohleman FG, Heaton EA, *et al.* 2004. Leaf photosynthesis and carbohydrate dynamics of soybeans grown throughout their life-cycle under Free-Air Carbon dioxide Enrichment. *Plant, Cell and Environment* **27**: 449–458.

Rogers A, Ely K, Davidson K. **2020**. Plant Physiology, Alder and Willow Species, Seward Peninsula, Alaska, 2019. Next Generation Ecosystem Experiments Arctic Data Collection, Oak Ridge National Laboratory, U.S. Department of Energy, Oak Ridge, Tennessee, USA. Dataset accessed on 2023-03-08 at https://doi.org/10.5440/1696801

Rogers A, Ely K, Serbin S, Lasota S, Lieberman-Cribbin W. **2017b**. Leaf Mass Area, Leaf Carbon and Nitrogen Content, Barrow, Alaska, 2012-2016. Next Generation Ecosystem Experiments Arctic Data Collection, Oak Ridge National Laboratory, U.S. Department of Energy, Oak Ridge, Tennessee, USA. Dataset accessed on 2023-03-13 at https://doi.org/10.5440/1336812

Rogers A, Ely K, Serbin S. **2017e**. Leaf Photosynthetic Parameters Vcmax and Jmax and Supporting Gas Exchange Data, Barrow, Alaska, 2012-2016. Next Generation Ecosystem Experiments Arctic Data Collection, Oak Ridge National Laboratory, U.S. Department of Energy, Oak Ridge, Tennessee, USA. Dataset accessed on 2023-03-14 at https://doi.org/10.5440/1336809

Rogers A, Ely K, Davidson K. 2023. Stomatal response of six Arctic plant species, Utqiagvik (Barrow), Alaska, 2022. Next Generation Ecosystem Experiments Arctic Data Collection, Oak Ridge National Laboratory, U.S. Department of Energy, Oak Ridge, Tennessee, USA. Dataset accessed on 2023-03-14

Rogers A, McDonald K, Muehlbauer MF, Hoffman A, Koenig K, Newman L, Taghavi S, Lelie D. **2012**. Inoculation of hybrid poplar with the endophytic bacterium Enterobacter sp. 638 increases biomass but does not impact leaf level physiology. *GCB Bioenergy* **4**: 364–370.

Rogers A, Medlyn BE, Dukes JS, Bonan G, von Caemmerer S, Dietze MC, Kattge J, Leakey ADB, Mercado LM, Niinemets Ü, *et al.* 2017a. A roadmap for improving the representation of photosynthesis in Earth system models. *New Phytologist* **213**: 22–42.

Rogers A, Medlyn BE, Dukes JS, Bonan G, von Caemmerer S, Dietze MC, Kattge J, Leakey ADB, Mercado LM, Niinemets Ü, *et al.* 2017c. A roadmap for improving the representation of photosynthesis in Earth system models. *New Phytologist* **213**: 22–42.

Rogers A, Serbin SP, Ely K, Wu J, Wolfe BT, Dickman LT, Collins AD, Detto M, Grossiord C, McDowell N, *et al.* 2021. Diurnal leaf gas exchange survey, Feb2016-May2016, PA-SLZ, PA-PNM: Panama.

Rogers A, Serbin SP, Ely KS, Sloan VL, Wullschleger SD. **2017d**. Terrestrial biosphere models underestimate photosynthetic capacity and CO 2 assimilation in the Arctic. *New Phytologist* **216**: 1090–1103.

Rogers A, Serbin SP, Way DA. **2022**. Reducing model uncertainty of climate change impacts on high latitude carbon assimilation. *Global Change Biology* **28**: 1222–1247.

Rogers A. **2014**. The use and misuse of V c,max in Earth System Models. *Photosynthesis Research* **119**: 15–29.

Ropars P, Boudreau S. **2012**. Shrub expansion at the forest–tundra ecotone: spatial heterogeneity linked to local topography. *Environmental Research Letters* **7**: 015501.

Sabot MEB, Kauwe MG, Pitman AJ, Medlyn BE, Ellsworth DS, Martin-StPaul N, Wu J, Choat B, Limousin J, Mitchell PJ, *et al.* 2022. One Stomatal Model to Rule Them All? Towards Improved Representation of Carbon and Water Exchange in Global Models. *Journal of Advances in Modeling Earth Systems*.

Sade N, Gebremedhin A, Moshelion M. **2012**. Risk-taking plants: Anisohydric behavior as a stress-resistance trait. *Plant Signaling & Behavior* **7**: 767–770.

Sala A, Tenhunen JD. **1996**. Simulations of canopy net photosynthesis and transpiration in Quercus ilex L. under the influence of seasonal drought. *Agricultural and Forest Meteorology* **78**: 203–222.

Salmon VG, Breen AL, Kumar J, Lara MJ, Thornton PE, Wullschleger SD, Iversen CM. **2019**. Alder Distribution and Expansion Across a Tundra Hillslope: Implications for Local N Cycling. *Frontiers in Plant Science* **10**: 1099.

Salvucci ME, Anderson JC. **1987**. Factors Affecting the Activation State and the Level of Total Activity of Ribulose Bisphosphate Carboxylase in Tobacco Protoplasts. *Plant Physiology* **85**: 66–71.

Sanchez A, Hughes N, Smith W. **2013**. Water-Use Efficiency Declines during Autumn Leaf Senescence in Three Deciduous Tree Species. *International Journal of Plant Biology* **4**: e7.

Sang Y, Wang C, Huo H. **2011**. Inter-specific and seasonal variations in photosynthetic capacity and water use efficiency of five temperate tree species in Northeastern China. *Scandinavian Journal of Forest Research* **26**: 21–29.

Santiago LS, Mulkey SS. **2003**. A Test of Gas Exchange Measurements on Excised Canopy Branches of Ten Tropical Tree Species. *Photosynthetica* **41**: 343–347.

Šantrůček J, Šimáňová E, Karbulková J, Šimková M, Schreiber L. **2004**. A new technique for measurement of water permeability of stomatous cuticular membranes isolated from Hedera helix leaves. *Journal of Experimental Botany* **55**: 1411–1422.

Sato H, Kumagai T, Takahashi A, Katul GG. **2015**. Effects of different representations of stomatal conductance response to humidity across the African continent under warmer CO_2 -enriched climate conditions. *Journal of Geophysical Research: Biogeosciences* **120**: 979–988.

Schlesinger WH, Jasechko S. **2014**. Transpiration in the global water cycle. *Agricultural and Forest Meteorology* **189–190**: 115–117.

Scholander PF, Hammel HT, Hemmingsen EA, Bradstreet ED. **1964**. HYDROSTATIC PRESSURE AND OSMOTIC POTENTIAL IN LEAVES OF MANGROVES AND SOME OTHER PLANTS. *Proceedings of the National Academy of Sciences* **52**: 119–125.

Schulze E-D, Čermák J, Matyssek M, Penka M, Zimmermann R, Vasicek F, Gries W, Kučera J. **1985**. Canopy transpiration and water fluxes in the xylem of the trunk of Larix and Picea trees—a comparison of xylem flow, porometer and cuvette measurements. *Oecologia* **66**: 475–483.

Schulze E-D, Hall AE. **1982**. Stomatal Responses, Water Loss and CO2 Assimilation Rates of Plants in Contrasting Environments. In: Lange OL, Nobel PS, Osmond CB, Ziegler H, eds. Physiological Plant Ecology II: Water Relations and Carbon Assimilation. Berlin, Heidelberg: Springer Berlin Heidelberg, 181–230.

Schuster A-C, Burghardt M, Alfarhan A, Bueno A, Hedrich R, Leide J, Thomas J, Riederer M. **2016**. Effectiveness of cuticular transpiration barriers in a desert plant at controlling water loss at high temperatures. *AoB PLANTS* **8**: plw027.

Schuster WSF, Griffin KL, Roth H, Turnbull MH, Whitehead D, Tissue DT. **2008**. Changes in composition, structure and aboveground biomass over seventy-six years (1930-2006) in the Black Rock Forest, Hudson Highlands, southeastern New York State. *Tree Physiology* **28**: 537–549.

Schuur EAG, McGuire AD, Schädel C, Grosse G, Harden JW, Hayes DJ, Hugelius G, Koven CD, Kuhry P, Lawrence DM, *et al.* 2015. Climate change and the permafrost carbon feedback. *Nature* **520**: 171–179.

Schwartz MD, others. **2003**. *Phenology: an integrative environmental science*. Springer.

Sellers P, Randall D, Collatz G, Berry J, Field C, Dazlich D, Zhang C, Collelo G, Bounoua L. **1996**. A revised land surface parameterization (SiB2) for atmospheric GCMs. Part I: Model formulation. *Journal of climate* **9**: 676–705.

Sellers PJ, Dickinson RE, Randall DA, Betts AK, Hall FG, Berry JA, Collatz GJ, Denning AS, Mooney HA, Nobre CA, *et al.* 1997. Modeling the Exchanges of Energy, Water, and Carbon Between Continents and the Atmosphere. *Science* **275**: 502–509.

Serbin S, Rogers A, Yang D, Davidson K, Ely K. **2023**. Leaf structural and chemical traits, and vegetation temperature and height, Seward Peninsula, Alaska, 2019.

Serbin SP, Anderson JA, Davidson KJ, Rogers A. **2020**. *Combining plant physiology and remote sensing to enable detection of concealed activities that are sensed through overlying vegetation*. Defense Advanced Research Projects Agency. Biological Technologies Office.

Serbin SP, Singh A, McNeil BE, Kingdon CC, Townsend PA. **2014**. Spectroscopic determination of leaf morphological and biochemical traits for northern temperate and boreal tree species. *Ecological Applications* **24**: 1651–1669.

Sharkey TD, Bernacchi CJ, Farquhar GD, Singsaas EL. **2007**. Fitting photosynthetic carbon dioxide response curves for C $_3$ leaves. *Plant, Cell & Environment* **30**: 1035–1040.

Singsaas EL, Ort DR, DeLUCIA EH. **2000**. Diurnal regulation of photosynthesis in understory saplings: Diurnal regulation of photosynthesis. *New Phytologist* **145**: 39–49.

Sirri NF, Libalah MB, Momo Takoudjou S, Ploton P, Medjibe V, Kamdem NG, Mofack G, Sonké B, Barbier N. **2019**. Allometric Models to Estimate Leaf Area for Tropical African Broadleaved Forests. *Geophysical Research Letters* **46**: 8985–8994.

Slot M, Nardwattanawong T, Hernández GG, Bueno A, Riederer M, Winter K. **2021**. Large differences in leaf cuticle conductance and its temperature response among 24 tropical tree species from across a rainfall gradient. *New Phytologist* **232**: 1618–1631.

Slot M, Winter K. **2017**. In situ temperature relationships of biochemical and stomatal controls of photosynthesis in four lowland tropical tree species. *Plant, Cell & Environment* **40**: 3055–3068.

Smith NG, Dukes JS. **2013**. Plant respiration and photosynthesis in global-scale models: incorporating acclimation to temperature and CO 2. *Global Change Biology* **19**: 45–63.

Smith NG, Keenan TF, Colin Prentice I, Wang H, Wright IJ, Niinemets Ü, Crous KY, Domingues TF, Guerrieri R, Yoko Ishida F, *et al.* 2019. Global photosynthetic capacity is optimized to the environment (S Niu, Ed.). *Ecology Letters* **22**: 506–517.

Sobol' IM. **1967**. On the distribution of points in a cube and the approximate evaluation of integrals. *Zhurnal Vychislitel'noi Matematiki i Matematicheskoi Fiziki* **7**: 784–802.

Souza DC, Jardine KJ, Rodrigues JVFC, Gimenez BO, Rogers A, McDowell N, Walker AP, Higuchi N, Sampaio-Filho IJ, Chambers J. **2021**. Canopy Position Influences the Degree of Light Suppression of Leaf Respiration in Abundant Tree Genera in the Amazon Forest. *Frontiers in Forests and Global Change* **4**: 723539.

Speckman H. **2019**. AquaFlux: Swift and Transparent Analysis of Plant-level Transpiration.

Sperlich D, Barbeta A, Ogaya R, Sabaté S, Peñuelas J. **2016**. Balance between carbon gain and loss under long-term drought: impacts on foliar respiration and photosynthesis in *Quercus ilex* L. *Journal of Experimental Botany* **67**: 821–833.

Sperry JS, Alder NN, Eastlack SE. **1993**. The Effect of Reduced Hydraulic Conductance on Stomatal Conductance and Xylem Cavitation. *Journal of Experimental Botany* **44**: 1075–1082.

Sperry JS, Love DM. **2015**. What plant hydraulics can tell us about responses to climate-change droughts. *New Phytologist* **207**: 14–27.

Sperry JS, Venturas MD, Anderegg WRL, Mencuccini M, Mackay DS, Wang Y, Love DM. **2017**. Predicting stomatal responses to the environment from the optimization of photosynthetic gain and hydraulic cost: A stomatal optimization model. *Plant, Cell & Environment* **40**: 816–830.

Sperry JS. **2013**. Cutting-edge research or cutting-edge artefact? An overdue control experiment complicates the xylem refilling story: Xylem-refilling artefacts. *Plant, Cell & Environment* **36**: 1916–1918.

Stinziano J, Harjoe M, Roback C, Toliver N, Rogers A, Hanson DT. **2020**. *Photosynthetic capacity exhibits diurnal variation, implications for terrestrial biosphere models and gas exchange measurements*. Preprints.

Stokes VJ, Morecroft MD, Morison JIL. **2010**. Comparison of leaf water use efficiency of oak and sycamore in the canopy over two growing seasons. *Trees* **24**: 297–306.

Streck NA. **2003**. Stomatal response to water vapor pressure deficit: an unsolved issue. *Current Agricultural Science and Technology* **9**.

Su Y-S, Yajima M. **2015**. R2Jags.

Sulman BN, Salmon VG, Iversen CM, Breen AL, Yuan F, Thornton PE. **2021**. Integrating arctic plant functional types in a land surface model using above- and belowground field observations. *Journal of Advances in Modeling Earth Systems*.

Tang A-C, Boyer JS. **2008**. Xylem tension affects growth-induced water potential and daily elongation of maize leaves. *Journal of Experimental Botany* **59**: 753–764.

Tape KD, Hallinger M, Welker JM, Ruess RW. **2012**. Landscape Heterogeneity of Shrub Expansion in Arctic Alaska. *Ecosystems* **15**: 711–724.

Tardieu F, Davies WJ. **1993**. Integration of hydraulic and chemical signalling in the control of stomatal conductance and water status of droughted plants. *Plant, Cell & Environment* **16**: 341–349.

Terashima I, Miyazawa S-I, Hanba YT. **2001**. Why are Sun Leaves Thicker than Shade Leaves? — Consideration based on Analyses of CO2 Diffusion in the Leaf. *Journal of Plant Research* **114**: 93–105.

Thomas DS, Eamus D, Bell D. **1999**. Optimization theory of stomatal behaviour: II. Stomatal responses of several tree species of north Australia to changes in light, soil and atmospheric water content and temperature. *Journal of Experimental Botany* **50**: 393–400.

Thomas HJD, Myers-Smith IH, Bjorkman AD, Elmendorf SC, Blok D, Cornelissen JHC, Forbes BC, Hollister RD, Normand S, Prevéy JS, *et al.* 2019. Traditional plant functional groups explain variation in economic but not size-related traits across the tundra biome (PM van Bodegom, Ed.). *Global Ecology and Biogeography* **28**: 78–95.

Thornton PE, Rosenbloom NA. **2005**. Ecosystem model spin-up: Estimating steady state conditions in a coupled terrestrial carbon and nitrogen cycle model. *Ecological Modelling* **189**: 25–48.

Thornton PE, Zimmermann NE. **2007**. An Improved Canopy Integration Scheme for a Land Surface Model with Prognostic Canopy Structure. *Journal of Climate* **20**: 3902–3923.

Tobin AK, Rogers WJ. **1992**. Metabolic interactions of organelles during leaf development. In: Tobin AK, ed. SEMINAR SERIES-SOCIETY FOR EXPERIMENTAL BIOLOGY. Plant organelles. Cambridge: Cambridge University Press, 293–323.

Tombesi S, Nardini A, Frioni T, Soccolini M, Zadra C, Farinelli D, Poni S, Palliotti A. **2015**. Stomatal closure is induced by hydraulic signals and maintained by ABA in drought-stressed grapevine. *Scientific Reports* **5**: 12449.

Torn MS, Dengel S. **2021**. AmeriFlux FLUXNET-1F US-NGB NGEE Arctic Barrow.

Torn MS, Dengel S. **2022**. AmeriFlux FLUXNET-1F US-NGC NGEE Arctic Council.

Troch PA, Martinez GF, Pauwels VRN, Durcik M, Sivapalan M, Harman C, Brooks PD, Gupta H, Huxman T. **2009**. Climate and vegetation water use efficiency at catchment scales. *Hydrological Processes* **23**: 2409–2414.

Tukey JW. **1949**. Comparing Individual Means in the Analysis of Variance. *Biometrics* **5**: 99.

Turnbull MH, Whitehead D, Tissue DT, Schuster WSF, Brown KJ, Griffin KL. **2001**. Responses of leaf respiration to temperature and leaf characteristics in three deciduous tree species vary with site water availability. *Tree Physiology* **21**: 571–578.

Tuzet A, Perrier A, Leuning R. **2003**. A coupled model of stomatal conductance, photosynthesis and transpiration: Coupled model of stomatal conductance, photosynthesis and transpiration. *Plant, Cell & Environment* **26**: 1097–1116.

Tyree MT, Sperry JS. **1989**. Vulnerability of Xylem to Cavitation and Embolism. *Annual review of plant biology,* **40**: 19–36.

Van Bodegom PM, Douma JC, Witte JPM, Ordoñez JC, Bartholomeus RP, Aerts R. **2012**. Going beyond limitations of plant functional types when predicting global ecosystem-atmosphere fluxes: exploring the merits of traits-based approaches: Merits of traits-based vegetation modelling. *Global Ecology and Biogeography* **21**: 625–636.

Van De Weg MJ, Shaver GR, Salmon VG. **2013**. Contrasting effects of long term versus short-term nitrogen addition on photosynthesis and respiration in the Arctic. *Plant Ecology* **214**: 1273–1286.

van Schaik CP, Terborgh JW, Wright SJ. **1993**. The Phenology of Tropical Forests: Adaptive Significance and Consequences for Primary Consumers. *Annual Review of Ecology and Systematics* **24**: 353–377.

Vehtari A, Gelman A, Simpson D, Carpenter B, Bürkner P-C. **2021**. Rank-Normalization, Folding, and Localization: An Improved Rˆ for Assessing Convergence of MCMC (with Discussion). *Bayesian Analysis* **16**.

Venturas MD, Mackinnon ED, Jacobsen AL, Pratt RB. **2015**. Excising stem samples underwater at native tension does not induce xylem cavitation: No evidence for a tension-cutting artefact. *Plant, Cell & Environment* **38**: 1060–1068.

Venturas MD, Sperry JS, Hacke UG. **2017**. Plant xylem hydraulics: What we understand, current research, and future challenges: Plant xylem hydraulics. *Journal of Integrative Plant Biology* **59**: 356–389.

Verhoef A, Egea G. **2014**. Modeling plant transpiration under limited soil water: Comparison of different plant and soil hydraulic parameterizations and preliminary implications for their use in land surface models. *Agricultural and Forest Meteorology* **191**: 22–32.

Verryckt LT, Van Langenhove L, Ciais P, Courtois EA, Vicca S, Peñuelas J, Stahl C, Coste S, Ellsworth DS, Posada JM, *et al.* 2020. Coping with branch excision when measuring leaf net photosynthetic rates in a lowland tropical forest. *Biotropica* **52**: 608–615.

von Caemmerer S, Farquhar GD. **1981**. Some relationships between the biochemistry of photosynthesis and the gas exchange of leaves. *Planta* **153**: 376–387.

Von Caemmerer S. **2013**. Steady-state models of photosynthesis: Steady-state models of photosynthesis. *Plant, Cell & Environment* **36**: 1617–1630.

Walker AP, Beckerman AP, Gu L, Kattge J, Cernusak LA, Domingues TF, Scales JC, Wohlfahrt G, Wullschleger SD, Woodward FI. **2014**. The relationship of leaf photosynthetic traits - V_{cmax} and J_{max} - to leaf nitrogen, leaf phosphorus, and specific leaf area: a meta-analysis and modeling study. *Ecology and Evolution* **4**: 3218–3235.

Walker AP, Johnson AL, Rogers A, Anderson J, Bridges RA, Fisher RA, Lu D, Ricciuto DM, Serbin SP, Ye M. **2021**. Multi-hypothesis comparison of Farquhar and Collatz photosynthesis models reveals the unexpected influence of empirical assumptions at leaf and global scales. *Global Change Biology* **27**: 804–822.

Walker DA, Daniëls FJA, Matveyeva NV, Šibík J, Walker MD, Breen AL, Druckenmiller LA, Raynolds MK, Bültmann H, Hennekens S, *et al.* 2018. Circumpolar Arctic Vegetation Classification. *Phytocoenologia* **48**: 181–201.

Wang H, Atkin OK, Keenan TF, Smith NG, Wright IJ, Bloomfield KJ, Kattge J, Reich PB, Prentice IC. **2020**. Acclimation of leaf respiration consistent with optimal photosynthetic capacity. *Global Change Biology* **26**: 2573–2583.

Wang Q, He Q, Zhou G. **2018**. Applicability of common stomatal conductance models in maize under varying soil moisture conditions. *Science of The Total Environment* **628–629**: 141–149.

Wang Q, Iio A, Tenhunen J, Kakubari Y. **2008**. Annual and seasonal variations in photosynthetic capacity of Fagus crenata along an elevation gradient in the Naeba Mountains, Japan. *Tree Physiology* **28**: 277–285.

Wang Q, Tenhunen J, Falge E, Bernhofer Ch, Granier A, Vesala T. **2004**. Simulation and scaling of temporal variation in gross primary production for coniferous and deciduous temperate forests: Physiological effects on temperate forest GPP. *Global Change Biology* **10**: 37–51.

Wang X, Chen JM, Ju W, Zhang Y. **2022**. Seasonal Variations in Leaf Maximum Photosynthetic Capacity and Its Dependence on Climate Factors Across Global FLUXNET Sites. *Journal of Geophysical Research: Biogeosciences* **127**: e2021JG006709.

Wang Y, Sperry JS, Anderegg WRL, Venturas MD, Trugman AT. **2020**. A theoretical and empirical assessment of stomatal optimization modeling. *New Phytologist* **227**: 311–325.

Wardle K, Short KC. **1983**. Stomatal Responses and the Senescence of Leaves. *Annals of Botany* **52**: 411–412.

Way DA, Montgomery RA. **2015**. Photoperiod constraints on tree phenology, performance and migration in a warming world. *Plant, Cell & Environment* **38**: 1725–1736.

Way DA, Pearcy RW. **2012**. Sunflecks in trees and forests: from photosynthetic physiology to global change biology. *Tree Physiology* **32**: 1066–1081.

Wehr R, Munger JW, McManus JB, Nelson DD, Zahniser MS, Davidson EA, Wofsy SC, Saleska SR. **2016**. Seasonality of temperate forest photosynthesis and daytime respiration. *Nature* **534**: 680–683.

Wheeler JK, Huggett BA, Tofte AN, Rockwell FE, Holbrook NM. **2013**. Cutting xylem under tension or supersaturated with gas can generate PLC and the appearance of rapid recovery from embolism: Sampling induced embolism. *Plant, Cell & Environment* **36**: 1938–1949.

White MA, Thornton PE, Running SW. **1997**. A continental phenology model for monitoring vegetation responses to interannual climatic variability. *Global Biogeochemical Cycles* **11**: 217–234.

Wilkinson S, Davies WJ. **2002**. ABA-based chemical signalling: the co-ordination of responses to stress in plants: ABA-based chemical signalling. *Plant, Cell & Environment* **25**: 195–210.

Williamson VG, Milburn JA. **1995**. Cavitation events in cut stems kept in water: implications for cut flower senescence. *Scientia Horticulturae* **64**: 219–232.

Wilson KB, Baldocchi DD, Hanson PJ. **2000a**. Spatial and seasonal variability of photosynthetic parameters and their relationship to leaf nitrogen in a deciduous forest. *Tree Physiology* **20**: 565–578.

Wilson KB, Baldocchi DD, Hanson PJ. **2000b**. Quantifying stomatal and non-stomatal limitations to carbon assimilation resulting from leaf aging and drought in mature deciduous tree species. *Tree Physiology* **20**: 787–797.

Wilson KB, Baldocchi DD, Hanson PJ. **2001**. Leaf age affects the seasonal pattern of photosynthetic capacityand net ecosystem exchange of carbon in a deciduous forest: Leaf age and net ecosystem exchange of carbon. *Plant, Cell & Environment* **24**: 571–583.

Wingler A, Marès M, Pourtau N. **2004**. Spatial patterns and metabolic regulation of photosynthetic parameters during leaf senescence. *New Phytologist* **161**: 781–789.

Winton M. **2006**. Amplified Arctic climate change: What does surface albedo feedback have to do with it? *Geophysical Research Letters* **33**: L03701.

Wolf A, Anderegg WRL, Pacala SW. **2016**. Optimal stomatal behavior with competition for water and risk of hydraulic impairment. *Proceedings of the National Academy of Sciences* **113**: E7222–E7230.

Wolfe BT, Sperry JS, Kursar TA. **2016**. Does leaf shedding protect stems from cavitation during seasonal droughts? A test of the hydraulic fuse hypothesis. *New Phytologist* **212**: 1007–1018.

Wolz KJ, Wertin TM, Abordo M, Wang D, Leakey ADB. **2017**. Diversity in stomatal function is integral to modelling plant carbon and water fluxes. *Nature Ecology & Evolution* **1**: 1292–1298.

Wong SC, Cowan IR, Farquhar GD. **1979**. Stomatal conductance correlates with photosynthetic capacity. *Nature* **282**: 424–426.

Wong SC, Cowan IR, Farquhar GD. **1985**. Leaf Conductance in Relation to Rate of CO2 Assimilation. *Plant Physiology* **78**: 821–825.

Wright IJ, Leishman MR, Read C, Westoby M. **2006**. Gradients of light availability and leaf traits with leaf age and canopy position in 28 Australian shrubs and trees. *Functional Plant Biology* **33**: 407.

Wright IJ, Reich PB, Westoby M, Ackerly DD, Baruch Z, Bongers F, Cavender-Bares J, Chapin T, Cornelissen JHC, Diemer M, *et al.* 2004. The worldwide leaf economics spectrum. *Nature* **428**: 821–827.

Wu J, Albert LP, Lopes AP, Restrepo-Coupe N, Hayek M, Wiedemann KT, Guan K, Stark SC, Christoffersen B, Prohaska N, *et al.* 2016. Leaf development and demography explain photosynthetic seasonality in Amazon evergreen forests. *Science* **351**: 972–976.

Wu J, Rogers A, Albert LP, Ely K, Prohaska N, Wolfe BT, Oliveira RC, Saleska SR, Serbin SP. **2019a**. Leaf reflectance spectroscopy captures variation in carboxylation capacity across species, canopy environment and leaf age in lowland moist tropical forests. *New Phytologist* **224**: 663–674.

Wu J, Serbin SP, Ely KS, Wolfe BT, Dickman LT, Grossiord C, Michaletz ST, Collins AD, Detto M, McDowell NG, *et al.* 2019b. The response of stomatal conductance to seasonal drought in tropical forests. *Global Change Biology* **26**: 823–839.

Wu J, Serbin SP, Xu X, Albert LP, Chen M, Meng R, Saleska SR, Rogers A. **2017**. The phenology of leaf quality and its within-canopy variation is essential for accurate modeling of photosynthesis in tropical evergreen forests. *Global Change Biology* **23**: 4814–4827.

Wullschleger SD, Epstein HE, Box EO, Euskirchen ES, Goswami S, Iversen CM, Kattge J, Norby RJ, van Bodegom PM, Xu X. **2014**. Plant functional types in Earth system models: past experiences and future directions for application of dynamic vegetation models in high-latitude ecosystems. *Annals of Botany* **114**: 1–16.

Xiao Y, Sloan J, Hepworth C, Osborne CP, Fleming AJ, Chen X, Zhu X. 2021. Estimating uncertainty: A Bayesian approach to modelling photosynthesis in C3 leaves. *Plant, Cell & Environment* 44: 1436–1450.

Xie J, Zha T, Zhou C, Jia X, Yu H, Yang B, Chen J, Zhang F, Wang B, Bourque CP-A, *et al.* 2016. Seasonal variation in ecosystem water use efficiency in an urban-forest reserve affected by periodic drought. *Agricultural and Forest Meteorology* **221**: 142–151.

Xu L, Baldocchi DD. **2003**. Seasonal trends in photosynthetic parameters and stomatal conductance of blue oak (Quercus douglasii) under prolonged summer drought and high temperature. **23**: 13.

Xu X, Medvigy D, Powers JS, Becknell JM, Guan K. **2016**. Diversity in plant hydraulic traits explains seasonal and inter-annual variations of vegetation dynamics in seasonally dry tropical forests. *New Phytologist* **212**: 80–95.

Yang D, Meng R, Morrison BD, McMahon A, Hantson W, Hayes DJ, Breen AL, Salmon VG, Serbin SP. **2020**. A Multi-Sensor Unoccupied Aerial System Improves Characterization of Vegetation Composition and Canopy Properties in the Arctic Tundra. *Remote Sensing* **12**: 2638.

Yang D, Morrison BD, Davidson KJ, Lamour J, Li Q, Nelson PR, Hantson W, Hayes DJ, Swetnam TL, McMahon A, *et al.* 2022. Remote sensing from unoccupied aerial systems:

Opportunities to enhance Arctic plant ecology in a changing climate. *Journal of Ecology* **110**: 2812–2835.

Yang D, Morrison BD, Hantson W, Breen AL, McMahon A, Li Q, Salmon VG, Hayes DJ, Serbin SP. **2021**. Landscape-scale characterization of Arctic tundra vegetation composition, structure, and function with a multi-sensor unoccupied aerial system. *Environmental Research Letters* **16**: 085005.

Yang X, Ricciuto DM, Thornton PE, Shi X, Xu M, Hoffman F, Norby RJ. **2019**. The Effects of Phosphorus Cycle Dynamics on Carbon Sources and Sinks in the Amazon Region: A Modeling Study Using ELM v1. *Journal of Geophysical Research: Biogeosciences* **124**: 3686–3698.

Yang X, Tang J, Mustard JF, Wu J, Zhao K, Serbin S, Lee J-E. **2016**. Seasonal variability of multiple leaf traits captured by leaf spectroscopy at two temperate deciduous forests. *Remote Sensing of Environment* **179**: 1–12.

Yin X, Struik PC. **2009**. C 3 and C 4 photosynthesis models: An overview from the perspective of crop modelling. *NJAS: Wageningen Journal of Life Sciences* **57**: 27–38.

Youngflesh C, Che-Castaldo C, Hardy TW. **2022**. MCMCvis.

Zeng X. **2001**. Global Vegetation Root Distribution for Land Modeling. *Journal of Hydrometeorology* **2**: 525–530.

Zhang J, Jiang H, Song X, Jin J, Zhang X. **2018**. The Responses of Plant Leaf CO2/H2O Exchange and Water Use Efficiency to Drought: A Meta-Analysis. *Sustainability* **10**: 551.

Zhang Q, Ficklin DL, Manzoni S, Wang L, Way D, Phillips RP, Novick KA. **2019**. Response of ecosystem intrinsic water use efficiency and gross primary productivity to rising vapor pressure deficit. *Environmental Research Letters* **14**: 074023.

Zhou S-X, Medlyn B, Sabaté S, Sperlich D, Prentice IC, Whitehead D. **2014**. Short-term water stress impacts on stomatal, mesophyll and biochemical limitations to photosynthesis differ consistently among tree species from contrasting climates. *Tree Physiology* **34**: 1035–1046.

Zhou S-X, Medlyn BE, Prentice IC. **2016**. Long-term water stress leads to acclimation of drought sensitivity of photosynthetic capacity in xeric but not riparian *Eucalyptus* species. *Annals of Botany* **117**: 133–144.

Zhu G-F, Li X, Su Y-H, Lu L, Huang C-L. **2011**. Seasonal fluctuations and temperature dependence in photosynthetic parameters and stomatal conductance at the leaf scale of Populus euphratica Oliv. *Tree Physiology* **31**: 178–195.

Zona D, Lafleur PM, Hufkens K, Gioli B, Bailey B, Burba G, Euskirchen ES, Watts JD, Arndt KA, Farina M, *et al.* 2022. Pan-Arctic soil moisture control on tundra carbon sequestration and plant productivity. *Global Change Biology*: gcb.16487.

Zona D, Lipson DA, Richards JH, Phoenix GK, Liljedahl AK, Ueyama M, Sturtevant CS, Oechel WC. **2014**. Delayed responses of an Arctic ecosystem to an extreme summer:

impacts on net ecosystem exchange and vegetation functioning. *Biogeosciences* **11**: 5877–5888.

Appendix 1: Supporting information for Chapter 2

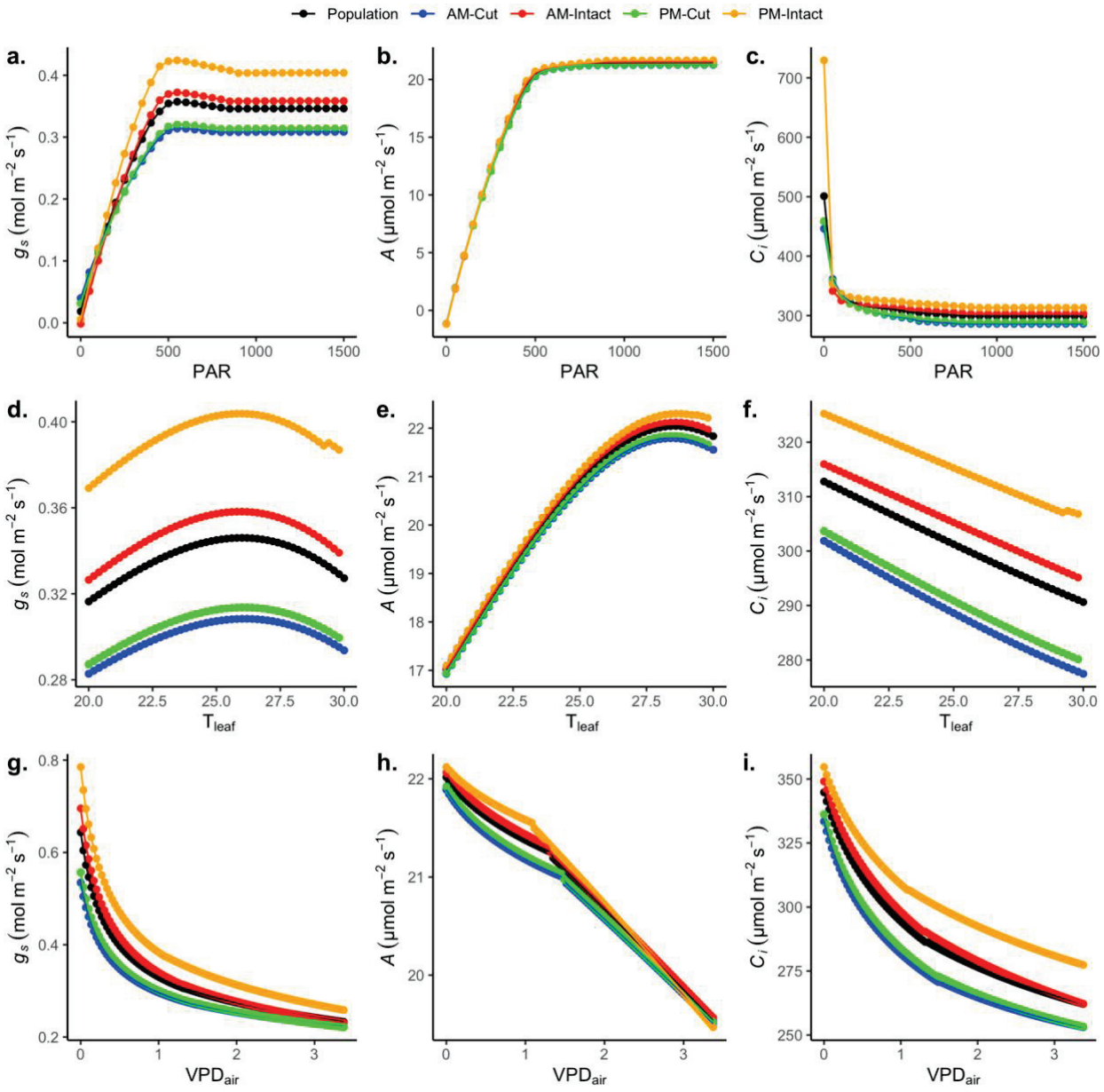

Figure A1.1: Diagnostic plots for stomatal conductance (g_s) (a, d, g), A (b, e, h), and C_i (c, f, i) across an expected range of irradiance (a-c), leaf temperature (d-f) and VPD_{air} (g-i). For all simulations, T_{leaf} = 26, PAR= 1100, RH= 70%, wind= 2 ms^{-1}, and P_{atm}= 101.16 KPa, unless otherwise stipulated. g_0 and g_1 values were as follows, population: g_0 = 0.037, g_1 = 2.66; AM-cut: g_0 = 0.055, g_1 = 2.02; AM-intact: g_0 = 0.048, g_1 = 2.17; PM-cut: g_0 = 0.019, g_1 = 3.01; PM-intact: g_0 = 0.028, g_1 = 3.41; Shape of the responses were as expected and indicate that the model is performing well.

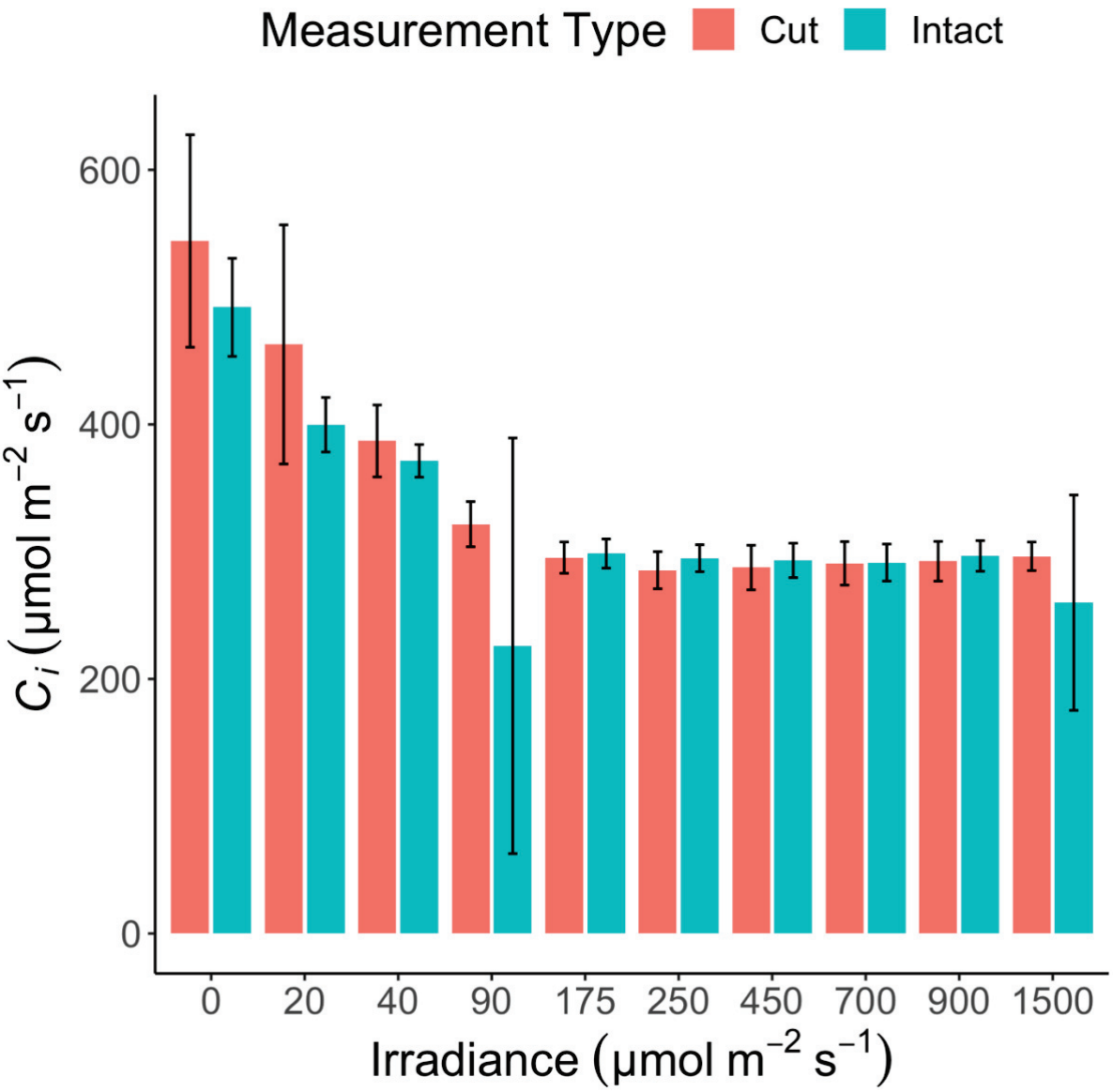

Figure A1.2: Comparison of values of C_i at each level of irradiance within a stomatal response curve. At each level there was no significant ($p < 0.05$) difference in C_i between pairs of cut and intact branches. Error bars represent ± 2 SE.

Table A1.1: Parameters used in the coupled photosynthesis, conductance, and energy balance models used for simulations in this study.

Parameter	Description	Default Value (units)	Source
R	Ideal gas constant	8.314 ($J\ mol^{-1}\ K^{-1}$)	-
O2	O_2 concentration in	210 (ppm)	-
TRef	Reference temperature for Kc, Ko, Rd, GammaStar Vcmax, Jmax	298.16 (K)	-
Patm	Atmospheric pressure	101 (kPa)	-
JmaxRef	Maximum electron transport rate	255.87 ($\mu mol\ m^{-2}\ s^{-1}$)	This study
JmaxHa	Energy of activation for Jmax	43540 ($J\ mol^{-1}$)	Bernacchi et al. (2001)*
JmaxHd	Energy of deactivation for Jmax	152040 ($J\ mol^{-1}$)	Bernacchi et al. (2001)*
JmaxS	Entropy term for Jmax	495 ($J\ mol^{-1}\ K^{-1}$)	Bernacchi et al. (2001)*
VcmaxRef	Maximum rate of Rubisco for carboxylation	158.43 ($\mu mol\ m^{-2}\ s^{-1}$)	This study
VcmaxHa	Energy of activation for Vcmax	65330 ($J\ mol^{-1}$)	Bernacchi et al. (2001)*
VcmaxHd	Energy of deactivation for Vcmax	149250 ($J\ mol^{-1}$)	Bernacchi et al. (2001)*
VcmaxS	Entropy term for Vcmax	485 ($J\ mol^{-1}\ K^{-1}$)	Bernacchi et al. (2001)*
RdRef	Respiration value at the reference temperature	1.13 ($\mu mol\ m^{-2}\ s^{-1}$)	This study
RdHa	Energy of activation for Rd	150650 ($J\ mol^{-1}$)	Bernacchi et al. (2001)*
KcRef	Michaelis-Menten constant of Rubisco for CO2 at the reference temperature	404.9 ($\mu mol\ mol^{-1}$)	Bernacchi et al. (2001)*
KcHa	Energy of activation for Kc	79430 ($J\ mol^{-1}$)	Bernacchi et al. (2001)*
KoRef	Michaelis-Menten constant of Rubisco for CO2 at the reference temperature	278.4 ($\mu mol\ mol^{-1}$)	Bernacchi et al. (2001)*
KoHa	Energy of activation for Ko	36380 ($J\ mol^{-1}$)	Bernacchi et al. (2001)*
GstarRef	CO2 compensation point in absence of respiration	42.75	Bernacchi et al. (2001)*
GstarHa	Enthalpy of activation for Gstar	37830 ($\mu mol\ mol^{-1}$)	Bernacchi et al. (2001)*
abso	Absorptance of the leaf in the photosynthetic active radiation wavelengths	0.85 (ratio)	-
aQY	Apparent quantum yield	0.425 (ratio)	-
Theta	Theta is the empirical curvature factor for the response of J to PFD	0.7 (ratio)	-

*Bernacchi, C.J., Singsaas, E.L., Pimentel, C., Portis Jr, A.R. and Long, S.P. (2001), Improved temperature response functions for models of Rubisco-limited photosynthesis. Plant, Cell & Environment, 24: 253-259. doi:10.1111/j.1365-3040.2001.00668.x

Table A1.2: Biochemical and functional properties estimated for each treatment group. Values in parentheses are the standard error of the mean.

Property	AM	PM	Cut	Intact
LMA ($g\ m^{-2}$)	88.44 (15.66)	89.14 (16.92)	91.23 (14.80)	86.35 (17.32)
FM/DM ($g\ g^{-1}$)	2.72 (0.39)	2.85 (0.60)	2.75 (0.39)	2.83 (0.60)
V_{cmax} ($\mu mol\ m^{-2}\ s^{-1}$)	138.97 (31.87)	178.90 (66.26)	162.19 (60.7)	154.68 (50.84)
R_{dark} ($\mu mol\ m^{-2}\ s^{-1}$)	1.17 (0.19)	1.10 (0.17)	1.18 (0.18)	1.09 (0.18)

Table A1.3: Fixed effects components from the mixed effects model comparing photosynthetic parameters to leaf structural properties. None of the four models tested yielded a significant effect.

Model	Numerator df	Denominator df	F-value	p-value
$g_0 \sim$ LMA	1	299	0.121	0.728
$g_1 \sim$ LMA	1	299	1.100	0.295
$g_0 \sim$ FM/DM	1	299	0.011	0.916
$g_1 \sim$ FM/DM	1	299	0.057	0.812

Appendix 2: Supporting information for Chapter 3

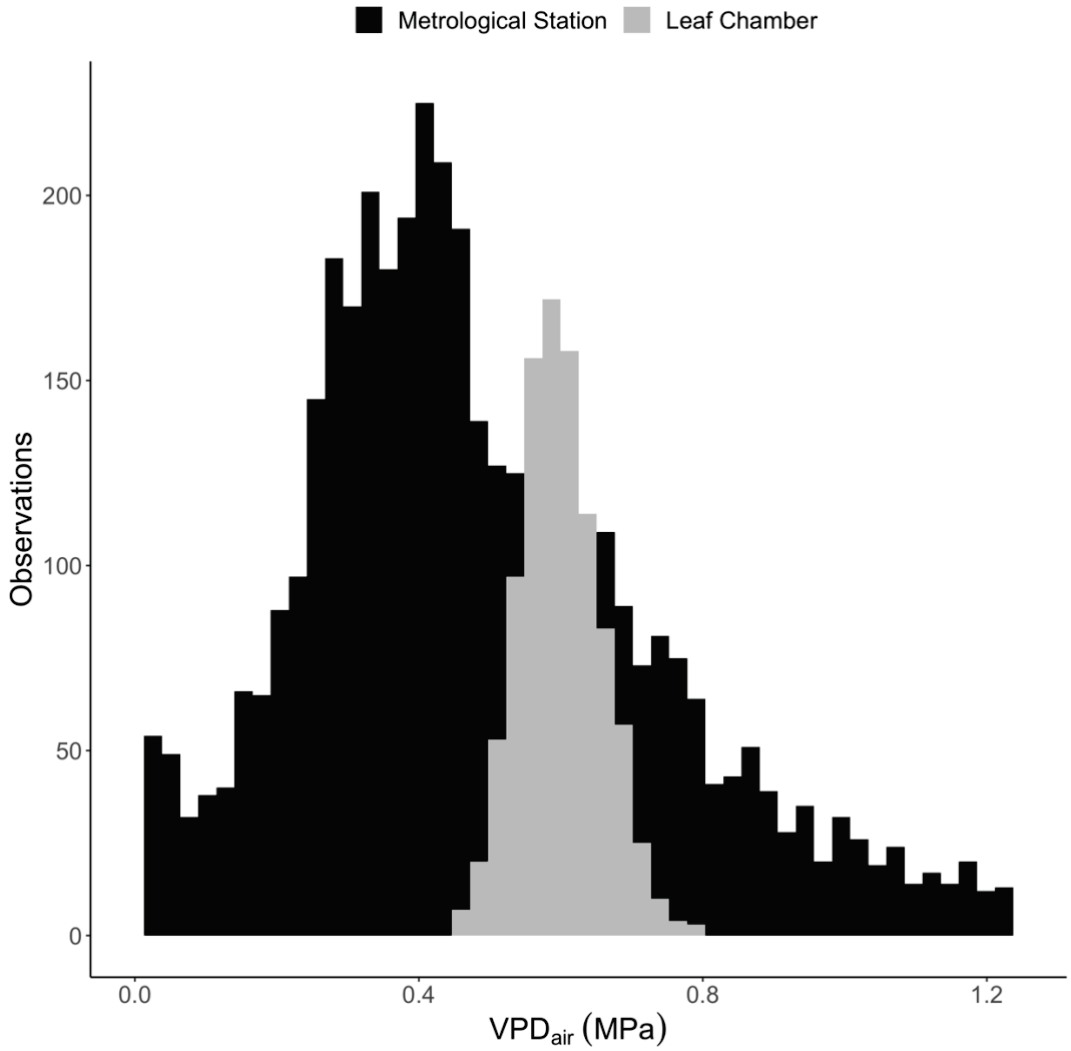

Figure A2.1: Histograms of the atmospheric vapor pressure deficit (VPD_{air}) observed during survey gas exchange measurements. Black bars represent data collected by the STRI metrological station positioned on top of the canopy crane from 06:00-18:30 for the duration of the study. Grey bars represent conditions inside the cuvette of the LI-6800 during survey measurements.

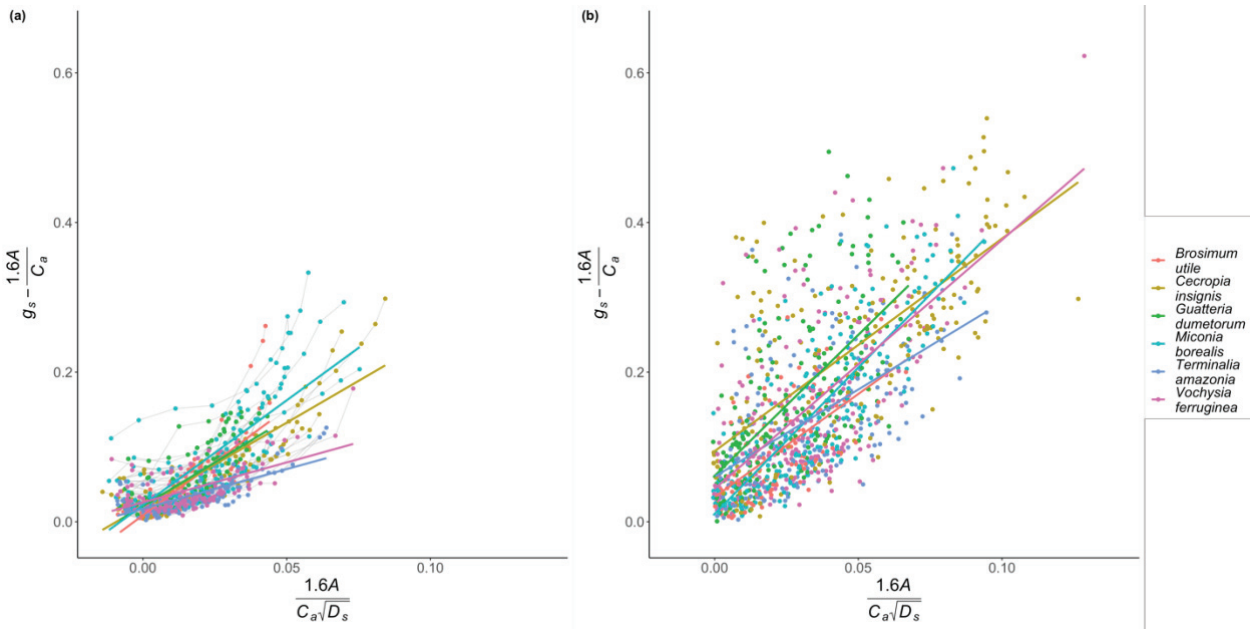

Figure A2.2: Regression of stomatal response from the two different measurement methods. Observations are of from (a) response curve data, and (b) survey derived data. For the response curve data, points which were collected on the same leaf are connected by a grey line. Regressions follow the linear form

$$g_s - \frac{1.6*A}{C_a} = g_0 + g_1 * \frac{1.6*A}{(\sqrt{D}*C_a)}$$

where the stomatal slope (g_1) directly acts as the slope between stomatal conductance (g_s), net photosynthesis (A), atmospheric CO_2 concentration (C_a), and the vapor pressure deficit at the leaf surface (VPD), while the intercept is given as g_0.

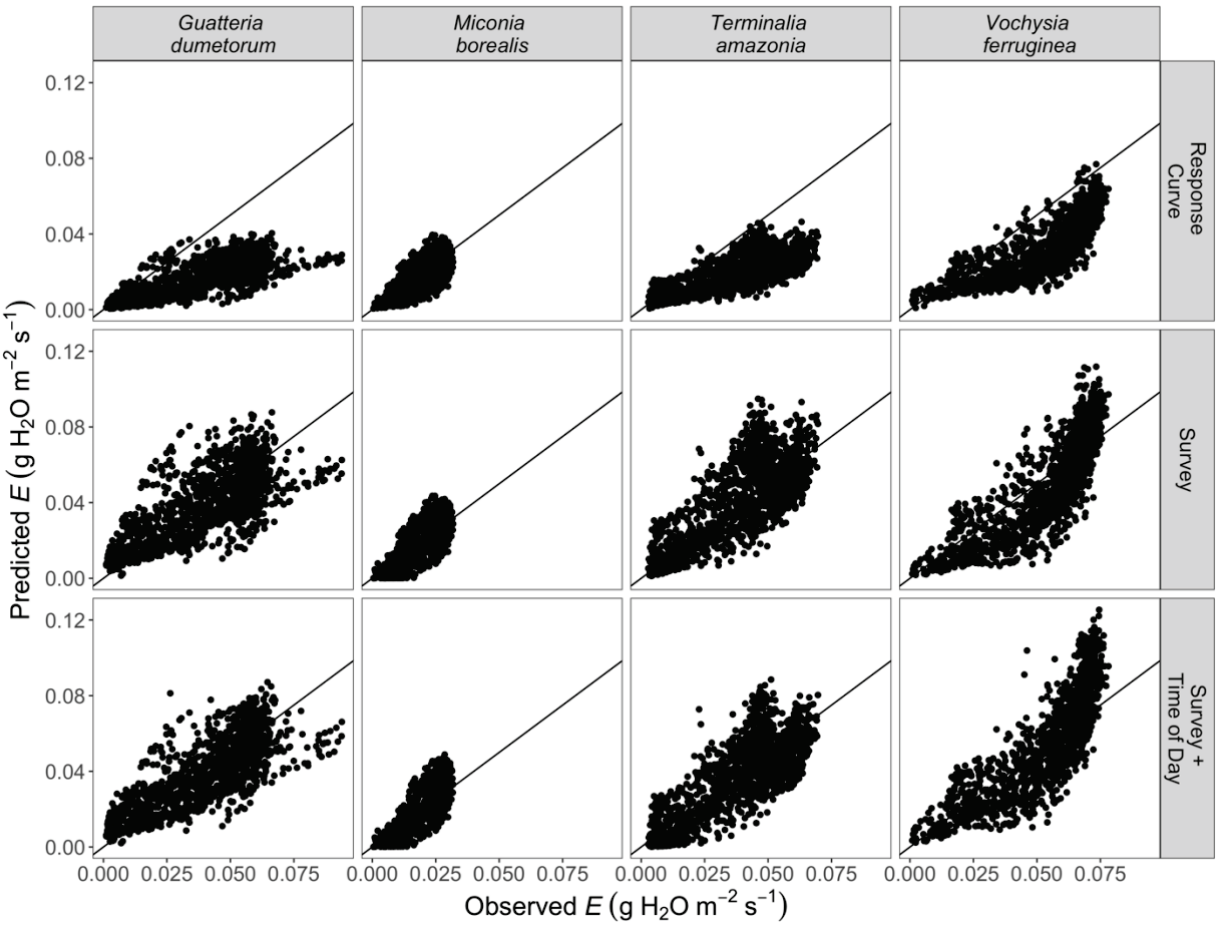

Figure A2.3: Observed versus predicted fluxes of canopy scale transpiration (*E*) for *Guatteria dumetorum*, *Miconia borealis*, *Terminalia amazonia*, and *Vochysia ferruginea* using three different methods to derive stomatal parameters. Observed data are scaled from sapflux measurements.

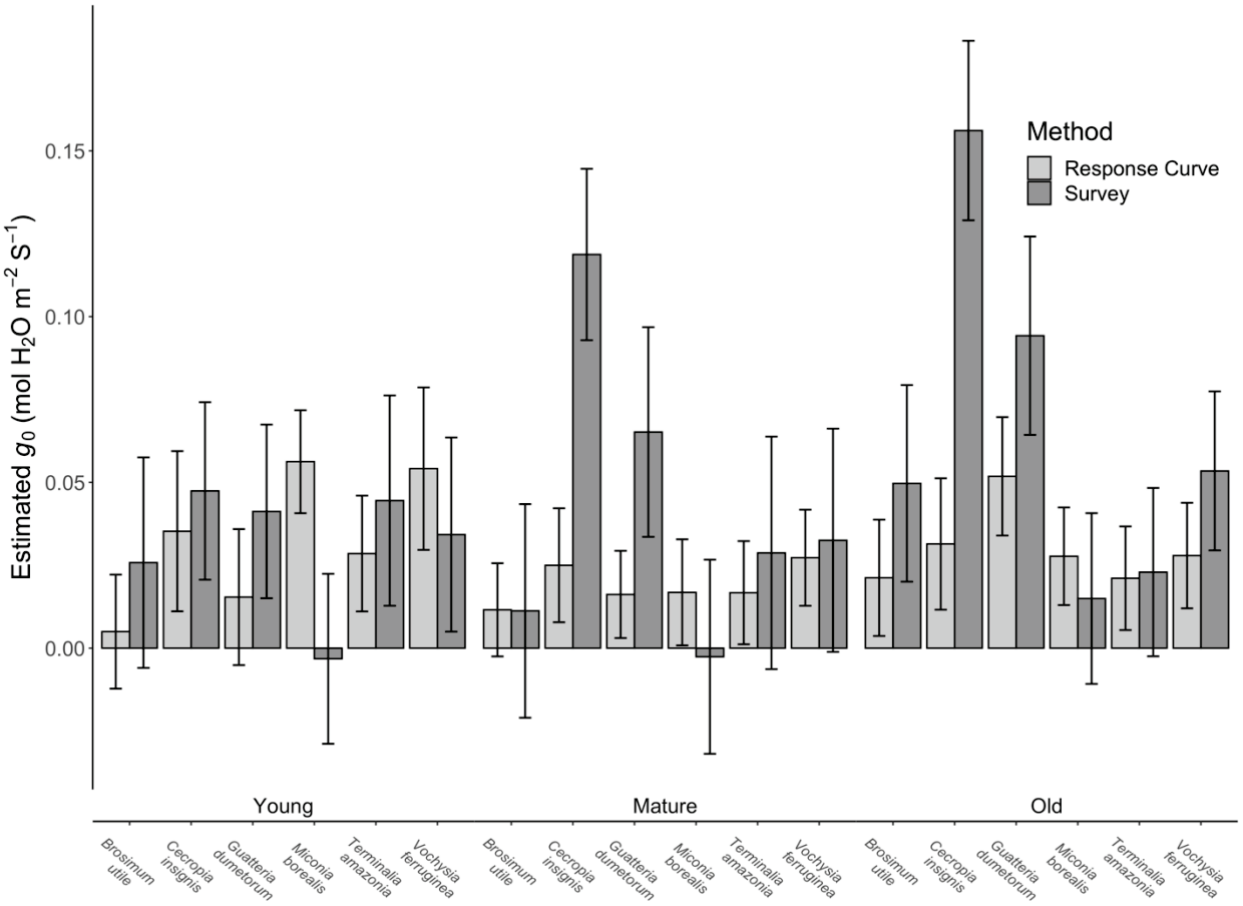

Figure A2.4: Stomatal intercept (g_0) estimates by species, phenological stage, and measurement method. Elevated g_0 for the survey method is apparent in four of the six species. There does not appear to be a consistent pattern between phenological stage and g_0 for either of the methods. Error bars represent ± 2 SE of the mean.

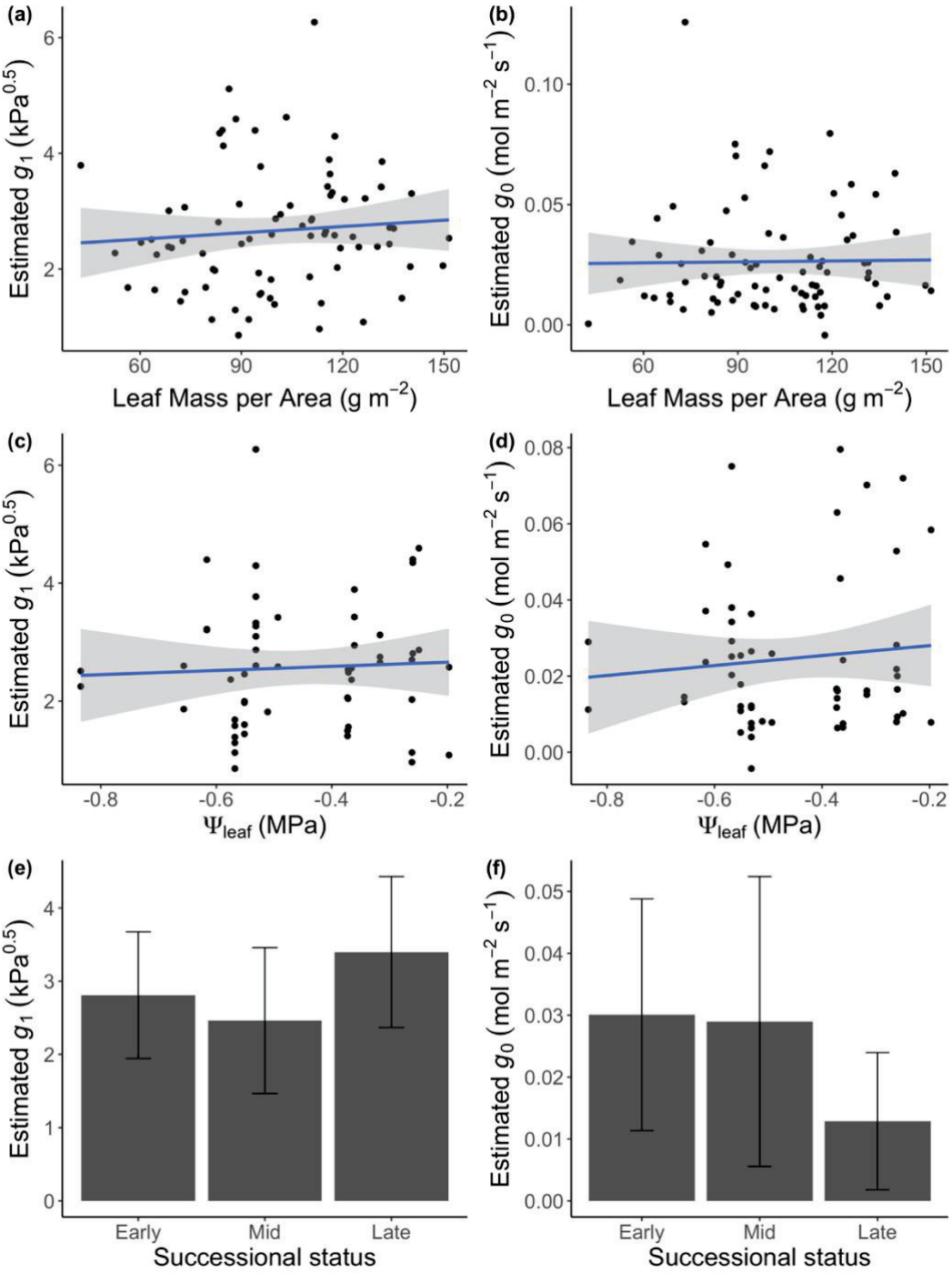

Figure A2.5: Relationships between estimated stomatal and leaf functional traits. Response curve derived stomatal slope (g_1) and stomatal intercept (g_0) versus (a-b) LMA, (c-d) predawn leaf water potential (Ψ_{leaf}), and (e-f) successional stage. An analysis of variance indicates that none of the relationships shown are significant. Error bars represent ± 1 SD of the mean.

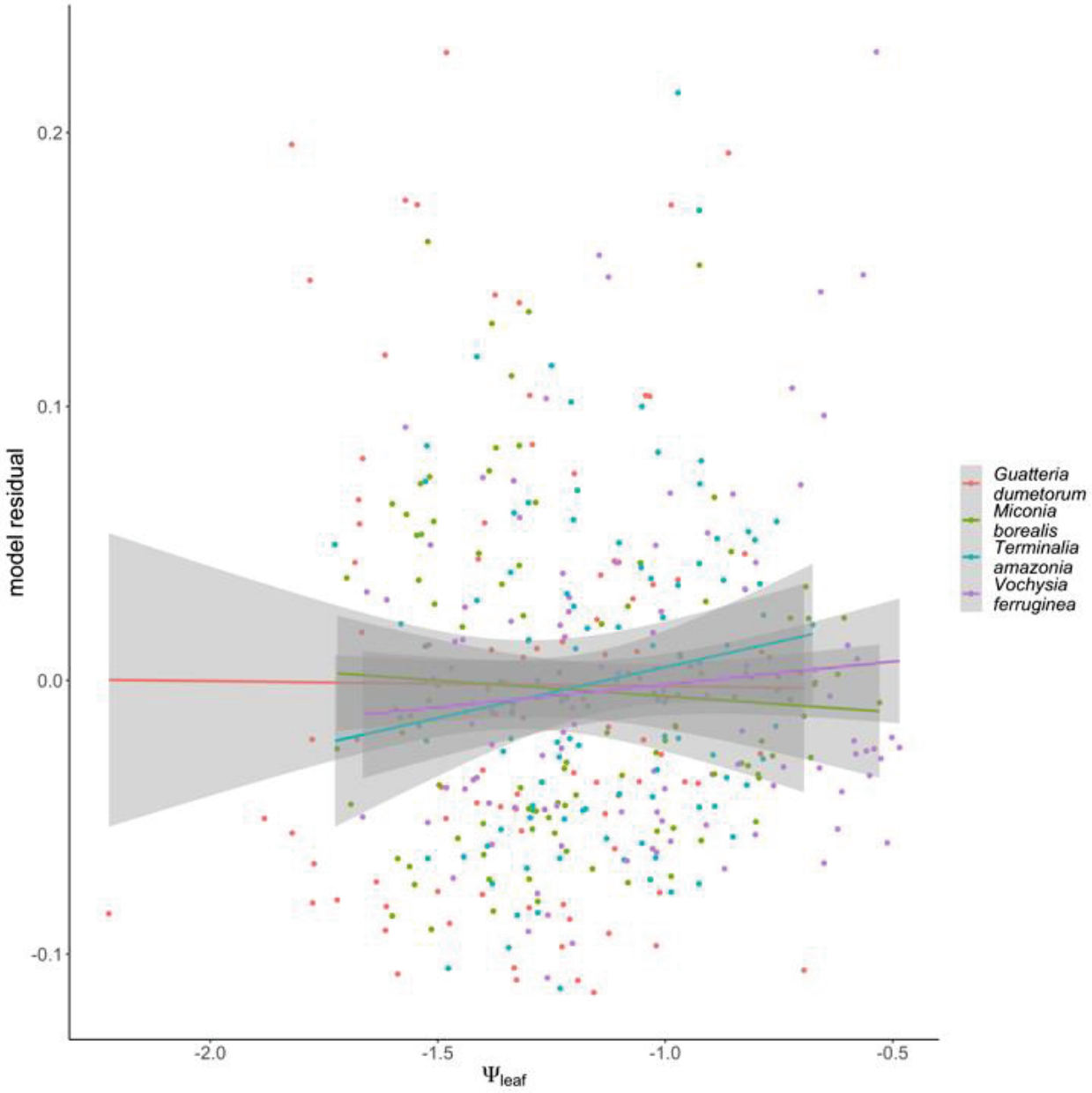

Figure A2.6: The relationship between leaf water potential (Ψ_{leaf}) and model residual (difference between observed and predicted stomatal conductance [g_s]) for the survey model including a time-of-day effect. Grey shroud around the lines of best fit indicates the interval of prediction, the expected range for a new value given the data.

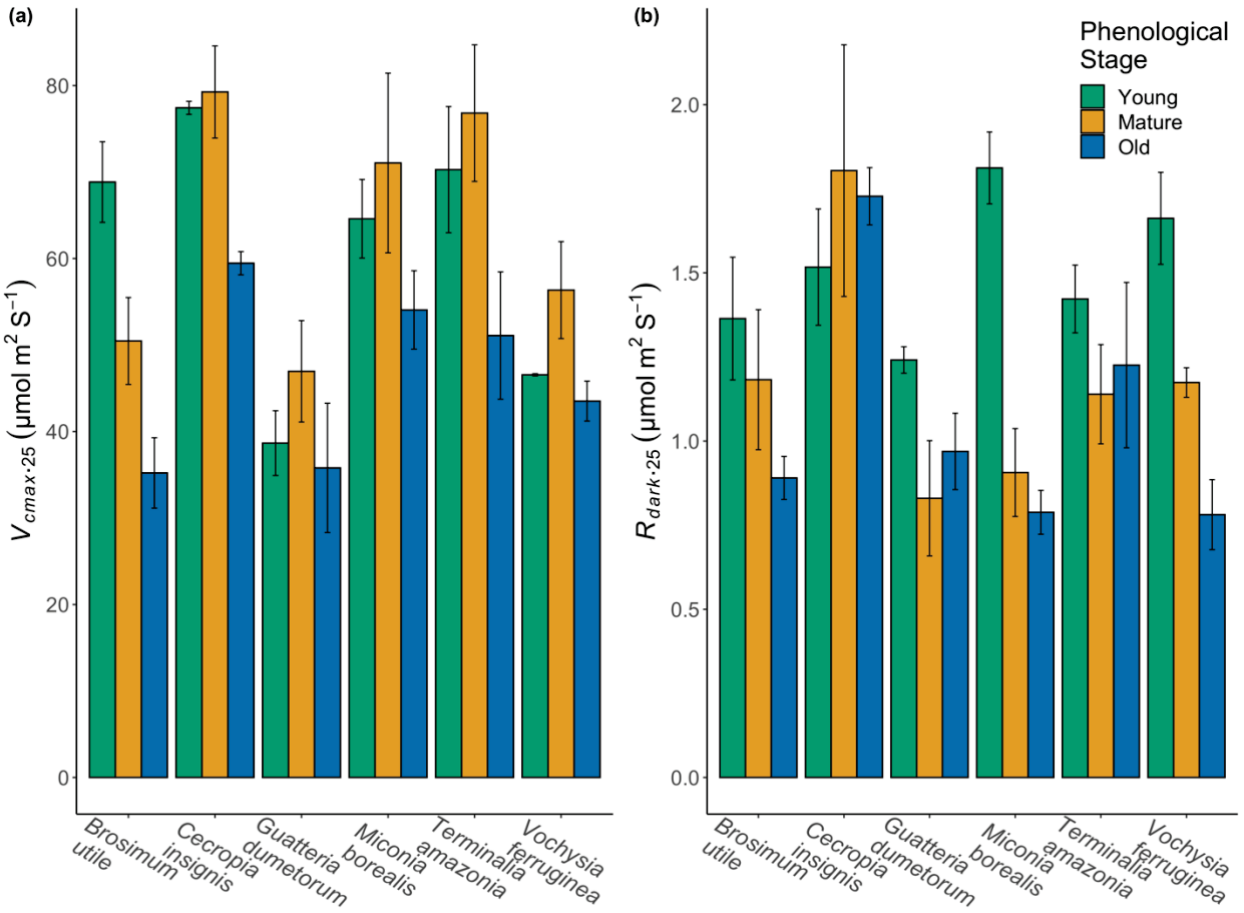

Figure A2.7: Relationship between leaf phenological stage and photosynthetic traits. (a) the maximum carboxylation capacity of Rubisco normalized to 25°C ($V_{cmax.25}$), and (b) the dark respiration rate normalized to 25°C ($R_{dark.25}$) by species and phenological stage. Analysis of Variance and post-hoc Tukey tests indicates that variation in both $V_{cmax.25}$, and $R_{dark.25}$ is significant to the species and phenological stage levels. Error bars represent ± 2 SE of the mean.

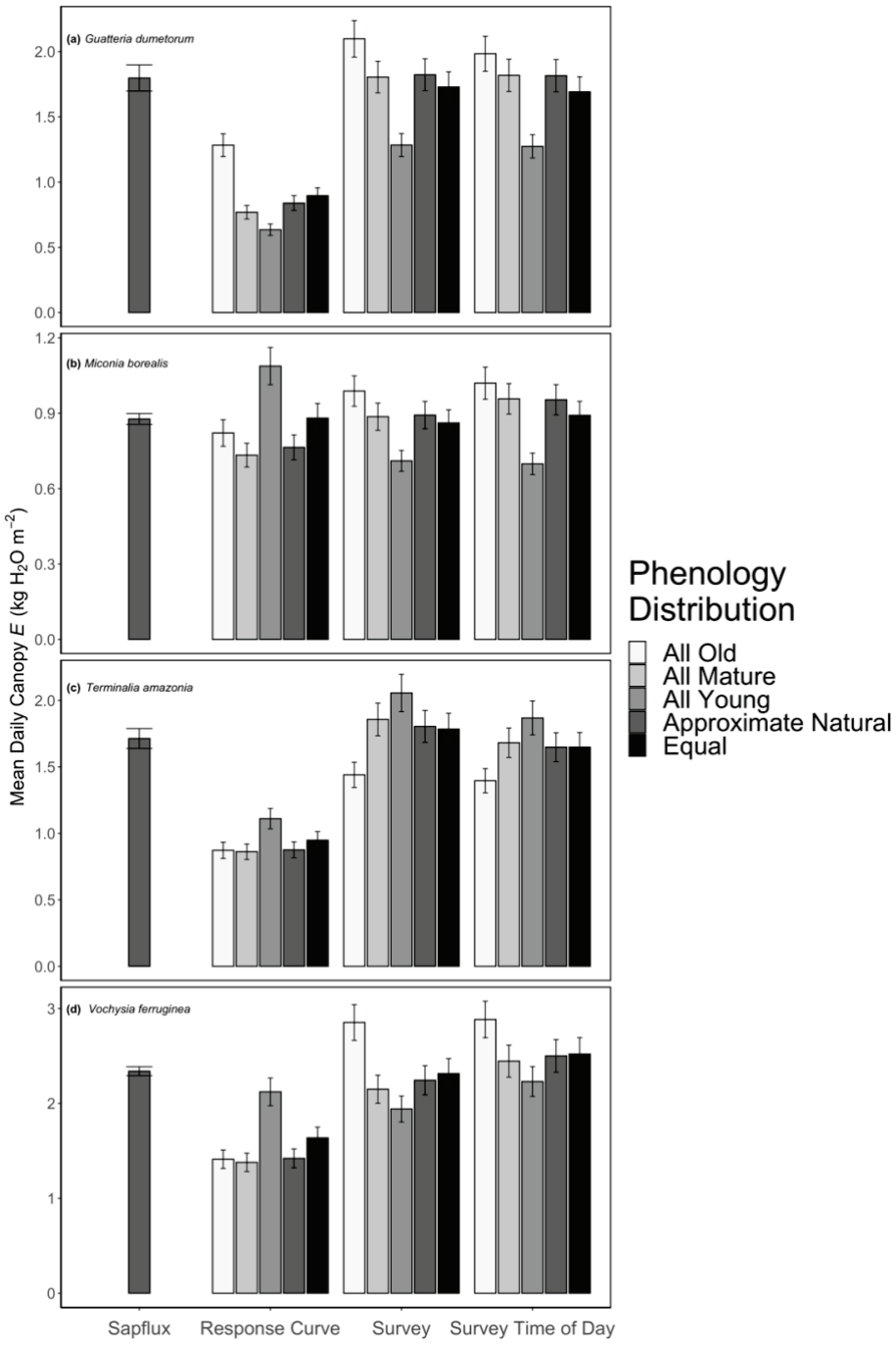

Figure A2.8: Simulations of daily canopy transpiration (*E*) by species when using different leaf phenology distributions. Distributions are as follows; All Old (0% young, 0% mature, 100% old), All Mature (0% young, 100% mature, 0% old), All Young (100% young, 0% mature, 0% old), Approximate Natural (15% young, 80% mature, 5% old), Equal (33.3% young, 33.3% mature, 33.3% old). X axis labels indicate which model was used to derive the conductance parameters for each simulation. Error bars represent ± 2 SE of the mean.

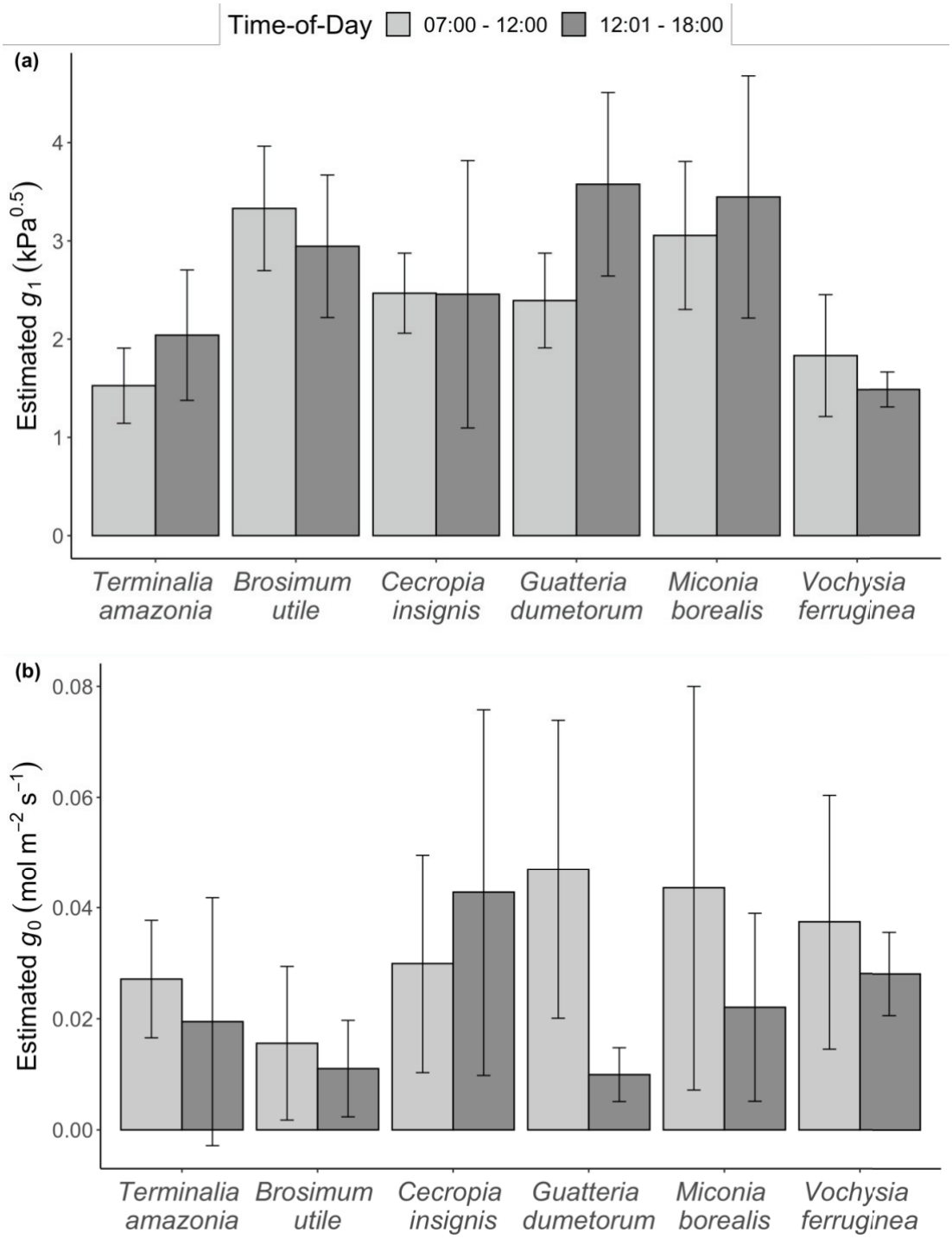

Figure A2.9: Comparison of fitted values of stomatal slope (g_1) and stomatal intercept (g_0)by species for curves conducted at different times of day. Data in panel (a) were collected in the morning (07:00-12:00), while data in panel (b) were collected in the afternoon (12:01-18:00). t-tests indicate that none of the within species comparisons shown are significant. Error bars represent ± 1 SD of the mean.

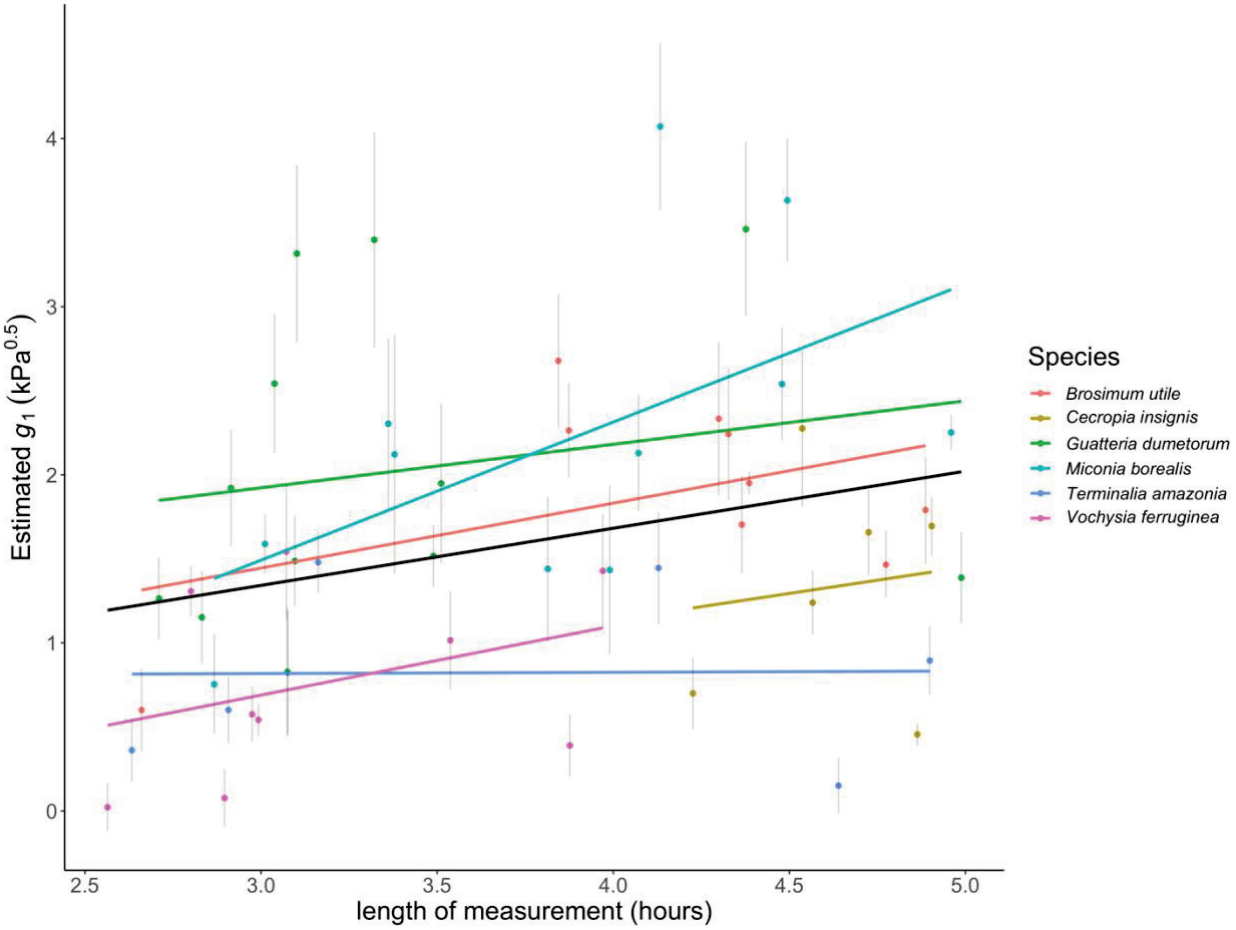

Figure A2.10: Estimated stomatal slope (g_1) versus length of response curve measurement. Colored lines corresponded to species specific slopes, while black line is the line of best fit for all the data. Error bars on each point represent ± 2 SE of the estimate. Across all species estimated g_1 increased with measurement time.

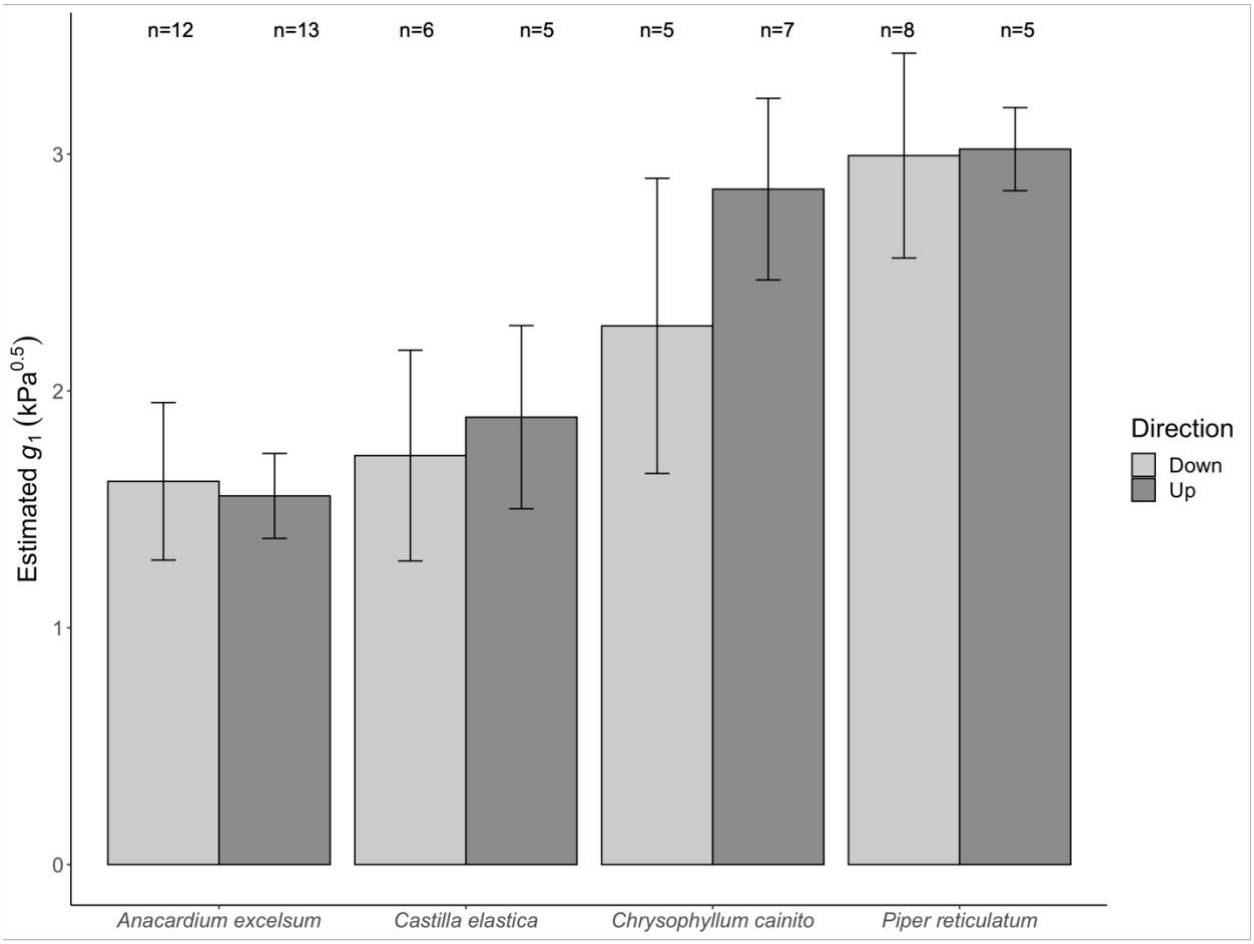

Figure A2.11: Stomatal slope (g_1) as estimated from response curves collected with decreasing (saturating to 0 µmol photosynthetic photon flix density) and increasing (0 µmol photosynthetic photon flix density to saturating) levels of irradiance. t-tests indicate that None of the within species g_1 estimates were significantly different. Error bars represent ± 2 SE of the mean.

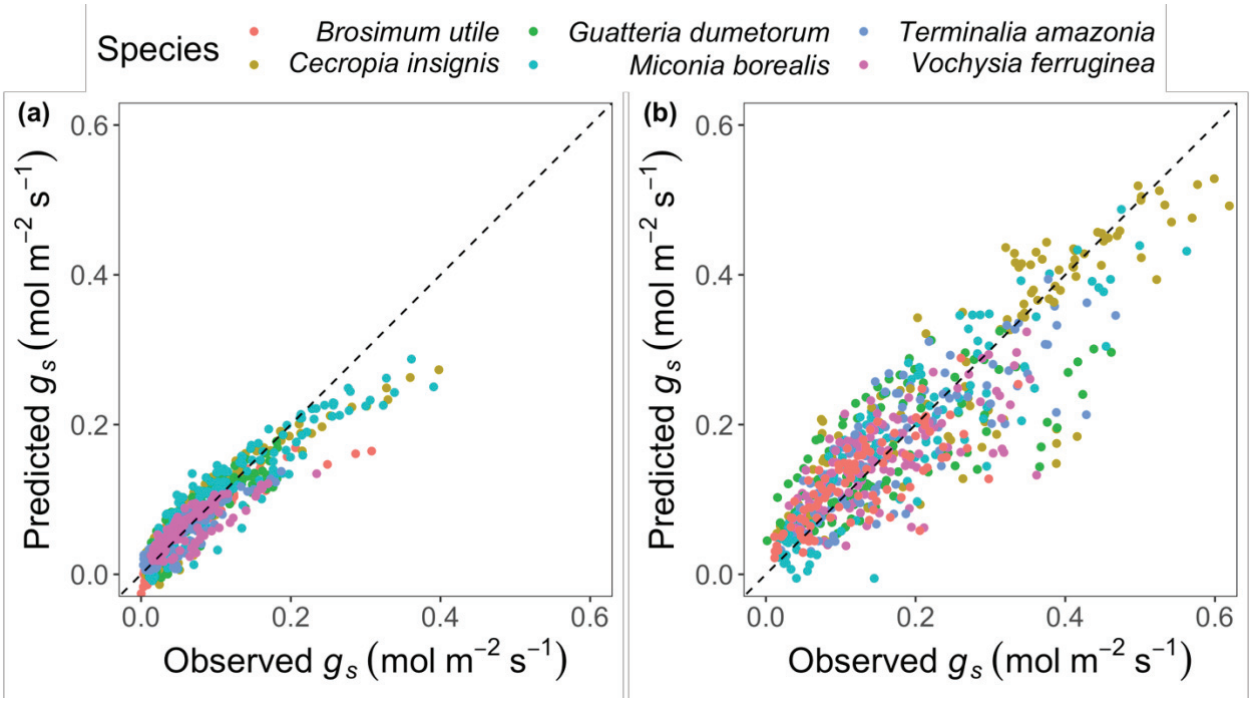

Figure A2.12: Observed verses predicted stomatal conductance (g_s) from the calibration phase of model development. Plots for (a) the curve derived data, and (b) the survey derived data used to build the models of stomatal slope (g_1) and stomatal intercept (g_0). From these calibration plots it is apparent that the curve model has a bias at high g_s levels, while the survey model has considerably more error at all levels of g_s.

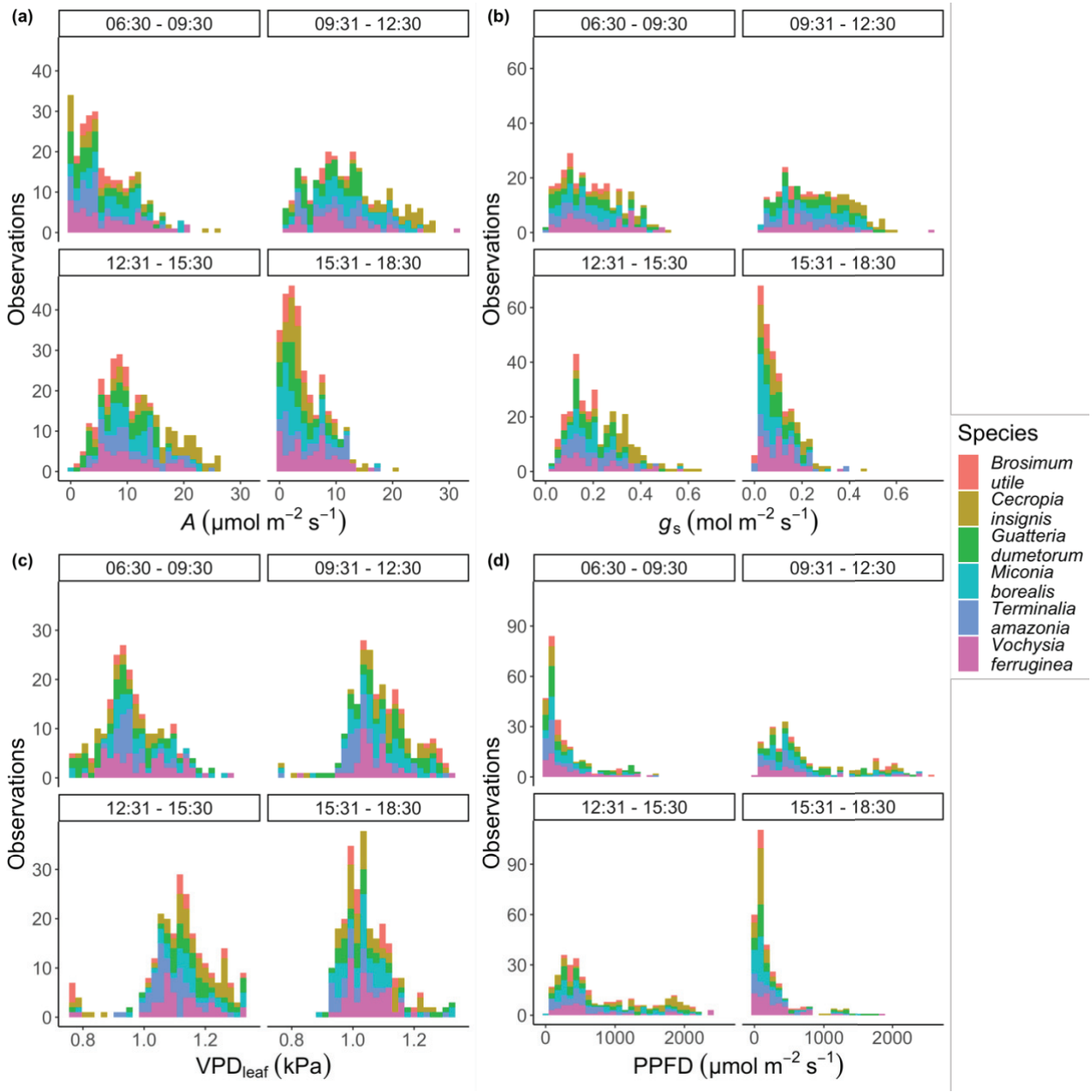

Figure A2.13: Range and distribution of individual observations of leaf-level conditions collected during survey gas exchange. (a) photosynthesis (A), (b) stomatal conductance (g_s), (c) vapor pressure deficit at the leaf surface (VPD_{leaf}), and (d) photosynthetic photon flux density (PPFD), divided out by time of day and by species.

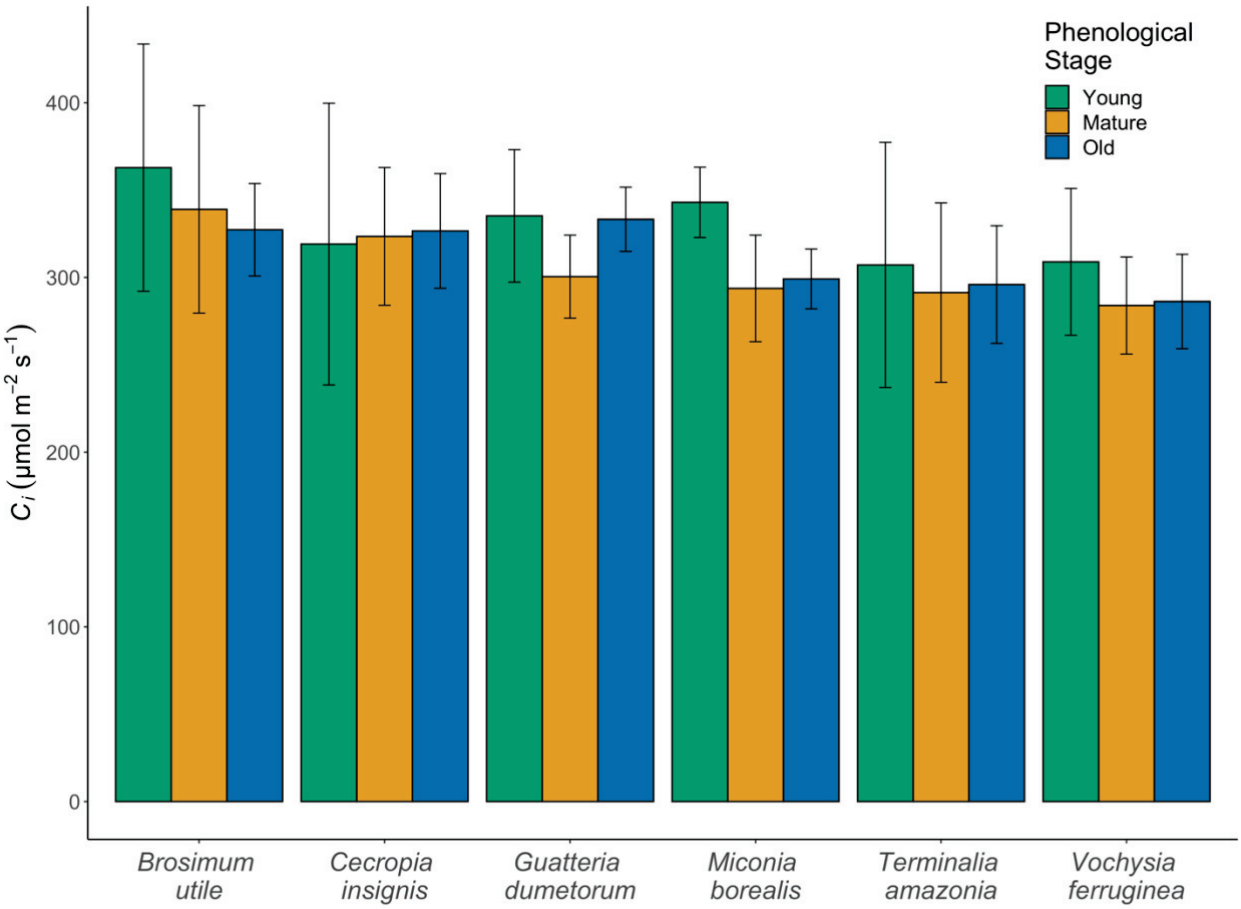

Figure A2.14: Mean estimated intercellular carbon mole fraction (C_i) by species and leaf age. Data are from response curve measurements and are an average across all irradiance levels. Error bars represent ± 2 SE of the mean.

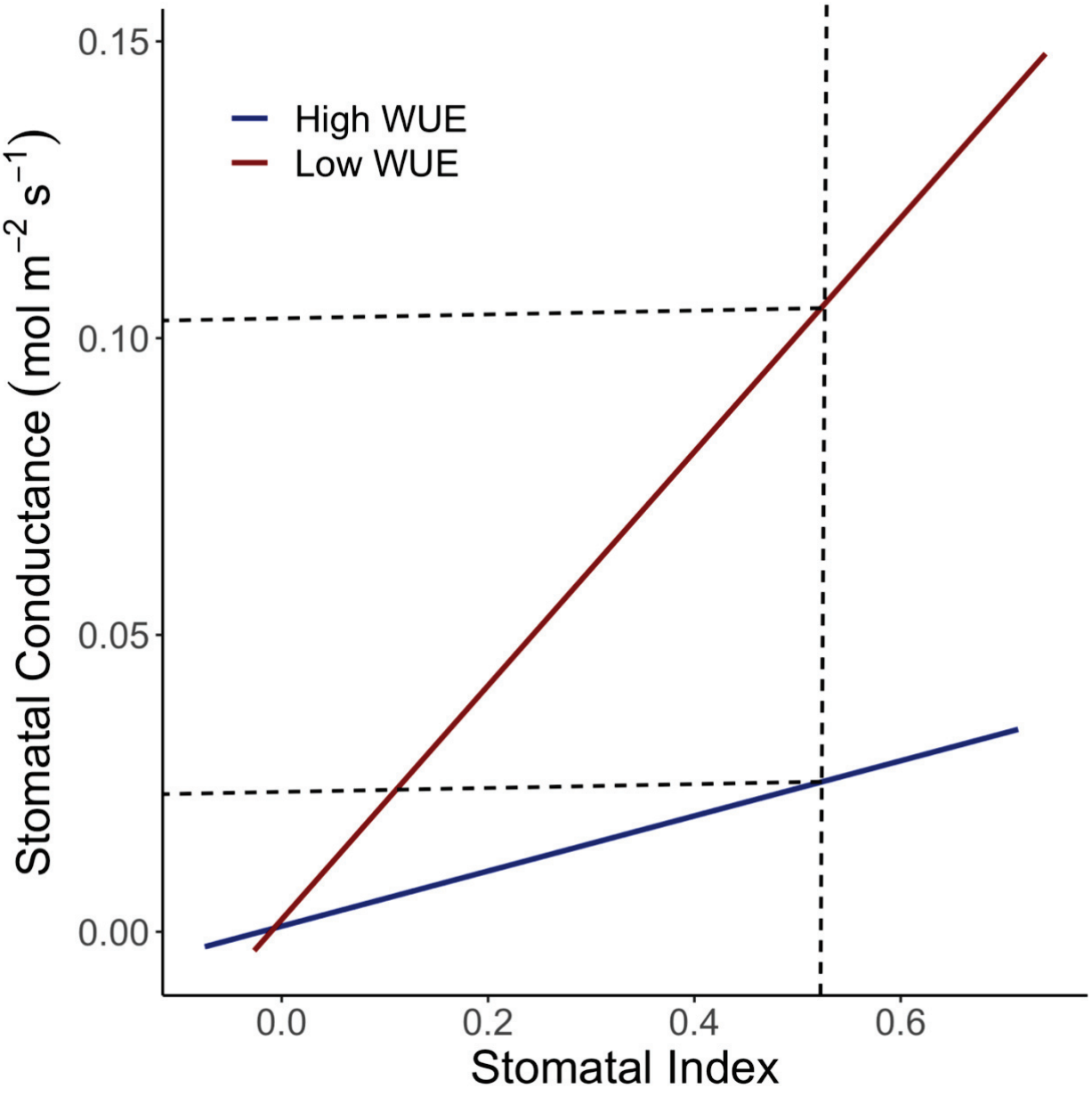

Figure A2.15: Conceptual illustration of the link between stomatal slope, and water use efficiency (WUE). At the same value of stomatal index (a term representing A at a combination of leaf-level environmental conditions) on the x axis (vertical dashed line) the two data series have different levels of stomatal conductance (g_s) (horizontal dashed lines).

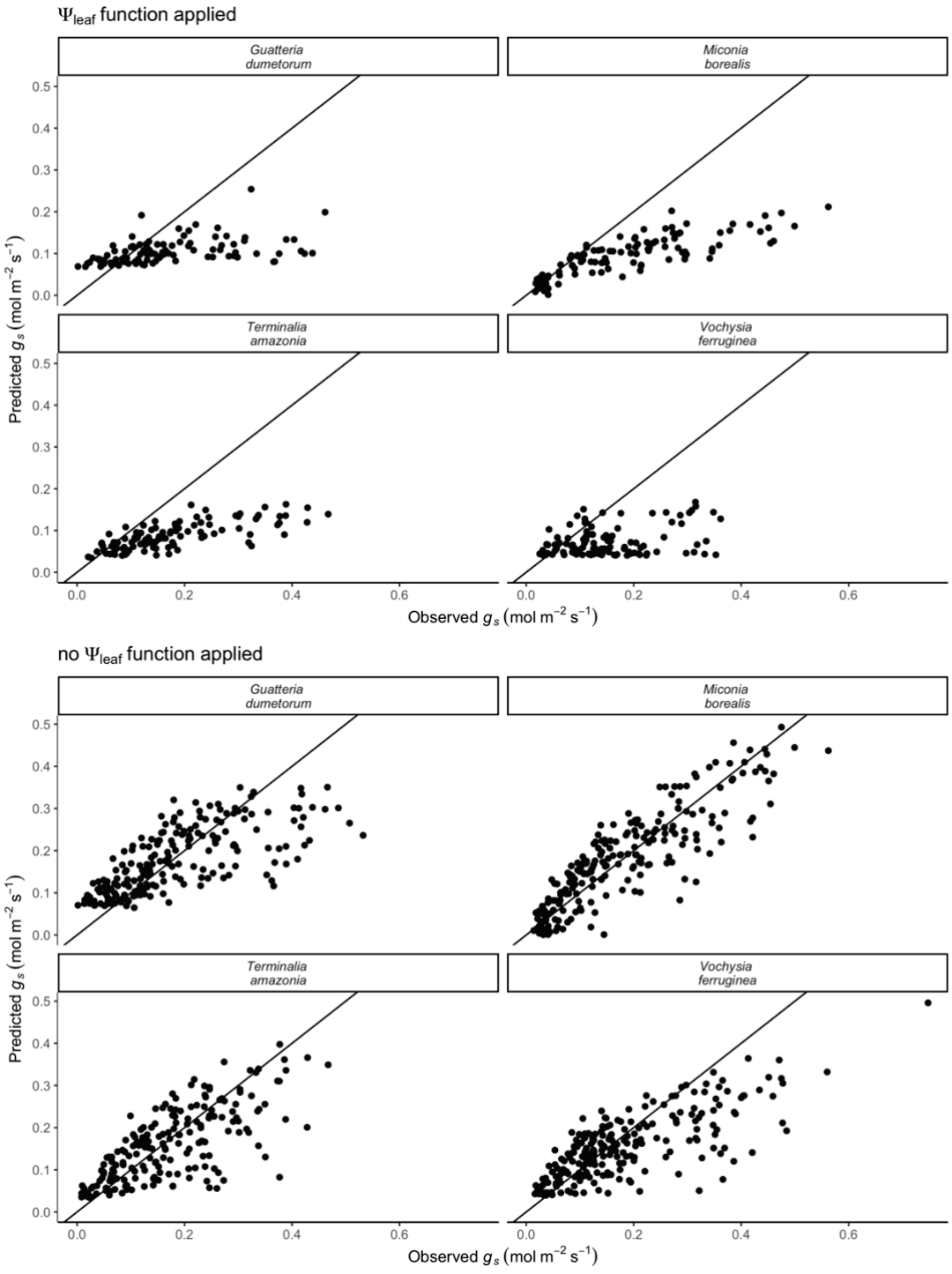

Figure A2.16: Observed vs predicted stomatal conductance (g_s) when a leaf water potential (Ψ_{leaf}) penalty is applied (upper panels), and when no penalty is applied (lower panels). All plots use survey collected data and the survey model.

Note A2.1: Description of mixed effects models and their parameter estimates.

USO Model: $g_s = g_0 + 1.6\left(1 + \frac{g_1}{\sqrt{D}}\right)\frac{A}{C_a}$

Response curve model: $g_{s,l,i} = \left(g_0 + \mu_{0,species_l:stage_l} + a_l\right) + 1.6\left(1 + \frac{\left(g_1 + \mu_{1,species_l:stage_l} + b_l\right)}{\sqrt{D}}\right)\frac{A}{C_a} + \varepsilon_{l,i}$

Survey model: $g_{s,t,i} = \left(g_0 + \mu_{0,species_t:stage_t} + a_t\right) + 1.6\left(1 + \frac{\left(g_1 + \mu_{1,species_t} + b_t\right)}{\sqrt{D}}\right)\frac{A}{C_a} + \varepsilon_{t,i}$

Survey + time-of-day model: $g_{s,t,i} = \left(g_0 + \mu_{0,species_t:stage_t} + a_t\right) + 1.6\left(1 + \frac{\left(g_1 + \mu_{1,species_t:quarter_i} + b_t\right)}{\sqrt{D}}\right)\frac{A}{C_a} + \varepsilon_{t,i}$

Where $g_{s,l,i}$ and $g_{s,t,i}$ are the ith stomatal conductance to water vapor measured on leaf *l* and on canopy position *t*, respectively. g_0 represents the population reference intercept of the model. $\mu_{0,species:stage}$ represents the fixed interactive effect of species and phenological stage on g_0. g_1 represents the population reference "slope" for the model. $\mu_{1,species}$ and $\mu_{1,species:quarter}$ represents the fixed effect of species and the interactive fixed effect of species and time-of-day (e.g., 6:30-09:30, 09:30-12:30, 12:31-15:30, and 15:31-18:30) respectively on g_1 such that each combination of species and of the four measurement periods have a fixed mean g_1.

a_l and a_t are the random effect of the leaf or canopy position, respectively, on g_0. The random effects represent the fact that $g_0$for each leaf or canopy position might deviate from the reference $g_0$corresponding to other individuals of the same age and the same species. Similarly, bl and bt are the random effects of the leaf or canopy position on g_1, respectively. $\varepsilon_{l,i}$ and $\varepsilon_{t,i}$ are the residual of the models. It is assumed that the variables a and b are independent and identically distributed and that $a \sim N(0, \sigma_a^2)$, $b \sim N(0, \sigma_b^2)$ and $\varepsilon_i \sim N(0, \sigma_i^2)$.

Table A2.1: Parameter estimates and their standard error for the response curve model.

Parameter	Value	SE
$\mu_{0,BROSUT:YOUNG}$	0.005	0.009
$\mu_{0,CECRIN:YOUNG}$	0.035	0.012
$\mu_{0,GUATDU:YOUNG}$	0.015	0.010
$\mu_{0,MICOBO:YOUNG}$	0.056	0.008
$\mu_{0,TERMAM:YOUNG}$	0.029	0.009
$\mu_{0,VOCHFE:YOUNG}$	0.054	0.012
$\mu_{0,BROSUT:MATURE}$	0.012	0.007
$\mu_{0,CECRIN:MATURE}$	0.025	0.009
$\mu_{0,GUATDU:MATURE}$	0.016	0.007
$\mu_{0,MICOBO:MATURE}$	0.017	0.008
$\mu_{0,TERMAM:MATURE}$	0.017	0.008
$\mu_{0,VOCHFE:MATURE}$	0.027	0.007
$\mu_{0,BROSUT:OLD}$	0.021	0.009
$\mu_{0,CECRIN:OLD}$	0.031	0.010
$\mu_{0,GUATDU:OLD}$	0.052	0.009
$\mu_{0,MICOBO:OLD}$	0.028	0.007
$\mu_{0,TERMAM:OLD}$	0.021	0.008
$\mu_{0,VOCHFE:OLD}$	0.028	0.008
$\mu_{1,BROSUT:YOUNG}$	3.447	0.295
$\mu_{1,CECRIN:YOUNG}$	0.645	0.423
$\mu_{1,GUATDU:YOUNG}$	2.861	0.353
$\mu_{1,MICOBO:YOUNG}$	3.081	0.236
$\mu_{1,TERMAM:YOUNG}$	0.317	0.313
$\mu_{1,VOCHFE:YOUNG}$	-0.074	0.432
$\mu_{1,BROSUT:MATURE}$	1.719	0.281
$\mu_{1,CECRIN:MATURE}$	1.860	0.261
$\mu_{1,GUATDU:MATURE}$	1.476	0.254
$\mu_{1,MICOBO:MATURE}$	1.638	0.263
$\mu_{1,TERMAM:MATURE}$	1.017	0.260
$\mu_{1,VOCHFE:MATURE}$	0.837	0.242
$\mu_{1,BROSUT:OLD}$	2.214	0.378
$\mu_{1,CECRIN:OLD}$	2.252	0.307
$\mu_{1,GUATDU:OLD}$	1.999	0.319
$\mu_{1,MICOBO:OLD}$	1.855	0.250
$\mu_{1,TERMAM:OLD}$	0.941	0.289
$\mu_{1,VOCHFE:OLD}$	0.867	0.323
σ_a^2	0.016	-
σ_b^2	0.482	-
$\sigma_{l,i}^2$	0.015	-

Table A2.2: Parameter estimates and their standard error for the survey model.

Parameter	Value	SE
$\mu_{0,BROSUT:YOUNG}$	0.026	0.016
$\mu_{0,CECRIN:YOUNG}$	0.047	0.013
$\mu_{0,GUATDU:YOUNG}$	0.041	0.013
$\mu_{0,MICOBO:YOUNG}$	-0.003	0.013
$\mu_{0,TERMAM:YOUNG}$	0.045	0.016
$\mu_{0,VOCHFE:YOUNG}$	0.034	0.015
$\mu_{0,BROSUT:MATURE}$	0.011	0.016
$\mu_{0,CECRIN:MATURE}$	0.119	0.013
$\mu_{0,GUATDU:MATURE}$	0.065	0.016
$\mu_{0,MICOBO:MATURE}$	-0.003	0.015
$\mu_{0,TERMAM:MATURE}$	0.029	0.018
$\mu_{0,VOCHFE:MATURE}$	0.033	0.017
$\mu_{0,BROSUT:OLD}$	0.050	0.015
$\mu_{0,CECRIN:OLD}$	0.156	0.014
$\mu_{0,GUATDU:OLD}$	0.094	0.015
$\mu_{0,MICOBO:OLD}$	0.015	0.013
$\mu_{0,TERMAM:OLD}$	0.023	0.013
$\mu_{0,VOCHFE:OLD}$	0.053	0.012
$\mu_{1,BROSUT}$	3.044	0.459
$\mu_{1,CECRIN}$	2.866	0.179
$\mu_{1,GUATDU}$	3.317	0.434
$\mu_{1,MICOBO}$	4.149	0.264
$\mu_{1,TERMAN}$	2.834	0.307
$\mu_{1,VOCHFE}$	2.573	0.356
σ_a^2	0.026	-
σ_b^2	0.36	-
$\sigma_{t,i}^2$	0.068	-

Table A2.3: Parameter estimates and their standard error for the survey + time-of-day model.

Parameter	Value	SE
$\mu_{0,BROSUT:YOUNG}$	0.029	0.015
$\mu_{0,CECRIN:YOUNG}$	0.060	0.013
$\mu_{0,GUATDU:YOUNG}$	0.044	0.012
$\mu_{0,MICOBO:YOUNG}$	0.004	0.012
$\mu_{0,TERMAM:YOUNG}$	0.033	0.015
$\mu_{0,VOCHFE:YOUNG}$	0.046	0.014
$\mu_{0,BROSUT:MATURE}$	0.019	0.015
$\mu_{0,CECRIN:MATURE}$	0.132	0.012
$\mu_{0,GUATDU:MATURE}$	0.071	0.015
$\mu_{0,MICOBO:MATURE}$	0.011	0.014
$\mu_{0,TERMAM:MATURE}$	0.017	0.017
$\mu_{0,VOCHFE:MATURE}$	0.046	0.016
$\mu_{0,BROSUT:OLD}$	0.056	0.014
$\mu_{0,CECRIN:OLD}$	0.169	0.013
$\mu_{0,GUATDU:OLD}$	0.090	0.014
$\mu_{0,MICOBO:OLD}$	0.022	0.012
$\mu_{0,TERMAM:OLD}$	0.018	0.012
$\mu_{0,VOCHFE:OLD}$	0.059	0.011
$\mu_{1,BROSUT:Morning}$	3.869	0.587
$\mu_{1,CECRIN:Morning}$	3.362	0.439
$\mu_{1,GUATDU:Morning}$	5.946	0.585
$\mu_{1,MICOBO:Morning}$	4.121	0.411
$\mu_{1,TERMAN:Morning}$	3.940	0.734
$\mu_{1,VOCHFE:Morning}$	3.532	0.422
$\mu_{1,BROSUT:PreNoon}$	3.257	0.543
$\mu_{1,CECRIN:PreNoon}$	2.792	0.198
$\mu_{1,GUATDU:PreNoon}$	3.532	0.458
$\mu_{1,MICOBO:PreNoon}$	4.223	0.257
$\mu_{1,TERMAN:PreNoon}$	3.446	0.320
$\mu_{1,VOCHFE:PreNoon}$	2.753	0.366
$\mu_{1,BROSUT:PostNoon}$	2.429	0.465
$\mu_{1,CECRIN:PostNoon}$	2.715	0.188
$\mu_{1,GUATDU:PostNoon}$	1.829	0.469
$\mu_{1,MICOBO:PostNoon}$	3.641	0.319
$\mu_{1,TERMAN:PostNoon}$	2.477	0.313
$\mu_{1,VOCHFE:PostNoon}$	1.481	0.394
$\mu_{1,BROSUT:Evening}$	1.511	0.877
$\mu_{1,CECRIN:Evening}$	1.156	0.482
$\mu_{1,GUATDU:Evening}$	1.328	0.899
$\mu_{1,MICOBO:Evening}$	2.594	0.648
$\mu_{1,TERMAN:Evening}$	3.248	0.459
$\mu_{1,VOCHFE:Evening}$	1.131	0.524
σ_a^2	0.052	-
σ_b^2	0.485	-
$\sigma_{t,i}^2$	0.054	-

Note A2.2: Description of the leaf scale photosynthesis, conductance, and energy balance model from the R package LeafGasExchange (Lamour & Serbin, 2021)

To simulate leaf surface temperature (T_{leaf}), CO_2 concentration (C_s), and leaf surface vapor pressure deficit (VPD_{leaf}) the model uses a leaf energy budget model published by Muir, (2019, 2020) which iteratively estimates T_{leaf}, intercellular CO_2 concentration (C_i), and boundary layer conductance (g_{bw}). This is accomplished by first assuming $T_{leaf} = T_{air} + 1$ ºC, C_s = atmospheric CO_2 concentration (C_a), then solving for A, g_s, C_i, $T_{leaf,}$ and g_{bw} accounting for the temperature dependencies of the photosynthetic parameters (Bernacchi et al., 2001, 2003; Leuning, 2002).The model then compares the resulting estimation of T_{leaf} to the prior value, and if the values differ by less than 0.1 ºC, assumes the model has converged. If the values differ by more than 0.1 ºC, the model is rerun using the updated values of Tleaf, C_s, and VPD_{leaf}.

Stomatal conductance is simulated using the USO model (Medlyn et al., 2011) presented in Equation A2.1. Photosynthesis is simulated using the FvCB assimilation model (Farquhar et al., 1980) which assumes that net photosynthesis (A) is the minimum of carboxylation limited assimilation (A_c) and RuBp regeneration limited assimilation (A_j), less the respiration rate that is not attributable to the photorespiratory pathway (R_{dark}). The model uses parameters for the maximum rate of electron transport at 25°C ($J_{max.25}$), maximum rate of carboxylation at 25°C ($V_{c,max.25}$), and the leaf dark respiration rate at 25°C ($R_{dark.25}$) which are scaled to T_{leaf} using an Arrhenius function or a modified Arrhenius function (Bernacchi et al., 2001, 2003; Leuning, 2002). The model also scales $V_{c,max.25}$ between canopy layers with cumulatively increasing LAI using the exponential decline function presented in Lloyd et al., (2010). While traditionally models consider a third limitation on photosynthesis, the export limited assimilation rate, also known as the rate of triose phosphate utilization (A_p), there is a growing body of evidence suggesting that this limitation is unlikely to limit photosynthesis under current growth conditions (Rogers et al., 2021). Therefore, I chose not to implement this limitation in the model.

Equation A2.1:
$$g_s = g_0 + 1.6\left(1 + \frac{g_1}{\sqrt{D}}\right)\frac{A}{C_s}$$

Note S3: Description of the leaf water potential (Ψ_{leaf}) penalty function introduced by Wolf *et al*., (2016) and tested by Anderegg *et al*., (2017).

To evaluate an additional constraint on the USO model, I tested if the inclusion of a function linking Ψ_{leaf} imposed hydraulic limitation on potential g_{sw} improved modeled rates. Here I applied the function in Equation A2.2 to Equation A2.1 to arrive at Equation A2.3 and a new predicted rate of g_s.

Equation A2.2: $$f\Psi_{leaf} = e^{-\left(\frac{\Psi_{leaf}}{c}\right)^{b}}$$

Equation A2.3: $$g_{sw} = g_0 + 1.6\left(1 + \frac{g_1}{\sqrt{D}}\right)\frac{A}{C_s} * f\Psi_{leaf}$$

Here Ψ_{leaf} is the observed Ψ_{leaf} (MPa) after each measurement of g_s, and b and c are species specific values, derived from Weibull functions of xylem conductivity Ψ_{stem} obtained from Wu et al., (2019), where Ψ_{leaf} is assumed to corollate with Ψ_{stem} such that at Ψ_{leaf} = 0 MPa, the rate of hydraulic conductance is maximized (Sperry et al., 2017). Values for b and c along with a diagnostic plot showing the functional decline in potential g_{sw} as a function of Ψ_{leaf} are reported below.

Table A2.4: Species specific Weibull function values corresponding to xylem conductivity versus stem water potential (Ψ_{stem}). Data are reproduced from Wu et al., (2019).

Species	*b* parameter	*c* parameter
Guatteria dumetorum	1.3	2.1
Miconia borealis	1.6	1.5
Terminalia amazonia	1.2	2.0
Vochysia ferruginea	1.0	3.5

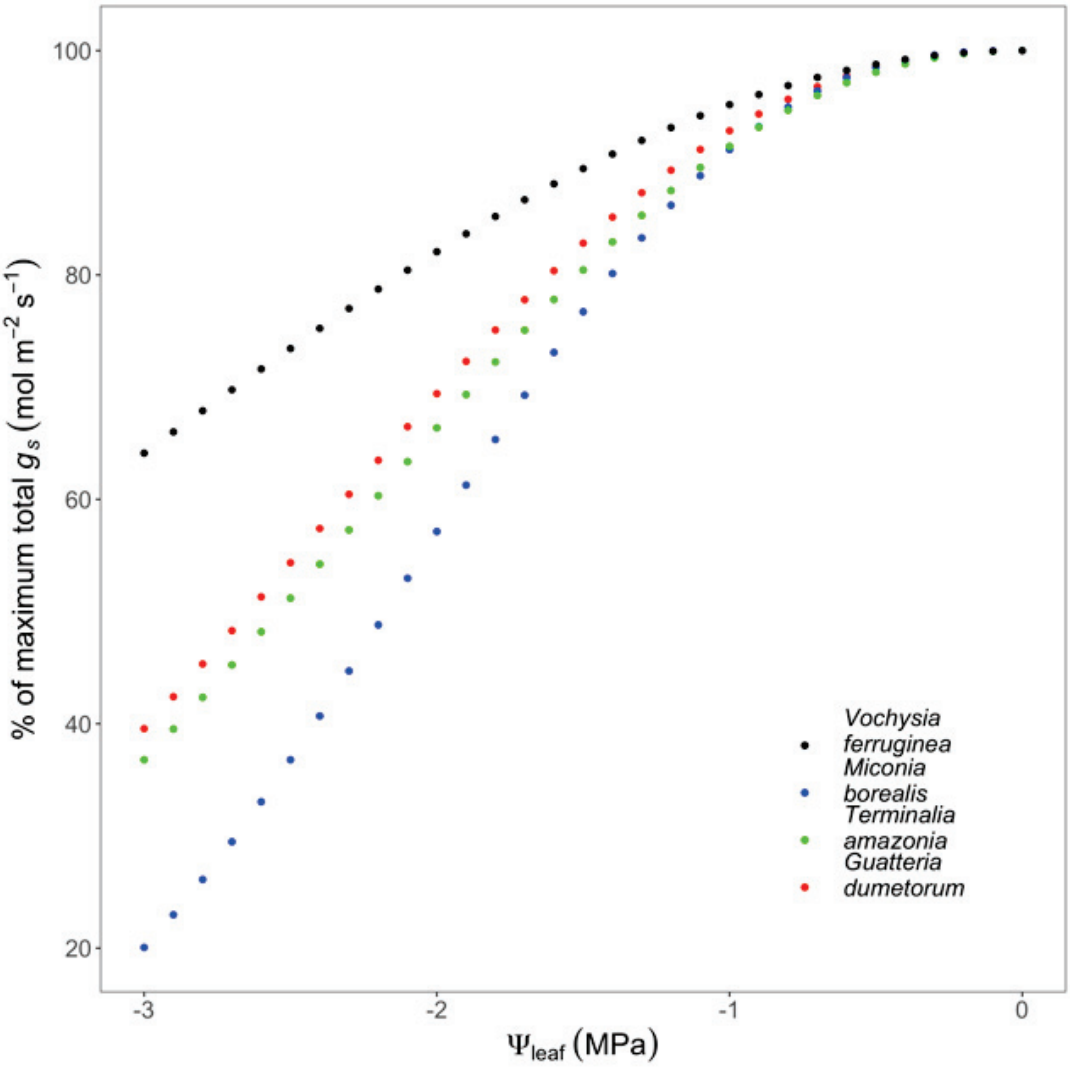

Figure A2.17: Reduction in potential stomatal conductance (g_s)between Equation A2.1 (100% at any Ψ_{leaf}) and Equation A2.3 as a function of Ψ_{leaf} for four species.

Appendix 3: Supporting information for Chapter 4

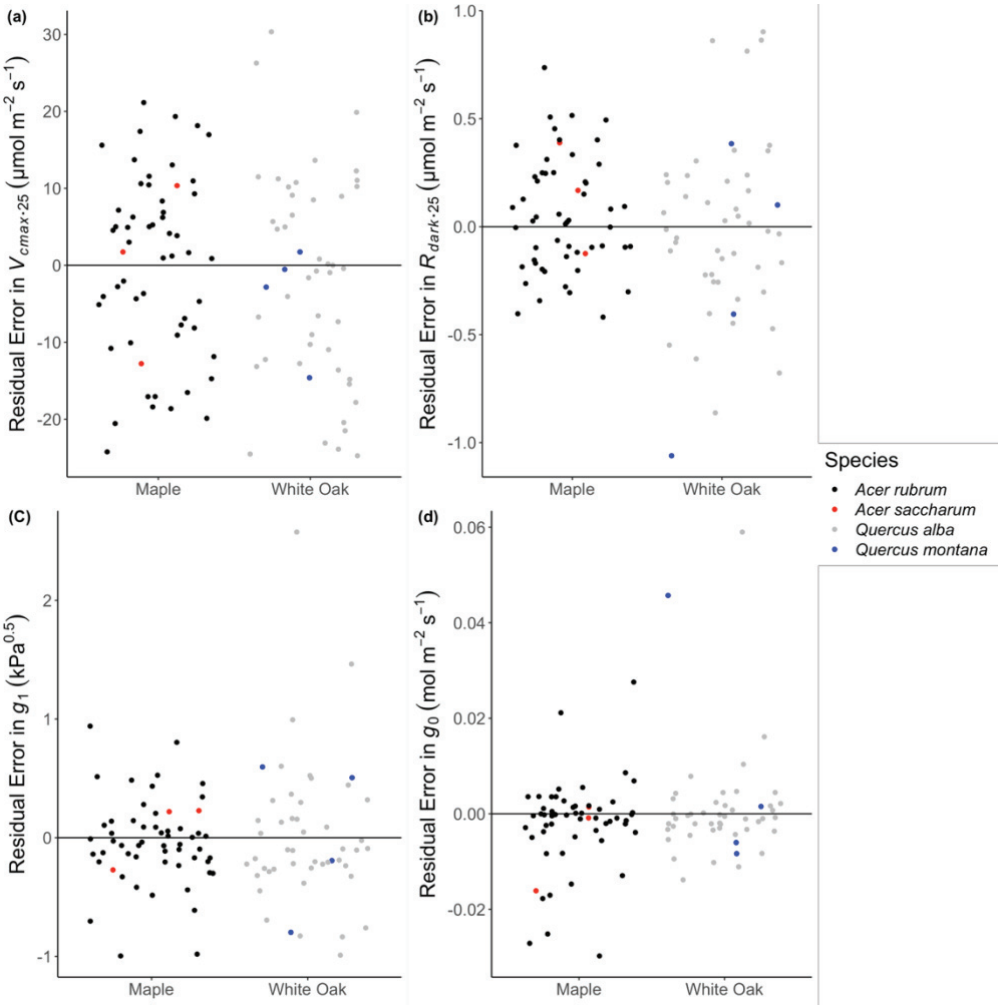

Figure A3.1: Evaluation of individual residuals for the maple and white oak species-groups. (a) the maximum carboxylation capacity of Rubisco normalized to 25°C ($V_{cmax.25}$), (b) dark respiration rate normalized to 25°C ($R_{dark.25}$), (c) the stomatal slope parameter (g_1) and (d) stomatal intercept parameter (g_0) of the unified stomatal optimization model (Medlyn et al. 2011). All residuals are shown relative to their species-group means.

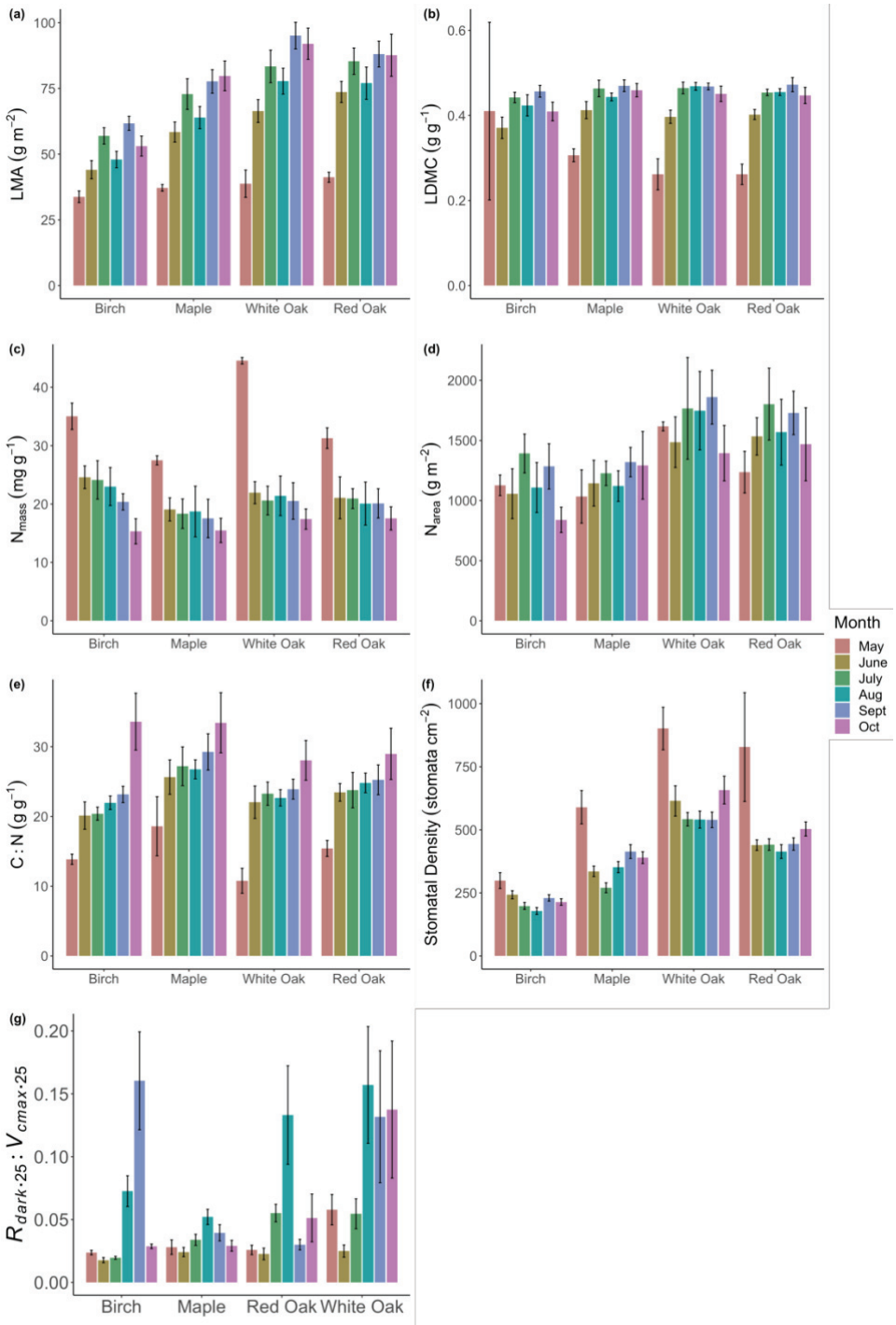

Figure A3.2: Average monthly estimates of (a) leaf mass per area (LMA), (b) leaf dry matter content (LDMC), (c) elemental nitrogen per unit mass (N_{mass}), (d) elemental nitrogen per unit area (N_{area}), (e) ratio of foliar carbon to nitrogen (C:N), (f) stomatal density, and (g) the ratio between the dark respiration rate normalized to 25°C ($R_{dark.25}$) and the maximum carboxylation capacity of Rubisco normalized to 25°C ($V_{cmax.25}$) by species-group for the 2021 growth season. Error bars represent ± 2 SE of the mean.

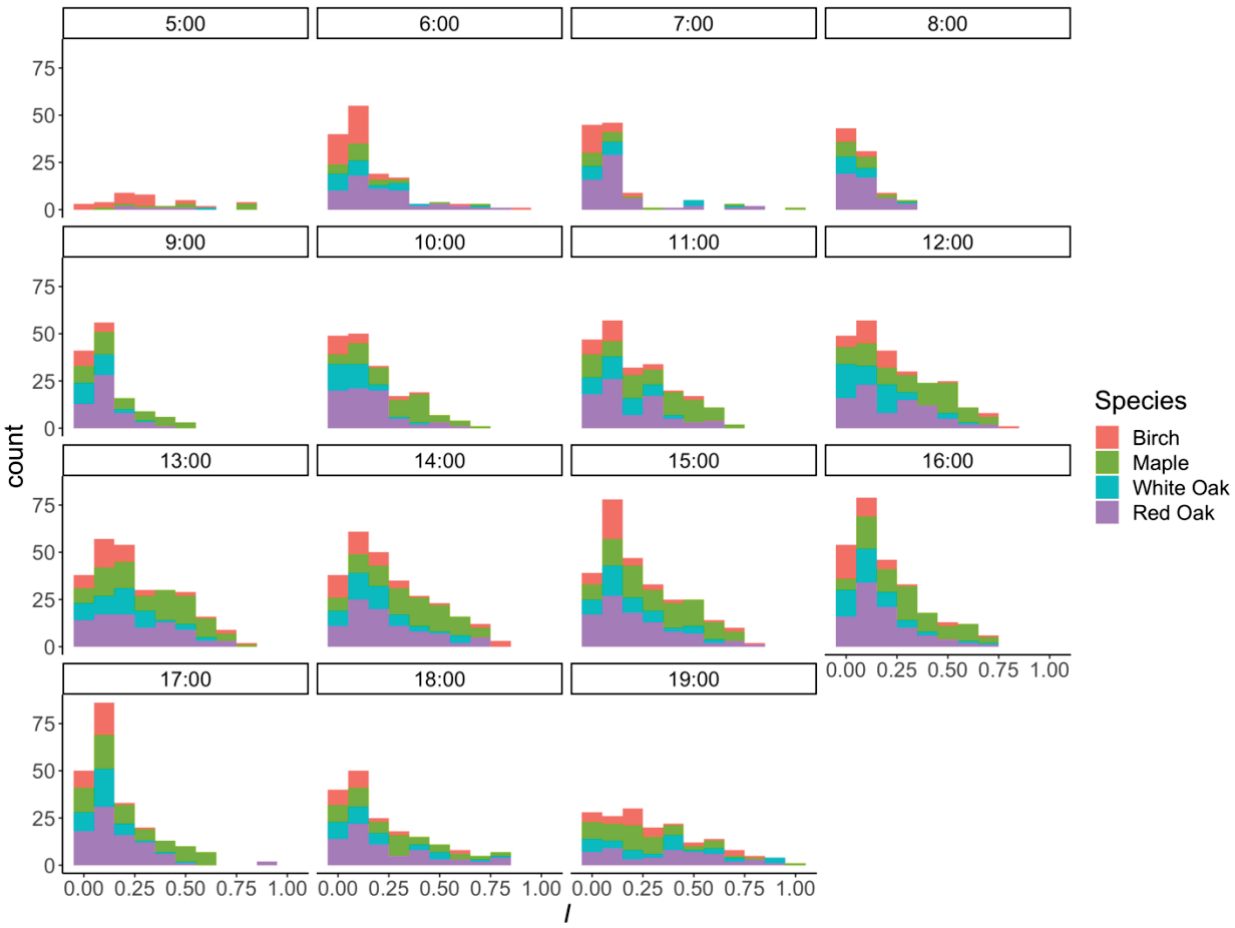

Figure A3.3: Frequency distributions of the level of the relative strength of the stomatal limitation on photosynthesis (*I,* where $I = 0$ represents no stomatal limitation on photosynthesis while a value of $I = 1$ represents complete stomatal limitation on photosynthesis). Observations divided by hour for each of the 15 hours where mean PAR ≥ 100 between May 15 and October 15, 2021 at the Black Rock Forest site.

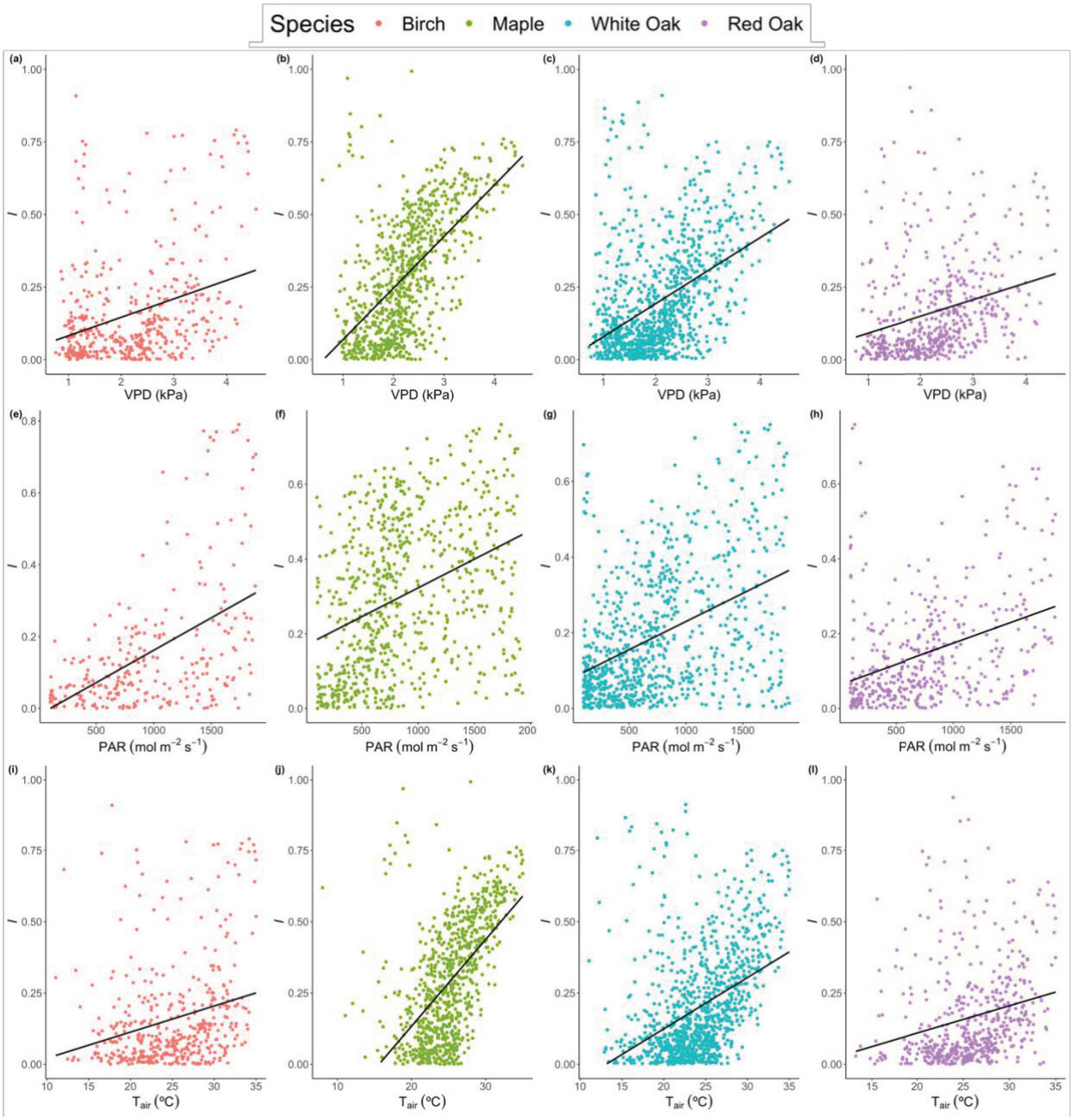

Figure A3.4: Relationships between (a-d) leaf to air VPD, (e-h) PAR, and (i-l) air temperature, and the level of stomatal limitation on photosynthesis (*I,* where $I = 0$ represents no stomatal limitation on photosynthesis while a value of $I = 1$ represents complete stomatal limitation on photosynthesis) for all observations where $I > 0$. All linear relationships shown are significant ($p < 0.05$), with the black line representing a line of best fit.

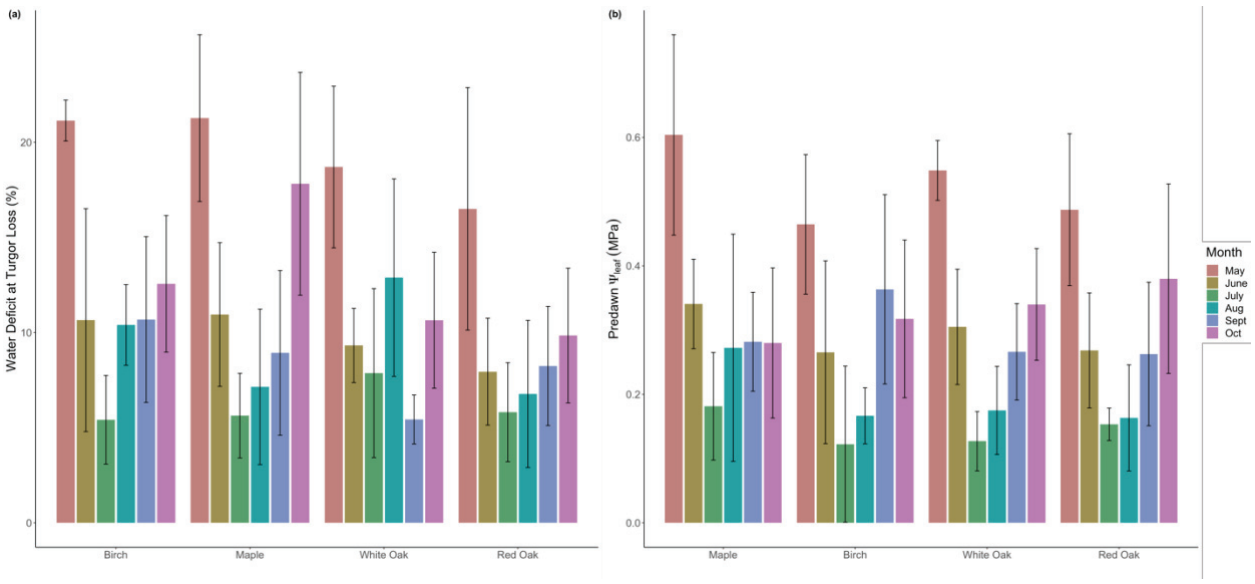

Figure A3.5: Average monthly (a) relative water deficit at turgor loss, and (b) predawn Ψ_{leaf} by species-group for the 2021 growth season. Error bars represent ± 2 SE of the mean.

Table A3.1: Group specific parameters used in the coupled photosynthesis, conductance, and energy balance models used for simulations in this study.

Parameter	Description	Birch (units)	Maple (units)	White Oak (units)	Red Oak (units)	Data Source
JmaxRef	Maximum electron transport rate	VcmaxRef * 1.74 (μmol m^{-2} s^{-1})	VcmaxRef * 1.32 (μmol m^{-2} s^{-1})	VcmaxRef * 1.25 (μmol m^{-2} s^{-1})	VcmaxRef * 1.50 (μmol m^{-2} s^{-1})	This study
JmaxHa	Energy of activation for Jmax	48500 (J mol^{-1})	50400 (J mol^{-1})	46100 (J mol^{-1})	55900 (J mol^{-1})	Dreyer et al. (2001)*
JmaxHd	Energy of deactivation for Jmax	193000 (J mol^{-1})	154000 (J mol^{-1})	280000 (J mol^{-1})	88300 (J mol^{-1})	Dreyer et al. (2001)*
JmaxS	Entropy term for Jmax	622 (J mol^{-1} K^{-1})	494 (J mol^{-1} K^{-1})	888 (J mol^{-1} K^{-1})	284 (J mol^{-1} K^{-1})	Dreyer et al. (2001)*
VcmaxHa	Energy of activation for Vcmax	60800 (J mol^{-1})	69700 (J mol^{-1})	67600 (J mol^{-1})	61100 (J mol^{-1})	Dreyer et al. (2001)*
VcmaxHd	Energy of deactivation for Vcmax	40100 (J mol^{-1})	404000 (J mol^{-1})	144000 (J mol^{-1})	247000 (J mol^{-1})	Dreyer et al. (2001)*
VcmaxS	Entropy term for Vcmax	1285 (J mol^{-1} K^{-1})	1285 (J mol^{-1} K^{-1})	151 (J mol^{-1} K^{-1})	778 (J mol^{-1} K^{-1})	Dreyer et al. (2001)*
RdHa	Energy of activation for Rd	21100 (J mol^{-1})	24950 (J mol^{-1})	27950 (J mol^{-1})	41550 (J mol^{-1})	Dreyer et al. (2001)*
Parameter	**Description**	**Common Value for all Species (units)**				**Data Source**
R	Ideal gas constant	8.314 (J mol^{-1} K^{-1})				-
O2	Atmospheric O_2 concentration	210 (ppm)				-
TRef	Reference temperature	298.16 (K)				-
Patm	Atmospheric pressure	101 (kPa)				-
KcRef	Michaelis-Menten constant of Rubisco for CO2 at the reference temperature	404.9 (μmol mol^{-1})				Bernacchi et al. (2001)†
KcHa	Energy of activation for Kc	79430 (J mol^{-1})				Bernacchi et al. (2001)†
KoRef	Michaelis-Menten constant of Rubisco for CO2 at the reference temperature	278.4 (μmol mol^{-1})				Bernacchi et al. (2001)†
KoHa	Energy of activation for Ko	36380 (J mol^{-1})				Bernacchi et al. (2001)†
GstarRef	CO2 compensation point in absence of respiration	42.75 (μmol mol^{-1})				Bernacchi et al. (2001)†
GstarHa	Enthalpy of activation for Gstar	37830 (μmol mol^{-1})				Bernacchi et al. (2001)†

*Dreyer E, Le Roux X, Montpied P, Daudet FA, Masson F. 2001. Temperature response of leaf photosynthetic capacity in seedlings from seven temperate tree species. *Tree Physiology* 21: 223–232. doi:10.1093/treephys/21.4.223

†Bernacchi, C.J., Singsaas, E.L., Pimentel, C., Portis Jr, A.R. and Long, S.P. (2001), Improved temperature response functions for models of Rubisco-limited photosynthesis. Plant, Cell & Environment, 24: 253-259. doi:10.1111/j.1365-3040.2001.00668.x

Table A3.2: Values for mean monthly photosynthetic and conductance parameters by species-group. Each sample represents an independent leaf-level estimate. Values in parentheses are the standard error of the group and month mean estimates.

Group	Month	Sample size	$V_{cmax.25}$ (µmol m^{-2} s^{-1})	$R_{dark.25}$ (µmol m^{-2} s^{-1})	g_1 ($kPa^{0.5}$)	g_0 (mol m^{-2} s^{-1})
Birch	May	10	33.68 (4.58)	2.01 (0.15)	0.67 (0.37)	0.056 (0.012)
	June	11	45.52 (2.89)	0.88 (0.08)	2.72 (0.22)	0.018 (0.008)
	July	12	54.04 (2.93)	0.96 (0.13)	2.59 (0.3)	0.047 (0.011)
	Aug	12	34.96 (3.87)	0.79 (0.08)	2.7 (0.22)	0.023 (0.008)
	Sept	12	38.35 (1.76)	1.09 (0.04)	2.69 (0.2)	0.023 (0.007)
	Oct	12	11.59 (2.97)	1.18 (0.02)	2.03 (0.38)	0.048 (0.01)
Maple	May	10	29.15 (3.09)	1.53 (0.14)	1.83 (0.2)	0.047 (0.007)
	June	11	22.18 (3.29)	0.84 (0.09)	1.08 (0.17)	0.004 (0.005)
	July	12	32.18 (2.49)	0.76 (0.11)	1.15 (0.21)	0.004 (0.007)
	Aug	11	28.56 (3.27)	0.64 (0.06)	1.6 (0.15)	0.004 (0.005)
	Sept	12	36.83 (3.09)	0.92 (0.06)	1.76 (0.12)	0.008 (0.004)
	Oct	12	33.81 (5.62)	1.1 (0.09)	1.82 (0.17)	0.027 (0.006)
White Oak	May	9	15.6 (1.61)	2.23 (0.42)	0.48 (0.41)	0.059 (0.008)
	June	10	40.44 (5.12)	1.68 (0.29)	0.59 (0.26)	0.017 (0.005)
	July	12	46.12 (8.58)	0.96 (0.06)	0.95 (0.27)	0.008 (0.006)
	Aug	12	25.15 (3.69)	1.2 (0.09)	0.74 (0.2)	0.006 (0.004)
	Sept	11	21.02 (3.71)	1.28 (0.07)	0.99 (0.2)	0.009 (0.003)
	Oct	12	16.8 (3.17)	1.27 (0.11)	1.38 (0.25)	0.011 (0.005)
Red Oak	May	10	23.62 (3.7)	2.72 (0.15)	1.88 (0.36)	0.071 (0.005)
	June	11	33.01 (3.74)	1.7 (0.18)	1.19 (0.25)	0.008 (0.003)
	July	12	58.62 (8.51)	1.19 (0.11)	1.85 (0.32)	0.003 (0.005)
	Aug	12	40.89 (3.92)	0.94 (0.08)	1.91 (0.22)	0.005 (0.004)
	Sept	12	49.64 (5.22)	1.1 (0.05)	3.16 (0.21)	0.003 (0.003)
	Oct	12	43.94 (5.52)	1.24 (0.1)	3.32 (0.28)	0.011 (0.005)

Appendix 4: Supporting information for Chapter 5

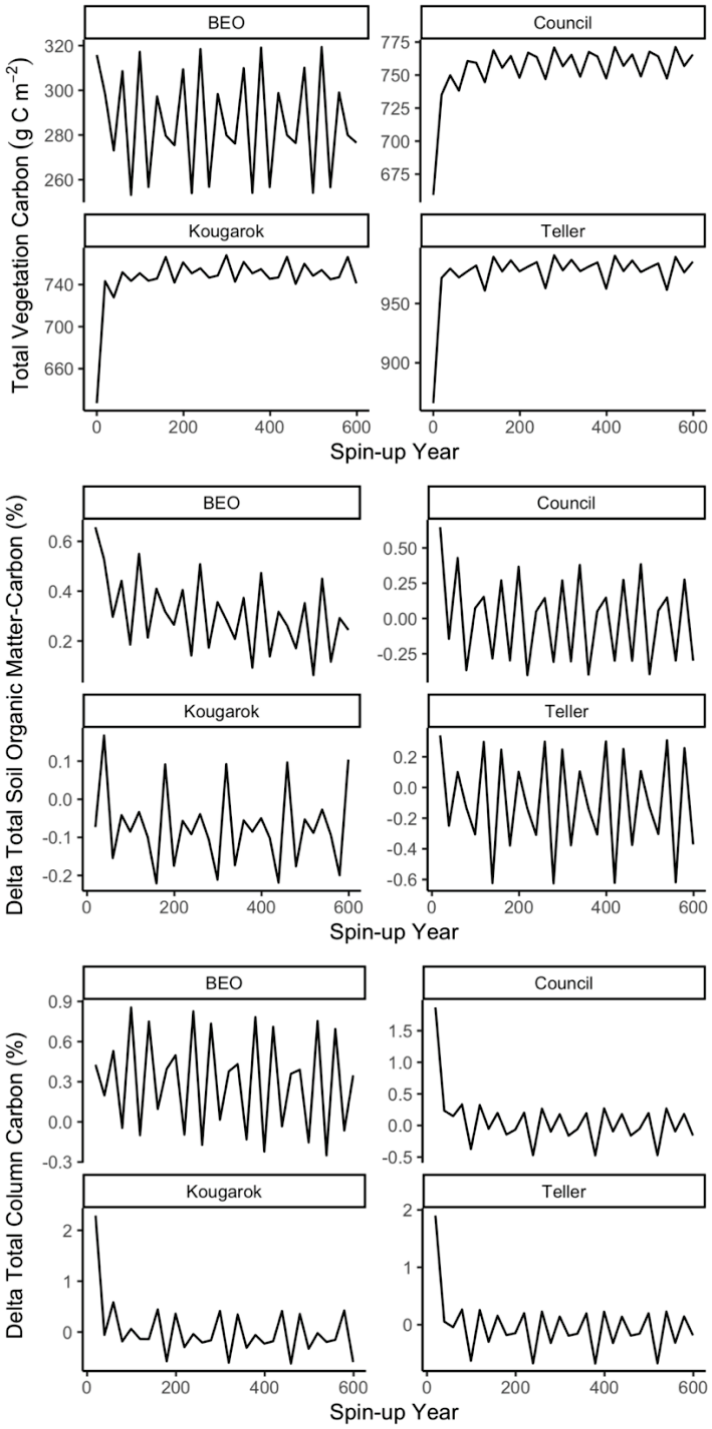

Figure A4.1: Model output for carbon dynamics during regular spin up phase. Carbon stocks are considered properly mixed and stabilized when disequilibrium of total ecosystem carbon is < 3%.

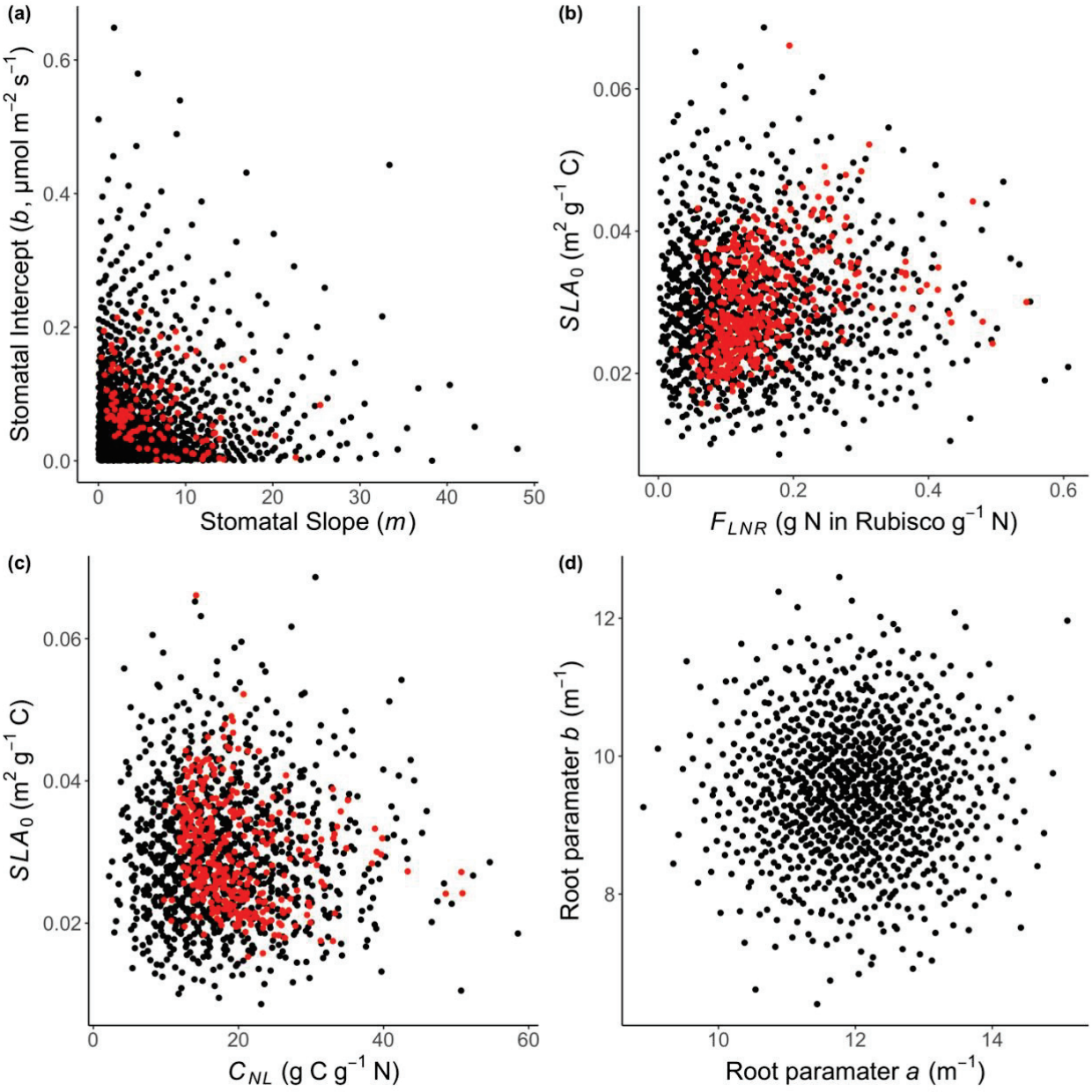

Figure A4.2: Relationships between parameters used in ensemble simulations. Data shown in red are actual observed data collected in this study, while data in black are parameters used in the ensemble simulations.

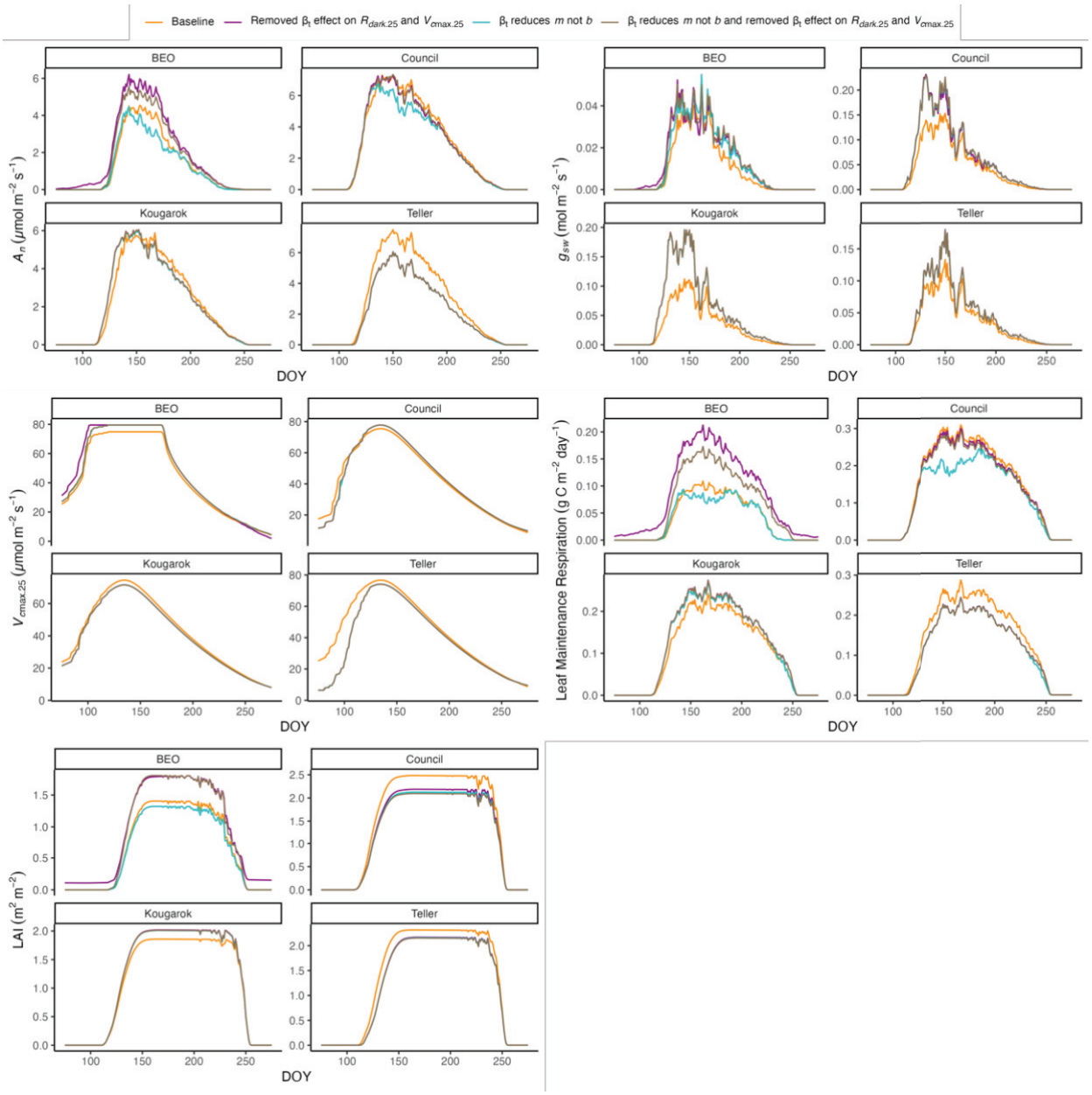

Figure A4.3: Above ground responses for simulations in which different β_t factor functions were tested. Average daily (a) photosynthetic carbon assimilation (μmol m^{-2} s^{-1}; A_n), (b) stomatal conductance (mol m^{-2} s^{-1}; g_s), (c) maximum carboxylation capacity of the enzyme rubisco normalized to 25°C (μmol m^{-2} s^{-1} ;$V_{cmax.25}$), (d) leaf maintenance respiration (g C m^{-2} day^{-1}), and (e) leaf area index (m^2 m^{-2}; LAI). Data in orange are simulations in which the β_t function has not been modified (MS-4), data in magenta represent the model where the direct effect of β_t on photosynthesis and respiration has been removed (MS-5), data in teal represent the model where β_t has been applied to the stomatal slope (m), rather than the stomatal intercept (b) (MS-6), and data in brown represent the model where the direct effect of β_t on photosynthesis and respiration has been removed and effect of β_t has been switched from b to m (MS-7). In all simulations, the fraction of leaf nitrogen in rubisco (F_{LNR}), the leaf carbon-to-nitrogen ratio (CN_L), the top of canopy specific leaf area (SLA_0), the root depth distribution parameters (ra and rb), m and b have been modified to correspond with field observations. Each subpanel represents one of the simulations sites.

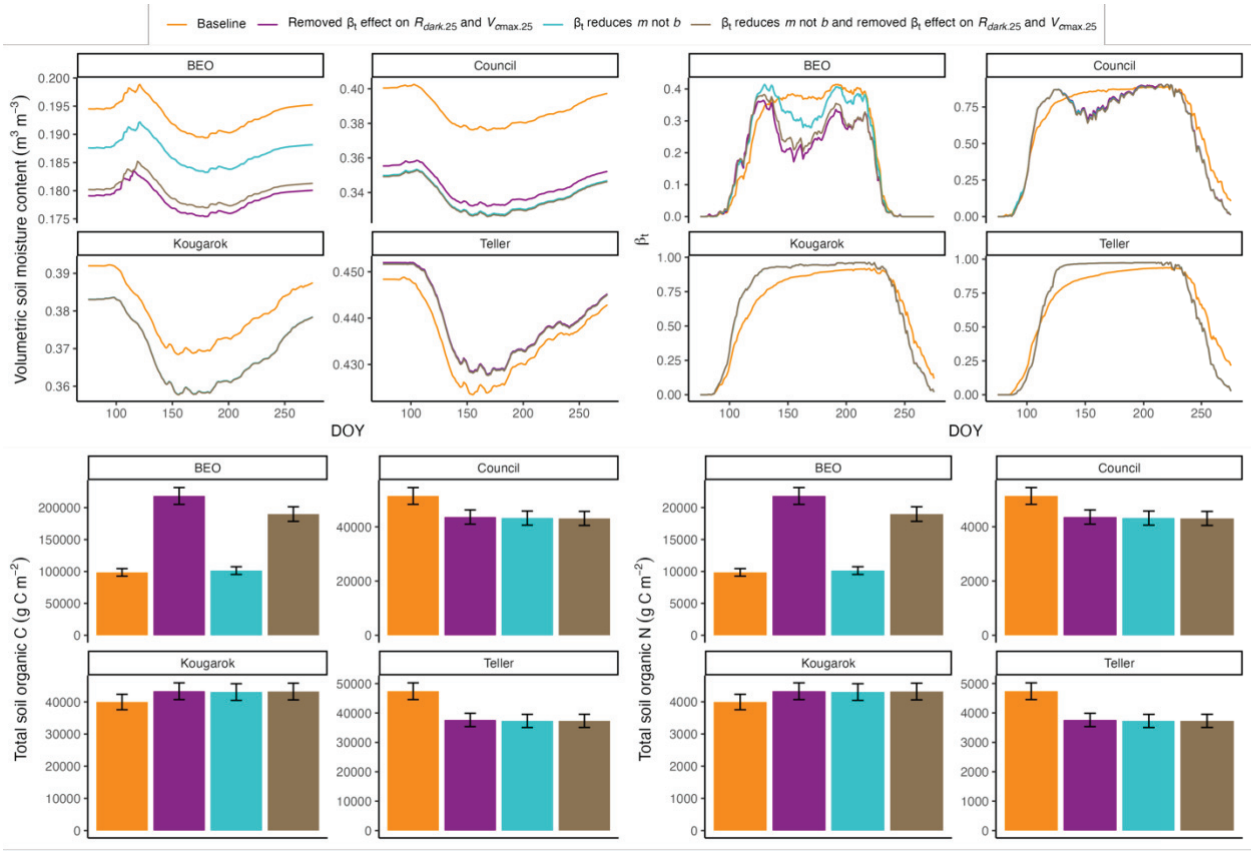

Figure A4.4: Below ground responses for simulations in which different β_t factor functions were tested. Average daily (a) volumetric soil moisture content (m^3 m^{-3} H_2O), (b) soil moisture stress factor (unitless; β_t), (c) total soil organic carbon (g C m^{-2}), and (d) total soil organic nitrogen (g N m^{-2}). Data in orange are simulations in which the β_t function has not been modified (MS-4), data in magenta represent the model where the direct effect of β_t on photosynthesis and respiration has been removed (MS-5), data in teal represent the model where β_t has been applied to the stomatal slope (m), rather than the stomatal intercept (b) (MS-6), and data in brown represent the model where the direct effect of β_t on photosynthesis and respiration has been removed and effect of β_t has been switched from b to m (MS-7). In all simulations, the fraction of leaf nitrogen in rubisco (F_{LNR}), the leaf carbon-to-nitrogen ratio (CN_L), the top of canopy specific leaf area (SLA_0), the root depth distribution parameters (ra and rb), m and b have been modified to correspond with field observations. Each subpanel represents one of the simulations sites. Error bars for the upper panels represent ± 2 SE of the mean annual value.

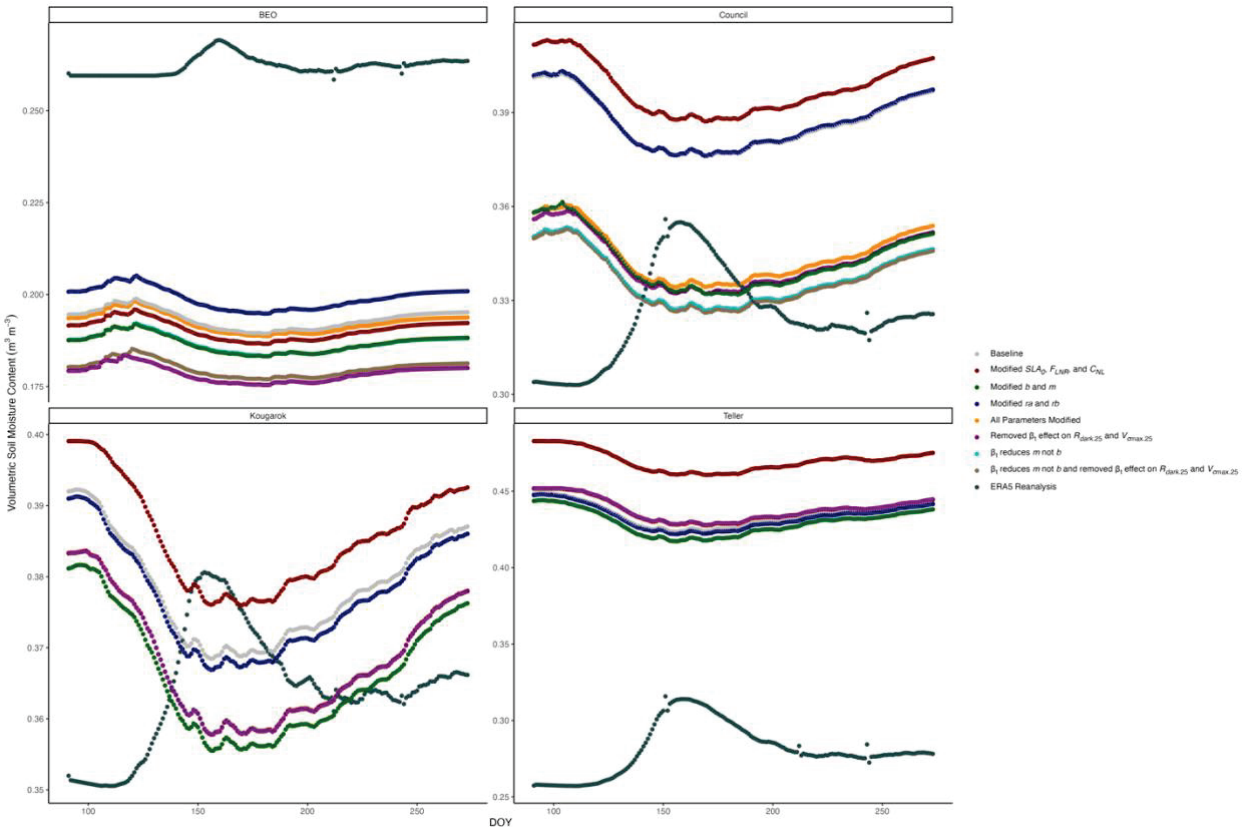

Figure A4.5: Comparison of model predicted, and observed, site level soil moisture content by day of year (DOY). Data in light grey represent the model with no modifications (MS-0), data in red are simulations in which the fraction of leaf nitrogen in rubisco (F_{LNR}), the leaf carbon-to-nitrogen ratio (CN_L) and the top of canopy specific leaf area (SLA_0) have been modified (MS-1), data in green are simulations in which the stomatal slope (m) and intercept (b) have been modified (MS-2), data in blue are simulations in which the root depth distribution parameters (ra and rb) have been modified (MS-3), and data in orange are simulations in all seven parameters were modified (MS-4), data in magenta represent the model where the direct effect of β_t on photosynthesis and respiration has been removed (MS-5), data in teal represent the model where β_t has been applied to the m, rather than b (MS-6), and data in brown represent the model where the direct effect of β_t on photosynthesis and respiration has been removed and effect of β_t has been switched from b to m (MS-7). Data in dark grey come from the ERA5-Land reanalysis product.

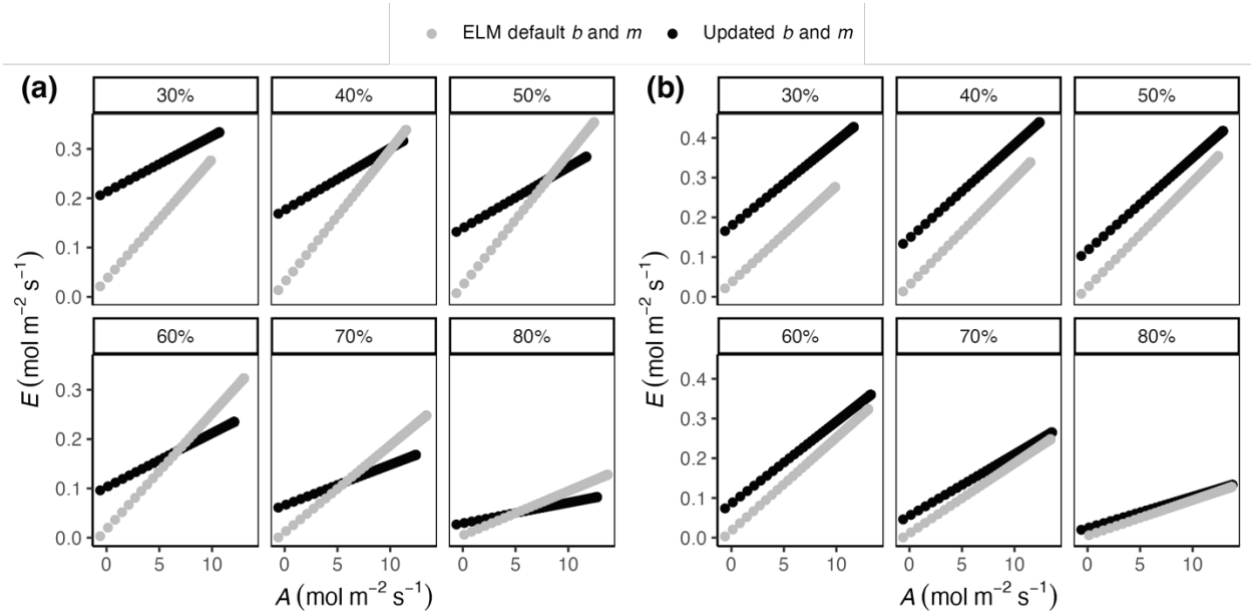

Figure A4.6: Theoretical relationships between assimilation rate (*A*) and transpiration rate (*E*) when ELM default and updated parameters for stomatal slope (*m*) and intercept (*b*) are used. For all simulations PAR ranged from 2000 µmol m^{-2} s^{-1} to 0 µmol m^{-2} s^{-1} in increments of 10 µmols, air temperature= 17ºC, and air CO_2 concentration = 400 ppm. Relative humidity for each simulation is indicated by the heading of the sub-panel. Simulations for the shrub PFT (a) used ($V_{cmax.25}$ = 68.01 µmol m^{-2} s^{-1}, m = 4.19, and b = 0.0590 mol m^{-2} s^{-1}, updated; $V_{cmax.25}$ = 68.01 µmol m^{-2} s^{-1}, m = 9, and b = 0.01 mol m^{-2} s^{-1}, default) while simulations for the grass PFT (b) used ($V_{cmax.25}$ = 85.40 µmol m^{-2} s^{-1}, m = 7.9, and b = 0.0495 mol m^{-2} s^{-1}, updated; $V_{cmax.25}$ = 68.01 µmol m^{-2} s^{-1}, m = 9, and b = 0.01 mol m^{-2} s^{-1}, default).

Table A4.1: Updated PFT specific values for F_{LNR} to account for corrections to α_{R25} and F_{NR} as recommended by Rogers, (2014). α_{R25} = 7.3 μmol CO2 g^{-1} Rubisco s^{-1} and F_{NR}= 6.22 g Rubisco g^{-1} N in Rubisco.

PFT	Default F_{LNR} (g N in rubisco g^{-1} N)	Updated F_{LNR} (g N in rubisco g^{-1} N)
needleleaf evergreen temperate tree	0.0509	0.0743
needleleaf evergreen boreal tree	0.042	0.0613
needleleaf deciduous boreal tree	0.07	0.1022
broadleaf evergreen tropical tree	0.058	0.0847
broadleaf evergreen temperate tree	0.0515	0.0752
broadleaf deciduous tropical tree	0.0716	0.1046
broadleaf deciduous temperate tree	0.1007	0.147
broadleaf deciduous boreal tree	0.1007	0.147
broadleaf evergreen shrub	0.0517	0.0755
broadleaf deciduous temperate shrub	0.12	0.1752
broadleaf deciduous boreal shrub	0.1365	0.1993
c3 arctic grass	0.1365	0.1993
c3 non-arctic grass	0.1	0.146
c4 grass	0.058	0.0847
c3 crop	0.1	0.146
c3 irrigated	0.1758	0.2567
corn	0.293	0.4278
irrigated corn	0.293	0.4278
spring temperate cereal	0.4102	0.599
irrigated spring temperate cereal	0.4102	0.599
winter temperate cereal	0.4102	0.599
irrigated winter temperate cereal	0.4102	0.599
soybean	0.4102	0.599
irrigated soybean	0.4102	0.599

Table A4.2: Description of the nine model simulations and their differences.

Simulation	*Unmodified parameters*	*Modified parameters*	*Modifications to β_t*
MS-0 (Baseline)	m, b, SLA_0, F_{LNR}, C_{NL}, r_a, and r_b	-	-
MS-1	m, b, r_a, and r_b	SLA_0, F_{LNR}, and C_{NL}	-
MS-2	SLA_0, F_{LNR}, C_{NL}, r_a, and r_b	m, and b	-
MS-3	m, b, SLA_0, F_{LNR}, and C_{NL},	r_a, and r_b	-
MS-4	-	m, b, SLA_0, F_{LNR}, C_{NL}, r_a, and r_b	-
MS-5	-	m, b, SLA_0, F_{LNR}, C_{NL}, r_a, and r_b	$A_n = (V_{cmax.25}) - (R_d)$ $g_s = \left(\frac{A_n * h_s}{C_a/P_{atm}} * m\right) + (b * \beta_t)$
MS-6	-	m, b, SLA_0, F_{LNR}, C_{NL}, r_a, and r_b	$A_n = (V_{cmax.25} * \beta_t) - (R_d * \beta_t)$ $g_s = \left(\frac{A_n * h_s}{C_a/P_{atm}} * (m * \beta_t)\right) + b$
MS-7	-	m, b, SLA_0, F_{LNR}, C_{NL}, r_a, and r_b	$A_n = (V_{cmax.25}) - (R_d)$ $g_s = \left(\frac{A_n * h_s}{C_a/P_{atm}} * (m * \beta_t)\right) + b$

Table A4.3: Probability density functions used to simulate prior distributions for ensemble model.

Model Parameter	Distribution	Distribution Parameter 1	Distribution Parameter 2
Stomatal slope	Gamma	Shape = 0.9257495	Rate = 0.1401035
Stomatal intercept	Gamma	Shape = 0.7854005	Rate = 9.779488
Leaf carbon-to-nitrogen ratio	Gamma	Shape = 4.275006	Rate = 0.2320171
Fraction of leaf nitrogen in rubisco	Beta	Shape 1 = 1.511528	Shape 2 = 8.54082
Top of canopy specific leaf area	Gamma	Shape = 9.683385	Rate = 323.69
Root distribution parameter a	Normal	Mean = 12	SD = 1
Root distribution parameter b	Normal	Mean = 9.5	SD = 1

Appendix 5: Supporting information for Chapter 6

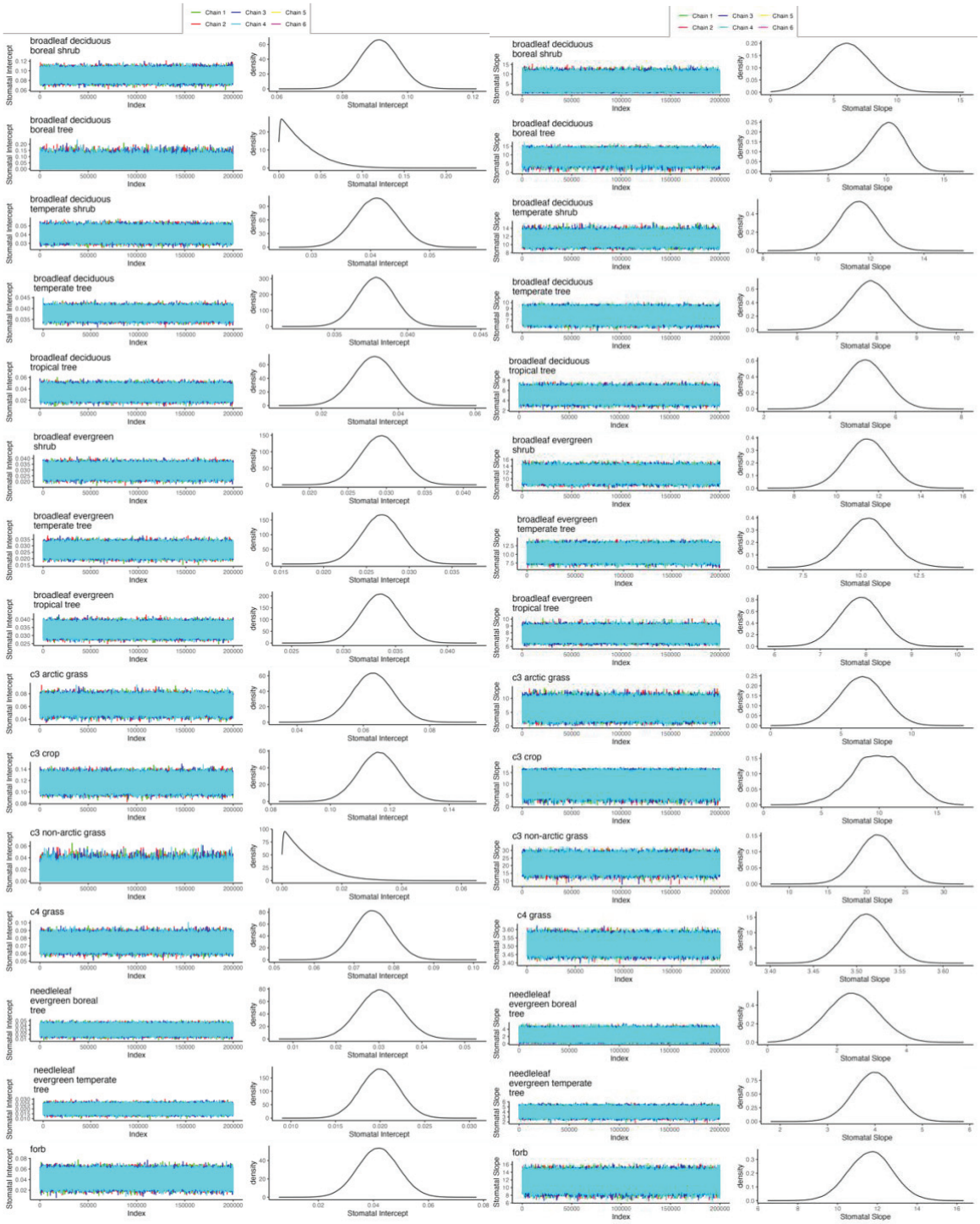

Figure A5.1: Caterpillar plots of posterior chains and histograms of posterior distributions for PFT specific slope and intercept using the BWB model and informative priors.



Figure A5.2: Caterpillar plots of posterior chains and histograms of posterior distributions for PFT specific slope and intercept using the Medlyn model and informative priors.

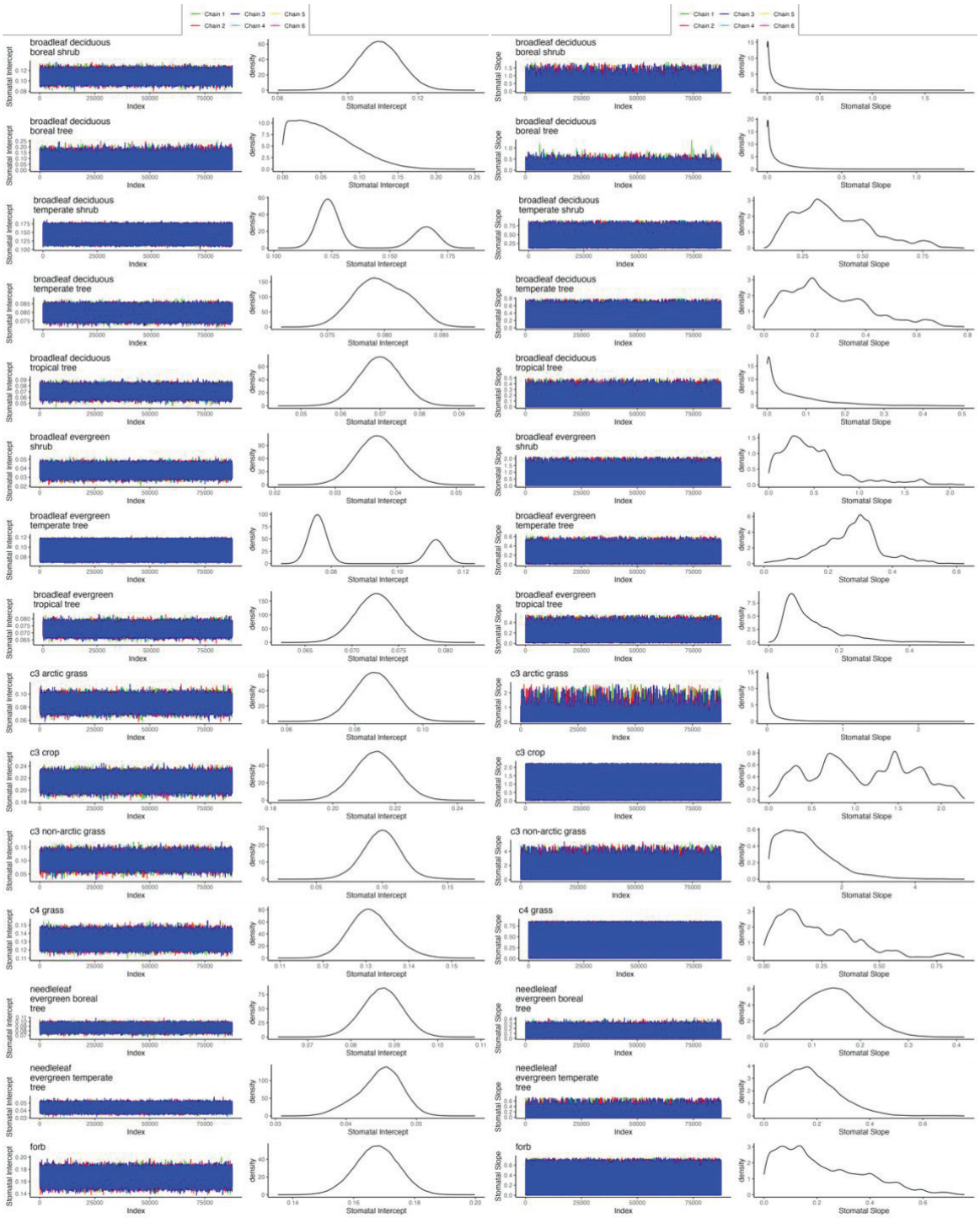

Figure A5.3: Caterpillar plots of posterior chains and histograms of posterior distributions for PFT specific slope and intercept using the Lamour model and informative priors.



Figure A5.4: Caterpillar plots of posterior chains and histograms of posterior distributions for PFT specific slope and intercept using the BWB model and uninformative priors.



Figure A5.5: Caterpillar plots of posterior chains and histograms of posterior distributions for PFT specific slope and intercept using the Medlyn model and uninformative priors.

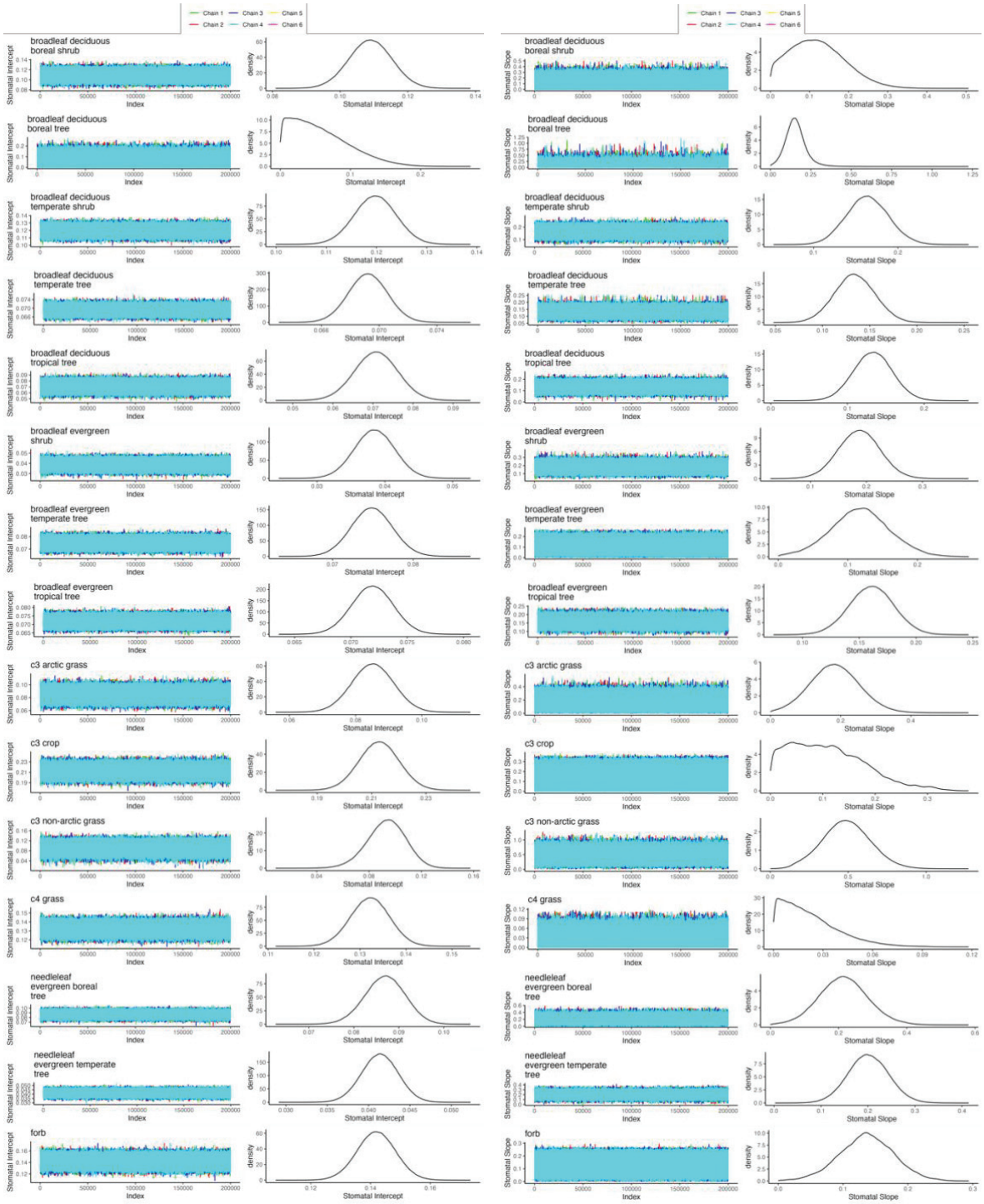

Figure A5.6: Caterpillar plots of posterior chains and histograms of posterior distributions for PFT specific slope and intercept using the Lamour model and uninformative priors.

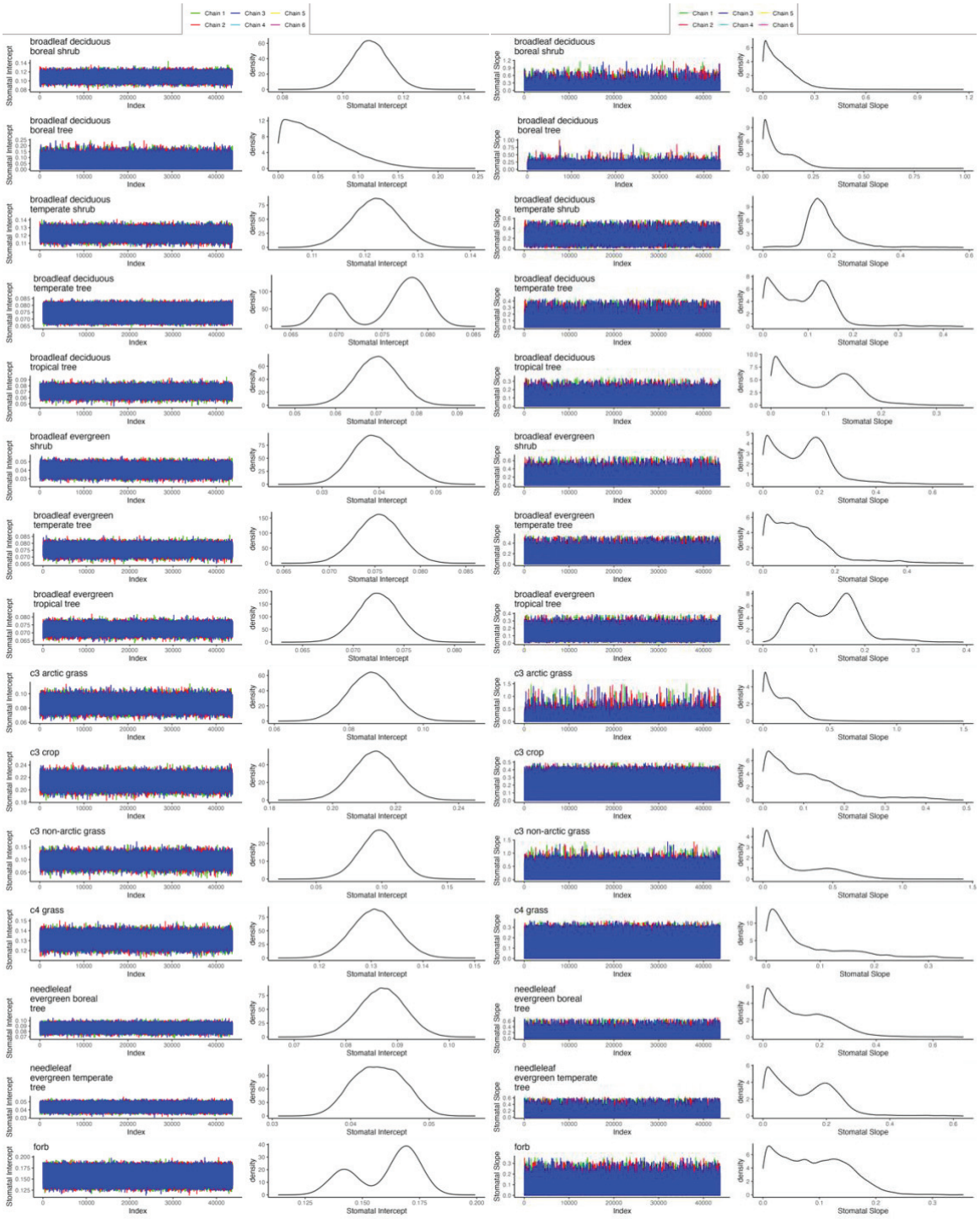

Figure A5.7: Caterpillar plots of posterior chains and histograms of posterior distributions for PFT specific slope and intercept using the Lamour model and uninformative priors for slope an intercept, but informative priors for $R_{d.25}$.

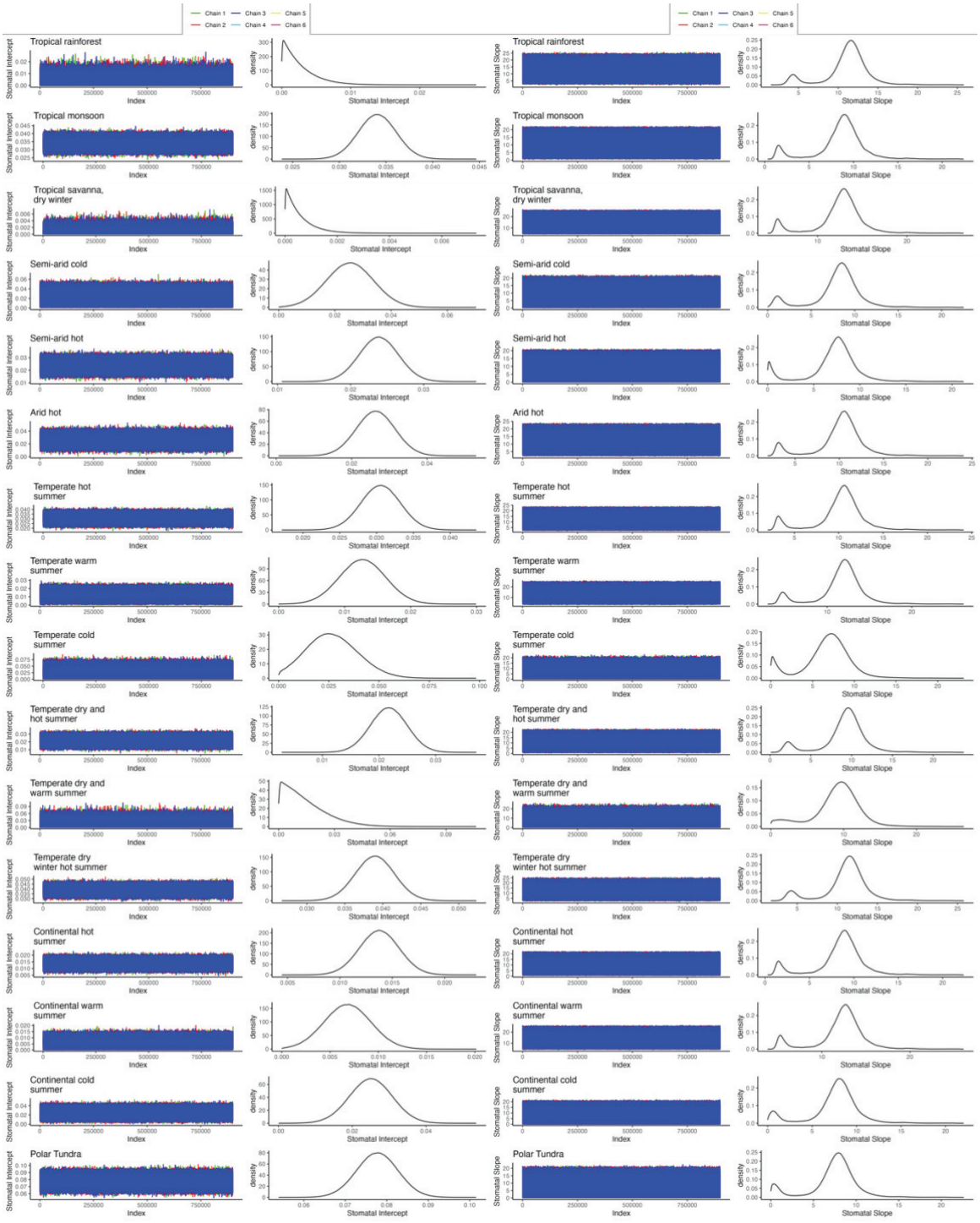

Figure A5.8: Caterpillar plots of posterior chains and histograms of posterior distributions for climate zone specific slope and intercept using the BWB model and uninformative priors.

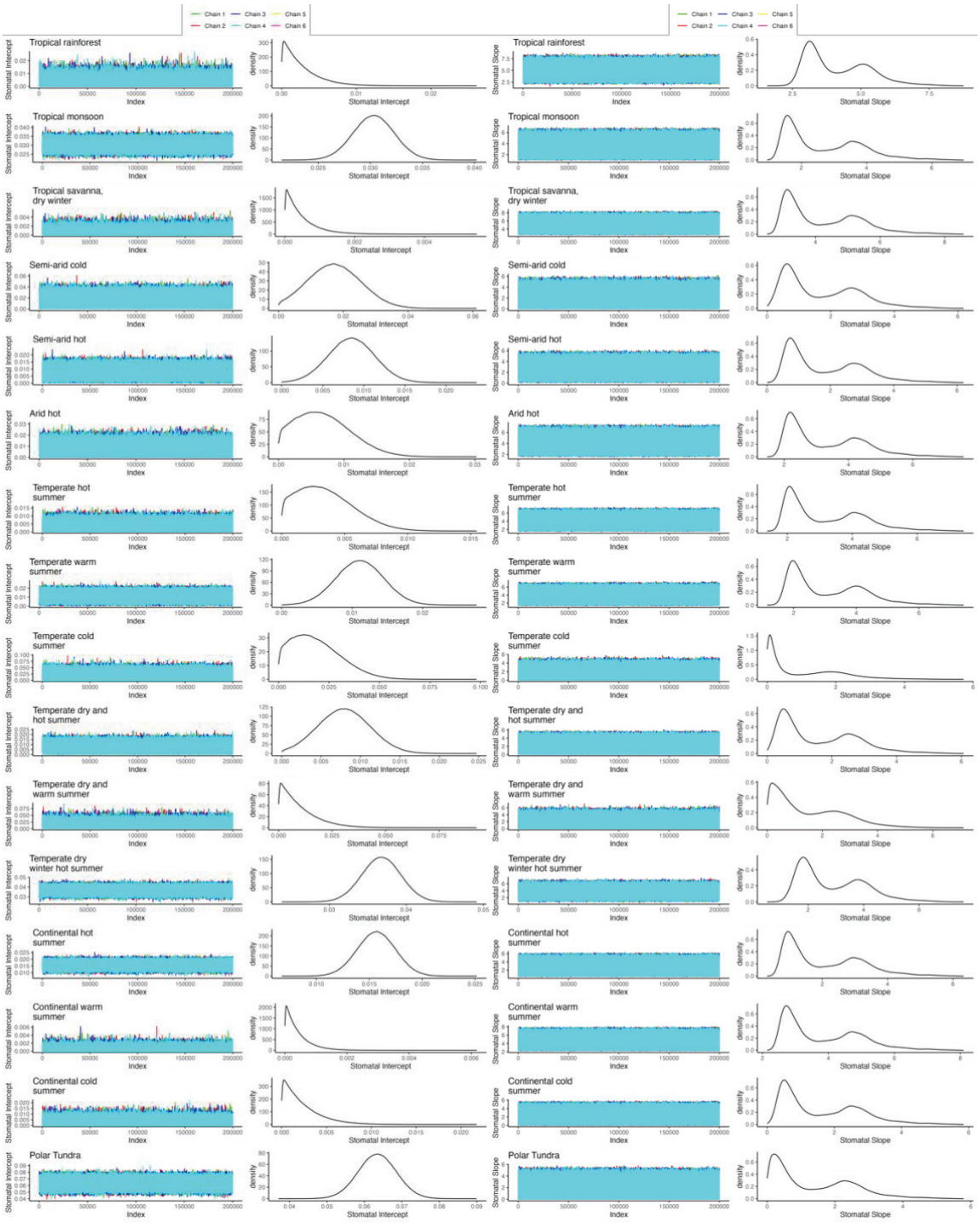

Figure A5.9: Caterpillar plots of posterior chains and histograms of posterior distributions for climate zone specific slope and intercept using the Medlyn model and uninformative priors.



Figure A5.10: Caterpillar plots of posterior chains and histograms of posterior distributions for climate zone specific slope and intercept using the Lamour model and uninformative priors.

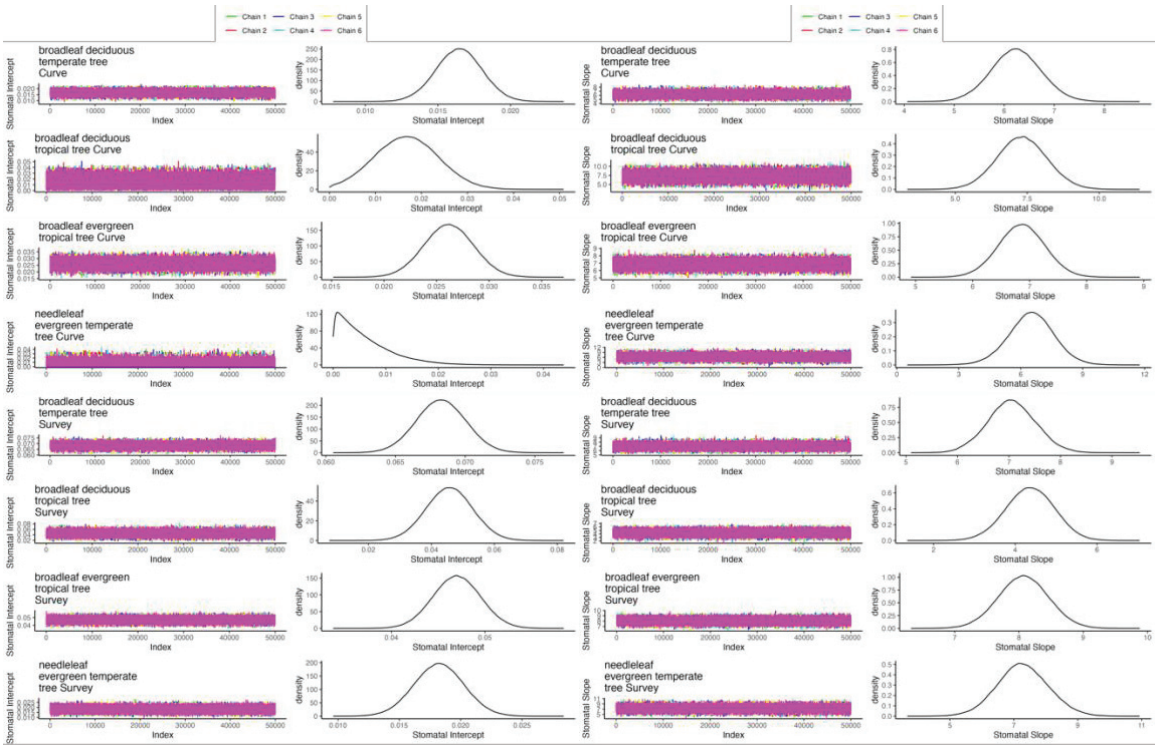

Figure A5.11: Caterpillar plots of posterior chains and histograms of posterior distributions for measurement method specific slope and intercept using the BWB model and uninformative priors.

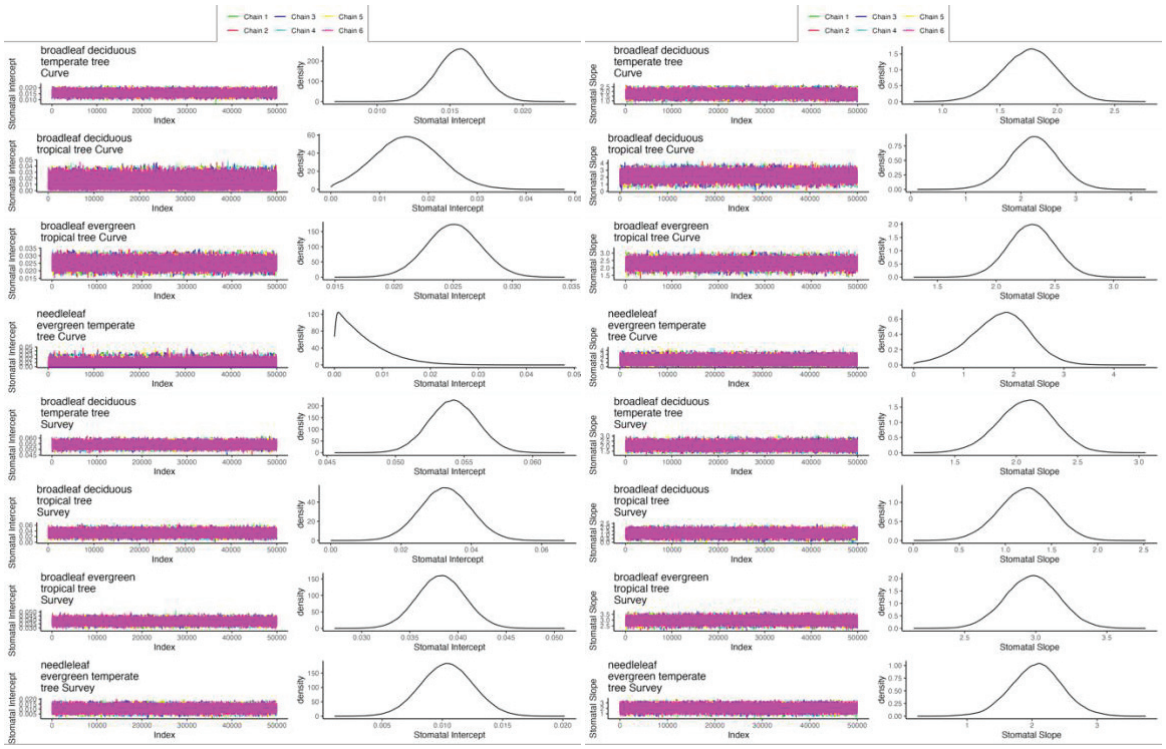

Figure A5.12: Caterpillar plots of posterior chains and histograms of posterior distributions for measurement method specific slope and intercept using the Medlyn model and uninformative priors.

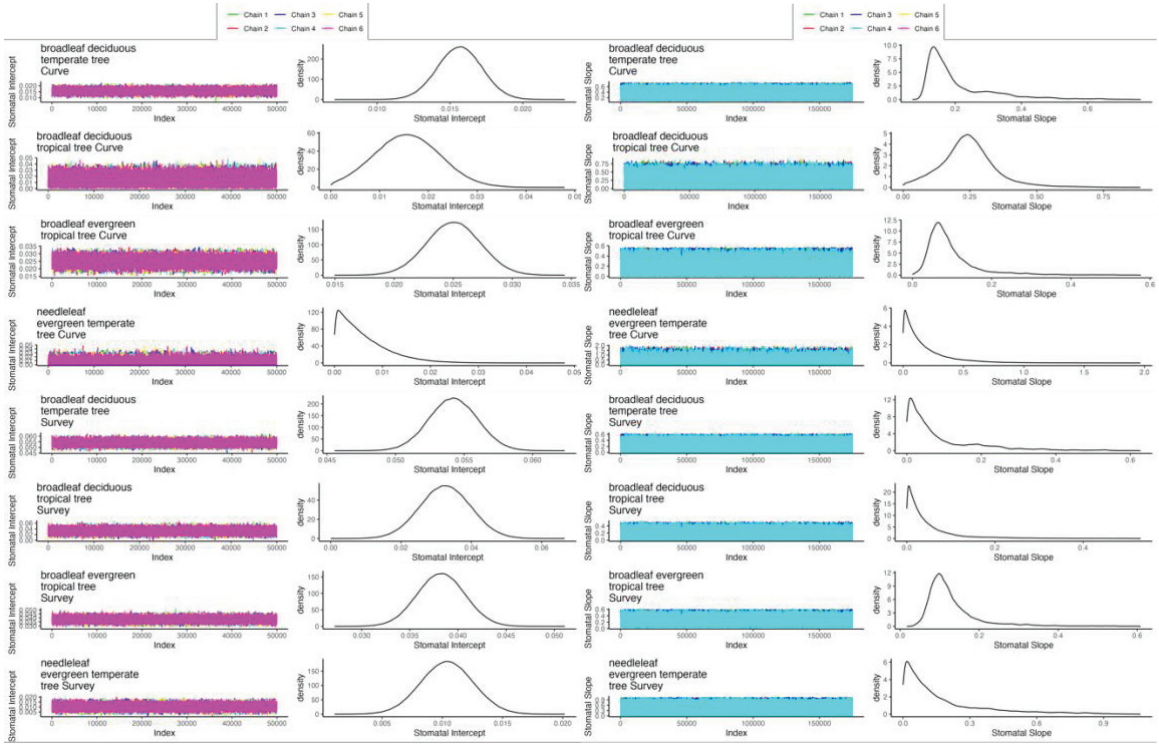

Figure A5.13: Caterpillar plots of posterior chains and histograms of posterior distributions for measurement method specific slope and intercept using the Lamour model and uninformative priors.

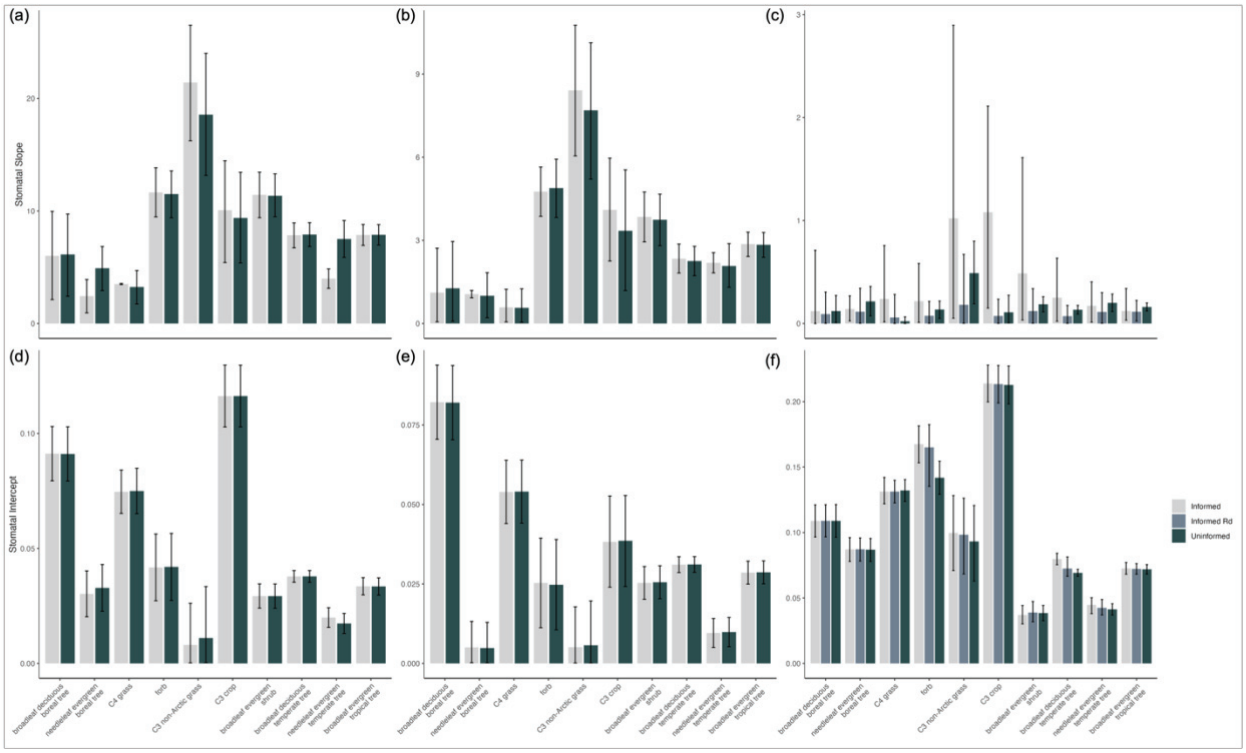

Figure A5.14: The effect of using informative versus uninformative priors on PFT specific estimates of (a-c) stomatal slope and intercept (d-f). Panels (a) and (d) correspond to the BWB model, panels (b) and (e) correspond to the Medlyn model, and panels (c) and (f) correspond to the Lamour model. For a full description of the models and the different priors used see Table 6.1.

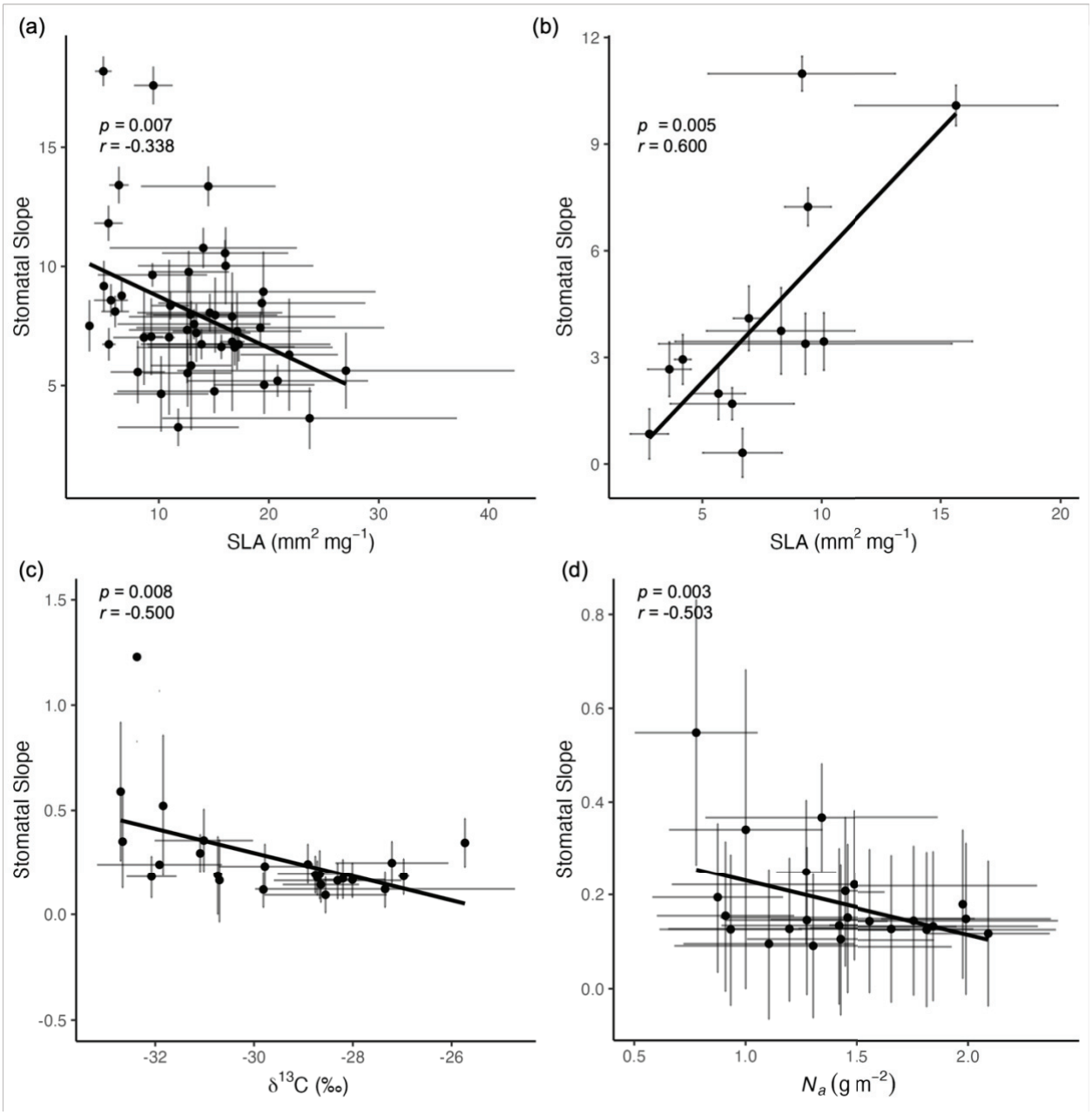

Figure A5.15: PFT specific correlations between estimated stomatal slope and leaf traits which were significant ($p \leq 0.0125$). Relationship between SLA and stomatal slope for (a) broadleaf evergreen tropical tree using the BWB model, and (b) broadleaf evergreen shrub using the Medlyn model. Relationship between ^{13}C isotope discrimination and stomatal slope for the Lamour model in (c) the broadleaf evergreen tropical tree PFT. Relationship between N_a and stomatal slope for the Lamour model in (d) the broadleaf deciduous temperate tree PFT. Horizontal error bars are ± 2 SE of the mean species-specific trait estimate. Vertical error bars are the 95% credible interval for the species level estimate of stomatal slope. The reported *r* value is the Pearson correlation coefficient.

Table A5.1: Links to the datasets used in this study, and their associated manuscripts. Information such as number of species and manipulation correspond to the subset of data from the original source which was included in this analysis.

Dataset	Manuscript Link	Data Link	Location	Method	Number of Species	Number of PFTs	Manipulation
Albert *et al* 2018	https://doi.org/10.1111/nph.15056	https://doi.org/10.5061/dryad.h83t0	Amazonas, Brazil	Curve, Survey	5	1	sun vs shade, leaf age
Aparecido *et al* 2020	https://doi.org/10.1111/ele.13516	https://doi.org/10.5061/dryad.j9kd51c8h	Arizona, US	Survey	9	3	natural drought
Baker *et al* 2020	https://doi.org/10.1093/aobpla/plz056	https://doi.org/10.5061/dryad.cr54775	Idaho, US	Survey	1	1	natural drought
Davidson *et al* 2022	http://dx.doi.org/10.1093/treephys/tpac006	http://dx.doi.org/10.15486/ngt/1783681	New York, US	Curve	1	1	excision
Davidson *et al* 2023a	https://doi.org/10.6073/pasta/400eae2df484707ced77d2c2563e3c6c	https://doi.org/10.1111/nph.19137	New York, US	Curve	6	1	seasonality
Davidson *et al* 2023b	-	https://doi.org/10.5440/1975097	Alaska, US	Curve	2	1	none
Heyduk *et al* 2016	https://doi.org/10.1093/jxb/erv536	https://doi.org/10.5061/dryad.pm4m5	Southeastern US	Survey	1	1	drought
Hogan *et al* 2021	http://dx.doi.org/10.1093/treephys/tpab151	https://doi.org/10.6073/pasta/27f6332609eb1ef6d398c7855855f2e3	Florida, US	Survey	6	1	none
Lamour *et al* 2021	https://doi.org/10.1111/gcb.16103 https://doi.org/10.1111/nph.18684	http://dx.doi.org/10.15486/ngt/1781004	Colón, Panama	Survey, Curve	17	3	leaf age
Lamour *et al* 2022	-	https://doi.org/10.15486/ngt/1896884	Panamá, Panama	Survey, Curve	5	1	vertical variation
Lin *et al* 2015	https://doi.org/10.1038/nclimate2550	https://figshare.com/articles/dataset/Optimal_stomatal_behaviour_around_the_world/1304289	Multiple	Survey	108	12	none
Rogers & Ely 2023	-	https://doi.org/10.5440/1975125	Alaska, US	Curve	6	2	none
Rogers *et al* 2022	https://doi.org/10.1111/gcb.14820	http://dx.doi.org/10.15486/ngt/1411972	Colón & Panamá, Panama	Survey	17	2	none
Schmiege *et al* 2020	https://doi.org/10.1093/treephys/tpaa123	https://doi.org/10.5061/dryad.1g1jwstss	Lam Dong, Vietnam	Curve	7	2	common garden
Verryckt *et al* 2020	https://doi.org/10.1111/btp.12774	https://doi.org/10.5061/dryad.v9s4mw6rg	Regina, French Guiana	Survey	5	1	excision
Wei *et al* 2022	https://doi.org/10.1111/1365-2435.14007	https://doi.org/10.5061/dryad.dncjsxm1d	Alberta, Canada	Survey	2	1	natural drought
Williams *et al* 2020	https://doi.org/10.1111/1365-2435.13613	https://doi.org/10.5061/dryad.ngf1vhhr9	Guanacaste, Costa Rica	Survey	14	4	artificial drought
Williams *et al* 2021	-	https://doi.org/10.6073/pasta/18acf7c9de8f7bcf5ff4ff274ec67e93	Massachusetts, US	Survey	15	1	disturbance
Wolz *et al* 2017	https://doi.org/10.1038/s41559-017-0238-z	https://www.nature.com/articles/s41559-017-0238-z	Illinois, US	Survey	6	2	none
Yang *et al* 2020	https://doi.org/10.1029/2019JG005624	https://doi.org/10.5061/dryad.b2rbnzs9k	Arizona, US	Survey	17	2	none

Table A5.2: Model summary for the PFT specific models using uninventive priors. Columns composed to PFT, parameter estimated, stomatal model used, priors used, parameter mean estimate, standard deviation of the estimate, and 2.5%, 50% and 97.5% quantiles for the estimate. For a full description of the models see Table 6.1.

PFT	Parameter	Model	Priors	mean	SD	2.50%	50%	97.50%
C3 Arctic grass	Stomatal Intercept	BWB	Uninformative slope	0.063	0.006	0.051	0.063	0.075
broadleaf deciduous boreal shrub	Stomatal Intercept	BWB	Uninformative slope	0.091	0.006	0.079	0.091	0.103
broadleaf deciduous boreal tree	Stomatal Intercept	BWB	Uninformative slope	0.027	0.024	0.001	0.021	0.088
needleleaf evergreen boreal tree	Stomatal Intercept	BWB	Uninformative slope	0.033	0.005	0.023	0.033	0.043
C4 grass	Stomatal Intercept	BWB	Uninformative slope	0.075	0.005	0.065	0.075	0.085
forb	Stomatal Intercept	BWB	Uninformative slope	0.042	0.007	0.027	0.042	0.057
C3 non-Arctic grass	Stomatal Intercept	BWB	Uninformative slope	0.011	0.009	0	0.009	0.033
C3 crop	Stomatal Intercept	BWB	Uninformative slope	0.116	0.007	0.103	0.116	0.13
broadleaf evergreen shrub	Stomatal Intercept	BWB	Uninformative slope	0.029	0.003	0.024	0.029	0.035
broadleaf deciduous temperate shrub	Stomatal Intercept	BWB	Uninformative slope	0.041	0.004	0.034	0.041	0.048
broadleaf deciduous temperate tree	Stomatal Intercept	BWB	Uninformative slope	0.038	0.001	0.035	0.038	0.04
broadleaf evergreen temperate tree	Stomatal Intercept	BWB	Uninformative slope	0.027	0.002	0.022	0.027	0.031
needleleaf evergreen temperate tree	Stomatal Intercept	BWB	Uninformative slope	0.017	0.002	0.013	0.017	0.022
broadleaf deciduous tropical tree	Stomatal Intercept	BWB	Uninformative slope	0.034	0.006	0.023	0.034	0.045
broadleaf evergreen tropical tree	Stomatal Intercept	BWB	Uninformative slope	0.033	0.002	0.03	0.034	0.037
C3 Arctic grass	Stomatal Slope	BWB	Uninformative slope	6.396	1.51	3.406	6.406	9.342
broadleaf deciduous boreal shrub	Stomatal Slope	BWB	Uninformative slope	6.142	1.868	2.423	6.169	9.728

Table A5.2 (cont.): Model summary for the PFT specific models using uninventive priors. Columns composed to PFT, parameter estimated, stomatal model used, priors used, parameter mean estimate, standard deviation of the estimate, and 2.5%, 50% and 97.5% quantiles for the estimate. For a full description of the models see Table 6.1.

PFT	Parameter	Model	Priors	mean	SD	2.50%	50%	97.50%
broadleaf deciduous boreal tree	Stomatal Slope	BWB	Uninformative slope	9.978	1.699	6.23	10.116	12.938
needleleaf evergreen boreal tree	Stomatal Slope	BWB	Uninformative slope	4.916	0.992	2.932	4.926	6.84
C4 grass	Stomatal Slope	BWB	Uninformative slope	3.249	0.752	1.739	3.266	4.709
forb	Stomatal Slope	BWB	Uninformative slope	11.507	1.065	9.394	11.526	13.559
C3 non-Arctic grass	Stomatal Slope	BWB	Uninformative slope	18.566	2.778	13.171	18.539	24.014
C3 crop	Stomatal Slope	BWB	Uninformative slope	9.383	2.006	5.383	9.397	13.439
broadleaf evergreen shrub	Stomatal Slope	BWB	Uninformative slope	11.354	0.978	9.495	11.339	13.303
broadleaf deciduous temperate shrub	Stomatal Slope	BWB	Uninformative slope	11.606	0.74	10.163	11.605	13.063
broadleaf deciduous temperate tree	Stomatal Slope	BWB	Uninformative slope	7.911	0.54	6.845	7.909	8.967
broadleaf evergreen temperate tree	Stomatal Slope	BWB	Uninformative slope	10.422	0.963	8.484	10.433	12.322
needleleaf evergreen temperate tree	Stomatal Slope	BWB	Uninformative slope	7.514	0.831	5.881	7.51	9.148
broadleaf deciduous tropical tree	Stomatal Slope	BWB	Uninformative slope	5.07	0.642	3.798	5.072	6.329
broadleaf evergreen tropical tree	Stomatal Slope	BWB	Uninformative slope	7.887	0.463	6.976	7.886	8.792
C3 Arctic grass	$R_{d.25}$	Lamour	Uninformative slope Informative $R_{d.25}$	3.981	1.435	1.36	3.932	6.891
broadleaf deciduous boreal shrub	$R_{d.25}$	Lamour	Uninformative slope Informative $R_{d.25}$	3.408	1.183	0.981	3.452	5.604

Table A5.2 (cont.): Model summary for the PFT specific models using uninventive priors. Columns composed to PFT, parameter estimated, stomatal model used, priors used, parameter mean estimate, standard deviation of the estimate, and 2.5%, 50% and 97.5% quantiles for the estimate. For a full description of the models see Table 6.1.

PFT	Parameter	Model	Priors	mean	SD	2.50%	50%	97.50%
broadleaf deciduous boreal tree	$R_{d.25}$	Lamour	Uninformative slope Informative $R_{d.25}$	2.159	1.602	0.132	1.811	6.157
needleleaf evergreen boreal tree	$R_{d.25}$	Lamour	Uninformative slope Informative $R_{d.25}$	5.307	0.742	3.807	5.317	6.747
C4 grass	$R_{d.25}$	Lamour	Uninformative slope Informative $R_{d.25}$	1.482	0.451	0.752	1.432	2.503
forb	$R_{d.25}$	Lamour	Uninformative slope Informative $R_{d.25}$	1.97	0.604	0.655	2.128	2.845
C3 non-Arctic grass	$R_{d.25}$	Lamour	Uninformative slope Informative $R_{d.25}$	1.533	0.597	0.283	1.558	2.698
C3 crop	$R_{d.25}$	Lamour	Uninformative slope Informative $R_{d.25}$	6.377	0.641	5.107	6.356	7.731
broadleaf evergreen shrub	$R_{d.25}$	Lamour	Uninformative slope Informative $R_{d.25}$	0.352	0.369	0.042	0.211	1.436
broadleaf deciduous temperate shrub	$R_{d.25}$	Lamour	Uninformative slope Informative $R_{d.25}$	2.344	0.41	1.348	2.441	2.955
broadleaf deciduous temperate tree	$R_{d.25}$	Lamour	Uninformative slope Informative $R_{d.25}$	0.809	0.729	0.047	0.444	2.195
broadleaf evergreen temperate tree	$R_{d.25}$	Lamour	Uninformative slope Informative $R_{d.25}$	1.493	0.325	0.795	1.516	2.068
needleleaf evergreen temperate tree	$R_{d.25}$	Lamour	Uninformative slope Informative $R_{d.25}$	0.694	0.447	0.105	0.585	1.824
broadleaf deciduous tropical tree	$R_{d.25}$	Lamour	Uninformative slope Informative $R_{d.25}$	0.839	0.384	0.205	0.803	1.675
broadleaf evergreen tropical tree	$R_{d.25}$	Lamour	Uninformative slope Informative $R_{d.25}$	0.591	0.399	0.088	0.467	1.45

Table A5.2 (cont.): Model summary for the PFT specific models using uninventive priors. Columns composed to PFT, parameter estimated, stomatal model used, priors used, parameter mean estimate, standard deviation of the estimate, and 2.5%, 50% and 97.5% quantiles for the estimate. For a full description of the models see Table 6.1.

PFT	Parameter	Model	Priors	mean	SD	2.50%	50%	97.50%
C3 Arctic grass	Stomatal Intercept	Lamour	Uninformative slope Informative $R_{d.25}$	0.086	0.006	0.074	0.086	0.098
broadleaf deciduous boreal shrub	Stomatal Intercept	Lamour	Uninformative slope Informative $R_{d.25}$	0.109	0.006	0.097	0.109	0.121
broadleaf deciduous boreal tree	Stomatal Intercept	Lamour	Uninformative slope Informative $R_{d.25}$	0.05	0.037	0.002	0.043	0.135
needleleaf evergreen boreal tree	Stomatal Intercept	Lamour	Uninformative slope Informative $R_{d.25}$	0.087	0.005	0.078	0.087	0.096
C4 grass	Stomatal Intercept	Lamour	Uninformative slope Informative $R_{d.25}$	0.131	0.004	0.123	0.131	0.14
forb	Stomatal Intercept	Lamour	Uninformative slope Informative $R_{d.25}$	0.165	0.012	0.135	0.168	0.182
C3 non-Arctic grass	Stomatal Intercept	Lamour	Uninformative slope Informative $R_{d.25}$	0.098	0.015	0.068	0.099	0.126
C3 crop	Stomatal Intercept	Lamour	Uninformative slope Informative $R_{d.25}$	0.213	0.007	0.199	0.213	0.228
broadleaf evergreen shrub	Stomatal Intercept	Lamour	Uninformative slope Informative $R_{d.25}$	0.039	0.004	0.032	0.039	0.047
broadleaf deciduous temperate shrub	Stomatal Intercept	Lamour	Uninformative slope Informative $R_{d.25}$	0.122	0.004	0.114	0.122	0.131
broadleaf deciduous temperate tree	Stomatal Intercept	Lamour	Uninformative slope Informative $R_{d.25}$	0.072	0.005	0.067	0.07	0.081
broadleaf evergreen temperate tree	Stomatal Intercept	Lamour	Uninformative slope Informative $R_{d.25}$	0.076	0.003	0.071	0.076	0.081
needleleaf evergreen temperate tree	Stomatal Intercept	Lamour	Uninformative slope Informative $R_{d.25}$	0.042	0.003	0.037	0.042	0.049
broadleaf deciduous tropical tree	Stomatal Intercept	Lamour	Uninformative slope Informative $R_{d.25}$	0.071	0.005	0.06	0.071	0.081

Table A5.2 (cont.): Model summary for the PFT specific models using uninventive priors. Columns composed to PFT, parameter estimated, stomatal model used, priors used, parameter mean estimate, standard deviation of the estimate, and 2.5%, 50% and 97.5% quantiles for the estimate. For a full description of the models see Table 6.1.

PFT	Parameter	Model	Priors	mean	SD	2.50%	50%	97.50%
broadleaf evergreen tropical tree	Stomatal Intercept	Lamour	Uninformative slope Informative $R_{d.25}$	0.072	0.002	0.068	0.072	0.076
C3 Arctic grass	Stomatal Slope	Lamour	Uninformative slope Informative $R_{d.25}$	0.114	0.101	0.002	0.086	0.351
broadleaf deciduous boreal shrub	Stomatal Slope	Lamour	Uninformative slope Informative $R_{d.25}$	0.092	0.085	0.002	0.067	0.306
broadleaf deciduous boreal tree	Stomatal Slope	Lamour	Uninformative slope Informative $R_{d.25}$	0.073	0.068	0.001	0.051	0.232
needleleaf evergreen boreal tree	Stomatal Slope	Lamour	Uninformative slope Informative $R_{d.25}$	0.115	0.099	0.002	0.089	0.342
C4 grass	Stomatal Slope	Lamour	Uninformative slope Informative $R_{d.25}$	0.059	0.07	0.001	0.034	0.283
forb	Stomatal Slope	Lamour	Uninformative slope Informative $R_{d.25}$	0.076	0.06	0.002	0.06	0.215
C3 non-Arctic grass	Stomatal Slope	Lamour	Uninformative slope Informative $R_{d.25}$	0.182	0.195	0.002	0.103	0.671
C3 crop	Stomatal Slope	Lamour	Uninformative slope Informative $R_{d.25}$	0.074	0.065	0.002	0.053	0.237
broadleaf evergreen shrub	Stomatal Slope	Lamour	Uninformative slope Informative $R_{d.25}$	0.121	0.094	0.003	0.108	0.338
broadleaf deciduous temperate shrub	Stomatal Slope	Lamour	Uninformative slope Informative $R_{d.25}$	0.131	0.064	0.015	0.137	0.266
broadleaf deciduous temperate tree	Stomatal Slope	Lamour	Uninformative slope Informative $R_{d.25}$	0.071	0.054	0.002	0.059	0.176
broadleaf evergreen temperate tree	Stomatal Slope	Lamour	Uninformative slope Informative $R_{d.25}$	0.086	0.067	0.002	0.075	0.23

Table A5.2 (cont.): Model summary for the PFT specific models using uninventive priors. Columns composed to PFT, parameter estimated, stomatal model used, priors used, parameter mean estimate, standard deviation of the estimate, and 2.5%, 50% and 97.5% quantiles for the estimate. For a full description of the models see Table 6.1.

PFT	Parameter	Model	Priors	mean	SD	2.50%	50%	97.50%
needleleaf evergreen temperate tree	Stomatal Slope	Lamour	Uninformative slope Informative $R_{d.25}$	0.113	0.088	0.002	0.095	0.301
broadleaf deciduous tropical tree	Stomatal Slope	Lamour	Uninformative slope Informative $R_{d.25}$	0.077	0.057	0.002	0.069	0.192
broadleaf evergreen tropical tree	Stomatal Slope	Lamour	Uninformative slope Informative $R_{d.25}$	0.115	0.056	0.024	0.112	0.225
C3 Arctic grass	$R_{d.25}$	Lamour	Uninformative slope Uninformative $R_{d.25}$	1.874	1.367	0.074	1.62	5.037
broadleaf deciduous boreal shrub	$R_{d.25}$	Lamour	Uninformative slope Uninformative $R_{d.25}$	2.902	1.217	0.45	2.959	5.128
broadleaf deciduous boreal tree	$R_{d.25}$	Lamour	Uninformative slope Uninformative $R_{d.25}$	1.771	1.561	0.052	1.348	5.791
needleleaf evergreen boreal tree	$R_{d.25}$	Lamour	Uninformative slope Uninformative $R_{d.25}$	5.188	0.596	3.99	5.198	6.323
C4 grass	$R_{d.25}$	Lamour	Uninformative slope Uninformative $R_{d.25}$	1.007	0.572	0.076	0.97	2.201
forb	$R_{d.25}$	Lamour	Uninformative slope Uninformative $R_{d.25}$	0.956	0.284	0.362	0.967	1.484
C3 non-Arctic grass	$R_{d.25}$	Lamour	Uninformative slope Uninformative $R_{d.25}$	1.591	0.352	0.837	1.613	2.214
C3 crop	$R_{d.25}$	Lamour	Uninformative slope Uninformative $R_{d.25}$	6.203	0.322	5.563	6.206	6.824
broadleaf evergreen shrub	$R_{d.25}$	Lamour	Uninformative slope Uninformative $R_{d.25}$	0.044	0.042	0.001	0.031	0.155
broadleaf deciduous temperate shrub	$R_{d.25}$	Lamour	Uninformative slope Uninformative $R_{d.25}$	2.544	0.131	2.288	2.544	2.801
broadleaf deciduous temperate tree	$R_{d.25}$	Lamour	Uninformative slope Uninformative $R_{d.25}$	0.125	0.083	0.007	0.113	0.314

Table A5.2 (cont.): Model summary for the PFT specific models using uninventive priors. Columns composed to PFT, parameter estimated, stomatal model used, priors used, parameter mean estimate, standard deviation of the estimate, and 2.5%, 50% and 97.5% quantiles for the estimate. For a full description of the models see Table 6.1.

PFT	Parameter	Model	Priors	mean	SD	2.50%	50%	97.50%
broadleaf evergreen temperate tree	$R_{d.25}$	Lamour	Uninformative slope Uninformative $R_{d.25}$	1.33	0.184	0.974	1.328	1.695
needleleaf evergreen temperate tree	$R_{d.25}$	Lamour	Uninformative slope Uninformative $R_{d.25}$	0.391	0.208	0.036	0.381	0.818
broadleaf deciduous tropical tree	$R_{d.25}$	Lamour	Uninformative slope Uninformative $R_{d.25}$	0.753	0.392	0.073	0.739	1.55
broadleaf evergreen tropical tree	$R_{d.25}$	Lamour	Uninformative slope Uninformative $R_{d.25}$	0.06	0.055	0.002	0.044	0.205
C3 Arctic grass	Stomatal Intercept	Lamour	Uninformative slope Uninformative $R_{d.25}$	0.085	0.006	0.073	0.085	0.098
broadleaf deciduous boreal shrub	Stomatal Intercept	Lamour	Uninformative slope Uninformative $R_{d.25}$	0.109	0.006	0.096	0.109	0.121
broadleaf deciduous boreal tree	Stomatal Intercept	Lamour	Uninformative slope Uninformative $R_{d.25}$	0.057	0.041	0.002	0.05	0.152
needleleaf evergreen boreal tree	Stomatal Intercept	Lamour	Uninformative slope Uninformative $R_{d.25}$	0.087	0.004	0.078	0.087	0.095
C4 grass	Stomatal Intercept	Lamour	Uninformative slope Uninformative $R_{d.25}$	0.132	0.004	0.124	0.132	0.14
forb	Stomatal Intercept	Lamour	Uninformative slope Uninformative $R_{d.25}$	0.142	0.006	0.129	0.142	0.154
C3 non-Arctic grass	Stomatal Intercept	Lamour	Uninformative slope Uninformative $R_{d.25}$	0.093	0.015	0.063	0.094	0.121
C3 crop	Stomatal Intercept	Lamour	Uninformative slope Uninformative $R_{d.25}$	0.213	0.007	0.198	0.213	0.227
broadleaf evergreen shrub	Stomatal Intercept	Lamour	Uninformative slope Uninformative $R_{d.25}$	0.038	0.003	0.033	0.038	0.044
broadleaf deciduous temperate shrub	Stomatal Intercept	Lamour	Uninformative slope Uninformative $R_{d.25}$	0.12	0.004	0.112	0.12	0.128

Table A5.2 (cont.): Model summary for the PFT specific models using uninventive priors. Columns composed to PFT, parameter estimated, stomatal model used, priors used, parameter mean estimate, standard deviation of the estimate, and 2.5%, 50% and 97.5% quantiles for the estimate. For a full description of the models see Table 6.1.

PFT	Parameter	Model	Priors	mean	SD	2.50%	50%	97.50%
broadleaf deciduous temperate tree	Stomatal Intercept	Lamour	Uninformative slope Uninformative $R_{d.25}$	0.069	0.001	0.067	0.069	0.072
broadleaf evergreen temperate tree	Stomatal Intercept	Lamour	Uninformative slope Uninformative $R_{d.25}$	0.075	0.003	0.07	0.075	0.08
needleleaf evergreen temperate tree	Stomatal Intercept	Lamour	Uninformative slope Uninformative $R_{d.25}$	0.041	0.002	0.037	0.041	0.046
broadleaf deciduous tropical tree	Stomatal Intercept	Lamour	Uninformative slope Uninformative $R_{d.25}$	0.071	0.005	0.06	0.071	0.081
broadleaf evergreen tropical tree	Stomatal Intercept	Lamour	Uninformative slope Uninformative $R_{d.25}$	0.072	0.002	0.068	0.072	0.076
C3 Arctic grass	Stomatal Slope	Lamour	Uninformative slope Uninformative $R_{d.25}$	0.184	0.07	0.049	0.183	0.324
broadleaf deciduous boreal shrub	Stomatal Slope	Lamour	Uninformative slope Uninformative $R_{d.25}$	0.121	0.07	0.009	0.116	0.272
broadleaf deciduous boreal tree	Stomatal Slope	Lamour	Uninformative slope Uninformative $R_{d.25}$	0.156	0.064	0.044	0.152	0.297
needleleaf evergreen boreal tree	Stomatal Slope	Lamour	Uninformative slope Uninformative $R_{d.25}$	0.215	0.072	0.074	0.214	0.36
C4 grass	Stomatal Slope	Lamour	Uninformative slope Uninformative $R_{d.25}$	0.022	0.017	0.001	0.019	0.064
forb	Stomatal Slope	Lamour	Uninformative slope Uninformative $R_{d.25}$	0.136	0.042	0.05	0.136	0.218
C3 non-Arctic grass	Stomatal Slope	Lamour	Uninformative slope Uninformative $R_{d.25}$	0.49	0.154	0.191	0.487	0.8
C3 crop	Stomatal Slope	Lamour	Uninformative slope Uninformative $R_{d.25}$	0.109	0.071	0.006	0.101	0.275
broadleaf evergreen shrub	Stomatal Slope	Lamour	Uninformative slope Uninformative $R_{d.25}$	0.187	0.037	0.114	0.187	0.26

Table A5.2 (cont.): Model summary for the PFT specific models using uninventive priors. Columns composed to PFT, parameter estimated, stomatal model used, priors used, parameter mean estimate, standard deviation of the estimate, and 2.5%, 50% and 97.5% quantiles for the estimate. For a full description of the models see Table 6.1.

PFT	Parameter	Model	Priors	mean	SD	2.50%	50%	97.50%
broadleaf deciduous temperate shrub	Stomatal Slope	Lamour	Uninformative slope Uninformative $R_{d.25}$	0.164	0.025	0.116	0.164	0.214
broadleaf deciduous temperate tree	Stomatal Slope	Lamour	Uninformative slope Uninformative $R_{d.25}$	0.134	0.022	0.092	0.134	0.176
broadleaf evergreen temperate tree	Stomatal Slope	Lamour	Uninformative slope Uninformative $R_{d.25}$	0.118	0.042	0.034	0.118	0.201
needleleaf evergreen temperate tree	Stomatal Slope	Lamour	Uninformative slope Uninformative $R_{d.25}$	0.201	0.043	0.117	0.2	0.286
broadleaf deciduous tropical tree	Stomatal Slope	Lamour	Uninformative slope Uninformative $R_{d.25}$	0.133	0.026	0.083	0.133	0.183
broadleaf evergreen tropical tree	Stomatal Slope	Lamour	Uninformative slope Uninformative $R_{d.25}$	0.161	0.02	0.122	0.161	0.199
C3 Arctic grass	Stomatal Intercept	Medlyn	Uninformative slope	0.054	0.006	0.041	0.054	0.066
broadleaf deciduous boreal shrub	Stomatal Intercept	Medlyn	Uninformative slope	0.082	0.006	0.07	0.082	0.094
broadleaf deciduous boreal tree	Stomatal Intercept	Medlyn	Uninformative slope	0.022	0.021	0.001	0.016	0.078
needleleaf evergreen boreal tree	Stomatal Intercept	Medlyn	Uninformative slope	0.005	0.003	0	0.004	0.013
C4 grass	Stomatal Intercept	Medlyn	Uninformative slope	0.054	0.005	0.044	0.054	0.064
forb	Stomatal Intercept	Medlyn	Uninformative slope	0.025	0.007	0.011	0.025	0.039
C3 non-Arctic grass	Stomatal Intercept	Medlyn	Uninformative slope	0.006	0.005	0	0.004	0.02
C3 crop	Stomatal Intercept	Medlyn	Uninformative slope	0.039	0.007	0.024	0.039	0.053
broadleaf evergreen shrub	Stomatal Intercept	Medlyn	Uninformative slope	0.026	0.003	0.02	0.026	0.031
broadleaf deciduous temperate shrub	Stomatal Intercept	Medlyn	Uninformative slope	0.032	0.004	0.025	0.032	0.039

Table A5.2 (cont.): Model summary for the PFT specific models using uninventive priors. Columns composed to PFT, parameter estimated, stomatal model used, priors used, parameter mean estimate, standard deviation of the estimate, and 2.5%, 50% and 97.5% quantiles for the estimate. For a full description of the models see Table 6.1.

PFT	Parameter	Model	Priors	mean	SD	2.50%	50%	97.50%
needleleaf evergreen temperate tree	Stomatal Slope	Medlyn	Uninformative slope	2.077	0.404	1.308	2.071	2.885
broadleaf deciduous tropical tree	Stomatal Slope	Medlyn	Uninformative slope	1.479	0.313	0.862	1.481	2.089
broadleaf evergreen tropical tree	Stomatal Slope	Medlyn	Uninformative slope	2.842	0.228	2.391	2.843	3.285

ProQuest Number: 30815092

INFORMATION TO ALL USERS
The quality and completeness of this reproduction is dependent on the quality
and completeness of the copy made available to ProQuest.



Distributed by ProQuest LLC (2024).
Copyright of the Dissertation is held by the Author unless otherwise noted.

This work may be used in accordance with the terms of the Creative Commons license
or other rights statement, as indicated in the copyright statement or in the metadata
associated with this work. Unless otherwise specified in the copyright statement
or the metadata, all rights are reserved by the copyright holder.

This work is protected against unauthorized copying under Title 17,
United States Code and other applicable copyright laws.

Microform Edition where available © ProQuest LLC. No reproduction or digitization
of the Microform Edition is authorized without permission of ProQuest LLC.

ProQuest LLC
789 East Eisenhower Parkway
P.O. Box 1346
Ann Arbor, MI 48106 - 1346 USA